EMERGING INFECTIOUS DISEASES®

CDC
Centers for Disease Control and Prevention

Zoonotic Infections

July 2021

***Parmigianino. Portrait of Antea*, c. 1531–1534.** Oil on canvas. 53.1 in × 34.6 in. Museo di Capodimonte, Naples, Italy, by kind permission of Ministero della Cultura–Museo e Real Bosco di Capodimonte.

EMERGING INFECTIOUS DISEASES®

Emerging Infectious Diseases is published monthly by the Centers for Disease Control and Prevention, 1600 Clifton Rd NE, Mailstop H16-2, Atlanta, GA 30329-4027, USA. Telephone 404-639-1960; email, eideditor@cdc.gov

EMERGING INFECTIOUS DISEASES®

Zoonotic Infections **July 2021**

On the Cover

Parmigianino. *Portrait of Antea*, c. 1531–1534. Oil on canvas. 53.1 in × 34.6 in. Museo di Capodimonte, Naples, Italy, by kind permission of Ministero della Cultura–Museo e Real Bosco di Capodimonte.

About the Cover p. 2003

Synopses

Research

Medscape EDUCATION ACTIVITY

EMERGING INFECTIOUS DISEASES®
July 2021

Dispatches

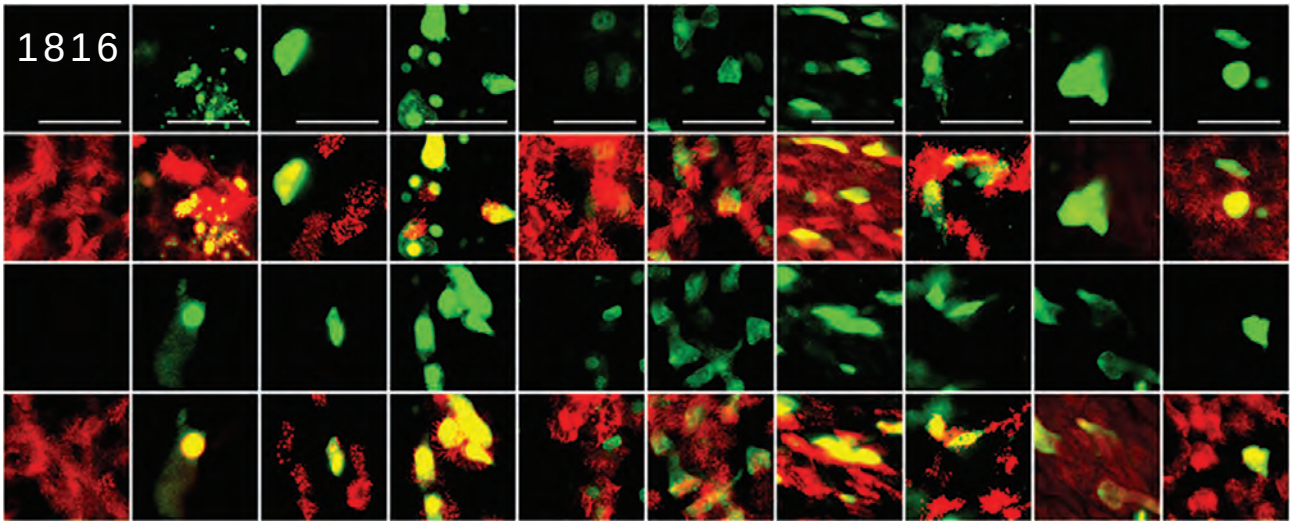

Research Letters

EMERGING INFECTIOUS DISEASES®
July 2021

About the Cover

Etymologia

1987

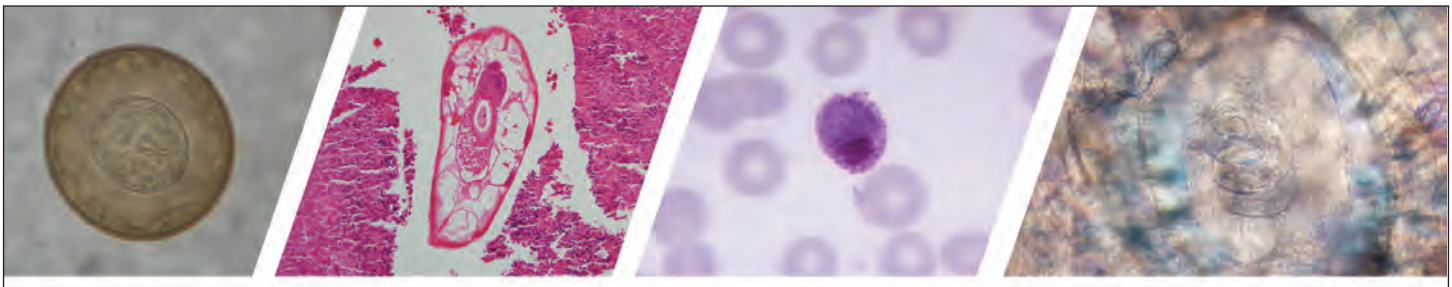

DPDx

Diagnostic Assistance and Training in Laboratory Identification of Parasites

A free service of CDC available to laboratorians, pathologists, and other health professionals in the United States and abroad

- Diagnosis from photographs of worms, histological sections, fecal, blood, and other specimen types
- Expert diagnostic review
- Formal diagnostic laboratory report
- Submission of samples via secure file share

Visit the DPDx website for information on laboratory diagnosis, geographic distribution, clinical features, parasite life cycles, and training via Monthly Case Studies of parasitic diseases.

www.cdc.gov/dpdx
dpdx@cdc.gov

U.S. Department of Health and Human Services
Centers for Disease Control and Prevention

CS272346-DE

Industry Sectors Highly Affected by Worksite Outbreaks of Coronavirus Disease, Los Angeles County, California, USA, March 19–September 30, 2020

Zuelma Contreras, Van Ngo, Marifi Pulido, Faith Washburn, Gayane Meschyan, Fruma Gluck, Karen Kuguru, Roshan Reporter, Condessa Curley, Rachel Civen, Dawn Terashita, Sharon Balter, Umme-Aiman Halai

Worksites with on-site operations have experienced coronavirus disease (COVID-19) outbreaks. We analyzed data for 698 nonresidential, nonhealthcare worksite COVID-19 outbreaks investigated in Los Angeles County, California, USA, during March 19, 2020–September 30, 2020, by using North American Industry Classification System sectors and subsectors. Nearly 60% of these outbreaks occurred in 3 sectors: manufacturing (n = 184, 26.4%), retail trade (n = 137, 19.6%), and transportation and warehousing (n = 73, 10.5%). The largest number of outbreaks and largest number and highest incidence rate of outbreak-associated cases occurred in manufacturing. Furthermore, 7 of the 10 industry subsectors with the highest incidence rates were within manufacturing. Approximately 70% of outbreak-associated case-patients reported Hispanic ethnicity. Facilities employing more on-site staff had larger and longer outbreaks. Identification of highly affected industry sectors and subsectors is necessary for targeted public health planning, outreach, and response, including ensuring vaccine access, to reduce burden of COVID-19 in vulnerable workers.

Worksites that have had on-site operations during the coronavirus disease (COVID-19) pandemic have been vulnerable to COVID-19 outbreaks. The effect of COVID-19 on essential workers in food manufacturing has been well-described, but limited data exist on the burden of COVID-19 in other industry sectors (*1*). The high-density, fast-paced environments of food production facilities pose a barrier to proper adherence to COVID-19 prevention measures, such as social distancing, use of face coverings, and cleaning of shared spaces (*2*). These challenges are not unique to food production facilities. Furthermore, factors distinctive to other sectors, such as increased contact with the public, could similarly increase the risk of COVID-19 worksite exposure. A closer examination of the COVID-19 burden in multiple industry sectors, particularly within their specific subsectors, is warranted to provide a more complete characterization of the risk and impact of COVID-19 exposure in worksites.

In Los Angeles County, California, USA, the first COVID-19 worksite outbreak was identified by the Los Angeles County Department of Public Health (LACDPH; Los Angeles, CA, USA) on March 19, 2020; by September 30, 2020, LACDPH had investigated 698 worksite outbreaks. Safer at home orders required all nonessential businesses in Los Angeles County to close operations during March 16–May 8, 2020, when some businesses opened under modified operations. The number of COVID-19 worksite outbreaks mirrored trends in community transmission. Worksite outbreak numbers increased until mid-July, followed by a gradual decrease until September 30. This analysis identifies the industries that were most affected by COVID-19 outbreaks in Los Angeles County during March 19–September 30, 2020, and describes worksite outbreak characteristics to understand the risk of exposure at the various worksites and to help guide public health outbreak prevention and response strategies.

Methods

Outbreak Identification

This analysis included COVID-19 outbreaks at nonresidential worksites in Los Angeles County but

Author affiliation: Los Angeles County Department of Public Health, Los Angeles, California, USA

DOI: https://doi.org/10.3201/eid2707.210425

excluded healthcare settings, homelessness services, and emergency medical services because outbreaks in these settings are investigated under different public health protocols. We excluded outbreaks in Pasadena and Long Beach because they have their own health departments. Initially, a worksite outbreak was identified when ≥5 suspected or laboratory-confirmed COVID-19 cases occurred within 14 days, with ≥1 case being laboratory-confirmed. On May 29, upon increased testing capacity and development of state definitions, a worksite outbreak was subsequently defined as ≥3 laboratory-confirmed cases occurring within 14 days. A county health officer order was issued requiring worksites to report any suspected outbreaks that might meet the definition. All reported, suspected outbreaks were investigated by LACDPH to determine if the cluster met outbreak criteria, including presence of epidemiologic links between cases indicating worksite transmission. Persons with COVID-19 were determined to be outbreak-associated cases on the basis of timing of symptoms or positive test result, exposure at the worksite during the investigation period, and absence of verifiable COVID-19 exposure outside the worksite.

Outbreak Investigation Procedures

Worksite outbreaks were investigated by an investigation team consisting of a public health investigator or public health nurse, a physician, and an environmental health inspector. Guidance on COVID-19 best practices was issued by the outbreak investigator to the worksite; guidance included recommendations on isolation of cases, contact investigation in the workplace, testing of close contacts, entry screening, physical distancing, masking, and cleaning/disinfection protocols. In addition, we conducted telephone conferences, as well as on-site visits, if needed, to assess worksite compliance with COVID-19 safety protocols. Worksites that failed to comply risked closure. Worksites were required to submit case line lists to LACDPH, and these lists were used for documentation and tracking of outbreak-associated cases at each site. The public health investigator regularly communicated with the site contact during each worksite outbreak (3–5 times/wk) to monitor for additional cases until at least 2 weeks after the last outbreak-associated case.

Analysis of Outbreak Data

We classified outbreaks by industry sector and subsector as described by the North American Industry Classification System used for classifying businesses (*3*). We calculated the outbreak-associated case incidence rate (IR) per 100,000 persons by using average annual employment data from the 2019 Quarterly Census of Employment and Wages (QCEW) for Los Angeles County (*4*). Because IR denominators include only employees, we excluded cases in nonemployees from IR calculations. We calculated outbreak duration by using symptom onset or test date, whichever was earlier, of the first and last outbreak-associated case. We calculated the Spearman correlation coefficient (ρ) to assess the strength and direction of association between the number of staff and number of outbreak-associated cases, as well as outbreak duration. We used descriptive statistics to summarize data. χ^2 tests were used to assess differences in case characteristics between sectors. All analyses were conducted by using SAS version 9.4 (https://www.sas.com).

Results

Worksite Outbreaks by Industry Sector

This analysis included 698 worksite outbreaks identified by LACDPH during March 19–September 30, 2020, of which 14% (n = 96) were still under investigation at the time of analysis. A total of 7,625 cases were associated with these outbreaks. We provide descriptive statistics for worksite outbreaks by North American Industry Classification System sector (Table 1). Most outbreaks occurred in manufacturing (n = 184, 26.4%), retail trade (n = 137, 19.6%), and transportation and warehousing (n = 73, 10.5%). Outbreak-associated cases were highest in manufacturing (n = 3,319, 43.5%), transportation and warehousing (n = 980, 12.9%), and retail trade (n = 871, 11.4%).

A total of 62 cases in nonemployees were excluded from IR calculations. Most (n = 15) nonemployee cases were in students within the educational services sector and children in daycare (n = 38) within the healthcare and social assistance sector. The remaining 9 nonemployee cases were spread across multiple different sectors and identified as being in vendors/contractors working on-site during the outbreak. The overall outbreak-associated IR was 171.8. The highest IRs were for manufacturing (980.8), transportation and warehousing (425.1), and wholesale trade (304.0). The overall median cases per outbreak was 6 (range 3–277), median on-site staff per outbreak was 95 (range 3–8,585), and median outbreak duration was 13 (range 0–189) days. The number of on-site employees showed a moderately positive correlation with the number of outbreak-associated cases (ρ = 0.49), as well as outbreak duration (ρ = 0.54) ($p<0.05$).

Table 1. Descriptive statistics for worksite outbreaks of coronavirus disease, by North American Industry Classification System industry sector, Los Angeles County, California, USA, March 19–September 30, 2020*

Sector	No. (%) outbreaks	No. (%) outbreak-associated cases	Average no. employed annually†	Outbreak-associated incidence‡	Median duration of outbreaks, d (min–max)	Median no. outbreak-associated cases (min–max)	Median no. staff at outbreak sites (min–max)
Overall total	698 (100.0)	7,625 (100.0)	4,439,578	171.8	13.0 (0–189)	6.0 (3–277)	95.0 (3–8,585)
Accommodation and food services	71 (10.2)	346 (4.5)	448,709	77.1	9.0 (0–71)	4.0 (3–16)	29.0 (3–180)
Administrative and support and waste management and remediation services	14 (2.0)	100 (1.3)	278,535	35.9	11.0 (1–85)	6.0 (3–17)	40.0 (11–239)
Arts, entertainment, and recreation	3 (0.4)	63 (0.8)	107,967	58.4	41.0 (13–62)	22.0 (3–38)	302.0 (134–1,500)
Construction	27 (3.9)	257 (3.4)	149,695	171.7	7.0 (1–83)	6.0 (3–81)	50.0 (7–3,000)
Educational services	11 (1.6)	62 (0.8)	380,928	12.3	7.0 (0–53)	5.0 (3–14)	69.5 (22–249)
Finance and insurance	9 (1.3)	66 (0.9)	134,635	49.0	11.0 (1–30)	4.0 (3–22)	18.0 (4–201)
Healthcare and social assistance§	29 (4.2)	199 (2.6)	777,828	20.7	11.0 (0–35)	6.0 (3–27)	68.0 (10–347)
Information	10 (1.4)	46 (0.6)	210,439	21.9	7.0 (1–23)	4.0 (3–9)	58.5 (20–140)
Manufacturing	184 (26.4)	3,319 (43.5)	338,308	980.8	20.0 (3–189)	9.0 (3–277)	153.5 (5–7,000)
Mining, quarrying, and oil and gas extraction	1 (0.1)	3 (0.0)	1,895	158.3	9.0 (9–9)	3.0 (3–3)	22.0 (22–22)
Other services (except public administration)	10 (1.4)	66 (0.9)	154,961	42.6	11.0 (2–36)	6.0 (3–13)	31.0 (8–120)
Professional, scientific, and technical services	10 (1.4)	50 (0.7)	299,007	16.7	6.5 (1–21)	4.0 (3–16)	20.0 (3–216)
Public administration	44 (6.3)	483 (6.3)	174,522	276.2	12.0 (2–117)	6.0 (3–67)	160.0 (6–1,200)
Real estate and rental and leasing	8 (1.2)	36 (0.5)	88,646	38.4	7.5 (0–11)	5.0 (3–7)	22.0 (6–115)
Retail trade	137 (19.6)	871 (11.4)	416,640	208.3	12.0 (0–141)	5.0 (3–25)	99.0 (5–8,585)
Transportation and warehousing	73 (10.5)	980 (12.9)	230,039	425.1	23.0 (0–158)	9.0 (3–125)	255.0 (4–2,083)
Utilities	3 (0.4)	14 (0.2)	28,370	49.3	10.0 (5–11)	3.0 (3–8)	19.0 (10–71)
Wholesale trade	54 (7.7)	664 (8.7)	218,454	304.0	18.0 0–79)	8.0 (3–87)	84.0 (9–600)

*Max, maximum; min, minimum.
†Denominator data were derived from 2019 Quarterly Census of Employment and Wages for Los Angeles County.
‡Per 100,000 persons. Incidence rate calculations excluded cases in nonemployees (n = 62).
§Full name of sector is healthcare and social assistance, but analysis includes only worksites in social assistance.

Outbreak-Associated Case-Patient Characteristics

Of 7,625 outbreak-associated case-patients, 79% (n = 6,047) were ≥18 years of age and had demographic and outcome information available for analysis. Outbreak-associated case-patients were predominantly ≤50 years of age, male, and Hispanic; there were some differences by sector (p<0.05) (Table 2). The other services sector, comprised primarily of repair and maintenance businesses, was the only sector in which most (55.7%) case-patients were ≥50 years of age. The sectors that had <50% male case-patients were healthcare and social assistance (22.1%); finance and insurance (35.7%); and professional, scientific, and technical services (44.4%). The proportion of Hispanic persons was highest in manufacturing (78.9%), followed by accommodation and food services (72.3%) and arts, entertainment, and recreation (71.4%). A few sectors had a lower proportion of cases in Hispanic persons than in non-Hispanic persons: educational services (37.0%); professional, scientific, and technical services (46.7%); and public administration (38.7%). A total of 243 hospitalizations (4%) and 37 deaths (0.6%) occurred; no differences were observed by sector or race/ethnicity (p>0.05).

Worksite Outbreaks by Industry Subsector

We further analyzed worksite outbreaks by industry subsectors. Among the 69 subsectors represented in our data, most outbreaks were in food and beverage stores (n = 75, 10.7%; sector: retail trade), followed by food manufacturing (n = 70, 10.0%; sector: manufacturing) and food services and drinking places (n = 64, 9.2%; sector: accommodation and food services). The highest number of outbreak-associated cases among subsectors were in food manufacturing (n = 1,515, 19.9%; sector: manufacturing); warehousing and storage (n = 621, 8.8%; sector: transportation and warehousing); and apparel manufacturing (n = 595, 7.8%; sector: manufacturing). Subsectors within the manufacturing, transportation and warehousing, and public administration sectors had the highest IRs (Table 3). The top 3 subsectors by IR were food

manufacturing (3,779.2), warehousing and storage (2,853.2), and apparel manufacturing (2,185.7).

Discussion

The manufacturing, transportation and warehousing, and retail trade sectors had the highest number of COVID-19 outbreaks and outbreak-associated cases among 698 worksite outbreaks in Los Angeles County. Manufacturing had the highest IR, which was >5 times the overall IR and twice that of the next highest sector. Among the top 10 subsectors by IR, 7 were from the manufacturing sector. Many worksites within the most affected subsectors were among those designated as essential critical infrastructure in California, enabling continued on-site operations through the pandemic. In addition, some nonessential manufacturing worksites redirected operations to the production of essential goods. Continued in-person operations probably contributed to increased risk of COVID-19 exposure and transmission at these facilities. Four of 5 outbreak-associated case-patients within manufacturing were Hispanic, the highest number for any sector. Worksite outbreak data can help identify vulnerable workers and enable public health departments to target policies and response, including ensuring vaccine access, to employees most affected by COVID-19.

These findings are supported by an analysis in Utah that reported similar results in manufacturing (*5*). In contrast, construction was not a highly affected sector in Los Angeles County on the basis of number of outbreaks, outbreak-associated cases, or IR. Jurisdictional differences in affected industries might vary by workforce distribution, reporting practices, and local outbreak identification and investigation procedures. This analysis identified affected subsectors, which might be essential for public health departments planning in diverse sectors (e.g., manufacturing) that require subsector-specific considerations. The food manufacturing subsector had the highest IR among subsectors in our analysis and is known to be a high-risk industry (*1*). This study identified additional manufacturing subsectors, such as apparel manufacturing and electrical equipment, appliance, and component manufacturing, which had among the highest IRs.

Facilities with more on-site staff are at risk for larger and longer COVID-19 outbreaks and should develop and implement strict safety protocols to prevent worksite exposure and transmission. In addition to having the most outbreak-associated cases, manufacturing and transportation and warehousing had among the most on-site employees and longest outbreak durations. The high-density environments and close contact in production lines, long shifts, shared equipment, and common spaces might increase risk for exposure in manufacturing and warehousing settings (*6*). In addition, practices such as use of shared

Table 2. Coronavirus disease outbreak–associated case demographics and health outcomes, by North American Industry Classification System industry sectors, Los Angeles County, California, USA, March 19–September 30, 2020*

Sector	Male sex†	Age ≥50 y†	Hispanic†	Hospitalizations	Deaths
Overall total	3,570/5,929 (60.2)	1,773/6,047 (29.3)	2,511/3,567 (70.4)	243/6,047 (4.0)	37/6,047 (0.6)
Accommodation and food services	135/263 (51.3)	62/267 (23.2)	99/137 (72.3)	9/267 (3.4)	1/267 (0.4)
Administrative and support and waste management and remediation services	58/89 (65.2)	30/89 (33.7)	29/43 (67.4)	5/89 (5.6)	0/89 (0.0)
Arts, entertainment, and recreation	16/26 (61.5)	13/26 (50.0)	15/21 (71.4)	4/26 (15.4)	1/26 (3.8)
Construction	156/160 (97.5)	36/167 (21.6)	57/92 (62.0)	4/167 (2.4)	0/167 (0.0)
Educational services	29/55 (52.7)	15/55 (27.3)	10/27 (37.0)	2/55 (3.6)	0/55 (0.0)
Finance and insurance	20/56 (35.7)	20/56 (35.7)	21/33 (63.6)	5/56 (8.9)	0/56 (0.0)
Health care and social assistance§	31/140 (22.1)	42/143 (29.4)	47/93 (50.5)	7/143 (4.9)	2/143 (1.4)
Information	21/33 (63.6)	9/33 (27.3)	8/13 (61.5)	0/33 (0.0)	0/33 (0.0)
Manufacturing	1,514/2,689 (56.3)	1,002/2,754 (36.4)	1,325/1,680 (78.9)	138/2,754 (5.0)	25/2,754 (0.9)
Mining, quarrying, and oil and gas extraction	1/1 (100.0)	1/1 (100.0)	0/0 (0.0)	0/1 (0.0)	0/1 (0.0)
Other services (except public administration)	45/61 (73.8)	34 (55.7)	26/37 (70.3)	1/61 (1.6)	0/61 (0.0)
Professional, scientific, and technical services	20/45 (44.4)	10/46 (21.7)	14/30 (46.7)	0/46 (0.0)	0/46 (0.0)
Public administration	208/292 (71.2)	54/294 (18.4)	74/191 (38.7)	9/294 (3.1)	2/294 (0.7)
Real estate and rental and leasing	21/32 (65.6)	10/32 (31.3)	12/19 (63.2)	0/32 (0.0)	0/32 (0.0)
Retail trade	377/656 (57.5)	131/676 (19.4)	262/394 (66.5)	19/676 (2.8)	1/676 (0.1)
Transportation and warehousing	498/787 (63.3)	153/796 (19.2)	326/483 (67.5)	25/796 (3.1)	3/796 (0.4)
Utilities	8/12 (66.7)	2/13 (15.4)	6/9 (66.7)	1/13 (7.7)	0/13 (0.0)
Wholesale trade	412/532 (77.4)	149/538 (27.7)	180/265 (67.9)	14/538 (2.6)	2/538 (0.4)

*Values are no. in category/total no. (%).
†$p<0.05$ by χ^2 test.
‡Full name of sector is health care and social assistance, but analysis includes only worksites in social assistance.

Table 3. Descriptive statistics for 10 North American Industry Classification System Industry subsector that had the highest outbreak-associated incidence rates for coronavirus disease, Los Angeles County, California, USA, March 19–September 30, 2020*

Subsector	Sector	No. (%) outbreaks	No. (%) outbreak-associated cases	Average no. employed annually†	Outbreak-associated incidence‡	Median no. outbreak-associated cases (min–max)
Food manufacturing	Manufacturing	71 (10.2)	1,592 (20.9)	40,088	3,971.3	11.0 (3–277)
Warehousing and storage	Transportation and Warehousing	35 (5.0)	621 (8.1)	21,765	2,853.2	10.0 (3–125)
Apparel manufacturing	Manufacturing	15 (2.1)	595 (7.8)	27,223	2,185.7	16.0 (3–184)
Beverage and tobacco product manufacturing	Manufacturing	6 (0.9)	99 (1.3)	6,357	1,557.3	10.5 (5–50)
Electrical equipment, appliance, and component manufacturing	Manufacturing	7 (1.0)	130 (1.7)	8,694	1,495.3	7.0 (3–68)
Plastics and rubber products manufacturing	Manufacturing	10 (1.4)	92 (1.2)	11,476	801.7	7.5 (3–22)
Furniture and related product manufacturing	Manufacturing	11 (1.6)	97 (1.3)	12,263	791.0	7.0 (4–24)
Chemical manufacturing	Manufacturing	9 (1.3)	141 (1.8)	19,656	717.3	8.0 (3–58)
Couriers and messengers	Transportation and Warehousing	14 (2.0)	213 (2.8)	32,195	655.4	16.0 (5–31)
Justice, public order, and safety activities	Public Administration	37 (5.3)	443 (5.8)	72,265	611.6	6.0 (3–67)

*Only rates for subsectors with ≥20 cases are included. Max, maximum; min, minimum.
†Denominator data were derived from 2019 Quarterly Census of Employment and Wages for Los Angeles County.
‡Per 100,000 persons. Incidence rate calculations excluded cases in nonemployees (n = 62).

transportation and frequent off-site worker interaction might contribute to this risk (*6*). Poor ventilation and sanitation have been well-documented in apparel manufacturing (*7*). Worksites within retail trade also had a high burden of COVID-19 outbreaks. Food and beverage stores had the most outbreaks within retail trade. Workers in these settings are particularly at risk for COVID-19 exposure because of their increased contact with the public (*6*).

Differences in worksite compliance with COVID-19 prevention protocols could also account for the higher COVID-19 burden seen in some industries. LACDPH site inspections, conducted in response to public complaints, have noted lower compliance with COVID-19 reopening and safety protocols in apparel manufacturing compared to restaurants (subsector: food services and drinking places) and grocery stores (subsector: food and beverage stores). Recommendations such as physical distancing might be more challenging to implement in manufacturing sites because of interdependent workflow processes and less modifiable physical environments. In addition, food facilities such as grocery stores and restaurants that routinely interact with public health departments because of permit requirements or regular inspections might have more knowledge and experience responding to DPH recommendations, which could contribute to higher compliance in these settings. Limited data has been published on compliance with COVID-19 prevention measures and potential barriers to compliance by industry. A closer and more systematic analysis of compliance with infection control measures by industry sector/subsector is needed.

Hispanic persons comprised 70% of outbreak-associated case-patients, which is almost twice the proportion of Hispanic persons employed in Los Angeles County in the 18 industry sectors represented in this analysis (40%) (*8*). This finding is consistent with findings of previous studies (*1*,*5*). Racial/ethnic minorities are overrepresented within essential industries, which often have higher risk working conditions as described above. In addition, Hispanic persons might experience more language barriers and are less likely to have access to paid leave and flexible work schedules (*9*,*10*). Community case rates of COVID-19 in Los Angeles County by race/ethnicity reflect an overall disproportionate burden on Hispanic persons, and the daily IR for Hispanic persons is more than twice that for white residents (*11*). Regardless of whether workplace exposure has driven community transmission or vice versa, a controlled worksite environment provides an opportunity to mitigate transmission within highly affected communities.

One limitation of our study is that the analysis includes only outbreaks reported to LACDPH, which underestimates the actual number of outbreaks. Because 14% of the investigations were ongoing, some outbreak-associated cases might not yet be documented. Employers might not have knowledge of employee symptom status, health outcomes, and testing results such that cases, outbreaks, hospitalizations, and deaths would remain unknown and unreported. Worksites that conducted facilitywide

testing voluntarily or based on LACDPH recommendations probably identified a higher number of cases. Of the 6,047 outbreak-associated cases that had demographic and outcome information available for analysis, 41% were missing race/ethnicity data. However, missing data are assumed to be random across industries.

Outbreak-associated cases represent a fraction of cases in employees that might have occurred in each sector/subsector. Although outbreak-associated case-patients are more likely to have been exposed at the worksite, some non-worksite acquired cases were probably included.

The IR might be underestimated because of inclusion of persons in the denominator who were not captured in the numerator if they became case-patients. Residents of Pasadena and Long Beach were included in the QCEW IR denominator for Los Angeles County, but outbreaks in these cities were excluded. Denominator data were based on 2019 QCEW average annual employment data, which was probably higher than employment in 2020 during the pandemic. However, this difference was probably less pronounced in sectors such as manufacturing that are composed of mostly essential businesses that continued operations. In addition, outbreaks in healthcare settings, homelessness services, and emergency medical services were excluded, underestimating the risks in the health care and social assistance and public administration sectors the most. Finally, the IR might also have been affected by persons who were not captured in the denominator (e.g., QCEW does not capture informal employment, which is more common in certain sectors).

This study highlights key sectors that have been affected by COVID-19 outbreaks and would benefit most from public health outreach and education. A better understanding of employer- and employee-level barriers that decrease compliance with public health measures and directives in specific industries is needed. COVID-19 safety protocols tailored to each industry that are culturally and linguistically appropriate to the employees at the worksite must be developed. Local champions can help build trust and support communication efforts.

Public health departments should cultivate and maintain relationships with labor representatives, worker advocates, and trade associations so that they can remain engaged with public health priorities and can help implement health directives when needed. Public health departments must continue to target essential workers in the affected industries in vaccination efforts to address gaps in vaccine access and barriers to uptake. The burden of disease, as well as the highest ethnic minority representation within manufacturing, underscores this sector as a priority area in Los Angeles County. The COVID-19 pandemic has highlighted infrastructure disparities and labor challenges faced by the Los Angeles County workforce and is an opportunity to improve worker safety and well-being across all industries.

Acknowledgments

We thank the staff of the Los Angeles County Department of Public Health, including public health analysts, investigators, inspectors, nurses, and physicians, for responding to and investigating worksite outbreaks of COVID-19 in Los Angeles County.

About the Author

Dr. Contreras is an epidemiologist in the Acute Communicable Disease Control Division, Los Angeles County Department of Public Health, Los Angeles, CA. Her primary research interests are epidemiology and prevention of vector-borne diseases.

References

1. Waltenburg MA, Rose CE, Victoroff T, Butterfield M, Dillaha JA, Heinzerling A, et al.; CDC COVID Emergency Response Team. Coronavirus disease among workers in food processing, food manufacturing, and agriculture workplaces. Emerg Infect Dis. 2021;27:243–9. https://doi.org/10.3201/eid2701.203821
2. Dyal JW, Grant MP, Broadwater K, Bjork A, Waltenburg MA, Gibbins JD, et al. COVID-19 among workers in meat and poultry processing facilities—19 states, April 2020. MMWR Morb Mortal Wkly Rep. 2020;69:557–61. https://doi.org/10.15585/mmwr.mm6918e3
3. US Census Bureau. North American Industry Classification System. Washington (DC): US Department of Commerce; 2020 [cited 2021 Apr 13]. https://www.census.gov/eos/www/naics
4. US Bureau of Labor Statistics. Quarterly Census of Employment and Wages. Washington, DC: US Department of Labor; 2020 [cited 2021 Apr 13]. https://www.bls.gov/cew/downloadable-data-files.htm#NAICS_BASED
5. Bui DP, McCaffrey K, Friedrichs M, LaCross N, Lewis NM, Sage K, et al. Racial and ethnic disparities among COVID-19 cases in workplace outbreaks by industry sector—Utah, March 6–June 5, 2020. MMWR Morb Mortal Wkly Rep. 2020;69:1133–8. https://doi.org/10.15585/mmwr.mm6933e3
6. Centers for Disease Control and Prevention. Manufacturing Workers and Employers. Interim Guidance from CDC and the Occupational Safety and Health Administration (OSHA) [cited 2021 Apr 13]. https://www.cdc.gov/coronavirus/2019-ncov/community/guidance-manufacturing-workers-employers.html#exposure-risk
7. Shadduck-Hernández J, Pech Z, Martinez M, Nuncio M. Dirty Threads, Dangerous Factories: Health and Safety

in Los Angeles' Fashion Industry. Los Angeles (CA): Garment Worker Center, UCLA Labor Center, UCLA Labor Occupational Safety and Health Program; 2016 [cited 2021 Apr 13]. https://garmentworkercenter.org/wp-content/uploads/2016/12/DirtyThreads.pdf
8. US Census Bureau. QWI Explorer. Suitland, MD: US Department of Commerce, US Census Bureau; 2020 [cited 2021 Apr 13]. https://qwiexplorer.ces.census.gov/static/explore.html#x=0&g=0
9. Tai DB, Shah A, Doubeni CA, Sia IG, Wieland ML. The disproportionate impact of COVID-19 on racial and ethnic minorities in the United States. Clin Infect Dis. 2021;72:703–6. https://doi.org/10.1093/cid/ciaa815
10. Hawkins D, Davis L, Kriebel D. COVID-19 deaths by occupation, Massachusetts, March 1–July 31, 2020. Am J Ind Med. 2021;64:238–44. https://doi.org/10.1002/ajim.23227
11. County of Los Angeles Public Health. LA County Daily COVID-19 Data. Los Angeles, CA; 2020 [cited 2021 Apr 13]. http://publichealth.lacounty.gov/media/coronavirus/data/index.htm

Address for correspondence: Zuelma Contreras, Acute Communicable Disease Control Division, Los Angeles County Department of Public Health, 313 N Figueroa St, Rm 212, Los Angeles, CA 90012, USA; email: zcontreras@ph.lacounty.gov

Risks and Preventive Strategies for *Clostridioides difficile* Transmission to Household or Community Contacts during Transition in Healthcare Settings

Ramin Asgary, Jessica A. Snead, Nabeel A. Wahid, Vicky Ro, Marina Halim, Judy C. Stribling

The burden of *Clostridioides difficile* infection (CDI) has greatly increased. We evaluated the risks for CDI transmission to community members after hospitalized patients are discharged. We conducted a systematic literature review in MEDLINE/PubMed, EMBASE, CINAHL plus EBSCO, Web of Science, Cochrane Library, and gray literature during January 2000–February 2019 and identified 4,798 citations were identified. We eliminated 4,554 citations through title and abstract screening; 217 additional citations did not meet full criteria. We reviewed texts for the 27 remaining articles qualitatively for internal/external validity. A few identified studies describing risks to community members lacked accurate risk measurement or preventative strategies. Primary data are needed to assess efficacy of and inform current expertise-driven CDI prevention practices. Raising awareness among providers and researchers, conducting clinical and health services research, linking up integrated monitoring and evaluation processes at hospitals and outpatient settings, and developing and integrating CDI surveillance systems are warranted.

Clostridioides (the genus name of this bacterium was changed from *Clostridium* to *Clostridioides* during 2018) *difficile* infection (CDI) is responsible for almost half a million infections and ≈29,000 deaths in the United States annually (*1*). During 2000–2014, the number of hospitalizations from CDI increased from 134,518 to 361,945, and the financial contribution to inpatient healthcare expenditure increased from $0.5 billion to $3.9 billion (*2*). Risk factors for CDI and colonization include older age, recent hospitalization, recent use of antimicrobial drugs, and use of proton-pump inhibitors (*3*). Transmission of *C. difficile* occurs through the spread of spores primarily through environmental contamination, hands of healthcare personnel, and asymptomatic carriers (*4*). Several well-established guidelines recommend strategies in the inpatient setting to prevent and treat CDI. Prevention methods strongly recommended in the guidelines within an acute-care setting include isolating patients with CDI in private rooms with private toilets, using gloves and gowns when entering rooms with CDI patients, using soap and water when entering or exiting a CDI patient room, and cleaning reusable equipment with a sporicidal disinfectant (*4*). For treatment, the 2017 update by the Infectious Diseases Society of America (IDSA) and the Society for Healthcare Epidemiology of America (SHEA) recommends stopping causing antimicrobial drugs and using oral vancomycin or fidaxomicin, or intravenous metronidazole as a less preferred alternative, in most cases of CDI (*4*).

Although classically believed to be a hospital-acquired infection, *C. difficile* has also proven to be a major community pathogen. Although the 2017 IDSA/SHEA update recognizes the role of CDI in the community, it gives no specific prevention strategies to use at home (*4*). Community-acquired *C. difficile* might account for more than one third of total CDI cases, and patients tend to be younger and have less recent exposure to antimicrobial drugs and less exposure to healthcare settings than other persons who have CDI (*5*,*6*).

Author affiliations: George Washington University, Washington, DC, USA (R. Asgary); Weill Cornell Medical College of Cornell University, New York, New York, USA (R. Asgary, N.A. Wahid, J.C. Stribling); New York Presbyterian Hospital of Cornell University, New York (J.A. Snead, N.A. Wahid, M. Halim); Columbia University Vagelos College of Physicians and Surgeons, New York (V. Ro)

DOI: https://doi.org/10.3201/eid2707.200209

Because many patients hospitalized for CDI are discharged before completing full-course treatment or complete resolution of diarrhea, a common conundrum is deciding what prevention strategies are effective to be recommended at home after discharge to prevent the spread of infection to household or community contacts. Although substantial data and consensus guidelines exist for effective prevention strategies in the inpatient setting, similar data appear more sparse in the community setting. In this study, we systematically assessed data regarding the rate and role of the spread of *C. difficile* from an index hospitalized patient to the patient's household members and community contacts. We also aimed to identify potential effective preventive strategies within the community.

Methods

For this study, we defined the population of interest as patients who had positive test results for CDI and who had another household member or contact with a patient who had been previously given a diagnosis of and treatment for *C. difficile* diarrhea. We defined a positive test result for CDI as a patient who had diarrhea sample that had positive results in a glutamate dehydrogenase antigen test, both toxin A and B tests, or a nucleic acid amplification test in the setting of either negative glutamate dehydrogenase test result or toxin A and B test results, or positive stool culture, regardless of diarrhea symptoms (i.e., active CDI vs. asymptomatic carrier).

Data Sources and Searches

We conducted a systematic review of literature in the databases MEDLINE, EMBASE, CINAHL plus EBSCO, Web of Science, PubMed, and The Cochrane Library, as well as gray literature, including abstracts/proceeding of gastroenterology, infectious disease, and related professional societies annual meeting, and guidelines by professional associations, all published during January 1, 2000–February 19, 2019. In addition to the primary literature search, we performed a snowballing method and checked references cited in current guidelines and the most relevant articles from our search. We developed a list of key search terms (Table 1) during multiple brainstorming sessions (involving clinicians, contributors, and a specialized librarian) and through an extensive review of Medical Subject Headings (MeSH) terms from relevant articles identified through preliminary searches in PubMed. We divided the search terms into 2 search buckets, 1 centered around "*Clostridium difficile*" (all related MeSH terms and possible text words) and 1 centered around "carrier state" and "cross infection" (all related MeSH terms and possible text words). Furthermore, we used the OVID Medline strategy (Appendix, https://wwwnc.cdc.gov/EID/article/27/7/20-0209-App1.pdf) to search all databases by using appropriate thesaurus terms and natural language. The study was registered at the PROSPERO Registry as no. CRD42019118021 (study protocol provided in the Appendix).

Inclusion criteria were studies that defined laboratory testing for *C. difficile* detection or used and measured diarrheal episodes or used any test to detect infection; measured or included a contact or an exposure with patients previously given a diagnosis of *C. difficile* diarrhea in hospital settings; measured outcomes among outpatient or community persons who were exposed in the form of rates or number of events; and mentioned or described an actual intervention (treatment such as antimicrobial drugs for the CDI index case, which is hypothesized to decrease the period of infectiousness and subsequent transmission or a prevention strategy, such as handwashing and surface cleaning with sporidicial

Table 1. Search terms and databases used for systematic review of *Clostridioides difficile* infection*

Bibliographic database	Search terms/condition	Search terms/carrier state
OVID MEDLINE	*Clostridium difficile*, *Clostridium* Infections, *Clostridium* adj4 poisoning, *Clostridium* Perfringen, *Clostridium sordell**, Infect* adj3 perfringen*	Carrier State, carrier and state, Cross infection, Cross and Infect*, infect* adj2 nosocomial
EMBASE	*Clostridium difficile*, *Clostridium* difficills*, *Clostridium* Infection, Clostridial Disease, Clostridial Infection* Clostridi*adj4 poisonin*, Clostridi* perfringen*, Clostridi* Sordell*	Carrier State, Cross Infection, Infect* and Cross, Infect* adj2 nosocomial
Web of Science	*Clostridium difficile*, *Clostridium* Infections, *Clostridium* Infection, *Clostridium* Poisoning, *Clostridium perfringens*, *Clostridicum* Perfringen, *Clostridium* Sordellii	Carrier State, Cross Infection, Nosocomial Infection, Nosocomial Infections
Cochrane Library	*Clostridium difficile*, *Clostridium* Infections, *Clostridium* Poisoning, *Clostridium perfringens*, *Clostridium sordellii*	Carrier State, Cross Infection, Nosocomial Infection, Nosocomial Infections
Gray literature	*Clostridium* Infection	Cross Infection

*Filters/limits were limit 2000–present and English language. Asterisks indicate truncation for other variations or modified versions of a searched word (e.g., shortened, misspelled, or differently spelled versions). This search includes all versions of *Clostridi* and *Clostridium difficile*, including *Clostridioides*, which also are shown in citations used for this paper.

antiseptic and contact isolation). Exclusion criteria were nonhuman studies, studies not published in English, studies that did not specifically describe the study population, and studies that did not describe any form of CDI infection or did not reference any treatment or prevention strategy.

Data Extraction, Quality Assessment, and Data Synthesis and Analysis

We designed a 4-stage screening process to select the most relevant literature for review. First, we developed search terms along with a search algorithm and searched databases for articles containing the key search terms in their title or abstract. Second, we reviewed the titles and abstracts of these articles for exclusion and inclusion criteria. We examined whether a study had an index patient who had diarrhea caused by CDI in the hospital, an exposure that existed outside the hospital, an outcome after that exposure measured with laboratory tests or clinical diagnosis, and an intervention (either preventive or therapeutic) that was applied to the index patient or other exposed persons to protect against subsequent CDI at the community level. If there was no intervention, we set to record the rates of postexposure infection among contacts. Third, we qualitatively reviewed the full texts of the remaining articles that had not been excluded to confirm that they met the inclusion and exclusion criteria and to assess them for their sample size, outcome measures, biases, comparison of rates and outcomes, efficacy of their treatment or preventive measures, and internal/external validity.

We also applied a snowballing method by reviewing references and citations to current guidelines and panel of expert recommendations selected for the full text review. At the end of this process, we retrospectively read through all 217 articles from phase 2, even though they did not fully meet the inclusion criteria, to ensure that all potential relevant information was captured. We then organized and reported findings according to the Preferred Reporting Items for Systematic Reviews and Meta-Analysis guidelines (*7*). A dedicated librarian with expertise in conducting systematic review performed the database search and imported search results into Covidence software (https://www.covidence.org) for review. Two reviewers screened the articles from stages 1 and 2 independently. Another tie-breaker reviewer looked at the articles that were discordant. The texts of remaining articles were reviewed by ≥2 reviewers.

Results

We found 4,798 articles through our search strategy. We compiled more detailed descriptions of search hits from specific databases (Table 2). After applying the exclusion criteria, we eliminated 4,554 articles through title and abstract screening. We screened the abstracts for the remaining 244 articles for inclusion criteria; we eliminated 217 of those for not meeting the full criteria. The full text of the remaining 27 articles were read to confirm eligibility (Figure).

None of the articles evaluated transmission of *C. difficile* from an infected person in the hospital to someone in the community, long-term acute care facility, nursing home, or subacute rehabilitation center. Some common reasons for eliminating articles included nonclinical studies that used computer modeling to study transmission, studies that only included exposure occurring within instead of outside the hospital, and studies that had no interventions described to prevent transmission. For example, one study interviewed 1,013 patients who had confirmed community-acquired *C. difficile* and showed that 11 patients had a household member with active CDI (*6*). Of patients with community-acquired CDI and no outpatient healthcare exposure, the odds ratio of having a household member with active CDI was 6.8 (95% CI 0.7–65.9) compared with patients who had high-level outpatient healthcare exposure (*6*). However, the study did not verify the

Table 2. Results of literature review search on prevention and treatment/management of *Clostridioides difficile* infection to family members and community from an index hospital patient, by database, September 2019

Database	Search strategy for prevention	Search strategy for management	Results	Key features of search engine
PubMed	Full search	Full search	2,215	Index to articles in medical journals and other selected biomedical literature
Cochrane Library	Full search	Full search	435	Database of systematic reviews of primary research in human healthcare and health policy
Web of Science	Search limited to 50 terms	Search limited to 50 terms	1,494	Helpful for topics that border on social science
EMBASE	Full search	Full search	1,653	European alternative to PubMed; helpful for topics with an international focus
Gray literature	Full search	Full search	1	Manifold document types produced on all levels of government, academics, business and industry in print and electronic formats.

infectious status of the index patient and did not examine what was performed to prevent transmission to household contacts.

Another study examined household transmission for 2,222 patients who had confirmed *C. difficile* infection diagnosed at the Centre Hospitalier Universitaire de Sherbooke (Sherbooke, Quebec, Canada). The study identified 1,061 spouses and 501 children <25 years of age living with the index patients (*8*). Five spouses and 3 children developed *C. difficile* infection within a year after discharge of the index patients (attack rate 4.71 cases/1,000 persons for spouses and 5.99 cases/1,000 persons for children of index cases). Similar to the study of Chitnis et al. (*6*), this study did not define what isolation or prophylactic measures were taken to reduce transmission to household contacts. However, a more recent study by Miller et al. conducted among 194,424 enrollees, published after our original search was completed, indicated a 12.47 incidence rate ratio among household contacts of DCI patients discharged from tertiary care centers (*9*). In addition, Loo et al. evaluated probable transmission rates of 1.5% and possible transmission rates of 7.5% for household contacts of 51 CDI patients (*10*).

Some studies reported community-acquired CDI, but did not explicitly report an exposure to hospitalized patients who had *C. difficile* infection (*11*,*12*). For example, Bloomfield and Riley reported estimated rates of community acquired *C. difficile* infection in North America ranging from 20% to 32% (*12*). This study also showed that nonhuman reservoirs, including animals and food, have shown positive results for *C. difficile* infection. However, these findings have yet to be replicated by additional studies. Another source of community-associated *C. difficile* infection studied was healthcare exposure. For example, Chitnis et al. (*6*) showed that 82% of their patients had some exposure to healthcare within 12 weeks before infection, including outpatient dental or physician office visits and dialysis. They also showed known traditional risk factors: 64% used antimicrobial drugs within 12 weeks before infection, and 27.7% used proton pump inhibitors (Table 3).

We identified consensus articles from organizations, such as the International Infection Control Council, IDSA, and SHEA. In addition, the American Nursing Association endorses the approach of the Centers for Disease Control and Prevention, which in return endorses IDSA guidelines. Many recommendations were guided by expert opinion, rather than primary research on CDI transmission from the hospital setting to the community. Although many of the guidelines are not guided by primary research results, we highlighted some current inpatient practices for treating and preventing transmission of CDI in the inpatient setting (Table 4, https://wwwnc.cdc.gov/EID/article/27/7/20-0209-T4.htm).

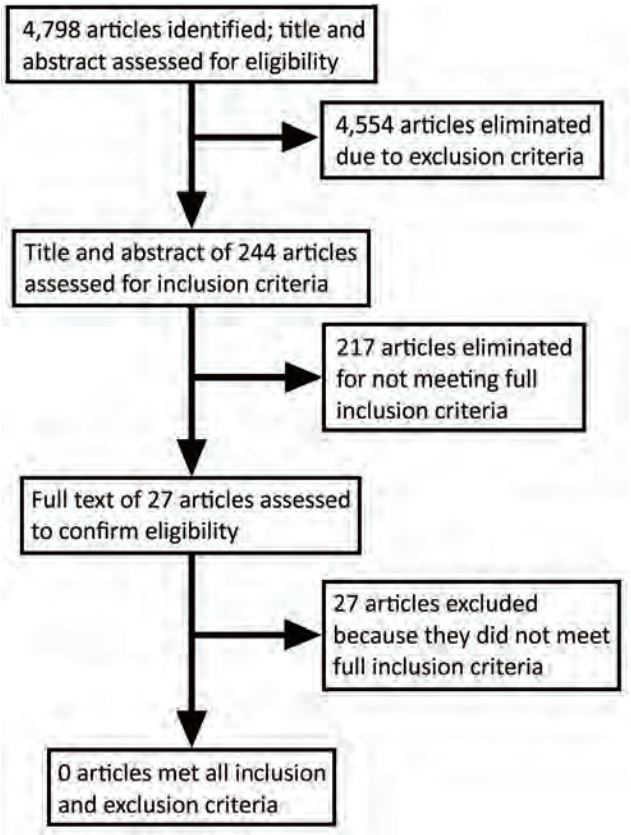

Figure. Process of selecting studies suitable for inclusion in the final review of the literature on prevention and treatment/management of *Clostridioides difficile* infection to family members and community from an index hospital patient, by database, September 2019.

Discussion

Increasingly, the extent and role of hospital-acquired infections, excessive use of antimicrobial drugs, drug-resistant bacterial infections, and decreased efficacy of common and available antimicrobial drugs as serious threat to individual and population health, and health agencies in the United States and elsewhere have called for measures to address these factors (*17*). *C. difficile* continues to be among the highest burden of hospital-acquired infections, such that IDSA, SHEA (*4*), the American College of Gastroenterology (*13*), and the European Society of Clinical Microbiology and Infectious Diseases (*14*,*15*), have all published guidelines for the preventing and managing of *C. difficile* in inpatient 11settings. Available

Table 3. Results of qualitative assessment of studies evaluating risk for CDI in the community*

Study (reference)	Study type	Year	No. persons/studies	Setting	Actual risk/assumed risk	Intervention
Pépin et al. (*8*)	Retrospective	2012	2,222 *C. difficile* patients	Household contacts	Children attack rate: 4.71 cases/1,000 persons; spouse attack rate: 5.99 cases/1,000 persons	None
Chitnis et al. (*6*)	Retrospective and telephone interview	2013	984 community-acquired *C. difficile* patients	Household contacts	Odds of community-acquired CDI if no outpatient healthcare exposure: 6.8 (95% CI 0.7–65.9); odds of community-acquired CDI if low level outpatient healthcare exposure: 6.9 (95% CI 0.9–56.7)	None
Durovic et al. (*11*)	Narrative review	2018	24 studies	Other healthcare facilities and community	Not measured	None
Bloomfield and Riley (*12*)	Narrative review	2016	NA	Household contacts	Estimated rate of community acquired CDI in North America: 20%–32%	None
Loo et al. (*10*)	Prospective	2016	51	Household contacts	Probable transmission: 1.5%; possible transmission: 7.5%	None, but type of soap for handwashing was recorded
Miller et al. (*9*)	Case–control	2020	194,424 enrollees	Household contacts	IRR 12.47 (95% CI 8.86–16.97)	None

*CDI, *Clostridioides difficile* infection; IRR, incidence rate ratio.

data demonstrate the considerable extent of *C. difficile* in the community (*12*), evidence of *C. difficile* on household surfaces among patients who have recurrent CDI (*18*), a rate of probable transmission of 1.5% and a rate of possible transmission of 7.5% for household contacts of discharged CDI patients (*10*). More recently, the incidence rate ratio of CDI was reported as 12.47 for household contacts of discharged patients who have CDI (*9*). However, no systematic data provide evidence of effective prevention strategies at the community level and with household contacts of index patients discharged from the hospital. Consequently, practitioners often do not provide specific prevention recommendations for CDI to patients or family members outside the hospital. Consequently, practitioners often do not provide specific prevention recommendations for CDI to patients or family members outside the hospital.

In this systematic review, we applied a comprehensive search strategy in a variety of search engines to cover complementary areas of the literature relevant to CDI prevention and treatment, including the gray literature and data from related professional associations. Through this extensive search, we were not able to find any publications that evaluated strategies to prevent or manage CDI among contact family or community members of an index patient. Therefore, we state that no data are currently available to demonstrate whether the prevention and management strategies that are widely used and included in proposed guidelines for inpatient or hospital setting are efficacious, feasible, or effective to prevent transmission outside the hospital.

The reasons for this lack of data are likely multifactorial. A fragmented healthcare system does not provide opportunities to identify and record outpatient episodes and related illnesses associated with inpatient CDI diagnosis. In addition, no systematic approach has been established to collect data at the patient level through providers, and no public health tracing or follow-up process with family members exists. Departments of health at the state level do not routinely collect data related to CDI patients or subsequent infections (*19*). The providers caring for index or subsequently exposed patients often lack the instruction or support necessary for evaluating patients after hospital discharge and their family or community contacts. There might be low rates of secondary symptomatic infections in the household setting. Furthermore, there is probably a lack of recognition of the burden of CDI among outpatient health providers, and laboratory report systems are not in place to send reminders. Potential consequences of this lack of strong data include inadvertent transmission of CDI from the community back to the healthcare environment, increased financial cost to health system from treating preventable cases of secondary CDI, and probably an increasing

number of multidrug-resistant CDI. The Institute of Medicine has emphasized the burden of hospital-acquired infections and the need for systematic approaches and delineated framework and processes for moving forward (*20*,*21*).

We have provided a summary of current practices in the inpatient settings because we realize that in the absence of primary data, the recommended approaches need to include all levels of evidence to direct the actual practice. Nevertheless, the role of primary approaches, such as antimicrobial drug stewardship, could not be overemphasized. Furthermore, we suggest that a range of overarching initiatives is needed to address the risk and subsequent burden of transmission of CDI to the community. Perhaps the most useful area to focus on is the development of a monitoring and evaluation process in the hospital setting that can ensure that relevant data are available to outpatient providers at the time of discharging the index patient. Proper data collection processes should be added into the current system of collecting and monitoring health data by developing tools and reinforcing accurate documentation and tracking of CDI cases and their sequelae. A direct link between providers in the outpatient and hospital settings to identify and address subsequent CDI should not be overlooked. Simple strategies, such as follow-up telephone calls and gathering information from family members, could help determine the possibility or the extent of the disease at the patient level through similar initiatives commonly used for post-surgical interventions (*22*–*27*).

There is also a need for direct primary research on the feasibility and efficacy of specific CDI prevention and management strategies after hospital discharge. Prevalence studies evaluating outcomes at individual and household levels, and interventional cohorts, including different types of preventive or management strategies for CDI should be considered because they are likely to provide useful data.

We did not include studies published in languages other than English. However, our preliminary search did not identify this limitation as a major gap in evidence. Data regarding the efficacy of prevention strategies at the community level might exit in the form of reports and proposals developed in departments of health in or outside the United States that were not captured in our extensive systematic review.

Our systematic review indicates a need for research that evaluates the efficacy and effectiveness of various CDI prevention and management strategies after infected patients are discharged from inpatient settings. Ultimately, this research will enable the field of CDI and multidrug-resistant infections to transition from one that is largely extrapolative and expertise driven to one that is more evidence based. The current guidelines do not give any recommendations on how to prevent and manage CDI among family members and community contacts after hospital discharge of an index patient. However, guidelines do recommend assessment and monitoring, clearly emphasizing the need for good data and evidence. There are clearly challenges at the research and practice level that need to be systematically addressed. To start, perhaps there is a need to appropriately raise awareness of the problem among clinical providers and researchers. Concurrently, conducting related clinical and population level research, setting up and connecting monitoring and evaluation programs at hospital and outpatient settings, and developing CDI-related data within public health surveillance are warranted.

About the Author

Dr. Asgary is a clinical associate professor of Medicine at Weill Cornell College of Medicine, New York, NY, and associate professor of global health at George Washington University, Washington, DC. His primary research interests are health services, general medicine, and global health.

References

1. Lessa FC, Winston LG, McDonald LC; Emerging Infections Program C. difficile Surveillance Team. Burden of *Clostridium difficile* infection in the United States. N Engl J Med. 2015;372:2369–70. https://doi.org/10.1056/NEJMoa1408913
2. Lee RM, Fishman NO. Increasing economic burden of inpatient *Clostridium difficile* infection in the United States: national trends in epidemiology, outcomes, and cost of care from 2000 to 2014. Open Forum Infect Dis. 2017;4(Suppl 1):S392. https://doi.org/10.1093/ofid/ofx163.976
3. Loo VG, Bourgault A-M, Poirier L, Lamothe F, Michaud S, Turgeon N, et al. Host and pathogen factors for *Clostridium difficile* infection and colonization. N Engl J Med. 2011;365:1693–703. https://doi.org/10.1056/NEJMoa1012413
4. McDonald LC, Gerding DN, Johnson S, Bakken JS, Carroll KC, Coffin SE, et al. Clinical practice guidelines for *Clostridium difficile* infection in adults and children: 2017 update by the Infectious Diseases Society of America (IDSA) and Society for Healthcare Epidemiology of America (SHEA). Clin Infect Dis. 2018;66:987–94. https://doi.org/10.1093/cid/ciy149
5. Khanna S, Pardi DS, Aronson SL, Kammer PP, Orenstein R, St Sauver JL, et al. The epidemiology of community-acquired *Clostridium difficile* infection: a population-based study. Am J Gastroenterol. 2012;107:89–95. https://doi.org/10.1038/ajg.2011.398
6. Chitnis AS, Holzbauer SM, Belflower RM, Winston LG, Bamberg WM, Lyons C, et al. Epidemiology of community-associated *Clostridium difficile* infection, 2009 through 2011.

JAMA Intern Med. 2013;173:1359–67. https://doi.org/10.1001/jamainternmed.2013.7056
7. Moher D, Liberati A, Tetzlaff J, Altman DG; PRIMSA Group. Preferred reporting items for systematic reviews and meta-analyses: the PRIMSA statement. PLoS Med. 2009; 6:e1000097. https://doi.org/10.1371/journal.pmed.1000097
8. Pépin J, Gonzales M, Valiquette L. Risk of secondary cases of *Clostridium difficile* infection among household contacts of index cases. J Infect. 2012;64:387–90. https://doi.org/10.1016/j.jinf.2011.12.011
9. Miller AC, Segre AM, Pemmaraju SV, Sewell DK, Polgreen PM. Association of household exposure to primary *Clostridioides difficile* infection with secondary infection in family members. JAMA Netw Open. 2020;3:e208925. https://doi.org/10.1001/jamanetworkopen.2020.8925
10. Loo VG, Brassard P, Miller MA. Household transmission of *Clostridium difficile* to family members and domestic pets. Infect Control Hosp Epidemiol. 2016;37:1342–8. https://doi.org/10.1017/ice.2016.178
11. Durovic A, Widmer AF, Tschudin-Sutter S. New insights into transmission of *Clostridium difficile* infection: narrative review. Clin Microbiol Infect. 2018;24:483–92. https://doi.org/10.1016/j.cmi.2018.01.027
12. Bloomfield LE, Riley TV. Epidemiology and risk factors for community-associated *Clostridium difficile* infection: a narrative review. Infect Dis Ther. 2016;5:231–51. https://doi.org/10.1007/s40121-016-0117-y
13. Surawicz CM, Brandt LJ, Binion DG, Ananthakrishnan AN, Curry SR, Gilligan PH, et al. Guidelines for diagnosis, treatment, and prevention of *Clostridium difficile* infections. Am J Gastroenterol. 2013;108:478–98, quiz 499. https://doi.org/10.1038/ajg.2013.4
14. Tschudin-Sutter S, Kuijper EJ, Durovic A, Vehreschild MJ, Barbut F, Eckert C, et al.; Committee. Guidance document for prevention of *Clostridium difficile* infection in acute healthcare settings. Clin Microbiol Infect. 2018;24:1051–4. https://doi.org/10.1016/j.cmi.2018.02.020
15. Debast SB, Bauer MP, Kuijper EJ; European Society of Clinical Microbiology and Infectious Diseases. European Society of Clinical Microbiology and Infectious Diseases: update of the treatment guidance document for *Clostridium difficile* infection. Clin Microbiol Infect. 2014;20(Suppl 2):1–26. https://doi.org/10.1111/1469-0691.12418
16. Sartelli M, Di Bella S, McFarland LV, Khanna S, Furuya-Kanamori L, Abuzeid N, et al. 2019 update of the WSES guidelines for management of *Clostridioides* (*Clostridium*) *difficile* infection in surgical patients. World J Emerg Surg. 2019;14:8. https://doi.org/10.1186/s13017-019-0228-3
17. Balsells E, Filipescu T, Kyaw MH, Wiuff C, Campbell H, Nair H. Infection prevention and control of *Clostridium difficile:* a global review of guidelines, strategies, and recommendations. J Glob Health. 2016;6:020410. https://doi.org/10.7189/jogh.06.020410
18. Shaughnessy MK, Bobr A, Kuskowski MA, Johnston BD, Sadowsky MJ, Khoruts A, et al. Environmental contamination in households of patients with recurrent *Clostridium difficile* infection. Appl Environ Microbiol. 2016;82:2686–92. https://doi.org/10.1128/AEM.03888-15
19. New York State Department of Health. Communicable disease reporting requirements, February 2011 [cited 2019 Oct 20]. https://www.health.ny.gov/forms/instructions/doh-389_instructions.pdf.
20. US Institute of Medicine. Forum on emerging infections. Antimicrobial resistance; issues and options. Harrison PF, Lederberg J, editors. Washington (DC): National Academies Press; 1998.
21. US Institute of Medicine Forum on Microbial Threats. Antibiotic resistance: implications for global health and novel intervention strategies: Workshop summary. Washington (DC): National Academies Press; National Academies Press; 2010 [cited 2019 Nov 4]. https://www.ncbi.nlm.nih.gov/pubmed/21595116
22. Halwani MA, Turnbull AE, Harris M, Witter F, Perl TM. Postdischarge surveillance for infection following cesarean section: a prospective cohort study comparing methodologies. Am J Infect Control. 2016;44:455–7. https://doi.org/10.1016/j.ajic.2015.10.023
23. Koek MB, Wille JC, Isken MR, Voss A, van Benthem BH. Post-discharge surveillance (PDS) for surgical site infections: a good method is more important than a long duration. Euro Surveill. 2015;20:21042. https://doi.org/10.2807/1560-7917.ES2015.20.8.21042
24. Staszewicz W, Eisenring M-C, Bettschart V, Harbarth S, Troillet N. Thirteen years of surgical site infection surveillance in Swiss hospitals. J Hosp Infect. 2014;88:40–7. https://doi.org/10.1016/j.jhin.2014.06.003
25. Horan TC, Andrus M, Dudeck MA. CDC/NHSN surveillance definition of health care-associated infection and criteria for specific types of infections in the acute care setting. Am J Infect Control. 2008;36:309–32. https://doi.org/10.1016/j.ajic.2008.03.002
26. Lima JL, de Aguiar RA, Leite HV, Silva HH, de Oliveira WM, Sacramento JP, et al. Surveillance of surgical site infection after cesarean section and time of notification. Am J Infect Control. 2016;44:273–7. https://doi.org/10.1016/j.ajic.2015.10.022
27. Petherick ES, Dalton JE, Moore PJ, Cullum N. Methods for identifying surgical wound infection after discharge from hospital: a systematic review. BMC Infect Dis. 2006;6:170. https://doi.org/10.1186/1471-2334-6-170

Address for correspondence: Ramin Asgary, Weill Cornell Medical College, 525 E 68th St, Baker 20th, F2008, New York, NY 10065, USA; email: ga263@columbia.edu

Transboundary Spread of *Brucella canis* through Import of Infected Dogs, the Netherlands, November 2016–December 2018

Marloes A.M. van Dijk, Marc Y. Engelsma, Vanessa X.N. Visser, Ingrid Keur, Marjolijn E. Holtslag, Nicole Willems, Björn P. Meij, Peter T.J. Willemsen, Jaap A. Wagenaar, Hendrik I.J. Roest,[1] Els M. Broens[1]

Brucella canis had not been isolated in the Netherlands until November 2016, when it was isolated from a dog imported from Romania. Including this case, 16 suspected cases were notified to the authorities during the following 25 months. Of these 16 dogs, 10 were seropositive; tracking investigations found another 8 seropositive littermates. All seropositive animals were rescue dogs imported from Eastern Europe. *B. canis* was cultured from urine, blood, and other specimens collected from the dogs. Genotyping of isolates revealed clustering by litter and country. Isolating *B. canis* in urine indicates that shedding should be considered when assessing the risk for zoonotic transmission. This case series proves introduction of *B. canis* into a country to which it is not endemic through import of infected dogs from *B. canis*–endemic areas, posing a threat to the naive autochthonous dog population and humans.

Canine brucellosis is caused by the bacterium *Brucella canis*. Reproductive disorders such as late abortion, stillbirth, epididymitis, and sperm anomalies are most frequently observed (*1*). Other clinical signs are lymphadenitis (*1*,*2*) and musculoskeletal disease (e.g., discospondylitis) (*3*). In addition, the infection can remain subclinical (*2*). *B. canis* is mostly transmitted vertically from bitch to offspring or venereally through vaginal discharge and semen; urine has also been implicated as a possible mode of transmission (*1*,*4*,*5*).

B. canis is a zoonotic pathogen; humans can become infected through direct contact with secreta and excreta of infected dogs (*6*,*7*) or through laboratory exposure (*8*,*9*). Clinical signs in humans vary from subclinical infection (*10*) to fever, malaise, splenomegaly, and lymphadenopathy (*7*). Human cases of *B. canis* infection are reported infrequently. However, the prevalence of human *B. canis* infections is probably underestimated; the diagnosis might be missed because of nonspecific clinical signs and the absence of accurate serologic tests for *B. canis* antibodies in humans (*6*,*11*). In the United States, a seroprevalence of 3.6% was found among persons occupationally exposed to dogs. Two seropositive persons had clinical symptoms of brucellosis, and both reported contact with *B. canis*–seropositive dogs (*10*). In addition, an outbreak involving 6 seropositive persons, 5 of whom had clinical symptoms, was described after contact with a seropositive litter (*6*). In general, *B. canis* appears to cause less severe clinical symptoms in humans than other *Brucella* spp. (*12*). However, the public health relevance of *B. canis* needs further investigation before a proper risk assessment can be performed.

B. canis is considered endemic in the southern United States, Central America, and South America and has been reported from Canada, Asia, Africa, and Europe (*7*,*13*). Sporadic cases originating from northwestern Europe have been reported and were at least partially caused by importing an infected dog (*13*,*14*). Recent papers have expressed concerns about the introduction of *B. canis* in countries to which it is not

Author affiliations: Utrecht University Faculty of Veterinary Medicine, Utrecht, the Netherlands (M.A.M. van Dijk, N. Willems, B.P. Meij, J.A. Wagenaar, E.M. Broens); Wageningen Bioveterinary Research, Lelystad, the Netherlands (M.Y. Engelsma, M.E. Holtslag, P.T.J. Willemsen, J.A. Wagenaar, H.I.J. Roest); Netherlands Food and Consumer Product Safety Authority, Utrecht (V.X.N. Visser, I. Keur); Ministry of Agriculture, Nature and Food Quality, The Hague, the Netherlands (H.I.J. Roest)

DOI: https://doi.org/10.3201/eid2707.201238

[1]These senior authors contributed equally to this article.

endemic through infected dogs (*15*,*16*). Brucellosis in dogs is, in contrast to livestock, not notifiable to the World Organisation for Animal Health (OIE) or the European Union (EU directive 64/432/EEG). In the Netherlands, brucellosis is notifiable in humans and all mammal species (*17*,*18*). *B. canis* had not been isolated in the Netherlands until November 2016, when it was isolated from a dog imported from Romania that had discospondylitis. Raised awareness following this first case resulted in multiple notifications at the Incidence Crisis Centre (NVIC) of the Netherlands Food and Consumer Product Safety Authority (NVWA). This study describes the follow-up of these notifications and the implications for animal and human health.

Methods

Notifications and Study Period

Animal owners, veterinarians, and laboratories in the Netherlands are obliged to notify suspicions of brucellosis to the competent authority, the NVWA, according to Dutch legislation (*17*,*18*). Suspicions are mostly based on clinical signs compatible with brucellosis and a history of importation. In this study, we include all notified and related *B. canis* cases during November 2016–December 2018, provided there was a clinical suspicion (e.g., routine tests for export or import excluded), and diagnostic tests were performed at the National Reference Laboratory (NRL; Wageningen Bioveterinary Research, Lelystad, the Netherlands). No mandatory control measures for pets are in place once a positive case has been identified.

Tracking Investigations

Upon notification, NVIC began investigations to track potential transmission by taking samples from suspected dogs and (if applicable) contact dogs or littermates for serologic and bacteriologic (blood and urine) evaluation. Contact dogs were defined as any dog imported with, cohabiting with, or regularly spending time with the suspected dog. Dogs were considered positive if they tested positive for *B. canis* antibodies or when the bacterium was cultured from blood, urine, or infection sites. In case of euthanasia of a seropositive dog, postmortem examination was performed by the NRL, and samples of various tissues were collected for culture. Diagnostic tests were performed by the NRL.

Detection of *B. canis* Antibodies

Serum samples were tested for *B. canis*–specific antibodies by the 2-Mercapto-ethanol serum agglutination test as described by Alton et al. (*19*) as reference method with an in-house derived positive rabbit anti–*B. canis* control serum (NRL in-house validation). Interpretation of the antibody titer is <1:50 negative, 1:50–1:100 inconclusive, ≥1:200 positive (*19*).

Detection of *B. canis*

Culture

We isolated *Brucella* spp. from clinical and tissue samples according to the OIE protocol (*20*). All laboratory work with potential *Brucella*-contaminated samples was performed within a Biosafety Level (BSL) 3 facility. Suspected colonies were confirmed as *Brucella* spp. by matrix-assisted laser desorption/ionization time-of-flight mass spectrometry on the Bruker MALDI Biotyper (Bruker, https://www.bruker.com) by using an extended in-house *Brucella* spp. database (*21*) and PCR.

DNA Isolation, PCR, and Genotyping

DNA from tissue samples was extracted by using the DNeasy Blood and Tissue Kit (QIAGEN, https://www.qiagen.com). DNA isolation from *Brucella*-suspected colonies was performed by suspending the colony in 200 μL nuclease-free water (Sigma-Aldrich, https://www.sigmaaldrich.com) and boiling at 100°C for 8 min, followed by centrifugation for 2 min at 20,000 × *g*. We performed real-time PCR targeting the IS711 sequences of *Brucella* spp. (*22*). Colonies and tissue samples were considered positive after real-time PCR if the results showed a cycle threshold (C_t) value of ≤36 (with sigmoid curve), inconclusive if C_t value was >36 but <40 (with inconclusive sigmoid curve), and negative if C_t value was ≥40 or there was no C_t at all.

For in silico multiple-locus variable number tandem repeat analysis (MLVA) and multilocus sequence typing (MLST), we constructed fragmented libraries by using Nextera DNA sample preparation kit (Illumina, https://www.illumina.com), as earlier published (*21*). Next generation whole-genome sequencing was performed by paired-end sequencing (300-bp reads) by using the Illumina technology on the MiSeq instrument (Illumina). We performed de novo assembly of the quality filtered reads by using ABySS-pe version 1.3.3 (*23*). Reads were aligned by using Bowtie2 version 0.2 (http://bowtie-bio.sourceforge.net/bowtie2/index.shtml) to the assembled contigs and the contig sequences were manually verified by using Tablet version 14.04.10 (*24*). We performed in silico MLVA-16 clustering according to the algorithm as described previously (*25*) by using

Bionumerics version 7.6 (Applied Maths, https://www.applied-maths.com) and assigning MLVA-type from DNA-sequence with software (*26*) or manually. MLST typing was performed in silico with a set of MLST specific primers (*27*) and the assembled contigs as input, by using the PubMLST.org database (*28*). For the analysis of *B. canis* genotypes, we compared them to genotypes from the publicly available database MLVA bank (*26*). Of note, the background of reference genotypes is unknown (e.g., import history of the dogs); therefore, these genotypes might not originate from the country in which they were isolated. If >1 isolate was recovered from different materials or time points from a dog in our study, 1 isolate per time point was sequenced with ≤2 isolates per dog to assess carriage of different genotypes (*29*,*30*).

Results

Including the first case of canine brucellosis in the Netherlands, 16 suspected cases were notified to NVIC in the study period (Table 1). The reasons for notification are variable: 7 dogs had a seropositive test result at the NRL, 7 dogs had a clinical complaint compatible with *B. canis* infection, and 2 cases had a *B. canis*–seropositive culture (Table 1). Of the 16 dogs, 15 had a history of importation. A total of 10 tested seropositive at the NRL, 4 tested seronegative, and 2 had an inconclusive antibody titer initially but were considered negative during follow-up (retesting after ≥3 weeks) (Table 1). The 10 seropositive dogs (hereafter referred to as notified seropositive cases) had been imported into the Netherlands 2–32 (median 9) months before notification. Tracking investigations into the 10 notified seropositive cases identified 11 littermates and 13 other contact dogs (Table 1). Of the 11 littermates, 8 were tested by the NRL and all (8/8) were seropositive. Of the 13 contact dogs, 6 were tested by the NRL; 5 were seronegative and 1 had an inconclusive titer (1:50). This dog lived together with notified case dog #12; they had shared an enclosure for 1.5 years with another seronegative contact dog (<1:50). The dog was euthanized because of geriatric health issues and was thus lost to follow-up. Thus, the total number of seropositive cases in this study was 18 (10 notified seropositive cases and 8 littermates) (Table 2, https://wwwnc.cdc.gov/EID/article/27/7/20-1238-T2.htm).

Of these 18 dogs, 14 (78%) had musculoskeletal disease with such clinical signs as lameness and neck or back pain; discospondylitis was diagnosed in 11.

Table 1. Overview of *Brucella canis* notifications and tracking investigations, the Netherlands, November 2016–December 2018*

Notification no.	Notifying party	Reason for notification	Clinical diagnosis or complaint	Serologic results (NRL)	Tracking investigation		Case ID
					Litter (positive/tested/identified), littermates	Contact dogs (positive/tested/identified)	
1	VMDC	*B. canis* positive culture	Discospondylitis	≥1:400	NA	0/1/1	1
2	VMDC	Clinical complaint	Epididymitis	<1:50	NA	NA	
3	VMDC	Clinical complaint	Discospondylitis	≥1:400	Litter 1 (2/2/2), 2 littermates	NA	2, 3–4
4	VP	Clinical complaint	Discospondylitis	≥1:400	Litter 2 (5/5/8), 5 littermates	NA	5, 6–10
5	NRL	Seropositive	Discospondylitis	1:200	NA	0/3/5	11
6	VP	Clinical complaint	Discospondylitis	1:100	NA	NA	
7	NRL	Seropositive	Discospondylitis	≥1:400	NA	1 (inconclusive)/2/3	12
8	NRL	Seropositive	Neck pain	1:100	NA	NA	
9	NRL	Seropositive	Back pain	≥1:400	Litter 3 (1/1/1), 1 littermate	0/0/2	13, 14
10	NRL	Seropositive	Behavioral problem	≥1:400	NA	0/0/2	15
11	NRL	Seropositive	Discospondylitis	≥1:400	NA	NA	16
12	VP	Clinical complaint	Lameness	<1:50	NA	NA	
13	VMDC	*B. canis* positive culture	Lameness	≥1:400	NA	NA	17
14	VP	Clinical complaint	Lameness	<1:50	NA	NA	
15	VP	Clinical complaint	Epididymitis	<1:50	NA	NA	
16	NRL	Seropositive	Discospondylitis	≥1:400	NA	NA	18

*ID, identification; NA, not applicable; NRL, National Reference Laboratory; VMDC, Veterinary Microbiological Diagnostic Center, Utrecht University; VP, veterinary practitioner.

Information regarding onset of clinical signs was available for 7 of these 13 dogs and occurred 0–3 months after import. One dog had a behavioral problem and 3, all littermates identified through tracking investigations, showed no clinical signs.

All dogs were mixed-breed rescue dogs imported from Romania (n = 7), Bulgaria (n = 10) and Croatia (n = 1). Among them were 9 female dogs, of which 7 were neutered, and 9 male dogs, of which 8 were neutered.

We collected blood, urine, or samples from the infection site from 16 of 18 seropositive dogs for culture; 10 dogs tested positive on these clinical samples (Table 2). Three dogs (nos. 3, 9, and 17) were euthanized because of deteriorating clinical symptoms linked to brucellosis; postmortem examination and cultures revealed growth of *B. canis* in collected tissue samples in 2 of 3 dogs (Table 2). This brings the total number of culture-positive cases in this study to 11 (10 from clinical samples and 1 exclusively from postmortem tissue samples) (Table 2). We cultured isolates from blood (6 samples), urine (5 samples), lymph nodes (3 samples), spleen (2 samples), lung (1 sample), synovial fluid (1 sample), and intervertebral disc (1 sample) (Table 2).

Genotyping was performed for 14 isolates; from 3 dogs, >1 isolate was recovered at different time points. Genotyping of isolates confirmed a close relation between isolates from the same litter (Figure, https://wwwnc.cdc.gov/EID/article/27/7/20-1238-F1.htm). Isolates from dogs imported from Bulgaria show high similarity. Isolates from litter 3 imported from Romania show high similarity, and the isolate from dog#3 clusters with a reference strain from Romania. Only the isolate from dog 1 does not cluster with any other (reference) strain from Romania. On the basis of in silico MLVA-16 analyses, the 2 isolates from dog 5 (samples taken with a 12-month interval) showed no difference in loci. The 2 isolates from dog 9 (3-month interval) showed 1 locus difference (MLVA Bruce16: first isolate 7 repeats, second 8 repeats). The 2 isolates from dog 8 (6-month interval) showed 2 loci difference (MLVA Bruce09: first isolate 7 repeats, second 6 repeats; Bruce16: first isolate 8 repeats, second 9 repeats).

Discussion

Brucellosis in dogs is not notifiable to the OIE or the European Union; therefore, prevalence data on canine brucellosis in different countries are scarce. Literature does confirm occurrence of *B. canis* in stray dogs in Bulgaria (*31*,*32*) and reports bacterial isolates from dogs in Romania (*16*,*33*). Buhmann et al. give an overview of test results for *B. canis* on the basis of data from a large laboratory in Europe receiving samples from 20 different countries in Europe. However, the background of the dogs (i.e., country of origin) is unknown, which makes it difficult to assess the risk of importing dogs from specific countries of origin (*13*).

The Netherlands imports an estimated 21,000 dogs legally per year (unpublished report, NVWA, 2018). According to the TRAde Control and Expert System (TRACES, https://webgate.ec.europa.eu/sanco/traces), a mean of 3,433 (range 2,925–3,950) dogs per year were imported from Romania, 724 (range 557–986) dogs per year from Bulgaria, and 20 (range 9–34) dogs per year from Croatia for the period 2015–2018. This case series underlines the risk of importing dogs from countries to which *B. canis* is endemic. Because *B. canis* was never isolated in the Netherlands before and most dogs showed clinical signs of infection shortly after arrival, all cases are considered import cases. This supposition is supported by the analysis of the genotypes, which showed clustering of isolates within litter and country. Minor differences between genotypes (1 or 2 loci) were seen in isolates from the same dog or litter, which might be explained by coinfection or within-host evolution (*29*,*30*).

The clustering of isolates within a litter confirms vertical transmission of *B. canis*. The most common transmission route of *B. canis* is venereal. Most dogs in our study (15/18) were neutered, which reduced the risk for transmission through genital secretions. Urinary shedding has been implicated as a possible transmission route for dogs cohabiting with male dogs (*4*,*5*). Bacteriuria has been demonstrated in both sexes; however, female dogs appear to shed a lower number of bacteria per milliliter (*5*). Serikawa et al. demonstrated up to 10^6 bacteria/mL urine in male dogs, which supports potential transmission of *B. canis* through urinary shedding (*4*). To our knowledge, all studies on urinary shedding have been conducted with intact animals. Shedding by neutered dogs is believed to be less likely (*34*), but evidence to confirm this does not exist. In our case series, shedding of *B. canis* in urine was found in 4/13 (31%) neutered dogs and 1/3 (33%) intact dogs, indicating that shedding by neutered dogs does occur and should be taken into account. Further research into the number of bacteria shed through urine of neutered dogs infected with *B. canis* is warranted to assess the risk for transmission to other animals or humans.

The diagnosis of a *B. canis* infection in dogs is hampered by subclinical disease and nonspecific clinical signs. In addition, both serologic testing and bacterial isolation have their limitations because of the nature of the disease (*34*). To avoid spread of canine

brucellosis, dogs should be tested before international movement (*7*). This process should involve a combination of tests at different times (*34*). However, freedom of trade between European Union member states hampers the unilateral introduction of mandatory control measures.

The zoonotic risk associated with the dogs infected with *B. canis* in our case series relates mostly to owners, veterinary personnel, and laboratory technicians. Laboratory personnel were put at risk by the positive cultures of dogs 1 and 17, because routine diagnostic procedures were done under BSL-2 conditions, whereas BSL-3 is mandatory for all *Brucella* spp. The risk level of the technicians involved was assessed by medical microbiologists of the Municipal Health Service in line with national guidelines (*35*). To our knowledge, no human infections were linked to the cases documented in this study. However, with the ongoing import of dogs from areas to which *B. canis* is endemic, aspiring dog owners, veterinary personnel, and laboratory technicians will continue to be at risk. Without mandatory testing or control measures, the competent authority in the Netherlands can only inform owners on the poor prognosis and the zoonotic risk and discuss the options of euthanasia or neutering of sexually intact dogs.

In conclusion, this case series proves introduction of *B. canis* in a country to which it is not endemic through import of infected dogs from *B. canis*–endemic areas, posing a threat to the naive autochthonous dog population and to humans. The extent of this threat is hard to estimate because of lack of prevalence data and mandatory testing combined with challenges in diagnosing the infection. Furthermore, the case series indicates that shedding of *B. canis* in urine by neutered dogs occurs and should be considered when assessing the risk for transmission.

Surveillance of zoonotic pathogens in companion animals in the Netherlands was funded by the Dutch Ministry of Agriculture, Nature and Food Quality and the Dutch Ministry of Health, Welfare and Sport. Confirmation and laboratory work done at Wageningen Bioveterinary Research was financed by the Ministry of Agriculture, Nature and Food Quality (project no. WOT-01-002-006.01).

About the Author

Dr. van Dijk is a veterinarian enrolled in a residency program in veterinary microbiology at the Department of Biomolecular Health Sciences, Faculty of Veterinary Medicine, Utrecht University, the Netherlands. She is coordinator of the surveillance program for zoonoses and antimicrobial resistance in companion animals in the Netherlands.

References

1. Wanke MM. Canine brucellosis. Anim Reprod Sci. 2004; 82-83:195–207. https://doi.org/10.1016/j.anireprosci.2004.05.005
2. Keid LB, Chiebao DP, Batinga MCA, Faita T, Diniz JA, Oliveira TMFS, et al. *Brucella canis* infection in dogs from commercial breeding kennels in Brazil. Transbound Emerg Dis. 2017;64:691–7. https://doi.org/10.1111/tbed.12632
3. Kerwin SC, Lewis DD, Hribernik TN, Partington B, Hosgood G, Eilts BE. Diskospondylitis associated with *Brucella canis* infection in dogs: 14 cases (1980–1991). J Am Vet Med Assoc. 1992;201:1253–7.
4. Serikawa T, Muraguchi T. Significance of urine in transmission of canine brucellosis. Nippon Juigaku Zasshi. 1979;41:607–16. https://doi.org/10.1292/jvms1939.41.607
5. Carmichael LE, Joubert JC. Transmission of *Brucella canis* by contact exposure. Cornell Vet. 1988;78:63–73.
6. Lucero NE, Corazza R, Almuzara MN, Reynes E, Escobar GI, Boeri E, et al. Human *Brucella canis* outbreak linked to infection in dogs. Epidemiol Infect. 2010;138:280–5. https://doi.org/10.1017/S0950268809990525
7. Hensel ME, Negron M, Arenas-Gamboa AM. Brucellosis in Dogs and Public Health Risk. Emerg Infect Dis. 2018;24:1401–6. https://doi.org/10.3201/eid2408.171171
8. Marzetti S, Carranza C, Roncallo M, Escobar GI, Lucero NE. Recent trends in human *Brucella canis* infection. Comp Immunol Microbiol Infect Dis. 2013;36:55–61. https://doi.org/10.1016/j.cimid.2012.09.002
9. Dentinger CM, Jacob K, Lee LV, Mendez HA, Chotikanatis K, McDonough PL, et al. Human *Brucella canis* infection and subsequent laboratory exposures associated with a puppy, New York City, 2012. Zoonoses Public Health. 2015;62:407–14. https://doi.org/10.1111/zph.12163
10. Krueger WS, Lucero NE, Brower A, Heil GL, Gray GC. Evidence for unapparent *Brucella canis* infections among adults with occupational exposure to dogs. Zoonoses Public Health. 2014;61:509–18. https://doi.org/10.1111/zph.12102
11. Yagupsky P, Morata P, Colmenero JD. Laboratory diagnosis of human brucellosis. Clin Microbiol Rev. 2019;33:e00073-19. https://doi.org/10.1128/CMR.00073-19
12. Glynn MK, Lynn TV. Brucellosis. J Am Vet Med Assoc. 2008;233:900–8. https://doi.org/10.2460/javma.233.6.900
13. Buhmann G, Paul F, Herbst W, Melzer F, Wolf G, Hartmann K, et al. Canine brucellosis: insights into the epidemiologic situation in Europe. Front Vet Sci. 2019;6:151. https://doi.org/10.3389/fvets.2019.00151
14. Holst BS, Löfqvist K, Ernholm L, Eld K, Cedersmyg M, Hallgren G. The first case of *Brucella canis* in Sweden: background, case report and recommendations from a northern European perspective. Acta Vet Scand. 2012;54:18. https://doi.org/10.1186/1751-0147-54-18
15. Egloff S, Schneeberger M, Gobeli S, Krudewig C, Schmitt S, Reichler IM, et al. *Brucella canis* infection in a young dog with epididymitis and orchitis. Schweiz Arch Tierheilkd. 2018;160:743–8. https://doi.org/10.17236/sat00190
16. Whatmore AM, Perrett L, Friggens M. Second UK isolation of *Brucella canis*. Vet Rec. 2017;180:617. https://doi.org/10.1136/vr.j3004
17. Dutch Government Gazette. Animal health and welfare act [in Dutch]. 1992 [cited 2020 Mar 25]. https://wetten.overheid.nl/BWBR0005662/2019-01-01
18. Dutch Government Gazette. Order on the prevention, control and monitoring of infectious animal diseases, zoonoses and TSEs (TRCJZ/2005/1411) [in Dutch]. 2005;120:17 [cited 2020 Mar 25]. https://zoek.officielebekendmakingen.nl/stcrt-2005-120-p17-SC70318.html

19. Alton GG, Jones LM, Angus RD, Verger JM. Techniques for the brucellosis laboratory. Paris: Institut national de la recherche agronomique; 1988. p. 171–2.
20. World Organisation for Animal Health. Brucellosis. In: Manual of diagnostic tests and vaccines for terrestrial animals. 2018 [cited 2020 Mar 25]. https://www.oie.int/fileadmin/Home/eng/Health_standards/tahm/3.01.04_BRUCELLOSIS.pdf
21. Kroese MV, Beckers L, Bisselink YJWM, Brasseur S, van Tulden PW, Koene MGJ, et al. *Brucella pinnipedialis* in grey seals (*Halichoerus grypus*) and harbor seals (*Phoca vitulina*) in the Netherlands. J Wildl Dis. 2018;54:439–49. https://doi.org/10.7589/2017-05-097
22. Maio E, Begeman L, Bisselink Y, van Tulden P, Wiersma L, Hiemstra S, et al. Identification and typing of *Brucella* spp. in stranded harbour porpoises (*Phocoena phocoena*) on the Dutch coast. Vet Microbiol. 2014;173:118–24. https://doi.org/10.1016/j.vetmic.2014.07.010
23. Simpson JT, Wong K, Jackman SD, Schein JE, Jones SJM, Birol I. ABySS: a parallel assembler for short read sequence data. Genome Res. 2009;19:1117–23. https://doi.org/10.1101/gr.089532.108
24. Milne I, Stephen G, Bayer M, Cock PJA, Pritchard L, Cardle L, et al. Using Tablet for visual exploration of second-generation sequencing data. Brief Bioinform. 2013;14:193–202. https://doi.org/10.1093/bib/bbs012
25. Al Dahouk S, Flèche PL, Nöckler K, Jacques I, Grayon M, Scholz HC, et al. Evaluation of *Brucell*a MLVA typing for human brucellosis. J Microbiol Methods. 2007;69:137–45. https://doi.org/10.1016/j.mimet.2006.12.015
26. Grissa I, Bouchon P, Pourcel C, Vergnaud G. On-line resources for bacterial micro-evolution studies using MLVA or CRISPR typing. Biochimie. 2008;90:660–8. https://doi.org/10.1016/j.biochi.2007.07.014
27. Whatmore AM, Perrett LL, MacMillan AP. Characterisation of the genetic diversity of *Brucella* by multilocus sequencing. BMC Microbiol. 2007;7:34. https://doi.org/10.1186/1471-2180-7-34
28. Jolley KA, Bray JE, Maiden MCJ. Open-access bacterial population genomics: BIGSdb software, the PubMLST.org website and their applications. Wellcome Open Res. 2018;3:124. https://doi.org/10.12688/wellcomeopenres.14826.1
29. Gyuranecz M, Rannals BD, Allen CA, Jánosi S, Keim PS, Foster JT. Within-host evolution of *Brucella canis* during a canine brucellosis outbreak in a kennel. BMC Vet Res. 2013;9:76. https://doi.org/10.1186/1746-6148-9-76
30. Yang Y, Wang Y, Poulsen E, Ransburgh R, Liu X, An B, et al. Genotyping *Brucella canis* isolates using a highly discriminatory multilocus variable-number tandem-repeat analysis (MLVA) assay. Sci Rep. 2017;7:1067. https://doi.org/10.1038/s41598-017-01114-7
31. Taleski V, Zerva L, Kantardjiev T, Cvetnic Z, Erski-Biljic M, Nikolovski B, et al. An overview of the epidemiology and epizootology of brucellosis in selected countries of Central and Southeast Europe. Vet Microbiol. 2002;90:147–55. https://doi.org/10.1016/S0378-1135(02)00250-X
32. Tcherneva E, Rijpens N, Naydensky C, Herman L. Repetitive element sequence based polymerase chain reaction for typing of *Brucella* strains. Vet Microbiol. 1996;51:169–78. https://doi.org/10.1016/0378-1135(96)00036-3
33. Fretin D, Whatmore AM, Al Dahouk S, Neubauer H, Garin-Bastuji B, Albert D, et al. Brucella suis identification and biovar typing by real-time PCR. Vet Microbiol.2008;131:376–85. https://doi.org/10.1016/j.vetmic. 2008.04.003
34. Greene CE, Carmichael LE. Canine brucellosis. In: Greene CE, editor. Infectious diseases of the dog and cat. 4th ed. Philadelphia: Elsevier Health Sciences; 2011. p. 398–411.
35. National Institute for Public Health and the Environment, National Coordination Centre for Communicable Disease Control. Guideline brucellosis [in Dutch]. 2007 [cited 2019 Jun 13]. https://lci.rivm.nl/richtlijnen/brucellose

Address for correspondence: Els M. Broens, Department of Biomolecular Health Sciences, Faculty of Veterinary Medicine, Utrecht University, Yalelaan 1, 3584 TD, Utrecht, the Netherlands; email: e.m.broens@uu.nl

Severe Acute Respiratory Syndrome Coronavirus 2 P.2 Lineage Associated with Reinfection Case, Brazil, June–October 2020

Paola Cristina Resende, João Felipe Bezerra, Romero Henrique Teixeira Vasconcelos, Ighor Arantes, Luciana Appolinario, Ana Carolina Mendonça, Anna Carolina Paixao, Ana Carolina Duarte, Thauane Silva, Alice Sampaio Rocha, Ana Beatriz Machado Lima, Alex Pauvolid-Corrêa, Fernando Couto Motta, Dalane Loudal Florentino Teixeira, Thiago Franco de Oliveira Carneiro, Francisco Paulo Freire Neto, Isabel Diniz Herbster, Anderson Brandao Leite, Irina Nastassja Riediger, Maria do Carmo Debur, Felipe Gomes Naveca, Walquiria Almeida, Mirian Livorati, Gonzalo Bello,[1] Marilda M. Siqueira[1]

A 37-year-old healthcare worker from the northeastern region of Brazil experienced 2 clinical episodes of coronavirus disease. Infection with severe acute respiratory syndrome coronavirus 2 was confirmed by reverse transcription PCR in samples collected 116 days apart. Whole-genome sequencing revealed that the 2 infections were caused by the most prevalent lineage in Brazil, B.1.1.33, and the emerging lineage P.2. The first infection occurred in June 2020; Bayesian analysis suggests reinfection at some point during September 14–October 11, 2020, a few days before the second episode of coronavirus disease. Of note, P.2 corresponds to an emergent viral lineage in Brazil that contains the mutation E484K in the spike protein. The P.2 lineage was initially detected in the state of Rio de Janeiro, and since then it has been found throughout the country. Our findings suggest not only a reinfection case but also geographic dissemination of the emerging Brazil clade P.2.

The efficiency and persistence of natural protective immunity caused by severe acute respiratory syndrome coronavirus 2 (SARS-CoV-2) infection or vaccination are currently unknown. Reinfection cases have been reported in different countries (*1*), but the differentiation between cases of reinfection and viral persistence remains a challenge. The detection of 2 coronavirus disease (COVID-19) episodes ≥90 days apart and caused by 2 different lineages of SARS-CoV-2 remains the most reliable evidence of reinfection (*2*). In this article, we describe a reinfection case and highlight details about the genomic features of the 2 COVID-19 episodes. In addition, we demonstrate that the virus in the second episode was related to the emerging variant of interest (VOI) designated as lineage P.2, which is currently circulating throughout Brazil.

Methods

Case Description

A 37-year-old female physician with no underlying conditions reported 2 episodes of COVID-19 in the state of Rio Grande do Norte in the northeastern region of Brazil. The first episode occurred in June 2020 and the second in October 2020; a total of 116 days occurred between the 2 episodes.

On June 17, the case-patient, who lives in Rio Grande do Norte and works in the neighboring state of Paraíba, experienced symptoms such as headache, runny nose, diarrhea, and myalgia, and her illness was classified as a mild COVID-19 case with no complications

Author affiliations: Instituto Oswaldo Cruz, Rio de Janeiro, Brazil (P.C. Resende, I. Arantes, L. Appolinario, A.C. Mendonça, A.C. Paixao, A.C. Duarte, T. Silva, A.S. Rocha, A.B.M. Lima, A. Pauvolid-Corrêa, F.C. Motta, G. Bello, M.M. Siqueira); Universidade Federal da Paraíba, João Pessoa, Brazil (J.F. Bezerra, R.H.T. Vasconcelos); Texas A&M University, College Station, Texas, USA (A. Pauvolid-Corrêa); Laboratório Central do Estado da Paraíba, João Pessoa (L.F. Teixeira, T.F. de Oliveira Carneiro); Universidade Federal do Rio Grande do Norte, Natal, Brazil (F.P.F. Neto); Maternidade Escola Januario Cicco, Natal (I.D. Herbster); Laboratório Central do Estado do Alagoas, Maceió, Brazil (A.B. Leite); Laboratório Central do Estado do Paraná, Curitiba, Brazil (I.N. Riediger, M.C. Debur); Instituto Leônidas e Maria Deane, on behalf of the COVIDNORTE team, Manaus, Brazil (F.G. Naveca); Ministério da Saúde do Brasil, Brasilia, Brazil (W. Almeida, M. Livorati)

DOI: https://doi.org/10.3201/eid2707.210401

[1]These authors share senior authorship.

(*3*). A nasopharyngeal swab specimen was collected on June 23, 6 days after the onset of symptoms. A second nasopharyngeal swab specimen was collected on September 16 as part of a follow-up procedure. On October 11, the patient experienced intense headache, ageusia, anosmia, and fatigue, which were suggestive of a new COVID-19 episode. This second infection was mild and also evolved without complications. On October 13, 2 days after the second onset of symptoms, a third nasopharyngeal swab specimen was collected.

Ethics

This study was approved by the FIOCRUZ-IOC Ethics Committee (68118417.6.0000.5248 and CAAE 32333120.4.0000.5190) and the Ministry of Health of Brazil SISGEN (A1767C3). In addition, the case-patient read and signed the free and informed consent form.

Procedures

First and third nasopharyngeal swab specimens were initially processed by the Public Health Central Laboratory of the state of Paraíba; the second nasopharyngeal swab specimen was processed by the Institute of Tropical Medicine of the Federal University of Rio Grande do Norte in northeastern Brazil. For the first and third specimens, viral RNA was extracted by using QIAamp Viral RNA Mini Kit (QIAGEN, https://www.qiagen.com), according to the manufacturer's instructions. RNA samples were tested for SARS-CoV-2 by real-time reverse transcription PCR (rRT-PCR) using a molecular kit design for the targets envelope gene and internal control human RNase P gene (*4*). For the second nasopharyngeal swab specimen, we extracted RNA by using Extracta kit Viral DNA and RNA (MVXA-P016) (Loccus, https://loccus.com.br) and tested for SARS-CoV-2 by using a rRT-PCR probe for the targets N1, N2, and Rnase P (Integrated DNA Technologies, https://www.idtdna.com) (*5*). For confirmation and complementary analysis, positive samples were sent to the Laboratory of Respiratory Viruses and Measles at Fiocruz, Brazil's National Reference Laboratory and the World Health Organization Reference Laboratory for Coronavirus.

According to the technical note of the Ministry of Health of Brazil 52/2020-CGPNI/DEIDT/SVS/MS, ≥2 rRT-PCR–positive swab samples collected ≥90 days apart, independent of clinical conditions, are required to confirm a SARS-CoV-2 reinfection. As the routine procedure for confirmation of reinfection cases, the 2 positive results obtained for this patient were confirmed by rRT-PCR. The RNA was obtained by using QIAamp Viral RNA Mini Kit (QIAGEN), according to the manufacturer's instructions. Molecular detection of SARS-CoV-2 was performed by using a rRT-PCR Biomanguinhos SARS-CoV-2 kit for the targets E, N1, N2, and Rnase P (*4*,*5*) using the Applied Biosystems 7500 Real-Time PCR (Thermo Fisher Scientific, https://www.thermofisher.com).

For supplementary analysis, the nasopharyngeal swab specimens were submitted for the qualitative detection of SARS-CoV-2 antigens by using the Panbio COVID-19 Ag rapid test device (Abbott, https://www.abbott.com), according to the manufacturer's instructions. Both clinical samples were also submitted to virus isolation in cell cultures as previously described (*6*). Next, 200 μL of the viral transport medium of positive specimens were inoculated in VERO E6 cells flasks and inspected daily for cytopathic effect (CPE) in a total of two 4-day blind passages. SARS-CoV-2 CPE was confirmed by rRT-PCR of culture supernatant. In cases in which no CPE was observed, rRT-PCR was performed on day 4 to confirm absence of virus replication.

In addition, we tested the serum sample from the case-patient's second episode of COVID-19 for IgG by the Abbott chemiluminescent microparticle immunoassay (CMIA) using nucleocapsid protein, as well as for SARS-CoV-2–specific neutralizing antibodies by plaque reduction neutralization test (PRNT) (*7*) for confirmation. For PRNT, an aliquot of serum sample inactivated at 56°C for 30 minutes was tested in VERO CCL-81 cells in duplicate at serial 2-fold dilutions to determine 90% endpoint titers against 4 infectious SARS-CoV-2 lineages, including B.1 (GISAID [https://www.gisaid.org] accession no. EPI_ISL_414045), P.1 (accession no. EPI_ISL_1402431), P.2 (accession no. EPI_ISL_1402429), and B.1.1.7 (accession no. EPI_ISL_1402430). Serum samples were considered seropositive when a serum dilution of at least 1:10 reduced ≥90% of the formation of SARS-CoV-2 viral plaques ($PRNT_{90}$) (*7*).

We performed whole-genome sequencing by using the RNA extracted manually using the QIAamp Viral RNA Mini Kit (QIAGEN). The SARS-CoV-2 genomes were recovered by using Illumina or ONT Nanopore sequencing protocols previously established and used by the Fiocruz COVID-19 Genomic Surveillance Network to recover high-quality genomes (P.C. Resende, unpub. data, https://doi.org/10.1101/2020.04.30.069039). The FASTQ reads obtained were imported into the CLC Genomics Workbench version 20.0.4 (QIAGEN), trimmed, and mapped against the reference sequence EPI_ISL_402124 from GISAID. The alignment was refined by using the InDels and Structural Variants module, then the Local Realignment module and the final consensus obtained. Maximum-likelihood phylogenetic analysis of all SARS-CoV-2 whole genomes from the state of Paraíba was conducted by using PhyML (*8*).

We conducted Bayesian phylogeographic analysis in BEAST version 1.10 (*9*).

Results

Diagnostic Laboratory Findings

The first and third nasopharyngeal swab specimens, collected on June 23 and October 13, 2020, tested positive for SARS-CoV-2 by rRT-PCR, whereas the second nasopharyngeal swab specimen, collected on September 8, tested negative. Both positive specimens had high viral load, presumed by the low cycle threshold (C_t) values by rRT-PCR (Table, https://wwwnc.cdc.gov/EID/article/27/7/21-0401-T1.htm). The 2 positive samples were confirmed by using the rRT-PCR protocol and the Ag-RDT Panbio COVID-19 Antigen Test (Abbott) directly from the clinical sample.

This case was confirmed as a reinfection according to the Ministry of Health of Brazil criteria for reinfection confirmation, which stipulates 2 positive rRT-PCR results separated by ≥90 days. The 2 positive samples were collected 116 days apart. Viral isolation from the specimen collected in the second episode of COVID-19 was negative for infectious virus in VERO E6 cells culture after 2 passages.

Serum sample collected 2 months after the second episode tested positive for IgG by CMIA, which uses the nucleocapsid protein of SARS-CoV-2. However, when the same serum sample was tested by PRNT for B.1, P.1, P.2, and B.1.1.7 lineages, neutralizing antibodies were under the detectable level of our assay; $PRNT_{90}$ titers for all 4 lineages were <10.

Genomic Findings

To distinguish between reinfection and long-term viral persistence, we recovered the SARS-CoV-2 whole genomes from the 2 positive nasopharyngeal swab specimens (accession nos. EPI_ISL_792561 and EPI_ISL_792562) of the reinfection case plus 76 SARS-CoV-2 positive cases detected in the same state of Paraíba during April 6–November 27, 2020 (EPI_ISL_792563 to EPI_ISL_792638). We performed maximum-likelihood phylogenetic analysis of all SARS-CoV-2 whole genomes from the state of Paraíba by using PhyML (*8*); this analysis revealed 2 different viral lineages in the 2 COVID-19 episodes. In the first episode, we detected the lineage B.1.1.33, whereas lineage P.2 (alias for B.1.1.28.2) was detected in the third clinical specimen (from the second episode) (Figure 1), according to PANGO lineage classification (*10*). The SARS-CoV-2 B.1.1.33 lineage was also detected in other samples from the state of Paraíba (Figure 1) and represent the most prevalent viral variant circulating in Brazil during the early epidemic phase (*11*,*12*). Of note, sequences recovered from the reinfection case and from 2 additional cases in the state of Paraíba harbor the substitution S-E484K (G23012A) and were classified as lineage P.2, which was initially detected in the state of Rio de Janeiro (*13*).

To better characterize the P.2 virus detected in the second SARS-CoV-2–positive nasopharyngeal swab specimen, we aligned it against all B.1.1.28 (an ancestor of P.2) whole genomes available in the GISAID EpiCoV database as of December 20, 2020. In addition, we also selected 8 P.2 whole-genome sequences from the states of Alagoas (n = 2), Amazonas (n = 1), and Parana (n = 5) available in the Fiocruz COVID-19 Genomic Surveillance Network database (accession nos. EPI_ISL_792560, EPI_ISL_792639, EPI_ISL_792642, EPI_ISL_792645, EPI_ISL_792646, and EPI_ISL_792650–52). The new maximum-likelihood phylogenetic tree revealed that the lineage P.2 recovered from the reinfection case branched in a highly supported (approximate-likelihood ratio test = 1) subclade with 46 additional sequences sampled during October–December, 2020, in the states of Rio de Janeiro, Paraíba, Alagoas, Parana, and Amazonas (Figure 2, panel A). We identified 5 lineage-defining single-nucleotide polymorphisms: C100U (5′ untranslated region), T10667G (NSP5_L205V), C11824T (NSP6), G23012A (S_E484K), and G28628T (N_A119S) that distinguish P.2 sequences from all other B.1.1.28 sequences available in Brazil.

To further investigate the spatiotemporal emergence of the VOI P.2 and the viral strain detected in the reinfection case, we conducted a Bayesian phylogeographic analysis of all 47 SARS-CoV-2 sequences in Brazil that branched within such clade. We estimated time-scaled trees by using a strict molecular clock model with a uniform substitution rate prior (8–10 × 10^{-4} substitutions/site/year), a general time-reversible plus invariable sites plus gamma nucleotide substitution model, and the Bayesian skyline coalescent prior as implemented in BEAST version 1.10 (*9*). Bayesian reconstructions traced the origin of the lineage P.2 in the state of Rio de Janeiro (PSP = 0.97) on August 27 (95% highest posterior density credible interval July 14–September 18) and its subsequent dispersion from Rio de Janeiro to other states in the southern and northeastern regions of the country (Figure 2, panel B). This phylogeographic reconstruction also supports a dissemination event from the state of Paraíba to the state of Amazonas and the branching of the P.2 sequence from the reinfection case with that from Amazonas with high support (PP = 1) (Figure 2, panel B). The most recent common ancestor of P.2 sequences from the reinfection case and the state of Amazonas was dated to September 29 (95% highest posterior density credible interval

September 14–October 11), a few days before the onset of reinfection symptoms on October 11.

Discussion

We demonstrate that this reinfection case in Brazil corresponds to a primary infection with the lineage B.1.1.33 and a reinfection with the VOI P.2, which harbors the mutation S-E484K. The age of the common ancestor of the P.2 virus of the reinfection case and a nonrelated virus sampled in the state of Amazonas provide a maximum limit for the reinfection episode during September 14–October 11. The estimated period excludes the possibility of long-term persistence of the P.2 virus since primary infection (before June 23, 2020).

Of note, the reinfection case reported here coincides with a recently reported case in the state of Bahia that also described a primary infection with the B.1.1.33 variant and reinfection with the P.2 viral variants (*14*). These studies also confirm that the P.2 initially described in the state of Rio de Janeiro (*13*) is more widely distributed across different states in Brazil. Our analysis supports that the P.2 lineage probably emerged in Rio de Janeiro around late August, but defining the precise location and time of emergence of this novel lineage will require a denser sampling from different states in Brazil from the second half of 2020.

The mutation E484K is located in the receptor-binding domain and has also been recently described in multiple SARS-CoV-2 VOI and variants of concern rapidly spreading in the Americas, Europe, and Africa (*15*). The rapid dissemination of these variants, combined with the ability of viruses harboring the mutation E484K to potentially escape from neutralizing antibodies mounted for older lineages (*13*,*16*), should raise concern about the potential effect on infectivity, pathogenicity, and reinfection.

We also speculate that the reinfection case described resulted from a weak and transient protective immunity that occurred after primary infection. Consistent with this notion, despite the positive result for IgG by CMIA in the serum sample collected 2 months after the second SARS-CoV-2 infection, $PRNT_{90}$ titers for all 4 lineages of SARS-CoV-2 tested, including P.2, were below the detectable level. The prevalence of neutralizing antibodies also varies among patients and low levels or absence of neutralizing antibody has been reported in mildly affected COVID-19

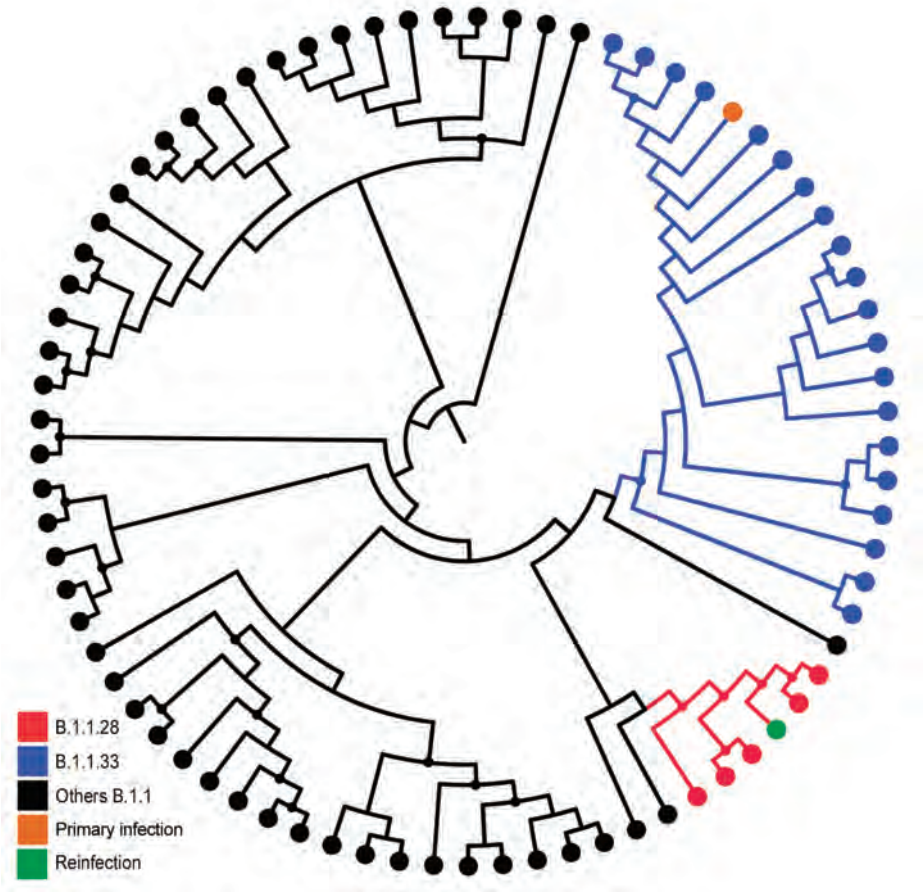

Figure 1. Maximum-likelihood tree of severe acute respiratory syndrome coronavirus 2 whole-genome sequences from Paraíba in study of reinfection case, Brazil, June–October 2020. Branching pattern of whole-genome sequences (29779 nt) from Paraíba (n = 77) are shown classified within lineages B.1.1.28 (red), B1.1.33 (blue), and others B.1.1 (black). Sequences derived from the primary infection and reinfection are highlighted with different colors as indicated. Nodes with high statistical support (approximate-likelihood ratio test ≥9.0) are marked by the smaller circular shapes.

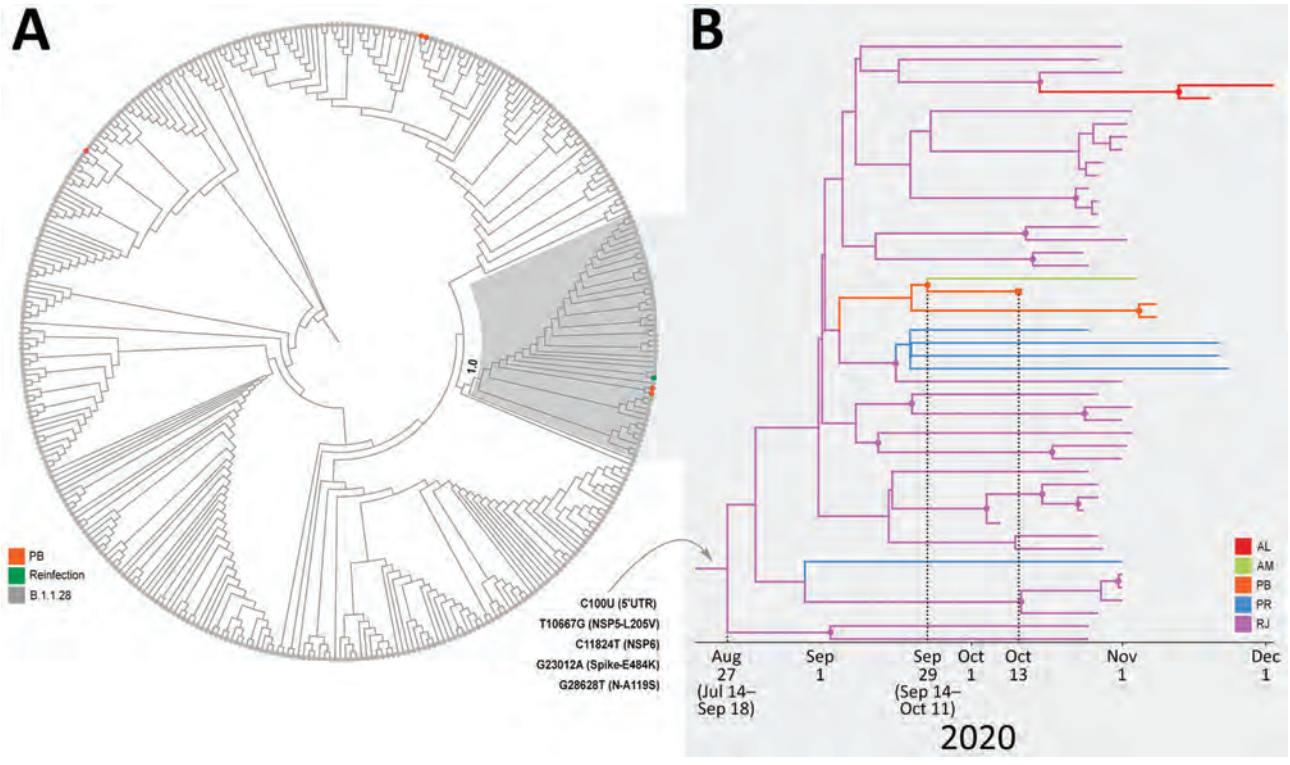

Figure 2. Emergence of the P.2 clade in study of severe acute respiratory syndrome coronavirus 2 (SARS-CoV-2) reinfection case, Brazil. A) Maximum-likelihood phylogenetic tree of B.1.1.28 SARS-CoV-2 whole-genome sequences (29,779-nt) from Brazil (n = 376). Shaded box highlights the P.2 clade (n = 47), and its statistical support (approximate-likelihood ratio test = 1.0) is indicated in the cladogram. Sequences from Paraíba are indicated in orange and sequences from the reinfection case are indicated by green. B) Time-scaled Bayesian maximum clade credibility tree of SARS-CoV-2 whole-genome sequences from the P.2 clade (n = 47). Branches are colored according to the most probable location state of their descendent nodes as indicated. The 5 lineage-defining single-nucleotide polymorphisms are indicated at the maximum clade credibility tree root node. Circular shapes mark nodes with high statistical support (posterior probability≥9.0), and a square tip shape indicates the sequence from reinfection case. AL, Alagoas; AM, Amazonas; PB, Paraíba; PR, Parana; RJ, Rio de Janeiro; UTR, untranslated region.

convalescent patients (*17*). In a study conducted with SARS-CoV-2–infected healthcare workers, neutralizing activity rapidly declined and might even be lost beginning 2 months after disease onset (*18*).

Whether reinfected persons might contribute substantially to the onwards transmission of SARS-CoV-2 in the population is currently unclear. The negative results from viral isolation after 2 sequential passages of nasopharyngeal swab specimens suggests absence (or low levels) of infectious virus in the second episode of COVID-19. Viral isolation prevalence among COVID-19 patient samples varies and is usually lower in mild infections with high C_t values (*17*).

Our results demonstrate that previous exposure to SARS-CoV-2 might not guarantee immunity, and that sequential infections might not mount detectable neutralizing antibodies in all cases. These findings reinforce the need to maintain nonpharmacologic protective measures not only by persons who test negative but also for those who have already tested positive for SARS-CoV-2. Characterization of the immune response in persons who become reinfected with SARS-CoV-2 will be crucial to learn more about the role of viral and host factors on this rare phenotype.

This article was preprinted at https://virological.org/t/spike-e484k-mutation-in-the-first-sars-cov-2-reinfection-case-confirmed-in-brazil-2020/584.

Acknowledgments

We are thankful for all that contribute to the EpiCoV database from the GISAID initiative with high-quality SARS-CoV-2 genomes. All genomes used in this study are described in the Appendix Table (https://wwwnc.cdc.gov/EID/article/27/7/21-0401-App1.xlsx). We gratefully acknowledge the authors from the originating laboratories responsible for obtaining the specimens, as well as the submitting laboratories where the genome data were generated and shared via GISAID, on which this research is based. All submitters of data may be contacted directly via https://www.gisaid.org.

We thank the funding support from General Laboratories Coordination of Brazilian Ministry of Health; the Coordination of Health Surveillance and Reference Laboratories of Oswaldo Cruz Foundation; Ministério da Ciência, Tecnologia, Inovações e Comunicações/Conselho Nacional de Desenvolvimento Científico e Tecnológico - CNPq/Ministério da Saúde–MS/FNDCT/SCTIE/Decit (grants no. 402457/2020-9 and 403276/2020-9); Inova Fiocruz/Fundação Oswaldo Cruz (grants no. VPPCB-007-FIO-18-2-30; FAPERJ: E26/210.196/2020; FAPEAM (PCTI-EmergeSaude/AM call 005/2020 and Rede Genomica de Vigilancia em Saude–REGESAM). We also appreciate the support of the Fiocruz COVID-19 Genomic Surveillance Network (http://www.genomahcov.fiocruz.br), the Respiratory Viruses Genomic Surveillance Network of the General Laboratory Coordination, Brazilian Ministry of Health, Brazilian Central Laboratory States, the Multi-user Research Facility of Biosafety Level 3 Platform of the Oswaldo Cruz Institute and Fiocruz Diagnoses Unit Rio de Janeiro.

About the Author

Dr. Paola Cristina Resende is a public health researcher at the Fundação Oswaldo Cruz (FIOCRUZ), Brazil, and a member of the Fiocruz COVID-19 Genomic Surveillance Network. Her primary research interests are genetic epidemiology and molecular evolution of viruses.

References

1. Babiker A, Marvil CE, Waggoner JJ, Collins MH, Piantadosi A. The importance and challenges of identifying SARS-CoV-2 reinfections. J Clin Microbiol. 2021; 59:e02769–20.
2. Brazilian Ministry of Health, Health Surveillance Secretariat. TECHNICAL NOTE Nº 52/2020-CGPNI/DEIDT/SVS/MS [in Portuguese]. In: Department of Immunization and Communicable Diseases. General Coordination of the National Immunization Program, editors. Bairro Asa Norte: Brazil DF; 2020. p. 4.
3. National Institutes of Health. Clinical spectrum of SARS-CoV-2 infection. December 17, 2020 [cited 2021 Mar 29]. https://www.covid19treatmentguidelines.nih.gov/overview/clinical-spectrum
4. Biomanginhos FIOCRUZ. Kit Molecular SARS-CoV-2 (information and consultation of manuals) [in Portuguese] [cited 2020 Apr 15]. https://www.bio.fiocruz.br/index.php/br/produtos/reativos/testes-moleculares/novo-coronavirus-sars-cov2
5. Food and Drug Administration. CDC 2019-novel coronavirus (2019-nCoV) real-time RT-PCR diagnostic panel [cited 2020 Dec 1]. https://www.fda.gov/media/134922/download
6. Basile K, McPhie K, Carter I, Alderson S, Rahman H, Donovan L, et al. Cell-based culture of SARS-CoV-2 informs infectivity and safe de-isolation assessments during COVID-19. Clin Infect Dis. 2020 Oct 24 [Epub ahead of print].
7. Deshpande GR, Sapkal GN, Tilekar BN, Yadav PD, Gurav Y, Gaikwad S, et al. Neutralizing antibody responses to SARS-CoV-2 in COVID-19 patients. Indian J Med Res. 2020;152:82–7. https://doi.org/10.4103/ijmr.IJMR_2382_20
8. Guindon S, Dufayard JF, Lefort V, Anisimova M, Hordijk W, Gascuel O. New algorithms and methods to estimate maximum-likelihood phylogenies: assessing the performance of PhyML 3.0. Syst Biol. 2010;59:307–21. https://doi.org/10.1093/sysbio/syq010
9. Suchard MA, Lemey P, Baele G, Ayres DL, Drummond AJ, Rambaut A. Bayesian phylogenetic and phylodynamic data integration using BEAST 1.10. Virus Evol. 2018;4:vey016. https://doi.org/10.1093/ve/vey016
10. Rambaut A, Holmes EC, O'Toole Á, Hill V, McCrone JT, Ruis C, et al. A dynamic nomenclature proposal for SARS-CoV-2 lineages to assist genomic epidemiology. Nat Microbiol. 2020;5:1403–7. https://doi.org/10.1038/s41564-020-0770-5
11. Candido DS, Claro IM, de Jesus JG, Souza WM, Moreira FRR, Dellicour S, et al.; Brazil-UK Centre for Arbovirus Discovery, Diagnosis, Genomics and Epidemiology (CADDE) Genomic Network. Evolution and epidemic spread of SARS-CoV-2 in Brazil. Science. 2020;369:1255–60. https://doi.org/10.1126/science.abd2161
12. Resende PC, Delatorre E, Gräf T, Mir D, Motta FC, Appolinario L, et al. Evolutionary dynamics and dissemination pattern of the SARS-CoV-2 lineage B.1.1.33 during the early pandemic phase in Brazil. Front Microbiol. 2020 Feb 17 [Epub ahead of print]. https://doi.org/10.3389/fmicb.2020.615280
13. Voloch CM, da Silva Francisco R Jr, de Almeida LGP, Cardoso CC, Brustolini OJ, Gerber AL, et al. Covid19-UFRJ Workgroup, LNCC Workgroup, Adriana Cony Cavalcanti. Genomic characterization of a novel SARS-CoV-2 lineage from Rio de Janeiro, Brazil. J Virol. 2021 Mar 1 [Epub ahead of print]. https://doi.org/10.1128/JVI.00119-21
14. Nonaka CKV, Franco MM, Gräf T, de Lorenzo Barcia CA, de Ávila Mendonça RN, de Sousa KAF, et al. Genomic evidence of SARS-CoV-2 reinfection involving E484K spike mutation, Brazil. Emerg Infect Dis. 2021 Feb 19 [Epub ahead of print]. https://doi.org/10.3201/eid2705.210191
15. Latif AA, Mullen JL, Alkuzweny M, Tsueng G, Cano M, Haag E, et al. S:E484K mutation report. 2020 [cited 2021 Mar 25]. https://outbreak.info/situation-reports?muts=S%3AE484K
16. Liu Z, VanBlargan LA, Bloyet L-M, Rothlauf PW, Chen RE, Stumpf S, et al. Identification of SARS-CoV-2 spike mutations that attenuate monoclonal and serum antibody neutralization. Cell Host Microbe. 2021;29:477–488.e4. https://doi.org/10.1016/j.chom.2021.01.014
17. Walsh KA, Jordan K, Clyne B, Rohde D, Drummond L, Byrne P, et al. SARS-CoV-2 detection, viral load and infectivity over the course of an infection. J Infect. 2020;81:357–71. https://doi.org/10.1016/j.jinf.2020.06.067
18. Marot S, Malet I, Leducq V, Zafilaza K, Sterlin D, Planas D, et al.; Sorbonne Université SARS-CoV-2 Neutralizing Antibodies Study Group. Rapid decline of neutralizing antibodies against SARS-CoV-2 among infected healthcare workers. Nat Commun. 2021;12:844. https://doi.org/10.1038/s41467-021-21111-9

Address for correspondence: Paola Cristina Resende, Instituto Oswaldo Cruz (IOC), Fiocruz, Laboratorio de Virus Respiratorios e Sarampo, Pavilhao Helio e Peggy Pererira (HPP), Av Brasil, 4365, Manguinhos, Rio de Janeiro, RJ, Brazil; email: paola@ioc.fiocruz.br

Seroprevalence of SARS-CoV-2 among Blood Donors and Changes after Introduction of Public Health and Social Measures, London, UK

Gayatri Amirthalingam, Heather Whitaker, Tim Brooks, Kevin Brown, Katja Hoschler, Ezra Linley, Ray Borrow, Colin Brown, Nick Watkins, David J. Roberts, Danielle Solomon, Charlotte M. Gower, Olivier le Polain de Waroux, Nick J. Andrews, Mary E. Ramsay

We describe results of testing blood donors in London, UK, for severe acute respiratory disease coronavirus 2 (SARS-CoV-2) IgG before and after lockdown measures. Anonymized samples from donors 17–69 years of age were tested using 3 assays: Euroimmun IgG, Abbott IgG, and an immunoglobulin receptor-binding domain assay developed by Public Health England. Seroprevalence increased from 3.0% prelockdown (week 13, beginning March 23, 2020) to 10.4% during lockdown (weeks 15–16) and 12.3% postlockdown (week 18) by the Abbott assay. Estimates were 2.9% prelockdown, 9.9% during lockdown, and 13.0% postlockdown by the Euroimmun assay and 3.5% prelockdown, 11.8% during lockdown, and 14.1% postlockdown by the receptor-binding domain assay. By early May 2020, nearly 1 in 7 donors had evidence of past SARS-CoV-2 infection. Combining results from the Abbott and Euroimmun assays increased seroprevalence by 1.6%, 2.3%, and 0.6% at the 3 timepoints compared with Euroimmun alone, demonstrating the value of using multiple assays.

The first confirmed cases of coronavirus disease (COVID-19) in the United Kingdom were identified at the end of January 2020. As cases increased across all regions, surveillance data indicated that the epidemic was progressing more rapidly in London than the rest of the United Kingdom. In response to the increase in cases, hospitalizations, and deaths, the United Kingdom introduced a series of measures to limit transmission, beginning March 12, 2020 (week 11); persons with a continuous cough or fever were advised to self-isolate for 7 days, school trips abroad were cancelled, and at-risk groups were advised to avoid cruises. These measures culminated in the implementation of legally enforceable public health and social measures (i.e., lockdown) beginning March 23 (week 13) (*1*).

Despite the reporting of a range of surveillance data in England, including laboratory-confirmed cases, primary-care consultations, hospital and intensive care unit (ICU) admissions, and deaths (*2*), much remains unknown about the magnitude of infection with severe acute respiratory syndrome coronavirus 2 (SARS-CoV-2) virus in the population, the key drivers of transmission, and the incidence of asymptomatic or mildly symptomatic infection within the UK population thus far.

Serologic estimates are critical to better understand epidemiologic trends and help inform policy options to control disease. These estimates also provide a denominator for estimating severity measures, such as infection fatality and infection hospitalization ratios, and to help clarify the epidemiology of COVID-19 in the population.

Early in the pandemic, data from population-based seroepidemiologic studies were limited (N. Bobrovitz et al., unpub. data, https://doi.org/10.1101/2020.05.10.20097451), and how the prevalence of SARS-CoV-2 infection varies by age was not well understood. Much remains unknown about the dynamics of the antibody response to SARS-CoV-2. The existing serologic assays target different viral

Author affiliations: Public Heath England, London, UK (G. Amirthalingam, H. Whitaker, K. Brown, K. Hoschler, C. Brown, D. Solomon, C.M. Gower, O. le Polain de Waroux, N.J. Andrews, M.E. Ramsay); Public Health England, Porton Down, UK (T. Brooks); Public Health England, Manchester, UK (R. Borrow); National Health Service Blood and Transplant, Cambridge, UK (N. Watkins); National Health Service Blood and Transplant, Oxford, UK (D.J. Roberts); Radcliffe Department of Medicine, University of Oxford, Oxford (D.J. Roberts)

DOI: https://doi.org/10.3201/eid2707.203167

proteins, and IgG responses to these proteins are likely to appear at different stages of the immune response, potentially resulting in some assays preferentially identifying those persons seroconverting earlier or later in the course of an infection (*3*); these differences are an important factor when interpreting data from seroprevalence studies. In this article, we describe the results of testing whole blood donors in London, UK, who were anonymously tested as part of the national public health response to COVID-19. These tests were conducted using 3 different serologic assays at 3 timepoints during the epidemic that reflect transmission prelockdown, perilockdown, and immediately post lockdown.

Methods

Data Collection

Sample Selection

A program of collecting plasma samples each week through the National Health Service Blood and Transplant Services from healthy 17–69 year old persons donating whole blood was initiated on March 23, 2020, at epidemiologic week 13. The minimum interval between serial donations was 12 weeks for men and 16 weeks for women. An average of 10,683 whole blood donations were received per month in London during March–July 2020.

Given the evidence of the scale of the epidemic in London, enhanced testing of London donors was implemented with donor samples from London collected during week 13 (period 1, beginning March 23), weeks 15–16 (period 2), and week 18 (period 3). Approximately 1,000 fully anonymized donations were obtained for each collection. The demographic information available from each donor included age, sex, and area of residence.

Blood donors are healthy persons who are excluded from donating if they experienced any acute illness for ≥2 weeks before donating blood. In addition, specific donor exclusion criteria for coronavirus have been introduced (14 days postinfection at the time of the study, which was extended to 28 days starting June 8) (*4*). Given the standard symptomatic period, the exclusion criteria described and the fact that antibodies might take ≥2 weeks to be detectable, prevalence estimates among blood donors probably reflect infection prevalence ≥2–4 weeks before samples were taken.

To undertake the validation of test sensitivity, samples from recovering case-patients are required. To obtain convalescent serum samples from case-patients in the community, Public Health England (PHE) initiated an active request for samples from persons with PCR-confirmed cases reported early in the epidemic. These persons were asked to attend their general practitioner approximately 3–5 weeks after illness onset to provide a convalescent serum sample (N.L. Boddington et al., unpub. data, https://doi.org/10.1101/2020.05.18.20086157). Crucially, these cases were detected in the containment phase, when testing was based on epidemiologic factors such as travel. These cases should therefore be a better reflection of mild and asymptomatic infections that would not otherwise be picked up by routine testing, which was based predominantly on testing hospitalized patients at the 3 timepoints.

To evaluate specificity, serum samples collected before the circulation of SARS-CoV-2 also were tested. This testing was done on residual serum samples taken in 2018 and provided by the Sero-Epidemiology Unit (SEU) at PHE, Manchester (*5*), and the Royal College of General Practitioners Research and Surveillance Centre (*6*). All samples were processed and stored at the SEU.

Serologic Assays

We tested samples on 2 commercial assays according to the manufacturers' instructions. Initial testing was conducted by using the SARS-CoV-2 ELISA IgG assay from Euroimmun (https://www.euroimmun.com) targeting the S1 domain, including the receptor-binding domain (RBD); testing was conducted by using the SARS-CoV-2 IgG for use on the Architect platform (Abbott, https://www.molecular.abbott) targeting the nucleoprotein. Samples were tested individually and reported according to the manufacturers' criteria. We defined Euroimmun results of 0.8 to <1.1 as equivocal and ≥1.1 as reactive. We defined Abbott results of ≥1.4 as reactive; we also defined an equivocal range of 0.8 to <1.4 for presentation of validation data.

The third assay was an in-house assay developed in the Virus Reference Department at PHE, also used retrospectively. For this ELISA, we purchased the commercial recombinant RBD subunit of the SARS-CoV-2 spike protein from SinoBiological Inc. (https://www.sinobiological.com), which we expressed in HEK293 cell culture with a C-terminal mouse Fc tag (Arg319-Phe541(V367F) (GenBank accession no. YP_009724390.1). We coated Nunc MaxiSorp (Nunc, https://www.thermofisher.com) flat-bottomed, polystyrene, 96-well microtiter plates by diluting 20 ng recombinant protein per well in sterile phosphate-buffered saline; pH 7.2 ± SD 0.05 (Gibco,

https://www.thermofisher.com) at 4°C–8°C for a minimum of 16 hours. We diluted serum at a final dilution factor of 1 in 100. We detected the binding of IgG on the plate surface by using an anti-human IgG horseradish peroxidase antibody conjugate (Sigma-Aldrich, https://www.sigmaaldrich.com) and 3,3′,5,5′-etramethylbenzidine (Europa Bioproducts Ltd, https://www.europa-bioproducts.com). We analyzed samples in duplicate and evaluated optical density at 450 nm (OD_{450}) data by dividing average OD_{450} values for individual samples by average OD_{450} of a known calibrator with negative antibody levels (T/N ratio). We defined results of 4 to <5 as equivocal and ≥5 as reactive. We defined samples as reactive for each assay independently.

Assay Validation

Because of the speed with which the assays have been developed, limited validation has been conducted by the manufacturers. We therefore used panels created by PHE and managed by the SEU to validate the assays (*7*,*8*)

Population Data

We weighted overall prevalence estimates for age. We based these estimates on population data from the Office for National Statistics (*9*).

Statistical Analysis

We calculated observed prevalence ($prev_{obs}$) by age group, sex, and time with 95% exact CIs. In these calculations, all results falling into the equivocal range of the assays were included as negative. Analyses were conducted in Stata 14 (StataCorp, https://www.stata.com).

We corrected observed prevalence to account for the sensitivity and specificity of the assays by using an adjusted prevalence ($prev_{adj}$) related to the observed prevalence as follows:

$$Prev_{obs} = Se \times prev_{adj} + (1 - Sp) \times (1 - prev_{adj}),$$

where Se denotes sensitivity, Sp denotes specificity, and $prev_{obs}$ denotes the observed prevalence (*10*,*11*). We solved this relationship within a Bayesian model, along with the sampling distribution for reactive tests $n^{+} \approx \text{binomial}(N, prev_{obs})$ and using a beta(0.5,0.5) prior for the adjusted prevalence $prev_{adj}$. We included sensitivity and specificity, which were based on positivity in convalescent and baseline serum samples, in our Bayesian model each by way of a conjugate beta-binomial model with a beta(0.5,0.5) prior, thus accounting for uncertainty of their actual value. We generated uncertainty and credible intervals by using Markov Chain Monte Carlo simulations with 500,000 iterations after a burn-in of 1,000 iterations and a thinning interval of 5, using the NIMBLE package in R software (*12*,*13*).

Results

The overall test positivity based on the Euroimmun assay was 2.9% (95% CI 1.8%–4.4%) in week 13, 9.9% (95% CI 8.2%–11.8%) in weeks 15–16, and 13.0% (95% CI 11.0%–15.3%) in week 18. Consecutive differences between the proportion reactive at the 3 timepoints reduced over time, from 7.0% (95% CI 4.8%–9.1%) during week 13 to weeks 15–16 to 3.2% (95% CI 0.4%–5.9%) during weeks 15–16 to week 18 (Figure 1; Appendix Table 1, https://wwwnc.cdc.gov/EID/article/27/7/20-3167-App1.pdf).

In comparison, results from the RBD and Abbott assays had higher positivity at week 13, RBD at 3.5% (95% CI 1.9%–5.9%) and Abbot at 3.0% (95% CI 1.4%–5.6%), compared with a positivity of 2.9% with the Euroimmun assay (Figure 1; Appendix Table 1). The number of samples tested using each assay varied considerably for this first timepoint. At week 18 the RBD test had highest positivity at 14.1% (95% 12.0%–16.5%) and Abbott the lowest at 12.3% (95% CI 10.3%–14.6%) (Figure 1; Appendix Table 1), although the differences in positivity estimated by the 3 assays were not significantly different at each of the 3 periods, producing overlapping CIs. We tested a smaller number of donor samples from week 13 using the Abbott assay. The geographic spread of these samples was a little more concentrated in inner London compared with the overall sample collection (Appendix Table 2) but reasonably representative in terms of age (Appendix Table 3).

After adjustment for sensitivity and specificity, Euroimmun had the highest adjusted prevalence in week 18 at 14.9%, compared with 13.3% for the Abbott assay and 13.4% for the RBD assay (Appendix Table 1). In weeks 15–16, adjusted prevalence was similar among the 3 assays: 10.9% for RBD, 11.0% for Euroimmun, and 11.3% for the Abbott assay. In week 13, adjusted prevalence was lowest for RBD at 1.5% and highest for the Abbott at 3.1%.

Venn diagrams show the results for samples tested by all assays for the 3 timepoints (Figure 2). Unadjusted prevalence based on a highly specific endpoint requiring all assays to be reactive was 1.0%, 8.5% and 11.6% at the 3 timepoints, whereas if based on a highly sensitive endpoint of any assay reactive prevalence was 6.5%, 13.6%, and 14.8%. The RBD assay gave the most reactive results, but this tendency can be explained by its lower specificity (Appendix, Appendix Table 5). If a criterion of reactive by Abbott or

Euroimmun were used (to maintain good specificity and increase sensitivity), then unadjusted prevalence would be 4.5%, 12.2%, and 13.6% for the 3 timepoints. These values compare with an unadjusted prevalence of 2.9%, 9.9%, and 13.0% for the Euroimmun assay alone. To adjust prevalence based on assay combinations, the sensitivity and specificity of these combinations is also required, but the validation data did not have all assays tested on the same negative samples to enable this calculation.

The analysis shows an important age effect, a decreasing prevalence with increasing age group at weeks 15–16 (Figure 3; Appendix Table 3), based on the Euroimmun assay. Comparisons by age were not interpretable for the earlier timepoint (week 13) because of the low number of donor samples from persons in older age groups. At week 18, the difference in prevalence by age group was less pronounced, showing little difference between age groups <50 years and an increased prevalence in older age groups. When comparing age effects by assay, this effect was most pronounced in the RBD assay results and least pronounced in the Abbott assay results (Appendix Table 3).

Although prevalence estimates from all 3 assays indicate a slightly higher prevalence among men than women in week 13 (Appendix Table 6), a more pronounced gender effect appears to have occurred by weeks 15–16, when prevalence was higher in younger women than in men and older women. This difference was no longer observed by week 18, when prevalence was similar.

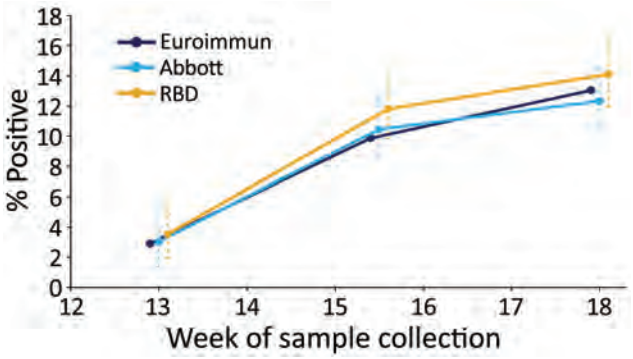

Figure 1. Percentage of reactive test results (unadjusted) for severe acute respiratory syndrome coronavirus 2 Ig in serum samples, by assay and epidemiologic week of sample collection (weeks 13, 15–16, and 18), London, UK, 2020. Error bars indicate 95% CIs. RBD, receptor-binding domain.

Discussion

We demonstrate the value of using 3 serologic assays targeting different proteins for evaluating seroprevalence of SARS-CoV-2 and for understanding the evolution of the epidemic in London and the effects of physical distancing measures. Our results show that overall trends in prevalence estimates are similar across all 3 assays; however, we observed some notable differences. The sensitivity analysis indicates that the assay targeting the nucleoprotein identifies early infections; the assays targeting the spike protein are more reliable in picking up late infections. These results are similar to observations made by other groups (*14*). Including samples that were positive on the nucleoprotein-based assay with those reactive on a spike-based assay increased unadjusted prevalence by 1.6%, 2.3%, and 0.6% for the 3 periods.

Understanding the changes in sensitivity of serologic assays over time is also critical in interpreting seroprevalence data, particularly taking into account recent data that have indicated differential waning patterns for antibodies that have different targets (*14*). These findings also demonstrate the value in combining data from different serologic assays with different target proteins for determining seroprevalence.

We show that, in London, ≈14% donors had evidence of infection by week 18, the highest for any

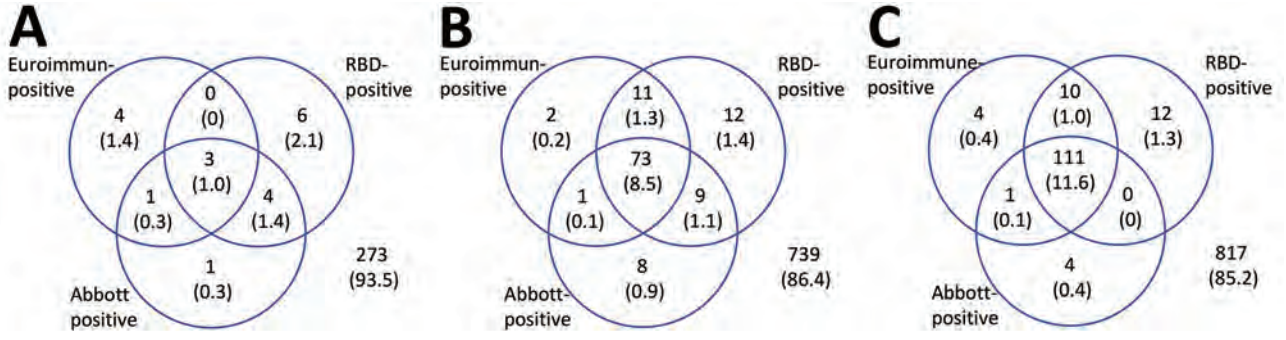

Figure 2. Results for serum samples tested for severe acute respiratory syndrome coronavirus 2 Ig with all 3 assays, by epidemiologic week of sample collection, London, UK, 2020. A) Week 13 (week beginning March 23); B) weeks 15–16; C) week 18. Values are no. (%) of reactive test results. RBD, receptor-binding domain.

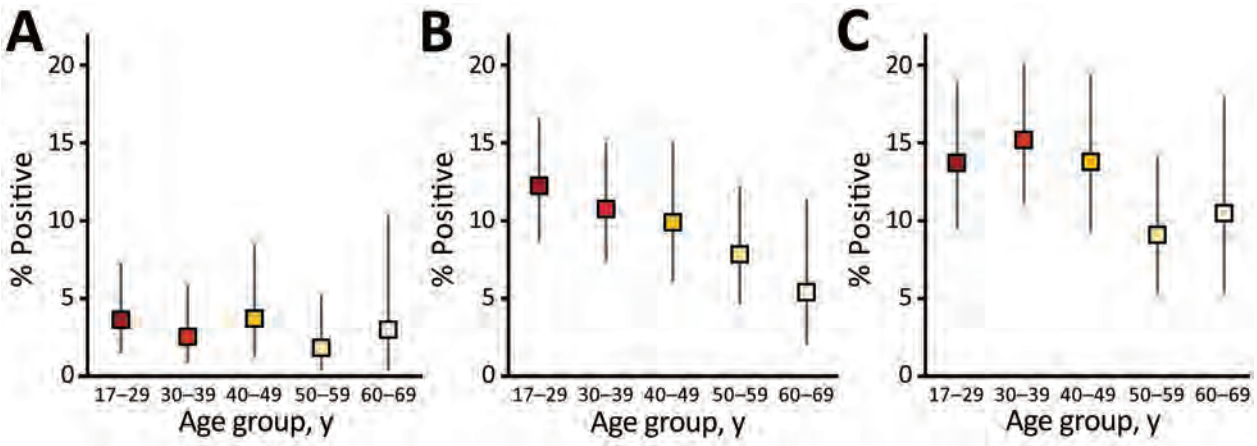

Figure 3. Percentage of reactive Euroimmun test results for severe acute respiratory syndrome coronavirus 2 Ig, by age group (unadjusted prevalence) and epidemiologic week of sample collection, London, United Kingdom, 2020. A) Week 13 (week beginning March 23); B) weeks 15–16; C) week 18.

region of England. This pattern is consistent with data from other surveillance systems, including numbers of cases, hospitalizations, and deaths (*15*). These results also confirm transmission slowed substantially after lockdown measures were put in place, plateauing from weeks 15–16 to 18. Given the time required to develop an antibody response and the fact that donors are excluded from donating for a minimum of 14 days after an acute illness, these prevalence estimates reflect the situation ≥2–4 weeks before the collection date. Therefore, increases observed from weeks 13 to 15–16 reflect the situation before the effects of lockdown measures fully taking effect, and results from early May reflect incidence from early to mid-April.

Our analysis shows a very pronounced age difference among adult age groups, particularly for samples taken in weeks 15–16, which probably reflect the epidemic dynamics under normal social-mixing patterns in a high-transmission situation (*16*), given the fact that these results were too early to have been affected by lockdown. Those findings suggest that young adults in London were infected earlier in the epidemic and older age groups affected later. The mixing patterns during lockdown have substantially changed, including less frequent contact with persons in the same age groups (i.e., less age-assortative mixing); fewer daily contacts overall; and more intergenerational mixing among persons >30 years of age, probably reflecting household compositions in these age groups (*17*). These patterns might explain, in part, some of the observed differences in trends by age group.

For prevalence by sex, data from London suggest that young adult women had a higher risk for infection than men of the same age, particularly before lockdown measures were implemented. However, after lockdown, those differences became less pronounced. This finding might support the hypothesis that women of childbearing age were acquiring infection before men of a similar age group. Evidence to support the idea that children are key drivers of transmission is limited (*17*), and further work is needed to address potential explanations for such a difference, including higher intensity of exposure to children, higher frequencies of occupational caring roles for women compared with men, or both.

The availability of large volumes of donor samples on a weekly basis provided an attractive and valuable source of samples for seroprevalence estimates. However, adult donors are not representative of the general population and are likely to be less ethnically diverse, of higher socioeconomic status, and healthier than the wider population (*18*,*19*), all of which might lead to an underestimate in population prevalence. Although donors ≥70 years of age were excluded from donation, increased pathogenicity of SARS-CoV-2 with age might have resulted in an increased proportion of infected older donors being hospitalized and thus not available for blood donation. This tendency could result in an underestimate of seroprevalence in the oldest age groups.

Changes in the precise locations of sampling within regions at different periods have been observed, and this lack of consistent sampling needs to be considered when interpreting any changes over time. For example, because of limited volumes, a smaller number of donor samples from week 13 were tested using the Abbott assay. We demonstrate similar results for using 3 different assays independently and adjusting for the estimated sensitivity

and specificity of the assays. We did not attempt to estimate adjusted prevalence on a combination of assays results or on the basis of changing assays cutoffs because more validation data on using multiple assays would be needed, and those data would probably indicate a pattern similar to that observed with the individual assays.

A range of interactions might have contributed to our results; further work is needed to understand the effect of age on antibody kinetics and the effect of age on different aspects of various assays, including sensitivity over time. These factors highlight the complexity inherent in interpreting seroprevalence surveys.

Despite those limitations, these results from testing blood donors have provided valuable intelligence regarding the progression of the epidemic among adults in London. Our results show that using multiple serologic assays targeting different proteins is probably informative as we try to determine the interplay between antibody kinetics and transmission dynamics in the population over time. Seroepidemiologic studies that rely on a single assay or have a single target risk incomplete ascertainment of the actual number of infections within the population.

Acknowledgments

We would like to acknowledge all the National Health Service Blood and Transplant staff and donors who contributed to the supply, processing, and donation of samples for this study, and in particular Su Brailsford, Ruth Allen, Sabine Taylor, Anthony Dhaliwal, and Belinda Singleton. We are also grateful to Charles Beck and Mona Dave from Public Health England (PHE) Field Services, who assisted with sourcing the convalescent samples for assay validation, and to Joshua Nagell-Smith and Richard Vipond, who developed the Material Transfer Agreements with National Health Service Blood and Transplant. Sample management was provided by Simon Tonge, Kevin Potts, Jamie Ellis, and Arif Nissar at the PHE Sero-Epidemiology Unit, Manchester. In the laboratories, we would like to acknowledge Stephen Taylor, Emma Hobbs, April Roberts, Sara Speight, Joanna Bacon, Steve Thomas, Chris Moon, Daniel Bailey, Silvia D'Arcangelo, Ashley Otter, Matthew Catton, Deborah Fox McKee, Prem Perumal, Abbie Bown, Cathy Rowe, and Richard Vipond for all their work in validating and running the Euroimmun assay service at the Rare and Imported Pathogens Laboratory, PHE, Porton Down; Shabnam Jamarani, Arham Khawar, and Vasiliki Zianta for work on the Abbott assay at the Clinical Service Unit, PHE, Colindale; Thivya Kankeyan for her technical work in the development of the receptor-binding domain assay at the Respiratory Virus Unit of PHE, Colindale, and we are especially grateful to Christine Carr, Sammy Ho, and Monali Patel for their contribution to validation as well as application of the receptor-binding domain assay in this study. We would also like to thank the staff in the Clinical Specimen Reception Unit at PHE, Colindale.

Funding was provided by PHE.

About the Author

Dr. Gayatri Amirthalingam is a consultant medical epidemiologist in the Immunisation and Countermeasures Division at Public Health England. Her primary research interests include maternal immunization, particularly maternal pertussis vaccination and evaluation of impact and effectiveness of vaccine programs.

References

1. Public Health England. Guidance on social distancing for everyone in the UK. 2020 [cited 2020 Sep 7] https:// www.gov.uk/government/publications/covid-19-guidance-on-social-distancing-and-for-vulnerable-people/guidance-on-social-distancing-for-everyone-in-the-uk-andprotecting-older-people-and-vulnerable-adults
2. Public Health England. National COVID-19 surveillance reports [cited 2020 Sep 7]. https://www.gov.uk/government/publications/national-covid-19-surveillance-reports 2020
3. To KK, Tsang OT, Leung WS, Tam AR, Wu TC, Lung DC, et al. Temporal profiles of viral load in posterior oropharyngeal saliva samples and serum antibody responses during infection by SARS-CoV-2: an observational cohort study. Lancet Infect Dis. 2020;20:565–74. https://doi.org/10.1016/S1473-3099(20)30196-1
4. Joint United Kingdom Blood Transfusion and Tissue Transplantation Services Professional Advisory Committee. Donor selection guidelines. 2020 [cited 2020 Sep 7]. https://www.transfusionguidelines.org/dsg/wb/latest-updates
5. Hardelid P, Andrews NJ, Hoschler K, Stanford E, Baguelin M, Waight PA, et al. Assessment of baseline age-specific antibody prevalence and incidence of infection to novel influenza A/H1N1 2009. Health Technol Assess. 2010;14:115–92. https://doi.org/10.3310/hta14550-03
6. de Lusignan S, Lopez Bernal J, Zambon M, Akinyemi O, Amirthalingam G, Andrews N, et al. Emergence of a Novel Coronavirus (COVID-19): Protocol for Extending Surveillance Used by the Royal College of General Practitioners Research and Surveillance Centre and Public Health England. JMIR Public Health Surveill. 2020;6:e18606. https://doi.org/10.2196/18606
7. Public Health England. COVID-19: laboratory evaluations of serological assays [cited 2020 Sep 7]. https://www.gov.uk/government/publications/covid-19-laboratory-evaluations-of-serological-assays
8. Jeffery-Smith A, Dun-Campbell K, Janarthanan R, Fok J, Crawley-Boevey E, Vusirikala A, et al. Infection and transmission of SARS-CoV-2 in London care homes reporting no cases or outbreaks of COVID-19: Prospective observational cohort study, England 2020. Lancet Reg Health Eur. 2021;3:100038; Epub ahead of print. https://doi.org/10.1016/j.lanepe.2021.100038

9. Office for National Statistics. Population estimates [cited 2020 Sep 7]. https://www.ons.gov.uk/peoplepopulation and community/populationandmigration/populationestimate
10. Diggle PJ. Estimating prevalence using an imperfect test. Epidemiol Res Int. 2011;2011:608719. https://doi.org/10.1155/2011/608719
11. Lewis FI, Torgerson PR. A tutorial in estimating the prevalence of disease in humans and animals in the absence of a gold standard diagnostic. Emerg Themes Epidemiol. 2012;9:9. https://doi.org/10.1186/1742-7622-9-9
12. de Valpine P, Turek D, Paciorek CJ, Anderson-Bergman C, Temple Land D, Bodik R. Programming with models: writing statistical algorithms for general model structures with NIMBLE. J Comput Graph Stat. 2017;26:403–17. https://doi.org/10.1080/10618600.2016.1172487
13. Team ND. Nimble: MCMC, particle filtering, and programmable hierarchical modeling [cited 2020 Sep 7]. https://cran.r-project.org/package=nimble
14. Chia WN, Tan CW, Foo R, Kang AEZ, Peng Y, Sivalingam V, et al. Serological differentiation between COVID-19 and SARS infections. Emerg Microbes Infect. 2020;9:1497–505. https://doi.org/10.1080/22221751.2020.1780951
15. Jarvis CI, Van Zandvoort K, Gimma A, Prem K, Klepac P,Rubin GJ, et al.; CMMID COVID-19 working group. Quantifying the impact of physical distance measures on the transmission of COVID-19 in the UK. BMC Med. 2020;18:124. https://doi.org/10.1186/s12916-020-01597-8
16. Mossong J, Hens N, Jit M, Beutels P, Auranen K, Mikolajczyk R, et al. Social contacts and mixing patterns relevant to the spread of infectious diseases. PLoS Med. 2008;5:e74. https://doi.org/10.1371/journal.pmed.0050074
17. Viner RM, Mytton OT, Bonell C, Melendez-Torres GJ, Ward J, Hudson L, et al. Susceptibility to SARS-CoV-2 infection among children and adolescents compared with adults: a systematic review and meta-analysis. JAMA Pediatr. 2021;175:143–56. https://doi.org/10.1001/jamapediatrics.2020.4573
18. Rosenberg ES, Tesoriero JM, Rosenthal EM, Chung R, Barranco MA, Styer LM, et al. Cumulative incidence and diagnosis of SARS-CoV-2 infection in New York. Ann Epidemiol. 2020;48:23–29.e4. https://doi.org/10.1016/j.annepidem.2020.06.004
19. Xu X, Sun J, Nie S, Li H, Kong Y, Liang M, et al. Seroprevalence of immunoglobulin M and G antibodies against SARS-CoV-2 in China. Nat Med. 2020;26:1193–5. https://doi.org/10.1038/s41591-020-0949-6

Address for correspondence: Gayatri Amirthalingam, Immunisation and Counter Measures Division, National Infection Service, Public Health England, 61 Colindale Ave, London NW9 5EQ, UK; email: gayatri.amirthalingam@phe.gov.uk

Psychobehavioral Responses and Likelihood of Receiving COVID-19 Vaccines during the Pandemic, Hong Kong

Kin On Kwok, Kin Kit Li, Arthur Tang, Margaret Ting Fong Tsoi, Emily Ying Yang Chan, Julian Wei Tze Tang, Angel Wong, Wan In Wei, Samuel Yeung Shan Wong

To access temporal changes in psychobehavioral responses to the coronavirus disease (COVID-19) pandemic, we conducted a 5-round (R1–R5) longitudinal population-based online survey in Hong Kong during January–September 2020. Most respondents reported wearing masks (R1 99.0% to R5 99.8%) and performing hand hygiene (R1 95.8% to R5 97.7%). Perceived COVID-19 severity decreased significantly, from 97.4% (R1) to 77.2% (R5), but perceived self-susceptibility remained high (87.2%–92.8%). Female sex and anxiety were associated with greater adoption of social distancing. Intention to receive COVID-19 vaccines decreased significantly (R4 48.7% to R5 37.6%). Greater anxiety, confidence in vaccine, and collective responsibility and weaker complacency were associated with higher tendency to receive COVID-19 vaccines. Although its generalizability should be assumed with caution, this study helps to formulate health communication strategies and foretells the initial low uptake rate of COVID-19 vaccines, suggesting that social distancing should be maintained in the medium term.

Since the World Health Organization declared coronavirus disease (COVID-19) a pandemic on March 11, 2020 (*1*), COVID-19 has infiltrated every continent in the world (*2*). Hong Kong, a densely populated city located on the southern coast of China with ≈7.5 million citizens and a mean daily number of 12.5 social encounters per individual (*3*), recorded its first laboratory-confirmed COVID-19 case in late January 2020 (*4*). Since then, Hong Kong has been adopting a suppress-and-lift strategy, under which lifting and reimposing of restrictions occured based on epidemiologic thresholds (*5*). As of April 9, 2021, Hong Kong had recorded 11,550 confirmed cases and 205 deaths (crude case-fatality rate 1.8%) (*6*), and the fourth wave of COVID-19 epidemic had just ended. After more available data on phase 3 clinical trials of candidate vaccines (*7*) became available and the vaccine was authorized for emergency use, the COVID-19 vaccination program in Hong Kong began in late February 2021.

Surveillance of psychobehavioral responses during the epidemic plays an essential role to convey risk communication messages to the public. Previously, we reported that the general population in Hong Kong had high levels of perceived risk and mild anxiety during the early phase of the COVID-19 epidemic; the prompt government interventions with widely adopted individual precautionary measures might be the determinants to slow down the transmission early in the outbreak (*8*). After that initial analysis, which was based on cross-sectional data (*8*), global researchers have applied similar protocols for the general public in Japan (*9*), Saudi Arabia (*10*), Italy (*11*) and the United Kingdom (*12*). However, the temporal variations of psychobehavioral responses have not been examined.

In addition to psychobehavioral responses, unique to COVID-19 is its unprecedented massive epidemic size compared with other recent outbreaks, such that vaccination becomes the exit strategy. However, despite vaccine availability, vaccine doubters may hamper the global effort against COVID-19 (*13*). Unraveling the reasons behind vaccine hesitancy and monitoring its trends over time will support the design of interventions to boost COVID-19 vaccine uptake.

We report a longitudinal analysis of 5 representative population-based surveys of adults in Hong Kong

Author affiliations: The Chinese University of Hong Kong, Hong Kong (K.O. Kwok, M.T.F. Tsoi, E.Y.Y. Chan, A. Wong, W.I. Wei, S.Y.S. Wong); City University of Hong Kong, Hong Kong (K.K. Li); Sungkyunkwan University, Seoul, South Korea (A. Tang); University of Leicester, Leicester, UK (J.W.T. Tang)

DOI: https://doi.org/10.3201/eid2707.210054

on their psychological, behavioral, and vaccine-related responses, conducted during the first 2 waves of the COVID-19 epidemic. Our main objectives were tracking major psychobehavioral responses (including risk perception, psychological distress, and adoption of precautionary measures) over time and examining the determinants of the intention to receive the COVID-19 vaccine. As a complement, other psychobehavioral responses (such as knowledge about COVID-19) were also reported. These findings should have major implications for infection control policies and targeted mental health recommendations. Hong Kong has a high-income economy but had major social unrest in the prepandemic period in the population (*14*); thus, the experience in Hong Kong may act as a reference for other similar populations to prepare for future epidemics.

Methods

Respondent Recruitment

We established a community cohort within 36 hours after the first COVID-19 confirmed case was identified in Hong Kong. District councilors shared an online survey link through channels in which they convey information to their targeted residents (*8*). We arranged 5 follow-up rounds (denoted as R1–R5) of online surveys of the community cohort during January–September 2020, each lasting for 3–6 weeks: R1, January 23–February 13; R2, March 6–April 14; R3, May 8–June 14; R4, July 15–August 7; and R5, August 8–September 15. Respondents were compensated with cash vouchers in Hong Kong dollars (HKD): HKD 10 for R1, HKD 20 for R2, and HKD 30 for R3–R5.

Study Instrument

The study instrument was based on a questionnaire used during the initial phase of the COVID-19 epidemic in Hong Kong (*8*). In each round, we administered questions soliciting key information on demographics, health conditions, travel history, risk perceptions toward COVID-19, anxiety and burnout, confidence in the local government and doctors, knowledge about COVID-19 transmission, and adoption and perceived effectiveness of preventive measures. In response to the funding commitments for COVID-19 vaccine development (*15*), starting with R4, we embedded vaccine-related questions along 2 dimensions: intention to receive COVID-19 vaccines when available and vaccine hesitancy.

Psychological Responses

Risk perceptions toward COVID-19 included perceived susceptibility (of oneself and one's family members), assuming no precautionary measure, and perceived severity. Starting with R3, we asked respondents to report their perceived susceptibility based on the situation during which they completed the survey (1, very likely; 5, very unlikely). In addition, respondents rated the level of disease severity of COVID-19 and other noncommunicable diseases and infectious diseases (1, very bad; 5, not bad at all).

We measured anxiety with the Chinese–Cantonese version of the Hospital, Anxiety and Depression Scale—Anxiety (*16*). Respondents rated 7 statements on the basis of their feelings in the preceding 7 days on a 4-point scale; a higher score indicated stronger anxiety (summative score: 0–7, normal; 8–10, borderline abnormal; 11–21, abnormal).

We measured burnout with a single-item measure: "Overall, based on your definition of burnout, how would you rate your level of burnout when facing COVID-19?" (1, "I have no symptoms of burnout"; 5, "I feel completely burned out and often wonder if I can go on facing COVID-19; I am at the point where I may need some changes or may need to seek some sort of help"). This single-item measure was refined from a nonproprietary validated burnout measure (*17*) to fit the current context and was asked starting with R3.

Behavioral Responses

Respondents rated the adoption (yes/no) (Appendix Table 1, https://wwwnc.cdc.gov/EID/article/27/7/21-0054-App1.pdf) and perceived effectiveness (1, very effective; 5, not very effective) (Appendix Table 2) of 17 precautionary measures against COVID-19. For the likelihood of COVID-19 vaccine uptake, respondents answered this question "If COVID-19 vaccines are available, how likely will you receive them?" (0, definitely not; 10, definitely). We measured vaccine hesitancy with a validated 15-item tool (*18*) with 3 items on each of 5 psychological antecedents (the 5Cs): confidence, defined as trust in the safety and effectiveness of the vaccine, the system that delivers the vaccine, and the motivations of policymakers who decide on the need of the vaccine; complacency, defined as not perceiving the disease as high risk and vaccination as necessary; constraints, defined as barriers to vaccination; calculation, defined as persons' engagement in extensive information searching; and collective responsibility, defined as willingness to protect others through herd immunity. We used an average score for each antecedent. For collective responsibility, one reverse item, "When everyone is vaccinated, I don't have to get vaccinated, too," was excluded from the calculation.

The vaccine-related items did not include any specific information about pharmaceutical companies or manufacturing countries.

Statistical Analysis

We summarized responses using descriptive statistics. To examine the overall linear trends in the responses and to account for the correlation diminishment resulting from responses from the same respondents across time, we adopted the generalized estimation equation framework featuring an autoregressive structure for within-subject correlations. To compare the proportion of responses in 2 time points, we used a partially overlapping samples *z*-test (*19*).

We adopted a multivariate regression model under the generalized estimation equation framework to identify the associated factors for higher tendency for social distancing (i.e., ≥5 social distancing measures) and higher uptake tendency for COVID-19 vaccines (i.e., ≥7 of 10 for the "likelihood of receiving COVID-19 vaccines" question). We reported adjusted odds ratios (aORs) and 95% CIs and specified a statistical significance of $p \leq 0.05$. We conducted the analysis in R software version 4.0.3 (https://www.r-project.org). This study was approved by the Survey Behavioral Research Ethics Committee of The Chinese University of Hong Kong (reference no. SBRE-20-037).

Results

Study Timeline

The 5 study rounds intertwined epidemic waves 1 and 2 in Hong Kong (*20*) at different disease stages (Figure 1): the initial phase (R1), amid epidemic waves (R2 and R4), during the relative quiescence between 2 waves (R3), and the decaying phase of wave 2 (R5). The government-initiated interventions (such as school closure and compulsory mask-wearing) and the call for COVID-19 vaccine were also presented (Figure 1). The data collection was completed before any announcement of the safety and efficacy trials of the candidate vaccines. We received 2,478 attempts to complete the survey in R1, of which 1,715 provided complete responses (*8*) and 1,054 indicated willingness to participate in future studies. The sample sizes for R2–R5 ranged from 441 to 644 (Figure 2).

Respondent Characteristics

The cohort consisted of more female persons (68.5%–69.8%) and young adults (18–44 years of age) (78.6%–81.0%) than other categories. Most were well educated: 78.9%–82.5% had at least postsecondary level education (Appendix Table 3). Most respondents were free from chronic diseases (87.1%–88.8%) and perceived themselves to be in good health (73.1%–78.1%) (Appendix Table 4).

Risk Perception over Time

We identified significant temporal variation of risk perception toward COVID-19 (Appendix Table 5). Assuming no precaution measures, respondents perceived themselves likely to be infected with COVID-19 (87.2%–92.8%). This proportion dropped to 19.3%–42.0% when the current situations were considered, when institutionalized interventions were in place and personal protective measures were conducted en masse (Appendix Table 1).

Perceived severity decreased significantly ($p<0.001$) over the study period, from 97.4% (R1) of respondents considering COVID-19 to be serious to 77.2% (R5). The perceived chance of having COVID-19 cured increased significantly ($p<0.001$) by more than 3-fold, from 16.6% (R1) to 57.2% (R5). An increasing time trend ($p<0.001$) was also observed for perceived survival chance if infected, from 18.6% (R1) to 67.2% (R5).

Psychological Distress

The mean Hospital, Anxiety and Depression Scale—Anxiety score remained borderline abnormal throughout the study, ranging from 8.99 (R1) to 7.61 (R5). There was a substantial increase in the proportion of normal respondents in terms of anxiety ($p<0.001$), from 35.6% (R1) to 51.7% (R5) (Appendix Table 6). This anxiety metric echoed the significant drop in the frequency of thinking about COVID-19 ($p<0.001$), from 76.2% (R1) to 48.6% (R5). Despite this ease in anxiety level, the proportion of respondents worrying specifically about COVID-19 (85.7%–96.8%) and having their daily lives affected a lot by COVID-19 (45.7%–61.8%) remained high throughout the study (Appendix Table 6). Meanwhile, ≈40% of the respondents have shown symptoms of burnout toward COVID-19 since R3.

Adoption of Precautionary Measures

The adoption of individual precautionary measures remained high throughout the study (Appendix Table 1). Most respondents reported they wore masks (R1, 99.0%; R5, 99.8%), covered mouth and nose when coughing or sneezing (R1, 96.9%; R5, 98.4%), performed hand hygiene using hand sanitizer or alcohol gel (R1, 95.8%; R5, 97.7%), and disinfected their homes (R1, 78.6%; R5, 88.5%). Hand hygiene and

home disinfection measures showed a significant increasing trend across time.

The adoptions of social distancing across rounds were consistently from moderate to high (Appendix Table 1). About one third of respondents avoided public transportation (R1, 38.0% to R5, 35.6%; p = 0.11) and work (R1, 24.6% to R5, 35.4%; p<0.001) across waves. Upward significant trends were observed among respondents in avoiding social activities (R1, 63.8% to R5, 85.7%; p<0.001) and contacting with persons with fever or symptoms of respiratory diseases (R1, 92.9% to R5, 95.1%; p<0.05).

Factors associated with greater adoption of social-distancing were being female (aOR 1.30, 95% CI 1.09–1.56); living in the New Territories, a suburb of Hong Kong (aOR for the 2 territories 1.40–1.42); and

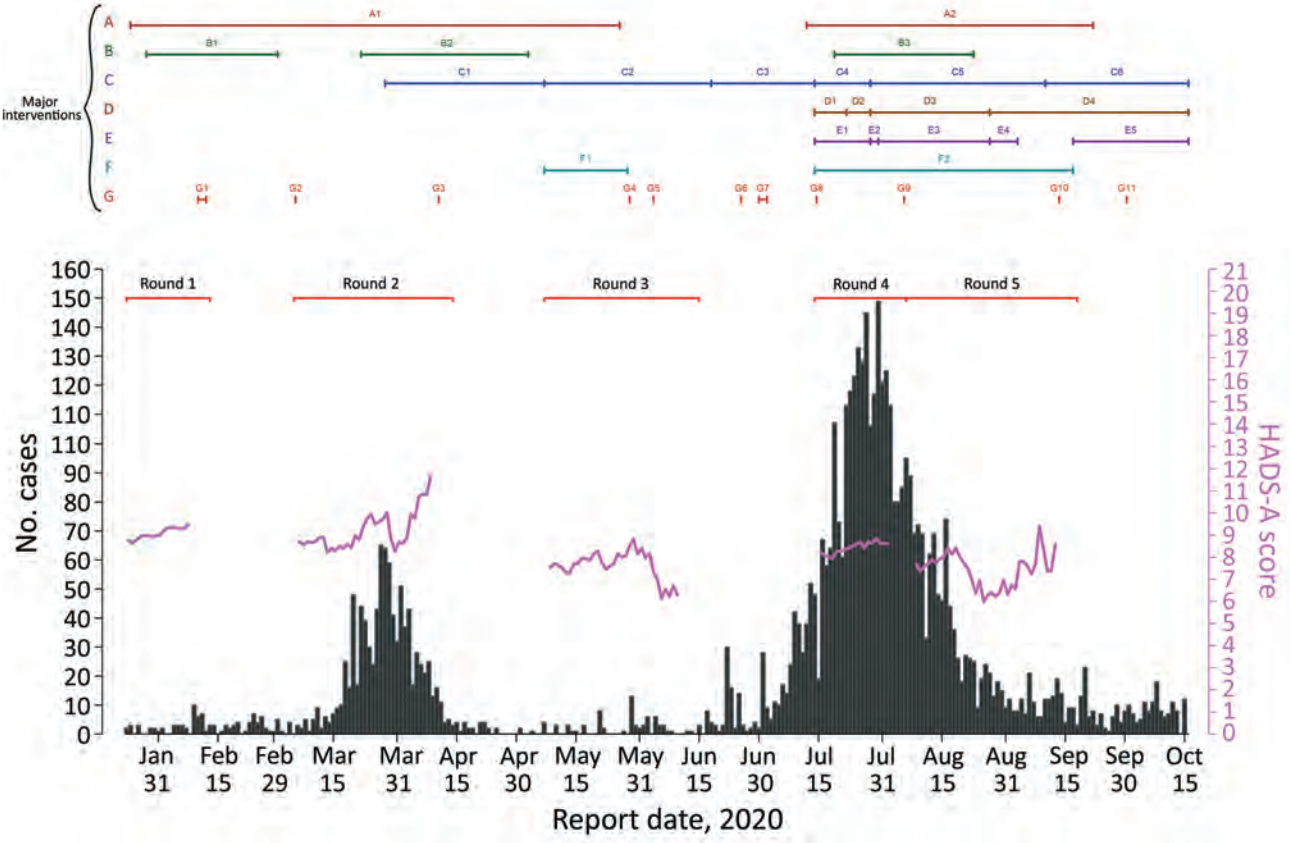

Figure 1. Coronavirus disease (COVID-19) incidence and anxiety level by report date from survey of psychobehavioral responses to the COVID-19 pandemic, showing timeline of major interventions, Hong Kong, 2020. A, school closures: A1, closure, Jan 25–May 26; A2, early start of summer holiday, Jul 13–Sep 22. B, government work-from-home arrangement: B1, Jan 29–Mar 1; B2, Mar 23–May 3; B3, Jul 20–Aug 23. C, group size limits on gatherings in public places: C1, limit 4, Mar 29–May 7; C2, limit 8s, May 8–Jun 18; C3, limit 50, Jun 19–Jul 14; C4, limit 4, Jul 15–Jul 28; C5, limit 2, Jul 29–Sep 10; C6, limit 4 persons, Sep 11–present (as of 2020 October 5). D, compulsory mask wearing: D1, on public transportation, Jul 15–present; D2, also in public indoor areas, Jul 23–present; D3, also in public outdoor areas, Jul 29–present (exemption for country parks or when engaging in strenuous physical activities in public outdoor spaces, Aug 28–present). E, regulations applied to restaurants, Mar 28–present: ≤50% of premises capacity; tables ≥1.5 m apart; no more than 2, 4, or 8 persons per table; compulsory mask wearing except when consuming food or drink; compulsory body temperature screening before entry; hand sanitizer on premises; suspension of dine-in service for the following periods: E1, 6 pm–4:59 am, Jul 15–Jul 28; E2, at all times, Jul 29–30; E3, 6 pm–4:59 am, Jul 31–Aug 27; E4, 9 pm–4:59 am, Aug 28–Sep 3; E5, 12 am–4:59 am, Sep 18–present. F, business closures: F1, bathhouses, party rooms, clubs, karaoke clubs, May 8–May 28; F2, bathhouses, party rooms, clubs, karaoke clubs (all reopened Sep 17), swimming pools (beginning Jul 29), sports premises (Jul 29–Aug 28), clubhouses (reopened Aug 28), beauty parlors (reopened Aug 28), massage establishments (reopened Sep 4), places of public entertainment (reopened Aug 28), places for amusement (reopened Sep 4), fitness centers (reopened Sep 4), and amusement game and mahjong-tin kau establishments (reopened Sep 11). G, vaccine development timeline: G1, World Health Organization (WHO) Convention of Global Research and Innovation, Feb 11–12; G2, WHO Global Research Roadmap prioritizing vaccine development, Jun 3; G3, draft landscape of candidate vaccines, Apr 11; G4, launch of COVID-19 Access Pool for sharing data for vaccine development, May 29; G5, funding commitment at Global Vaccine Summit for immunization in low-income countries, Jun 4; G6, call for USD 31.3 billion for therapeutics and vaccine development, Jun 26; G7, second summit on COVID-19 research and innovation, Jul 1–2; G8, engaging >150 countries in financing vaccines, Jul 15; G9, outline of global vaccine procurement, Aug 6; G10, WHO guidance on vaccine allocation between and within countries, Sep 14; G11, WHO calls for vaccine manufacturers to apply for prequalification, Oct 1. HADS-A, Hospital, Anxiety and Depression Scale—Anxiety.

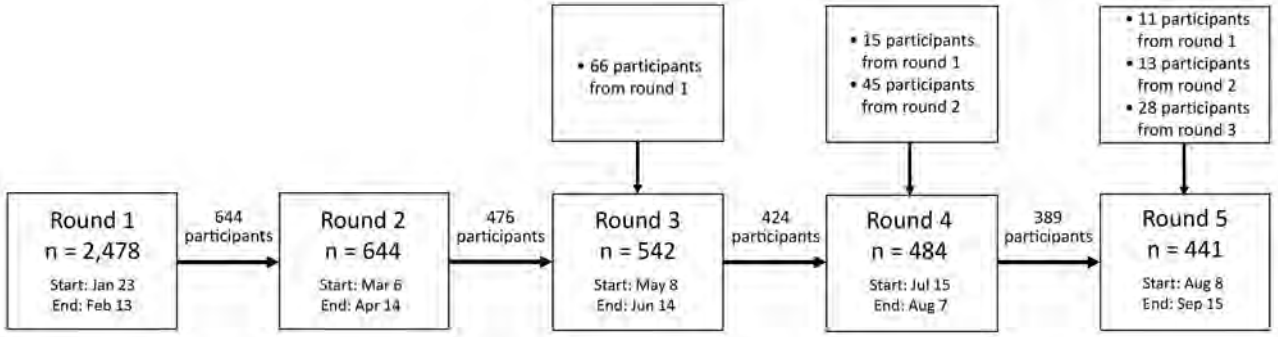

Figure 2. Timeline and participant recruitment for survey of psychobehavioral responses to the coronavirus disease pandemic, Hong Kong, 2020. To qualify for the survey, participants had to be ≥18 years of age and reside in Hong Kong for ≥5 days/week in the preceding month. The numbers in the box for each round refer to the number of respondents who indicated willingness to participate in the respective survey round; they may or may not have completed the questionnaire.

being anxious (aOR 1.47, 95% CI 1.23–1.76) (Appendix Table 7). Respondents with chronic conditions (aOR 0.72, 95% CI 0.54–0.95) and those reporting having neutral understanding of COVID-19, compared with those who said they understood COVID-19 not well/not well at all (aOR 0.73, 95% CI 0.62–0.85), were less likely to practice social distancing (Appendix Table 7).

Likelihood of COVID-19 Vaccine Uptake

Respondents' intention to receive COVID-19 vaccine decreased significantly from R4 (48.7%, 95% CI 44.0–53.4) to R5 (37.6%, 95% CI 32.9–42.4), with particularly low rates among persons ≥55 years of age (Appendix Table 8). Factors associated with higher tendency for receiving COVID-19 vaccines were anxiety (borderline abnormal: aOR 1.53, 95% CI 1.04–2.23; abnormal: aOR 1.87, 95% CI 1.19–2.93), complacency (aOR 0.72, 95% CI 0.62–0.85), confidence (aOR 1.71, 95% CI 1.48–1.99), and collective responsibility (aOR 1.31, 95% CI 1.10–1.55). Compared with persons 18–24 years of age, persons ≥55 years of age were less likely to receive COVID-19 vaccine (aOR 0.47, 95% CI 0.23–0.98) (Appendix Table 8).

We also researched the trends of other psychobehavioral responses. We compiled responses for comparing perceived severity across diseases (Appendix, Appendix Table 9), confidence in government and doctors (Appendix, Appendix Table 10), knowledge of COVID-19 (Appendix, Appendix Table 11), and perceived effectiveness of precautionary measures (Appendix, Appendix Table 2).

Discussion

Our 5-round longitudinal online survey analyzed the temporal changes in community responses throughout the first 2 COVID-19 epidemics in Hong Kong. Overall, perceived susceptibility (assuming no precautionary measure taken) remained high: self-susceptibility (87.2%–92.8%) was substantially higher than that observed for the 2003 SARS epidemic (23.0%) (*21*) and the 2009 influenza pandemic (58.1%) (*22*) in the same population. However, in terms of perceived severity, the proportions dropped dramatically across time but were still higher than those observed in other highly affected locations (United Kingdom, 20.7% [*12*]; Kerala state, India, 55.7% [*23*]). The proportions of persons with an abnormal level of anxiety also dropped over the study period, from 34.3% to 22.0%. We observed consistently high levels of precautionary measures, such as mask wearing, hand hygiene, and home disinfection throughout the study period. Greater anxiety was associated with higher tendency of social distancing. The projected COVID-19 vaccine uptake rate dropped from 48.7% (R4) to 37.6% (R5). Greater anxiety, confidence in the vaccine, and collective responsibility and lower complacency contributed to a greater likelihood of intended vaccination.

Implications of Results

Our results have 5 immediate public health implications. First, with the uncertain disease progression (e.g., emergence of new variants of coronavirus) and the changing institutionalized interventions, there should be continual monitoring of risk perception toward COVID-19 in the community. Risk perception is an indispensable determinant of behavioral change (*24*) and depends on the prevalence of the health risk concerned (*25*). Our findings show varying risk perception over time during the pandemic, illustrating a perceived severity of COVID-19 that significantly decreased over time. Inferring from the large difference between naive (assuming no precautionary measures) and current (based on the current situation) scenarios, perceived susceptibility is sensitive to the disease progression and interventions in place.

Although such temporal trend of risk perception was also observed in past pandemics (*26*), the absolute level of risk perception was not.

Second, surveillance and encouragement of social distancing should be maintained in the medium to long term, given the low projected uptake rate of COVID-19 vaccine. In Hong Kong, the reproductive number peaked at 2.39 in wave 1 and 3.04 in wave 2 (*20*), which (based on early data) corresponded approximately to requiring 56.1%–66.9% of the population to be immune to confer herd immunity (*27*). Because the projected vaccine uptake rates (R4, 48.7%; R5, 37.6%) fell short of the required level, relatively small-scale upcoming epidemics compared with the previous waves are expected. With more persons being vaccinated, there might be more social interactions, so persons should be encouraged to maintain social distancing (such as avoiding unnecessary gatherings). Meanwhile, further research should focus on disease transmission during a mix of social distancing in place and vaccine hesitancy in the population.

Third, risk communications in Hong Kong should target complacency, vaccine confidence, and collective responsibility to boost the COVID-19 vaccine uptake. We reported a low intention for uptake of the would-be vaccines, which declined over time in Hong Kong. A similar situation was observed in the United States, where the projected vaccine uptake rate dropped from 74.1% in April 2020 to 56.2% in December 2020 (*28*). Such low uptake intention among older persons in our study (R4, 29.4%; R5, 31.4%) is particularly worrisome because older age is a risk factor for death from COVID-19 (*29*).

The extent to which our findings on the predictors of uptake intention can be generalized to other countries or regions requires further investigation. Unique to Hong Kong were the low COVID-19 infection rate and low level of confidence in government measures. The weak uptake intention reported in this study was uncommon compared with other countries (71.5% overall for 19 countries) (*30*). The low infection rate, along with the decreasing perceived severity toward COVID-19, might weaken the urgency for vaccination, which may also apply to places such as Taiwan, Japan, and Australia. However, the social unrest in Hong Kong in late 2019 might have led to distrust in the government (*31*), which could subsequently lower vaccination intention (*32*) and trigger maintenance of personal precautionary measures. One possible explanation is that, when moderated by distrust in government, persons tend to rely on personal protective measures (such as wearing facemasks and maintaining social distancing) but become skeptical to institutional protective measures (such as vaccines). Distrust in governments during the pandemic may also influence vaccine hesitancy in other regions, such as Brazil and Poland (*33*). Nevertheless, given the projected low vaccine uptake rate in this study, it may be insufficient to reach herd immunity in the near future, if ever, in Hong Kong. Therefore, taking the vaccine or not may have little bearing on relaxing government interventions in the medium term. In addition, from findings in other regions, trust in the government itself (*34*) and the information provided by the government (*30*) increased preventive practices, specifically accepting vaccines, during pandemics (*30*). Therefore, effective health communication is particularly crucial for the Hong Kong government. To rebuild trust, public health authorities need to possess competence, objectivity, fairness, consistency, transparency, sincerity, and faith (*35*). In addition, organizations aside from government and healthcare providers, such as professional bodies and religious groups, may help deliver pro-vaccine messages (*36*).

Fourth, our results help to prioritize the content in promotional messaging. It is worth investing resources on promotional messaging, particularly when few respondents in R4 (overall, 16.7%; 18–24 y, 24.7%; 25–34 y, 14.5%; 35–44 y, 15.5%; 45–54 y, 11.5%; ≥55 y, 17.6%) and R5 (overall, 10.5%; 18–24 y, 12.8%; 25–34 y, 7.4%; 35–44 y, 12.1%; 45–54 y, 6.1%; ≥55 y, 20.0%) indicated an absolute "yes" for receiving COVID-19 vaccines (measured on a 11-point Likert scale) and when there was antibody waning after receiving the vaccine. The decreasing confidence metric from R4 to R5 highlighted the need to build trust among the public toward the logistics of vaccine development, licensing, generating recommendations, and distribution (*37*). Before the government authorizes the use of a COVID-19 vaccine, establishment of an advisory panel will help determine factors that the government should consider, such as performance (safety, efficacy, and effectiveness) and characteristics (number of doses, formulation, and presentation and packaging) of the available vaccine (*38*). Moreover, to increase the collective responsibility and perceived vaccine necessity, the government should foster understanding of the vaccine among the public with transparent communication, including more engagement with different stakeholders in the community and populations who are disproportionately affected by the pandemic to listen to their concerns. Leveraging knowledge, skills, and expertise from these communications will provide a robust assessment to underpin the vaccination campaign. Although calculations and constraints

in the 5Cs model were not associated with the vaccine uptake likelihood at this stage, continuous examination in these 2 constructs will help refine future vaccination campaigns to engage citizens in cost–benefit calculations and increase their vaccine availability, affordability and accessibility.

Fifth, the psychological distress arising from burnout should be weighed together with the well-established anxiety. This pandemic is ongoing and has lasted much longer than the SARS epidemic, so more persons are developing syndromes of emotional exhaustion. The interplay between 2 psychological distresses, burnout and anxiety, is worth investigating during the ongoing pandemic. Our study showed that almost half of respondents had burnout symptoms in a short 4-month window from June through September 2020. This symptom did not contribute to the likelihood of COVID-19 vaccination in the last 2-point survey. However, the current general measure of burnout was not able to pinpoint the sources of burnout, such as financial stress, social isolation, the disease itself, or their combinations, for a detailed analysis. Nevertheless, the burnout phenomenon among persons coping with a long-term pandemic (*39*) suggests the need to reexamine the temporal association among social-distancing adoption, vaccination, and burnout.

Our study's first limitation is that the survey may have been subject to recall and social conformity biases, but its longitudinal design enabled us to track the same respondents over time, reducing self-control bias. Second, caution should be exercised when generalizing our findings to other regions because Hong Kong was exposed to other disease outbreaks recently, such as 1997 avian influenza (*40*), 2003 SARS (*41*), and 2009 pandemic influenza (*42*). Nevertheless, our COVID-19 experience after those past outbreaks may be precedent to other countries, after the current COVID-19 pandemic. Third, our survey was conducted before the safety and efficacy data of the COVID-19 vaccines were released. The actual uptake rates might be affected by possible vaccination side effects events, such as the recent reported deaths after taking the vaccines in Hong Kong (*43*–*45*).

In conclusion, our findings highlight the importance of continuous longitudinal assessment of community psychobehavioral responses during the COVID-19 pandemic. Monitoring those responses can help public health authorities tailor health communication strategies to achieve the desired behavioral outcomes (vaccination and adoption of precautionary measures) to control future epidemic waves.

Acknowledgments

We thank Henry Chan and Sui Ting Fong for technical support.

K.O. Kwok acknowledges support from Health and Medical Research Fund (reference nos. INF-CUHK-1, 17160302, 18170312), General Research Fund (reference nos. 14112818, 24104920), Wellcome Trust Fund (United Kingdom, 200861/Z/16/Z), and Group Research Scheme of The Chinese University of Hong Kong.

About the Author

Dr. Kwok is an assistant professor affiliated with the JC School of Public Health and Primary Care at The Chinese University of Hong Kong, Hong Kong, China. His primary research interests include infectious disease epidemiology and infection control, with a current focus on mitigating emerging infectious disease outbreaks from the mathematic, epidemiologic, and behavioral perspectives.

References

1. World Health Organization. Archived: WHO timeline—COVID-19 [cited 2020 Dec 24]. https://www.who.int/news/item/27-04-2020-who-timeline---covid-19
2. World Health Organization. WHO coronavirus disease (COVID-19) dashboard [cited 2020 Dec 24]. https://covid19.who.int
3. Kwok KO, Cowling B, Wei V, Riley S, Read JM. Temporal variation of human encounters and the number of locations in which they occur: a longitudinal study of Hong Kong residents. J R Soc Interface. 2018;15:20170838. https://doi.org/10.1098/rsif.2017.0838
4. Kwok KO, Wong V, Wei VWI, Wong SYS, Tang JW-T. Novel coronavirus (2019-nCoV) cases in Hong Kong and implications for further spread. J Infect. 2020;80:671–93. https://doi.org/10.1016/j.jinf.2020.02.002
5. Kwok KO, Huang Y, Tsoi MTF, Tang A, Wong SYS, Wei WI, et al. Epidemiology, clinical spectrum, viral kinetics and impact of COVID-19 in the Asia-Pacific region. Respirology. 2021;26:322–33. https://doi.org/10.1111/resp.14026
6. Centre for Health Protection. Countries/areas with reported cases of coronavirus disease-2019 (COVID-19). 2021 [cited 2021 Apr 9]. https://www.chp.gov.hk/files/pdf/statistics_of_the_cases_novel_coronavirus_infection_en.pdf
7. World Health Organization. Draft landscape and tracker of COVID-19 candidate vaccines [cited 2020 Dec 24]. https://www.who.int/publications/m/item/draft-landscape-of-covid-19-candidate-vaccines
8. Kwok KO, Li KK, Chan HHH, Yi YY, Tang A, Wei WI, et al. Community responses during early phase of COVID-19 epidemic, Hong Kong. Emerg Infect Dis. 2020;26:1575–9. https://doi.org/10.3201/eid2607.200500
9. Stickley A, Matsubayashi T, Sueki H, Ueda M. COVID-19 preventive behaviours among people with anxiety and depressive symptoms: findings from Japan. Public Health. 2020;189:91–3. https://doi.org/10.1016/j.puhe.2020.09.017
10. Alanezi F, Aljahdali A, Alyousef S, Alrashed H, Alshaikh W, Mushcab H, et al. Implications of public understanding of COVID-19 in Saudi Arabia for fostering effective communication through awareness framework. Front

Public Health. 2020;8:494. https://doi.org/10.3389/fpubh.2020.00494
11. Vai B, Cazzetta S, Ghiglino D, Parenti L, Saibene G, Toti M, et al. risk perception and media in shaping protective behaviors: insights from the early phase of COVID-19 Italian outbreak. Front Psychol. 2020;11:563426. https://doi.org/10.3389/fpsyg.2020.563426
12. Bowman L, Kwok KO, Redd R, Yi Y, Ward H, Wei WI, et al. Comparing public perceptions and preventive behaviors during the early phase of the COVID-19 pandemic in Hong Kong and the United Kingdom: cross-sectional survey study. J Med Internet Res. 2021;23:e23231. https://doi.org/10.2196/23231
13. Coustasse A, Kimble C, Maxik K. COVID-19 and vaccine hesitancy: a challenge the United States must overcome. J Ambul Care Manage. 2021;44:71–5. https://doi.org/10.1097/JAC.0000000000000360
14. Ni MY, Yao XI, Leung KSM, Yau C, Leung CMC, Lun P, et al. Depression and post-traumatic stress during major social unrest in Hong Kong: a 10-year prospective cohort study. Lancet. 2020;395:273–84. https://doi.org/10.1016/S0140-6736(19)33160-5
15. Coalition for Epidemic Preparedness Innovations. $2 billion required to develop a vaccine against the COVID-19 virus. 2020 [cited 2021 Jan 4]. https://cepi.net/news_cepi/2-billion-required-to-develop-a-vaccine-against-the-covid-19-virus-2/
16. Leung CM, Wing YK, Kwong PK, Lo A, Shum K. Validation of the Chinese-Cantonese version of the hospital anxiety and depression scale and comparison with the Hamilton Rating Scale of Depression. Acta Psychiatr Scand. 1999;100:456–61. https://doi.org/10.1111/j.1600-0447.1999.tb10897.x
17. Dolan ED, Mohr D, Lempa M, Joos S, Fihn SD, Nelson KM, et al. Using a single item to measure burnout in primary care staff: a psychometric evaluation. J Gen Intern Med. 2015;30:582–7. https://doi.org/10.1007/s11606-014-3112-6
18. Betsch C, Schmid P, Heinemeier D, Korn L, Holtmann C, Böhm R. Beyond confidence: development of a measure assessing the 5C psychological antecedents of vaccination. PLoS One. 2018;13:e0208601. https://doi.org/10.1371/journal.pone.0208601
19. Derrick B, Dobson-Mckittrick A, Toher D, White P. Test statistics for comparing two proportions with partially overlapping samples; 2015 [cited 2021 Jan 4]. https://uwe-repository.worktribe.com/output/805270
20. Kwok KO, Wei WI, Huang Y, Kam KM, Chan YYE, Riley S, et al. Evolving epidemiological characteristics of COVID-19 in Hong Kong from January to August 2020: retrospective study. J Med Internet Res. 2021;23:326645. https://doi.org/10.2196/26645
21. Leung GM, Quah S, Ho L-M, Ho S-Y, Hedley AJ, Lee H-P, et al. A tale of two cities: community psychobehavioral surveillance and related impact on outbreak control in Hong Kong and Singapore during the severe acute respiratory syndrome epidemic. Infect Control Hosp Epidemiol. 2004;25:1033–41. https://doi.org/10.1086/502340
22. Mak K-K, Lai C-M. Knowledge, risk perceptions, and preventive precautions among Hong Kong students during the 2009 influenza A (H1N1) pandemic. Am J Infect Control. 2012;40:273–5. https://doi.org/10.1016/j.ajic.2011.10.023
23. Jose R, Narendran M, Bindu A, Beevi N, L M, Benny PV. Public perception and preparedness for the pandemic COVID 19: A Health Belief Model approach. Clin Epidemiol Glob Health. 2021;9:41–6. https://doi.org/10.1016/j.cegh.2020.06.009
24. Gaube S, Lermer E, Fischer P. The concept of risk perception in health-related behavior theory and behavior change. In: Raue M, Streicher B, Leimer E, editors. Perceived safety. Cham (Switzerland): Springer International Publishing; 2019. p. 101–18.
25. El-Toukhy S. Parsing susceptibility and severity dimensions of health risk perceptions. J Health Commun. 2015;20:499–511. https://doi.org/10.1080/10810730.2014.989342
26. Yeung NCY, Lau JTF, Choi KC, Griffiths S. Population responses during the pandemic phase of the influenza A(H1N1)pdm09 epidemic, Hong Kong, China. Emerg Infect Dis. 2017;23:813–5. https://doi.org/10.3201/eid2305.160768
27. Kwok KO, Lai F, Wei WI, Wong SYS, Tang JWT. Herd immunity—estimating the level required to halt the COVID-19 epidemics in affected countries. J Infect. 2020;80:e32–3. https://doi.org/10.1016/j.jinf.2020.03.027
28. Szilagyi PG, Thomas K, Shah MD, Vizueta N, Cui Y, Vangala S, et al. National trends in the US public's likelihood of getting a COVID-19 vaccine—April 1 to December 8, 2020. JAMA. 2021;325:396–8. https://doi.org/10.1001/jama.2020.26419
29. Zhou F, Yu T, Du R, Fan G, Liu Y, Liu Z, et al. Clinical course and risk factors for mortality of adult inpatients with COVID-19 in Wuhan, China: a retrospective cohort study. Lancet. 2020;395:1054–62. https://doi.org/10.1016/S0140-6736(20)30566-3
30. Lazarus JV, Ratzan SC, Palayew A, Gostin LO, Larson HJ, Rabin K, et al. A global survey of potential acceptance of a COVID-19 vaccine. Nat Med. . 2021;27:225–8. https://doi.org/10.1038/s41591-020-1124-9
31. Legido-Quigley H, Asgari N, Teo YY, Leung GM, Oshitani H, Fukuda K, et al. Are high-performing health systems resilient against the COVID-19 epidemic? Lancet. 2020;395:848–50. https://doi.org/10.1016/S0140-6736(20)30551-1
32. Miyachi T, Takita M, Senoo Y, Yamamoto K. Lower trust in national government links to no history of vaccination. Lancet. 2020;395:31–2. https://doi.org/10.1016/S0140-6736(19)32686-8
33. Lazarus JV, Ratzan S, Palayew A, Billari FC, Binagwaho A, Kimball S, et al. COVID-SCORE: A global survey to assess public perceptions of government responses to COVID-19 (COVID-SCORE-10). PLoS One. 2020;15:e0240011. https://doi.org/10.1371/journal.pone.0240011
34. Min C, Shen F, Yu W, Chu Y. The relationship between government trust and preventive behaviors during the COVID-19 pandemic in China: exploring the roles of knowledge and negative emotion. Prev Med. 2020;141:106288. https://doi.org/10.1016/j.ypmed.2020.106288
35. World Health Organization Europe. Vaccination and trust (2017). 2019 [cited 2021 Apr 7]. https://www.euro.who.int/en/health-topics/disease-prevention/vaccines-and-immunization/publications/2017/vaccination-and-trust-2017
36. Lee C, Whetten K, Omer S, Pan W, Salmon D. Hurdles to herd immunity: distrust of government and vaccine refusal in the US, 2002–2003. Vaccine. 2016;34:3972–8. https://doi.org/10.1016/j.vaccine.2016.06.048
37. Opel DJ, Salmon DA, Marcuse EK. Building trust to achieve confidence in COVID-19 vaccines. JAMA Netw Open. 2020;3:e2025672. https://doi.org/10.1001/jamanetworkopen.2020.25672
38. World Health Organization. Principles and considerations for adding a vaccine to a national immunization programme. 2015 [cited 2021 Jan 1]. https://www.who.int/

immunization/programmes_systems/policies_strategies/vaccine_intro_resources/nvi_guidelines/en
39. Carvalho Aguiar Melo M, de Sousa Soares D. Impact of social distancing on mental health during the COVID-19 pandemic: an urgent discussion. Int J Soc Psychiatry. 2020;66:625–6. https://doi.org/10.1177/0020764020927047
40. Chan PKS. Outbreak of avian influenza A(H5N1) virus infection in Hong Kong in 1997. Clin Infect Dis. 2002;34 (Suppl 2):S58–64. https://doi.org/10.1086/338820
41. Hung LS. The SARS epidemic in Hong Kong: what lessons have we learned? J R Soc Med. 2003;96:374–8. https://doi.org/10.1177/014107680309600803
42. Kwok KO, Davoudi B, Riley S, Pourbohloul B. Early real-time estimation of the basic reproduction number of emerging or reemerging infectious diseases in a community with heterogeneous contact pattern: using data from Hong Kong 2009 H1N1 pandemic influenza as an illustrative example. PLoS One. 2015;10:e0137959. https://doi.org/10.1371/journal.pone.0137959
43. Cheng S. Two more deaths, another nine temporary facial paralysis cases after Covid vaccinations. 2021 [cited 2021 Apr 10]. https://hongkongfp.com/2021/03/25/two-more-deaths-another-nine-temporary-facial-paralysis-cases-after-covid-vaccinations
44. Magramo K, Choy G, Tsang E. Coronavirus: chronically ill Hongkonger dies days after getting BioNTech Covid-19 vaccine, while experts push for return of international travel. 2021 [cited 2021 Apr 10]. https://www.scmp.com/news/hong-kong/health-environment/article/3126158/coronavirus-tourism-lawmaker-urges-hong-kong
45. The Standard. Another man died after receiving Sinovac vaccine. 2021 [cited 2021 Apr 10]. https://www.thestandard.com.hk/breaking-news/section/4/168423/Another-man-died-after-receiving-Sinovac-vaccine

Address for correspondence: Kin On Kwok, Rm 419, 4/F, JC School of Public Health and Primary Care Building, Prince of Wales Hospital, Shatin, New Territories, Hong Kong; email: kkokwok@cuhk.edu.hk; Wan In Wei, Rm 429, 4/F, JC School of Public Health and Primary Care Building, Prince of Wales Hospital, Shatin, New Territories, Hong Kong; email: vivian1628@cuhk.edu.hk

etymologia

Clyde Partin

Sunda Pangolin [ˈsün də ˈpaNG gōl ən]

The Sunda or Malayan pangolin (*Manis javanica*) achieved notoriety during the coronavirus disease pandemic because of flawed evidence suggesting that pangolins could be intermediate hosts. Genetic analysis later demonstrated that the spike protein angiotensin-converting enzyme-2 receptor-binding domain of the pangolin had marginal viral avidity and thus was an unlikely infectious conduit. Pangolins are edentate mammals possessing short powerful forelimbs suitable for excavating ants and termites.

Linnaeus named the genus *Manis*, derived from *manes*, Latin for "spirits" or "ghosts or shades of the dead," which refers to their noncuddly reptilian persona and solitary nocturnal foraging. Covered by keratin scales, pangolins, when threatened, assume a rolled up position, described by the Malayan word pengguling (one who rolls up). Native to Java (thus *javanica*), their habitat includes Southeast Asia, especially the Indomalayan archipelago and Sunda Islands. Humans hunt pangolins for their meat, consume their blood as an elixir, and use their scales and other body parts as ingredients for crafting leather products and nonefficacious medications.

Figure. Covered in tough keratin scales interspersed with strands of fur, the pangolin, also known as a scaly anteater, assumes an impenetrable rolled-up position when threatened. Note the short muscular forelimbs. Pangolins are endangered and World Pangolin Day is the third Saturday in February. Photo of a young Chinese pangolin (*Manis pentadactyla*) by Te-Chuan Chan (Taipei Zoo, Taiwan) and Wen-Ta Li (Pangolin International Biomedical Consultant Ltd., Taiwan)

Sources

1. Frutos R, Serra-Cobo J, Chen T, Devaux CA. COVID-19: time to exonerate the pangolin from the transmission of SARS-CoV-2 to humans. Infect Genet Evol. 2020;84:104493. https://doi.org/10.1016/j.meegid.2020.104493
2. ITIS Report. Manus Linnaeus, 1758 [cited 2021 Mar 21]. https://www.itis.gov/servlet/SingleRpt/SingleRpt?search_topic= TSN&search_value=584905#null
3. Animal source of the coronavirus continues to elude scientists. Nature. May 18, 2020 [cited 2021 Mar 21]. https://www.nature.com/articles/d41586-020-01449-8
4. Wang Y, Turvey ST, Leader-Williams N. Knowledge and attitudes about the use of pangolin scale products in traditional Chinese medicine (TCM). People and Nature. 2020;2:903–12 [cited 2021 May 14]. https://doi.org/10.1002/pan3.10150.

Address for correspondence: Clyde Partin, Department of Medicine, Emory University School of Medicine, 1365 Clifton Rd NE, Atlanta, GA 30322-1007, USA; email: wpart01@emory.edu

Author affiliation: Emory University School of Medicine, Atlanta, Georgia, USA

DOI: https://doi.org/10.3201/eid2707.ET2707

Susceptibility of Well-Differentiated Airway Epithelial Cell Cultures from Domestic and Wild Animals to Severe Acute Respiratory Syndrome Coronavirus 2

Mitra Gultom, Matthias Licheri, Laura Laloli, Manon Wider, Marina Strässle, Philip V'kovski,[1] Silvio Steiner, Annika Kratzel, Tran Thi Nhu Thao, Lukas Probst, Hanspeter Stalder, Jasmine Portmann, Melle Holwerda, Nadine Ebert, Nadine Stokar-Regenscheit, Corinne Gurtner, Patrik Zanolari, Horst Posthaus, Simone Schuller, Amanda Vicente-Santos, Andres Moreira-Soto, Eugenia Corrales-Aguilar, Nicolas Ruggli, Gergely Tekes, Veronika von Messling, Bevan Sawatsky, Volker Thiel, Ronald Dijkman

Severe acute respiratory syndrome coronavirus 2 (SARS-CoV-2) has spread globally, and the number of worldwide cases continues to rise. The zoonotic origins of SARS-CoV-2 and its intermediate and potential spillback host reservoirs, besides humans, remain largely unknown. Because of ethical and experimental constraints and more important, to reduce and refine animal experimentation, we used our repository of well-differentiated airway epithelial cell (AEC) cultures from various domesticated and wildlife animal species to assess their susceptibility to SARS-CoV-2. We observed that SARS-CoV-2 replicated efficiently only in monkey and cat AEC culture models. Whole-genome sequencing of progeny viruses revealed no obvious signs of nucleotide transitions required for SARS-CoV-2 to productively infect monkey and cat AEC cultures. Our findings, together with previous reports of human-to-animal spillover events, warrant close surveillance to determine the potential role of cats, monkeys, and closely related species as spillback reservoirs for SARS-CoV-2.

During the past 2 decades we have observed zoonotic outbreaks of severe acute respiratory syndrome coronavirus (SARS-CoV) in 2003 and Middle East respiratory syndrome coronavirus (MERS-CoV) in 2012 (*1*,*2*). These outbreaks have been followed by the current pandemic caused by the 2019 zoonotic emergence of severe acute respiratory syndrome coronavirus 2 (SARS-CoV-2), the etiologic agent of coronavirus disease (COVID-19) (*3*,*4*). Humans are currently seen as the main hosts, but the zoonotic

Author affiliations: Institute for Infectious Diseases, University of Bern, Bern, Switzerland (M. Gultom, M. Licheri, L. Laloli, M. Wider, M. Strässle, L. Probst, M. Holwerda, R. Dijkman); University of Bern Department of Infectious Diseases and Pathobiology, Bern (M. Gultom, L. Laloli, M. Strässle, P. V'kovski, S. Steiner, A. Kratzel, T.T.N. Thao, H. Stalder, J. Portmann, M. Holwerda, N. Ebert, N. Stokar-Regenscheit, C. Gurtner, H. Posthaus, V. Thiel, R. Dijkman); Institute of Virology and Immunology, Bern and Mittelhäusern, Switzerland (M. Gultom, L. Laloli, M. Strässle, P. V'kovski, S. Steiner, A. Kratzel, T.T.N. Thao, H. Stalder, J. Portmann, M. Holwerda, N. Ebert, V. Thiel, R. Dijkman); University of Bern Graduate School for Biomedical Science, Bern (M. Gultom, L. Laloli, S. Steiner, A. Kratzel, T.T.N. Thao, L. Probst, M. Holwerda); Institute of Veterinary Bacteriology, University of Bern, Bern (M. Strässle); Institute of Animal Pathology, University of Bern, Bern (N. Stokar-Regenscheit, C. Gurtner, H. Posthaus); Clinic for Ruminants, Vetsuisse Faculty, University of Bern, Bern (P. Zanolari); University of Bern Department of Clinical Veterinary Medicine, Bern (S. Schuller); Virology-Research Center for tropical diseases (CIET), University of Costa Rica, Montes de Oca, Costa Rica (A. Vicente-Santos, A. Moreira-Soto, E. Corrales-Aguilar); Institute of Virology, Charité-Universitätsmedizin Berlin, Corporate Member of Freie Universität Berlin, Humboldt-Universität zu Berlin, and Berlin Institute of Health, Berlin, Germany (A. Moreira-Soto); Institute of Virology, Justus Liebig University Giessen, Giessen, Germany (G. Tekes); Federal Institute for Vaccines and Biomedicines, Langen, Germany (V. von Messling, B. Sawatsky)

DOI: https://doi.org/10.3201/eid2707.204660

[1]Current affiliation: Institute for Infectious Diseases, University of Bern, Bern, Switzerland.

origins and intermediate and potential spillback host reservoirs of SARS-CoV-2 are not yet well defined. Several reports indicate that SARS-CoV-2 spillover events from human to other animal species can occur (*5*–*7*). These zoonotic events are likely driven by close human–animal interactions and the conservation of crucial receptor binding motif (RBM) residues in the angiotensin-converting enzyme 2 (ACE2) orthologs, potentially facilitating SARS-CoV-2 entry (*8*,*9*). This knowledge gap highlights the need to assess the potential host spectrum for SARS-CoV-2 to support current pandemic mitigation strategies.

Besides their use in determining the host spectrum, animal models will be needed for viral pathogenesis studies, as well as for testing novel antiviral drugs, immunotherapies, and vaccines against SARS-CoV-2. Typically, in such studies a large variety of animal species are tested for susceptibility (*10*–*12*). However, such experiments have several drawbacks, including the availability of diverse animal models and the need for dedicated personnel, housing facilities, and most important, ethics approval. Some of these factors are especially limiting when applied to wildlife and livestock animals, such as pigs, cattle, and other ruminants; when working with companion animals and nonhuman primates, there are additional socioemotional and ethical considerations.

In this study, we evaluated the susceptibility of several mammal species to SARS-CoV-2 by recapitulating the initial stages of infection in a controlled in vitro model, in compliance with the reduction, refinement, and replacement principles in animal experimentation, while at the same time circumventing traditional in vivo experimental constraints. We used a unique well-differentiated airway epithelial cell (AEC) culture repository from the primary tracheobronchial airway tissue of 12 mammal species comprising companion animals, animal model candidates, livestock, and wild animals to assess their susceptibility to SARS-CoV-2 infection. To control for the quality of the AEC, we used influenza viruses that have known broad host tropism (*13*–*15*).

Materials and Methods

Conventional Cell Culture

We cultured Vero E6 cells in Dulbecco Modified Eagle medium supplemented with 10% volume/volume percent (vol/vol) heat-inactivated fetal bovine serum, 1 mmol/L sodium pyruvate, 1x GlutaMAX, 100 μg/mL streptomycin, 100 IU/mL penicillin, 1% vol/vol nonessential amino acids, and 15 mmol/L HEPES buffering agent (GIBCO; https://www.thermofisher.com). We maintained cells at 37°C in a humidified incubator with 5% CO_2.

Establishment of Animal AEC Culture Repository

We isolated tracheobronchial epithelial cells from 12 different animal species from postmortem tracheobronchial tissue that was obtained from slaughterhouses, veterinary hospitals, or domestic or international research institutes that euthanize their animals for diagnostic purposes or as part of their licensed experimental work in accordance with local regulations and ethics guidelines. We isolated and cultured the cells as described elsewhere (*16*). To establish well-differentiated AEC cultures from diverse mammal species, we introduced several modifications to the composition of the air-liquid interface (ALI) medium (Table 1). We maintained all animal ALI cultures at 37°C in a humidified incubator with 5% CO_2. While the differentiated ALI cultures were developing over 3–4 wk, we changed media every 2–3 d.

Virus Propagation

We propagated SARS-CoV-2 (SARS-CoV-2/München-1.1/2020/929) virus stock in Vero E6 cells for 48 h then cleared virus-containing supernatant from cell debris by centrifuging for 5 min at 500 × g before aliquoting and storing it at –80°C. We determined viral titer by plaque forming unit (PFU) assay on Vero E6 cells as described elsewhere (*17*). We prepared working stocks of influenza A virus (IAV) A/Hamburg/4/2009 strain in the pHW2000 reverse genetic backbone by propagating the rescued virus in MDCK-II cells for 72 h in the infection medium, which was composed of Eagle Minimum Essential Medium, supplemented with 0.5% of bovine serum albumin, 100 μg/mL streptomycin and 100 IU/mL penicillin solution, 1 μg/mL trypsin acetylated from bovine pancreas (Sigma-Aldrich, https://www.sigmaaldrich.com), and 15 mmol/L HEPES buffer. We determined viral titer by 50% tissue culture infective dose ($TCID_{50}$) assay on MDCK-II cells as described elsewhere (*18*,*19*). We propagated influenza D virus (IDV, D/bovine/Oklahoma/660/2013 strain) stocks in the human rectal tumor cell line HRT-18G (ATCC [American Type Culture Collection] CRL11663, https://www.atcc.org) for 96 h in the infection medium, with the adjustment of using 0.25 μg/mL of trypsin. We determined viral titer by $TCID_{50}$ assay on HRT-18G cells as described elsewhere (*20*).

Infection of Animal AEC Cultures

We infected well-differentiated AEC cultures from 12 different species with 30.000 PFU of SARS-CoV-2, or 10.000 $TCID_{50}$ of either IAV or IDV, as described

Table. Optimized epidermal growth factor, retinoic acid, hydrocortisone, and DAPT concentration in the air-liquid interface medium for differentiation of the animal airway epithelial cell cultures*

Animal species	No. donors	Source	End concentration additives in ALI medium			
			EGF	RA	HC	DAPT
Monkey (*Rhesus macaque*)	2	Paul-Ehrlich-Institut, Langen, Germany	5 ng/mL	50 nM	0.48 μg/mL	NS
Ferret (*Mustela putorius furo*)	2	Paul-Ehrlich-Institut, Langen, Germany	12.5 ng/mL	100 nM	0.48 μg/mL	2.5 μM
Cat (*Felis catus*)	2	Justus-Liebig-University, Giessen, Germany	25 ng/mL	50 nM	0.072 μg/mL	NS
Dog (*Canis lupus familiaris*)	1	Institute of Animal Pathology, Bern, Switzerland	25 ng/mL	50 nM	0.072 μg/mL	NS
Rabbit (*Oryctolagus cuniculus*)	1	Slaughterhouse, Bern, Switzerland	25 ng/mL	50 nM	0.48 μg/mL	NS
Pig (*Sus scrofa domesticus*)	2	Institute of Virology and Immunology, Mittelhäusern, Switzerland	25 ng/mL	70 nM	0.072 μg/mL	NS
Cattle (*Bos taurus*)	1	Institute of Animal Pathology, University of Bern, Switzerland	25 ng/mL	50 nM	0.48 μg/mL	2.5 μM
Goat (*Capra aegagrus hircus*)	2	Slaughterhouse, Bern, Switzerland	12.5 ng/mL	50 nM	0.48 μg/mL	2.5 μM
Bactrian camel (*Camelus bactrianus*)	1	Institute of Animal Pathology, University of Bern, Switzerland	5 ng/mL	50 nM	0.072 μg/mL	NS
Llama (*Llama glama*)	2	Institute of Animal Pathology, University of Bern, Switzerland	5 ng/mL	50 nM	0.072 μg/mL	NS
Bat (*Sturnira lilium*)	1	Costa Rica, (CIET-315–2013; permit 1841/14)	5 ng/mL	50 nM	0.48 μg/mL	NS
Bat (*Carollia perspicillata*)	1	Costa Rica (CIET-315–2013; permit 1841/14)	5 ng/mL	50 nM	0.48 μg/mL	NS

*ALI, air-liquid interface; DAPT, N-[N-(3,5-difluorophenacetyl-l-alanyl)]-S-phenylglycine t-butyl ester (a γ-secretase inhibitor); EGF, epidermal growth factor; HC, hydrocortisone; NS, not added as supplement; RA, retinoic acid.

elsewhere (*16*). We monitored progeny virus release at 24-h intervals for 96 h, through the application of 100 μL of HBSS onto the apical surface and incubated 10 min before collection. We diluted collected apical washes 1:1 with virus transport medium and stored them at –80°C for later analysis. After the collection of the apical washes, we exchanged the basolateral medium with fresh ALI medium. We repeated each experiment as 2 independent biologic replicates using AEC cultures established from either 1 or 2 biologic donors of each species depending on the availability of procured animal tissue (Table 1).

Immunofluorescence Analysis

We fixed virus-infected animal AEC cultures with 4% vol/vol neutral-buffered formalin at 96 hours postinfection (hpi) for SARS-CoV-2 or 48 hpi for IAV- or IDV-infected AEC cultures and processed them as described elsewhere (*16*). To detect SARS-CoV-2, we incubated fixed animal AEC cultures with a Rockland (https://rockland-inc.com) 200-401-A50 rabbit polyclonal antibody against SARS-CoV nucleocapsid protein, which has previously been shown to cross-react with SARS-CoV-2 (*17*). We used an Abcam (https://www.abcam.com) ab128193 mouse antibody against IAV clone C43 nucleoprotein to detect IAV-infected cells and a custom-made rabbit polyclonal antibody against the nucleoprotein of influenza D/bovine/Oklahoma/660/2013 strain (GenScript, https://www.genscript.com) to detect IDV-infected cells. To visualize the distribution of ACE2 in the AEC cultures, we used Abcam ab15348 and Biorbyt (https://www.biorbyt.com) orb582208 rabbit polyclonal antibodies against ACE2. We used Alexa Fluor 488 conjugated donkey anti–rabbit or anti–mouse IgG (H + L) as secondary antibodies. We used Alexa Fluor 647-conjugated anti-β-tubulin (9F3) rabbit mAb (Thermo Fisher Scientific) to visualize cilia and Alexa Fluor 594 mouse anti-ZO1 1A12 monoclonal antibody to visualize tight junctions. We counterstained all samples using DAPI (4′,6-diamidino-2-phenylindole; Thermo Fisher Scientific) to visualize the nuclei. We performed imaging using a Thermo Fisher EVOS FL Auto 2 imaging system equipped with a plan apochromat 40×/0.95 air objective; we processed images using Fiji software packages (https://fiji.sc) (*21*) and assembled figures using the FigureJ plugin (https://github.com/mutterer/figurej) (*22*). We adjusted brightness and contrast of images to be identical to their corresponding controls.

Quantitative Real-Time Reverse Transcription PCR

We extracted viral RNA from 100 μL of 1:1 diluted apical wash using the NucleoMag VET (Macherey-Nagel AG, https://www.mn-net.com), according to the manufacturer's guidelines, on a Kingfisher Flex

purification system (Thermo Fisher Scientific). We amplified 2 μL of extracted RNA using TaqMan Fast Virus 1-Step Master Mix (Thermo Fisher Scientific) according to the manufacturer's protocol. We used a forward primer, adapted from primers described elsewhere (*23*): 5′-ACAGGTACGTTAATAGTTAATAGCGTACTTCT-3′, reverse 5′- ACAATATTGCAGCAGTACGCACA-3′, and probe 5′-FAM-ATCCTTACTGCGCTTCGA-MGB-Q530-3′(Microsynth,https://www.microsynth.ch), targeting the envelope gene of SARS-CoV-2 (GenBank accession no. MN908947.3). As a positive control, we included a serial dilution of in vitro–transcribed RNA containing regions of the RNA-dependent RNA polymerase, envelope, and N genes derived from a SARS-CoV-2 synthetic construct (GenBank accession no. MT108784) to determine the genome copy number. We performed measurements and analysis using an Applied Biosystems ABI7500 instrument and associated software package (Thermo Fisher Scientific).

Titration of SARS-CoV-2 in the Apical Washes

To quantify SARS-CoV-2, we titrated apical washes by plaque assay on Vero E6 cells. In brief, we seeded 1×10^5 cells/well in 24-well plates 1 d before titration and inoculated them with 10-fold serial dilutions of virus solutions. We removed inoculums 1 hpi and replaced them with overlay medium consisting of Dulbecco Modified Eagle Medium supplemented with 1.2% Avicel (DuPont, https://www.pharma.dupont.com), 10% heat-inactivated fetal bovine serum, 100 μg/mL streptomycin, and 100 IU/mL penicillin. We incubated cells at 37°C with 5% CO_2 for 48 h and fixed them with 4% vol/vol neutral buffered formalin before staining with crystal violet (*24*).

ACE2 Homology Analysis

To analyze ACE2 homology among different species, we retrieved the available ACE2 protein sequences for humans (GenBank accession no. NM_001371415.1), rhesus macaques (accession no. NM_001135696.1), cats (accession no. XM_023248796.1), ferrets (accession no. NM_001310190.1), dogs (accession no. NM_001165260.1), rabbits (accession no. XM_002719845.3), pigs (accession no. NM_001123070.1), cattle (accession no. XM_005228428.4), goats (accession no. NM_001290107.1), and Bactrian camels (accession no. XM_010968001.1). We acquired the ACE2 sequences for *Carollia perspicillata* bats from a study of SARS-CoV and SARS-CoV-2 infection among bats (*25*). We obtained the corresponding ACE2 sequences for llamas and *Sturnira lilium* bats (accession nos. MW863647 and MW863648) by reverse transcription PCR amplification of ACE2 mRNA, as described elsewhere (*26*). We performed sequence analysis and protein alignment using the ClustalW (https://www.genome.jp/tools-bin/clustalw) plugin in Geneious Prime (https://www.geneious.com) with the default settings. We selected ACE2 protein residues interacting with SARS-CoV-2 RBM based on previously described critical ACE2 residues interacting with SARS-CoV-2 receptor binding domains (*27*,*28*).

Whole-Genome Sequencing Using Oxford Nanopore MinION

We performed sequencing on viral RNA isolated from SARS-CoV-2 stock and the 96 hpi apical washes of SARS-CoV-2–infected monkey and cat AEC cultures according to the ARTIC platform nCoV19 protocols (*29*,*30*). We used the version 2 protocol as a basis for the reverse transcription and tiled multiplex PCR reaction using the ARTIC nCoV-2019 V3 primer pool (Appendix 1, https://wwwnc.cdc.gov/EID/article/27/7/20-4660-App1.xlsx), but we used the version 3 protocol for the downstream library preparation. We generated sequencing libraries using the EXP-NBD196 Native Barcoding Expansion 96 kit (Oxford Nanopore Technologies, https://nanoporetech.com) and sequenced on an Oxford Nanopore Technologies MinION R9.4.1 flow cell for 48 h, according to the manufacturer's instructions. We used Oxford Nanopore MinION software version 20.06.4 to perform data acquisition and real-time high-accuracy basecalling. We performed demultiplexing and read filtering according to the ARTIC platform nCoV19 pipeline (https://artic.network/ncov-2019) and the experimental Medaka pipeline (https://community.artic.network/t/medaka-longshot-pipeline/107) to perform consensus calling. We aligned and further analyzed consensus sequences in Geneious 11.1.5 using SARS-CoV-2/Wuhan-Hu-1 (GenBank accession no. MN908947.3) as the reference sequence.

Results

To evaluate the susceptibility of a diverse set of animal species to SARS-CoV-2 infection, we infected a total of 12 different well-differentiated mammal AEC culture models and monitored the viral replication kinetics at both 33°C and 37°C. Quantification of the viral RNA load at both temperatures showed a progressive 4-log fold increase in viral RNA load at 72 and 96 hpi in rhesus macaque and cat AEC cultures. In contrast, for the remaining animal AEC cultures we detected either a continuous or declining level of viral RNA load throughout the entire time course (Figure 1, panels A, B; Appendix 2, https://wwwnc.cdc.gov/EID/article/27/7/20-4660-App2.pdf, Figure 1,

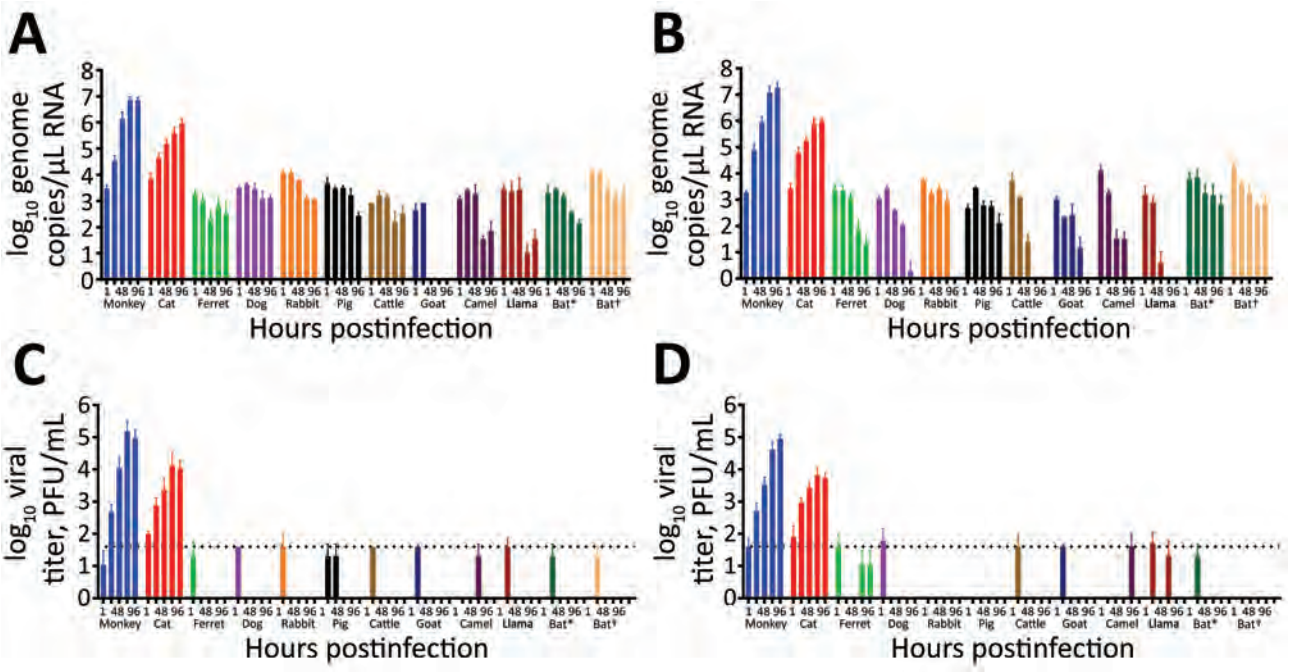

Figure 1. Severe acute respiratory syndrome coronavirus 2 replication kinetics in diverse mammal species. We inoculated well-differentiated animal airway epithelial cell cultures derived from the tracheobronchial epithelial cells with 30.000 PFU of severe acute respiratory syndrome coronavirus 2 at either 33°C (panels A, C) or 37°C (panels B, D). We removed inoculated virus at 1 hour postinfection and washed the apical side 3 times. We further incubated cultures for 96 h. At the indicated time postinfection, we assessed apical virus release by quantitative reverse transcription PCR targeting the E gene (panels A, B) and plaque titration assays on Vero E6 cells (panels C, D). Error bars represent the average of 2 independent biologic replicates using airway epithelial cell cultures established from 1 or 2 biologic donors. The dotted lines on panels C and D indicate the detection limit of the assay. **Sturnira lilium* bat; †*Carollia perspicillata* bat.

panels B, C). Because molecular assays cannot discern between infectious and noninfectious viruses, we also performed viral titration assays with the corresponding apical washes (*31*). This corroborated our previous finding that only AEC cultures from rhesus macaques and cats displayed a progressive increase in viral SARS-CoV-2 titers over time, and we detected no sustained productive virus infection above the detectable threshold beyond 24 hpi in most species (Figure 1, panels C, D; Appendix 2 Figure 1, panels D, E). The viral titers we observed in the rhesus macaque and cat AEC cultures were comparable to those we previously observed in human AEC cultures, where we also observed a 4-log fold rise in progeny-released virus in the apical side (*17*). Although ferrets have previously been shown to be susceptible to SARS-CoV-2, we observed no viral replication in AEC cultures derived from the tracheobronchial regions of ferrets. Instead, we detected only low levels of SARS-CoV-2 viral titers at 72 and 96 hpi at 37°C, in agreement with findings from in vivo studies in ferrets showing a dose-dependent and limited SARS-CoV-2 infection restricted to the upper respiratory tract (*32*–*34*). We further analyzed SARS-CoV-2 infection in the animal AEC cultures by staining for SARS-CoV-2 nucleocapsid protein on formalin-fixed AEC cultures to visualize intracellular presence of the virus. This process revealed SARS-CoV-2 antigen-positive cells in rhesus macaque and cat AEC cultures at 96 hpi, but no SARS-CoV-2 antigen-positive cells were observed in the other animal AEC cultures, including those of ferrets (Figure 2; Appendix 2 Figure 1, panel A). This further confirmed that only monkey and cat AEC support efficient replication of SARS-CoV-2 among the animals we studied.

Because productive progeny virus production was only observed in the well-differentiated tracheobronchial epithelial cell cultures from rhesus macaques and cats, we wondered whether this was because of incompatibility with the cellular receptor used by SARS-CoV-2 for cellular entry (*27*,*35*). To assess whether this corresponds to the amino acid sequence conservation of RBM in ACE2, we performed in silico analysis on the ACE2 protein sequences of the species included in this study (*27*,*28*). This process revealed that the amino acid identity of the ACE2 RBM regions interacting with the receptor-binding domain of SARS-CoV-2 in humans were more similar

to those in rhesus macaques and cats than in other species (Appendix 2 Figure 2, panel A).

Apart from receptor compatibility as a limiting factor for virus infection, it has been demonstrated previously that partially differentiated AEC cultures are poorly permissive to respiratory virus infection (*36*). To investigate whether the lack of replication in ferret cells, for example, was not caused by poor differentiation of our cell cultures, we validated the AEC cultures by infecting culture samples with the 2009 pandemic IAV A/Hamburg/4/2009 and ruminant-associated IAV D/bovine/Oklahoma/660/2013 strains. Both viruses are members of *Orthomyxoviridae* and are known to have a broad host spectrum, including ferrets (*13*–*15*,*37*). We inoculated the AEC cultures from 12 different species (rhesus macaque, cat, ferret, dog, rabbit, pig, cattle, goat, llama, camel, and 2 neotropical bats) with 10.000 $TCID_{50}$ of either IAV or IDV and incubated them at either 33°C or 37°C. At 48 hpi, we fixed the AEC cultures and processed them by

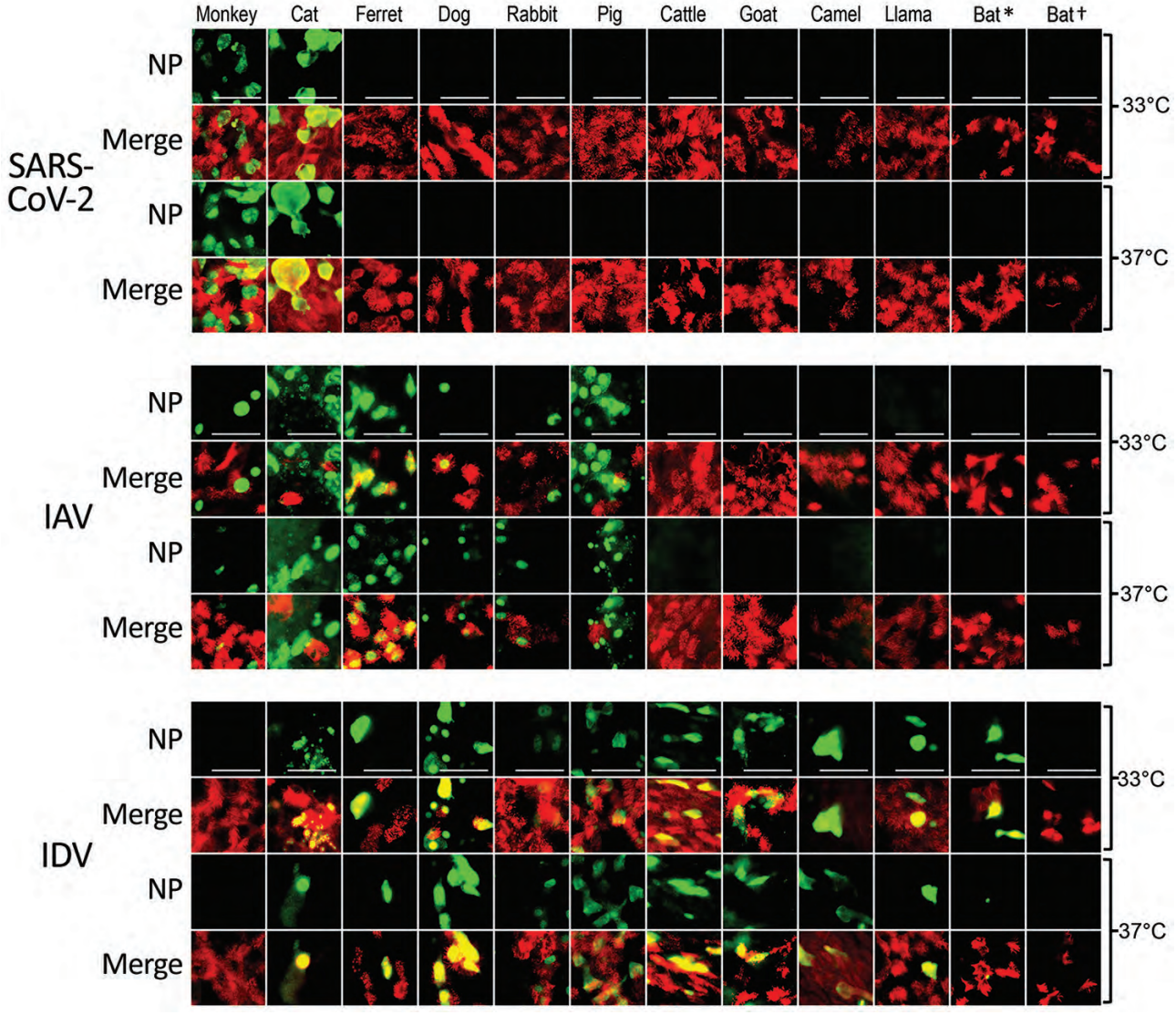

Figure 2. Tropisms of SARS-CoV-2, IAV, and IDV in infected airway epithelial cell cultures from diverse mammal species. We inoculated well-differentiated animal airway epithelial cell cultures with either 30.000 PFU of SARS-CoV-2 (SARS-CoV-2/München-1.1/2020/929), 10.000 50% tissue culture infective dose of IAV/Hamburg/4/2009, or IDV (D/bovine/Oklahoma/660/2013). We incubated virus-infected airway epithelial cell cultures at 33°C or 37°C and formalin-fixed them at 96 hours postinfection (for SARS-CoV-2) or 48 hours postinfection (for influenza viruses). After fixation, we stained virus-infected cultures using antibodies against either SARS-CoV-2, IAV, or IDV NP (green), and β-tubulin (cilia, red). We acquired images using an EVOS FL Auto 2 Imaging System equipped with a 40x air objective. Scale bar indicates 50 μm. **Sturnira lilium* bat; †*Carollia perspicillata* bat. IAV, influenza A virus; IDV, influenza D virus; NP, nucleocapsid protein; SARS-CoV-2, severe acute respiratory syndrome coronavirus 2.

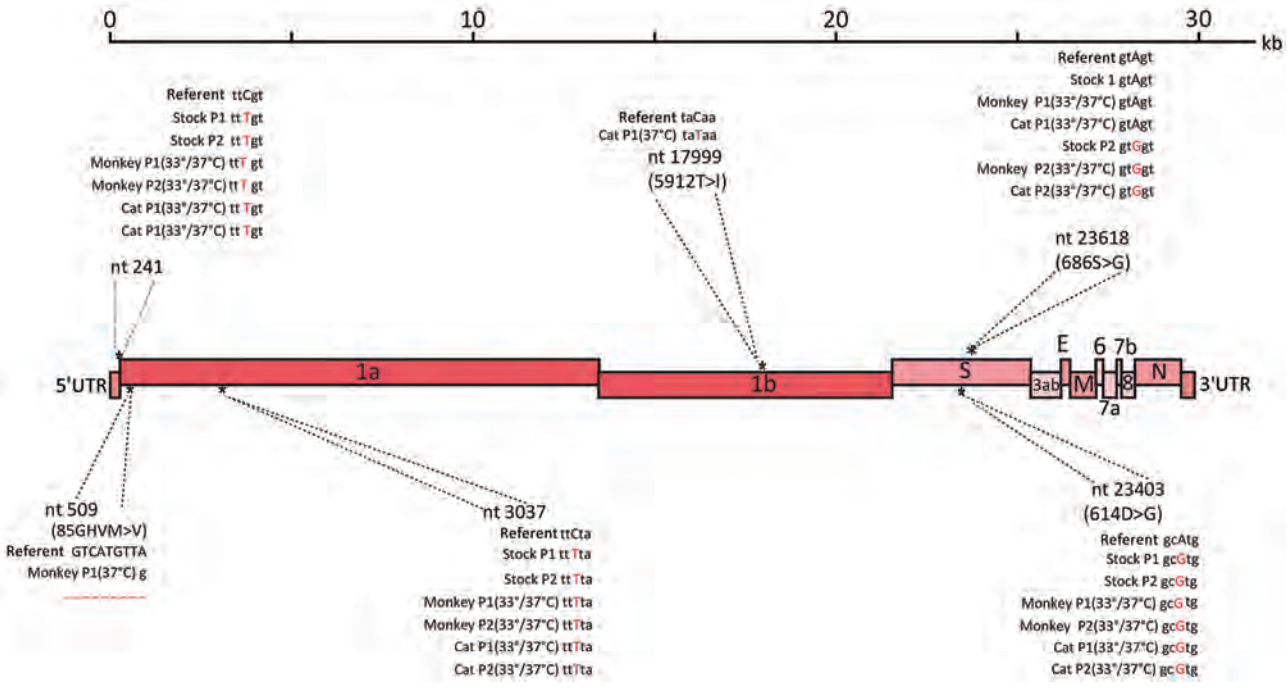

Figure 3. Whole-genome sequencing analysis using Nanopore sequencing technology (Oxford Nanopore Technologies, https://nanoporetech.com). A graphical representation of variants found in the severe acute respiratory syndrome coronavirus 2 (SARS-CoV-2) stock P1 and P2, as well as the apical washes from SARS-CoV-2–infected monkey and cat airway epithelial cell cultures with either P1 or P2 stock 96 hpi at 33°C or 37°C. SARS-CoV-2/Wuhan-Hu-1 (GenBank accession no. MN908947.3) was used as the reference sequence. P, passage; UTR, untranslated region.

immunofluorescence assays. This analysis showed that, in contrast with SARS-CoV-2 testing results, IAV antigen-positive cells could be detected in AEC cultures from companion animals and from animals commonly used for testing, such as ferret, monkey, rabbit, and pigs (Figure 2; Appendix 2 Figure 1, panel A) (*38*). For IDV infections, we observed antigen-positive cells in all AEC models, except for rhesus macaques and 1 of the neotropical bat species, indicating that AEC cultures were all well-differentiated and susceptible to virus infection.

In the immunofluorescence analysis, we also incorporated an antibody against β-tubulin marker to discern ciliated and nonciliated cell populations. For both rhesus macaques and cats, SARS-CoV-2 antigen–positive cells predominantly overlapped with the nonciliated cell populations, at either incubation temperature. Using polyclonal antibodies against ACE2, we found that the cellular receptor expression in rhesus macaques and cats predominantly overlapped with SARS-CoV-2 cell tropism, similar to ACE2 distribution in human AEC cultures (Appendix 2 Figure 2, panel B) (*17*). Unfortunately, because of limited availability of well-differentiated AEC cultures, we could not assess the ACE2 expression in goat, cattle, and rabbit AEC cultures. Nevertheless, for most species, including ferrets, that did not support efficient replication of SARS-CoV-2, we observed that ACE2 was expressed on the cell surface (Appendix 2 Figure 2, panel B). This finding suggests that ACE2 expression alone does not per se confer permissiveness to SARS-CoV-2.

It has previously been shown that SARS-CoV-2 can undergo rapid genetic changes in vitro (*39*). Because we observed efficient replication in rhesus macaque and cat AEC cultures, we assessed whether any mutations suggestive of viral adaptation had occurred. We performed whole-genome sequencing (Oxford Nanopore Technologies) on the viral inoculum used, as well as on the progeny viruses collected from the rhesus macaque and cat AEC cultures incubated at 33°C or 37°C after 1 passage, at 96 hpi. This inoculum was from either passage 1 or passage 2 virus stocks from the SARS-CoV-2/München-1.1/2020/929 isolate we had received. In the viral sequences in the 96 hpi samples from virus-infected rhesus macaque and cat AEC cultures, we observed no obvious signs of nucleotide transitions that led to nonsynonymous mutations compared to the respective inoculums (Figure 3), regardless of temperature and animal species. This finding highlights that the currently circulating SARS-CoV-2 D614G variant can productively infect rhesus macaque and cat AEC.

Discussion

Our study used an in vitro AEC culture repository composed of various domestic and wildlife animal species to assess the spectrum of potential intermediate and spillback host reservoirs for SARS-CoV-2. Inoculation of AEC cultures from rhesus macaque, cat, ferret, dog, rabbit, pig, cattle, goat, llama, camel, and 2 neotropical bat species with SARS-CoV-2 revealed that tracheobronchial cells only from rhesus macaque monkeys and cats supported efficient replication of SARS-CoV-2. Whole-genome sequencing indicated that the currently circulating SARS-CoV-2 D614G variant can efficiently infect rhesus macaque and cat AEC. Our data highlight that these 2 animals are potential models for evaluating therapeutic mitigation strategies for circulating viral variants. Our findings, in conjunction with information from previously documented spillover events, indicate that close surveillance of these animals and closely related species, whether in the wild, captivity, or households, is warranted.

To date, there have been several reports published evaluating the suitability of animal models, including cats, rhesus macaques, dogs, pigs, rabbit and ferrets, for testing SARS-CoV-2 infection (*32*,*33*,*40*–*43*). We observed that SARS-CoV-2 did not efficiently replicate in tracheobronchial AEC derived from rabbits and ferrets, although ferrets are used as an animal model for SARS-CoV-2. This finding may be because viral infections in rabbits and ferrets are mainly restricted to the nasal conchae, are dose-dependent and, in addition, the origin of the cells used as input for the AEC cultures may not recapitulate the cells of the nasal mucosa (*34*,*40*,*42*,*43*). Differences exist in cellular composition and host determinant expression levels along proximal and distal regions of the respiratory tract (*44*). In addition, SARS-CoV-2 might use a different cellular receptor in ferrets, although ACE2 could be detected on the cell surface (Appendix 2 Figure 2, panel B) (*45*). Therefore, it would be of interest to complement our current repository with AEC cultures from different anatomic regions of animals such as rabbits and ferrets and to evaluate whether ACE2 is the cellular receptor employed by SARS-CoV-2 in these various animal species.

It has been proposed that SARS-CoV-2 spillover into humans, as with SARS-CoV, originally occurred from bats, either directly or through an intermediate reservoir (*3*,*46*). With >1,400 bat species comprising >20% of all mammal species, we restricted our experiments with SARS-CoV-2 to our established AEC cultures from the 2 neotropical bat species *C. perspicillata* and *S. lilium* (M. Gultom et al., unpub. data). We showed that these 2 neotropical bats express ACE2 but are not susceptible to SARS-CoV-2, suggesting that they are not likely reservoir hosts for SARS-CoV-2 despite the detection of other coronaviruses and presumptive ACE2 receptor usage by SARS-CoV-2 in closely related bat species (*25*,*47*). In fact, a 2020 study described susceptibility to SARS-CoV-2 infection in fruit bats (*Rousettus aegyptiacus*) (*33*). Future research should therefore include AEC cultures from this bat species, as well as from horseshoe bat species (genus *Rhinolophus*), which have previously been characterized as reservoir hosts for viruses with a close genetic relationship to the coronavirus associated with the 2003 SARS outbreak (*33*,*46*). In summary, our results highlight that in vitro well-differentiated animal AEC culture models can be used as an alternative to traditional animal experimentation models to evaluate and provide insight into the host spectrum of SARS-CoV-2.

Acknowledgments

We gratefully thank Lia van der Hoek for critical reading of the manuscript and helpful discussions. Moreover, we would like to thank Doreen Muth, Marcel Müller, and Christian Drosten for providing us Vero E6 cells and the SARS-CoV-2/München-1.1/2020/929 virus isolate; Martin Schwemmle for providing us the influenza A/Hamburg/4/2009 (H1N1pdm09) virus reverse genetic system; and Feng Li for sharing the influenza D/bovine/Oklahoma/660/2013 virus isolate.

This study was supported by research grants from the European Commission (Marie Sklodowska-Curie Innovative Training Network HONOURS; grant agreement no. 721367), the Swiss National Science Foundation (SNSF grants 310030_179260, 31CA30_196062, and 31CA30_196644), the Federal Food Safety and Veterinary Office (FSVO grant 1.20.02), the German Research Foundation (DFG, SFB 1021, project B01), and Federal Ministry of Education and Research (BMBF; grant RAPID, #01KI1723A).

About the Author

Ms. Gultom is a PhD student at the University of Bern, Bern, Switzerland. Her research interest lies with the establishment of primary airway epithelial cell cultures to study emerging respiratory viruses.

References

1. Drosten C, Günther S, Preiser W, van der Werf S, Brodt H-R, Becker S, et al. Identification of a novel coronavirus in patients with severe acute respiratory syndrome. N Engl J Med. 2003;348:1967–76. https://doi.org/10.1056/NEJMoa030747
2. Zaki AM, van Boheemen S, Bestebroer TM, Osterhaus ADME, Fouchier RAM. Isolation of a novel coronavirus from a man with pneumonia in Saudi Arabia. N Engl J Med. 2012; 367:1814–20. https://doi.org/10.1056/NEJMoa1211721

3. Zhou P, Yang X-L, Wang X-G, Hu B, Zhang L, Zhang W, et al. A pneumonia outbreak associated with a new coronavirus of probable bat origin. Nature. 2020;579:270–3. https://doi.org/10.1038/s41586-020-2012-7
4. Li Q, Guan X, Wu P, Wang X, Zhou L, Tong Y, et al. Early transmission dynamics in Wuhan, China, of novel coronavirus–infected pneumonia. N Engl J Med. 2020;382:1199–207. https://doi.org/10.1056/NEJMoa2001316
5. Oreshkova N, Molenaar RJ, Vreman S, Harders F, Oude Munnink BB, Hakze-van der Honing RW, et al. SARS-CoV-2 infection in farmed minks, the Netherlands, April and May 2020. Euro Surveill. 2020;25:2001005. https://doi.org/10.2807/1560-7917.ES.2020.25.23.2001005
6. Leroy EM, Ar Gouilh M, Brugère-Picoux J. The risk of SARS-CoV-2 transmission to pets and other wild and domestic animals strongly mandates a one-health strategy to control the COVID-19 pandemic. One Health. 2020;10:100133. https://doi.org/10.1016/j.onehlt.2020.100133
7. Segalés J, Puig M, Rodon J, Avila-Nieto C, Carrillo J, Cantero G, et al. Detection of SARS-CoV-2 in a cat owned by a COVID-19-affected patient in Spain. Proc Natl Acad Sci U S A. 2020;117:24790–3. https://doi.org/10.1073/pnas.2010817117
8. Liu Z, Xiao X, Wei X, Li J, Yang J, Tan H, et al. Composition and divergence of coronavirus spike proteins and host ACE2 receptors predict potential intermediate hosts of SARS-CoV-2. J Med Virol. 2020;92:595–601. https://doi.org/10.1002/jmv.25726
9. Lam SD, Bordin N, Waman VP, Scholes HM, Ashford P, Sen N, et al. SARS-CoV-2 spike protein predicted to form complexes with host receptor protein orthologues from a broad range of mammals. Sci Rep. 2020;10:16471. https://doi.org/10.1038/s41598-020-71936-5
10. Vergara-Alert J, van den Brand JMA, Widagdo W, Muñoz M V, Raj S, Schipper D, et al. Livestock susceptibility to infection with Middle East respiratory syndrome coronavirus. Emerg Infect Dis. 2017;23:232–40. https://doi.org/10.3201/eid2302.161239
11. Kalthoff D, Grund C, Harder TC, Lange E, Vahlenkamp TW, Mettenleiter TC, et al. Limited susceptibility of chickens, turkeys, and mice to pandemic (H1N1) 2009 virus. Emerg Infect Dis. 2010;16:703–5. https://doi.org/10.3201/eid1604.091491
12. Weingartl HM, Copps J, Drebot MA, Marszal P, Smith G, Gren J, et al. Susceptibility of pigs and chickens to SARS coronavirus. Emerg Infect Dis. 2004;10:179–84. https://doi.org/10.3201/eid1002.030677
13. O'Donnell CD, Subbarao K. The contribution of animal models to the understanding of the host range and virulence of influenza A viruses. Microbes Infect. 2011;13:502–15. https://doi.org/10.1016/j.micinf.2011.01.014
14. Parrish CR, Murcia PR, Holmes EC. Influenza virus reservoirs and intermediate hosts: dogs, horses, and new possibilities for influenza virus exposure of humans. J Virol. 2015;89:2990–4. https://doi.org/10.1128/JVI.03146-14
15. Asha K, Kumar B. Emerging influenza D virus threat: what we know so far! J Clin Med. 2019;8:192. https://doi.org/10.3390/jcm8020192
16. Gultom M, Laloli L, Dijkman R. Well-differentiated primary mammalian airway epithelial cell cultures In: Maier HJ, Bickerton E, editors. Coronaviruses: methods and protocols. New York: Springer; 2020.
17. V'kovski P, Gultom M, Kelly JN, Steiner S, Russeil J, Mangeat B, et al. Disparate temperature-dependent virus-host dynamics for SARS-CoV-2 and SARS-CoV in the human respiratory epithelium. PLoS Biol. 2021;19:e3001158. https://doi.org/10.1371/journal.pbio.3001158
18. Edinger TO, Pohl MO, Yángüez E, Stertz S. Cathepsin W is required for escape of influenza A virus from late endosomes. MBio. 2015;6:e00297. https://doi.org/10.1128/mBio.00297-15
19. Hierholzer JC, Killington RA, Stokes A. Preparation of antigens. Mahy BWJ, Kangro HO, editors. Virology methods manual. London: Academic Press. 1996. p. 25–46.
20. Holwerda M, Kelly J, Laloli L, Stürmer I, Portmann J, Stalder H, et al. Determining the replication kinetics and cellular tropism of influenza D virus on primary well-differentiated human airway epithelial cells. Viruses. 2019;11:377. https://doi.org/10.3390/v11040377
21. Schindelin J, Arganda-Carreras I, Frise E, Kaynig V, Longair M, Pietzsch T, et al. Fiji: an open-source platform for biological-image analysis. Nat Methods. 2012;9:676–82. https://doi.org/10.1038/nmeth.2019
22. Mutterer J, Zinck E. Quick-and-clean article figures with FigureJ. J Microsc. 2013;252:89–91. https://doi.org/10.1111/jmi.12069
23. Corman VM, Landt O, Kaiser M, Molenkamp R, Meijer A, Chu DKW, et al. Detection of 2019 novel coronavirus (2019-nCoV) by real-time RT-PCR. Euro Surveill. 2020;25:2000045. https://doi.org/10.2807/1560-7917.ES.2020.25.3.2000045
24. Jonsdottir HR, Dijkman R. Characterization of human coronaviruses on well-differentiated human airway epithelial cell cultures. In: Maier HJ, Bickerton E, Britton P, editors. Coronaviruses: methods and protocols. New York: Springer; 2015. p. 73–87.
25. Yan H, Jiao H, Liu Q, Zhang Z, Xiong Q, Wang B-J, et al. ACE2 receptor usage reveals variation in susceptibility to SARS-CoV and SARS-CoV-2 infection among bat species. Nat Ecol Evol. 2021;5:600–8. https://doi.org/10.1038/s41559-021-01407-1
26. Hou Y, Peng C, Yu M, Li Y, Han Z, Li F, et al. Angiotensin-converting enzyme 2 (ACE2) proteins of different bat species confer variable susceptibility to SARS-CoV entry. Arch Virol. 2010;155:1563–9. https://doi.org/10.1007/s00705-010-0729-6
27. Lan J, Ge J, Yu J, Shan S, Zhou H, Fan S, et al. Structure of the SARS-CoV-2 spike receptor-binding domain bound to the ACE2 receptor. Nature. 2020;581:215–20. https://doi.org/10.1038/s41586-020-2180-5
28. Wang Q, Zhang Y, Wu L, Niu S, Song C, Zhang Z, et al. Structural and functional basis of SARS-CoV-2 entry by using human ACE2. Cell. 2020;181:894–904.e9. https://doi.org/10.1016/j.cell.2020.03.045
29. Quick J. nCoV-2019 sequencing protocol v2 (GunIt). 2020 [cited 2020 Sep 28]. https://dx.doi.org/10.17504/protocols.io.bdp7i5rn
30. Quick J. nCoV-2019 sequencing protocol v3 (LoCost). 2020 [cited 2020 Sep 28]. https://protocols.io/view/ncov-2019-sequencing-protocol-v3-locost-bh42j8ye
31. Bullard J, Dust K, Funk D, Strong JE, Alexander D, Garnett L, et al. Predicting infectious severe acute respiratory syndrome coronavirus 2 from diagnostic samples. Clin Infect Dis. 2020;71:2663–6. https://doi.org/10.1093/cid/ciaa638
32. Shi J, Wen Z, Zhong G, Yang H, Wang C, Huang B, et al. Susceptibility of ferrets, cats, dogs, and other domesticated animals to SARS-coronavirus 2. Science. 2020;368:1016–20. https://doi.org/10.1126/science.abb7015
33. Schlottau K, Rissmann M, Graaf A, Schön J, Sehl J, Wylezich C, et al. SARS-CoV-2 in fruit bats, ferrets, pigs, and chickens: an experimental transmission study. Lancet Microbe. 2020;1:e218–25. https://doi.org/10.1016/S2666-5247(20)30089-6
34. Ryan KA, Bewley KR, Fotheringham SA, Slack GS, Brown P, Hall Y, et al. Dose-dependent response to infection with SARS-CoV-2 in the ferret model and evidence

of protective immunity. Nat Commun. 2021;12:81. https://doi.org/10.1038/s41467-020-20439-y
35. Matsuyama S, Nagata N, Shirato K, Kawase M, Takeda M, Taguchi F. Efficient activation of the severe acute respiratory syndrome coronavirus spike protein by the transmembrane protease TMPRSS2. J Virol. 2010;84:12658–64. https://doi.org/10.1128/JVI.01542-10
36. Zhang L, Peeples ME, Boucher RC, Collins PL, Pickles RJ. Respiratory syncytial virus infection of human airway epithelial cells is polarized, specific to ciliated cells, and without obvious cytopathology. J Virol. 2002;76:5654–66. https://doi.org/10.1128/JVI.76.11.5654-5666.2002
37. Hause BM, Ducatez M, Collin EA, Ran Z, Liu R, Sheng Z, et al. Isolation of a novel swine influenza virus from Oklahoma in 2011 which is distantly related to human influenza C viruses. PLoS Pathog. 2013;9:e1003176. https://doi.org/10.1371/journal.ppat.1003176
38. Wu NH, Yang W, Beineke A, Dijkman R, Matrosovich M, Baumgärtner W, et al. The differentiated airway epithelium infected by influenza viruses maintains the barrier function despite a dramatic loss of ciliated cells. Sci Rep. 2016;6:39668. https://doi.org/10.1038/srep39668
39. Ogando NS, Dalebout TJ, Zevenhoven-Dobbe JC, Limpens RWAL, van der Meer Y, Caly L, et al. SARS-coronavirus-2 replication in Vero E6 cells: replication kinetics, rapid adaptation and cytopathology. J Gen Virol. 2020;101:925–40. https://doi.org/10.1099/jgv.0.001453
40. Kim Y-I, Kim S-G, Kim S-M, Kim E-H, Park S-J, Yu K-M, et al. Infection and rapid transmission of SARS-CoV-2 in ferrets. Cell Host Microbe. 2020;27:704–709.e2. https://doi.org/10.1016/j.chom.2020.03.023
41. Munster VJ, Feldmann F, Williamson BN, van Doremalen N, Pérez-Pérez L, Schulz J, et al. Respiratory disease in rhesus macaques inoculated with SARS-CoV-2. Nature. 2020;585:268–72. https://doi.org/10.1038/s41586-020-2324-7
42. Richard M, Kok A, de Meulder D, Bestebroer TM, Lamers MM, Okba NMA, et al. SARS-CoV-2 is transmitted via contact and via the air between ferrets. Nat Commun. 2020;11:3496. https://doi.org/10.1038/s41467-020-17367-2
43. Mykytyn AZ, Lamers MM, Okba NMA, Breugem TI, Schipper D, van den Doel PB, et al. Susceptibility of rabbits to SARS-CoV-2. Emerg Microbes Infect. 2021;10:1–7. https://doi.org/10.1080/22221751.2020.1868951
44. Hou YJ, Okuda K, Edwards CE, Martinez DR, Asakura T, Dinnon KH III, et al. SARS-CoV-2 reverse genetics reveals a variable infection gradient in the respiratory tract. Cell. 2020;182:429–446.e14. https://doi.org/10.1016/j.cell.2020.05.042
45. Gramberg T, Hofmann H, Möller P, Lalor PF, Marzi A, Geier M, et al. LSECtin interacts with filovirus glycoproteins and the spike protein of SARS coronavirus. Virology. 2005;340:224–36. https://doi.org/10.1016/j.virol.2005.06.026
46. Li W, Shi Z, Yu M, Ren W, Smith C, Epstein JH, et al. Bats are natural reservoirs of SARS-like coronaviruses. Science. 2005;310:676–9. https://doi.org/10.1126/science.1118391
47. Góes LGB, Campos ACA, Carvalho C, Ambar G, Queiroz LH, Cruz-Neto AP, et al. Genetic diversity of bats coronaviruses in the Atlantic Forest hotspot biome, Brazil. Infect Genet Evol. 2016;44:510–3. https://doi.org/10.1016/j.meegid.2016.07.034

Address for correspondence: Ronald Dijkman, Institute for Infectious Diseases, University of Bern, Friedbühlstrasse 51, 3001 Bern, Switzerland; email: ronald.dijkman@ifik.unibe.ch

Multiplex Real-Time Reverse Transcription PCR for Influenza A Virus, Influenza B Virus, and Severe Acute Respiratory Syndrome Coronavirus 2

Bo Shu,[1] Marie K. Kirby,[1] William G. Davis, Christine Warnes, Jimma Liddell, Ji Liu, Kai-Hui Wu, Norman Hassell, Alvaro J. Benitez, Malania M. Wilson, Matthew W. Keller, Benjamin L. Rambo-Martin, Yamundow Camara, Jörn Winter, Rebecca J. Kondor, Bin Zhou, Stacey Spies, Laura E. Rose, Jonas M. Winchell, Brandi M. Limbago, David E. Wentworth,[2] John R. Barnes[2]

Severe acute respiratory syndrome coronavirus 2 (SARS-CoV-2) emerged in late 2019, and the outbreak rapidly evolved into the current coronavirus disease pandemic. SARS-CoV-2 is a respiratory virus that causes symptoms similar to those caused by influenza A and B viruses. On July 2, 2020, the US Food and Drug Administration granted emergency use authorization for in vitro diagnostic use of the Influenza SARS-CoV-2 Multiplex Assay. This assay detects influenza A virus at $10^{2.0}$, influenza B virus at $10^{2.2}$, and SARS-CoV-2 at $10^{0.3}$ 50% tissue culture or egg infectious dose, or as few as 5 RNA copies/reaction. The simultaneous detection and differentiation of these 3 major pathogens increases overall testing capacity, conserves resources, identifies co-infections, and enables efficient surveillance of influenza viruses and SARS-CoV-2.

An outbreak of pneumonia of unknown etiology in Wuhan, China, was reported to the World Health Organization on December 31, 2019 (*1*). Researchers determined that the illness, later known as coronavirus disease (COVID-19), was caused by a previously unidentified betacoronavirus, severe acute respiratory syndrome coronavirus 2 (SARS-CoV-2) (*2*). SARS-CoV-2 rapidly spread around the world, and on March 11, 2020, the World Health Organization declared a pandemic (*3*). By January 2021, SARS-CoV-2 had infected >96 million persons and caused >2 million deaths worldwide (*4*).

The high demand for molecular testing for SARS-CoV-2 has contributed to global shortages of diagnostic resources, including reagents, enzymes used in reverse transcription PCR (RT-PCR), plastic consumables, and staff availability (*5*,*6*). Efficient diagnostic tests can reduce strain on the testing system and decrease turnaround time. To improve testing efficiency, we developed the Centers for Disease Control and Prevention (CDC) Influenza SARS-CoV-2 (Flu SC2) Multiplex Assay, which is selective for influenza A and B viruses and SARS-CoV-2. This quadruplex real-time RT-PCR (rRT-PCR) simultaneously detects and distinguishes RNA of influenza A virus, influenza B virus, and SARS-CoV-2 in upper and lower respiratory specimens. To monitor specimen quality control, the assay also detects the *Homo sapiens* (human) RNase P (RP) gene. Because the Flu SC2 Multiplex Assay can test 93 samples in a 96-well plate, this technology improves the throughput of SARS-CoV-2 testing by 3-fold compared with the CDC 2019-nCoV Real-Time RT-PCR Diagnostic Panel (*7*). The Flu SC2 Multiplex Assay also simultaneously detects influenza A and B viruses, thereby reducing the overall strain on testing facilities, especially during influenza season. Continued testing and surveillance of influenza viruses during the COVID-19 pandemic provide

Author affiliations: Centers for Disease Control and Prevention, Atlanta, Georgia, USA (B. Shu, M.K. Kirby, W.G. Davis, C. Warnes, J. Liddell, J. Liu, K.-H. Wu, N. Hassell, A.J. Benitez, M.M. Wilson, M.W. Keller, B.L. Rambo-Martin, Y. Camara, J. Winter, R.J. Kondor, B. Zhou, S. Spies, L.E. Rose, J.M. Winchell, B.M. Limbago, D.E. Wentworth, J.R. Barnes); Battelle Memorial Institute, Atlanta (W.G. Davis, J. Liddell); Leidos Inc, Atlanta (Y. Camara)

DOI: https://doi.org/10.3201/eid2707.210462

[1]These first authors contributed equally to this article.

[2]These senior authors contributed equally to this article.

critical guidance on selection of candidate vaccine strains; these processes also identify antiviral resistance genes and novel influenza viruses that have pandemic potential (*8*).

We evaluated existing and novel SARS-CoV-2 primers and probes to identify the optimal SC2 assay components for this quadruplex rRT-PCR (Appendix Table 1, https://wwwnc.cdc.gov/EID/article/27/7/21-0462-App1.pdf). The SC2 assay components are selective for the 3′ region of the SARS-CoV-2 genome from the carboxy terminus of the nucleocapsid (N) gene into the 3′ untranslated region (UTR). The primer and probe sequences for the influenza A (InfA), influenza B (InfB), and RP targets are identical to those used in the singleplex assays of the US Food and Drug Administration (FDA)–approved CDC Human Influenza Virus Real-Time RT-PCR Detection and Characterization Panel [510(k) no. K200370] (*9*). The Flu SC2 Multiplex Assay is selective for the matrix (M) gene segment of the influenza A virus, the nonstructural (NS) gene segment of the influenza B virus, and the human ribonuclease P/MRP subunit P30 gene; the InfA assay is designed for universal detection of all influenza A viruses and InfB assay is designed for universal detection of all influenza B viruses (*10*–*14*). The InfA assay was recently updated to address evolutionary changes and reactivity challenges; the updated CDC Human Influenza Virus Real-Time RT-PCR Diagnostic Panel was cleared by FDA in 2020 (*9*). On July 2, 2020, FDA granted an emergency use authorization (EUA) for in vitro diagnostic use of the Flu SC2 Multiplex Assay (*15*).

Multiplex detection of RNA from influenza A virus, influenza B virus, and SARS-CoV-2 can increase testing capacity and reduce use of reagents. The increased throughput can preserve staff resources and reduce turnaround time. The Flu SC2 Multiplex Assay and similar panels identify co-infections or alternative causes of influenza-like and COVID-19–like illnesses. The Flu SC2 Multiplex Assay can enable collection of critical data on influenza A and B viruses and SARS-CoV-2, as well as the prevalence of co-infection among these respiratory viruses.

Materials and Methods

Influenza Viruses and SARS-CoV-2

Influenza viruses were grown to high titer in Madin-Darby Canine Kidney cells or embryonated chicken eggs. Infectious virus titer in the cell culture supernatant or allantoic fluid was measured by using 50% tissue culture infectious dose ($TCID_{50}$) or 50% egg infectious dose (EID_{50}) (*16*). The SARS-CoV-2 virus (2019-nCoV/USA-WA1/2020; GenBank accession no. MT576563) was grown to high titer in Vero cells; the infectious virus titer in the cell culture supernatant was measured by using $TCID_{50}$ (*16*). Total nucleic acids were extracted by using the EZ1 DSP Virus Kit on the EZ1 Advanced XL automated extractor (QIAGEN, https://www.qiagen.com).

Primers and Probes

Primers and probes were selected from highly conserved regions of the SARS-CoV-2 genome based on ≈4,000 sequences available in GISAID (https://www.gisaid.org) in March 2020 (Table 1). Primer Express 3.0.1 software (Thermo Fisher Scientific, https://www.thermofisher.com) was used to design primers that had annealing temperatures of ≈60°C and probes that had annealing temperatures of ≈68°C.

The multiplex assay probes were synthesized by using ZEN or TAO Double-Quenched Probes labeled at the 5′ end using reporter 6-carboxyfluorescein (FAM) for InfA, Yakima Yellow for InfB, Texas Red-XN for SARS-CoV-2, and Cyanine 5 (Cy 5) for RP targets (Integrated DNA Technologies, Inc., https://www.idtdna.com). The InfA and InfB probes were quenched with ZEN between nucleotides 9 and 10 and with Iowa Black FQ at the 3′ end; the SARS-CoV-2 and RP probes were quenched with TAO between nucleotides 9 and 10 and with Iowa Black RQ at the 3′ end (Integrated DNA Technologies, Inc.). Primers and Taqman hydrolysis probes were synthesized by Integrated DNA Technologies and the CDC Biotechnology Core Facility Branch (Division of Scientific Resources, National Center for Emerging and Zoonotic Infectious Diseases; Atlanta, Georgia, USA).

rRT-PCR Reaction Conditions

The rRT-PCR reactions of the Flu SC2 Multiplex Assay were optimized and conducted by using the TaqPath 1-Step Multiplex Master Mix (No Rox) (Thermo Fisher Scientific) and the 7500 Fast Dx Real-Time PCR Instrument (Thermo Fisher Scientific). The final volume of 25 μL included 6.25 μL of TaqPath 1-Step Multiplex Master Mix (No Rox) and 5 μL RNA. We used final concentrations of 400 nmol for the InfA F1 and F2 primers, 600 nmol for the InfA R1 primer, and 200 nmol for the InfA R2 primer; all other primers had final concentrations of 800 nmol. Probes had a final concentration of 200 nmol. Reaction conditions for the multiplex rRT-PCR were based on conditions for the CDC rRT-PCR Flu Panel, but we reduced the reverse transcription step from 30 min to 15 min (*9*,*17*). We used the following thermocycling conditions for

Table 1. Primers and probes used in the Influenza SARS-CoV-2 Multiplex Assay*

Primer or probe	Oligonucleotide sequence, 5′→3′	Target gene or region	Nucleotide position†	Concentration, μM‡
InfA				
Forward primer 1	CAA GAC CAA TCY TGT CAC CTC TGAC	Matrix protein	143–167	3.33
Forward primer 2	CAA GAC CAA TYC TGT CAC CTY TGAC		143–167	3.33
Reverse primer 1	GCA TTY TGG ACA AAV CGT CTA CG		248–226	5
Reverse primer 2	GCA TTT TGG ATA AAG CGT CTA CG		248–226	1.67
InfB				
Forward primer	TCC TCA AYT CAC TCT TCG AGC G	Nonstructural protein	746–767	6.67
Reverse primer	CGG TGC TCT TGA CCA AAT TGG		848–828	6.67
RP				
Forward primer	AGA TTT GGA CCT GCG AGC G	Human RNase P	50–67	6.67
Reverse primer	GAG CGG CTG TCT CCA CAA GT		50–67	6.67
SARS-CoV-2				
Forward primer	CTG CAG ATT TGG ATG ATT TCT CC	Nucleoprotein–3′ untranslated region	29463–29485	6.67
Reverse primer	CCT TGT GTG GTC TGC ATG AGT TTA G		29554–29530	6.67
InfA probe§	TGC AGT CCT /ZEN/ CGC TCA CTG GGC ACG	Matrix protein	224–201	1.67
InfB probe¶	CCA ATT CGA /ZEN/ GCA GCT GAA ACT GCG GTG	Nonstructural protein	790–817	1.67
RP probe#	TTC TGA CCT /TAO/ GAA GGC TCT GCG CG	Human RNase P	71–93	1.67
SARS-CoV-2 probe**	ATT GCA ACA /TAO/ ATC CAT GAG CAG TGC TGA CTC	Nucleoprotein–3′ untranslated region	29491–29520	1.67

*Multiplex real-time reverse transcription PCR for influenza A virus, influenza B virus, and SARS-CoV-2. InfA, influenza A; InfB, influenza B; RP, RNase P; SARS-CoV-2, severe acute respiratory syndrome coronavirus 2.
†Nucleotide positions are indicated as location in the coding domain sequences for the ribonuclease P/MRP subunit p30 (human; GenBank accession no. NM-004613), M gene (GISAID accession no. EPI 1312561) of A/Brisbane/02/2018-H1N1 (InfA), NS gene (GenBank accession no. CY232070) of B/Colorado/06/2017 (InfB), or Wuhan-Hu-1 (SARS-CoV-2; GenBank accession no. NC045512).
‡Multiplex assay is supplied with a tube of primers mixed in 1.5 mL aqueous solution and a tube of probes mixed in 1.5 mL aqueous solution.
§Probe labeled with the reporter molecule 6-carboxyfluorescein at the 5′ end, a ZEN quencher between nt 9 and 10, and an Iowa Black FQ quencher at the 3′ end (Integrated DNA Technologies, Inc., https://www.idtdna.com). Probe and primer sequences are identical to InfA sequences used by the CDC Human Influenza Real-Time RT-PCR Diagnostic Panel [510(k) no. K200370] (*9*).
¶Probe labeled with Yakima Yellow reporter at the 5′ end, a ZEN quencher between nt 9 and 10, and an Iowa Black FQ quencher at the 3′ end (Integrated DNA Technologies, Inc.). Probe and primer sequences identical to InfB sequences used by the CDC Human Influenza Virus Real-Time RT-PCR Detection and Characterization Panel [510(k) no. K200370] (*9*).
#Probe labeled with the CY5 reporter at the 5′ end, a TAO quencher between nt 9 and 10, and an Iowa Black RQ quencher at the 3′ end (Integrated DNA Technologies, Inc.). Probe and primer sequences identical to RP sequences in the CDC Human Influenza Virus Real-Time RT-PCR Detection and Characterization Panel [510(k) no. K200370].
**Probe labeled with the Texas Red-XN reporter at the 5′ end, a TAO quencher between nt 9 and 10, and an Iowa Black RQ quencher at the 3′ end (Integrated DNA Technologies, Inc.)

rRT-PCR: 25°C for 2 min, 50°C for 15 min, *Taq* activation at 95°C for 2 min, 45 cycles at 95°C for 15 sec, and 55°C for 30 sec. We conducted comparator reactions using influenza singleplex rRT-PCR and the CDC 2019-nCoV Real-Time RT-PCR Diagnostic Panel, as described previously (*7*,*10*,*17*).

Analytical Sensitivity and Specificity

A quantified synthetic RNA material (Armored RNA Quant CDC-9; Asuragen, Inc., https://asuragen.com) was used to test analytical sensitivity. The synthetic RNA included primer–probe region sequences derived from the M gene of A/Brisbane/02/2018_(H1N1)pdm09 (GISAID accession no. EPI1799928), for the InfA target, the NS gene of B/Colorado/06/2017_Victoria (GISAID accession no. EPI1056634) for the InfB target, and the *Homo sapiens* (human) ribonuclease P/MRP subunit P30 gene for the RP target. We used RNA extracted from propagated, A/Illinois/20/2018_(H1N1)pdm09 (GISAID accession no. EPI1220313; GenBank accession no. MH359945), and B/Colorado/06/2017_Victoria viruses to test the analytical sensitivity of the InfA and InfB targets. We used Twist Synthetic SARS-CoV-2 RNA Control 2 (Twist Bioscience, https://www.twistbioscience.com) and RNA extracted from propagated SARS-CoV-2 virus (2019-nCoV/USA-WA1/2020) to assess analytical sensitivity of the SARS-CoV-2 target.

We evaluated assay specificity by using a panel of influenza A virus, influenza B virus, and SARS-CoV-2. This panel included influenza A(H1/H3) variant viruses that usually circulate among swine and have caused outbreaks and pandemics in human populations (*18*–*22*).

We used a collection of influenza C viruses, coronaviruses, and human noninfluenza respiratory pathogens to test the analytical specificity of the Flu SC2 Multiplex Assay. We also tested the specificity of the SARS-CoV-2 target with an RNA transcript

generated from a clone representing nt 27768–29738 of the severe acute respiratory syndrome coronavirus (SARS-CoV)/Urbani genome, which contains the entire N gene through the 3′-terminus, and a full SARS-CoV viral genome.

To test sensitivity to co-infection, we created a serial dilution with nucleic acids extracted from A/Illinois/20/2018_(H1N1)pdm09, B/Colorado/06/2017_Victoria, 2019-nCoV/USA-WA1/2020, and adenocarcinomic human alveolar basal epithelial cells (A549). We tested the dilution by the Flu SC2 Multiplex Assay, influenza A and influenza B singleplex rRT-PCR from the CDC rRT-PCR Flu Dx Panel Influenza A/B Typing Kit, and the N1 component of the CDC 2019-nCoV Real-Time RT-PCR Diagnostic Panel.

In Silico Analysis

We tested the specificity and sensitivity of each primer and probe oligonucleotide sequence for the SARS-CoV-2 target of the Flu SC2 Multiplex Assay by BLAST analysis (http://blast.ncbi.nlm.nih.gov/blast.cgi) against the nr/nt database and the National Center for Biotechnology Iinformation and GISAID β Coronaviridae nucleotide database. We analyzed results and assessed for potential non–SARS-CoV-2 matches (Appendix). We compared the primer and probe sequences with SARS-CoV-2 variant sequences available in GISAID on January 19, 2021, including 501Y.V1, a B.1.1.7 variant from the United Kingdom; 501Y.V2, a B.1.351 variant from South Africa; and 501Y.V3, a P.1 variant from Brazil.

Assay Performance with Clinical Specimens

We evaluated the clinical performance of the Flu SC2 Multiplex Assay using 104 upper and lower respiratory specimens, including oral swab, throat swab, nasopharyngeal swab, oropharyngeal swab, and sputum samples. Total nucleic acids were extracted from 120 μL of each clinical specimen by using the EZ1 DSP Virus Kit on the EZ1 Advanced XL automated extractor (QIAGEN). The extracted material was eluted in 120 μL elution buffer. Specimens were tested with the Flu SC2 Multiplex Assay, the CDC Human Influenza Real-Time RT-PCR Diagnostic Panel: Influenza A/B Typing Kit version 2 [510 (k) no. K200370], or the CDC 2019-nCoV Real-Time RT-PCR Diagnostic Panel, as described previously (*7*,*9*).

Results

Developing the SARS-CoV-2 Target

We identified candidate SARS-CoV-2 targets and evaluated them by an in silico screening process. This process identified targets with very few mismatches across the available SARS-CoV-2 genomes and accounted for RNA structural elements known to be essential for related betacoronaviruses. In total, we tested 17 SARS-CoV-2 assay designs in singleplex format; we subsequently tested a subset of these candidates using the multiplex format, including published targets in the RNA-dependent RNA polymerase and E gene regions (Appendix Table 1) (*23*). We selected for the assay the SARS-CoV-2 target with the highest levels of sensitivity and specificity and that accurately identified residual clinical respiratory specimens.

The SARS-CoV-2 assay is selective for the 3′ region of the SARS-CoV-2 genome from the carboxy terminus of the of the N gene into the 3′-UTR (Appendix Figure). This region is expressed at high levels in infected cells and is highly conserved because it encodes a cis-acting RNA pseudoknot essential for the transcription and replication of closely related betacoronaviruses (*24*).

Analytical Sensitivity of Flu SC2 Multiplex Assay

We determined the analytical sensitivity of the Flu SC2 Multiplex Assay by calculating the limits of detection using extracted RNA from influenza A virus, influenza B virus, and SARS-CoV-2. We used serial 10-fold dilutions of extracted RNA to identify an endpoint for detection with each primer and probe set included in the multiplex assay (data not shown). After a detection range was established, we tested serial 5-fold dilutions of extracted RNA from each virus at titers near the limit of detection (LOD) with the Flu SC2 Multiplex Assay, the CDC 2019-nCoV Real-Time RT-PCR Diagnostic Panel, or the CDC rRT-PCR Flu Dx Panel: Influenza A/B Typing Kit version 2 [510 (k) no. K200370] (Table 2). We determined the limits of detection to be $10^{2.0}$ $TCID_{50}$ for influenza A, $10^{2.2}$ EID_{50} for influenza B, and $10^{0.3}$ $TCID_{50}$ for SARS-CoV-2 (Table 2). These values correspond to $10^{-0.3}$ $TCID_{50}$ for each influenza A reaction, $10^{-0.1}$ EID_{50} for influenza B, and $10^{-2.0}$ $TCID_{50}$ for SARS-CoV-2 (i.e., 5 μl RNA/reaction). We confirmed the LOD through further testing of 20 replicate viral isolates mixed with A549 cells at the established LOD and at a 5-fold dilution step above the established LOD; this process demonstrated that the multiplex assay can detect >95% of samples at the lowest detectable concentrations (Table 3; Appendix Table 2). The SD across the 20-replicate experiment was very low, demonstrating the consistency of the multiplex results even at the LOD (Table 3).

We used an engineered RNA construct (Armored RNA Quant CDC-9; Asuragen, Inc.) containing the

Table 2. Sensitivity of the Influenza SARS-CoV-2 Multiplex Assay compared with singleplex assays*

Viral titers†	Cycle threshold value‡					
	Multiplex			Singleplex		
A/Illinois/20/2018_(H1N1)pdm09						
$10^{4.1}$	23.50	23.59	23.17	24.97	24.97	24.66
$10^{3.4}$	26.57	26.50	26.81	27.71	27.49	27.50
$10^{2.7}$	29.90	30.20	30.15	30.50	29.97	29.74
$10^{2.0}$	35.58	35.24	36.17	32.32	32.43	33.63
$10^{1.3}$	42.23	37.28	0	36.01	34.61	34.96
B/Colorado/06/2017_Victoria						
$10^{4.3}$	24.47	24.44	24.31	25.80	25.68	25.93
$10^{3.6}$	27.57	27.45	27.71	28.84	28.98	29.30
$10^{2.9}$	31.09	30.17	30.47	32.10	32.10	32.38
$10^{2.2}$	34.38	33.49	34.43	35.19	35.49	35.99
$10^{1.5}$	39.75	0	0	0	0	0
2019-nCoV/USA-WA1/2020						
$10^{2.4}$	25.41	25.8	25.42	26.48	26.57	26.46
$10^{1.7}$	28.69	28.87	28.5	30.26	29.77	29.51
$10^{1.0}$	31.31	31.42	31.32	32.74	33.17	32.27
$10^{0.3}$	35.14	36.36	34.58	36.10	35.34	35.81
$10^{-0.4}$	0	0	0	37.16	0	0

*Multiplex PCR is selective for influenza A virus, influenza B virus, and SARS-CoV-2. Boldface type indicates limits of detection. SARS-CoV-2, severe acute respiratory syndrome coronavirus 2.
†Viral titers are in relation to 50% tissue culture infectious dose, except for B/Colorado/06/2017, which is in relation to 50% egg infectious dose.
‡The multiplex cycle threshold values were derived from Influenza SARS-CoV-2 Multiplex Assay. The singleplex cycle threshold values were derived from the InfA (for influenza A), InfB (for influenza B), or N1 singleplex assays (for SARS-CoV-2). The N1 singleplex assay is a component of the CDC 2019-nCoV Real-Time RT-PCR Diagnostic Panel (*7*). The InfA and InfB singleplex assays are components of the CDC Human Influenza Virus Real-Time RT-PCR Detection and Characterization Panel [510(k) no. K200370] (*9*). Each assay was performed in triplicate.

target sequences for the InfA, InfB, and RP assays to test the copy number sensitivity of the multiplex assay through serial dilutions. We assessed copy number sensitivity of the SARS-CoV-2 assay by using a serial dilution of a synthetic SARS-CoV-2 genome (GenBank accession no. MN908947.3; Twist Bioscience). All targets in the assay could detect as few as 5 RNA copies per reaction (Table 4).

Analytical Specificity of Flu SC2 Multiplex Assay

Initially, the Flu SC2 Multiplex Assay was screened using no template control reactions; we found no intramolecular or intermolecular nonspecific interactions that resulted in any products (data not shown). The specificity of the primers and probes was evaluated with viral RNA from 13 influenza A, 2 influenza B, and 1 SARS-CoV-2 isolate. The viral RNAs were tested at high and low titers; each assay accurately detected the corresponding viral target (Table 5). We observed no cross-reactivity among the 4 targets within the assays, nor did we observe any bleed-through fluorescence imaging from neighboring channels when testing the individual assays (Table 5).

To confirm that the SARS-CoV-2 assay was specific to that virus, we tested 6 known human coronaviruses, 2 alphacoronaviruses, 2 group A betacoronaviruses, and 2 group B betacoronavirus (i.e., SARS-CoV and Middle East respiratory syndrome coronavirus [MERS-CoV]), as well as an RNA transcript including the entire SARS-CoV N gene region through the 3′ UTR. No cross-reactivity was observed, demonstrating the high specificity of the assay (Appendix Table 3).

Table 3. Confirmation of established limits of detection of the Influenza SARS-CoV-2 Multiplex Assay*

Viral titer†	Influenza A		Influenza B		SARS-CoV-2	
	No. (%) positive	Mean C_t ±SD	No. (%) positive	Mean C_t ±SD	No. (%) positive	Mean C_t ±SD
A/Illinois/20/2018_(H1N1)pdm09						
$10^{2.7}$	20 (100)	29.71 ±0.51	0	NA	0	NA
$10^{2.0}$	20 (100)	33.55 ±1.15	0	NA	0	NA
B/Colorado/06/2017_Victoria						
$10^{2.9}$	0	NA	20 (100)	29.80 ±0.74	0	NA
$10^{2.2}$	0	NA	20 (100)	32.70 ±0.48	0	NA
2019-nCoV/USA-WA1/2020						
$10^{1.0}$	0	NA	0	NA	20 (100)	32.59 ±0.78
$10^{0.3}$	0	NA	0	NA	19 (95)	34.71 ±1.03

*Multiplex real-time reverse transcription PCR for influenza A virus, influenza B virus, and SARS-CoV-2. Boldface type indicates limits of detection. C_t, cycle threshold; NA, not applicable; SARS-CoV-2, severe acute respiratory syndrome coronavirus 2; SD, standard deviation.
†Viral titers are in relation to 50% tissue culture infectious dose, except for B/Colorado/06/2017, which is in relation to 50% egg infectious dose.

Table 4. Evaluation of the Influenza SARS-CoV-2 Multiplex Assay sensitivity using quantified synthetic RNAs*

RNA copies/reaction	Cycle threshold values											
	Influenza A			Influenza B			SARS-CoV-2			RNase P (human)		
50,000	23.72	24.02	23.86	22.02	21.59	21.88	20.05	20.26	20.08	22.02	22.13	21.69
5,000	27.01	27.38	28.01	25.17	25.03	25.04	24.03	24.12	24.15	25.12	24.68	25.09
500	31.74	31.73	32.48	28.52	28.02	28.88	27.25	28.01	27.60	28.19	28.02	28.11
50	35.60	35.34	36.65	32.58	31.58	31.17	31.89	31.33	32.93	31.47	31.54	30.59
5	36.50	38.40	0	33.76	34.65	36.15	34.24	34.03	34.25	34.33	35.42	39.02

*Multiplex real-time reverse transcription PCR for influenza A virus, influenza B virus, and SARS-CoV-2. Influenza A, Influenza B, and RP targets were quantified using Armored RNA Quant CDC-9 (Asuragen, Inc., https://asuragen.com), which includes the M gene of influenza A virus strain A/Brisbane/02/2018_H1N1, the NS gene of influenza B virus strain B/Colorado/06/2017, and RP; the SARS-CoV-2 target was quantified using Twist Synthetic SARS-CoV-2 RNA (Twist Bioscience, https://www.twistbioscience.com). SARS-CoV-2, severe acute respiratory syndrome coronavirus 2.

To further evaluate the specificity of the multiplex assay, we also tested common respiratory pathogens and genetic near neighbors of viruses selected for by the assay. Nucleic acids from high titer viral preparations were extracted and tested with the Flu SC2 Multiplex Assay; no cross-reactivity was observed (Appendix Table 4).

An extensive in silico BLAST analysis of the primer and probe sequences for the SARS-CoV-2 target confirmed that the assay is specific to SARS-CoV-2; no evidence of non–SARS-CoV-2 target matches was found (Figure; Appendix Table 5). These results demonstrate that Flu SC2 Multiplex Assay is specific to

Table 5. Evaluation of the Influenza SARS-CoV-2 Multiplex Assay specificity*

Virus strain	Lineage	GISAID accession no.	Con†	Cycle threshold value								
				Influenza A			Influenza B			SARS-CoV-2		
Influenza A												
A/Florida/81/2018	A(H1N1) pdm09	EPI1310819	$10^{8.1}$	13.97	14.00	14.02	0	0	0	0	0	0
			$10^{3.1}$	27.48	28.16	27.74	0	0	0	0	0	0
A/Kansas/14/2017	A(H3N2)	EPI1653963	$10^{8.5}$	13.62	13.66	13.68	0	0	0	0	0	0
			$10^{5.5}$	25.07	25.00	25.01	0	0	0	0	0	0
A/Ohio/35/2017	A(H1N2)v	EPI1056728	$10^{6.9}$	14.71	14.90	14.84	0	0	0	0	0	0
			$10^{1.9}$	30.91	31.25	30.99	0	0	0	0	0	0
A/chicken/Pennsylvania/298101-4/2004	A(H2N2)	EPI229365	$10^{9.5}$	15.60	15.66	15.74	0	0	0	0	0	0
			$10^{3.5}$	33.40	33.20	34.71	0	0	0	0	0	0
A/Ohio/13/2017	A(H3N2)v	EPI1056648	$10^{6.6}$	20.85	20.96	20.86	0	0	0	0	0	0
			$10^{1.6}$	35.48	35.49	33.98	0	0	0	0	0	0
A/canine/Florida/43/2004	A(H3N2)	EPI98471	$10^{8.1}$	19.61	19.69	19.44	0	0	0	0	0	0
			$10^{4.1}$	34.10	35.45	36.87	0	0	0	0	0	0
A/equine/Ohio/01/2003	A(H3N8)	DQ124188§	$10^{8.4}$	16.50	16.70	16.68	0	0	0	0	0	0
			$10^{3.4}$	31.01	31.55	31.07	0	0	0	0	0	0
A/Northern pintail/Washington/40964/2014	A(H5N2)	EPI860995	$10^{9.4}$	16.39	16.43	16.49	0	0	0	0	0	0
			$10^{4.4}$	36.89	36.45	34.43	0	0	0	0	0	0
A/gyrfalcon/Washington/41088-6/2014	A(H5N8)	EPI569393	$10^{9.75}$	14.12	14.10	14.13	0	0	0	0	0	0
			$10^{4.75}$	29.60	29.38	29.90	0	0	0	0	0	0
A/chicken/California/32213–1/2000	A(H6N2)	EPI1915583	$10^{9.2}$	14.97	15.05	15.08	0	0	0	0	0	0
			$10^{3.2}$	34.19	32.52	32.49	0	0	0	0	0	0
A/feline/New York/16-040082-1/2016	A(H7N2)	EPI985440	$10^{10.2}$	15.76	15.94	16.00	0	0	0	0	0	0
			$10^{5.2}$	28.16	28.30	28.46	0	0	0	0	0	0
A/Taiwan/1/2017	A(H7N9)	EPI917065	$10^{9.5}$	16.69	16.90	16.99	0	0	0	0	0	0
			$10^{3.5}$	32.20	33.11	32.53	0	0	0	0	0	0
A/Bangladesh/0994/2011	A(H9N2)	EPI445991	$10^{10.5}$	18.03	18.14	18.21	0	0	0	0	0	0
			$10^{4.5}$	34.25	35.32	36.90	0	0	0	0	0	0
Influenza B												
B/Maryland/15/2016	B(Victoria)	EPI1255266	$10^{8.5}$	0	0	0	13.46	13.49	13.47	0	0	0
			$10^{2.5}$	0	0	0	30.82	31.07	31.20	0	0	0
B/Phuket/3073/2013	B (Yamagata)	EPI1799818	$10^{8.9}$	0	0	0	13.66	13.67	13.68	0	0	0
			$10^{2.9}$	0	0	0	31.87	31.77	32.18	0	0	0
SARS-CoV-2												
2019-nCoV/USA-WA1/2020	Betacoronavirus	MT 576563	$10^{4.5}$	0	0	0	0	0	0	18.34	18.55	18.41
			$10^{0.5}$	0	0	0	0	0	0	33.11	34.15	34.88

*Multiplex real-time reverse transcription PCR for influenza A virus, influenza B virus, and SARS-CoV-2. Evaluation conducted in triplicate. Con, concentration; SARS-CoV-2, severe acute respiratory syndrome coronavirus 2.
‡Concentration in relation to 50% tissue culture infectious dose.
§GenBank accession number.

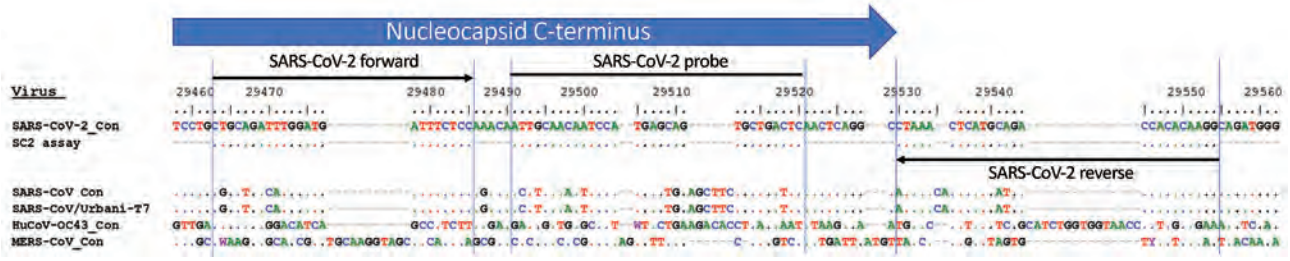

Figure. Alignment of SARS-CoV-2-specific PCR with consensus sequences for SARS-CoV-2, SARS-CoV, MERS-CoV, and HuCoV-OC43. Consensus sequence for SARS-CoV/Urbani-T7 was reverse transcribed from SARS-CoV strain Urbani (GenBank accession no. AY278741). HuCoV-OC43, human coronavirus OC43 consensus sequence; MERS-CoV, Middle East respiratory syndrome coronavirus; SARS-CoV, severe acute respiratory syndrome coronavirus; SARS-CoV-2, severe acute respiratory syndrome coronavirus 2.

influenza A viruses, influenza B viruses, and SARS-CoV-2; it does not detect other respiratory pathogens or close relatives, including SARS-CoV.

An in silico analysis compared the genomes of the emerging SARS-CoV-2 variants B.1.1.7, B.1.351, and P.1 with the sequence of the SARS-CoV-2 target. This analysis demonstrated that during January 2021, most (>99.5%) of the variant virus sequencing data was identical to the SARS-CoV-2 target sequence; of the genomes that had <100% match, none except 2 sequences displayed >1 mismatch for any region of the assay (Appendix Table 6). Therefore, the Flu SC2 Multiplex Assay should accurately detect the B.1.1.7, B.1.351, and P.1 SARS-CoV-2 variants.

Co-Infection Sensitivity of Flu SC2 Multiplex Assay

We evaluated the analytical sensitivity of the multiplex assay in the context of a mock co-infection scenario by testing a mixture of nucleic acids extracted from influenza A, influenza B, SARS-CoV-2, and A549 cells with the Flu SC2 Multiplex Assay and the InfA, InfB, and N1 singleplex assays (*7*,*9*). The results demonstrated that the multiplex assay can detect all 4 targets simultaneously at comparable or higher sensitivity levels than each singleplex comparator (Appendix Table 7).

Performance on Clinical Specimens

We evaluated the clinical performance of the multiplex assay by using residual clinical respiratory specimens. Nucleic acids were extracted from 104 prospective and retrospective clinical specimens, including 33 SARS-CoV-2–positive, 30 influenza A–positive, 30 influenza B–positive, and 11 negative residual clinical samples. The samples were tested with the Flu SC2 Multiplex Assay; the results were in 100% agreement with the expected value for each specimen (Table 6; Appendix Tables 8, 9).

Discussion

SARS-CoV-2 emerged in December 2019 and quickly spread, causing the COVID-19 pandemic. As the SARS-CoV-2 infection rate increased, the demand for viral diagnostic testing also increased. The Flu SC2 Multiplex Assay increases throughput and uses less reagent than the CDC 2019-nCoV Real-Time RT-PCR Diagnostic Panel, thus improving SARS-CoV-2 testing efficiency. The multiplex assay enables laboratories to simultaneously test for influenza viruses and SARS-CoV-2, an application that is especially useful because influenza virus and SARS-CoV-2 infections cause similar signs and symptoms (*25*,*26*). Although not described in this article, additional enzyme master mix combinations, nucleic acid extraction platforms, and an alternative manufacturer were added to the assay EUA, further improving its utility (*15*,*27*). CDC granted the right of reference to all data submitted to the FDA for EUA authorization of the Flu SC2 Multiplex Assay. Several commercial providers have leveraged the data to produce multiplex kits, including the BioSearch Valuepanel (LGC BioSearch Technologies, https://www.biosearchtech.com), PrimeTime

Table 6. Clinical performance of the Influenza SARS-CoV-2 Multiplex Assay*

Specimen type (no.)	Influenza A–positive	Influenza B–positive	SARS-CoV-2–positive	Negative for all 3 viral targets
Influenza A (30)	30	0	0	0
Influenza B (30)	0	30	0	0
SARS-CoV-2 (33)	0	0	33	0
Negative for all 3 viral targets (11)	0	0	0	11

*Multiplex real-time reverse transcription PCR for influenza A virus, influenza B virus, and SARS-CoV-2. SARS-CoV-2, severe acute respiratory syndrome coronavirus 2; (+), positive.

SARS-CoV-2/Flu Test Integrated DNA Technologies, Inc., Accuplex (includes assay for human respiratory syncytial virus) (SeraCare Life Sciences, Inc., https://www.seracare.com), BioRad Reliance (Bio-Rad Laboratories, Inc., https://www.bio-rad.com), and FLU SC2 RT-PCR (InGenuityD Diagnostics, https://ingenuityd.com).

The analytical sensitivity of the Flu SC2 Multiplex Assay was evaluated; each component was comparable to the singleplex versions of each assay. The assay detects titers as low as $10^{2.2}$–$10^{0.3}$ $TCID_{50}$ or EID_{50} (or $10^{-2.0}$–$10^{-0.1}$ $TCID_{50}$ or EID_{50}/reaction) of influenza A viruses, influenza B viruses, and SARS-CoV-2, or as few as 5 RNA copies/reaction. We observed no cross-reactivity among the targets, even at high viral titers; none with the other 6 known human coronaviruses, including SARS-CoV and MERS-CoV; and none with influenza C cultured viruses or other common noninfluenza respiratory pathogens (*28*). The Flu SC2 assays manufactured by CDC are evaluated to ensure that the LOD of each lot is comparable with the LOD established in the EUA. Quality assessments ensure limited variability: lots that have a variance of >2 cycle thresholds from the EUA submission data against standard quality control virus dilution series are deemed unacceptable for distribution (data not shown). These standards ensure that sensitivity and specificity are maintained through the manufacturing process.

The SARS-CoV-2 target used by the multiplex panel was selected from a conserved and vital region of the N gene (*29*). Analytical evaluation and in silico analysis demonstrated the target is sensitive and specific to SARS-CoV-2 and will not detect other human coronaviruses, including SARS-CoV and MERS-CoV. The in silico analysis of 376,469 SARS-CoV-2 sequences available in GISAID in January 2021 indicated that >99.9% of the viruses have ≤1 mismatch within a single primer or probe of the SARS-CoV-2 assay (Appendix Table 5). An in silico analysis of genomes from the emerging SARS-CoV-2 B.1.1.7, B.1.351, and P.1 variants demonstrated that the target is identical to the genome sequence for >99.5% of these variant genomes (Appendix Table 6). The Flu SC2 Multiplex Assay should detect these emerging variants because the mutations associated with these variants are located within a different region of the genome than the target.

The Flu SC2 Multiplex Assay was evaluated using a reference panel developed by the FDA for assessing diagnostic nucleic acid amplification tests for SARS-CoV-2 (*30*,*31*). The panel consisted of reference SARS-CoV-2 material, blinded samples, and a protocol provided by the FDA. The evaluation included range finding and confirmatory studies for LOD, as well as blinded sample testing to establish specificity and further confirmation of the LODs. The LOD of the Flu SC2 Multiplex Assay using the FDA panel was 5.7×10^3 nucleic acid amplification test detectable units/mL, with no observable cross-reactivity with MERS-CoV (*32*).

In summary, the Flu SC2 Multiplex Assay demonstrates a high level of specificity and sensitivity. In a single reaction, it can detect and distinguish 3 major respiratory viruses as well as the human quality control target, thereby increasing the testing throughput. Additional advantages of the Flu SC2 Multiplex Assay include fewer freeze-thaw cycles, decreased potential for contamination through a reduction in the number of reactions, and fewer opportunities for pipetting errors. With this multiplex assay, users can rapidly test large amounts of samples. Although the influenza season for 2020–21 had historically few cases, this assay will be beneficial in upcoming influenza seasons when influenza might co-circulate with SARS-CoV-2.

Acknowledgments

We acknowledge and thank the Laboratory and Testing Task Force team, including Kevin Karem, Wendi Kuhnert-Tallman, Jeff Johnson, Michele Owen, Christopher Elkins, Victoria Olson, Alison Laufer Halpin, and Sean Courtney, for guidance, resources, and feedback during the development of the Flu SC2 Multiplex Assay. We also acknowledge and thank the CDC Division of Scientific Resources, National Center for Emerging and Zoonotic Infectious Diseases, for their support with primer and probe synthesis during the development phase of the assay. Individual external experts were consulted to review the design and approach of the Flu SC2 Multiplex Assay; we acknowledge and thank Tom Slezak, Timothy Minogue, and Pardis Sabeti for their time and feedback. We would like to acknowledge and thank the public health laboratories that performed preliminary testing and feedback of the Flu SC2 Multiplex Assay, including Matthew Charles, Leslie Chapman, Christopher Vogt, and Jamie Pierce of the Illinois Department of Public Health Division of Laboratories; Peter Shult and Erik Reisdorf of the Wisconsin State Laboratory of Hygiene; Carol Loring of the New Hampshire Public Health Laboratories; and Rene C. Hull and Kirsten St. George of the Wadsworth Center, New York State Department of Health. Finally, we thank and acknowledge the authors, as well as the originating and submitting laboratories, who submitted sequences to the GISAID database (https://www.gisaid.org).

About the Authors

Drs. Shu and Kirby are biologists with the Genomics and Diagnostics Team in the Influenza Division, National Center for Immunization and Respiratory Diseases, Centers for Disease Control and Prevention, Atlanta, Georgia, USA. Their research interests include detection of influenza viruses and severe acute respiratory syndrome coronavirus 2.

References

1. World Health Organization. Pneumonia of unknown cause—China. 2020 [cited 2020 Jul 8]. https://www.who.int/csr/don/05-january-2020-pneumonia-of-unkown-cause-china/en/
2. Zhu N, Zhang D, Wang W, Li X, Yang B, Song J, et al.; China Novel Coronavirus Investigating and Research Team. A novel coronavirus from patients with pneumonia in China, 2019. N Engl J Med. 2020;382:727–33. https://doi.org/10.1056/NEJMoa2001017
3. Cucinotta D, Vanelli M. WHO declares COVID-19 a pandemic. Acta Biomed. 2020;91:157–60.
4. Dong E, Du H, Gardner L. An interactive web-based dashboard to track COVID-19 in real time. Lancet Infect Dis. 2020;20:533–4. https://doi.org/10.1016/S1473-3099(20)30120-1
5. Slabodkin G. FDA chief warns of supply pressure on reagents for coronavirus tests. MedTech Dive. 2020 [cited 2020 Sep 15]. https://www.medtechdive.com/news/fda-chief-warns-of-supply-pressure-on-reagents-for-coronavirus-tests/573999/
6. Wu KJ. It's like Groundhog Day: coronavirus testing labs again lack key supplies. The New York Times. 2020 Jul 23 [cited 2020 Sep 15]. https://www.nytimes.com/2020/07/23/health/coronavirus-testing-supply-shortage.html
7. Lu X, Wang L, Sakthivel SK, Whitaker B, Murray J, Kamili S, et al. US CDC real-time reverse transcription PCR panel for detection of severe acute respiratory syndrome coronavirus 2. Emerg Infect Dis. 2020;26:1654–65. https://doi.org/10.3201/eid2608.201246
8. Houser K, Subbarao K. Influenza vaccines: challenges and solutions. Cell Host Microbe. 2015;17:295–300. https://doi.org/10.1016/j.chom.2015.02.012
9. US Food and Drug Administration. 510 (k): CDC Human Influenza Virus Real-Time RT-PCR Diagnostic Panel. 2020 [2020 Mar 10]. https://www.accessdata.fda.gov/cdrh_docs/pdf20/K200370.pdf
10. US Food and Drug Administration. Human Influenza Virus Real-Time RT-PCR Detection and Characterization Panel: 510(k) 080570. 2008 [2008 Sep 26]. https://www.accessdata.fda.gov/cdrh_docs/pdf8/k080570.pdf
11. World Health Organization. CDC protocol of realtime RT-PCR for influenza H1N1. 2009 [2009 Apr 30]. https://www.who.int/csr/resources/publications/swineflu/realtimeptpcr/en/index.html
12. World Health Organization. Real-time RT-PCR protocol for the detection of avian influenza A(H7N9) virus. 2013 [2013 Apr 15]. https://www.who.int/influenza/gisrs_laboratory/cnic_realtime_rt_pcr_protocol_a_h7n9.pdf
13. US Food and Drug Administration. New traditional 510(k): CDC Human Influenza Virus Real-Time RT-PCR Diagnostic Panel. 2019 [2019 Mar 27]. https://www.accessdata.fda.gov/cdrh_docs/pdf19/K190302.pdf
14. Shu B, Kirby MK, Warnes C, Sessions WM, Davis WG, Liu J, et al. Detection and discrimination of influenza B Victoria lineage deletion variant viruses by real-time RT-PCR [Erratum in: Euro Surveill. 2020;25:201022e]. Euro Surveill. 2020;25:1900652. https://doi.org/10.2807/1560-7917.ES.2020.25.41.1900652
15. US Food and Drug Administration. Coronavirus (COVID-19) update: FDA authorizes additional COVID-19 combination diagnostic test ahead of flu season. 2020 [cited 2020 Jul 8]. https://www.fda.gov/news-events/press-announcements/coronavirus-covid-19-update-fda-authorizes-additional-covid-19-combination-diagnostic-test-ahead-flu
16. Szretter KJ, Balish AL, Katz JM. Influenza: propagation, quantification, and storage. Curr Protoc Microbiol. 2006;3:15G.1.1–15G.1.22.
17. Shu B, Wu KH, Emery S, Villanueva J, Johnson R, Guthrie E, et al. Design and performance of the CDC real-time reverse transcriptase PCR swine flu panel for detection of 2009 A (H1N1) pandemic influenza virus. J Clin Microbiol. 2011;49:2614–9. https://doi.org/10.1128/JCM.02636-10
18. Garten RJ, Davis CT, Russell CA, Shu B, Lindstrom S, Balish A, et al. Antigenic and genetic characteristics of swine-origin 2009 A(H1N1) influenza viruses circulating in humans. Science. 2009;325:197–201. https://doi.org/10.1126/science.1176225
19. Jhung MA, Epperson S, Biggerstaff M, Allen D, Balish A, Barnes N, et al. Outbreak of variant influenza A(H3N2) virus in the United States. Clin Infect Dis. 2013;57:1703–12. https://doi.org/10.1093/cid/cit649
20. Nelson MI, Gramer MR, Vincent AL, Holmes EC. Global transmission of influenza viruses from humans to swine. J Gen Virol. 2012;93:2195–203. https://doi.org/10.1099/vir.0.044974-0
21. Rajao DS, Vincent AL, Perez DR. Adaptation of human influenza viruses to swine. Front Vet Sci. 2019;5:347. https://doi.org/10.3389/fvets.2018.00347
22. Schicker RS, Rossow J, Eckel S, Fisher N, Bidol S, Tatham L, et al. Outbreak of influenza A(H3N2) variant virus infections among persons attending agricultural fairs housing infected swine—Michigan and Ohio, July–August 2016. MMWR Morb Mortal Wkly Rep. 2016;65:1157–60. https://doi.org/10.15585/mmwr.mm6542a1
23. Corman VM, Landt O, Kaiser M, Molenkamp R, Meijer A, Chu DK, et al. Detection of 2019 novel coronavirus (2019-nCoV) by real-time RT-PCR [Erratum in: Euro Surveill. 2020;25:20200409c; 2020;25:2007303; 2021;26:210204e]. Euro Surveill. 2020;25. https://doi.org/10.2807/1560-7917.ES.2020.25.3.2000045
24. Züst R, Miller TB, Goebel SJ, Thiel V, Masters PS. Genetic interactions between an essential 3′ cis-acting RNA pseudoknot, replicase gene products, and the extreme 3′ end of the mouse coronavirus genome. J Virol. 2008;82:1214–28. https://doi.org/10.1128/JVI.01690-07
25. Konala VM, Adapa S, Gayam V, Naramala S, Daggubati SR, Kammari CB, et al. Co-infection with influenza A and COVID-19. Eur J Case Rep Intern Med. 2020;7:001656. https://doi.org/10.12890/2020_001656
26. Konala VM, Adapa S, Naramala S, Chenna A, Lamichhane S, Garlapati PR, et al. A case series of patients coinfected with influenza and COVID-19. J Investig Med High Impact Case Rep. 2020;8:2324709620934674. https://doi.org/10.1177/2324709620934674
27. US Food and Drug Administration. Coronavirus disease 2019 (COVID-19) emergency use authorizations for medical devices: in vitro diagnostics EUAs. 2019 [cited 2021 Jan 11]. https://www.fda.gov/medical-devices/coronavirus-disease-2019-covid-19-emergency-use-authorizations-medical-devices/vitro-diagnostics-euas

28. Dominguez SR, Shrivastava S, Berglund A, Qian Z, Góes LGB, Halpin RA, et al. Isolation, propagation, genome analysis and epidemiology of HKU1 betacoronaviruses. J Gen Virol. 2014;95:836–48. https://doi.org/10.1099/vir.0.059832-0
29. Rangan R, Zheludev IN, Hagey RJ, Pham EA, Wayment-Steele HK, Glenn JS, et al. RNA genome conservation and secondary structure in SARS-CoV-2 and SARS-related viruses: a first look. RNA. 2020;26:937–59. https://doi.org/10.1261/rna.076141.120
30. BioSpectrum Asia. FDA sets up SARS-CoV-2 reference panel for diagnostic tests. 2020 [cited 2020 Sep 15]. https://www.biospectrumasia.com/news/30/16018/fda-sets-up-sars-cov-2-reference-panel-for-diagnostic-tests.html
31. US Food and Drug Administration. Coronavirus (COVID-19) update: FDA provides new tool to aid development and evaluation of diagnostic tests that detect SARS-CoV-2 infection. 2020 [cited 2020 Sep 15]. https://www.fda.gov/news-events/press-announcements/coronavirus-covid-19-update-fda-provides-new-tool-aid-development-and-evaluation-diagnostic-tests
32. US Food and Drug Administration. SARS-CoV-2 reference panel comparative data. 2020 [cited 2010 Sep 16]. https://www.fda.gov/medical-devices/coronavirus-covid-19-and-medical-devices/sars-cov-2-reference-panel-comparative-data

Address for correspondence: John R. Barnes, Centers for Disease Control and Prevention, 1600 Clifton Rd NE, Mailstop H23-12, Atlanta, GA 30329-4027, USA; email: fzq9@cdc.gov

Effects of Coronavirus Disease Pandemic on Tuberculosis Notifications, Malawi

Rebecca Nzawa Soko,[1] Rachael M. Burke,[1] Helena R.A. Feasey, Wakumanya Sibande, Marriott Nliwasa, Marc Y.R. Henrion, McEwen Khundi, Peter J. Dodd, Chu Chang Ku, Gift Kawalazira, Augustine T. Choko, Titus H. Divala, Elizabeth L. Corbett,[2] Peter MacPherson[2]

The coronavirus disease (COVID-19) pandemic might affect tuberculosis (TB) diagnosis and patient care. We analyzed a citywide electronic TB register in Blantyre, Malawi and interviewed TB officers. Malawi did not have an official COVID-19 lockdown but closed schools and borders on March 23, 2020. In an interrupted time series analysis, we noted an immediate 35.9% reduction in TB notifications in April 2020; notifications recovered to near prepandemic numbers by December 2020. However, 333 fewer cumulative TB notifications were received than anticipated. Women and girls were affected more (30.7% fewer cases) than men and boys (20.9% fewer cases). Fear of COVID-19 infection, temporary facility closures, inadequate personal protective equipment, and COVID-19 stigma because of similar symptoms to TB were mentioned as reasons for fewer people being diagnosed with TB. Public health measures could benefit control of both TB and COVID-19, but only if TB diagnostic services remain accessible and are considered safe to attend.

Tuberculosis (TB) is a major killer, causing ≈1.4 million deaths worldwide annually (*1*), making it second only to coronavirus disease (COVID-19) as the biggest cause of infectious disease deaths in 2020 (*2*). In addition to the direct health effects of COVID-19, the secondary effects of the COVID-19 pandemic, including lockdowns, economic turmoil, healthcare worker illness and attrition, overwhelmed health facilities, and fear of healthcare facilities, might affect delivery of health services (*3*). Concerns have been raised that COVID-19 could adversely affect TB disease diagnosis, treatment, and prevention, reversing recent progress in improving TB case detection and reducing deaths, although protective measures used for COVID-19 also could reduce TB transmission (*1*,*3*,*4*). Initial modeling published in May 2020 suggested that healthcare service disruption worldwide could lead to 6.3 million additional TB cases and 1.4 million additional TB deaths from 2020 through 2025 because of TB underdiagnosis and interruptions in TB treatment (*5*). Empirical data from settings with high TB burdens are urgently needed to examine the effects of COVID-19 on TB and to determine mitigation strategies (*4*).

According to the World Health Organization, Malawi is 1 of 30 countries that have high TB and HIV burdens (*1*). In Blantyre, in the southern region of Malawi, a citywide electronic TB register has been maintained in partnership by the Malawi Liverpool Wellcome Trust, Malawi National Tuberculosis Programme, and Blantyre District Health Office (*6*). We used these data to investigate the effects of COVID-19 on citywide TB case notifications. We hypothesized that the direct and indirect effects of the COVID-19 epidemic in Malawi would reduce TB case notifications and that effects might have been experienced disproportionately at different health system levels and by certain population groups, including persons living with HIV. Our primary objective was to estimate the number of missed TB case

Author affiliations: Malawi Liverpool Wellcome Clinical Research Programme, Blantyre, Malawi (R. Nzawa Soko, R.M. Burke, H.R.A. Feasey, W. Sibande, M. Nliwasa, M.Y.R. Henrion, M. Khundi, A.T. Choko, T.H. Divala, E.L. Corbett, P. MacPherson); London School of Hygiene and Tropical Medicine, London, UK (R. Nzawa Soko, R.M. Burke, H.R.A. Feasey, M. Khundi, T.H. Divala, E.L. Corbett, P. MacPherson); University of Malawi College of Medicine, Blantyre (M. Nliwasa); Liverpool School of Tropical Medicine, Liverpool, UK (M.Y.R. Henrion, P. MacPherson); University of Sheffield, Sheffield, UK (P.J. Dodd, C.C. Ku); District Health Office, Blantyre (G. Kawalazira)

DOI: https://doi.org/10.3201/eid2707.210557

[1]These first authors contributed equally to this article.

[2]These last authors contributed equally to this article.

notifications. Our secondary objective was to determine whether missed notifications were affected by sex, health facility, or HIV status. Finally, to investigate and explain the underlying causes of under notification of TB, we performed a qualitative study with TB officers, the cadre of healthcare workers who provide most TB services in Malawi.

Methods

Data Sources

To estimate population denominators for Blantyre District, we obtained age- and sex-specific background mortality rates and fertility rates from 2008–2020 World Population Prospect data (*7*). We used the cohort-component method to combine these data into local estimates from the 2008 and 2018 Malawi national population censuses.

In Blantyre, TB officers working at all primary health centers and the city's main hospital, Queen Elizabeth Central Hospital (QECH), record demographic and clinical characteristics of all TB patients who register for treatment by using an electronic case record form. Data collected includes date and clinic of registration, age, sex, HIV status, residential address, and TB characteristics, such as pulmonary versus extra-pulmonary TB and microbiological classification. Records are reconciled with the Ministry of Health National Tuberculosis Programme treatment registers every quarter. Each month, a randomly selected 5% sample of people who registered for TB treatment undergoes home tracing for data validation purposes.

Statistical Modeling

To investigate the effects of COVID-19 on TB case notification in Blantyre, we conducted an interrupted time series analysis (*8*). The Malawi government declared a state of emergency because of COVID-19 on March 23, 2020, and the first COVID-19 cases were diagnosed on April 2, 2020. We assumed that COVID-19 restrictions and the government and public response to the emerging epidemic would cause both an immediate step change in TB case notifications and a slope change leading to different month-by-month trends than those seen before COVID-19 (*8*). Using a negative binomial distribution to account for overdispersion, we modeled monthly counts of TB cases as a function of month, COVID-19, and month-given-COVID-19, with an offset term to account for underlying population (Appendix, https://wwwnc.cdc.gov/EID/article/27/7/21-0557-App1.pdf). We used TB notification data from June 2016, when the country began a universal test-and-treat program to provide antiretroviral therapy for persons with HIV and started using the Xpert MTB/RIF assay (*9*), which rapidly diagnoses *Mycobacterium tuberculosis*, the bacterium that causes TB disease, and rifampin resistance in <2 hours (*10*).

We estimated trends in TB case notification rates (CNRs) by using estimated Blantyre census population denominators to convert model-fitted monthly numbers of notified cases to annualized equivalent cases per 100,000 population. We used the model to predict TB CNRs from April 2020 on under a counterfactual situation in which COVID-19 had not occurred and background trends from April 2016 and March 2020 continued linearly. We defined numbers of missed TB cases as the difference between the observed numbers of notified cases and numbers expected under the counterfactual no–COVID-19 situation, acknowledging that some of the missed cases might be diagnosed later and thus be delayed rather than entirely missed. We estimated the 95% CI for the total number of missed TB cases through 1,000 parametric bootstrap replications. We took observed cases as-is and predicted cases under the counterfactual scenario from a normal distribution on the link scale with the mean equal to model prediction for given month under the counterfactual and SD equal to model SE for predictions for the given month under the counterfactual scenario.

For the secondary objective, we modeled the differential effect of COVID-19 on TB case notifications by sex, HIV status, and whether TB was diagnosed at the QECH or primary care level (Appendix). Because a small amount of data were missing for HIV status and sex, we performed multiple imputations using chained equations with predictive mean matching by using the mice package in R software (*11*).

All decisions about the expected effect model (i.e., a step and slope change), the date of change (i.e., April 2020), and the covariates in model 2 (i.e., age, sex, and primary care vs. QECH) were made a priori on the basis of knowledge about likely effects of COVID-19 and covariates known to differentially affect access to TB healthcare (*12*). To assess the statistical significance of the change in TB notifications concurrent with COVID-19 epidemic in Malawi, we extracted residuals from a regression that did not model changes due to COVID-19. We compared the sum of the residuals for the 9 months during the COVID-19 epidemic in Malawi, April–December 2020, with the distribution of this statistic from 1 million randomly permuted residuals. We also computed this statistic for all 9-month windows, excluding COVID-19 within the data.

Sensitivity Analysis

TB exhibits seasonality related to climate and weather conditions (*13*). Therefore, we performed a sensitivity analysis by adding seasonal effects to the interrupted time series model by using a harmonic term with 2 peaks every 12 months.

Qualitative Analysis

During October 21–December 14, 2020, we conducted in-depth interviews with 12 TB officers from healthcare facilities in Blantyre, 2 from QECH and 10 from primary healthcare centers, to ascertain the main reasons for changes in TB case notifications during the COVID-19 pandemic. A local social scientist with experience of qualitative interviewing conducted interviews in Chichewa, the local language. Data were recorded and simultaneously transcribed and translated to English. We developed a thematic framework from the initial 4 interviews, which we applied across all subsequent interviews. Coding and data analysis were done using NVIVO (QSR International, https://www.qsrinternational.com). Interviews were continued until saturation of themes was reached. We did not interview persons attending clinics to receive healthcare.

Ethics Approval

Participants provided oral consent for their data to be recorded in the enhanced surveillance dataset. A waiver of requirement for written consent was approved by London School of Hygiene and Tropical Medicine and College of Medicine, University of Malawi, both of which provided ethical approval for the Blantyre enhanced TB surveillance system and qualitative interviews. TB officer participants in the in-depth interviews provided informed written consent.

Results

Interrupted Time Series

During June 2016–December 2020, a total of 10,274 people starting TB treatment were notified in Blantyre. During June 2016–March 2020 (i.e., before COVID-19), annualized Blantyre TB CNRs fell by ≈1% per month, reaching a peak of 405 cases/100,000 persons in November 2016 and declining to 137 cases/100,000 persons in October 2019. A total of 9,199 TB cases were notified in Blantyre during the pre–COVID-19 period (June 2016 to December 2020), 3,561 among women and girls and 5,611 in men and boys; 27 cases were missing data on sex. Persons living with HIV represented 5,820 (63.3%) TB notifications and 3,279 (35.6%) HIV-negative persons were among notified TB cases; 100 TB cases had missing data or unknown HIV status. TB notifications were split almost evenly between QECH (4,889 notifications; 53.1%) and primary health facilities (4,310 notifications; 46.9%). Children ≤14 years of age comprised 920 (10%) notifications. The median age among adults with diagnosed TB was 35 (interquartile range [IQR] 28–44) years for women and 37 (IQR 30–45) years for men.

The declaration of a national COVID-19 disaster led to an abrupt 35.9% (95% CI 22.1%–47.3%) decline in TB notifications in April 2020 (Figure 1). However, subsequent TB notifications increased at a rate of 4.40% (95% CI 0.59%–8.36%) per month. The effect of the initial decline at the start of the COVID-19 pandemic was that observed Blantyre TB annualized CNRs pre–COVID-19, in March 2020, were 240 cases/100,000 persons and rates after the COVID-19 disaster declaration were 152 cases/100,000 persons in April 2020. By comparison, the predicted April CNR in the counterfactual scenario without COVID-19 was 230 cases/100,000 person-years. However, by November 2020, observed Blantyre TB CNRs were 205 cases/100,000 person-years and December 2020 rates were 156 cases/100,000 person-years, compared with a predicted CNR of 213 cases/100,000 person-years in November and 211 cases/100,000 person-years in December in the counterfactual scenario.

During April–December 2020, a total of 1,075 TB cases were notified in Blantyre, equivalent to 196 cases/100,000 person-years (Table 1). Under the counterfactual situation of no COVID-19 epidemic, we would expect 1,408 (95% CI 1,366–1,451) TB cases would have been notified, equivalent to annualized case notification rate of 221 cases/100,000 person-years. Therefore, we estimate that the COVID-19 epidemic directly and indirectly led to 333 (95% CI 291–376) fewer TB notifications, a 23.7% (95% CI 21.4%–26.0%) reduction in TB notifications.

As a secondary objective, we modeled which population groups were most affected by disruption to TB services (Figure 2). This model incorporated sex, HIV status, and healthcare facility (QECH vs. primary care clinics) and estimated that 352 (95% CI 319–385) TB cases were missed during April–December 2020. Men and boys accounted for a slightly larger number of missed TB diagnoses with 183 (95% CI 158–209) missed cases compared with 170 (95% CI 151–188) missed cases among women and girls. However, women and girls had a larger proportional decline, 30.7% (95% CI 28.4%–33.0%) than did men and boys, 20.9% (95% CI 18.5%–23.3%). Notifications at primary healthcare centers also were disproportionately reduced compared with hospital notifications, as were notifications for HIV-negative persons compared with those living with HIV (Table 2). The nonoverlapping confidence intervals for these groups indicated statistically significant

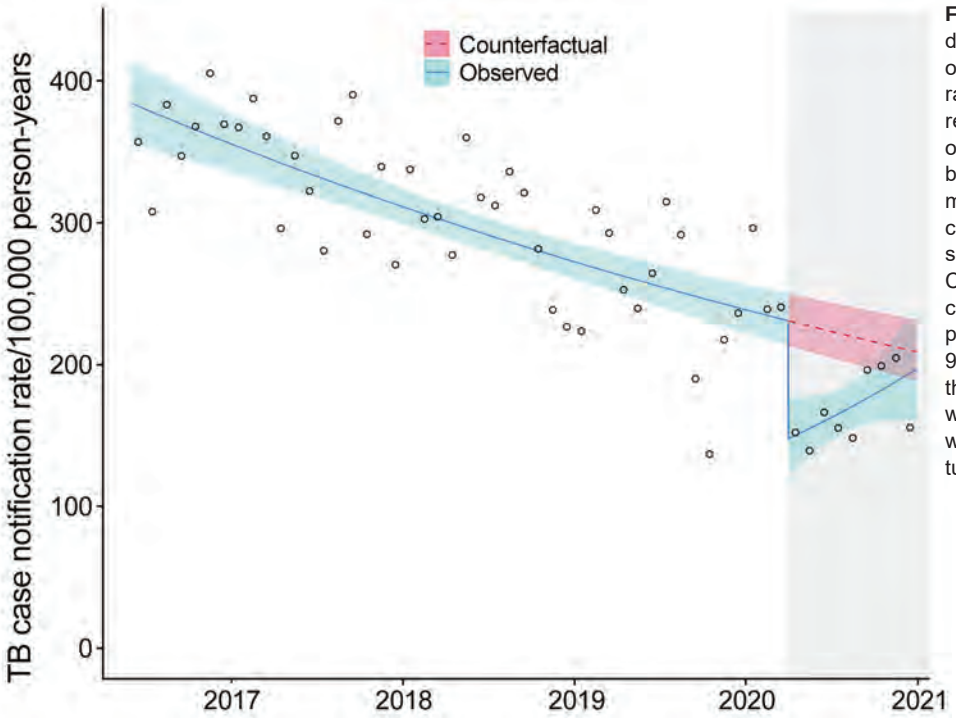

Figure 1. Effects of coronavirus disease (COVID-19) pandemic on monthly TB case notification rates in Blantyre, Malawi. Circles represent the observed number of cases each month. Solid blue line represents the fitted model with both step and slope change due to COVID-19; teal shaded area represents 95% CI. Pink dotted line represents counterfactual expected TB rates; pink shaded area represents 95% CI. Gray shaded area on the right indicates timeframe in which the COVID-19 emergency was declared in Malawi. TB, tuberculosis.

differences in effects of COVID-19 by gender, HIV status, and healthcare setting.

The drop in TB notifications during April–December 2020 was greater than that for any other 9-month period observed, and the sum of the residuals during this period was more negative than expected by random chance (p = 0.004). The sum of residuals in other 9-month periods was significantly more negative than anticipated from random resampling (p<0.05), indicating a unique statistically significant drop in cases during April–December 2020. Sensitivity analysis around seasonality of TB did not materially affect the conclusions.

Qualitative Results

Of the 12 in-depth interviews with healthcare providers, 9 participants were female and 3 were male; ages were 34–53 years. Most (10/12) participants had secondary-level education. Themes that emerged from the in-depth interviews related to both an overall reduction in persons attending health facilities and to TB-specific issues.

Reduced Attendance at Healthcare Facilities

In addition to reduced attendance at healthcare facilities among the general public from fear of being infected with COVID-19, participants mentioned that several healthcare workers tested positive for COVID-19 during the epidemic (Table 2). The facility-based COVID-19 outbreaks led to temporary closures for disinfection. Facility closures not only affected the number of persons attending the health facilities on the days of closure but also led to greater fear of

Table 1. Modeled effects of coronavirus disease pandemic on tuberculosis case notifications, April–December 2020, Blantyre, Malawi*

Models	Observed no. notified TB cases with COVID-19	Median counterfactual model-estimated no. notified TB cases without COVID-19 (95% CI)	% Difference (95% CI)	
			Absolute	Relative
Model 1				
Overall	1,075	1,408 (1,366–1,451)	333 (291–376)	23.7 (21.4–26.0)
Model 2				
Sex				
M	692	875 (848–901)	183 (156–209)	20.9 (18.5–23.3)
F	383	553 (534–571)	170 (151–188)	30.7 (28.4–33.0)
Primary health centers	488	761 (737–785)	273 (249–297)	35.9 (33.9–37.9)
Queen Elizabeth Central Hospital	587	666 (645–688)	79 (58–101)	11.9 (9.10–14.7)
HIV status				
HIV-positive	660	820 (796–845)	160 (136–185)	19.6 (17.2–21.9)
HIV-negative	415	607 (586–627)	192 (171–212)	31.6 (29.3–33.8)

*COVID-19, coronavirus disease; TB, tuberculosis.

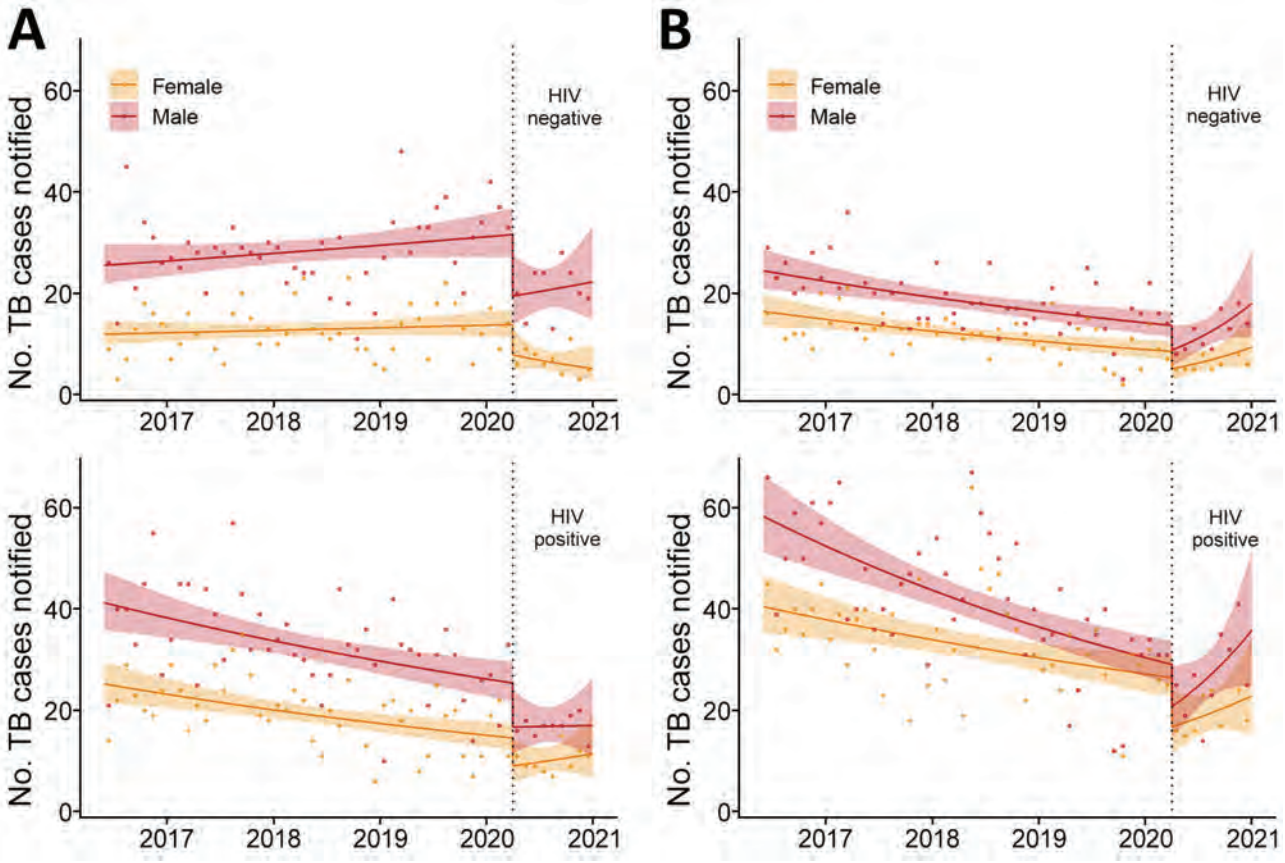

Figure 2. Effects of coronavirus disease (COVID-19) on monthly TB case notifications in Blantyre, Malawi, by HIV status, registration site, and sex. A) TB notifications at primary healthcare centers. B) TB notifications at Queen Elizabeth Central Hospital. Dots indicate observed number of cases per month. Solid lines indicate fitted model with both step and slope change due to COVID-19; shaded areas indicate 95% CI. Vertical dotted lines indicate time that COVID-19 emergency was declared in Malawi. TB, tuberculosis.

infection at healthcare facilities and, in 1 instance, rumors that the clinic was closed for a longer period than it was (Table 2). Finally, health facility worker strikes and sit-ins over risk allowance payments and lack of personal protective equipment (PPE) also resulted in temporary closures of facilities (Table 2).

Effects of COVID-19 Prevention Measures on Healthcare Access

Government COVID-19 prevention measures that required use of facemasks and social distancing also were reported to have contributed to reduced access to health services. Mandatory use of face masks at health facilities was introduced during the epidemic, but TB officers cited the inability to afford a mask and the feeling that masks "suffocate them" as reasons patients did not want to wear masks (Table 2). Patients who tried to attend facilities without having a mask were sent away (meaning that they were not seen by a healthcare worker) and often did not return (Table 2). Public transportation in Blantyre also had a limit on vehicle capacity, which led to doubled transport costs and limited clinic access (Table 2).

TB-Specific Issues

Because TB and COVID-19 both have symptoms of cough and fever, TB officers reported issues around TB testing. First, persons with fever and cough reportedly were afraid of being tested for COVID-19 if they went to healthcare facilities. TB officers said patients were more afraid of COVID-19 than TB because they knew that TB could be cured and that patients with COVID-19 might need to be placed under facility isolation (Table 2). The similarity of symptoms also led to persons who normally would have been tested for TB being turned away from healthcare facilities and told to go home and call the COVID-19 help line (Table 2).

Reduced Healthcare Worker Capacity

TB officers also spoke of their own fear of contracting COVID-19 from presumptive TB patients. TB officers reported changing how they interacted with

symptomatic persons, including interacting less directly and not supervising sputum collection as closely (Table 2). In addition, many TB officers reported that the lack of PPE in health facilities forced them to temporarily stop conducting TB tests or supervising sputum collection at all. For those patients who did submit sputum, results could be delayed because, as a TB officer reported, laboratory staff "were taught that sputum has the highest concentration of COVID-19" (Table 2).

Discussion

In addition to directly causing millions of deaths, the COVID-19 pandemic has directly and indirectly affected delivery of health services globally (*14*). In our analysis of the effects of the COVID-19 pandemic on TB notifications in Blantyre, Malawi, we found a substantial immediate decline in TB case notifications concurrent with the start of the COVID-19 epidemic in Malawi. Our findings are consistent

Table 2. Quotations from in-depth interviews with health officers about reasons for reduced tuberculosis notifications due to coronavirus disease epidemic in Malawi, June–December 2020*

Theme, quote no.	Participant no., sex	Quote
Fear of COVID-19 contagion at health facilities		
Q1	02, F	"People were afraid of getting infected if they come to the facility."
Q2	09, F	"… they were afraid saying that if the workers are found with COVID, so if we go there they will infect us."
COVID-19 related health facility closures		
Q3	03, F	"…they were told that the clinic had been shut down and people are not being assisted… which means people were just staying in their homes and the TB was just being spread amongst them."
Q4	02, F	"Our facility wasn't closed, but there was a certain week that we were just going but we were not working because there was no PPE, so people were afraid. There were no gloves, no masks how were we going to work? So a sit-in happened."
Q5	05, F	"Yes we had a strike at this hospital and the strike occurred in all health centres. The reason behind the strike was that COVID-19 was at its peak but we didn't have PPE which was putting us at risk."
Q6	07, M	"The first strike was against shortage of PPEs and the second strike was organized by Interns who were complaining that they are making them work on this dangerous disease of COVID-19 yet they are not being employed… And the other strike was about risk allowance."
Effects of COVID-19 prevention measures on healthcare access		
Q7	04, F	"…then government announced that wearing of mask is mandatory some people who couldn't manage wear the mask were making a decision of not going to the hospital instead, some were complaining that they suffocate in a mask."
Q8	08, F	"…all patients should be wearing masks when coming here but some patients were ignoring and when we send them back to go and get a mask some patients were ending up not coming back."
Q9	08, F	"Some people travel from far communities to come here and the increase in transport fare also influenced some people to fail to come to the hospital."
Similarity of TB and COVID-19 symptoms leading to reduced access to TB care		
Q10	02, F	"… sometimes they think that if they test positive [for COVID-19], people will discriminate them, they have fear of unknown. So during this period people weren't coming to say I have a cough, test me, they were just staying at home buying Bactrim and drinking it at home."
Q11	06, F	"the signs and symptoms of COVID-19 and TB were somehow similar so because the signs were similar people were scared to come to the hospital because they were assuming that instead of testing them for TB we will test them for COVID-19"
Q12	07, M	"They were communicating that if a person has fever then that is a sign of COVID-19 and that particular person is required to go into isolation so people were afraid to come to the hospital when they have fever because of the messages that they may be isolated with their families."
Q13	01, M	"… they were expecting that someone who has COVID-19 coughs and sneezes severely, and has fever and headaches, so when they ask about those, the same things that a TB patient presents, that was when those people were being sent back to go home and call the COVID-19 help line."
Reduced healthcare worker capacity to support TB testing		
Q14	05, F	"… we were no longer asking many questions once the person tells us that she has dry cough we were running away from that person… Because if the person has dry cough the first thing that we were thinking of is COVID-19."
Q15	11, F	"I was scared because it was difficult to know if the patient is coughing because of TB or COVID-19."
Q16	01, M	"… in the laboratory… the ones that are involved in the testing, they were refusing to handle sputum because they were taught that sputum has the highest concentration of COVID-19 so some were dodging which was resulting in delays."

*COVID-19, coronavirus disease; PPE, personal protective equipment; TB, tuberculosis.

with initial reports on COVID-19 effects on HIV and TB diagnosis and care from other settings (*15*–*22*). However, we show that, after an initial decline, TB CNRs increased and reached near prepandemic levels within 9 months. Overall, we estimate that 333 fewer cases of TB were notified, equivalent to 39 cases/100,000 persons, during April–December 2020 than would have been expected in the absence of the COVID-19 epidemic. For the affected persons, the missed or delayed diagnoses likely will have severe consequences, and for public health programs the consequences might hinder progress toward TB elimination. The reduction in TB case notifications also could be indicative of more general disruption of a range of primary healthcare services.

To put these results into context, Malawi has high HIV and TB burdens. Estimated prevalence of TB in urban Malawi was 988 cases/100,000 persons at the last national survey in 2013 (*4*). TB in Malawi is declining in response to concerted efforts from the national and district TB and the HIV programs. In June 2016, Malawi introduced a test-and-treat program for HIV, which involved starting antiretroviral therapy for persons who had positive HIV tests regardless of CD4 cell count. Malawi is coming close to achieving United Nations AIDS/HIV 90-90-90 goals (*23*). However, TB remains one of the leading causes of death and years of life lost in Malawi (*24*).

We hypothesize that the major reason for the drop in TB notifications during the COVID-19 pandemic is that persons with true TB disease had their TB diagnosis missed or at least delayed. This hypothesis is consistent with data from our qualitative interviews with TB officers, who noted that, in the immediate period after the Malawi COVID-19 epidemic began, access to health facilities was extremely challenging. Alternative explanations are that persons with diagnosed TB started on treatment, but their cases were not notified to the national program, or that the true incidence of TB declined. However, we consider these explanations unlikely. TB treatment cannot be accessed in Malawi outside of TB registration centers, and our electronic TB surveillance system is cross-referenced with paper ledgers that confirm the same trends in notifications. Reduced incidence of other respiratory pathogens, notably influenza, has resulted from the nonpharmaceutical interventions for COVID-19, which possibly also resulted in a decline in TB transmission. However, the prolonged interval between infection and onset of symptoms for TB makes an immediate effect on notifications in ≤3 months implausible, particularly because Malawi has had less stringent COVID-19 prevention measures than many other countries.

Our qualitative interviews indicate that, in addition to general restrictions on healthcare access during the COVID-19 epidemic, TB testing and notifications particularly were affected because of the similarity in clinical presentation of TB and COVID-19. The TB officers considered that persons with TB symptoms were less likely to attend facilities for fear of a COVID-19 diagnosis and possible consequences, such as isolation. In addition, TB officers believed that at least some persons with possible TB who went to healthcare facilities were turned away and directed to COVID-19–specific services where they would be unlikely to be assessed for TB. In countries with high TB burdens, alignment of COVID-19 and TB diagnosis, prevention, and care will likely lead to improved outcomes for both diseases.

Women and girls had disproportionately higher reductions in case notifications than men and boys, as did HIV-negative compared with HIV-positive patients and notifications from primary care clinics compared with the central hospital. We hypothesize that women and girls faced greater barriers to accessing healthcare during COVID-19 than men and boys because of greater requirements of women to stay home to school children; social gender norms, meaning that men were more likely to disregard COVID-19 public health restrictions; and perhaps economic requirements for men leave the house to work, meaning men could more easily continue to access TB services (*25*).

Primary healthcare centers were more affected than QECH, both in terms of initial step change (drop in TB cases notified at the start of COVID-19) and with slower recovery in the period after the initial phase of COVID-19 epidemic in Malawi. Reasons for the difference in reporting rates could include QECH being prioritized for PPE, thus remaining more functional than healthcare centers; in addition, patients with TB diagnosed at QECH tend to have more severe illness and potentially were unable to delay seeking healthcare.

TB cases among HIV-negative persons declined more than among persons living with HIV, which also could be associated with site of TB diagnosis. QECH has the largest number of HIV-positive persons registered for antiretroviral therapy in the city, and so persons living with HIV may have accessed TB services through the ART clinic. Alternatively, persons living with HIV can have more severe TB symptoms and be less able to defer healthcare seeking.

Limitations to our study include uncertainty around the counterfactual conditions; during June

2016–March 2020, TB case notifications were declining in Blantyre, and for the counterfactual condition, no COVID-19 scenario we modeled TB notifications as continuing to decline at the same rate. Since December 2020, Malawi has had a second wave of COVID-19. Our electronic enhanced surveillance data are entered in real time, but data are monitored and verified on a quarterly basis, so we do not yet have information on the effects of the second wave of COVID-19 in Malawi. Finally, we only interviewed healthcare workers; we did not directly capture perspectives of patients about their difficulties accessing healthcare.

Malawi is fortunate to have well-functioning TB and HIV programs that are more resilient to COVID-19 than programs in other countries. Malawi did not introduce any substantial restrictions on population movement and gathering due to COVID-19, so no legal restrictions hindered travel to TB clinics. Therefore, our data are not necessarily generalizable to other settings in southern Africa or elsewhere.

In conclusion, the effects of missed or delayed TB diagnoses likely will be severe for affected persons and households. However, the initial COVID-19–related decline in TB case notification was not sustained, and the Malawi National Tuberculosis Programme had a relatively quick recovery after the first wave of COVID-19. We observed a shorter period of disruption than earlier modeling of COVID-19 effects on TB assumed (*5*). COVID-19 or TB diagnosis, treatment, care, and public health measures should not be considered in isolation. Rather, public health and healthcare officials should seek opportunities to combine resources to tackle both COVID-19 and TB. Through improved infection prevention and control at health facilities, strengthened laboratory infrastructure, and community engagement to address stigma and provide sources of information about both diseases, communities can create a setting of universal health coverage.

Data and code to recreate analyses are freely available at https://github.com/rachaelmburke/tbcovidblantyre.

The Blantyre Enhanced TB Surveillance data is funded by Wellcome, through a grant to E.L.C. (no. 200901/Z/16/Z). R.M.B. is funded by grant no. 203905/Z/16/Z and P.M. by grant no. 206575/Z/17/Z from Wellcome. M.Y.R.H. is supported by a Wellcome Strategic Award to the Malawi Liverpool Wellcome Trust Clinical Research Programme (grant no. 206545/Z/17/Z). P.J.D. was supported by a fellowship from the UK Medical Research Council (no. MR/P022081/1); this UK-funded award is part of the European and Developing Countries Clinical Trials Partnership 2 (EDCTP2) program supported by the European Union. Wellcome had no role in design or conduct of this work, or the decision to publish.

About the Author

Dr. Burke is a medical doctor and research fellow at London School of Hygiene and Tropical Medicine and the Malawi Liverpool Wellcome Trust. She researches HIV–associated TB, public health effects of TB diagnostics and reducing deaths among hospitalized adults with HIV in southern Africa. Ms. Nwanza Soko is studying for her masters of science degree at London School of Hygiene and Tropical Medicine and is a data manager at Malawi Liverpool Wellcome Trust. Her research interest is TB epidemiology in Malawi.

References

1. World Health Organization. Global tuberculosis report 2020 [cited 2021 Jan 27]. https://www.who.int/publications/i/item/9789240013131
2. World Health Organization. Coronavirus disease (COVID-19) dashboard [cited 2021 Feb 25]. https://covid19.who.int
3. Khan MS, Rego S, Rajal JB, Bond V, Fatima RK, Isani AK, et al. Mitigating the impact of COVID-19 on tuberculosis and HIV services: a cross-sectional survey of 669 health professionals in 64 low and middle-income countries. PLoS One. 2021;16:e0244936. https://doi.org/10.1371/journal.pone.0244936
4. McQuaid CF, Vassall A, Cohen T, Fiekert K; COVID/TB Modelling Working Group. White RG. The impact of COVID-19 on TB: a review of the data. Int J TB Lung Disease. 2021 Mar 9 [Epub ahead of print]. https://theunion.org/news/the-impact-of-covid-19-on-tb-a-review-of-the-data
5. Stop TB. Partnership. The potential impact of the COVID-19 response on tuberculosis in high-burden countries: a modelling analysis [cited 2021 Feb 25]. http://www.stoptb.org/assets/documents/news/Modeling%20Report_1%20May%202020_FINAL.pdf?fbclid=IwAR1I4py4vDnzh-DTxErv4abXNF1NC4Dv-6iRbByE0GJSIsOe1_Lzycg2Svg
6. MacPherson P, Khundi M, Nliwasa M, Choko AT, Phiri VK, Webb EL, et al. Disparities in access to diagnosis and care in Blantyre, Malawi, identified through enhanced tuberculosis surveillance and spatial analysis. BMC Med. 2019;17:21. https://doi.org/10.1186/s12916-019-1260-6
7. United Nations. World population prospects 2019 [cited 2021 Feb 25]. https://population.un.org/wpp
8. Bernal JL, Cummins S, Gasparrini A. Interrupted time series regression for the evaluation of public health interventions: a tutorial. Int J Epidemiol. 2017;46:348–55.
9. Government of Malawi Ministry of Health. Malawi guidelines for clinical management of HIV in children and adults. 3rd edition. 2016 [cited 2021 Feb 1]. https://www.childrenandaids.org/sites/default/files/2017-04/Malawi_Clinical-HIV-Guidelines_2016.pdf
10. Centers for Disease Control and Prevention. Availability of an assay for detecting *Mycobacterium tuberculosis*, including rifampin-resistant strains, and considerations for its use—United States, 2013. MMWR Morb Mortal Wkly Rep. 2013;62:821–7.
11. van Buuren S, Groothuis-Oudshoorn K. mice: Multivariate Imputation by Chained Equations in R. J Stat Soft. 2011;45:1–67. https://doi.org/10.18637/jss.v045.i03

12. Horton KC, MacPherson P, Houben RMGJ, White RG, Corbett EL. Sex differences in tuberculosis burden and notifications in low- and middle-income countries: a systematic review and meta-analysis. PLoS Med. 2016; 13:e1002119. https://doi.org/10.1371/journal.pmed.1002119
13. Andrews JR, Cobelens F, Horsburgh CR, Hatherill M, Basu S, Hermans S, et al. Seasonal drivers of tuberculosis: evidence from over 100 years of notifications in Cape Town. Int J Tuberc Lung Dis. 2020;24:477–84. https://doi.org/0.5588/ijtld.19.0274
14. Hogan AB, Jewell BL, Sherrard-Smith E, Vesga JF, Watson OJ, Whittaker C, et al. Potential impact of the COVID-19 pandemic on HIV, tuberculosis, and malaria in low-income and middle-income countries: a modelling study. Lancet Glob Health. 2020;8:e1132–41. https://doi.org/10.1016/S2214-109X(20)30288-6
15. Adepoju P. Tuberculosis and HIV responses threatened by COVID-19. Lancet HIV. 2020;7:e319–20. https://doi.org/10.1016/S2352-3018(20)30109-0
16. de Souza CDF, Coutinho HS, Costa MM, Magalhães MAFM, Carmo RF. Impact of COVID-19 on TB diagnosis in northeastern Brazil. Int J Tuberc Lung Dis. 2020;24:1220–2. https://doi.org/10.5588/ijtld.20.0661
17. Pang Y, Liu Y, Du J, Gao J, Li L. Impact of COVID-19 on tuberculosis control in China. Int J Tuberc Lung Dis. 2020;24:545–7. https://doi.org/10.5588/ijtld.20.0127
18. Malik AA, Safdar N, Chandir S, Khan U, Khowaja S, Riaz N, et al. Tuberculosis control and care in the era of COVID-19. Health Policy Plan. 2020;35:1130–2. https://doi.org/10.1093/heapol/czaa109
19. Gupta A, Singla R, Caminero JA, Singla N, Mrigpuri P, Mohan A. Impact of COVID-19 on tuberculosis services in India. Int J Tuberc Lung Dis. 2020;24:637–9. https://doi.org/10.5588/ijtld.20.0212
20. Mohammed H, Oljira L, Roba KT, Yimer G, Fekadu A, Manyazewal T. Containment of COVID-19 in Ethiopia and implications for tuberculosis care and research. Infect Dis Poverty. 2020;9:131. https://doi.org/10.1186/s40249-020-00753-9
21. Reid MJA, Silva S, Arinaminpathy N, Goosby E. Building a tuberculosis-free world while responding to the COVID-19 pandemic. Lancet. 2020;396:1312–3. https://doi.org/10.1016/S0140-6736(20)32138-3
22. Abdool Karim Q, Abdool Karim SS. COVID-19 affects HIV and tuberculosis care. Science. 2020;369:366–8. https://doi.org/10.1126/science.abd1072
23. Avert. Malawi 90-90-90 progress. 20 August 2020 [cited 12 May 2021]. https://www.avert.org/infographics/malawi-90-90-90-progress
24. Vos T, Lim SS, Abbafati C, Abbas KM, Abbasi M, Abbasifard M, et al.; GBD 2019 Diseases and Injuries Collaborators. Global burden of 369 diseases and injuries in 204 countries and territories, 1990–2019: a systematic analysis for the Global Burden of Disease Study 2019. Lancet. 2020;396:1204–22. https://doi.org/10.1016/S0140-6736(20)30925-9
25. Chikovore J, Hart G, Kumwenda M, Chipungu GA, Desmond N, Corbett L. Control, struggle, and emergent masculinities: a qualitative study of men's care-seeking determinants for chronic cough and tuberculosis symptoms in Blantyre, Malawi. BMC Public Health. 2014;14:1053. https://doi.org/10.1186/1471-2458-14-1053

Address for correspondence: Rachael Burke, Malawi Liverpool Wellcome Clinical Research Programme, Queen Elizabeth Central Hospital, Chipatala Avenue, Blantyre, Malawi; email: rachael.burke@lshtm.ac.uk

Non–*C. difficile Clostridioides* Bacteremia in Intensive Care Patients, France

Guillaume Morel, Guillaume Mulier, Etienne Ghrenassia, Moustafa Abdel Nabey, Yacine Tandjaoui, Achille Kouatchet, Laura Platon, Frédéric Pène, Anne-Sophie Moreau, Amelie Seguin, Damien Contou, Romain Sonneville, David Rousset, Muriel Picard, Guillaume Dumas, Djamel Mokart, Bruno Megarbane, Guillaume Voiriot, Isabelle Oddou, Elie Azoulay, Lucie Biard, Lara Zafrani

Medscape EDUCATION ACTIVITY

In support of improving patient care, this activity has been planned and implemented by Medscape, LLC and Emerging Infectious Diseases. Medscape, LLC is jointly accredited by the Accreditation Council for Continuing Medical Education (ACCME), the Accreditation Council for Pharmacy Education (ACPE), and the American Nurses Credentialing Center (ANCC), to provide continuing education for the healthcare team.

Medscape, LLC designates this Journal-based CME activity for a maximum of 1.00 ***AMA PRA Category 1 Credit(s)™***. Physicians should claim only the credit commensurate with the extent of their participation in the activity.

Successful completion of this CME activity, which includes participation in the evaluation component, enables the participant to earn up to 1.0 MOC points in the American Board of Internal Medicine's (ABIM) Maintenance of Certification (MOC) program. Participants will earn MOC points equivalent to the amount of CME credits claimed for the activity. It is the CME activity provider's responsibility to submit participant completion information to ACCME for the purpose of granting ABIM MOC credit.

All other clinicians completing this activity will be issued a certificate of participation. To participate in this journal CME activity: (1) review the learning objectives and author disclosures; (2) study the education content; (3) take the post-test with a 75% minimum passing score and complete the evaluation at http://www.medscape.org/journal/eid; and (4) view/print certificate. For CME questions, see page 2007.

Release date: Jun 18, 2021; Expiration date: Jun 18, 2022

Learning Objectives

Upon completion of this activity, participants will be able to:

- Assess the background of patients with *Clostridioides* bacteremia (CB) in the current study
- Distinguish clinical features of severe CB in the current study
- Assess the microbiology of CB in the current study
- Identify risk factors for mortality due to CB in the current study

CME Editor

Dana C. Dolan, BS, Copyeditor, Emerging Infectious Diseases. *Disclosure: Dana C. Dolan, BS, has disclosed the following relevant financial relationships: employed by a commercial interest (spouse): Micro C Imaging.*

CME Author

Charles P. Vega, MD, Health Sciences Clinical Professor of Family Medicine, University of California, Irvine School of Medicine, Irvine, California. *Disclosure: Charles P. Vega, MD, has disclosed the following relevant financial relationships: served as an advisor or consultant for GlaxoSmithKline.*

Authors

Disclosures: ***Guillaume Morel, MD; Guillaume Mulier, MSc; Etienne Ghrenassia, MD; Moustafa Abdel-Nabey, MD; Yacine Tandjaoui, MD; Achille Kouatchet, MD;Laura Platon, MD; Anne-Sophie Moreau, MD; Amelie Seguin, MD; Damien Contou, MD; Romain Sonneville, MD, PhD; David Rousset, MD; Muriel Picard, MD; Guillaume Dumas, MD, PhD; Djamel Mokart, MD, PhD; Bruno Megarbane, MD, PhD; Guillaume Voiriot, MD; Isabelle Oddou, MD;*** *and* ***Lucie Biard, MD, PhD,*** *have disclosed no relevant financial relationships.* ***Frédéric Pène, MD, PhD,*** *has disclosed the following relevant financial relationships: served as an advisor or consultant for Gilead Sciences, Inc.; received grants for clinical research from Alexion Pharmaceuticals, Inc.* ***Elie Azoulay, MD, PhD,*** *has disclosed the following relevant financial relationships: served as an advisor or consultant for Gilead Sciences, Inc.; served as a speaker or a member of a speakers bureau for Astellas Pharma, Inc.; Gilead Sciences, Inc.; Merck Sharp & Dohme; received grants for clinical research from Ablynx NV; Alexion Pharmaceuticals, Inc.; Baxter; Fisher and Payckle, Gilead Sciences, Inc.; Jazz Pharmaceuticals, Inc.* ***Lara Zafrani, MD, PhD,*** *has disclosed the following relevant financial relationships: received grants for clinical research from: Jazz Pharmaceuticals, Inc.*

Author affiliations: Hautepierre Hospital—University Medical Center, Strasbourg, France (G. Morel); Hospital Saint Louis, APHP, Paris, France (G. Morel, G. Mulier, E. Ghrenassia, M.A. Nabey, E. Azoulay, L. Biard, L. Zafrani); Hospital Avicenne, Bobigny, France (Y. Tandjaoui); Teaching Hospital, Angers, France (A. Kouatchet); Lapeyronie University Hospital, Montpellier, France (L. Platon); Hospital Cochin, APHP, Paris (F. Pène); Salengro Hospital, Lille, France (A.-S. Moreau); University Hospital, Nantes, France (A. Seguin); Victor Dupouy Hospital, Argenteuil, France (D. Contou); Hospital Bichat, APHP, Paris (R. Sonneville); University Teaching Hospital, Toulouse, France (D. Rousset), Institut Universitaire du Cancer—Oncopole, Toulouse (M. Picard); Hospital Saint Antoine, APHP, Paris (G. Dumas); Paoli-Calmettes Institute, Marseille, France (D. Mokart); Hospital Lariboisiere, APHP, Paris (B. Megarbane); Hospital Tenon, APHP, Paris (G. Voiriot); University Medical Center, Strasbourg (I. Oddou); INSERM U976, Paris (L. Zafrani)

DOI: https://doi.org/10.3201/eid2707.203471

Usually responsible for soft tissue infections, *Clostridioides* species can also cause bacteremia, life-threatening infections often requiring intensive care unit (ICU) admission. We conducted a multicenter retrospective study to investigate *Clostridioides* bacteremia in ICUs to describe the clinical and biologic characteristics and outcomes in critically ill patients. We identified 135 patients with *Clostridioides* bacteremia, which occurred almost exclusively (96%) in patients with underlying conditions. Septic shock and digestive symptoms were the hallmarks of *Clostridioides* bacteremia in the ICU. We identified 16 different species of *Clostridioides*, among which *C. perfringens* accounted for 31% of cases. Despite the high sensitivity of *Clostridioides* to common antimicrobial drugs, mortality rates were high: 52% for ICU patients and 71% overall at 3 months. In multivariate analysis, the most important factor associated with increased risk for death was the presence of hemolysis. *Clostridioides* bacteremia often leads to multiple organ failures, which have high mortality rates.

Obligate anaerobic bacteremia is a rare event, accounting for ≈0.1%–10% of positive blood cultures; *Clostridioides* spp. bacteremia represents 8%–46% of the cases (*1*–*4*). *Clostridioides* (formerly *Clostridium*) species are ubiquitous, gram-positive, spore-forming (most species), and toxin-producing bacteria (*3*). The most well-known toxins, *C. perfringens* α and θ toxins, induce platelet aggregation, diffuse formation of thrombi, cell lysis, and gas gangrene (*5*). Anaerobic bacteria are not only found in the soil or rotting vegetation but also are commensal constituents of the human microbiome, especially in the gastrointestinal tract or genital organs of women (*3*,*6*). Humans are usually infected by direct entry of the bacteria through a wound (*C. tetani*, *C. perfringens*) or by contaminated food (*C. botulae*). However, contamination of a wound by spores is not sufficient to generate the infection because *Clostridioides* spp. need hypoxic and acidic conditions to proliferate. Conditions such as vascular trauma, atherosclerosis, or malignancies may induce tissue hypoxia. Moreover, the liberation of both α and θ toxin, which induce the formation of occlusive thrombi, may increase tissue hypoxia, sometimes leading to gas gangrene formation (*3*,*7*–*9*).

Thus, *Clostridioides* infections are especially known to cause myonecrosis with rapid extension and gas gangrene formation, which, if not treated rapidly, may be fatal. This outcome has largely been described in the context of war wounds, trauma, and surgery (*10*–*12*). Although *C. perfringens* is mostly involved in gas gangrene, other *Clostridioides* subspecies can also be responsible for such infections (*13*).

Clostridioides bacteria can also cause primary bacteremia, with or without gas gangrene (*2*,*6*). *Clostridioides* bacteremia are usually fulminant and life-threatening infections. Data focusing on *Clostridioides* bacteremia rely mainly on case reports (*14*–*16*), case series on selected populations (*17*,*18*), or larger epidemiologic series that contain microbiological data but few clinical descriptions (*2*,*19*,*20*). Although *Clostridioides* bacteremia often leads to sudden and massive organ failure requiring transfer to a hospital intensive care unit (ICU), no study has focused on *Clostridioides* bacteremia in the ICU. Therefore, we conducted a multicenter retrospective study of case-patients who were positive for all *Clostridioides* species except *C. difficile* to investigate *Clostridioides* bacteremia in the ICU; we described the clinical spectrum of critically ill patients, ICU admission conditions, microbiological characteristics, and outcomes. We aimed to identify risk factors associated with mortality.

Methods

Ethics

This study was approved by an Institutional Review Board (Comité d'Ethique de la Société de Réanimation de Langue Française no. CE-SRLF 18–38) in accordance with the French regulation on noninterventional studies, which waived the need for signed informed consent for patients included in this database. No data allowing identification of the patients included in the study were recorded. The study was conducted in accordance with the Declaration of Helsinki principles.

Study Population

We retrospectively recorded cases of *Clostridioides* bacteremia in the period July 2003–December 2018 in 15 ICUs in France. Patients were identified by review of ICU medical records and hospital microbiological databases; we selected only cases with ≥1 positive blood culture for all *Clostridioides* species except *C. difficile*. Blood samples had been collected with specific anaerobic blood culture bottles and incubated in automated systems, in accordance with routine practice (*21*). Anaerobes were identified using the API System (bioMérieux, https://www.biomerieux.com) until 2010; as of 2010, matrix-assisted laser desorption/ionization time-of-flight mass spectrometry methods were used in most of the centers to identify anaerobic bacteria (*3*,*22*). Antimicrobial susceptibility test results of *Clostridioides* species, evaluated by diffusion methods according to guidelines of the Comité

de l'Antibiogramme de la Société Française de Microbiologie, were also collected for our study.

We reviewed ICU medical records of selected patients for age, sex, underlying diseases, clinical and biologic symptoms at ICU admission, the need for organ support, antimicrobial drug treatment, and outcome. We recorded Charlson index, simplified acute physiology score (SAPS2), and sequential organ failure assessment (SOFA) scores as previously defined (*23*–*25*). We defined septic shock according to the Sepsis-3 consensus definition (*26*) and hemolysis as low hemoglobin level associated with other hemolysis parameters, such as an increase of lactate dehydrogenase (LDH) or unconjugated bilirubin and reduced haptoglobin levels.

Statistical Analysis

We described categorical variables as counts and percentages and quantitative variables as median and interquartile range. We estimated mortality rate at 28 days and 90 days after the date of bacteremia, as a binary variable, and examined factors associated with overall survival as a time-to-event endpoint. We defined overall survival as the time between the date of *Clostridioides* bacteremia and the date of death or last follow-up, whichever occurred first. We performed survival analysis using a Cox regression model, estimating hazard ratios (HR) and 95% CIs. We checked the proportional hazards (PH) assumption and the log-linearity assumptions for the models; if the PH assumption was not valid, we used time-dependent coefficient for time-varying effect over time; we used a step function, with time-intervals defined based on the Schoenfeld's residuals. Factors which were associated to OS with a $p<0.1$ in univariate analysis were candidates for a multivariate adjusted model. We selected the adjusted model using a backward stepwise procedure, based on the Akaike criterion. All tests were 2-sided; $p<0.05$ was considered significant. We performed analyses by using the R statistical platform version 3.6.1 (https://www.r-project.org).

Results

Clinical and Biologic Manifestations

In total, 135 patients with *Clostridioides* bacteremia were identified in 15 ICUs in France during the study period (Table 1); 60% (n = 81) of the patients were men. Median age at diagnosis was 64 years. Most (96%) patients had ≥1 underlying medical condition; among patients >65 years of age, diabetes mellitus, neoplasms, and chronic obstruction pulmonary disease (COPD) were the most frequent. Thirty-four (26%) patients had an underlying solid tumor from digestive (n = 14, 41%), gynecological (n = 7, 21%), and pancreatic or biliary (n = 4, 12%) origins. Three patients (9%) had urinary tract tumors, 2 (6%) neuroendocrine tumors, 1 (3%) an Ewing tumor, 1 (3%)

Table 1. Global characteristics of patients with *Clotristridioides* bacteremia, France*

Characteristic	Baseline population, n = 135	Survived, n -= 65	Died in ICU, n = 70
Age			
Age at diagnosis, median (IQR)	64 (51–75)	62 (50–70)	66 (54–79)
Age at diagnostic >65 y	67 (50)	27 (42)	40 (57)
Sex			
M	81 (60)	43 (66)	38 (54)
F	54 (40)	22 (33)	32 (46)
All underlying conditions	130 (96)	62 (95)	68 (97)
Diabetes mellitus	34 (26)	19 (31)	15 (22)
Neoplasm	34 (26)	17 (27)	17 (25)
Chronic obstructive pulmonary disease	33 (25)	15 (24)	18 (26)
Alcoholism	26 (20)	11 (18)	15 (22)
Heart failure	26 (20)	9 (15)	17 (25)
Hematological malignancy	19 (15)	7 (11)	12 (18)
Liver cirrhosis	13 (10)	4 (6)	9 (13)
Chronic renal failure	10 (8)	8 (13)	2 (3)
Arteriopathy	9 (7)	3 (5)	6 (9)
Autoimmune diseases	7 (5)	4 (6)	3 (4)
HIV	1 (1)	0	1 (1)
Other predisposing conditions			
Surgery or trauma in the previous 15 d	13 (10)	10 (16)	3 (4)
Digestive surgery	10 (77)	7 (70)	3 (100)
Trauma	3 (23)	3 (30)	0
Immunosuppressive agents			
Patients receiving Immunosuppressive agents	38 (28)	18 (28)	20 (29)
Steroids	20 (53)	9 (50)	11 (55)
Chemotherapy	20 (53)	9 (50)	11 (55)
Immunosuppressive drugs	10 (26)	6 (33)	4 (20)

*Data are no. (%) unless otherwise indicated.

oral cancer, and 1 (3%) testicular cancer. In all, 94% of tumors were active at the time of the bacteremia. Nineteen (15%) patients had also received diagnoses of hematological malignancies (7 lymphoma, 4 acute lymphoblastic leukemia, 4 myelodysplastic syndrome, 3 acute myeloid leukemia, and 1 myeloproliferative disorder); 3 of those patients had undergone bone marrow transplantation. Thirty-eight patients (28%) had been treated with immunosuppressive agents. In addition, 13 (10%) patients had experienced recent surgery or trauma, and these situations were associated with a better outcome in univariate analysis (Appendix Figure 1, http://wwwnc.cdc.gov/EID/article/27/7/20-3471-App1.pdf). However, this difference was not significant in multivariate analysis (HR 0.41, 95% CI 0.13–1.32; p = 0.13) (Figure 1).

Clostridioides bacteremia manifested with septic shock at ICU admission in 115 patients (85%), and 26 (19%) patients experienced a cardiac arrest in the ICU (Table 2). Indeed, *Clostridioides* bacteremia causes severe illness, as assessed by high SAPS2 and SOFA scores, high lactate levels, and substantial need for organ supports during an ICU stay. Of note, digestive symptoms were the main symptoms associated with *Clostridioides* bacteremia (62% of patients), whereas myonecrosis represented only 16% of ICU admissions. Acute hemolysis, a distinctive biologic signature of *Clostridioides* bacteremia, was present in 22 (17%) cases (Appendix Table 1). Median hemoglobin level was significantly lower in the hemolysis group (4.9, IQR 3.6–7.0) compared with the rate in patients without hemolysis (10.9, IQR 9.3–12.6; p<0.001). Multiple organ failure, experienced as hepatic cytolysis, acute kidney injury and thrombocytopenia (Table 2), was also common. Of note, aspartate aminotransferase levels were higher than alanine aminotransferase levels, which is commonly found in case of hemolysis. Twenty-seven patients (28%) had <4 × 10^9 leukocytes/L; 23 (85%) of those had an underlying solid tumor or a hematological malignancy.

Documentation of Infectious Species

In total, 16 different *Clostridioides* species were identified by blood cultures, including *C. perfringens* in one third of the patients (Table 3; Figure 2). In univariate analysis, documented *C. perfringens* infection was not associated with a worse outcome than other *Clostridioides* species (HR 0.78, CI 95% 0.49–1.23; p = 0.285) (Appendix Figure 2). Blood cultures were mainly performed by peripheral venipuncture (58%), followed by central venous catheter puncture (23%) and arterial catheter puncture (17%). One blood culture revealed *Clostridioides* bacteremia in 87% of cases. Of note, 49 cases of *Clostridioides* bacteremia were polymicrobial bacteremia, yielding the presence of ≥1 type of bacteria in blood cultures, balanced between gram-negative, gram-positive, and other anaerobic bacteria. Nine patients had both gram-negative and gram-positive bacteria cultures. Hematogenous spread with gas-forming abscess was one particular complication,

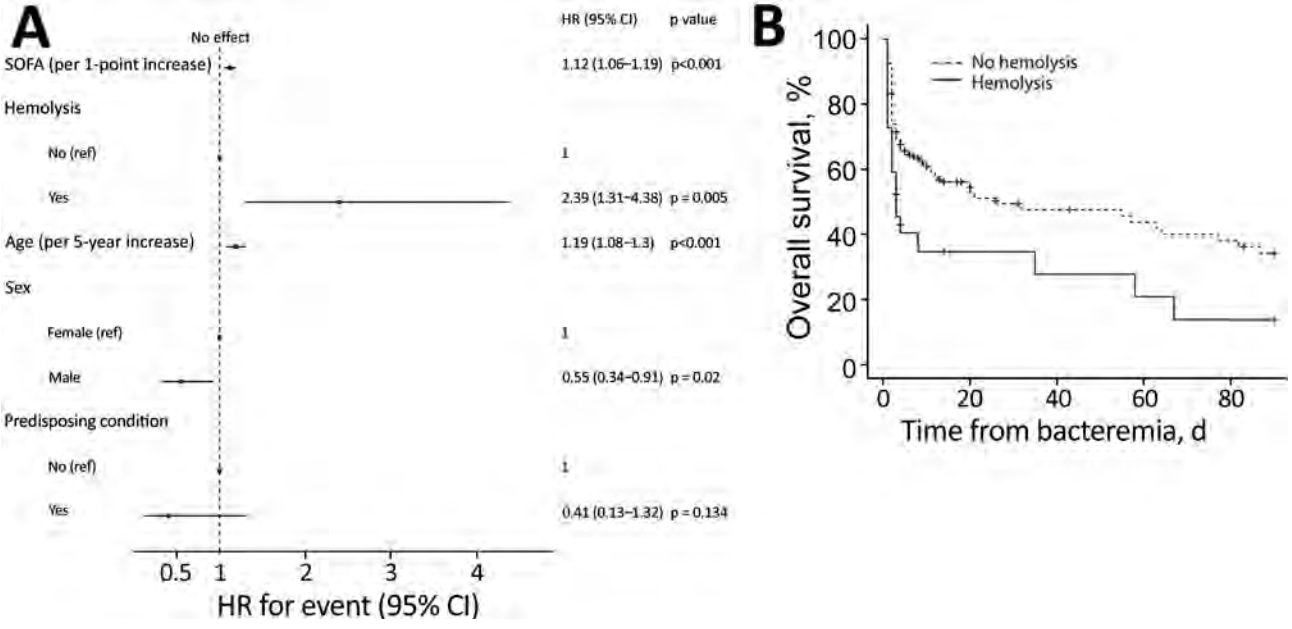

Figure 1. Survival analysis with Cox regression model for patients with *Clostridiodes* bacteremia, France. A) Forest plot of multivariate factors associated with overall survival. Predisposing conditions were trauma or surgery. B) Kaplan-Meier curve of mortality depending on hemolysis. HR, hazard ratio; ref, referent; SOFA, sequential organ failure assessment.

Table 2. Clinical and biologic characteristics of patients with *Clostridiodes* bacteremia, France*

Characteristic	All patients, n = 135		Survived, n = 65		Died in ICU, n = 70	
	No.	Result	No.	Result	No.	Result
Temperature	75	37 (36–39)	30	38.5 (37.3–39)	45	37 (35.6–38.7)
Clinical manifestations associated with bacteremia at ICU admission						
Septic shock	115	85%	49	75%	66	94%
Digestive symptoms	84	62%	42	65%	42	60%
Acute respiratory failure	41	30%	15	23%	26	37%
Coma	38	28%	6	9%	32	46%
Cardiac arrest	26	19%	2	3%	24	34%
Myonecrosis	21	16%	11	17%	10	14%
Prognostic scores at ICU admission						
Charlson score	135	5 (3–6)	65	5 (2–7)	70	4.5 (3–6)
SAPS2 score	106	63 (44–88)	47	45 (33–57)	59	82 (63–97)
SOFA score	105	10 (7–14)	47	8 (5–10)	58	12 (9–15)
Organ support in ICU						
Vasopressors, n = 132	108	82%	42	66%	66	97%
Mechanical ventilation, n = 133	105	79%	41	63%	64	94%
Renal-replacement therapy, n = 131	44	34%	17	26%	27	41%
Biologic parameters at ICU admission						
Leukocytes, $\times 10^9$/L	97	9.5 (2.8–17.8)	49	9.5 (6.1–20.2)	48	9.3 (1.6–16.0)
Platelets, $\times 10^9$/L	93	141 (76–214)	45	143 (73–217)	48	138 (84–206)
Hemoglobin, g/dL	92	10.3 (7.8–12.2)	45	10.2 (8.8–12.2)	47	10.3 (7.0–11.9)
Hemolysis, n = 130	22	17%	6	9%	16	24%
Acute renal failure, n = 107						
KDIGO classification 1	14	13%	10	20%	4	7%
KDIGO classification 2	34	32%	19	38%	15	26%
KDIGO classification 3	59	55%	21	42%	38	67%
Other						
Aspartate aminotransferase, U/L	80	92 (41–269)	38	71 (41–172)	42	134 (44–346)
Alanine aminotransferase, U/L	81	54 (25–142)	39	47 (21–125)	42	69 (27–152)
Bilirubin, µmol/L	69	22 (10–45)	34	27 (10.3–52.3)	35	19.5 (10.5–35.7)
Lactatemia, mmol/L	93	5.3 (2.3–8.8)	40	3.2 (1.5–5.2)	53	8 (4.9–12)
pH	93	7.29 (7.13–7.4)	40	7.38 (7.32–7.43)	53	7.18 (7.05–7.31)

*Results are given as percentages or median (interquartile range). ICU, intensive care unit; KDIGO, Kidney Disease: Improving Global Outcomes (https://kdigo.org); SAPS2, simplified acute physiology score (SAPS2); SOFA, sequential organ failure assessment.

found in 9 patients and leading to death in 5 in the ICU (Figure 3, panels A–C). As suggested by clinical symptoms, cases of bacteremia were mostly from the gastrointestinal tract (74%), followed by myonecrosis (16%) (Figure 3, panels D–E). In total, 110 (91%) of the patients were treated with antimicrobial drugs in the ICU, and 64 (47%) patients underwent surgery that was mostly gastrointestinal surgery (67% of surgery interventions).

Most strains of *Clostridioides* were sensitive to β-lactam drugs. *Clostridioides* species were sensitive to clindamycin in 69% of the cases. Two species (*C. tertium* and *C. septicum*) were resistant to metronidazole. We did not find any association between specific antimicrobial agents used to treat *Clostridioides* bacteremia and mortality (HR 1.01, 95% CI 0.57–1.77; p = 0.977) (Appendix Table 2).

Outcomes and Mortality Risk Factors

Although *Clostridioides* spp. were for the most part efficiently treated by common antimicrobial drugs, *Clostridioides* bacteremia remained very aggressive and life-threatening; the overall mortality rate at 6 months was 71%. Of 135 patients, 84 died; 70 (52%) of all patients died in the ICU. The 28-day mortality rate was 55% (95% CI 45%–64%), and the 90-day mortality rate was 71% (95% CI 60%–79%). The rapid need for hospitalization after the occurrence of the first symptoms (median days 0, IQR 0–1) highlighted the aggressiveness of *Clostridioides* bacteremia; direct ICU transfer was necessary in most cases (median time between hospitalization and ICU transfer 0 days, IQR 0–2). Median length of stay in ICU was 2 days for patients who did not survive (IQR 1.25–5.75) and 11 days for survivors (IQR 5–23).

In multivariate analysis for overall survival, factors associated with increased risk for death were increasing age (in 5-year increments) (HR 1.19, 95% CI 1.08–1.31; p<0.001), increasing SOFA score (per point) (HR 1.12, 95% CI 1.06–1.19; p<0.001), and presence of hemolysis (HR 2.39, 95% CI 1.31–4.38; p = 0.005). On the other hand, male sex was associated with a reduced risk for death (HR 0.56, 95% CI 0.34–0.91; p = 0.02) (Figure 2).

Discussion

In our study, we found that *Clostridioides* bacteremia is an aggressive and rapidly life-threatening infec-

tion, occurring mainly in patients with underlying conditions. Septic shock with digestive symptoms is the usual manifestation. Despite rapid transfer to the ICU, large use of organ support, and active antimicrobial treatment, *Clostridioides* bacteremia remains highly lethal; 52% of ICU patients died. Massive intravascular hemolysis, associated with fatal complications, should alert clinicians to the possibility of sepsis.

Data on *Clostridioides* bacteremia consist mainly of case reports (*14*–*16*,*27*) or case series that include a small number of patients (*17*,*28*–*30*). Larger publications focusing on anaerobic bacteremia do not provide details on patients' characteristics and outcomes (*2*,*19*). Furthermore, we could find no previous publications on *Clostridioides* bacteremia in ICU patients, even though anaerobic bacteremia is frequent in this population (*2*,*31*). Our study provides a thorough description of the clinical and biologic characteristics as well as the outcomes of this serious condition.

Table 3. Characteristics of non–*C. difficile* bacteria in cases of *Clostridioides* bacteremia, France

Characteristic	No. (%) patients		
	All patients, n = 135	Survived, n = 65	Died in ICU, n = 70
Clostridium species			
Perfringens	42 (31)	16 (25)	26 (37)
Ramosum	18 (13)	10 (15)	8 (11)
Any *Clostridioides* sp.	16 (12)	6 (9)	10 (14)
Tertium	14 (10)	9 (14)	5 (7)
Clostridiforme	12 (9)	8 (12)	4 (6)
Septicum	10 (7)	2 (3)	8 (11)
Innocuum	6 (4)	5 (8)	1 (1)
Butyricum	4 (3)	2 (3)	2 (3)
Paraputrificum	3 (2)	2 (3)	1 (1)
Baratii	2 (1)	1 (2)	1 (1)
Orbiscindens	2 (1)	1 (2)	1 (1)
Sporogenes	2 (1)	1 (2)	1 (1)
Cadaveris	1 (1)	0 (0)	1 (1)
Novyi	1 (1)	1 (2)	0 (0)
Sordellii	1 (1)	0 (0)	1 (1)
Symbosium	1 (1)	1 (2)	0 (0)
No. positive blood cultures for *Clostridioides* spp.			
1	117 (87)	52 (80)	65 (93)
2	13 (10)	9 (14)	4 (6)
3	5 (4)	4 (6)	1 (1)
Other microbes associated with *Clostridioides* bacteremia, n = 49		27	22
Gram-negative bacteria	33 (67)	20 (74)	13 (59)
Gram-positive bacteria	24 (49)	12 (44)	12 (55)
Candida fungemia	1 (2)	1 (4)	0 (0)
Effectiveness of tested antimicrobial drugs against *Clostridioides* species			
Penicillin, n = 84	83 (99)	37 (100)	46 (98)
Clindamycin, n = 67	46 (69)	22 (67)	24 (71)
Vancomycin, n = 67	67 (100)	33 (100)	34 (100)
Metronidazole, n = 84	82 (98)	36 (97)	46 (98)
Patients receiving drugs	110 (91)	64 (98)	46 (82)
Beta-lactams	102 (94)	60 (94)	42 (95)
Amoxicillin/clavulanic acid	9 (9)	6 (10)	3 (7)
Piperacillin/tazobactam	46 (45)	25 (42)	21 (50)
Cephalosporins	22 (22)	15 (25)	7 (17)
Carbapenems	26 (25)	15 (25)	11 (26)
Aminoglycoside	58 (54)	34 (53)	24 (55)
Anti–gram positive bacteria	46 (43)	29 (45)	17 (39)
Metronidazole	39 (36)	26 (41)	13 (30)
Others	10 (9)	5 (8)	5 (11)
Missing data	2	0	2
Origin of bacteremia			
Digestive origin	87 (74)	43 (70)	44 (79)
Bowel pathology	33 (28)	14 (23)	19 (34)
Mesenteric ischemia	25 (21)	7 (11)	18 (32)
Peritonitis	19 (16)	16 (26)	3 (5)
Pancreatic or biliary origin	10 (9)	6 (10)	4 (7)
Myonecrosis	19 (16)	11 (18)	8 (14)
Abscess	8 (7)	5 (8)	3 (5)
Pneumonia	3 (3)	2 (3)	1 (2)
Missing data	18	4	14

Our results are consistent with earlier reports; most *Clostridioides* bacteremia cases occur in patients >65 years of age, and prevalence is higher in men (*17*,*29*,*31*). Diseases such as diabetes, chronic kidney disease, heart failure, and COPD, which maintain a baseline degree of organ ischemia and cause chronic organ failure, can lead to *Clostridioides* proliferation and consequently to bacteremia (*1*,*19*,*29*,*31*). Cancer patients or patients with hematological malignancies are also at high risk (*18*,*32*). Chemotherapy-induced cytopenia may result in neutropenic enterocolitis (*33*); this impairment of the natural digestive barrier favors the development of *Clostridioides* bacteremia. Digestive symptoms that have been described as hallmarks of this condition (*1*,*17*,*29*) were frequently associated with *Clostridioides* bacteremia in the ICU. Of note, although *Clostridioides* bacteremia is mostly from digestive origins, myonecrosis was identified as the origin of the bacteremia in 16% of the cases in our study, which is consistent with previous reports (*17*,*18*,*29*,*31*).

Among *Clostridioides* species, *C. perfringens* was more often identified as the source of bacteremia, as previously published (*1*,*19*,*34*). Fifteen other *Clostridioides* species have been identified; distribution is similar to the one described by Leal et al. (*19*). In this study, we chose to exclude *C. difficile* infections because this pathogen is mainly responsible for healthcare-associated digestive infections. *C. difficile* can still present as extradigestive infections; however, few cases of bacteremia have been reported (*35*,*36*).

Data on incidence of anaerobic and *Clostridioides* bacteremia are conflicting. Some authors report an increasing incidence of anaerobic bacteremia since the 1990s, whereas other report decreasing trends (*2*,*6*,*20*,*37*). The incidence of anaerobic bacteremia depend on patients' age and underlying conditions (especially cancer or cardiovascular illness), and antibiotic selection pressure driven by antimicrobial drug use and environmental conditions. In addition, as suggested by Morris et al. (*38*), blood cultures for anaerobic bacteria may be influenced by patients' background and clinical symptoms. Indeed, in a recent study evaluating anaerobic bacteremia, 39.7% of the positive blood cultures were considered to be bloodstream infections; the remaining 60.3% were attributed to contaminants (*39*). The evolution of microbiologic techniques, including growing use of automated techniques and matrix-assisted laser desorption/ionization time-of-flight mass spectrometry, might have also influenced the increasing isolation of anaerobic bacteremia. Although we cannot rule out that some infections may have been overestimated, the severity of clinical presentations in our cohort suggests that these cases resulted from true bloodstream infections.

Of note, *Clostridioides* bacteremia can present either as a single microbial bacteremia or as a polymicrobial bacteremia (*2*,*28*,*30*,*31*). *Enterobacteriaceae* were the most commonly associated bacteria, followed by *Staphylococcus* species. Cultures for multiple microbes were positive for *Clostridioides* spp. in 18 patients. Comparable results were also found by Fujita et al. (*17*). *Clostridioides* species are largely susceptible to common antimicrobial drugs, except for clindamycin; susceptibility for clindamycin has been reported as reduced by 73%–96% (*1*,*3*,*5*,*19*,*31*). High susceptibility to penicillin should alert clinicians to rapidly initiate treatment in identified cases of *Clostridioides* bacteremia.

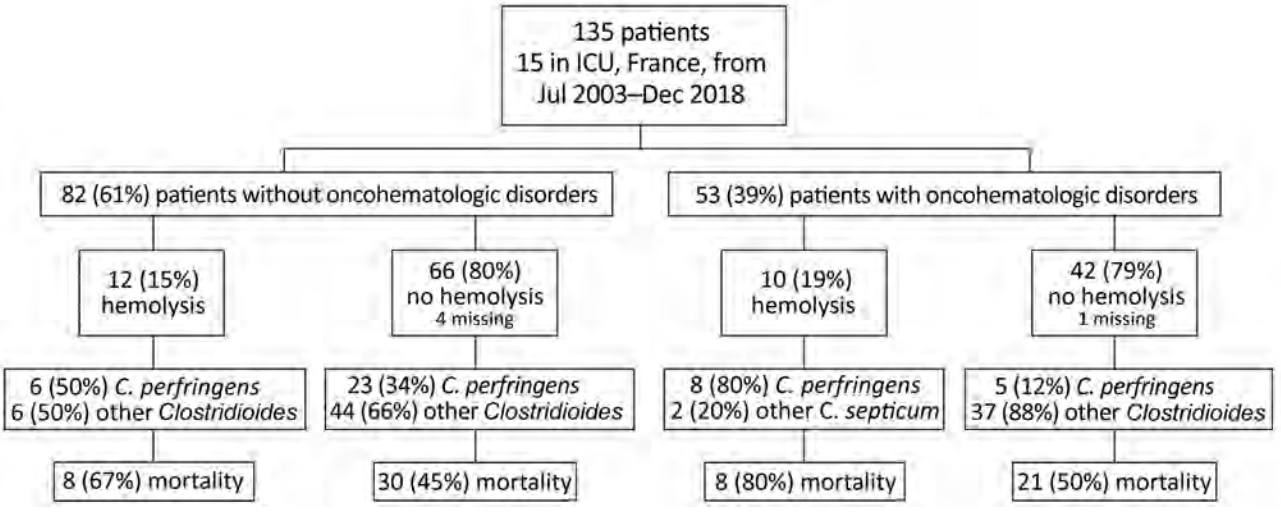

Figure 2. Flowchart of the repartition of *Clostridioides* bacteremia in patients in France according to the presence or absence of hemolysis. Hemolysis was associated with a high mortality rate.

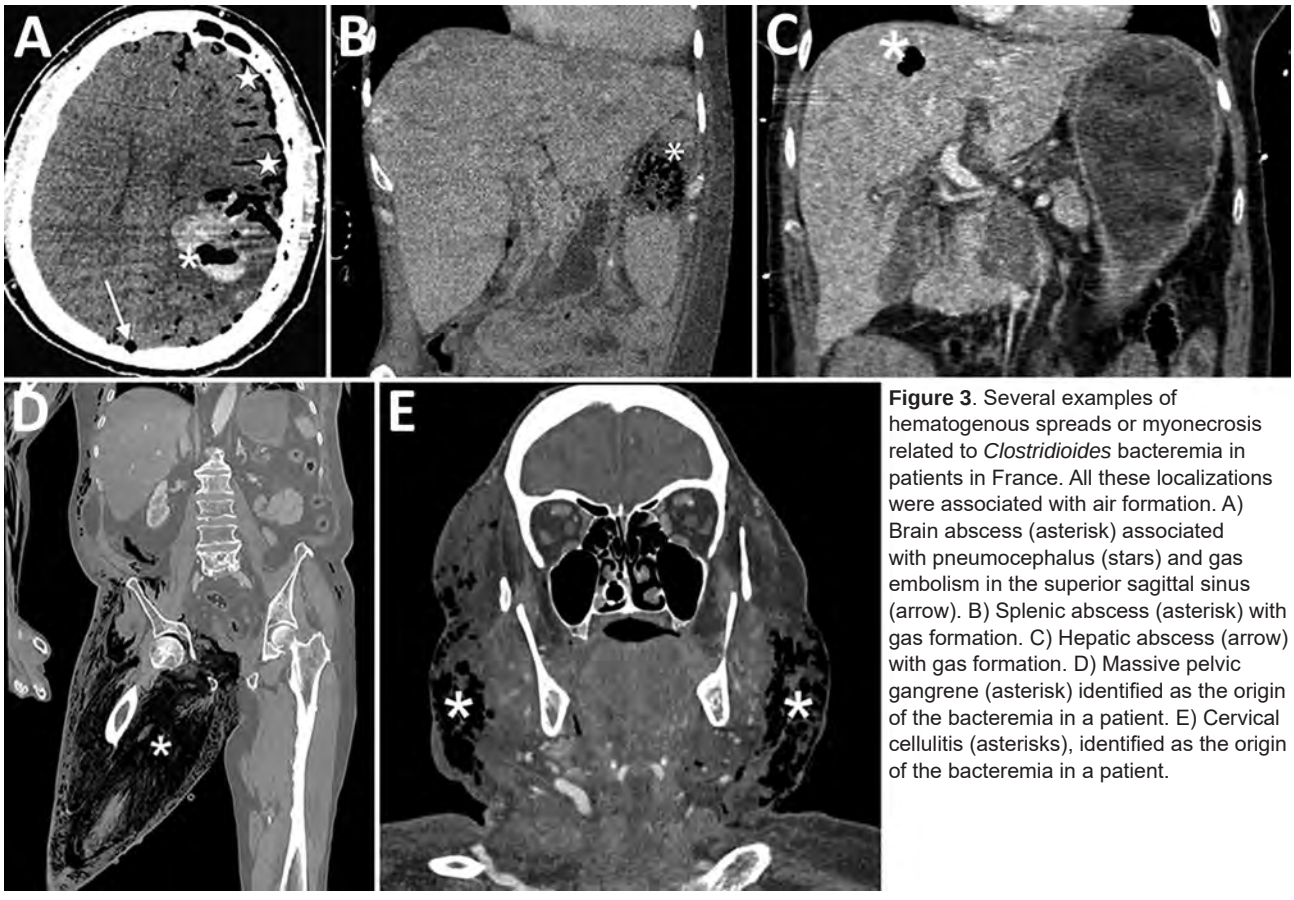

Figure 3. Several examples of hematogenous spreads or myonecrosis related to *Clostridioides* bacteremia in patients in France. All these localizations were associated with air formation. A) Brain abscess (asterisk) associated with pneumocephalus (stars) and gas embolism in the superior sagittal sinus (arrow). B) Splenic abscess (asterisk) with gas formation. C) Hepatic abscess (arrow) with gas formation. D) Massive pelvic gangrene (asterisk) identified as the origin of the bacteremia in a patient. E) Cervical cellulitis (asterisks), identified as the origin of the bacteremia in a patient.

Because 94% of the patients in our study received adequate antimicrobial drugs within 24 hours of ICU admission, we were not able to find any statistical association between early initiation of drugs and death. However, in a recent study published by Stabler et al. (*34*), adequate empiric antimicrobial therapy was associated with a better outcome. This result was also highlighted previously by Zahar et al. (*18*).

Mortality rates for *Clostridioides* bacteremia reported in the literature were 15%–48% (*17*–*19*,*28*–*31*), which is lower than the mortality rates reported in our study. Indeed, Yang (31) and Fujita (17) revealed that patients who developed shock and required transfer to the ICU had worse outcomes than other patients. In those studies, shock was statistically associated with increased deaths. The prognosis for *Clostridioides* bacteremia patients is also related to underlying conditions that predispose to *Clostridioides* bacteremia and possibilities of therapeutic interventions in addition to prompt and appropriate antimicrobial drugs. As demonstrated by Rechner et al. (*1*), patients who required medical intervention to treat *Clostridioides* bacteremia had lower survival rates than patients who were managed by surgery. Conversely, the presence of massive intravascular hemolysis is a marker of extreme severity, despite appropriate management (*16*,*40*). Hemolysis is induced by *Clostridioides* toxin A (*29*), which hydrolyzes phospholipids in erythrocyte membranes, causing spherocytosis and subsequent intravascular hemolysis. Present in 17% of patients in our cohort, hemolysis is associated with a dramatic increase in mortality rate and remains a strong prognostic factor identified in our study. Finally, *Clostridioides* bacteremia in the ICU is associated with a higher mortality rate than that for classic septic shock in the ICU (*41*,*42*), which makes *Clostridioides* bacteremia a particularly difficult infection to deal with in the ICU.

The first limitation of our study is its retrospective nature and the inherently associated bias, such as missing data and unidentified confounding factors that may have been overlooked in the data collection. However, because of the rarity of *Clostridioides* bacteremia, prospective studies would hardly be feasible. Second, there are no standardized ICU admission policies for these patients, and patient recruitment patterns may have influenced the findings. Given the rapidity of the onset of symptoms and the severity

of illness, rapid ICU management was the rule in the participating centers. However, we could not exclude that some patients, because of their advanced age or underlying conditions, were considered too sick for admission to the ICU and may have been denied intensive care.

In conclusion, *Clostridioides* bacteremia is an aggressive infection that often leads to failure of multiple organs, requiring prompt intensive care management. Particular attention should be paid to patients who have underlying conditions and are experiencing hemolysis. Early administration of antimicrobial agents active against *Clostridioides* bacteremia is essential, considering that most *Clostridioides* species are sensitive to β-lactams drugs. Even with prompt and appropriate management, however, *Clostridioides* bacteremia is associated with a high mortality rate in the ICU.

About the Author

Dr. Morel is a specialist in intensive care at the medical intensive care unit of Hautepierre Hospital—University Medical Center, Strasbourg, France. His primary expertise is in infectious diseases and immunocompromised patients.

References

1. Rechner PM, Agger WA, Mruz K, Cogbill TH. Clinical features of clostridial bacteremia: a review from a rural area. Clin Infect Dis. 2001;33:349–53. https://doi.org/10.1086/321883
2. Gajdács M, Ábrók M, Lázár A, Terhes G, Urbán E. Anaerobic blood culture positivity at a university hospital in Hungary: a 5-year comparative retrospective study. Anaerobe. 2020;63:102200. https://doi.org/10.1016/j.anaerobe.2020.102200
3. Gajdács M, Spengler G, Urbán E. Identification and antimicrobial susceptibility testing of anaerobic bacteria: Rubik's cube of clinical microbiology? Antibiotics (Basel). 2017;6:25. https://doi.org/10.3390/antibiotics6040025
4. Blairon L, De Gheldre Y, Delaere B, Sonet A, Bosly A, Glupczynski Y. A 62-month retrospective epidemiological survey of anaerobic bacteraemia in a university hospital. Clin Microbiol Infect. 2006;12:527–32. https://doi.org/10.1111/j.1469-0691.2006.01407.x
5. Stevens DL, Aldape MJ, Bryant AE. Life-threatening clostridial infections. Anaerobe. 2012;18:254–9. https://doi.org/10.1016/j.anaerobe.2011.11.001
6. Gajdács M, Urbán E. Relevance of anaerobic bacteremia in adult patients: a never-ending story? Eur J Microbiol Immunol (Bp). 2020;10:64–75. https://doi.org/10.1556/1886.2020.00009
7. Bryant AE, Chen RY, Nagata Y, Wang Y, Lee CH, Finegold S, et al. Clostridial gas gangrene. I. Cellular and molecular mechanisms of microvascular dysfunction induced by exotoxins of *Clostridium perfringens*. J Infect Dis. 2000;182:799–807. https://doi.org/10.1086/315756
8. Bryant AE, Chen RY, Nagata Y, Wang Y, Lee CH, Finegold S, et al. Clostridial gas gangrene. II. Phospholipase C–induced activation of platelet gpIIbIIIa mediates vascular occlusion and myonecrosis in *Clostridium perfringens* gas gangrene. J Infect Dis. 2000;182:808–15. https://doi.org/10.1086/315757
9. Ohyama K, Fujimoto M, Nakagomi Y, Ohta M, Yamori T, Kato K. Effect of cyproterone acetate on active and inactive renin secretion in patients with precocious puberty and genetic short stature. Horm Res. 1991;36:216–9. https://doi.org/10.1159/000182166
10. Takazawa T, Ohta J, Horiuchi T, Hinohara H, Kunimoto F, Saito S. A case of acute onset postoperative gas gangrene caused by *Clostridium perfringens*. BMC Res Notes. 2016;9:385. https://doi.org/10.1186/s13104-016-2194-0
11. North JP. Clostridial wound infections and gas gangrene; arterial damage as a modifying factor. Surgery. 1947;21:364–72.
12. MacLennan JD. The histotoxic clostridial infections of man. Bacteriol Rev. 1962;26:177–276. https://doi.org/10.1128/BR.26.2_Pt_1-2.177-274.1962
13. Srivastava I, Aldape MJ, Bryant AE, Stevens DL. Spontaneous *C. septicum* gas gangrene: a literature review. Anaerobe. 2017;48:165–71. https://doi.org/10.1016/j.anaerobe.2017.07.008
14. Shen A, Ologun GO, Behm R. Fulminant hepatic failure and fatal cerebral edema following *Clostridium perfringens* bacteremia: case report and review of literature. Cureus. 2017;9:e1714. https://doi.org/10.7759/cureus.1714
15. Wazir M, Jain AG, Nadeem M, Ur Rahman A, Everett G. *Clostridium tertium* bacteremia in a non-neutropenic patient with liver cirrhosis. Cureus. 2019;11:e4432. https://doi.org/10.7759/cureus.4432
16. Simon TG, Bradley J, Jones A, Carino G. Massive intravascular hemolysis from *Clostridium perfringens* septicemia: a review. J Intensive Care Med. 2014;29:327–33. https://doi.org/10.1177/0885066613498043
17. Fujita H, Nishimura S, Kurosawa S, Akiya I, Nakamura-Uchiyama F, Ohnishi K. Clinical and epidemiological features of *Clostridium perfringens* bacteremia: a review of 18 cases over 8 year-period in a tertiary care center in metropolitan Tokyo area in Japan. Intern Med. 2010;49:2433–7. https://doi.org/10.2169/internalmedicine.49.4041
18. Zahar JR, Farhat H, Chachaty E, Meshaka P, Antoun S, Nitenberg G. Incidence and clinical significance of anaerobic bacteremia in cancer patients: a 6-year retrospective study. Clin Microbiol Infect. 2005;11:724–9. https://doi.org/10.1111/j.1469-0691.2005.01214.x
19. Leal J, Gregson DB, Ross T, Church DL, Laupland KB. Epidemiology of *Clostridium* species bacteremia in Calgary, Canada, 2000–2006. J Infect. 2008;57:198–203. https://doi.org/10.1016/j.jinf.2008.06.018
20. De Keukeleire S, Wybo I, Naessens A, Echahidi F, Van der Beken M, Vandoorslaer K, et al. Anaerobic bacteraemia: a 10-year retrospective epidemiological survey. Anaerobe. 2016;39:54–9. https://doi.org/10.1016/j.anaerobe.2016.02.009
21. Kirn TJ, Weinstein MP. Update on blood cultures: how to obtain, process, report, and interpret. Clin Microbiol Infect. 2013;19:513–20. https://doi.org/10.1111/1469-0691.12180
22. Lévesque S, Dufresne PJ, Soualhine H, Domingo MC, Bekal S, Lefebvre B, et al. A side by side comparison of Bruker Biotyper and VITEK MS: utility of MALDI-TOF MS technology for microorganism identification in a public health reference laboratory. PLoS One. 2015;10:e0144878. https://doi.org/10.1371/journal.pone.0144878
23. Moreno R, Vincent JL, Matos R, Mendonça A, Cantraine F, Thijs L, et al. Working Group on Sepsis-

related Problems of the ESICM. The use of maximum SOFA score to quantify organ dysfunction/failure in intensive care. Results of a prospective, multicentre study. Intensive Care Med. 1999;25:686–96. https://doi.org/10.1007/s001340050931
24. Charlson ME, Pompei P, Ales KL, MacKenzie CR. A new method of classifying prognostic comorbidity in longitudinal studies: development and validation. J Chronic Dis. 1987;40:373–83. https://doi.org/10.1016/0021-9681(87)90171-8
25. Le Gall JR, Lemeshow S, Saulnier F. A new Simplified Acute Physiology Score (SAPS II) based on a European/North American multicenter study. JAMA. 1993;270:2957–63. https://doi.org/10.1001/jama.1993.03510240069035
26. Singer M, Deutschman CS, Seymour CW, Shankar-Hari M, Annane D, Bauer M, et al. The third international consensus definitions for sepsis and septic shock (Sepsis-3). JAMA. 2016;315:801–10. https://doi.org/10.1001/jama.2016.0287
27. Fukui M, Iwai S, Sakamoto R, Takahashi H, Hayashi T, Kenzaka T. *Clostridium paraputrificum* bacteremia in an older patient with no predisposing medical condition. Intern Med. 2017;56:3395–7. https://doi.org/10.2169/internalmedicine.8164-16
28. Lopez-Fabal MF, Sanz N, Ruiz-Bastian M, Barros C, Gomez-Garces JL. *Clostridium perfringens* bacteremia, an analysis of 28 cases over 10 years in a university hospital of Madrid [in Spanish]. Enferm Infecc Microbiol Clin. 2018;36:225–8. https://doi.org/10.1016/j.eimc.2017.02.002
29. Shindo Y, Dobashi Y, Sakai T, Monma C, Miyatani H, Yoshida Y. Epidemiological and pathobiological profiles of *Clostridium perfringens* infections: review of consecutive series of 33 cases over a 13-year period. Int J Clin Exp Pathol. 2015;8:569–77.
30. Shah M, Bishburg E, Baran DA, Chan T. Epidemiology and outcomes of clostridial bacteremia at a tertiary-care institution. ScientificWorldJournal. 2009;9:144–8. https://doi.org/10.1100/tsw.2009.21
31. Yang CC, Hsu PC, Chang HJ, Cheng CW, Lee MH. Clinical significance and outcomes of *Clostridium perfringens* bacteremia—a 10-year experience at a tertiary care hospital. Int J Infect Dis. 2013;17:e955–60. https://doi.org/10.1016/j.ijid.2013.03.001
32. Lark RL, McNeil SA, VanderHyde K, Noorani Z, Uberti J, Chenoweth C. Risk factors for anaerobic bloodstream infections in bone marrow transplant recipients. Clin Infect Dis. 2001;33:338–43. https://doi.org/10.1086/322595
33. Duceau B, Picard M, Pirracchio R, Wanquet A, Pène F, Merceron S, et al. Neutropenic enterocolitis in critically ill patients: spectrum of the disease and risk of invasive fungal disease. Crit Care Med. 2019;47:668–76. https://doi.org/10.1097/CCM.0000000000003687
34. Stabler S, Titécat M, Duployez C, Wallet F, Loïez C, Bortolotti P, et al. Clinical relevance of *Clostridium* bacteremia: an 8-year retrospective study. Anaerobe. 2020;63:102202. https://doi.org/10.1016/j.anaerobe. 2020.102202
35. Libby DB, Bearman G. Bacteremia due to *Clostridium difficile*—review of the literature. Int J Infect Dis. 2009;13:e305–9. https://doi.org/10.1016/j.ijid.2009.01.014
36. Urbán E, Terhes G, Gajdács M. Extraintestinal *Clostridioides difficile* infections: epidemiology in a university hospital in Hungary and review of the literature. Antibiotics (Basel). 2020;9:16. https://doi.org/10.3390/antibiotics9010016
37. Lassmann B, Gustafson DR, Wood CM, Rosenblatt JE. Reemergence of anaerobic bacteremia. Clin Infect Dis. 2007;44:895–900. https://doi.org/10.1086/512197
38. Morris AJ, Wilson ML, Mirrett S, Reller LB. Rationale for selective use of anaerobic blood cultures. J Clin Microbiol. 1993;31:2110–3. https://doi.org/10.1128/JCM.31.8.2110-2113.1993
39. Lafaurie M, d'Anglejan E, Donay JL, Glotz D, Sarfati E, Mimoun M, et al. Utility of anaerobic bottles for the diagnosis of bloodstream infections. BMC Infect Dis. 2020;20:142. https://doi.org/10.1186/s12879-020-4854-x
40. Dutton D, Gavrilova N. Massive intravascular hemolysis with organ failure due to *Clostridium perfringens*: evidence of intracytoplasmic *C. perfringens*. Blood. 2013;122:310. https://doi.org/10.1182/blood-2013-01-472407
41. Angus DC, Linde-Zwirble WT, Lidicker J, Clermont G, Carcillo J, Pinsky MR. Epidemiology of severe sepsis in the United States: analysis of incidence, outcome, and associated costs of care. Crit Care Med. 2001;29:1303–10. https://doi.org/10.1097/00003246-200107000-00002
42. Shankar-Hari M, Phillips GS, Levy ML, Seymour CW, Liu VX, Deutschman CS, et al.; Sepsis Definitions Task Force. Developing a new definition and assessing new clinical criteria for septic shock. JAMA. 2016;315:775–87. https://doi.org/10.1001/jama.2016.0289

Address for correspondence: Guillaume Morel, Medical Intensive Care Unit, Hospital Hautepierre—Hôpitaux Universitaires de Strasbourg, 1 Avenue Molière, BP 83049, 67098 Strasbourg CEDEX, France; email: guillaume.morel@chru-strasbourg.fr

Triclabendazole Treatment Failure for *Fasciola hepatica* Infection among Preschool and School-Age Children, Cusco, Peru[1]

Maria L. Morales, Melinda B. Tanabe, A. Clinton White, Jr., Martha Lopez, Ruben Bascope, Miguel M. Cabada

We conducted a retrospective cohort study of children who had chronic fascioliasis in the highlands of Peru to determine triclabendazole treatment efficacy. Children passing *Fasciola* eggs in stool were offered directly observed triclabendazole treatment (≥1 doses of 10 mg/kg). Parasitologic cure was evaluated by using microscopy of stool 1–4 months after each treatment. A total of 146 children who had chronic fascioliasis participated in the study; 53% were female, and the mean ± SD age was 10.4 ± 3.1 years. After the first treatment, 55% of the children achieved parasitologic cure. Cure rates decreased after the second (38%), third (30%), and fourth (23%) treatments; 17 children (11.6%) did not achieve cure after 4 treatments. Higher baseline egg counts and lower socioeconomic status were associated with triclabendazole treatment failure. Decreased triclabendazole efficacy in disease-endemic communities threatens control efforts. Further research on triclabendazole resistance and new drugs to overcome it are urgently needed.

Triclabendazole is the only medication recommended by the World Health Organization for treatment of *Fasciola hepatica* liver fluke infection in humans (*1*). Triclabendazole use in human infections was initially reported in Europe in 1986 (*2*). Several studies in Bolivia, Peru, and Egypt have documented efficacy of 80%–100% after 1 or 2 doses (*3*–*5*). The recommended triclabendazole treatment regimen is 1–2 doses of 10 mg/kg with a fatty meal in patients >6 years of age (*1*,*6*). Triclabendazole has been administered at higher doses and in children <6 years of age despite limited safety and efficacy data (*3*,*8*–*10*).

Author affiliations: Universidad Peruana Cayetano Heredia, Cusco, Peru (M.L. Morales, A.C. White Jr., M. Lopez, M.M. Cabada); University of Texas Medical Branch, Galveston, Texas, USA (M.B. Tanabe, A.C. White Jr., M.M. Cabada); Peruvian Ministry of Health, Cusco (R. Bascope)

DOI: https://doi.org/eid2707.203900

The widespread use of triclabendazole in livestock that have fascioliasis has been associated with decreasing efficacy. Triclabendazole resistance in cattle was first reported from Australia in 1995 (*11*). Since then, ≥11 countries have reported triclabendazole resistance in livestock (*12*). A reported case of triclabendazole resistance in a farmer from the Netherlands was described in 2012 (*13*). Other human cases have been described in Chile, Peru, Portugal, and Turkey (*14*–*16*). Decreasing triclabendazole efficacy is a threat to public health and livestock industry in disease-endemic regions. However, little is known about triclabendazole treatment failure rates in human fascioliasis (*12*).

We conducted a large epidemiologic study on the prevalence and effect of *F. hepatica* infection among children from 26 communities in the Cusco region of Peru; ≈10% of children had evidence of *Fasciola* infection (*16*). Children given a diagnosis of fascioliasis in that study were provided open-label treatment with triclabendazole. We retrospectively describe the outcomes of triclabendazole treatment among children with chronic fascioliasis from rural communities in Cusco, Peru.

Materials and Methods

Study Population

The initial study cohort consisted of children with chronic fascioliasis from 26 communities of the Ancahuasi, Zurite, and Anta Districts of the Cusco region in Peru (*16*). Informed consent was provided by parents of 2,958 children 3–16 years of age who had no history of previous treatment for *F. hepatica*

[1]Preliminary results from this study were presented at the 68th Annual Meeting of the American Society of Tropical Medicine and Hygiene, November 20–24, 2019, National Harbor, MD, USA.

infection to participate in an epidemiologic study. We studied children for evidence of *F. hepatica* infection by using a serum Fas2 ELISA for *Fasciola* antibodies (Bionoma, https://www.dnb.com) and microscopy of 3 consecutive stool samples by using 1 Kato-Katz test and 1 Lumbreras sedimentation test per specimen. The Lumbreras sedimentation test has been demonstrated to have high sensitivity for detecting helminths ova in human feces (*17*). We evaluated the likelihood of living under the US $3.75/day poverty line by using the Simple Poverty Scorecard validated for Peru (*18*). We calculated this likelihood by comparing the score obtained in a standardized household questionnaire against a table of probabilities of living under a certain poverty line assigned to questionnaire score intervals (*18*).

Intervention

The Ministry of Health offered triclabendazole treatment to all children who had ≥1 positive test result for *F. hepatica* infection. We defined chronic fascioliasis as having *Fasciola* eggs in ≥1 stool sample. Children who had chronic fascioliasis and received directly observed treatment with ≥1 triclabendazole dose and attended follow-up were included in the retrospective cohort. We defined a triclabendazole dose as the oral administration of 10 mg/kg with a fatty meal (≈350 calories).

The local Ministry of Health provided 250 mg scored triclabendazole tablets (Egaten; Novartis Pharma AG, https://www.novartis.com). The number of triclabendazole doses was determined by an expert panel advising the Ministry of Health with no input from the investigators. The selection was based on age, weight, and the number of treatment rounds previously received. Doses were rounded up to the next half or full tablet. Children whose parents did not consent for treatment before any round were referred to the local health center for follow up.

Assessment of Response

We tested children who received ≥1 dose of triclabendazole for treatment response by using microscopy for 3 stool samples collected between 1 and 4 months after treatment. We assessed response to treatment by using parasitologic cure and egg reduction rate. We defined parasitologic cure as the absence of *Fasciola* eggs in 3 stool samples each tested by using 1 Kato Katz test and 1 Lumbreras rapid sedimentation test (*17*). The arithmetic mean for the Kato Katz egg count was calculated for each child by using the values from the 3 stool samples tested. Some children who had negative Kato Katz test results (0 eggs/gram of stool) were given a diagnosis of chronic fascioliasis on the basis of only the Lumbreras rapid sedimentation test. We calculated the geometric mean egg count for the population before and after each treatment. The egg reduction rate (ERR) was calculated by using the formula: ERR = (geometric mean pretreatment egg count – geometric mean posttreatment egg count)/(geometric mean pretreatment egg count) × 100 and was presented as a percentage. Children who did not achieve parasitologic cure were offered additional treatment courses as needed to achieve cure. After the fourth triclabendazole treatment, children were considered to have failed treatment with triclabendazole and to harbor drug-resistant *F. hepatica* parasites.

Statistical Analysis

We used SPSS Statistics 25.0 (IBM Corp., https://www.ibm.com) for statistical analysis. For univariate analysis, we calculated frequencies, mean ± SD, median with interquartile range (IQR), and geometric means with 95% CIs to determine the distribution of the variables. Parasitologic cure after each round of treatment was recorded and used to estimate the efficacy of triclabendazole. We defined efficacy as the proportion of all children who were cured after each round and treatment regimen and calculated the egg reduction rate for each treatment round. Children who were lost to follow-up or whose parents refused further testing after treatment were excluded from the analysis of efficacy. We compared demographic information, socioeconomic status, and epidemiologic information between children with parasitologic cure and children without cure by using the Student t-test, Mann-Whitney U test, or χ^2 test when appropriate. A p value <0.05 was considered significant for all statistical tests.

Ethics

The study was approved by the Institutional Ethics Committee of Universidad Peruana Cayetano Heredia and the University of Texas Medical Branch. Informed consent was obtained in Quechua or Spanish language from the children's parents or guardians. In addition, children >6 years of age provided verbal assent before any study procedure in the parent study.

Results

A total of 228 (7.7%) of 2,958 children had ≥1 positive test result for *Fasciola*. A total of 166 (5.6%) children were passing eggs in the stool and met criteria for chronic fascioliasis, and 146 (88%) children met

criteria to participate in the retrospective cohort (Figure). Most (77/146, 53.0%) children female; mean ± SD age was 10.4 ± 3.1 years (Table 1) The geometric mean egg count was 25 (95% CI 19.5–32.2) eggs/gram of stool (range 0–820 eggs/gram of stool). Twenty children had an egg count of 0 eggs/gram of stool by the Kato Katz test but were given a diagnosis by the Lumbreras rapid sedimentation test, which is not quantitative. The median eosinophil count was 290 cells/μL (IQR 195–425 cells/μL). A total of 72% (104/146) of the children had a positive Fas2 ELISA result for *Fasciola* antibodies.

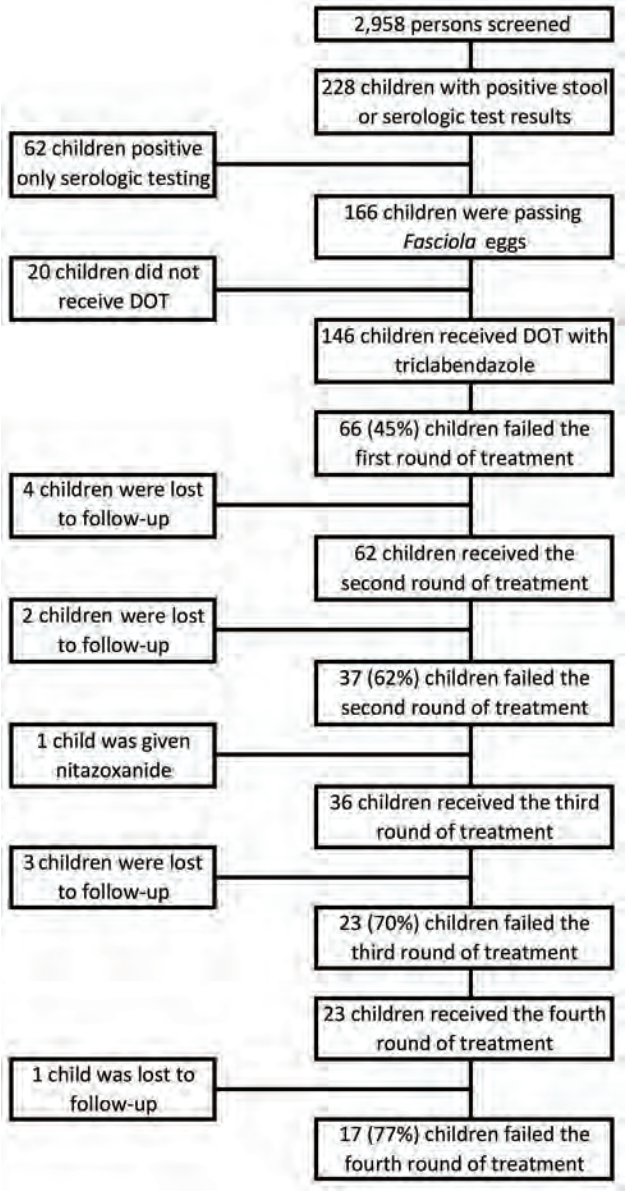

Figure. Flowchart of selection and treatment for participants in study of triclabendazole treatment failure for *Fasciola hepatica* infection among preschool and school-age children, Cusco, Peru. DOT, directly observed therapy.

First Treatment

During the initial round of treatment, 139/146 (95.2%) children received 1 dose of triclabendazole and 7/146 (4.8%) children received 2 doses separated by 24 hours. The median number of days from treatment to assessment of response was 88 (IQR 56–114). Overall, 80/146 (55%) children achieved parasitologic cure after the first round of treatment, including 75/139 (54%) treated with 1 dose of triclabendazole and 5/7 (71%) treated with 2 doses (Table 2).

Children who had a positive pretreatment Fas2 ELISA result (p = 0.026) and a higher egg count (p = 0.001) were more likely to fail the first round of triclabendazole (Table 3). The baseline geometric mean egg count of children who achieved parasitologic cure was less than half the geometric mean egg count of children who failed to be cured (17, 95% CI 11.9–24.5 vs. 40.9, 95% CI 30.3–55.4) eggs/gram of stool. No significant differences by age (p = 0.76), sex (p = 0.54), district (p = 0.9), socioeconomic score (p = 0.54), baseline height-for-age Z score (p = 0.19), or baseline hemoglobin level (p = 0.97) were evident between those who failed treatment and those who responded to the first round of treatment. The overall ERR after the first round of treatment was 84.8%. The ERR among those who failed the first round of treatment was 53%.

Second Treatment

A total of 4 (6.1%) of the 66 children eligible to receive a second round of treatment were lost to follow-up or their parents refused further treatment. The geometric mean egg count before the second round of treatment was 19 (95% CI 12.3–29.5) eggs/gram of stool (range 0–287 eggs/gram of stool). During the second round, 11 (17.7%) of 62 children received 1 dose of triclabendazole, 48 (77.0%) of 62 received 2 doses, and 3 (4.8%) of 62 received >2 doses. The median time between the second round of treatment and the assessment of response was 49 (IQR 34–65) days. Overall, 23 (38.0%) of 60 children achieved parasitologic cure after the second round of treatment, including 5 (46.0%) of 11 children who received 1 dose, 17 (37.0%) of 46 children who received 2 doses, and 1 (33.0%) of 3 children who received >2 doses. Two children did not provide stool samples for assessment of parasitologic cure. The overall ERR after the second round of treatment was 60.6%. However, the ERR for those who failed the second round of treatment was only 4.6%.

Third Treatment

A total of 36 (97.3%) of the 37 children eligible for a third round of treatment received triclabendazole

again and 33 (83.3%) of 36 children were prescribed treatment regimens containing ≥2 doses (Table 2). The geometric mean egg count before the third round of treatment was 35.8 (95% CI 22.9–56.4) eggs/gram of stool (range 0–387 eggs/gram of stool). Three children did not provide follow-up specimens. Parasitologic cure was achieved by 10 (30%) of 33 children. One child did not receive triclabendazole and was given nitazoxanide (500 mg 2×/d for 6 d) without achieving parasitologic cure. The overall ERR after the third round of treatment was 58%, and the ERR of those who failed the third round was 34.7%.

Fourth Treatment

A total of 23 children who failed treatment again were administered ≥2 doses of triclabendazole for a fourth round of treatment. One child did not provide a follow-up specimen. The pretreatment geometric mean egg count was 29.6 (95% CI 16–55.3) eggs/gram of stool (range 0–833 eggs/gram of stool). Parasitologic cure was achieved by 5 (23.0%) of 22 children. The overall ERR after the fourth round of triclabendazole was 23.6%. For children who were not cured, the geometric mean egg count increased by 89.3%.

Triclabendazole Failure

A total of 17 (11.6%) of 146 children given triclabendazole were considered to have failed triclabendazole treatment and harbored drug-resistant *F. hepatica* parasites. The median age of the children was 8.5 (IQR 6.4– 12.3) years and 10 (58.8%) of 17 were female. All households had less than a 50% likelihood of living under a US $3.75/day poverty line. Almost one third (6/17, 35.3%) were infected with other gastrointestinal parasites at enrollment. A total of 11 (65.0%) of 17 children received additional treatment courses without achieving parasitologic cure (Table 4). Children who were cured after the first round of treatment when compared with children who had drug-resistant parasites were less likely to live in Anta district, more likely to live under the poverty line, and more likely to have a lower baseline egg count (Table 3).

Table 1. Characteristics of participants in study of triclabendazole treatment failure for *Fasciola hepatica* infection for 146 preschool and school-age children, Cusco, Peru*

Characteristic	Value
Sex	
F	77 (52.7)
M	69 (47.3)
District	
Ancahuasi	81 (55.5)
Anta	53 (36.3)
Zurite	12 (8.2)
Other parasites†	
0	83 (56.8)
1	47 (32.2)
2	16 (11.0)
Fas2 ELISA test result‡	
Positive	104 (72.7)
Negative	39 (27.3)
Likelihood of poverty‡§	
≤50%	112 (83.0)
>50%	23 (17.0)
Eosinophil count, cells/μL‡	290 (195–425)
Baseline hemoglobin, g/dL¶	12.9 (12.2–13.7)
Baseline (IQR) HAZ‡	−1.57 (−2.16 to −0.94)
Median age ± SD, y	10.4 (± 3.14)
Geometric mean (95% CI) baseline egg count/g of stool	25 (19.5–32.2)

*Values are no. (%), median (IQR), or mean ± SD unless otherwise indicated. HAZ, height-for-age Z score; IQR, interquartile range.
†Gastrointestinal parasites.
‡Does not add up to 146 because of missing data.
§Likelihood of living at a level <US $3.75/day.
¶Uncorrected at enrollment.

Discussion

Fascioliasis imposes a large burden on impoverished human populations, and triclabendazole is the only medication recommended for treatment and control. In our cohort of children who had chronic fascioliasis, the efficacy of triclabendazole was low, especially after treatment with a single dose. The overall drug

Table 2. Triclabendazole treatment outcomes per round for study of triclabendazole treatment failure for *Fasciola hepatica* infection for 146 preschool and school-age children, Cusco, Peru

Round	Regimen, no. doses	Parasitologic cure, no. (%)	Parasitologic failure, no. (%)
1	1	75 (54)	64 (46)
	2	5 (71)	2 (29)
	Overall	80/146 (55)	66/146 (45)
2	1	5 (46)	6 (55)
	2	17 (37)	29 (63)
	>2	1 (33)	2 (67)
	Overall	23/60 (38)	37/60 (62)
3	1	0 (0)	3 (100)
	2	2 (67)	1 (33)
	>2	8 (30)	19 (70)
	Overall	10/33 (30)	23/33 (70)
4	2	0 (0)	3 (100)
	>2	5 (26)	14 (74)
	Overall	5/22 (22.7)	17/22 (77.3)

Table 3. Response to first round of triclabendazole treatment for *Fasciola hepatica* infection among preschool and school-age children compared with failure to respond to first or fourth round of treatment, Cusco, Peru*

Characteristic	Cured after first round, n = 80	Failed after first round, n = 66	p value†	Failed after fourth round, n = 17	p value†
District					
Anta	27 (34)	26 (39)	0.48	12 (71)	0.005
Other	53 (64)	40 (61)		5 (29)	
Fas2 ELISA result					
Negative	27 (35)	12 (18)	0.02	2 (12)	0.08
Positive	50 (65)	54 (82)		15 (88)	
Likelihood of poverty‡					
≤50%	56 (70)	56 (89)	0.08	17 (100)	0.03
>50%	16 (30)	7 (11)		0 (0)	
Other parasites§					
No	42 (53)	41 (62)	0.24	11 (65)	0.35
Yes	38 (48)	25 (38)		6 (35)	
Sex					
F	44 (55)	33 (50)	0.54	10 (59)	0.77
M	36 (45)	33 (50)		7 (41)	
Age, y, mean ± SD	10.5 ± 2.9	10.4 ± 3.4	0.85	9.0 ± 3.6	0.06
Baseline egg count, eggs/g of stool	33.3 (6.6–53.3)	48.3 (25–87.5)	0.001	60 (26–100)	0.005
Baseline hemoglobin, g/dL¶	12.9 (12.1–13.7)	12.9 (12.3–13.4)	0.97	12.3 (12–13)	0.08
Baseline HAZ#	−1.6 (−2.2 to −1.0)#	−1.5 (−2.0 to −0.9)#	0.19	−1.2 (−1.9 to −0.7)	0.17
Eosinophil count, cells/μL	300 (190–460)#	265 (197–412)	0.36	310 (230–500)	0.64

*Values are no. (%) or median (interquartile range) except as indicated. HAZ, height-for-age Z score.
†By Mann-Whitney U test.
‡Likelihood of living under US $3.75/day poverty line (*18*).
§Gastrointestinal parasites.
¶Uncorrected at enrollment.
#One or 2 persons were missing information for this variable.

efficacy after 1 round of treatment was 55%, and it decreased further after subsequent rounds to 38%, 30%, and 23%, respectively. Overall, 11% of the children failed to respond to ≥4 triclabendazole treatment rounds. The overall ERR rates were lower after each round of treatment and modest in children who failed each triclabendazole round. Higher pretreatment egg counts, higher socioeconomic status, and living in the Anta district were associated with failure to achieve parasitologic cure.

Factors underlying failutre of triclabendazole treatment for chronic fascioliasis might include poor medication quality and bioavailability. We used Egaten in this study, which is the human formulation of triclabendazole donated by Novartis Pharma to the Peruvian Ministry of Health. This medication was administered to children well before its expiration date. In addition, children received a standard fatty meal before each triclabendazole dose. Food increased triclabendazole bioavailability between 2-fold and 3-fold in pharmacokinetic studies (*8*). However, scarce information on triclabendazole population pharmacokinetics in *Fasciola*-infected persons from disease-endemic areas is available.

We based the chronic *Fasciola* diagnosis on the presence of eggs in stool and tested for parasitologic cure at 1–4 months posttreatment by using the same type and number of stool tests as those used to diagnose the infection. This period is within the duration of the migratory phase of *Fasciola* parasites when immature parasites have not reached the bile ducts or produce eggs. Thus, our approach in an area with moderate prevalence of fascioliasis and low intensity of infection decreased the possibility of reinfection as a cause of persistent positive results for stool microscopy (*19*).

The poor response to triclabendazole contrasts with previous reports from the highlands of South America. Maco et al. reported parasitologic cure rates of 100% after 2 doses of 7.5 mg/kg of triclabendazole in 24 hours and 95% after a single dose of 10 mg/kg of triclabendazole among children with fascioliasis in highlands of Peru (*5*). A study in the Altiplano of Bolivia, near the border with Peru, reported parasitologic cure rates of 78% and 98% among chronically infected children after 1 and 2 rounds of treatment with a single 10 mg/kg dose of triclabendazole, respectively (*3*). No recent large treatment studies are available from South America with which to compare our results, but increasing reports of triclabendazole failure in the area support the idea of decreasing effectiveness and raise concern for the lack of alternative medications.

A higher pretreatment egg count was found for children who failed ≥1 rounds of treatment. This observation has been described for other trematode infections, such as schistosomiasis. Black et al. studied a cohort of 200 men who had occupational exposure

to schistosomiasis in Lake Victoria, Kenya, and proposed that even with drug efficacies >90%, persons who had a high burden of infection might still be infected with enough surviving egg-producing parasites to have positive results for stool microscopy (*20*). The mesoendemic area we studied showed a moderate *Fasciola* prevalence, and egg burden was not as high as those described in hyperendemic areas around Lake Titicaca, where the egg count geometric mean can reach 700 eggs/gram of stool (*21*). For that reason, it is unlikely that triclabendazole failure could be explained by surviving parasites despite high drug efficacy.

Survival of juvenile parasites migrating through the liver has been proposed as a cause for persistent infection after treatment. In *Fasciola* infection models, juvenile parasites have reduced susceptibility to triclabendazole compared with established infection with mature parasites (*22*). No clinical trials of triclabendazole treatment of acute fascioliasis have been published, and the clinical experience in published case series is inconsistent. After 2 triclabendazole doses, some authors reported low efficacy (Ramadan et al., 55% efficacy [*23*]) and some authors reported high efficacy (Chen et al., 96% efficacy [*24*]). However, ascertainment bias is a major issue in acute fascioliasis case series because there is no consensus on case definition and treatment response measures. In our community-based study, only 0.4% of children had acute fascioliasis defined by negative stool test results, positive results for *Fasciola* antibodies, eosinophilia (>500 cells/μL), and elevated levels of aminotransferases (*16*). Thus, we believe that the potential contribution of the survival of migrating parasites to the persistence of infection in our treatment cohort is negligible.

Persons from Anta district and with <50% chance of living in poverty were more likely to fail a fourth round of treatment. The Anta district is the district closest to Cusco and has one of the lowest poverty levels in the province (*25*). We hypothesize that access to veterinary triclabendazole to give to cattle might be associated with higher urbanization and socioeconomic status in our cohort. It is likely that drug resistance emerges first in livestock under constant triclabendazole selective pressure but also under inconsistent dosing because of lack of quality control of veterinary products or training of farmers (*14*,*26*,*27*). Subsequently, the proportion of drug-resistant parasites shed by cattle in the environment might reach a threshold, leading to transmission to humans. However, further studies are needed to evaluate the association between drug resistance in cattle, environmental contamination with drug-resistant isolates, clonal expansion in intermediate hosts, and the emergence of triclabendazole resistance in humans.

A major limitation of this study was the lack of established dosing schemes. A consultant from the Ministry of Health made dosing decisions after reviewing the child's age, weight, and previous treatment courses. These decisions were outside the control of the study investigators and introduced some

Table 4. Clinical characteristics of 17 children who failed 4 rounds of triclabendazole treatment for *Fasciola hepatica* infection among preschool and school-age children, Cusco, Peru*

Child	Community	District	Age, y/sex	Other parasites	HAZ	Living under US $3.75/day	ERR, %†	Total drug dose, mg/kg‡	Additional treatment received
1	Anta	Anta	6.8/F	Yes	−0.6	25	0§	90	1 more round
2	Anta	Anta	14.1/M	No	−2.3	25	40	90	2 more rounds
3	Conchacalla	Anta	10.5/M	No	−1.8	13	67	210	Nitazoxanide
4	Conchacalla	Anta	3.2/F	No	−2.4	36	40	50	2 more rounds
5	Conchacalla	Anta	6.0/F	No	−0.4	36	0§	210	None
6	Inquilpata	Anta	8.5/M	No	−0.9	36	30	50	2 more rounds
7	Inquilpata	Anta	9.7/F	No	−1.2	36	43	50	2 more rounds
8	Inquilpata	Anta	3.3/M	Yes	−1.2	49	+275	210	None
9	Izcuchaca	Anta	13.9/F	No	−0.6	36	+574	150	1 more round
10	Izcuchaca	Anta	7.4/M	No	−0.6	25	63	150	1 more round
11	Mantoclla	Anta	7.3/F	Yes	−2.0	25	10	150	None
12	Mantoclla	Anta	9.2/F	Yes	−1.9	25	31	150	None
13	Caccahuara	Ancahuasi	13.1/F	No	−1.5	25	17	210	Nitazoxanide
14	Caccahuara	Ancahuasi	15.5/F	No	−1.9	13	+50	210	None
15	Caccahuara	Ancahuasi	7.8/M	No	−1.1	25	+100	210	Nitazoxanide
16	Chaquillccasa	Ancahuasi	11.5/M	Yes	−0.9	25	+250	210	None
17	Chaquillccasa	Ancahuasi	5.5/F	Yes	−2.1	49	63	210	1 more round

*ERR, egg reduction rate; HAZ, height-for-age Z score.
†Between baseline and after the fourth round of treatment, as estimated by the number of eggs in Kato Katz tests. + signs indicate the percent increase in the egg count.
‡Total cumulative dose received after the fourth round of treatment
§Diagnosed only by Lumbreras rapid sedimentation test and a negative Kato Katz test result.

heterogeneity in the dosing. However, after failing triclabendazole, some children received treatment with multiple doses, well above the recommended dosing regimens in the triclabendazole package insert. We did not note increased effectiveness with regimens containing >2 doses of triclabendazole, but the small numbers treated precluded a statistical comparison. A more cautious approach was used with children <6 years of age because fewer data support the safety of triclabendazole for this age group.

A potential limitation when evaluating drug efficacy is in the ability to distinguish persistent infections from reinfections in disease-endemic areas. In addition, the low sensitivity of stool microscopy and variability of egg shedding could hinder ascertainment of treatment outcomes, particularly ERR. Testing >1 stool sample and combination of microscopy methods was necessary to increase sensitivity. The timing for assessment of cure for fascioliasis has not been well established. Intervals between determination of treatment failure and the next round of treatment lasted several months for some children because of triclabendazole shortages. Thus, we cannot exclude increased parasite burdens before treatment among children caused by rapidly occurring reinfections. However, considering that we studied an area with a moderate infection prevalence, these reinfections probably occurred rarely if at all.

There are no established alternatives to triclabendazole for treatng fascioliasis. Nitazoxanide has been used in some studies. This drug was used for children who had repeated triclabendazole treatment failures but was not effective. In Egypt, Ramadan et al. reported a cure rate of 30% for nitazoxanide among persons who had acute fascioliasis who failed 2 triclabendazole doses (*23*). There are wide regional variations in reported nitazoxanide cure rates among *Fasciola*-infected persons (*28*,*29*). We previously reported a case series of triclabendazole-resistant fascioliasis in Cusco and noted a lack of nitazoxanide effectiveness among persons previously failing multiple triclabendazole treatments (*14*). Although we provided treatment with nitazoxanide to only 4 children with nitazoxanide in the current cohort study, our results do not support the use of nitazoxanide as rescue treatment for persistent *Fasciola* infections.

In this cohort, we have demonstrated decreased response rates to triclabendazole among children with chronic fascioliasis, including poor egg reduction rates and low parasitologic cure rates with single triclabendazole doses. In addition, we have documented high levels of drug resistance in children treated several times with increasing doses of triclabendazole. The absence of effective alternative medications and lack of interventions to overcome drug-resistance mechanisms are of concern in disease-endemic areas. Triclabendazole use stewardship in humans and livestock is urgently needed to prevent further decrease in infectiveness. In this setting, it is unclear whether mass drug administration control strategies might aggravate the problem. Ongoing research in the Cusco area is evaluating the mechanisms of triclabendazole resistance. Clinicians should be aware of alternative drugs and the interactions between triclabendazole-resistant parasites in livestock, human, and the environment that drive transmission to children.

Acknowledgments

We thank the Cusco Regional Health Directorate of the Peruvian Ministry of Health and Benicia Baca, Kelly Fernandez-Baca, Eulogia Arque, and Carolina Coto for participating in this study.

This study was supported by the National Institute for Allergy and Infectious Diseases, National Institutes of Health (grant no. 1R01AI104820–01).

About the Author

Ms. Morales is a registered nurse at the Universidad Peruana Cayetano Heredia, Cusco, Peru. Her primary research interests are public health and control programs for infectious diseases.

References

1. World Health Organization. Fascioliasis diagnosis, treatment and control strategy (updated 2014) [cited 2020 May 28]. https://www.who.int/foodborne_trematode_infections/fascioliasis/fascioliasis_diagnosis
2. Wessely K, Reischig HL, Heinerman M, Stempka R. Human fascioliasis treated with triclabendazole (Fasinex) for the first time. Trans R Soc Trop Med Hyg. 1988;82:743–4. https://doi.org/10.1016/0035-9203(88)90222-2
3. Villegas F, Angles R, Barrientos R, Barrios G, Valero MA, Hamed K, et al. Administration of triclabendazole is safe and effective in controlling fascioliasis in an endemic community of the Bolivian Altiplano. PLoS Negl Trop Dis. 2012;6:e1720. https://doi.org/10.1371/journal.pntd.0001720
4. el-Morshedy H, Farghaly A, Sharaf S, Abou-Basha L, Barakat R. Triclabendazole in the treatment of human fascioliasis: a community-based study. East Mediterr Health J. 1999;5:888–94.
5. Maco V, Marcos L, Delgado J, Herrera J, Nestares J, Terashima A, et al. Efficacy and tolerability of two single-day regimens of triclabendazole for fascioliasis in Peruvian children. Rev Soc Bras Med Trop. 2015;48:445–53. https://doi.org/10.1590/0037-8682-0148-2015
6. Centers for Disease Control and Prevention. *Fasciola*. Resources for health professionals and treatment (updated 2019) [cited 2020 May 28]. https://www.cdc.gov/parasites/fasciola/health_professionals/index.html

7. Talaie H, Emami H, Yadegarinia D, Nava-Ocampo AA, Massoud J, Azmoudeh M, et al. Randomized trial of a single, double and triple dose of 10 mg/kg of a human formulation of triclabendazole in patients with fascioliasis. Clin Exp Pharmacol Physiol. 2004;31:777–82. https://doi.org/10.1111/j.1440-1681.2004.04093.x
8. US Food and Drug Administration. Drug approval package: Egaten (triclabendazole) 2019 [cited 2020 May 28]. https://www.accessdata.fda.gov/drugsatfda_docs/nda/2018/208711Orig1s000TOC.cfm
9. Mollinedo S, Gutierrez P, Azurduy R, Valle F, Salas A, Mollinedo Z, et al. Mass drug administration of triclabendazole for *Fasciola hepatica* in Bolivia. Am J Trop Med Hyg. 2019;100:1494–7. https://doi.org/10.4269/ajtmh.19-0060
10. Bayhan GI, Özkan AT, Beyhan YE. The clinical characteristics of fascioliasis in pediatric patients. Turk Pediatri Ars. 2020;55:67–71.
11. Overend DJ, Bowen FL. Resistance of *Fasciola hepatica* to triclabendazole. Aust Vet J. 1995;72:275–6. https://doi.org/10.1111/j.1751-0813.1995.tb03546.x
12. Kelley JM, Elliott TP, Beddoe T, Anderson G, Skuce P, Spithill TW. Current threat of triclabendazole resistance in *Fasciola hepatica*. Trends Parasitol. 2016;32:458–69. https://doi.org/10.1016/j.pt.2016.03.002
13. Winkelhagen AJ, Mank T, de Vries PJ, Soetekouw R. Apparent triclabendazole-resistant human *Fasciola hepatica* infection, the Netherlands. Emerg Infect Dis. 2012;18:1028–9. https://doi.org/10.3201/eid1806.120302
14. Cabada MM, Lopez M, Cruz M, Delgado JR, Hill V, White AC Jr. Treatment failure after multiple courses of triclabendazole among patients with fascioliasis in Cusco, Peru: a case series. PLoS Negl Trop Dis. 2016;10:e0004361. https://doi.org/10.1371/journal.pntd.0004361
15. Branco EA, Ruas R, Nuak J, Sarmento A. Treatment failure after multiple courses of triclcabendazole in a Portuguese patient with fascioliasis. BMJ Case Rep. 2020;13:e232299. https://doi.org/10.1136/bcr-2019-232299
16. Cabada MM, Morales ML, Webb CM, Yang L, Bravenec CA, Lopez M, et al. Socioeconomic factors associated with *Fasciola hepatica* infection among children from 26 communities of the Cusco region of Peru. Am J Trop Med Hyg. 2018;99:1180–5. https://doi.org/10.4269/ajtmh.18-0372
17. Lopez M, Morales ML, Konana M, Hoyer P, Pineda-Reyes R, White AC Jr, et al. Kato-Katz and Lumbreras rapid sedimentation test to evaluate helminth prevalence in the setting of a school-based deworming program. Pathog Glob Health. 2016;110:130–4. https://doi.org/10.1080/20477724.2016.1187361
18. Schreiner M. A simple poverty scorecard for Peru 2009 [cited 2021 Jan 14]. http://www.simplepovertyscorecard.com/PER_2007_ENG.pdf
19. Keiser J, Engels D, Büscher G, Utzinger J. Triclabendazole for the treatment of fascioliasis and paragonimiasis. Expert Opin Investig Drugs. 2005;14:1513–26. https://doi.org/10.1517/13543784.14.12.1513
20. Black CL, Steinauer ML, Mwinzi PN, Evan Secor W, Karanja DM, Colley DG. Impact of intense, longitudinal retreatment with praziquantel on cure rates of schistosomiasis mansoni in a cohort of occupationally exposed adults in western Kenya. Trop Med Int Health. 2009;14:450–7. https://doi.org/10.1111/j.1365-3156.2009.02234.x
21. Esteban JG, Flores A, Angles R, Mas-Coma S. High endemicity of human fascioliasis between Lake Titicaca and La Paz valley, Bolivia. Trans R Soc Trop Med Hyg. 1999;93:151–6. https://doi.org/10.1016/S0035-9203(99)90289-4
22. Duthaler U, Smith TA, Keiser J. In vivo and in vitro sensitivity of *Fasciola hepatica* to triclabendazole combined with artesunate, artemether, or OZ78. Antimicrob Agents Chemother. 2010;54:4596–604. https://doi.org/10.1128/AAC.00828-10
23. Ramadan HK, Hassan WA, Elossily NA, Ahmad AA, Mohamed AA, Abd-Elkader AS, et al. Evaluation of nitazoxanide treatment following triclabendazole failure in an outbreak of human fascioliasis in Upper Egypt. PLoS Negl Trop Dis. 2019;13:e0007779. https://doi.org/10.1371/journal.pntd.0007779
24. Chen JX, Chen MX, Ai L, Xu XN, Jiao JM, Zhu TJ, et al. An outbreak of human fascioliasis gigantica in Southwest China. PLoS One. 2013;8:e71520. https://doi.org/10.1371/journal.pone.0071520
25. Instituto Nacional de Estadistica e Informatica. Provincial and district poverty map, 2013. Lima, Peru [in Spanish] [cited 2020 May 28]. https://www.inei.gob.pe/media/MenuRecursivo/publicaciones_digitales/Est/Lib1261/Libro.pdf
26. Sargison ND, Scott PR. Diagnosis and economic consequences of triclabendazole resistance in *Fasciola hepatica* in a sheep flock in south-east Scotland. Vet Rec. 2011;168:159. https://doi.org/10.1136/vr.c5332
27. Webster JP, Molyneux DH, Hotez PJ, Fenwick A. The contribution of mass drug administration to global health: past, present and future. Philos Trans R Soc Lond B Biol Sci. 2014;369:20130434. https://doi.org/10.1098/rstb.2013.0434
28. Lukambagire AH, Mchaile DN, Nyindo M. Diagnosis of human fascioliasis in Arusha region, northern Tanzania by microscopy and clinical manifestations in patients. BMC Infect Dis. 2015;15:578. https://doi.org/10.1186/s12879-015-1326-9
29. Zumaquero-Ríos JL, Sarracent-Pérez J, Rojas-García R, Rojas-Rivero L, Martínez-Tovilla Y, Valero MA, et al. Fascioliasis and intestinal parasitoses affecting school-children in Atlixco, Puebla State, Mexico: epidemiology and treatment with nitazoxanide. PLoS Negl Trop Dis. 2013;7:e2553. https://doi.org/10.1371/journal.pntd.0002553

Address for correspondence: Miguel M. Cabada, University of Texas Medical Branch, 301 University Blvd, RT 0435, Galveston, TX 77555, USA; email: micabada@utmb.edu

Novel Morbillivirus as Putative Cause of Fetal Death and Encephalitis among Swine

Bailey Arruda, Huigang Shen, Ying Zheng, Ganwu Li

Morbilliviruses are highly contagious pathogens. The *Morbillivirus* genus includes measles virus, canine distemper virus (CDV), phocine distemper virus (PDV), peste des petits ruminants virus, rinderpest virus, and feline morbillivirus. We detected a novel porcine morbillivirus (PoMV) as a putative cause of fetal death, encephalitis, and placentitis among swine by using histopathology, metagenomic sequencing, and in situ hybridization. Phylogenetic analyses showed PoMV is most closely related to CDV (62.9% nt identities) and PDV (62.8% nt identities). We observed intranuclear inclusions in neurons and glial cells of swine fetuses with encephalitis. Cellular tropism is similar to other morbilliviruses, and PoMV viral RNA was detected in neurons, respiratory epithelium, and lymphocytes. This study provides fundamental knowledge concerning the pathology, genome composition, transmission, and cellular tropism of a novel pathogen within the genus *Morbillivirus* and opens the door to a new, applicable disease model to drive research forward.

Paramyxoviridae encompasses a group of large (300–500 nm in diameter), enveloped, pleomorphic viruses with RNA genomes of 14.6–20.1 kb. The family comprises 4 subfamilies and 17 genera that contain >70 species and includes global human and animal viral pathogens of concern (*1*). Currently, the genus *Morbillivirus*, in subfamily *Orthomyxovirinae*, contains measles virus (MeV), rinderpest virus (RPV), peste des petits ruminants virus (PPRV), canine distemper virus (CDV), phocine distemper virus (PDV), cetacean morbillivirus (CMV), and feline morbillivirus (FeMV) (*2*,*3*).

Morbillivirus genomes encode 6 structural proteins in the following order: nucleocapsid (N) protein, phosphoprotein (P), matrix (M) protein, hemagglutinin (H) protein, fusion (F) protein, and large polymerase (L) protein (*2*). Two nonstructural proteins, C and V, are expressed from the P open reading frame and are thought to interfere with the innate immune response in at least a subset of members of the family *Paramyxoviridae* (*4*).

Morbilliviruses cause respiratory and gastrointestinal disease and profound immune suppression (*5*). Morbillivirus host species experience a similar pathogenesis; infection occurs through inhalation, direct contact with body fluids, or fomites or vertical transmission (*6*–*8*). Carnivore morbilliviruses readily invade the central nervous system (CNS), and all morbilliviruses produce intranuclear viral inclusion bodies containing nucleocapsid-like structures (*1*,*9*,*10*).

Paramyxoviruses known to naturally infect swine include porcine rubulavirus, Menangle virus, Nipah virus, and porcine parainfluenza virus (*11*–*16*). Less well-characterized paramyxoviruses associated with central nervous and respiratory disease in pigs also have been reported (*17*–*20*), but none of these viruses are classified in the genus *Morbillivirus*. Using histopathology, metagenomic sequencing, and RNA in situ hybridization (ISH), we identified a novel morbillivirus in swine as the putative cause of an outbreak of reproductive disease characterized by fetal mummification, encephalitis, and placentitis.

Materials and Methods

Clinical Background and Samples

In early 2020, the Iowa State University Veterinary Diagnostic Laboratory (Ames, IA, USA) received 22 porcine fetuses from 6 litters (A–F) that originated from a commercial breeding herd in northern Mexico for routine diagnostic investigation (Table 1). The breeding herd comprised 2,000 sows and reported reproductive clinical signs characterized by an increased percentage (18% reported) of mummified fetuses and stillbirths. For negative controls, we used fetal tissues from 2 litters from a 3,000-head sow farm in the United States that was experiencing increased mummified fetuses and stillborn fetuses.

Authors affiliation: Iowa State University, Ames, Iowa, USA

DOI: https://doi.org/10.3201/eid2707.203971

Table 1. Clinical data and gross pathology in instances of novel porcine morbillivirus among pig litters*

Litter ID	Sow parity	Crown to rump length, cm (condition of fetuses submitted)	Total born	No. mummified fetuses	No. stillbirths
A	6	24 (S)	13	0	4
B	4	24 (N)	12	0	4
C	6	29.5 (S)	NA	NA	NA
D	2	7 (M), 9 (M), 14 (M), 15 (M), 28 (Mod), 26 (Mod)	9	6	0
E	1	7 (M), 7 (M), 9 (M), 12 (M), 14 (M), 14 (M), 15 (M), 15 (M), 15 (M), 26 (Mod)	NA	NA	NA
F	1	16 (M), 23 (Mod), 19 (S)	9	3	0

*M, mummified fetus; Mod, fetus with moderate autolysis; N, neonatal mortality; NA, not available; S, stillborn fetus.

Pathology

At necropsy, we recorded the condition, including neonatal morality, mummified fetus, moderate autolysis, or stillbirth, and the crown-to-rump length (CRL) of each fetus or piglet in the case record (Appendix, https://wwwnc.cdc.gov/EID/article/27/7/20-3971-App1.pdf). We processed fixed tissues by standard technique, stained tissues by using hematoxylin and eosin, and performed histologic evaluations. We used sections from the paraffin blocks for ISH.

Porcine Morbillivirus ISH and PCR

At Iowa State University Veterinary Diagnostic Laboratory, we used RNAscope 2.5 HD Reagent Kit (Advanced Cell Diagnostics [ACD] bio-techne, https://acdbio.com) to perform RNA ISH according to the manufacturer's instructions for formalin-fixed paraffin-embedded samples (Appendix). We prepared fetal thoracic tissue homogenate from each litter, extracted nucleic acids, and performed PCR similar to previously described methods (*21*). We used fetal heart and lung to perform PCRs for porcine circovirus 2 and 3 (PCV2 and PCV3), porcine parovirus 1 (PPV1), and porcine reproductive and respiratory virus (PRRSV). We used kidney tissue for *Leptospira* sp. PCR (Appendix).

We developed a real-time reverse transcription PCR (RT-PCR) specific for PoMV by using the MBLV-900F and MBLV-988R primers and the MBL-959P probe (Appendix Table 2). In addition, we performed a previously described real-time RT-PCR (*22*) to rule out porcine rubulavirus coinfection (Appendix).

Metagenomics and Bioinformatics Analysis

We extracted total nucleic acid of 2 pooled fetal thoracic tissue samples and prepared sequencing libraries, as described previously (*23*). The first pool consisted of litters A and B; the second pool consisted of litters D and E. We used the MiSeq platform (Illumina, https://www.illumina.com) to sequence the libraries by using the MiSeq 600-Cycle Reagent Kit v3 (Illumina). We preprocessed raw sequencing reads and classified reads by using Kraken version 0.10.5-β (*24*) with the standard database. We used Kaiju version 1.6.2 (*25*) to classify unclassified reads, and used KronaTools-2.6 (*26*) to generate the interactive html charts for hierarchical classification results. We extracted reads of the virus of interest, morbillivirus, from the classification results for de novo assembly by using ABySS version 1.3.9 (*27*), iva version 1.0.8 (*28*), and Spades version 3.11.1 (*29*). We manually refined the resulting contigs, and then curated and elongated contigs by using BLAST (https://blast.ncbi.nlm.nih.gov), SeqMan Pro (https://seqman.software), and integrated genomics viewer for visualization (*30*). We closed the genome gap by conventional RT-PCR with specifically designed primers.

We used ClustalW (http://www.clustal.org) to generate multiplex sequence alignments. We constructed phylogenetic trees based on whole-genome sequences and amino acid sequences of the L protein from aligned sequences by the maximum likelihood model in MEGA version X (https://www.megasoftware.net). We used L protein sequences because paramyxoviruses currently are classified based on the sequence comparison of L protein, the RNA-dependent RNA polymerase. We evaluated the robustness of the phylogenetic tree by bootstrapping using 500 replicates. We used interactive Tree of Life (iTOL, https://itol.embl.de) to display, manipulate, and annotate bases of the whole-genome sequence and L protein amino acid sequence trees (*31*).

Genome Gap Closure and Whole Genome Sequencing

We used conventional RT-PCR to close the genome gap and confirm the genome sequence assembled from next-generation sequencing (NGS). We used 1 pair of primers to close the genome gap and 14 pairs to confirm the genome sequence (Appendix Table 2).

Results

Gross Pathology and Pathogen Detection

Among 22 porcine fetuses from the 6 litters (A–F) submitted for diagnostic investigation, CRL length varied from 7 to 29.5 cm (Table 1). We noted the litter identification, sow parity, CRL by individual fetus and piglet, and total number born and number of

affected fetuses in each litter as reported by the sow farm (Table 1). Submitted fetuses were 1 neonatal death, in which necropsy revealed aerated lungs; 3 stillbirths, all of which were full-term, fresh-type fetuses but had fetal atelectasis; 14 mummified fetuses, in which in utero death occurred with sufficient time for complete dehydration of tissue; and 4 fetuses with moderate autolysis, in which in utero death occurred without sufficient time for complete dehydration of tissue. Gross evaluation of stillbirths and the single neonatal death was unremarkable.

To address differential diagnoses, we used quantitative PCR (qPCR) to detect known swine viral and bacterial reproductive pathogens. We did not detect PCV2, PCV3, PRRSV, PPV1, or *Leptospira* sp. by qPCR or quantitative RT-PCR (qRT-PCR) in any litter.

Metagenomic Sequencing

We pooled samples of fetal thoracic tissue from litters A and B (A–B), both of which had encephalitis noted histologically. We also pooled fetal thoracic tissue from litters D and E (D–E), which had leukocytes in the epicardium noted histologically. We performed NGS on the 2 pooled samples by using the MiSeq platform (Illumina). After using an in-house bioinformatics analysis pipeline, we detected and identified 693 paramyxovirus-like reads in A–B and 118,772 in D–E. No reads of other pathogens were identified. De novo assembly obtained 2 contigs with 4,869 and 10,456 nt from pooled sample A–B and another 2 contigs from pooled sample D–E. The nucleotide sequences of the contigs from A–B and D–E were 100% identical but the contigs assembled from pooled sample D–E were slightly longer, 5,042 and 10,705 nt. Sequence analysis of the 4 contigs suggested the presence of a previously undescribed paramyxovirus of genus *Morbillivirus*. The 2 shortest contigs had <40% nt identity to PDV (GenBank accession no. KC802221) and CDV (GenBank accession no. AF014953) at the 3′ end. The 2 longer contigs had >60% nt identity to PDV and CDV at the 5′ end. We propose this paramyxovirus be named porcine morbillivirus (PoMV).

Genome Sequence Characterization

A complete genome sequence of PoMV (GenBank accession no. MT511667) was obtained by using RT-PCR to fill the gap between the 2 contigs. We designed 14 pairs of primers according to the obtained genome sequence and sequenced the RT-PCR products again, confirming the accuracy of the whole-genome sequence. The genome size of PoMV is 15,714 bases and has a G+C content of 45.19%. The 3′ leader sequence of the PoMV is 55 nt with 13/20 initial nt being highly conserved among morbilliviruses (Appendix Figure 1). PoMV has a 5′ trailer sequence of 41 nt, similar to other morbilliviruses that have a trailer sequence of 40 or 41 nt (Appendix Figure 1), except for FeMV, which has an unusually long trailer sequence of 400 nt. The last 11 nt of 5′ trailer sequences are conserved in all morbilliviruses.

The genome of PoMV contains 6 genes, 3′-N-P/V/C-M-F-H-L-5′, similar to other morbilliviruses. The pairwise alignment of the predicted gene and gene products in PoMV and other paramyxoviruses showed the highest nucleotide and amino acid identities with members of the genus *Morbillivirus* (Table 2). Nucleotide identities were 56.3%–66.6% for N, 44.3%–61.4% for P, 62.4%–68.4% for M, 50.2%–64.1% for F, 31.7%–52.7% for H, and 58.1%–68.1% for L; amino acid identities were 56.3%–70.3% for N, 26%–50.1% for P, 60.9%–78.8% for M, 42.2%–65.5% for F, 15.7%–45.4% for H, and 56.2%–75.8% for L. PoMV had the highest identities to PDV and CDV and the lowest to FeMV (Table 2).

We noted PoMV included the conserved N terminal motif MA(T/S)L in morbilliviruses containing the sequence MASL in the nucleoprotein (N) (Appendix Figure 2). We identified a leucine-rich motif at aa positions 4–11 and 70–77 in the N protein of PoMV (Appendix Figure 2). We identified 2 initiation codons in the P/V/C gene of PoMV; the first translates P and V and the second translates C. In addition, we identified a UC-rich editing site, ttaaaagggg, in the P/V/C gene of PoMV. We detected a conserved cleavage site, RRQKRF, ≈114 aa residues from the N terminus of the F protein. The F protein of PoMV also contains 9/10 Cys residues and 3 potential N-glycosylation sites.

Phylogenetic Analyses

We constructed phylogenetic trees by using the whole-genome sequences (Figure 1, panel A) and the predicted aa sequences of the L gene, the RNA-dependent RNA polymerase gene of PoMV and other members of *Paramyxoviridae* (Figure 1, panel B). In both phylogenetic trees, PoMV clustered with other morbilliviruses, with high bootstrap supporting a distinct subgroup (Figure 1). Both phylogenetic analyses also confirmed the findings from the results of pairwise alignment and demonstrated that PoMV was most closely related to CDV and PDV; closely related to CMV, PPRV, MeV, and RPV; and most distantly related to FeMV in the genus *Morbillivirus* (Figure 1). Overall, these data further support that PoMV is a previously undescribed member in the genus *Morbillivirus*, subfamily *Orthoparamyxovirinae*, and family *Paramyxoviridae*.

Histopathology and PoMV ISH

We performed histologic examination and RNA ISH by litter (Table 3). For all 6 litters, the positive control probe, Ss-PPIB, was positive and the negative control probe, DapB, was negative on the single slide assayed (data not shown). PoMV RNA was not detected by ISH in the cerebrum and cerebellum of 2 stillborn fetuses from unaffected litters used as negative controls (data not shown).

The single stillborn fetus submitted from litter A had multifocal areas of mineralization associated with neuronal necrosis and rarefaction in the cerebrum and brainstem (Figure 2, panel A). Cerebral vessels were occasionally surrounded by lymphocytes. Eosinophilic intranuclear and intracytoplasmic viral inclusion bodies were in neurons (Figure 2, panel A) and glial cells in the cerebrum and internal granular layer of the cerebellum. Rarely, respiratory epithelium lining bronchi and bronchioles contained intranuclear viral inclusion bodies. Histologic evaluation of the heart, spleen, and kidney was diagnostically unremarkable. Moderate autolysis of the liver

Table 2. Pairwise identities of predicted gene and gene products of porcine morbillivirus compared with other paramyxoviruses*

	N		P		M		F		A (H)		L	
Paramyxovirus	CS	AA	CS	AA	CS	AA	CS	AA	CS	AA	CS	AA
Morbillivirus (*Orthoparamyxovirinae*)												
CDV	65.8	69.0	61.4	48.3	67.3	77.6	62.5	64.2	52.7	45.4	68.1	75.2
PDV	66.6	70.3	61.3	50.1	68.0	78.8	62.4	62.6	51.5	44.6	67.5	75.8
CMV	62.7	66.4	57.2	43.9	68.4	77.9	64.1	65.5	48.2	39.9	65.3	72.0
PPRV	60.6	64.9	54.9	41.0	65.6	72.5	62.8	62.9	45.6	34.5	64.5	69.7
RPV	62.8	66.0	54.5	39.7	65.2	73.1	61.9	63.1	44.8	32.6	65.3	70.6
MeV	63.1	65.4	54.2	37.9	65.7	74.6	60.9	63.9	45.3	34.5	65.3	70.2
FeMV	56.3	56.3	44.3	26.0	62.4	60.9	50.2	42.2	31.7	15.7	58.1	56.2
Salemvirus (*Orthoparamyxovirinae*)												
Salem virus	50.7	45.0	33.5	21.2	53.8	47.9	45.9	35.5	27.1	11.9	52.6	46.8
Narmovirus (*Orthoparamyxovirinae*)												
TupPV	44.0	32.3	37.3	19.6	51.6	43.5	46.0	33.3	27.1	10.9	54.2	49.5
MosPV	43.7	36.0	36.7	20.9	54.1	48.8	46.0	35.9	30.1	10.9	54.4	49.6
Jeilongvirus (*Orthoparamyxovirinae*)												
Tailam virus	45.4	35.4	38.9	18.4	53.9	46.8	43.5	33.8	30.3	12.6	52.8	48.1
MmlPV	46.5	34.0	39.0	21.5	52.5	46.4	44.3	32.1	31.2	11.9	53.2	47.8
Henipavirus (*Orthoparamyxovirinae*)												
Nipah virus	42.1	30.3	34.4	18.8	52.7	45.2	45.3	32.1	30.8	11.7	51.2	46.2
Bat Paramyxovirus	42.9	33.1	34.6	16.9	52.8	43.3	46.4	32.6	26.8	9.4	51.1	45.0
Ferlavirus (*Orthoparamyxovirinae*)												
FdlPV	41.7	25.7	35.1	13.3	46.1	34.9	42.9	29.0	28.1	10.9	48.2	39.6
Aquaparramyxovirus (*Orthoparamyxovirinae*)												
AsaPV	38.8	23.0	30.4	11.4	45.2	36.7	43.2	30.4	29.1	9.9	47.9	39.0
Respirovirus (*Orthoparamyxovirinae*)												
BpiPV-3	37.1	20.2	31.5	12.8	45.0	35.7	40.9	25.8	30.4	11.7	48.2	37.3
HPIV-1	38.1	20.4	31.1	11.2	45.2	37.1	42.9	26.8	29.8	9.7	47.9	38.7
Pararubulavirus (*Rubulavirinae*)												
Tioman virus	38.5	24.7	33.6	15.3	38.3	23.3	38.5	23.5	30.3	9.6	40.9	29.4
Orthorubulavirus (*Rubulavirinae*)												
SipPV	37.5	23.7	34.5	11.9	37.7	18	38.1	24.1	30.2	10.1	41.1	29.3
PrPV	38.0	23.8	32.8	12.8	37.6	18.6	39.2	28.6	29.9	10.1	40.8	28.5
Orthoavulavirus (*Avulvirinae*)												
NDV	37.0	23.1	33.8	13.2	34.4	20.8	40.5	25.2	28.7	11.5	40.2	27.1
ApPV	37.3	24.5	33.2	ND	33.7	19.6	41.7	26.2	28.2	11.2	39.9	27.2
Paraavulavirus (*Avulvirinae*)												
AviPV-3	38.4	23.7	33.2	17.1	35.5	17.4	38.3	21.7	29.3	13.4	39.5	26.4
Mataavulavirus (*Avulvirinae*)												
AviPV-2	38.8	26.9	35.2	13.9	35.7	20.8	42.0	26.8	27.2	13.6	39.6	26.8
Synodovirus (*Metaparamyxovirinae*)												
WtlPV	34.9	18.2	ND	ND	39.2	23.7	40.8	27.1	27.1	10.6	44.0	34.3
Unassigned to a genus or subfamily												
WtPV	34.7	15.8	ND	ND	38.4	16.6	36.5	20.2	ND	8.2	41.8	26.3
WhPV	35.7	15.1	ND	ND	35.1	17.4	30.0	8.9	28.6	11.2	40.4	25.1
WpssPV	34.8	17.2	ND	ND	29.5	ND	35.7	19.0	27.3	8.7	42.7	26.7

*AA, amino acid sequence; AsaPV, Atlantic salmon paramyxovirus; APV, Antarctic penguin virus A; AviPV-2, avian avualavirus 2; AviPV-3, avian avualavirus 3; BpiPV-3, bovine parainfluenza virus 3; CDV, canine distemper virus; CMV, cetacean morbillivirus; CS, coding sequence; FdlPV, Fer-de-lance virus; FeMV, feline morbillivirus; HPIV-1, human parainfluenza virus 1; MeV, measles virus; MmlPV, Mount Mabu Lophuromys virus 1; MosPV, Mossman virus; ND, not detected; NDV, Newcastle disease virus (Avian avualavirus 1); PDV, phocine distemper virus; PPRV, peste des petits ruminants virus; PrPV, porcine rubulavirus; RPV, Rinderpest virus; SipPV, simian parainfluenza virus; TupPV, Tupaia paramyxovirus; WhPV, Wenling hoplichthys paramyxovirus; WpssPV, Wenzhou Pacific spadenose shark paramyxovirus; WtlPV, Wenling triplecross lizardfish paramyxovirus; WtPV, Wenling tonguesole paramyxovirus.

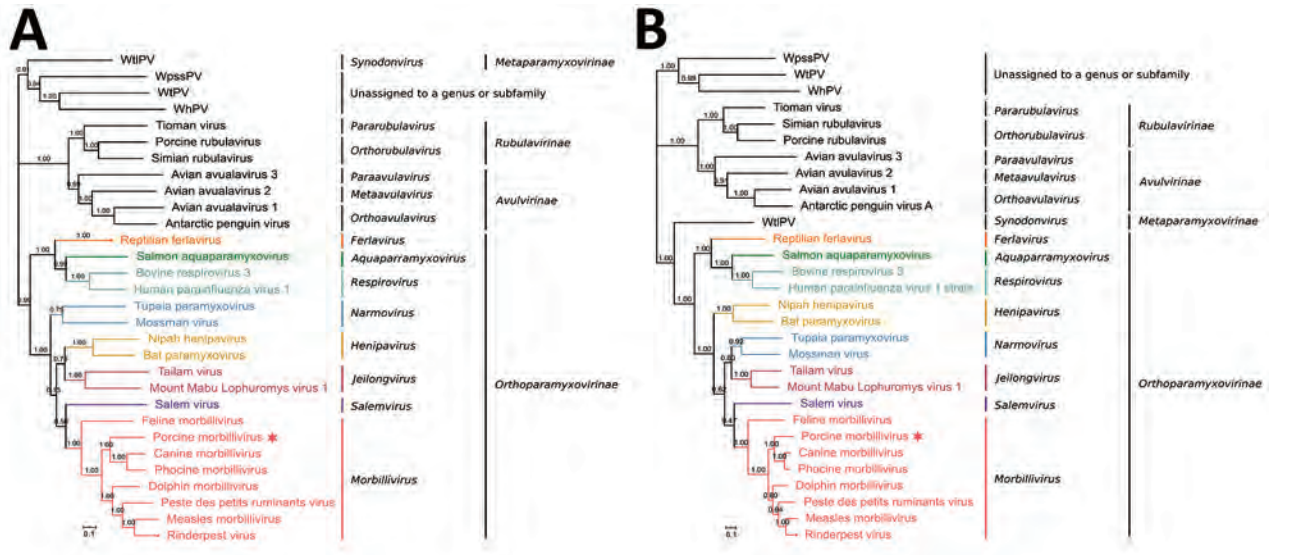

Figure 1. Phylogenetic analysis of novel porcine morbillivirus (PoMV, star) detected among infected swine. A) Phylogenetic analysis of whole genome sequence. B) Phylogenetic analysis of L amino acid sequence. The trees were constructed by maximum likelihood method with bootstrap values calculated from 500 trees and rooted on midpoint. Scale bars indicate nucleotide substitutions per site. WhPV, Wenling hoplichthys paramyxovirus; WpssPV, Wenzhou pacific spadenose shark paramyxovirus; WtlPV, Wenling triplecross lizardfish paramyxovirus; WtPV, Wenling tonguesole paramyxovirus.

precluded a thorough histologic evaluation. ISH detected extensive PoMV RNA in the cerebellum in the external granular layer, molecular layer, internal granular layer, and white matter (Figure 2, panel B) and in neurons and axons in the cerebrum (Figure 2C). We also detected PoMV RNA in clusters of respiratory epithelium lining bronchi and bronchioles, scattered lymphocytes and aggregates of lymphocytes in periarteriolar lymphoid sheaths in the spleen, and aggregates of tubular epithelium in rare tubules within the cortex of the kidney. ISH did not detect PoMV RNA in the heart or liver.

The single full-term piglet submitted from litter B had multifocal mineralization and rare satellitosis in the cerebrum (Figure 2, panel D). Adjacent to the lateral ventricle, marked neuropil rarefaction, mineralization, neuronal necrosis, and leukocyte infiltration were visible. Numerous viral inclusion bodies could be seen in neurons (Figure 2, panel D) and glial cells. Histologic evaluation of the cerebellum, lung, heart, spleen, liver, and kidney was diagnostically unremarkable. PoMV was detected by ISH in the gray matter of the cerebrum with extensive labeling; and in the white matter with less but still abundant labeling (Figure 2, panel E). PoMV also was detected by ISH in low to moderate numbers of respiratory epithelium in multifocal bronchi and bronchioles, and individual lymphocytes were noted in the spleen. PoMV RNA was not detected in the heart, kidney, or liver.

Litter C also was represented by a single stillbirth in which histologic evaluation of the cerebrum, cerebellum, lung, heart, and kidney was diagnostically unremarkable. Moderate autolysis of the liver and spleen precluded a thorough histologic evaluation. However, PoMV was detected by ISH in the endothelial cells of a single vessel in the cerebrum, scattered cells within alveolar septa and numerous lymphocytes within the spleen (Figure 2, panel F). PoMV was not detected by ISH in the heart.

Table 3. Summary of histopathology and RNA in situ hybridization in investigation of novel porcine morbillivirus in pig litters*

Litter	Cerebrum		Cerebellum		Lung		Heart		Spleen		Kidney		Liver		Placenta	
ID	Histo	ISH	Histo	ISH	Histo	ISH	Histo	ISH	Histo	ISH	Histo	ISH	Histo	ISH	Histo	ISH
A	N, M, I	+++	I	+++	I	++	U	Neg	U	+	U	+	Auto	Neg	NA	NA
B	N, M, I, S	+++	U	ND	U	++	U	Neg	U	+	U	Neg	U	Neg	NA	NA
C	U	+	U	ND	U	+	U	Neg	Auto	+++	U	ND	Auto	ND	NA	NA
D	NA	NA	NA	NA	U	++	L	Neg	Auto	+++	U	+	Auto	Neg	L	+
E	NA	NA	NA	NA	U	+++	L	+	NA	NA	U	+	NA	NA	NA	NA
F	U	ND	U	ND	U	++	U	Neg	U	Neg	U	ND	U	ND	L	+++

*Auto, autolysis; Histo, histopathology; I, inclusions; ID, identification; ISH, in situ hybridization; L, leukocytes; M, mineralization; N, necrosis; NA, not available; ND, not done; S, satellitosis; U, unremarkable; +, minimal labeling; ++, moderate labeling; +++, abundant labeling.

Litter D was represented by 3 mummified fetuses and 2 fetuses with moderate autolysis. In a single section of the heart from a fetus with moderate autolysis, we noted mononuclear leukocytes in the epicardium. Lung and kidney of fetuses with moderate autolysis were unremarkable. Autolysis of the spleen and liver from these fetuses and lung, kidney, and heart from mummified fetuses precluded histologic evaluation. Despite severe autolysis and mineralization, leukocytes were observed in the allantoic connective tissue of the placenta. PoMV was detected by ISH in the alveolar septa, bronchi, and bronchioles of the lung of both fetuses with moderate autolysis as well as bronchi and bronchioles of a mummified fetus. PoMV RNA also was detected in scattered lymphocytes in one fetus with moderate autolysis and abundant lymphocytes in the spleen of the other. Mononuclear leukocytes in the allantoic connective tissue and allantoic epithelium of the placenta also contained PoMV RNA (Figure 2, panel G) as did rare renal tubular epithelium and endothelium of a vessel adjacent to the renal pelvis in a mummified fetus (Figure 2, panel H). PoMV was not detected by ISH in the heart or liver of moderately autolyzed fetuses.

Litter E consisted of 9 mummified fetuses and 1 fetus with moderate autolysis. In a single section of 1 heart, the epicardium contained multifocal mononuclear leukocyte aggregates. The lung and kidney were unremarkable in the fetus with moderate autolysis. Autolysis of the heart, lung, and kidney of mummified fetuses precluded histologic evaluation. PoMV was detected by ISH extensively in the conducting airway epithelium and alveolar septa of the lung (Figure 2, panel I), renal tubules, and in rare leukocytes in the epicardium of the fetus with moderate autolysis. ISH was not performed on mummified fetal tissues.

Litter F was represented by a mummified fetus, a fetus with moderate autolysis, and a stillborn fetus. Abundant mononuclear leukocytes were expanding the allantoic connective tissue of the placenta. Histologic evaluation of the cerebrum, cerebellum, spleen, and liver of the stillborn fetus was diagnostically unremarkable. Kidney and lung of the stillborn and moderately autolyzed fetuses were unremarkable. The heart was unremarkable in all fetuses. Autolysis of the mummified fetus precluded evaluation of the lung and kidney. PoMV was detected in the epithelium of

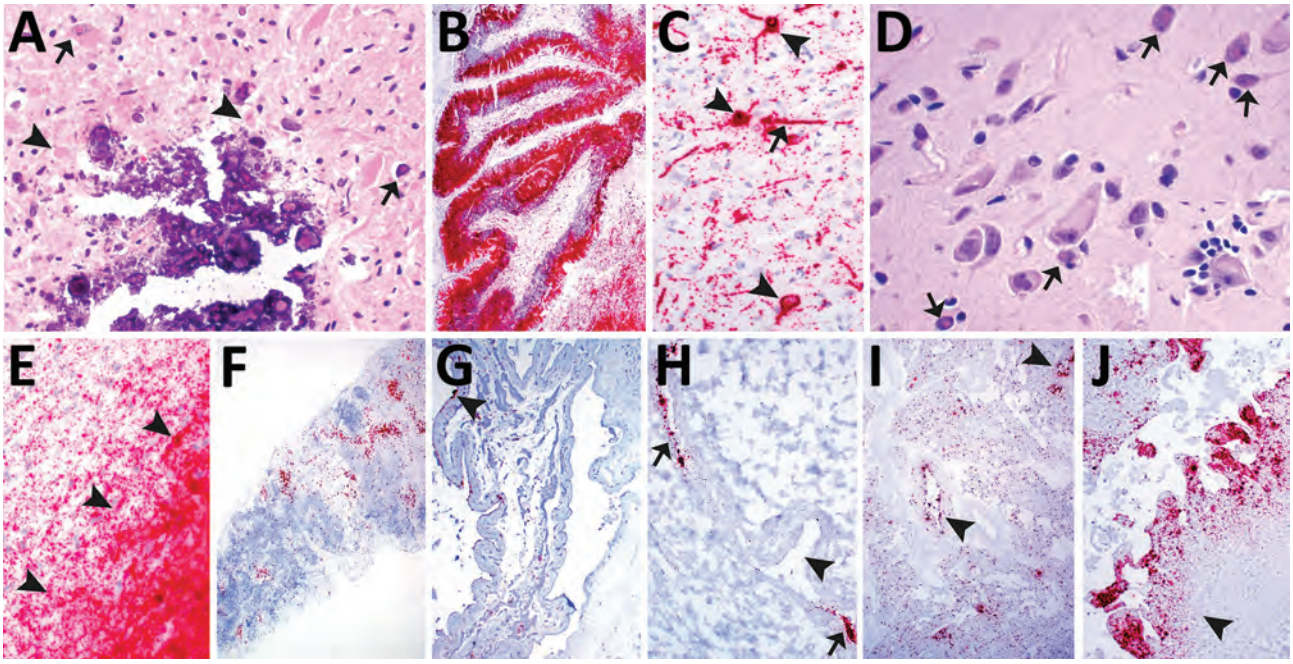

Figure 2. Histologic lesions and porcine morbillivirus (PoMV) RNA in situ hybridization (ISH, red) of tissue of infected swine. A) Histologic section of cerebrum from fetus A stained by hematoxylin and eosin. Arrowheads indicate neuronal necrosis; arrows indicate mineralization and viral inclusion bodies in a neuron and glial cell. B) Cerebellum of fetus A with extensive detection of PoMV by ISH. C) Cerebrum of fetus A; arrowheads indicate ISH labeling within the cytoplasmic and nuclear compartment of neurons; arrow indicates ISH labelling in an axon. D) Cerebrum of fetus B; arrows indicate multiple viral inclusion bodies in neurons; inset displays satellitosis. E) Cerebrum of fetus B showing extensive PoMV detection by ISH. Arrowheads indicate the border of white and gray matter. F) Detection of PoMV by ISH in the spleen of fetus C. G) Detection of PoMV by ISH in a placenta from litter D; arrowhead indicates allantoic epithelium. H) Detection of PoMV by ISH in a renal vessel of a fetus from litter D; arrows indicate the endothelium and arrowhead indicates the vessel lumen. I) Detection of PoMV by ISH in conducting airways (arrowheads) and alveolar septa in the lung of fetus from litter E. J) Detection of PoMV by ISH in the allantoic connective tissue of the placenta and leukocytes from litter F; arrowhead indicates infiltration of leukocytes.

conducting airways and alveolar septa of the mummified fetus and the fetus with moderate autolysis. We noted extensive labeling in the allantoic connective tissue and mononuclear leukocytes throughout the placenta (Figure 2, panel J). PoMV was not detected in the lung, heart, or spleen of the stillborn fetus or heart of the fetus with moderate autolysis.

PoMV Real-Time RT-PCR

Fetal thoracic tissues from litters A, B, D, and E were further subjected to real-time RT-PCR to approximate the viral load by litter. All were positive for PoMV with fetal thoracic tissues from litters A and E having a higher viral load. Litter A had a quantification cycle (C_q) value of 19.7; the C_q for litter E was 19.4. Fetal thoracic tissues from litters B and D had a lower viral load values; B had C_q of 23.4 and D had C_q of 20.2. PoMV was not detected by real-time RT-PCR in the fetal thoracic tissues of 2 litters of unaffected fetuses selected as negative controls. In addition, porcine rubulavirus was not detected in any sample by RT-PCR.

Discussion

We report a novel porcine morbillivirus, PoMV, as a cause of fetal death, encephalitis, and placentitis among 6 swine litters. The synchronous use of 3 independent and complementary lines of evidence, pathology, metagenomic sequencing, and in situ hybridization, aided in PoMV discovery. Although several paramyxoviruses have been found, the existence of a naturally occurring morbillivirus in swine previously was unknown. Analyses of predicted nt and aa sequences of 6 genes revealed that PoMV has the highest nucleotide (31.7%–68.1%) and amino acid (26%–75.2%) identities with members in the genus *Morbillivirus* in the N, P, M, F, H, and L genes (Table 2). Phylogenetic analyses based on the whole genome sequence (Figure 1, panel A) and amino acid sequence of the L gene (Figure 1, panel B) further demonstrated that PoMV forms a distinct cluster in morbillivirus and is most closely related to PDV and CDV.

Experimental inoculation of CDV and PPRV in domestic pigs has resulted in infection (*32*,*33*), but no morbillivirus previously has been known to infect swine naturally. Other viruses within the family *Paramyxoviridae* that infect swine include porcine rubulavirus (genus *Orthorubulavirus*, subfamily *Rubulavirunae*), Menangle virus (genus *pararubulavirus*, subfamily *Rubulavirunae*), Nipah virus (genus *Henipavirus*, subfamily *Orthoparamyxovirinae*), and porcine parainfluenza virus 1 (genus *Respirovirus*, subfamily *Orthoparamyxovirinae*). Among these, only porcine rubulavirus and Menangle virus are thought to cause fetal mummification and stillbirths, as observed with PoMV (*34*,*35*). Histologic lesions noted for PoMV are similar to Menangle virus and included encephalitis, viral inclusion bodies, and nonsuppurative myocarditis (*36*).

Similar to our findings with PoMV, MeV has been reported to be transmitted vertically resulting in premature stillbirth, stillbirth, premature birth, neonatal death, or congenital measles (*6*,*37*,*38*). Viral inclusion bodies have been observed in human congenital MeV infection and MeV was detected in placenta and splenic lymphocytes by immunohistochemistry (*39*). Herein, viral inclusion bodies were commonly observed in the cerebrum and cerebellum (Table 3; Figure 2, panels A,D) and rarely in the respiratory epithelium lining conducting airways. ISH demonstrated presence of PoMV in the placenta (Figure 2, panels G, J) and splenic lymphocytes (Figure 2, panel F), and in the cerebrum (Figure 2, panels C, E), cerebellum (Figure 2, panel B), lung (Figure 2, panel I), and to a lesser extent in the kidney (Figure 2, panel H) and heart. Of note, the degree of viral involvement within the monochorionic placenta and effects of MeV on human monozygotic twins was inconsistent; 1 in utero death at 32 weeks gestation and 1 surviving infant with no clinical signs of MeV infection (*39*). This observation, along with the placentation of swine, large litter size, and observations from other swine viral reproductive pathogens (*40*), likely accounts for the variable effects on litters, which were characterized by fetal and piglet death at various stages of gestation and resulted in fetal mummification, in utero death, and stillbirth, along with the variability of ISH staining observed among fetuses and between litters.

Cellular tropism of PoMV determined by ISH aligns with other morbilliviruses, including MeV. A common entry receptor for morbilliviruses is CD150 or signaling lymphocytic activation molecule (SLAM), which is expressed on activated lymphocytes, dendritic cell subsets, and macrophages and cells in the alveolar lumen and lining the alveolar epithelium (*41*–*44*). PoMV RNA was observed in the alveolar septa, lymphocytes of the spleen, and mononuclear leukocytes in the placenta and epicardium, which suggest that PoMV also might use CD150. Morbilliviruses infect epithelia by using nectin-4, which is expressed on the basolateral surface (*45*,*46*). We detected PoMV RNA in the allantoic epithelium of the placenta, epithelium of bronchi and bronchioles, and in rare instances the renal tubular epithelium. In addition, we detected PoMV in the endothelium of a cerebral and renal vessel, and the most extensive staining was in the cerebrum and cerebellum, including neurons. Previous studies have shown that no detectable expression of SLAM was found in human neurons (*47*) and extremely low

expression of nectin-4 was detected in central nervous system cells and tissues (*48*). In contrast, CD46 is a widely distributed complement regulatory protein expressed on all nucleated cells with labeling noted in the cerebral endothelium as well as ependymal cells, neurons, and oligodendrocytes (*47*). Accordingly, PoMV also could use CD46 as seen in some MeV strains.

Our study provides essential information about a newly discovered pathogen within the *Morbillivirus* genus, but much is left to learn. The geographic distribution and species susceptibility of PoMV currently is unknown. Virus isolation to facilitate research, in vitro studies evaluating cell entry receptors, and in vivo studies to further elucidate pathogenesis and generate samples of known status for diagnostic assay development and evaluation are needed. Nonetheless, this discovery opens the door to a new and possibly more applicable model of disease to drive research forward (*49*).

Acknowledgments

We thank the staff of Iowa State University Veterinary Diagnostic Laboratory for their assistance with tissue collection and processing, including Kaleigh Bell, Kevin Berkland, Sally Howard, Megan Jackson, Scott Kostohryz, Austin Kosusnik, Emily Kurtz, Haley McClure, Bonnie Snovelle, and Jerry Snyder; and the histology technicians, including Katherine Baber-Dillavou, Rosalyn Branaman, Dawn Fenneman, Victoria Green, Haley Lambert, and Linda Smith. We also thank Jennifer Groeltz-Thrush for performing the in situ hybridization assay.

About the Author

At the time of this study, Dr. Arruda was a diagnostic pathologist at the Iowa State University Veterinary Diagnostic Laboratory and associate professor in the Department of Veterinary Diagnostic and Production Animal Medicine. Her research focused on the ecology and pathophysiology of infectious diseases of swine. She has recently taken a research position at the US Agricultural Research Services focusing on the prevention and control of influenza A virus in swine.

References

1. Rima B, Balkema-Buschmann A, Dundon WG, Duprex P, Easton A, Fouchier R, et al.; ICTV Report Consortium. ICTV virus taxonomy profile: *Paramyxoviridae.* J Gen Virol. 2019;100:1593–4. https://doi.org/10.1099/jgv.0.001328
2. Pfeffermann K, Dörr M, Zirkel F, von Messling V. Morbillivirus pathogenesis and virus-host interactions. Adv Virus Res. 2018;100:75–98. https://doi.org/10.1016/bs.aivir.2017.12.003
3. Amarasinghe GK, Ayllón MA, Bào Y, Basler CF, Bavari S, Blasdell KR, et al. Taxonomy of the order Mononegavirales: update 2019. Arch Virol. 2019;164:1967–80. https://doi.org/10.1007/s00705-019-04247-4
4. Lamb RA, Parks GD. Paramyxoviridae: the viruses and their replication. In: Fields BN, Knipe DM, Howley PM, editors. Fields virology. 6th ed. Philadelphia: Lippincott Williams & Wilkins; 2013. p. 957–95.
5. Black FL. Epidemiology of Paramyxoviridae. In: Kingsbury DW, editor. The paramyxoviruses. In: Fraenkel-Conrat H and Wagner RR, series editors. The viruses. 1st ed. New York: Springer Science+Business Media; 1991. p. 509–36.
6. Chiba ME, Saito M, Suzuki N, Honda Y, Yaegashi N. Measles infection in pregnancy. J Infect. 2003;47:40–4. https://doi.org/10.1016/S0163-4453(03)00045-8
7. Furuse Y, Suzuki A, Oshitani H. Origin of measles virus: divergence from rinderpest virus between the 11th and 12th centuries. Virol J. 2010;7:52. https://doi.org/10.1186/1743-422X-7-52
8. de Vries RD, Ludlow M, de Jong A, Rennick LJ, Verburgh RJ, van Amerongen G, et al. Delineating morbillivirus entry, dissemination and airborne transmission by studying in vivo competition of multicolor canine distemper viruses in ferrets. PLoS Pathog. 2017;13:e1006371. https://doi.org/10.1371/journal.ppat.1006371
9. Rudd PA, Cattaneo R, von Messling V. Canine distemper virus uses both the anterograde and the hematogenous pathway for neuroinvasion. J Virol. 2006;80:9361–70. https://doi.org/10.1128/JVI.01034-06
10. Summers BA, Greisen HA, Appel MJ. Early events in canine distemper demyelinating encephalomyelitis. Acta Neuropathol. 1979;46:1–10. https://doi.org/10.1007/BF00684797
11. Stephan HA, Gay GM, Ramírez TC. Encephalomyelitis, reproductive failure and corneal opacity (blue eye) in pigs, associated with a paramyxovirus infection. Vet Rec. 1988;122:6–10. https://doi.org/10.1136/vr.122.1.6
12. Bowden TR, Westenberg M, Wang LF, Eaton BT, Boyle DB. Molecular characterization of Menangle virus, a novel paramyxovirus which infects pigs, fruit bats, and humans. Virology. 2001;283:358–73. https://doi.org/10.1006/viro.2001.0893
13. Mohd Nor MN, Gan CH, Ong BL. Nipah virus infection of pigs in peninsular Malaysia. Rev Sci Tech. 2000;19:160–5. https://doi.org/10.20506/rst.19.1.1202
14. Qiao D, Janke BH, Elankumaran S. Complete genome sequence and pathogenicity of two swine parainfluenzavirus 3 isolates from pigs in the United States. J Virol. 2010;84:686–94. https://doi.org/10.1128/JVI.00847-09
15. Lau SKP, Woo PCY, Wu Y, Wong AYP, Wong BHL, Lau CCY, et al. Identification and characterization of a novel paramyxovirus, porcine parainfluenza virus 1, from deceased pigs. J Gen Virol. 2013;94:2184–90. https://doi.org/10.1099/vir.0.052985-0
16. Palinski RM, Chen Z, Henningson JN, Lang Y, Rowland RRR, Fang Y, et al. Widespread detection and characterization of porcine parainfluenza virus 1 in pigs in the USA. J Gen Virol. 2016;97:281–6. https://doi.org/10.1099/jgv.0.000343
17. Janke BH, Paul PS, Landgraf JG, Halbur PG, Huinker CD. Paramyxovirus infection in pigs with interstitial pneumonia and encephalitis in the United States. J Vet Diagn Invest. 2001;13:428–33. https://doi.org/10.1177/104063870101300513
18. Greig AS, Johnson CM, Bouillant AM. Encephalomyelitis of swine caused by a haemagglutinating virus. VI. Morphology of the virus. Res Vet Sci. 1971;12:305–9. https://doi.org/10.1016/S0034-5288(18)34153-5
19. Sasahara J, Hayashi S, Kumagai T, Yamamoto Y, Hirasawa N, Munekata K, et al. On a swine virus disease newly discovered in Japan its characteristic traits of pneumonia: 1. Isolation of the virus. 2. Some properties of the virus. Virus. 1954;4:131–9. https://doi.org/10.2222/jsv1951.4.131

20. Lipkind M, Shoham D, Shihmanter E. Isolation of a paramyxovirus from pigs in Israel and its antigenic relationships with avian paramyxoviruses. J Gen Virol. 1986;67:427–39. https://doi.org/10.1099/0022-1317-67-3-427
21. Arruda B, Piñeyro P, Derscheid R, Hause B, Byers E, Dion K, et al. PCV3-associated disease in the United States swine herd. Emerg Microbes Infect. 2019;8:684–98. https://doi.org/10.1080/22221751.2019.1613176
22. Rivera-Benitez JF, García-Contreras AC, Reyes-Leyva J, Hernández J, Sánchez-Betancourt JI, Ramírez-Mendoza H. Efficacy of quantitative RT-PCR for detection of the nucleoprotein gene from different porcine rubulavirus strains. Arch Virol. 2013;158:1849–56. https://doi.org/10.1007/s00705-013-1672-0
23. Zhang J, Zheng Y, Xia XQ, Chen Q, Bade SA, Yoon KJ, et al. High-throughput whole genome sequencing of porcine reproductive and respiratory syndrome virus from cell culture materials and clinical specimens using next-generation sequencing technology. J Vet Diagn Invest. 2017;29:41–50. https://doi.org/10.1177/1040638716673404
24. Wood DE, Salzberg SL. Kraken: ultrafast metagenomic sequence classification using exact alignments. Genome Biol. 2014;15:R46. https://doi.org/10.1186/gb-2014-15-3-r46
25. Menzel P, Ng KL, Krogh A. Fast and sensitive taxonomic classification for metagenomics with Kaiju. Nat Commun. 2016;7:11257. https://doi.org/10.1038/ncomms11257
26. Ondov BD, Bergman NH, Phillippy AM. Interactive metagenomic visualization in a Web browser. BMC Bioinformatics. 2011;12:385. https://doi.org/10.1186/1471-2105-12-385
27. Simpson JT, Wong K, Jackman SD, Schein JE, Jones SJ, Birol I. ABySS: a parallel assembler for short read sequence data. Genome Res. 2009;19:1117–23. https://doi.org/10.1101/gr.089532.108
28. Hunt M, Gall A, Ong SH, Brener J, Ferns B, Goulder P, et al. IVA: accurate de novo assembly of RNA virus genomes. Bioinformatics. 2015;31:2374–6. https://doi.org/10.1093/bioinformatics/btv120
29. Bankevich A, Nurk S, Antipov D, Gurevich AA, Dvorkin M, Kulikov AS, et al. SPAdes: a new genome assembly algorithm and its applications to single-cell sequencing. J Comput Biol. 2012;19:455–77. https://doi.org/10.1089/cmb.2012.0021
30. Robinson JT, Thorvaldsdóttir H, Wenger AM, Zehir A, Mesirov JP. Variant review with the integrative genomics viewer. Cancer Res. 2017;77:e31–4. https://doi.org/10.1158/0008-5472.CAN-17-0337
31. Letunic I, Bork P. Interactive Tree Of Life (iTOL) v4: recent updates and new developments. Nucleic Acids Res. 2019;47(W1):W256–9. https://doi.org/10.1093/nar/gkz239
32. Gaskin JM. Canine distemper virus in domesticated cats and pigs. Adv Enzymol Relat Areas Mol Biol. 1974;40:803–6.
33. Schulz C, Fast C, Schlottau K, Hoffmann B, Beer M. Neglected hosts of small ruminant morbillivirus. Emerg Infect Dis. 2018;24:2334–7. https://doi.org/10.3201/eid2412.180507
34. Hernández-Jáuregui P, Ramírez Mendoza H, Mercado García C, Moreno-López J, Kennedy S. Experimental porcine rubulavirus (La Piedad-Michoacan virus) infection in pregnant gilts. J Comp Pathol. 2004;130:1–6. https://doi.org/10.1016/S0021-9975(03)00058-6
35. Love RJ, Philbey AW, Kirkland PD, Ross AD, Davis RJ, Morrissey C, et al. Reproductive disease and congenital malformations caused by Menangle virus in pigs. Aust Vet J. 2001;79:192–8. https://doi.org/10.1111/j.1751-0813.2001.tb14578.x
36. Philbey AW, Kirkland PD, Ross AD, Davis RJ, Gleeson AB, Love RJ, et al. An apparently new virus (family Paramyxoviridae) infectious for pigs, humans, and fruit bats. Emerg Infect Dis. 1998;4:269–71. https://doi.org/10.3201/eid0402.980214
37. Eberhart-Phillips JE, Frederick PD, Baron RC, Mascola L. Measles in pregnancy: a descriptive study of 58 cases. Obstet Gynecol. 1993;82:797–801.
38. Ali ME, Albar HM. Measles in pregnancy: maternal morbidity and perinatal outcome. Int J Gynaecol Obstet. 1997;59:109–13. https://doi.org/10.1016/S0020-7292(97)00196-3
39. Ohyama M, Fukui T, Tanaka Y, Kato K, Hoshino R, Sugawara T, et al. Measles virus infection in the placenta of monozygotic twins. Mod Pathol. 2001;14:1300–3. https://doi.org/10.1038/modpathol.3880478
40. Malgarin CM, Nosach R, Novakovic P, Suleman M, Ladinig A, Detmer SE, et al. Classification of fetal resilience to porcine reproductive and respiratory syndrome (PRRS) based on temporal viral load in late gestation maternal tissues and fetuses. Virus Res. 2019;260:151–62. https://doi.org/10.1016/j.virusres.2018.12.002
41. Cocks BG, Chang CC, Carballido JM, Yssel H, de Vries JE, Aversa G. A novel receptor involved in T-cell activation. Nature. 1995;376:260–3. https://doi.org/10.1038/376260a0
42. Tatsuo H, Ono N, Yanagi Y. Morbilliviruses use signaling lymphocyte activation molecules (CD150) as cellular receptors. J Virol. 2001;75:5842–50. https://doi.org/10.1128/JVI.75.13.5842-5850.2001
43. Lemon K, de Vries RD, Mesman AW, McQuaid S, van Amerongen G, Yüksel S, et al. Early target cells of measles virus after aerosol infection of non-human primates. PLoS Pathog. 2011;7:e1001263. https://doi.org/10.1371/journal.ppat.1001263
44. Mesman AW, de Vries RD, McQuaid S, Duprex WP, de Swart RL, Geijtenbeek TBH. A prominent role for DC-SIGN+ dendritic cells in initiation and dissemination of measles virus infection in non-human primates. PLoS One. 2012;7:e49573. https://doi.org/10.1371/journal.pone.0049573
45. Mühlebach MD, Mateo M, Sinn PL, Prüfer S, Uhlig KM, Leonard VHJ, et al. Adherens junction protein nectin-4 is the epithelial receptor for measles virus. Nature. 2011;480:530–3. https://doi.org/10.1038/nature10639
46 Noyce RS, Bondre DG, Ha MN, Lin LT, Sisson G, Tsao MS, et al. Tumor cell marker PVRL4 (nectin 4) is an epithelial cell receptor for measles virus. PLoS Pathog. 2011;7:e1002240. https://doi.org/10.1371/journal.ppat.1002240
47. McQuaid S, Cosby SL. An immunohistochemical study of the distribution of the measles virus receptors, CD46 and SLAM, in normal human tissues and subacute sclerosing panencephalitis. Lab Invest. 2002;82:403–9. https://doi.org/10.1038/labinvest.3780434
48. Berglund L, Björling E, Oksvold P, Fagerberg L, Asplund A, Szigyarto CA-K, Persson A, et al. A genecentric Human Protein Atlas for expression profiles based on antibodies. Mol Cell Proteomics. 2008;7:2019–27. https://doi.org/10.1074/mcp.R800013-MCP200
49. Swindle MM, Makin A, Herron AJ, Clubb FJ Jr, Frazier KS. Swine as models in biomedical research and toxicology testing. Vet Pathol. 2012;49:344–56. https://doi.org/10.1177/0300985811402846

Address for correspondence: Ganwu Li and Bailey Arruda, Iowa State University Veterinary Diagnostic Laboratory, 1850 Christensen Dr, Ames, IA 50011, USA; email: liganwu@iastate.edu and bailey.arruda@usda.gov

Whole-Genome Analysis of *Streptococcus pneumoniae* Serotype 4 Causing Outbreak of Invasive Pneumococcal Disease, Alberta, Canada

James D. Kellner, Leah J. Ricketson, Walter H.B. Demczuk, Irene Martin, Gregory J. Tyrrell, Otto G. Vanderkooi, Michael R. Mulvey

After the introduction of pneumococcal conjugate vaccines for children, invasive pneumococcal disease caused by *Streptococcus pneumoniae* serotype 4 declined in all ages in Alberta, Canada, but it has reemerged and spread in adults in Calgary, primarily among persons who are experiencing homelessness or who use illicit drugs. We conducted clinical and molecular analyses to examine the cases and isolates. Whole-genome sequencing analysis indicated relatively high genetic variability of serotype 4 isolates. Phylogenetic analysis identified 1 emergent sequence type (ST) 244 lineage primarily associated within Alberta and nationally distributed clades ST205 and ST695. Isolates from 6 subclades of the ST244 lineage clustered regionally, temporally, and by homeless status. In multivariable logistic regression, factors associated with serotype 4 invasive pneumococcal disease were being male, being <65 years of age, experiencing homelessness, having a diagnosis of pneumonia or empyema, or using illicit drugs.

Streptococcus pneumoniae causes both invasive and noninvasive disease. Since the introduction of 7-valent and 13-valent protein-polysaccharide conjugated pneumococcal vaccines (PCV7 and PCV13, respectively) for children, vaccine serotype disease has been nearly eliminated among children and reduced indirectly among adults through herd effect (*1*–*4*). PCV7, administered as a 3-dose primary series plus a booster (3+1 dosing schedule) was introduced in Alberta, Canada, in 2002, followed in 2010 by PCV13 (2+1 dosing schedule); both vaccines include serotype 4. In Alberta Province and throughout Canada, invasive pneumococcal disease (IPD) has continued to decline in children <5 years of age since 2010, after PCV13 vaccine introduction, but among older age groups, IPD incidence has remained steady (*5*,*6*). No pediatric cases of IPD caused by *S. pneumoniae* serotype 4 have been diagnosed in Calgary, Alberta, Canada, since 2007 (*3*), although recent data from Calgary showed low levels of serotype 4 carriage in children identified by using PCR but not by using conventional culture (*7*).

In 2011, IPD caused by *S. pneumoniae* serotype 4 began to increase in adults in the province of Alberta, particularly among persons who were homeless. A previous outbreak in Alberta in 2005–2007 included serotypes 5 and 8, primarily in persons experiencing homelessness and those using illicit drugs (*8*). Homelessness is overrepresented as a factor in adult IPD cases: 18.8% of adults with IPD are homeless, despite only 0.2% of adults in Calgary being homeless (*9*). We conducted this study to examine clinical and demographic factors associated with serotype 4 IPD and to conduct molecular characterization and phylogenetic analysis from whole-genome sequencing (WGS) data on the serotype 4 isolates collected during the outbreak. Our goal was to clarify the dynamics of an outbreak of serotype 4 IPD in a post-vaccine community setting where serotype 4 had previously been uncommon.

Author affiliations: University of Calgary, Calgary, Alberta, Canada (J.D. Kellner, L.J. Ricketson, O.G. Vanderkooi); Alberta Health Services, Calgary Zone, Calgary (J.D. Kellner, O.G. Vanderkooi); National Microbiology Laboratory, Public Health Agency of Canada, Winnipeg, Manitoba, Canada (W.H.B. Demczuk, I. Martin, M.R. Mulvey); University of Alberta, Edmonton, Alberta (G.J. Tyrrell); Alberta Precision Laboratories–Public Health, Edmonton (G.J. Tyrrell)

DOI: https://doi.org/10.3201/eid2707.204403

Methods

Population

An inception cohort including all adult case-patients with serotype 4 IPD was identified through population-based surveillance during 2010–2018 in Calgary (2018 population 1,648,385) and Edmonton, Alberta (2018 population 1,393,380). Epidemic curves were generated for Calgary and Edmonton from the number of cases of serotype 4 IPD reported each year during 2000–2018 (Figure 1). We performed WGS to analyze isolates from all patients. We included all adults (≥18 years of age) with IPD reported in the Calgary *S. pneumoniae* Epidemiology Research (CASPER) (*4*) study during 2010–2018 in the clinical analysis.

Data Collection and Ethics

IPD is a reportable disease to the Ministry of Health in Alberta; therefore, all culture-confirmed cases of serotype 4 IPD in Calgary and Edmonton were identified. All pneumococcal isolates identified by diagnostic microbiology laboratories in Alberta must be submitted to Alberta Precision Laboratories–Public Health for pneumococcal serotyping. Serotyping was performed by quellung reaction (*10*). Clinical information was obtained from chart reviews in Calgary as part of the CASPER study. Ethics approval was provided for the clinical study by the Conjoint Health Research Ethics Board of the University of Calgary.

Analysis of Clinical Factors

We collected clinical data on all pneumococcal disease cases in Calgary identified through the CASPER study. Clinical data were not available for cases from Edmonton, so we included only cases from Calgary in the clinical analysis. We used tests of proportions to compare serotype 4 IPD with non–serotype 4 IPD in a univariable analysis to determine clinical and demographic factors and outcomes. We used the Student 2-tailed t-test to compare risk by age as a continuous variable. We chose clinical, demographic, and outcome factors a priori on the basis of biologic plausibility and clinical relevance. For underlying health conditions we sorted patients into 3 groups: those having no underlying conditions increasing risk for IPD; those with underlying conditions but immunocompetent; and those with underlying conditions and immunocompromised, according to Public Health Agency of Canada recommendations for immunization (*11*). For factors with multiple possible responses (e.g., disease manifestation, underlying conditions), which were therefore not possible to collapse into 2 groups, we ran a Fisher χ^2 test to determine p value. However, although $p<0.05$ indicates a significant difference between ≥ 2 groups, it does not provide information on where the difference occurs.

We used stepwise multivariable logistic regression to analyze clinical and demographic factors and determine adjusted odds ratios and 95% CIs for factors associated with infection from IPD serotype 4 compared with IPD from all other serotypes. We included age as a dichotomous variable: <65 or ≥65 years of age. We did not include indigenous background, intensive care unit (ICU) admission, death, or hospitalization as variables in the model: indigenous status because it is a difficult factor to determine from chart reviews, which are often missing large amounts of data, but its effect was not significant in univariable analysis; ICU admission, death, and hospitalization because they are outcomes and we were interested in clinical factors associated with serotype

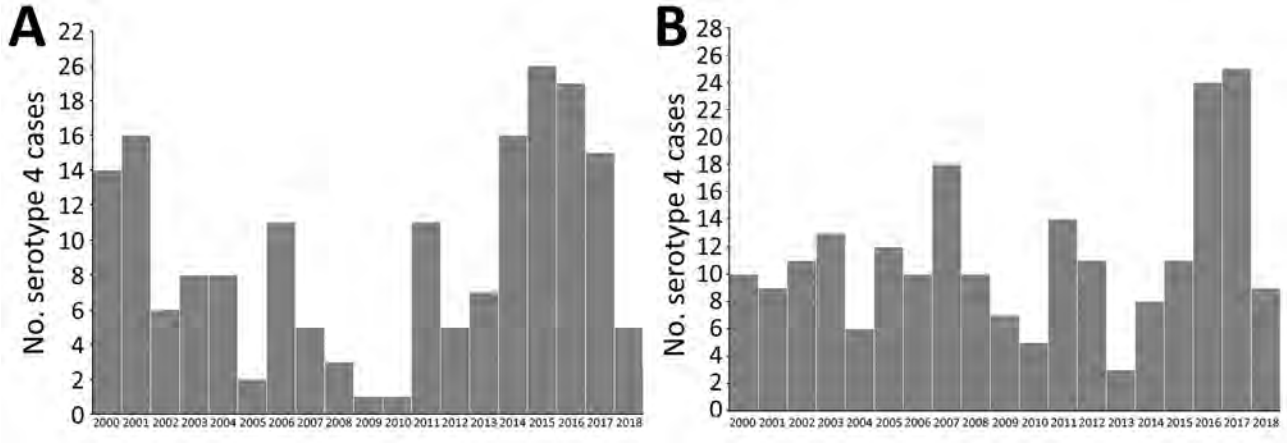

Figure 1. Epidemic curve for *Streptococcus pneumoniae* serotype 4 versus non–serotype 4 causing invasive pneumococcal disease, among adults >18 years of age, Alberta, Canada, 2010–2018. A) Calgary zone of Alberta Health Services; B) capital health zone (Edmonton) of Alberta Health Services.

4 IPD. We removed smoking status because of nonsignificance and a large amount of missing data.

Bacterial Identification

We screened isolates using optochin disk susceptibility (Oxoid, http://www.oxoid.com) and tube bile solubility analyses (*12*,*13*). We performed serotyping by quellung reaction using commercial antiserum (Statens Serum Institut, https://en.ssi.dk; SSI Diagnostica, https://www.ssidiagnostica.com) (*10*). We used PCR to test isolates for the presence of the *cpsA* gene if a quellung reaction was not observed (*14*); we verified species identification using *rpoB* (β subunit of RNA polymerase gene) sequence typing (*15*,*16*).

We determined antimicrobial susceptibilities using Sensititer STP6F (Trek Diagnostics, http://www.trekds.com) broth microdilution panels according to Clinical and Laboratory Standards Institute guidelines (*17*,*18*). We used meningitis resistance breakpoints for nonsusceptibility to penicillin (≥0.12 μg/mL), ceftriaxone and cefotaxime (≥2 μg/mL), and parenteral resistance breakpoints for cefuroxime (≥2 μg/mL).

Whole Genome Sequencing Analyses

We conducted WGS analyses on *S. pneumoniae* serotype 4 isolates from Calgary and Edmonton as well as background serotype 4 isolates collected from other provinces in Canada at the National Microbiology Laboratory in Winnipeg, Manitoba, as described elsewhere (*19*). We prepared DNA samples using Epicenter MasterPure Complete DNA and RNA Extraction Kit (Mandel Scientific, https://www.mandel.ca) and created libraries using Nextera sample preparation kits (Illumina, https://www.illumina.com) with 300 bp (n = 140) and 150 bp (n = 50) paired-end indexed reads generated on the Illumina NextSeq platform. We submitted read data for all *S. pneumoniae* serotype 4 isolates from Alberta to the National Center for Biotechnology Information Short Read Archive (BioProject accession no. PRJNA693536). We assessed the quality of the reads using FastQC version 0.11.4 (*20*) and assembled using Shovill (Galaxy version 1.0.4+galaxy0) programs (*21*).

We conducted core single-nucleotide variant (SNV) phylogenetic analysis by using a custom Galaxy version SNVPhyl version 1.0.1b Paired-End (*22*) phylogenomics workflow with minimum coverage = 7, minimum mean mapping quality = 30, and alternative allele ratio = 0.75; we removed highly recombinant regions containing >5 SNVs/500 bp. We visualized phylogenetic trees using FigTree version 1.4.3 (*23*). We determined phylogenetic clades by cluster analysis using ClusterPicker (*24*) with these settings: initial and main support thresholds = 0.9, genetic distance threshold = 0.045, and the large cluster threshold = 10. We used WGS data to identify the presence of macrolide (*ermB*, *ermTR*, *mefA/E*), tetracycline (*tetM*, *tetO*), chloramphenicol (*cat*), trimethoprim/sulfamethoxazole (*folA*, *folP*), penicillin (*pbp1a*, *pbp2b*, *pbp2x*), and fluoroquinolone (*gyrA* S81, *parC* S79/D83/N91) molecular antimicrobial resistance markers (*8*–*12*). We queried virulence factors including *pspA* (pneumococcal surface protein A), *ply* (pneumolysin), *pavA* and *pavB* (pneumococcal adhesion and virulence A and B), *lytA*, *lytB* and *lytC* (autolysins A, B and C), *nanA* and *nanB* (neuraminidase A and B), *rrgA* (pilus-1), *sipA* (pilus-2), *cbpA*, *cbpD*, *cbpG*, and *pce* (choline binding proteins A, D, G and E), *hasA* (hyaluronate lyase), and *zmpC* (immunoglobulin A1 protease) (*13*,*14*). We determined the presence or absence of molecular marker genes in the isolates by querying reference nucleotide sequences against assembled contig files using BLAST (*15*) with the E-value cutoff option set to 10e-100. We used the SNVPhyl workflow program to determine the number of 23S rRNA allele mutations, using an allele of *S. pneumoniae* R6 (locus tag sprr02) as a mapping reference and interrogating the allele counts at nucleotide position 2061 from the resultant variant call files (.vcf). We determined multilocus sequence type (MLST) allelic profiles in silico and queried them using the open-access PubMLST *S. pneumoniae* database (*25*) located at the University of Oxford to determine sequence types (ST).

Results

Populations

We identified 190 IPD serotype 4 cases in adults (96 from Calgary, 94 from Edmonton) during 2010–2018 and used WGS to analyze isolates obtained from those patients. A total of 1,008 adults sought treatment at Calgary hospitals with IPD during 2010–2018; of these, 100 (10%) cases involved serotype 4 IPD. For clinical analysis, we completed chart reviews for 97% of the 1,008 IPD cases. For cases without full chart reviews, we collected basic demographic information from notifiable disease reports and laboratory reports and included the information in the analysis when possible. Of the 30 cases without a full chart review, 57% were because of patient refusal to participate in the study. Twelve percent of chart reviews were missing large amounts of information because smoking status was not consistently reported; 56% of reviews lacked clear indication of indigenous status. We included the 967 patients with full information available in the multivariable analysis.

Epidemic Curves

In Calgary, after PCV7 introduction, serotype 4 had almost disappeared by 2009–2010. The outbreak among adults peaked in 2015–2016 (Figure 1, panel A). The number of cases of serotype 4 decreased and no cases occurred after July 2018, suggesting resolution of the outbreak. In Edmonton, the decline of serotype 4 after PCV7 introduction was less pronounced and the outbreak had 2 peaks, a smaller one in 2011 and a larger one in 2016–2017 (Figure 1). Serotype 4, which was originally prevalent, declined in the initial period after PCV7 introduction but then increased in 2011 after PCV13 was introduced.

Clinical Analysis

Homelessness, illicit drug use, alcohol abuse, and smoking were overrepresented as risk factors among patients with cases of serotype 4 IPD in data from the univariable analysis (Table 1). Persons with underlying conditions who were immunocompromised were underrepresented among those with serotype 4 IPD (Table 1). People with serotype 4 IPD were also younger (mean age 47.0 years, 95% CI 44.2–49.8 years) than those with non–serotype 4 IPD (mean age 58.4 years, 95% CI 57.2–59.5 years) during 2010–2018 (t-test p value <0.001). The most common diagnosis for serotype 4 IPD was bacteremic pneumonia (82%). All serotype 4 IPD cases that occurred during 2010–2018 were susceptible to penicillin, ceftriaxone, and erythromycin. In results from multivariable logistic regression, we found that being male, being <65 years of age, experiencing homelessness, having a diagnosis of pneumonia or empyema, or using illicit drugs were associated with serotype 4 IPD (Table 2). Alcohol abuse was not significantly associated with serotype 4 IPD in the multivariable logistic regression, indicating that the association seen in the univariable analysis was because of confounding by another factor (Table 2).

WGS

We conducted WGS analyses on 96 *S. pneumoniae* serotype 4 isolates from Calgary, 94 from Edmonton, and 37 background serotype 4 isolates from the National Microbiology Laboratory, collected from other provinces in Canada (*19*). Illumina MiSeq sequencing yielded an average 817,775 reads/genome, and average genome coverage was 91X. De novo assembly resulted in an average contig length of 45,875 nt and an N50 length of 85,135 nt.

The 190 *S. pneumoniae* serotype 4 genomes from Alberta clustered into 3 major phylogenetic clades (Figure 2); each clade was associated with an MLST. The largest number 93.7% (n = 159) of isolates were located in clade A and were MLST type ST244. Isolates in clade A were geographically relatively evenly distributed between Calgary (n = 69) and Edmonton (n = 90) and temporally after 2010 (n = 4); ≈19 isolates per year were found during 2011–2019. Clade B

Table 1. Results of univariable tests of proportions of patient demographics and clinical characteristics of *Streptococcus pneumoniae* serotype 4 versus non–serotype 4 causing IPD, Calgary, Alberta, Canada, 2010–2018*

Characteristics	Serotype 4, no. (%)	Non–serotype 4, no. (%)	% Difference (95% CI)	p value
Total cases, n = 990	100	890	NA	NA
Age ≥65 y	7 (7.5)	311 (34.9)	27.9 (22.0–33.8)	<0.001
Homelessness	47 (47.5)	129 (14.8)	32.6 (22.5–42.8)	<0.001
Illicit drug use	47 (58.0)	156 (22.5)	35.6 (24.4–46.8)	<0.001
Alcohol abuse	50 (61.7)	238 (34.2)	27.5 (16.3–38.6)	<0.001
Indigenous	13 (40.6)	105 (29.4)	11.2 (–6.4 to 28.9)	0.1862
Current or former smoker	85 (89.5)	579 (74.1)	15.3 (8.4–22.2)	0.001
Severity				
Death ≤30 d	7 (7.0)	114 (12.9)	5.9 (0.5–11.4)	0.09†
Hospitalization	88 (88.0)	775 (88.1)	0.1 (–6.6 to 6.8)	0.9
ICU admission	29 (29.6)	224 (25.9)	3.7 (–5.8 to 13.2)	0.4
Underlying condition an indication for pneumococcal vaccination‡ (*11*)				<0.001§
No underlying condition	46 (46.5)	279 (31.9)	NA	NA
Underlying condition, but immunocompetent	44 (44.4)	356 (40.7)	NA	NA
Underlying condition, immunocompromised	9 (9.1)	237 (27.4)	NA	NA
Primary diagnosis				0.02§
Bacteremia	1 (1.0)	89 (10.0)	NA	NA
Other IPD	1 (1.0)	38 (4.3)	NA	NA
Bacteremic pneumonia	82 (82.0)	613 (68.9)	NA	NA
Empyema	11 (11.0)	86 (9.7)	NA	NA
Pericarditis	7 (0.79)	1 (1.0)	NA	NA
Meningitis	4 (4.0)	56 (6.3)	NA	NA

*IPD, invasive pneumococcal disease; NA, not applicable.
†p value >0.05 but 95% CI does not cross 0, therefore significant.
‡Underlying conditions exclude alcohol and drug abuse.
§p value from χ^2 test; overall comparison made between groups but not for each level within groups because of multiple levels.

Table 2. Results of multivariable logistic regressions of clinical and demographic factors associated with *Streptococcus pneumoniae* serotype 4 versus non–serotype 4 causing IPD, Calgary, Alberta, Canada, 2010–2018 (n = 967)*

Factors associated with serotype 4†	Odds ratio (95% CI)	p value
Male sex	2.1 (1.2–3.7)	0.007
Age ≥65 y	0.3 (0.1–0.7)	0.003
Homelessness	2.4 (1.4–4.1)	0.001
Illicit drug use	2.3 (1.4–3.8)	0.001
Alcohol abuse	0.9 (0.5–1.5)	0.698
Underlying condition an indication for pneumococcal vaccination (*11*)		
No underlying condition increasing risk for IPD	Referent	Referent
Underlying condition, but immunocompetent	0.9 (0.6–1.5)	0.731
Underlying condition, immunocompromised	0.3 (0.1–0.7)	0.003
Primary diagnosis		
Bacteremia or other invasive condition‡	Referent	Referent
Pneumonia or empyema	3.6 (1.1–12.0)	0.034
Meningitis	2.8 (0.6–13.4)	0.202

*IPD, invasive pneumococcal disease.
†Smoking status included in initial model but result was not significant and a large amount of data was missing, so it was removed from final model.
‡For example, pericarditis, peritonitis, abscess, endophthalmitis.

included 2 isolates from Edmonton, collected in 2010 and 2012, and 1 from Calgary, collected in 2018, that were ST695, a triple-locus variant of ST244 and ancestor of newly emergent serotype 19A/ST695 clone (*26*). Clade C was associated with ST205 (n = 23) and ST15531 (n = 2), a single-locus variant of ST205. Twenty-three of the 24 isolates in clade C were collected from the Calgary region. Although another ST205 isolate from Edmonton and the TIGR4 reference strain (National Center for Biotechnology Information accession no. NC_003028.3) were proximal to clade C in the phylogenetic tree, ClusterPicker excluded them from the clade based on the clustering thresholds used. A further 2 isolates from Calgary and a third from Edmonton were distant phylogenetic outliers of ST2213, ST7776, and ST11662. Most national background isolates collected from other provinces (n = 36) clustered within the ST205 clade C lineage (n = 23), but the ST244 clade A lineage was predominantly associated with Alberta, with fewer national isolates present (n = 10) (Appendix Figure 1, https://wwwnc.cdc.gov/EID/article/27/7/20-4403-App1.pdf).

Further phylogenetic analysis of the ST244 isolates from Alberta identified 6 major clades with isolates clustered by city (Figure 3). Isolates from Edmonton mainly comprised clades A1 (19 of 21) and A2 (8 of 8), but isolates from the Calgary area comprised clades A3 (9 of 10), A4 (21 of 25), A5 (19 of 19), and A6 (5 of 5). Clade A1 emerged in Edmonton in 2011, and clade A2 followed 4 years later in 2015; in Calgary, clade A6 was first seen in 2011, followed by clades A4 in 2013, and A3 and A5 in 2014, with A5 expanding in 2015 (Appendix Figure 2).

Additional information about homelessness, death, ICU admittance, and risk factors was available for case-patients from Calgary. Clade A1 had the highest proportion of isolates associated with homelessness (7 of 9 isolates), whereas clade A4 had the lowest (7 of 21 isolates; Figure 3). There was also a relatively high number of isolates (3 of 5) in clade A6 and from the miscellaneous nonclustered strains from Calgary (10 of 14) associated with homelessness. Although only about half of the isolates in clade A5 were associated with homelessness (10 of 19), a subgroup of 7 highly related isolates associated with homelessness were identical to each other (no SNV difference). Among the ST205 isolates, 6 of the 23 Calgary isolates were associated with homelessness. We observed no clustering of isolates associated with the other background information (death, risk factors, or ICU admittance).

WGS Antimicrobial Susceptibility

Using in silico molecular characterization we found antimicrobial resistance determinants in 7 of the 190 *S. pneumoniae* serotype 4 isolates including single ParC D83 aa substitution (n = 2), *ermB* and *tetM* determinants (n = 1), sole *folA* I100L (n = 2), *folA* I100L, a *folP* amino acid insertion, and *tetM* (n = 1), and a SAMK motif in *pbp2x* and the *folA* I100L and *folP* insert (n = 1). All virulence factors we analyzed were present

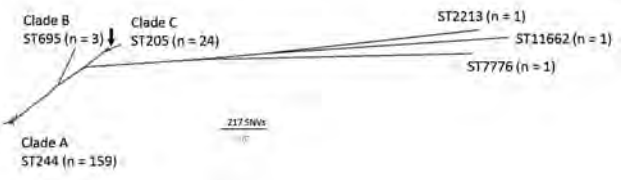

Figure 2. Maximum-likelihood core SNV unrooted phylogenetic tree of 190 *Streptococcus pneumoniae* serotype 4 isolates collected from patients in Alberta, Canada, 2010–2018. A total of 3,097 sites were used in the phylogeny, and 80.7% of the core genome was included. *S. pneumoniae* TIGR4 (arrow; National Center for Biotechnology Information accession number NC_003028.3) was used as a mapping reference. Cluster analysis did not group 1 ST205 isolate and TIGR4 with the other clade C strains. SNV, single nucleotide variant; ST, sequence type.

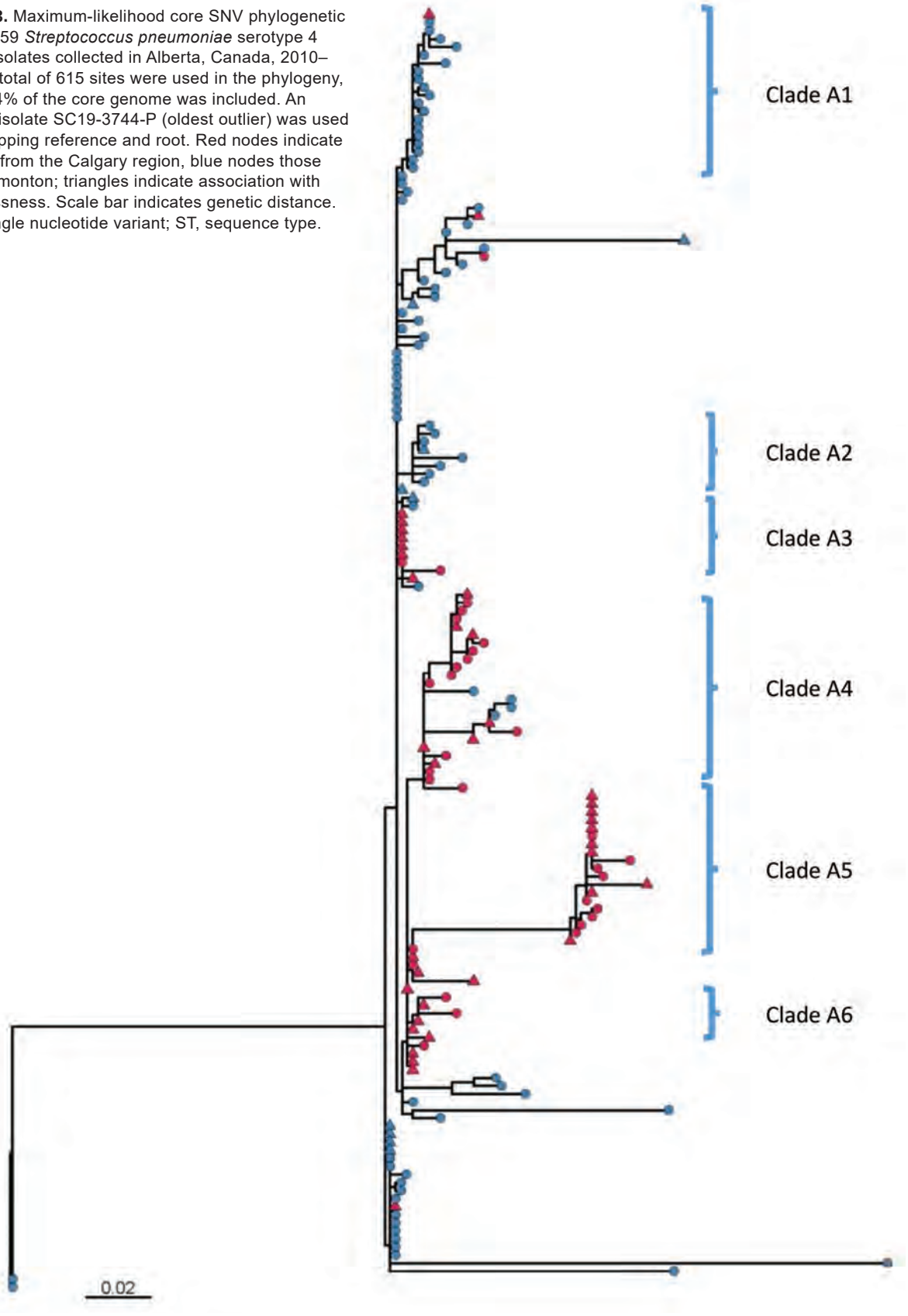

Figure 3. Maximum-likelihood core SNV phylogenetic tree of 159 *Streptococcus pneumoniae* serotype 4 ST244 isolates collected in Alberta, Canada, 2010–2018. A total of 615 sites were used in the phylogeny, and 97.4% of the core genome was included. An internal isolate SC19-3744-P (oldest outlier) was used as a mapping reference and root. Red nodes indicate isolates from the Calgary region, blue nodes those from Edmonton; triangles indicate association with homelessness. Scale bar indicates genetic distance. SNV, single nucleotide variant; ST, sequence type.

in the isolates except *cbpA* and *sipA* (pilus-2), which were absent in all strains; *rrgA* (pilus-1) or *zmpC* were absent in the phylogenetic outliers (n = 3).

Discussion

Outbreaks of IPD have been described most often in vulnerable populations and groups living in crowded conditions, but only a few serotypes have been described in association with outbreaks (*27*). Outbreaks of disease can be characterized as a temporal increase of disease from epidemiologically linked cases. The temporal relation can vary depending on the causative organism. Pneumococcal outbreaks may occur over a period of several years. In this study, phylogenetic analyses were used to support epidemiologic information linking a susceptible population with a particular serotype.

In Calgary we have observed 2 large outbreaks of IPD that particularly affected homeless persons. The one during 2005–2007 was largely caused by serotype 5, although an increase in serotype 8 was also observed (*8*). In the more recent outbreak during 2010–2018, the incidence of serotype 4 increased. Phylogenetic analysis indicated relatively high genetic variability among the serotype 4 isolates collected over this period. Previously, we conducted WGS on a small sample of serotype 5 cases associated with the 2005–2007 outbreak; results indicated that all isolates were from the same genetic clone (*8*). In our analysis of the predominant serotype 4 ST244 clone in Alberta, we observed higher diversity with some clustering regionally in Calgary and Edmonton, as well as some temporal clustering and clustering in homeless persons during 2014–2016. There were also some genetically diverse isolates of *S. pneumoniae* serotype 4 broadly disseminated throughout the community, including among persons who were not homeless. No clustering was observed by age group, gender, site of bacterial isolation, or disease severity, which may indicate that the rise in disease was not because of the emergence of a single, more transmissible clone of serotype 4. Because of the longer temporal period over which pneumococcal outbreaks occur, some degree of genetic drift is expected, with strains being disseminated among the susceptible population and sublineages emerging more acutely in pockets that facilitate transmission, forming diversified subclades within the overall outbreak. The relative diversity among subclades can be thought of as smaller outbreaks of more clonal strains within the overarching dissemination of the original strain.

From a genetic perspective, the phylogeny representing the nationwide breadth of serotype 4 strains had a maximum 1,472 SNVs and an average 192 SNVs between strains (Appendix Figure 1), in contrast with the larger overall outbreak lineage (clade A) with a maximum 148 SNVs and average 22 SNVs. Further clonality can be seen among the subclades with each having ≈5 SNVs difference within and ≈10 SNVs between subclades (Appendix Table). A recent report of an outbreak of serotype 5 IPD in British Columbia, Canada stated that its strains differed by only ≈10 SNVs over a 3.5-year period (*28*).

The rise of serotype 4 IPD cases occurred during a period of widespread PCV13 use in children, raising questions about the reservoirs of this strain. Before that period, during the period of PCV7 use in children, serotype 4 was largely controlled at all ages, reflecting direct immunity in vaccine recipients and indirect immunity in unvaccinated adults. The reemergence of serotype 4 cases, primarily among adults, suggests reduced herd immunity. When Alberta switched from PCV7 to PCV13 in 2010, there was also a switch from a 4-dose schedule of PCV7 to a 3-dose PCV13 schedule for children. This change raises a question about whether the reduced-dose schedule in children, although still providing direct protection, might be less effective in reducing nasopharyngeal carriage, leading to asymptomatic transmission and reduced herd immunity. A study of pneumococcal carriage among children in Calgary has previously shown the near elimination of serotype 4 carriage after the introduction of PCV7, supporting this possible explanation (*29*). More recent studies in children in 2016 and 2018, well after the introduction of PCV13, found that serotype 4 IPD was not identified in any sample tested by conventional culture but was identified in 3.5% of children by using PCR (*7*). It is also possible that PCV13 may not reduce nasopharyngeal carriage and asymptomatic carriage of all vaccine serotypes as effectively as PCV7 did, regardless of the change in number of doses. In support of this possibility, PCV13 has known limited effectiveness to reduce serotype 3 IPD and possibly nasopharyngeal carriage, as described in a 2019 review (*30*).

Serotype 4 IPD was associated with being male or a current user of illicit drugs or experiencing homelessness. Serotype 4 IPD case-patients had lower odds of having an immunocompromising illness, which may be partially associated with being younger, although the association remained when we adjusted for age. We previously reported that IPD is significantly overrepresented in homeless persons compared with the general population, regardless of season (*9*). Although the 23-valent pneumococcal polysaccharide vaccine is recommended for homeless persons in Canada, among those for whom

we were able to obtain records, vaccination rates were very low (*9*,*11*).

The main limitation of this study is that we had complete clinical data only from Calgary. In addition, the total population of the surveillance area was 3,041,765 and for a relatively rare disease like IPD, local random variation in prevalent serotypes may limit the generalizability of our results.

Similar to serotype 5 during the 2005–2007 outbreak, serotype 4 also migrated across a large geographic area in western Canada and was seen in Victoria, British Columbia (*31*,*32*). Pneumococcal outbreaks have been reported in overcrowded jails, homeless shelters, and care homes (*8*,*31*,*33*–*36*). One study found recurrent infections were 5-fold higher among persons who were homeless than those who were not (*37*). Another study found most outbreaks of pneumococcal disease occurred in crowded settings (*38*). It is clear that homelessness and drug use are risk factors for illness and should be considered indicators for vaccination. Although we acknowledge the challenge of delivering vaccines to homeless persons, on the basis of these results, we recommended a public health initiative, currently under consideration by public health officials in Alberta, to target the homeless population of Calgary for publicly funded vaccination with both PCV13 and 23-valent pneumococcal polysaccharide vaccine.

Acknowledgments

We acknowledge the research staff and students at National Microbiology Lab, Winnipeg. We also acknowledge the contributions in data collection and consolidation by the ACHIEVE research team (Shannon Pyra, Joslyn Gray, Nicole MacMillan, Ashley Choo, and Megan Neal) and the Provincial Public Health Laboratory of Alberta Health Services.

About the Author

Dr. Kellner is a pediatrician, subspecialist in pediatric infectious diseases, and clinical epidemiologist. He is professor and former chair of the Department of Pediatrics at the University of Calgary and the Calgary zone of Alberta Health Services. His research interests are in the field of vaccine preventable infections; his main interest is *Streptococcus pneumoniae*.

References

1. Pilishvili T, Lexau C, Farley MM, Hadler J, Harrison LH, Bennett NM, et al.; Active Bacterial Core Surveillance/ Emerging Infections Program Network. Sustained reductions in invasive pneumococcal disease in the era of conjugate vaccine. J Infect Dis. 2010;201:32–41. https://doi.org/10.1086/648593
2. Kaplan SL, Barson WJ, Lin PL, Romero JR, Bradley JS, Tan TQ, et al. Early trends for invasive pneumococcal infections in children after the introduction of the 13-valent pneumococcal conjugate vaccine. Pediatr Infect Dis J. 2013;32:203–7. https://doi.org/10.1097/INF.0b013e318275614b
3. Leal J, Vanderkooi OG, Church DL, Macdonald J, Tyrrell GJ, Kellner JD. Eradication of invasive pneumococcal disease due to the seven-valent pneumococcal conjugate vaccine serotypes in Calgary, Alberta. Pediatr Infect Dis J. 2012;31:e169–75. https://doi.org/10.1097/INF.0b013e3182624a40
4. Kellner JD, Vanderkooi OG, MacDonald J, Church DL, Tyrrell GJ, Scheifele DW. Changing epidemiology of invasive pneumococcal disease in Canada, 1998–2007: update from the Calgary-area *Streptococcus pneumoniae* research (CASPER) study. Clin Infect Dis. 2009;49:205–12. https://doi.org/10.1086/599827
5. Demczuk W, Griffith A, Singh R, Montes K, Sawatzky P, Martin I, et al. National laboratory surveillance of invasive streptococcal disease in Canada—annual summary 2017. Winnipeg, Manitoba (Canada): Public Health Agency of Canada; 2017.
6. Ricketson LJ, Kellner JD. Invasive pneumococcal disease (IPD) trends 1998 to mid-2019 in Calgary, Canada: an interrupted time series analysis: a CASPER study. International Symposium on Pneumococci and Pneumococcal Disease; 2022 Jun 19–23; Toronto, Ontario, Canada. Abstract 104 [cited 2020 Oct 19]. https://cslide.ctimeetingtech.com/isppd20/attendee/confcal/persons/120
7. Martin I, Lidder R, Ricketson LJ, Demczuk WH, LeBlanc JJ, Sadarangani M, et al. Molecular identification and serotyping of pneumococcal nasopharyngeal carriage vs culture and quellung serotyping in healthy children: a Calgary *S. pneumoniae* Epidemiology Research (CASPER) study. International Symposium on Pneumococci and Pneumococcal Disease; 2022 Jun 19–23; Toronto, Ontario, Canada. Abstract 348 [cited 2020 Oct 19] https://cslide.ctimeetingtech.com/isppd20/attendee/person/663
8. Vanderkooi OG, Church DL, MacDonald J, Zucol F, Kellner JD. Community-based outbreaks in vulnerable populations of invasive infections caused by *Streptococcus pneumoniae* serotypes 5 and 8 in Calgary, Canada. PLoS One. 2011;6:e28547. https://doi.org/10.1371/journal.pone.0028547
9. Lemay J-A, Ricketson LJ, Zwicker L, Kellner JD. Homelessness in adults with invasive pneumococcal disease (IPD) in Calgary, Canada. Open Forum Infect Dis. 2019;6:ofz362. https://doi.org/10.1093/ofid/ofz362
10. Austrian R. The quellung reaction, a neglected microbiologic technique. Mt Sinai J Med. 1976;43:699–709.
11. Public Health Agency of Canada. Pneumococcal vaccine: Canadian immunization guide [cited 2020 Dec 23]. https://www.canada.ca/en/public-health/services/publications/healthy-living/canadian-immunization-guide-part-4-active-vaccines/page-16-pneumococcal-vaccine.html#a3
12. Facklam R, Washington JA. *Streptococcus* and related catalase-negative Gram-positive cocci. In: Balows A, Hausler WJ, Hermann KL, Isenberg HD, Shadom HJ, editors. Manual of clinical microbiology. Washington: American Society for Microbiology; 1991. p. 238–57.
13. Spellerberg B, Brandt C. *Streptococcus*. In: Jorgensen JH, Carroll KC, Funke G, et al., editors. Manual of clinical microbiology, 11th ed. Washington: American Society for Microbiology; 2015. p. 383–402.

14. Pimenta FC, Roundtree A, Soysal A, Bakir M, du Plessis M, Wolter N, et al. Sequential triplex real-time PCR assay for detecting 21 pneumococcal capsular serotypes that account for a high global disease burden. J Clin Microbiol. 2013;51:647–52. https://doi.org/10.1128/JCM.02927-12
15. Drancourt M, Roux V, Fournier PE, Raoult D. rpoB gene sequence-based identification of aerobic Gram-positive cocci of the genera *Streptococcus*, *Enterococcus*, *Gemella*, *Abiotrophia*, and *Granulicatella*. J Clin Microbiol. 2004;42:497–504. https://doi.org/10.1128/JCM.42.2.497-504.2004
16. Clinical Laboratory and Standards Institute. Interpretive criteria for identification of bacteria and fungi by DNA target sequencing; approved guideline (MM18-A). Wayne (PA): The Institute; 2008.
17. Clinical and Laboratory Standards Institute. Methods for dilution antimicrobial susceptibility tests for bacteria that grow aerobically, 8th ed (M07–A8). Wayne (PA): The Institute; 2009.
18. Clinical Laboratory and Standards Institute. Performance standards for antimicrobial susceptibility testing; 22nd informational supplement (M100–S22). Wayne (PA): The Institute; 2012.
19. Demczuk WHB, Martin I, Hoang L, Van Caeseele P, Lefebvre B, Horsman G, et al. Phylogenetic analysis of emergent *Streptococcus pneumoniae* serotype 22F causing invasive pneumococcal disease using whole genome sequencing. PLoS One. 2017;12:e0178040. https://doi.org/10.1371/journal.pone.0178040
20. Andrews S. FastQC: a quality control tool for high throughput sequence data, version 0.11.4 [cited 2020 June 29] https://www.bioinformatics.babraham.ac.uk/projects/fastqc
21. Seemann T. Shovill: faster SPAdes assembly of Illumina reads. 2017. [cited 2020 June 21] https://github.com/tseemann/shovill
22. Petkau A, Mabon P, Sieffert C, Knox NC, Cabral J, Iskander M, et al. SNVPhyl: a single nucleotide variant phylogenomics pipeline for microbial genomic epidemiology. Microb Genom. 2017;3:e000116. https://doi.org/10.1099/mgen.0.000116
23. Rambaut A. FigTree: molecular evolution, phylogenetics and epidemiology, version 1.4.3 [cited 2020 June 15] http://tree.bio.ed.ac.uk/software/figtree
24. Ragonnet-Cronin M, Hodcroft E, Hué S, Fearnhill E, Delpech V, Brown AJ, et al.; UK HIV Drug Resistance Database. Automated analysis of phylogenetic clusters. BMC Bioinformatics. 2013;14:317. https://doi.org/10.1186/1471-2105-14-317
25. Jolley KA, Bray JE, Maiden MCJ. Open-access bacterial population genomics: BIGSdb software, the PubMLST.org website and their applications. Wellcome Open Res. 2018;3:124. https://doi.org/10.12688/wellcomeopenres.14826.1
26. Tyrrell GJ. The changing epidemiology of *Streptococcus pneumoniae* serotype 19A clonal complexes. J Infect Dis. 2011;203:1345–7. https://doi.org/10.1093/infdis/jir056
27. Hausdorff WP, Feikin DR, Klugman KP. Epidemiological differences among pneumococcal serotypes. Lancet Infect Dis. 2005;5:83–93. https://doi.org/10.1016/S1473-3099(05)70083-9
28. Miller RR, Langille MG, Montoya V, Crisan A, Stefanovic A, Martin I, et al. Genomic analysis of a serotype 5 *Streptococcus pneumoniae* outbreak in British Columbia, Canada, 2005–2009. Can J Infect Dis Med Microbiol. 2016;2016:5381871. https://doi.org/10.1155/2016/5381871
29. Kellner JD, Scheifele D, Vanderkooi OG, Macdonald J, Church DL, Tyrrell GJ. Effects of routine infant vaccination with the 7-valent pneumococcal conjugate vaccine on nasopharyngeal colonization with *streptococcus pneumoniae* in children in Calgary, Canada. Pediatr Infect Dis J. 2008;27:526–32. https://doi.org/10.1097/INF.0b013e3181658c5c
30. Linley E, Bell A, Gritzfeld JF, Borrow R. Should pneumococcal serotype 3 be included in serotype-specific immunoassays? Vaccines (Basel). 2019;7:4. https://doi.org/10.3390/vaccines7010004
31. Tyrrell GJ, Lovgren M, Ibrahim Q, Garg S, Chui L, Boone TJ, et al. Epidemic of invasive pneumococcal disease, western Canada, 2005-2009. Emerg Infect Dis. 2012;18:733–40. https://doi.org/10.3201/eid1805.110235
32. McKee G, Choi A, Madill C, Marriott J, Kibsey P, Hoyano D II. Outbreak of invasive *Streptococcus pneumoniae* among an inner-city population in Victoria, British Columbia, 2016-2017. Can Commun Dis Rep. 2018;44:317–22. https://doi.org/10.14745/ccdr.v44i12a02
33. Hoge CW, Reichler MR, Dominguez EA, Bremer JC, Mastro TD, Hendricks KA, et al. An epidemic of pneumococcal disease in an overcrowded, inadequately ventilated jail. N Engl J Med. 1994;331:643–8. https://doi.org/10.1056/NEJM199409083311004
34. DeMaria A Jr, Browne K, Berk SL, Sherwood EJ, McCabe WR. An outbreak of type 1 pneumococcal pneumonia in a men's shelter. JAMA. 1980;244:1446–9. https://doi.org/10.1001/jama.1980.03310130024022
35. Mercat A, Nguyen J, Dautzenberg B. An outbreak of pneumococcal pneumonia in two men's shelters. Chest. 1991;99:147–51. https://doi.org/10.1378/chest.99.1.147
36. Gleich S, Morad Y, Echague R, Miller JR, Kornblum J, Sampson JS, et al. *Streptococcus pneumoniae* serotype 4 outbreak in a home for the aged: report and review of recent outbreaks. Infect Control Hosp Epidemiol. 2000;21:711–7. https://doi.org/10.1086/501717
37. Plevneshi A, Svoboda T, Armstrong I, Tyrrell GJ, Miranda A, Green K, et al.; Toronto Invasive Bacterial Diseases Network. Population-based surveillance for invasive pneumococcal disease in homeless adults in Toronto. PLoS One. 2009;4:e7255. https://doi.org/10.1371/journal.pone.0007255
38. Zivich PN, Grabenstein JD, Becker-Dreps SI, Weber DJ. *Streptococcus pneumoniae* outbreaks and implications for transmission and control: a systematic review. Pneumonia (Nathan). 2018;10:11. https://doi.org/10.1186/s41479-018-0055-4

Address for correspondence: James D. Kellner, Department of Pediatrics, Alberta Children's Hospital, 28 Oki Dr NW, Calgary, AB T3B 6A8, Canada; email: Jim.Kellner@albertahealthservices.ca

Shiga Toxin–Associated Hemolytic Uremic Syndrome in Adults, France, 2009–2017

Benoît Travert,[1] Antoine Dossier,[1] Matthieu Jamme, Aurélie Cointe, Yahsou Delmas, Sandrine Malot, Alain Wynckel, Amélie Seguin, Claire Presne, Miguel Hie, Ygal Benhamou, David Ribes, Gabriel Choukroun, Steven Grangé, Alexandre Hertig, Emilie Cornec-Le Gall, Lionel Galicier, Eric Daugas, Lila Bouadma, François-Xavier Weill, Elie Azoulay, Fadi Fakhouri, Agnès Veyradier, Stéphane Bonacorsi, Julien Hogan, Véronique Frémeaux-Bacchi, Eric Rondeau, Patricia Mariani-Kurkdjian, Paul Coppo, Centre de Référence des Microangiopathies Thrombotiques[2]

We conducted a retrospective study on hemolytic uremic syndrome caused by Shiga toxin–producing *Escherichia coli* (STEC) in 96 adults enrolled in the cohort of the National Reference Center for Thrombotic Microangiopathies network in France during 2009–2017. Most infections were caused by STEC strains not belonging to the O157 or O104 serogroups. Thirty (31.3%) patients had multiple risk factors for thrombotic microangiopathy. In total, 61 (63.5%) patients required dialysis, 50 (52.1%) had a serious neurologic complication, 34 (35.4%) required mechanical ventilation, and 19 (19.8%) died during hospitalization. We used multivariate analysis to determine that the greatest risk factors for death were underlying immunodeficiency (hazard ratio 3.54) and severe neurologic events (hazard ratio 3.40). According to multivariate analysis and propensity score-matching, eculizumab treatment was not associated with survival. We found that underlying conditions, especially immunodeficiency, are strongly associated with decreased survival in adults who have hemolytic uremic syndrome caused by STEC.

Shiga toxin–producing *Escherichia coli* (STEC) infection is an environmental foodborne or waterborne disease that causes bloody diarrhea. Approximately 5%–20% of cases are complicated by hemolytic uremic syndrome (HUS) (*1*,*2*). Shiga toxins (Stx) can cause acute microvascular injury, leading to thrombotic microangiopathy (TMA), which is characterized by hemolytic anemia and thrombocytopenia, and in the scenario of HUS, associated with acute kidney injury (*3*). Researchers estimate that the global prevalence of STEC infection is ≈43.1 acute illnesses/100,000 person-years, causing ≈3,890 annual cases of STEC-associated HUS (*4*). STEC-associated HUS occurs mostly in children; sporadic cases are rare in adults.

Among children, STEC-associated HUS is the most frequent form of TMA and the leading cause of acute renal failure (*3*). In France, surveillance for STEC-associated HUS in children <15 years of age

Author affiliations: Centre de Référence des Microangiopathies Thrombotiques, Paris, France (B. Travert, A. Dossier, M. Jamme, Y. Delmas, S. Malot, A. Wynckel, A. Seguin, C. Presne, M. Hie, Y. Benhamou, G. Choukroun, S. Grangé, A. Hertig, L. Galicier, E. Azoulay, F. Fakhouri, A. Veyradier, V. Frémeaux-Bacchi, E. Rondeau, P. Coppo); Université de Paris, Paris (B. Travert, A. Dossier, A. Cointe, L. Galicier, E. Daugas, L. Bouadma, E. Azoulay, A. Veyradier, S. Bonacorsi, J. Hogan, V. Frémeaux-Bacchi, P. Mariani-Kurkdjian); Hôpital Bichat—Claude Bernard, Paris (B. Travert, A. Dossier, E. Daugas, L. Bouadma); Sorbonne-Université, Paris (M. Jamme, M. Hie, A. Hertig, E. Rondeau, P. Coppo); Hôpital Tenon, Paris (M. Jamme, E. Rondeau); Hôpital Robert-Debré, Paris (A. Cointe, S. Bonacorsi, J. Hogan, P. Mariani-Kurkdjian); Centre Hospitalier Universitaire de Bordeaux, Bordeaux, France (Y. Delmas); Hôpital Maison Blanche, Reims, France (A. Wynckel); Centre Hospitalier Universitaire de Caen, Caen, France (A. Seguin); Centre Hospitalier Universitaire d'Amiens, Amiens, France (C. Presne, G. Choukroun); Groupement Hospitalier Pitié-Salpêtrière, Paris (M. Hie, A. Hertig); Centre Hospitalier Universitaire de Rouen, Rouen, France (Y. Benhamou, S. Grangé); Centre Hospitalier Universitaire de Toulouse, Toulouse, France (D. Ribes); Centre Hospitalier Universitaire de Brest, Brest, France (E. Cornec-Le Gall); Hôpital Saint-Louis, Paris (L. Galicier, E. Azoulay); Institut Pasteur, Paris (F.-X. Weill); Centre Hospitalier Universitaire de Nantes, Nantes, France (F. Fakhouri); Hôpital Lariboisière, Paris (A. Veyradier); Hôpital Européen Georges Pompidou, Paris (V. Frémeaux-Bacchi); Hôpital Saint Antoine, Paris (P. Coppo)

DOI: https://doi.org/10.3201/eid2707.204638

[1]These first authors contributed equally to this article.

[2]Members of this group are listed at the end of this article.

has existed since 1996. This surveillance system comprises 32 pediatric healthcare centers, including all 21 university hospital units specializing in pediatric nephrology. These centers notify public health authorities of cases of STEC-associated HUS. The National Reference Center for *Escherichia coli*, *Shigella* and *Salmonella* at the Institut Pasteur (NRC-Ec; Paris, France) and its associated laboratory at the Robert Debré University Hospital (Paris, France) confirm and characterize STEC infections in children and adults. This surveillance network estimated the annual incidence of HUS in France to be 1.00 case/100,000 child-years, causing a ≈1% death rate during 2007–2016 (*5*).

Despite the much lower incidence of HUS among adults than children, most deaths caused by STEC-associated HUS occur among persons ≥60 years of age (*2*,*6*). The French national health authorities do not have a dedicated surveillance system for STEC-associated HUS in adults. In 2011, a large STEC outbreak in Europe sickened 3,816 persons in Germany, causing 845 cases of HUS and 54 deaths; 24 persons were affected in the Bordeaux region of France, including 9 who had HUS, 8 of whom were adults (*7*,*8*). The outbreak was linked to an atypical hybrid pathotype *E. coli* O104:H4 strain characterized by enteroaggregative and enterohemorrhagic virulence; the strain also produced an extended spectrum β-lactamase. Most (88%) patients involved in this outbreak, which was associated with consumption of organic fenugreek sprouts, were adults, and the median age was 42 years. Publicity surrounding this outbreak raised awareness of STEC-associated HUS in adults. However, cases of STEC-associated HUS in adults remain rare (*9*,*10*). Hence, the clinical characteristics of adult STEC-associated HUS and the effects of therapeutic strategies on outcome remain uncertain. We describe the epidemiologic and clinical features of adults with STEC-associated HUS, identify predictors of patient outcomes, and assess the effectiveness of therapeutic interventions in this population.

Methods

Study Design, Settings, and Data Sources

We conducted a retrospective cohort study of STEC-associated HUS cases in adults registered during January 2009–December 2017 in France by the Centre National de Référence des Microangiopathies Thrombotiques (CNR-MAT; https://www.cnr-mat.fr). We reviewed all medical files from the CNR-MAT database. This work was part of the TMA study approved by our institutional review board (Comité pour la protection des personnes Ile-de-France; approval no. CPP04807) in accordance with the Declaration of Helsinki and the French Data Protection Authority.

Diagnostic Criteria

The diagnosis of HUS required the coexistence of TMA (i.e., thrombocytopenia [platelet levels <150,000 cells/μL] and microangiopathic hemolytic anemia [hemoglobin levels <12 g/dL]) and an acute kidney injury (AKI). We included all TMA patients ≥18 years of age in the CNR-MAT cohort who had an AKI and a positive PCR result for the Stx genes *stx1*, *stx2*, or both. We considered patients to have fever if they had a temperature of ≥38°C within 24 hours after admission.

Microbiological Data

Participating laboratories conducted PCR specific for *stx1* and *stx2* on *E. coli* strains isolated from stool, blood, and urine samples. Laboratory technicians also cultured samples from *stx*-positive stools. To characterize the isolated STEC strains, technicians used an O-serogroup multiplex PCR selective for the 10 most frequent serogroups affecting humans in France: O157, O26, O145, O55, O103, O104, O111, O91, O121, and O80 (*11*). Strains belonging to other serogroups were characterized by PCR of the restriction fragment length polymorphism of the O operon, *rfb* (*rfb*-RFLP) (*12*). In April 2017, NRC-Ec and local laboratories also began to characterize strains using whole-genome sequencing, when available. If a strain was *stx*-positive but its serogroup was not identified by culture, we classified that strain as not isolated.

Variables

Participating laboratories and physicians submitted data on each patient's medical history, clinical and biological features, microbiological findings, and treatment at admission and during hospitalization (*13*). We retrospectively calculated each patient's age-weighted Charlson Comorbidity Index (CCI) (*14*) and classified AKI according to the Kidney Disease: Improving Global Outcomes (KDIGO) criteria published by the International Society of Nephrology (*15*). We investigated ADAMTS13 and complement alternative pathway (CAP) activity as previously described (*16*).

Treatments and Outcomes

Treatment consisted mainly of therapeutic plasma exchange (TPE) or best supportive care (BSC) according to the discretion of the treating physician. The C5 complement blocker eculizumab (Soliris; Alexion Pharmaceuticals, Inc., https://alexion.com) also

was given at the discretion of the treating physician; however, physicians were encouraged to discuss eculizumab use with a member of the CNR-MAT team. The primary outcome of this study was patient survival at the time of most recent follow-up.

Statistics

We reported qualitative variables as frequencies and percentages; we reported quantitative discrete and continuous variables as medians and interquartile ranges (IQRs). We estimated survival using the Kaplan-Meier method. We used Cox proportional hazards regression to identify factors independently associated with survival. The proportional hazard assumption was supported by a nonsignificant relationship between scaled Schoenfeld residuals and time and refuted by a significant relationship using an alpha (α) risk set at 5%. We reported the results using hazard ratios (HRs) and 95% CIs, using an α risk set at 5% statistical significance. To quantify the effect of eculizumab on survival, we calculated and compared the propensity scores of patients who did and did not use eculizumab (Appendix, https://wwwnc.cdc.gov/EID/article/27/7/20-4638-App1.pdf). We used R software version 3.6.1 (The R Project for Statistical Computing, https://www.r-project.org) for statistical analysis. For propensity score analysis, we used MatchIt package (*17*).

Results

Of the 4,048 patients in the CNR-MAT cohort, we first identified 61 adult STEC-associated HUS patients with complete data during January 2009–December 2017. After comparing the NRC-Ec and CNR-MAT surveillance data, we identified 35 additional patients to be included in the study cohort. In total, the study cohort comprised 96 patients (Appendix Figure 1). This cohort included patients from hospitals throughout France, most of which were part of the CNR-MAT network (Figure 1, panel A). The women-to-men ratio was 1.7 and median age was 60.5 years (IQR 47.0–71.0 years) (Figure 1, panel B). Geographic, temporal, and microbiological characteristics of the cases suggested an outbreak among 13 patients (Figure 1). The cohort also included 8 patients affected by the 2011 O104:H4 outbreak in France described previously (*8*). We found a patient in our cohort who was infected in a family cluster of STEC-associated HUS in 2014, but the strain could not be identified. We also found 4 patients (2 in Marne, 1 in Nord, 1 in Paris) who tested positive for STEC O91 in summer 2013 but did not share a known infection source.

In total, 69 (71.9%) patients had underlying conditions; the median CCI was 2.00 (IQR 1.00–4.25) (Table 1). Of the 96 patients, 27 (28.1%) had an underlying immunodeficiency and 30 (31.3%) had ≥1 condition that might contribute to TMA.

Most (83.3%) patients had diarrhea and nearly half (49.0%) had bloody diarrhea; 11 patients had severe colitis, including 4 who required emergency surgery (Table 2). All patients had renal impairment. In 2011, 2 patients with STEC O104:H4 infection had proteinuria (i.e., >1 g/L) but not serum creatinine elevation; these patients also had microangiopathic hemolytic anemia and peripheral thrombocytopenia (*8*). The other 94 patients all had AKI stage 1 or higher according to KDIGO criteria, of which 61 (63.5%) required dialysis. Of 12 patients who underwent kidney biopsy, 11 showed signs of TMA. Most (76%) patients had neurologic symptoms, mainly confusion (56.3%) and headache (18.8%). Approximately half (52.1%) of patients had a serious neurologic complication such as seizure, coma, or focal deficiency. In addition, 34 (35.4%) patients required mechanical ventilation. In total, 42 patients had high blood pressure (≥150/90 mm Hg) at admission; severe hypertension (≥170/110 mm Hg) subsequently developed in 11 patients and hypertensive retinopathy developed in 6 patients. Only 2 patients had hypotension (≤90/60 mm Hg) at admission. In total, 41 (42.7%) patients had cardiac events; in 26 of 43 cases with available data, patients had troponin levels above the defined threshold of their respective laboratory (Table 2).

CAP measurements during the acute phase of illness were recorded in 69 patients. Of these patients, 36 (52.2%) had values within the reference range (Table 2). Less than 10% of patients had low levels of C3, C4, factor H, or factor I, whereas 26 (38.8%) patients had low levels of CH50. CD46 levels were low in 65.7% (23/35) patients. Two patients had low levels of anti-factor H antibodies (242 and 800 arbitrary units) (Table 2). ADAMTS13 activity was detectable (≥10%) in all 69 patients in whom it was tested.

Among the 84 cases in which *stx* type was detected, *stx1*–/*stx2*+ was the most common genotype (85.7%). The *stx1*+/*stx2*– genotype was significantly associated with increased CCI and immunodeficiency (Appendix Table 1). As expected, the most common STEC isolation site was stool (93.8%), whereas only 10 patients had STEC-positive urine or blood samples. Seven (7.3%) patients had STEC-positive urine samples, including 5 who had a urologic infection without associated colitis. Four patients had STEC-positive blood samples, including 1 patient for whom STEC was identified in blood samples only. In total, 5 patients had a multisite infection.

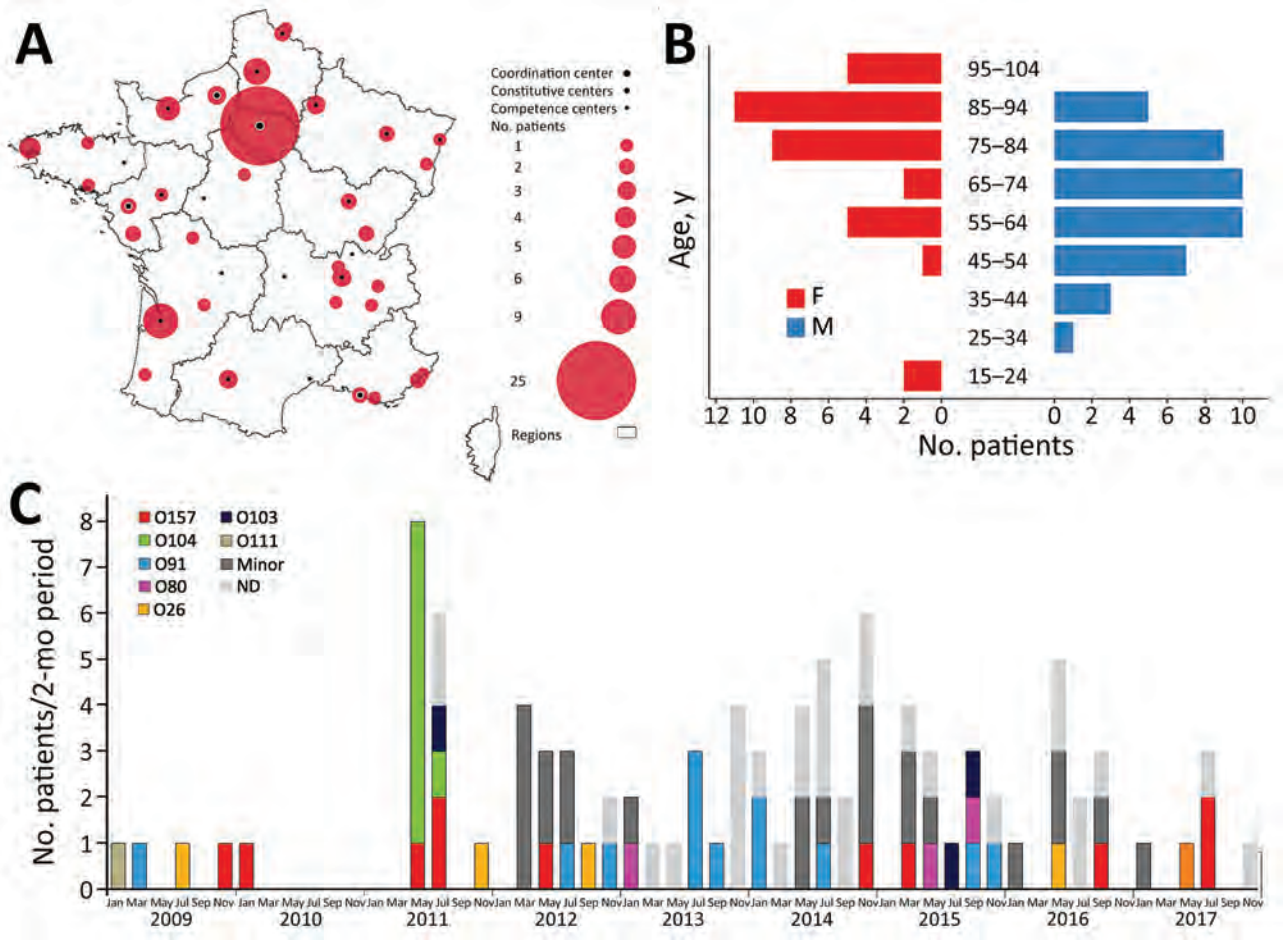

Figure 1. Distribution of adults with Shiga toxin–associated hemolytic uremic syndrome, France, 2009–2017. A) Geographic distribution of cases and thrombotic microangiopathy reference centers. The Centre National de Référence des Microangiopathies Thrombotiques is a national network comprising 1 coordination center, 5 constitutive centers, and 21 competence centers. B) Age and sex distribution of cases. C) Bimonthly distribution of cases according to serogroup. Of patients with minor serogroups, 4 had strains belonging to O106, 3 to O128, 3 to O174, 2 to O113, 1 to O100, 1 to O126, 1 to O148, 1 to O177, 1 to O78, 1 to O84, and 7 to an O serogroup not typable at the time of identification. ND, not determined.

Most (60; 62.5%) had a serogroup typable by the NRC-Ec; 7 (7.3%) patients had an untypable serogroup. The most common serogroups were O91 (12; 17.9%) and O157 (10; 14.9%) (Table 2). The STEC isolates from urine samples belonged to the O104, O91, O106, O126, O174, and O148 serogroups; isolates from blood samples belonged to the O80, O103, and O128 serogroups (Appendix Table 2).

In total, 19 (19.8%) patients died during hospitalization (Figure 2, panel A; Appendix Table 3). Patients died 3–152 days after admission and had a median follow-up period of 112 days (IQR 49–238). After follow-up, 1 patient had HELLP (hemolysis, elevated liver enzymes, low platelets) syndrome; the patient was STEC-negative at the time of the episode. None of the surviving patients had a further episode of TMA during follow-up.

Patients were treated mainly with BSC, TPE, or eculizumab; 3 patients also received immunoadsorption treatment (Appendix Table 4). Of the 61 patients who required dialysis, 17 (25.4%) died. At the end of the follow-up period, 6 (9.8%) patients still required dialysis, including 4 who had a follow-up period of >90 days. Patients who received dialysis were treated for a median duration of 13.5 days (IQR 8–28 days); 38 patients no longer required dialysis at the end of the follow-up period. After a median follow-up period of 34 days (IQR 23–75 days), the median serum creatinine value was 92 μmol/L (IQR 74–124 μmol/L). Of the 50 patients with a severe neurologic complication, 14 (28.0%) died. Of the 25 surviving patients with available data, 8 (32.0%) patients had neurologic sequelae, including persistent sensorimotor deficit (7, 28.0%), epilepsy (2, 8.0%), and cognitive impairment (2, 8.0%).

In total, 26 (27.1%) patients were treated with macrolides, including 3 who received the treatment to prevent infectious meningoencephalitis associated with eculizumab. Fifty-seven (59.4%) patients received β-lactam antimicrobial drugs, aminoglycosides, or quinolones; 22 (22.9%) patients received metronidazole.

After unadjusted analysis, we found that age (HR 1.04, 95% CI 1.01–1.07; p = 0.01), CCI (HR 1.15, 95% CI 1.03–1.28; p = 0.02) (Figure 2, panel B), underlying immunodeficiency (HR 4.36, 95% CI 1.72–11.07; p<0.01), and associated digestive disease (HR 4.07, 95% CI 1.63–10.14; p<0.01) were significantly associated with death of all causes (Table 3). We also found that severe neurologic events (HR 2.90, 95% CI 1.04–8.06; p = 0.04), mechanical ventilation (HR 2.71, 95% CI 1.09–6.74; p = 0.03), and dialysis (HR 5.57, 95% CI 1.29–24.16; p = 0.02) were predictive of death. High troponin levels and *stx* types were not associated with survival (Table 3). Most patients who died had STEC strains belonging to non-O104 and non-O157

Table 1. Characteristics of adults with Shiga toxin–associated hemolytic uremic syndrome, France, 2009–2017*

Characteristic	Value
Median age, y (IQR)	60.5 (47.00–71.00)
Sex	
M	35 (36.5)
F	61 (63.5)
Median age-weighted Charlson Comorbidity Index (IQR)	2.00 (1.00–4.25)
Tobacco use within previous 3 y	12 (12.5)
>1 underlying condition	69 (71.9)
Cardiovascular disease	48 (50.0)
Arterial hypertension	38 (39.6)
Diabetes mellitus	12 (12.5)
Venous thromboembolic disease	11 (11.5)
Heart disease†	20 (20.8)
CKD‡	15 (15.6)
History of kidney transplant	5 (5.2)
Stage 2 CKD	4 (4.2)
Stage 3 CKD	8 (8.3)
Stage 4 CKD	3 (3.1)
Digestive disorder§	29 (30.2)
Gastrointestinal disorder	18 (18.8)
Biliopancreatic disorder	9 (9.4)
Hepatic disorder	4 (4.2)
Autoimmune or inflammatory disease¶	11 (11.5)
Immunodeficiency	27 (28.1)
History of bone marrow or solid organ transplant#	8 (8.3)
Hematologic disease**	8 (8.3)
Active cancer††	8 (8.3)
HIV‡‡	3 (3.1)
Primary immunodeficiency§§	2 (2.1)
Neuropsychiatric disorder¶¶	18 (18.8)
Treatment	
Immunosuppressive treatment	12 (12.5)
Corticosteroids	11 (11.5)
Calcineurin inhibitors	7 (7.3)
Azathioprine or mycophenolate mofetil	7 (7.3)

*Values are no. (%) patients except as indicated. CKD, chronic kidney disease; IQR, interquartile range.
†8 patients had hypertensive disease, 4 had ischemic disease, 4 had hypertensive and ischemic disease, 2 had valvular cardiopathy, 1 had pulmonary hypertension, and 1 had unspecified heart disease.
‡According to Kidney Disease Improving Global Outcomes guidelines (*15*).
§8 patients had gastric, small bowel, or colonic resection; 2 had history of bariatric surgery; 3 had chronic diarrhea from diverticulosis; 1 had graft-versus-host disease; 1 had colonic endometriosis; 1 had microscopic colitis; 1 had AA amyloidosis; 1 had neurovegetative disorder (1 each); 3 had recurrent pyogenic cholangitis; 1 had sclerosing cholangitis; 2 had a double kidney-pancreas transplantation; 3 had chronic pancreatitis; 2 had cirrhosis; 1 had history of liver transplant; and 1 had autoimmune hepatitis.
¶2 patients had mixed connective tissue disease, 1 had systemic sclerosis, 1 had sclerosing cholangitis, 1 had microscopic polyangiitis, 3 had type 1 diabetes, 1 had multiple sclerosis, and 2 had psoriasis.
#3 patients had a history of kidney, 2 of double kidney–pancreas, 2 of bone marrow, and 1 of liver transplant.
**1 patient had acute myeloid leukemia, 1 had chronic lymphocytic leukemia, 1 had Hodgkin's lymphoma, 1 had clonal B-cell lymphocytosis, 1 had monoclonal gammopathy of undetermined significance, 1 had Waldenström's disease, 1 had myeloproliferative disorder, and 1 had myelodysplastic syndrome.
††3 patients had breast cancer, 1 had metastatic lung cancer, 1 had a gastrointestinal stromal cell tumor, 1 had bladder cancer, 1 had cervical cancer, and 1 had gastric cancer.
‡‡3 patients had AIDS, including 2 patients who received HIV diagnoses during treatment.
§§2 patients had hypogammaglobulinemia, including 1 patient who had ICF1 syndrome caused by a DNMT3b germinal mutation.
¶¶5 patients had stroke sequelae, 3 had Parkinson's disease, 1 had multiple sclerosis, 4 had cognitive impairment (including 1 patient who had Korsakoff syndrome and 1 who had vascular dementia), 1 had epilepsy, 1 had chronic polyradiculoneuropathy, and 5 had major depressive or bipolar disorder.

serogroups (Figure 2, panel C; Appendix Table 3). We found that overall survival was comparable among patients treated by different combinations of BSC, TPE, and eculizumab (p = 0.43 by log-rank test) (Table 3; Figure 2, panel D). The use of macrolides was not associated with survival (p = 0.77).

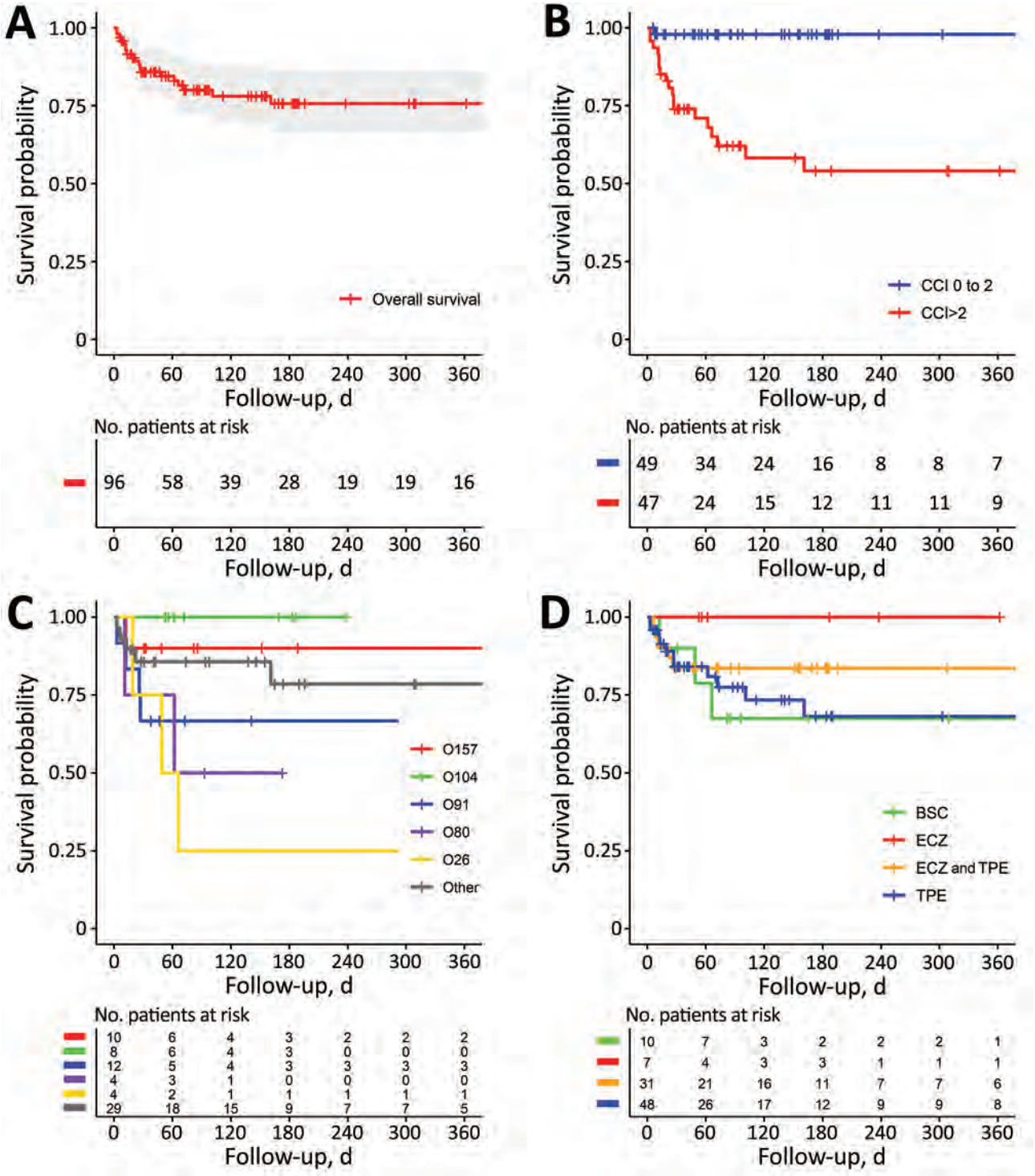

Figure 2. Kaplan-Meier survival plots of adults with Shiga toxin–associated hemolytic uremic syndrome, France, 2009–2017. A) Overall. B) By age-weighted Charlson comorbidity index. C) By STEC serogroup. D) By treatment. Plots show time from admission to death. p values determined using log-rank test. BSC, best standard of care; CCI, age-weighted Charlson comorbidity index; ECZ, eculizumab; TPE, therapeutic plasma exchange.

Multivariate analysis showed that underlying immunodeficiency (HR 3.54, 95% CI 1.24–10.14; p = 0.02) and severe neurologic events (HR 3.40, 95% CI 1.05–11.04; p = 0.04) were negatively associated with survival (Table 3). After adjustment of determinants retained for the multivariate analysis, we found that eculizumab was not associated with survival (HR 0.77, 95% 0.25–2.33; p = 0.64). Propensity score-matching also indicated that eculizumab was not associated with survival (p = 0.34) (Appendix Table 5, Figure 2).

Discussion

We found that 20% of adults who had STEC-associated HUS died during hospitalization, in agreement with previous findings (*9*,*10*); however, <1% of children who had STEC-associated HUS died in France during the same years, 2007–2016 (*5*). In addition, adults had cerebral involvement 3 times more frequently than children (*2*); 52.1% of adult patients had severe neurologic manifestations, similar to the observations of Karpac et al. (*10*). Renal recovery was slow and inconsistent; 4 patients still required dialysis 90 days after hospitalization (*9*). One third of patients required mechanical ventilation. These findings emphasize that, in adults, STEC-associated HUS is a severe systemic disease that can cause multiple organ failure. However, inclusion in the CNR-MAT registry relied on voluntary physician reporting; thus, this case series is not exhaustive and might disproportionately reflect the most severe cases. As previously observed for children (*18*), most cases in this cohort were sporadic and, for unclear reasons, in women. In regard to age distribution, STEC-associated HUS has a U curve from birth to old age (*6*,*9*,*10*,*19*). During the study period, 1,095 STEC-associated HUS cases in children were reported to Santé Publique France through the country's pediatric surveillance network (*5*). By comparison, this disease appears to be much rarer among adults, although underreporting is probable.

Our findings on underlying conditions and deaths by age group resemble those of the FoodNet registry of elderly adults with STEC-associated HUS (*9*). The risk for death from STEC-associated HUS increases for persons age >40 years, suggesting that young and middle-aged adults have similar clinical courses to those observed in children. We found a strong association between underlying conditions and decreased survival, especially for patients with immunodeficiency (*9*,*20*–*23*). The prevalence of antibodies against Stx decreases for persons >40 years of age (*24*), which might account for the more severe forms of STEC-associated HUS in elderly persons. The expression of glomerular globotriaosylceramide (Gb3), the main receptor of Stx, was thought to decrease with age; however, researchers now believe that expression levels remain stable throughout a person's lifetime (*25*). Renal and neurologic signs similar to those caused by HUS develop in immunocompromised mice after STEC inoculation or Stx exposure, whereas wild-type mice are naturally resistant to this disease (*26*,*27*). Together, these findings highlight the role of the immune system in preventing STEC-associated HUS. Immunodeficiency probably contributes to disease severity.

The 2011 outbreak in Europe illustrated that microbiological characteristics play a key role in STEC-associated HUS (*7*). The distribution of serotypes among adults in our study was slightly different than in a study on pediatric HUS in France in the same timeframe (*5*). Non-O157 strains were more prevalent in the pediatric series (*5*) and in ours, whereas O157 and O26 were more commonly observed among children than adults (23% among children vs. 15% among adults for O157; 11% among children vs. 6% among adults for O26) (*5*). A similar overall distribution was observed among children and adults with STEC infection in Norway (23% for O157, 10% for O26) (*28*). By contrast, serogroups O91 and O104 have been mainly found among adults (*29*,*30*). The data might have been skewed by the 2011 outbreak caused by a strain belonging to the O104 serogroup; this outbreak caused infections in younger persons who had fewer underlying conditions, which could account for the better outcomes of those patients. Other serogroups, especially O80, O26, and O91, are emerging and might be associated with increased pathogenicity (*2*,*18*). STEC O91 was also the most common serogroup among adults with STEC infections in Germany (*30*), which raises the question of increased pathogenicity in adults and in persons >40 years of age.

In agreement with previous reports of STEC-associated HUS in adults (*29*,*31*), we found that *stx1*+/*stx2*– strains were more prevalent among adults (14.3%) than had been previously documented among children (2.0%) (*5*). One possible explanation for this distribution might be that in some patients, HUS was concurrent with but unrelated to infection or colonization by *stx1*+/*stx2*– STEC; however, this scenario is unlikely because STEC-positive patients had typical features of HUS in an infectious context. We cannot exclude the possibility that the *stx2* gene could have been lost in human hosts during infection or ex vivo during subculture, as already described for STEC O26 (*32*). In this series, all *stx1*+/*stx2*– strains belonged to non-O157 serogroups. These findings are similar to those of Käppeli et al. (*29*), who found that 15.8% of cases of non-O157 STEC–associated HUS were caused

by *stx1*+/*stx2*– strains, which could suggest that different serogroups might pose different risks for HUS associated with particular *stx* genotypes. Last, most (83%) patients with *stx1*+/*stx2*– genotypes had underlying immunodeficiency; one explanation could be that immunodeficient patients are more susceptible to Stx1. The alleles *stx1* and *stx2c* have been associated with a lower risk for severe STEC infection and HUS (*28*). However, *stx1a* is associated with higher risk for severe STEC infection (*33*). We did not have data on *stx* subtypes in our study.

We observed CAP abnormalities similar to those previously reported in a cohort of 113 cases of STEC-associated HUS in children (*16*). We found that 65.7% of patients had low CD46 and 38.8% had low CH50 levels. However, a decrease in the concentration of complement factors, the interpretation of which remains equivocal, might be attributable to kidney damage and STEC-associated HUS (*16*). The presence of an inflammatory syndrome further complicates the interpretation of these data. In contrast to atypical HUS, pediatric STEC-associated HUS has not been linked to a constitutional or acquired dysregulation of the CAP. Screening for variants in complement genes is not usually conducted among children with STEC-associated HUS. Similarly, it seems unlikely that STEC infection reveals underlying CAP abnormalities in many adults.

We found that 7% of patients had STEC-positive urine samples, an underrecognized finding documented by Lavrek et al. (*34*). Although urine samples might be easily contaminated, especially in patients who have diarrhea, these findings encourage systematic STEC-specific PCR screening and culture confirmation of stool or other biological samples (in the event of extraintestinal *E. coli* infection) from adult TMA patients (*2*,*34*).

Because the effectiveness of specific treatments remains unclear, BSC is the cornerstone of STEC-associated HUS treatment (*2*,*35*,*36*). Univariate analysis indicated that TPE was not associated with overall survival improvement, although other studies have concluded differently (*37*–*39*). However, considering the substantial overlap between the signs and symptoms of STEC-associated HUS in adults and TMA of other etiologies, some researchers believe that plasma therapy should be given until TTP or atypical HUS are ruled out (*13*,*40*). Whether TPE should be continued after the determination of *stx* status remains unclear. As previously reported, we did not find a clear survival benefit from eculizumab (*38*,*41*). However, the small sample size and the strong differences between patients who did and did not receive eculizumab treatment preclude definitive conclusions.

The benefits of antimicrobial drugs in treating STEC-associated HUS are unclear (*42*,*43*). Previous studies suggest that the use of antimicrobial drugs during early stages of STEC infection is associated with the development of HUS. However, the effects of antimicrobial drugs administered after HUS diagnosis remain unknown (*42*). A retrospective study reported that azithromycin administered during STEC infection might reduce the duration of STEC carriage (*43*). We found that use of macrolides was not associated with survival. This observation might have been confounded by possible unreported administration of antimicrobial drugs before hospitalization, treatment for unstandardized indications at the discretion of the practitioner, or other variables. We also found that the prescription of multiple antimicrobial drugs was a common practice, especially in cases of severe infection.

In conclusion, STEC-associated HUS is rarer among adults than among children but causes more severe disease and death. Underlying conditions, especially immunodeficiency, are strongly associated with decreased survival. The severity of the disease, a probably underestimated prevalence, and the risk for outbreaks of emerging STEC-associated HUS provide strong arguments for active epidemiologic and microbiological surveillance of this disease.

Members of the Reference Center for Thrombotic Microangiopathies team: Jean-François Augusto, Elie Azoulay, Virginie Barbay, Ygal Benhamou, Dominique Bordessoule, Christophe Charasse, Anne Charvet-Rumpler, Dominique Chauveau, Gabriel Choukroun, Jean-Philippe Coindre, Paul Coppo, Elise Corre, Yahsou Delmas, Georges Deschenes, Alain Devidas, Antoine Dossier, Olivier Fain, Fadi Fakhouri, Véronique Frémeaux-Bacchi, Lionel Galicier, Steven Grangé, Bertrand Guidet, Jean-Michel Halimi, Mohamed Hamidou, Raoul Herbrecht, Miguel Hié, Frédéric Jacobs, Bérangère Joly, Tarik Kanouni, Gilles Kaplanski, Alexandre Lautrette, Véronique Le Guern, Bruno Moulin, Christiane Mousson, Mario Ojeda Uribe, Abdelkader Ouchenir, Nathalie Parquet, Frédéric Pène, Pierre Perez, Pascale Poullin, Claire Pouteil-Noble, Claire Presne, François Provôt, Eric Rondeau, Samir Saheb, Amélie Seguin, Aude Servais, Alain Stépanian, Agnès Veyradier, Cécile Vigneau, Alain Wynckel, and Patricia Zunic.

Acknowledgments

We thank Eric Alamartine, Sandrine Bedon Carte, Gilles Bernardin, Severin Cabasson, Vincent Cadiergue, Jean-François Cerfon, Thomas Crepin, Vincent Das, Philippe De Swardt, Geneviève Dumont, Alexandre Hertig, Jean Claude Lacherade, Olivier Leroy, Julie Le Scanff, Didier Perez, Emilie Pinçon, Jean-Pierre Quenot, Felipe Suarez, Rachel Tetaz,

Olivier Thaunat, Jean Marc Thouret, and Xavier Valette for their valuable collaboration with the CNR-MAT. These physicians played an active role in care of patients with STEC-associated HUS.

This work was partly funded by grants from the French Ministry of Health (Programme Hospitalier de Recherche Clinique [grant nos. P120118 and AOM12259]). B.T. has received a research grant from CSL Behring (https://www.cslbehring.com). E.R. and C.P. are members of the Advisory Board for Alexion Pharmaceuticals, Inc. (https://alexion.com). Y.D. has received lecture fees from Alexion Pharmaceuticals, Inc. and honorarium as advisory board member for Sanofi (https://www.sanofi.com). F.F. has received consultancy fees and speaker honoraria from F. Hoffmann-La Roche Ltd (https://www.roche.com); Alexion Pharmaceuticals, Inc.; Apellis Pharmaceuticals (https://apellis.com); Achillion Pharmaceuticals; Novartis AG (https://www.novartis.com); and Alnylam Pharmaceuticals, Inc. (https://www.alnylam.com). P.C. is member of the advisory boards of Alexion Pharmaceuticals, Inc.; Sanofi; Shire P.C.C. (http://shirepcc.com); Takeda Pharmaceutical Company Limited (https://www.takeda.com); and Octapharma AG (https://www.octapharma.com); he has received consultancy fees and speaker honoraria from Sanofi; Alexion Pharmaceuticals, Inc.; and Takeda Pharmaceutical Company Limited.

About the Author

Dr. Travert is a medical intern at Assistance Publique-Hôpitaux de Paris in Paris, France. His research interests include the epidemiology of STEC-associated HUS and environmental factors contributing to autoimmune diseases.

References

1. Karmali MA, Steele BT, Petric M, Lim C. Sporadic cases of haemolytic-uraemic syndrome associated with faecal cytotoxin and cytotoxin-producing *Escherichia coli* in stools. Lancet. 1983;321:619–20. https://doi.org/10.1016/S0140-6736(83)91795-6
2. Joseph A, Cointe A, Mariani Kurkdjian P, Rafat C, Hertig A. Shiga toxin–associated hemolytic uremic syndrome: a narrative review. Toxins (Basel). 2020;12:67. https://doi.org/10.3390/toxins12020067
3. Fakhouri F, Zuber J, Frémeaux-Bacchi V, Loirat C. Haemolytic uraemic syndrome. Lancet. 2017;390:681–96. https://doi.org/10.1016/S0140-6736(17)30062-4
4. Majowicz SE, Scallan E, Jones-Bitton A, Sargeant JM, Stapleton J, Angulo FJ, et al. Global incidence of human Shiga toxin–producing *Escherichia coli* infections and deaths: a systematic review and knowledge synthesis. Foodborne Pathog Dis. 2014;11:447–55. https://doi.org/10.1089/fpd.2013.1704
5. Bruyand M, Mariani-Kurkdjian P, Le Hello S, King L-A, Van Cauteren D, Lefevre S, et al.; Réseau Français Hospitalier de Surveillance du Shu Pédiatrique. Paediatric haemolytic uraemic syndrome related to Shiga toxin–producing *Escherichia coli*, an overview of 10 years of surveillance in France, 2007 to 2016. Euro Surveill. 2019;24:24. https://doi.org/10.2807/1560-7917.ES.2019.24.8.1800068
6. Gould LH, Demma L, Jones TF, Hurd S, Vugia DJ, Smith K, et al. Hemolytic uremic syndrome and death in persons with *Escherichia coli* O157:H7 infection, foodborne diseases active surveillance network sites, 2000–2006. Clin Infect Dis. 2009;49:1480–5. https://doi.org/10.1086/644621
7. Frank C, Werber D, Cramer JP, Askar M, Faber M, an der Heiden M, et al.; HUS Investigation Team. Epidemic profile of Shiga-toxin–producing *Escherichia coli* O104:H4 outbreak in Germany. N Engl J Med. 2011;365:1771–80. https://doi.org/10.1056/NEJMoa1106483
8. Delmas Y, Vendrely B, Clouzeau B, Bachir H, Bui H-N, Lacraz A, et al. Outbreak of *Escherichia coli* O104:H4 haemolytic uraemic syndrome in France: outcome with eculizumab. Nephrol Dial Transplant. 2014;29:565–72. https://doi.org/10.1093/ndt/gft470
9. Gould LH, Jordan JG, Dunn J, Apostol M, Griffin PM; Emerging Infections Program FoodNet Working Group. Postdiarrheal hemolytic uremic syndrome in persons aged 65 and older in FoodNet sites, 2000–2006. J Am Geriatr Soc. 2011;59:366–8. https://doi.org/10.1111/j.1532-5415.2011.03269.x
10. Karpac CA, Li X, Terrell DR, Kremer Hovinga JA, Lämmle B, Vesely SK, et al. Sporadic bloody diarrhoea-associated thrombotic thrombocytopenic purpura-haemolytic uraemic syndrome: an adult and paediatric comparison. Br J Haematol. 2008;141:696–707. https://doi.org/10.1111/j.1365-2141.2008.07116.x
11. Soysal N, Mariani-Kurkdjian P, Smail Y, Liguori S, Gouali M, Loukiadis E, et al. Enterohemorrhagic *Escherichia coli* hybrid pathotype O80:H2 as a new therapeutic challenge. Emerg Infect Dis. 2016;22:1604–12. https://doi.org/10.3201/eid2209.160304
12. Coimbra RS, Grimont F, Lenormand P, Burguière P, Beutin L, Grimont PA. Identification of *Escherichia coli* O-serogroups by restriction of the amplified O-antigen gene cluster (rfb-RFLP). Res Microbiol. 2000;151:639–54. https://doi.org/10.1016/S0923-2508(00)00134-0
13. Coppo P, Schwarzinger M, Buffet M, Wynckel A, Clabault K, Presne C, et al.; French Reference Center for Thrombotic Microangiopathies. Predictive features of severe acquired ADAMTS13 deficiency in idiopathic thrombotic microangiopathies: the French TMA reference center experience. PLoS One. 2010;5:e10208. https://doi.org/10.1371/journal.pone.0010208
14. Charlson M, Szatrowski TP, Peterson J, Gold J. Validation of a combined comorbidity index. J Clin Epidemiol. 1994;47:1245–51. https://doi.org/10.1016/0895-4356(94)90129-5
15. International Society of Nephrology. KDIGO clinical practice guideline for acute kidney injury. 2012 [cited 2020 Jul 31]. https://kdigo.org/wp-content/uploads/2016/10/KDIGO-2012-AKI-Guideline-English.pdf
16. Frémeaux-Bacchi V, Sellier-Leclerc A-L, Vieira-Martins P, Limou S, Kwon T, Lahoche A, et al. Complement gene variants and Shiga toxin–producing *Escherichia coli*-associated hemolytic uremic syndrome. Clin J Am Soc Nephrol. 2019;14:364–77. https://doi.org/10.2215/CJN.05830518
17. Ho D, Imai K, King G, Stuart EA. MatchIt: nonparametric preprocessing for parametric causal inference. J Stat Softw. 2011;42:1–28. https://doi.org/10.18637/jss.v042.i08
18. Griffin PM, Karmali MA. Emerging public health challenges of Shiga toxin–producing *Escherichia coli* related to changes in the pathogen, the population, and the environment. Clin Infect Dis. 2017;64:371–6. https://doi.org/10.1093/cid/ciw708

19. Carter AO, Borczyk AA, Carlson JAK, Harvey B, Hockin JC, Karmali MA, et al. A severe outbreak of *Escherichia coli* O157:H7–associated hemorrhagic colitis in a nursing home. N Engl J Med. 1987;317:1496–500. https://doi.org/10.1056/NEJM198712103172403
20. Ville S, Ydee A, Garandeau C, Canet E, Tissot A, Cantarovich D, et al. Shiga toxin-producing *Escherichia coli*–associated hemolytic uremic syndrome in solid organ transplant recipients. Kidney Int. 2019;96:1423–4. https://doi.org/10.1016/j.kint.2019.08.024
21. Farina C, Gavazzeni G, Caprioli A, Remuzzi G. Hemolytic uremic syndrome associated with verocytotoxin-producing *Escherichia coli* infection in acquired immunodeficiency syndrome. Blood. 1990;75:2465. https://doi.org/10.1182/blood.V75.12.2465a.2465a
22. Vera-Aguilera J, Duma N, Gast K, Alkhateeb H, Tande A, Leung N, et al. Hemolytic uremic syndrome associated with *Escherichia coli* O157 infection in an allogenic stem cell transplant recipient. Mayo Clin Proc Innov Qual Outcomes. 2018;2:387–91. https://doi.org/10.1016/j.mayocpiqo.2018.07.001
23. Manière L, Domenger C, Camara B, Giovannini D, Malvezzi P, Rostaing L. An atypical case of Shiga toxin producing–*Escherichia coli* hemolytic and uremic syndrome (STEC-HUS) in a lung transplant recipient. Case Rep Transplant. 2019;2019:9465040. https://doi.org/10.1155/2019/9465040
24. Karmali MA, Mascarenhas M, Petric M, Dutil L, Rahn K, Ludwig K, et al. Age-specific frequencies of antibodies to *Escherichia coli* verocytotoxins (Shiga toxins) 1 and 2 among urban and rural populations in southern Ontario. J Infect Dis. 2003;188:1724–9. https://doi.org/10.1086/379726
25. Ergonul Z, Clayton F, Fogo AB, Kohan DE. Shigatoxin-1 binding and receptor expression in human kidneys do not change with age. Pediatr Nephrol. 2003;18:246–53. https://doi.org/10.1007/s00467-002-1025-9
26. Brando RJF, Miliwebsky E, Bentancor L, Deza N, Baschkier A, Ramos MV, et al. Renal damage and death in weaned mice after oral infection with Shiga toxin 2–producing *Escherichia coli* strains. Clin Exp Immunol. 2008;153:297–306. https://doi.org/10.1111/j.1365-2249.2008.03698.x
27. Karpman D, Connell H, Svensson M, Scheutz F, Aim P, Svanborg C. The role of lipopolysaccharide and Shiga-like toxin in a mouse model of *Escherichia coli* O157:H7 infection. J Infect Dis. 1997;175:611–20. https://doi.org/10.1093/infdis/175.3.611
28. Brandal LT, Wester AL, Lange H, Løbersli I, Lindstedt B-A, Vold L, et al. Shiga toxin–producing *Escherichia coli* infections in Norway, 1992–2012: characterization of isolates and identification of risk factors for haemolytic uremic syndrome. BMC Infect Dis. 2015;15:324. https://doi.org/10.1186/s12879-015-1017-6
29. Käppeli U, Hächler H, Giezendanner N, Beutin L, Stephan R. Human infections with non-O157 Shiga toxin–producing *Escherichia coli*, Switzerland, 2000–2009. Emerg Infect Dis. 2011;17:180–5. https://doi.org/10.3201/eid1702.100909
30. Werber D, Beutin L, Pichner R, Stark K, Fruth A. Shiga toxin–producing *Escherichia coli* serogroups in food and patients, Germany. Emerg Infect Dis. 2008;14:1803–6. https://doi.org/10.3201/eid1411.080361
31. Adams NL, Byrne L, Smith GA, Elson R, Harris JP, Salmon R, et al. Shiga toxin–producing *Escherichia coli* O157, England and Wales, 1983–2012. Emerg Infect Dis. 2016;22:590–7. https://doi.org/10.3201/eid2204.151485
32. Bielaszewska M, Prager R, Köck R, Mellmann A, Zhang W, Tschäpe H, et al. Shiga toxin gene loss and transfer in vitro and in vivo during enterohemorrhagic *Escherichia coli* O26 infection in humans. Appl Environ Microbiol. 2007;73:3144–50. https://doi.org/10.1128/AEM.02937-06
33. Byrne L, Adams N, Jenkins C. Association between Shiga toxin–producing *Escherichia coli* O157:H7 stx gene subtype and disease severity, England, 2009–2019. Emerg Infect Dis. 2020;26:2394–400. https://doi.org/10.3201/eid2610.200319
34. Lavrek D, Lava SAG, Milani GP, Simonetti GD, Bianchetti MG, Giannini O. Hemolytic-uremic syndrome after *Escherichia coli* urinary tract infection in humans: systematic review of the literature. J Nephrol. 2018;31:919–24. https://doi.org/10.1007/s40620-018-0543-x
35. Michael M, Elliott EJ, Ridley GF, Hodson EM, Craig JC. Interventions for haemolytic uraemic syndrome and thrombotic thrombocytopenic purpura. Cochrane Database Syst Rev. 2009;1:CD003595. https://doi.org/10.1002/14651858.CD003595.pub2
36. Grisaru S, Xie J, Samuel S, Hartling L, Tarr PI, Schnadower D, et al.; Alberta Provincial Pediatric Enteric Infection Team. Associations between hydration status, intravenous fluid administration, and outcomes of patients infected with Shiga toxin–producing *Escherichia coli*: a systematic review and meta-analysis. JAMA Pediatr. 2017;171:68–76. https://doi.org/10.1001/jamapediatrics.2016.2952
37. Keenswijk W, Raes A, De Clerck M, Vande Walle J. Is plasma exchange efficacious in Shiga toxin–associated hemolytic uremic syndrome? A narrative review of current evidence. Ther Apher Dial. 2019;23:118–25. https://doi.org/10.1111/1744-9987.12768
38. Kielstein JT, Beutel G, Fleig S, Steinhoff J, Meyer TN, Hafer C, et al.; Collaborators of the DGfN STEC-HUS registry. Best supportive care and therapeutic plasma exchange with or without eculizumab in Shiga-toxin–producing *E. coli* O104:H4 induced haemolytic-uraemic syndrome: an analysis of the German STEC-HUS registry. Nephrol Dial Transplant. 2012;27:3807–15. https://doi.org/10.1093/ndt/gfs394
39. Padmanabhan A, Connelly-Smith L, Aqui N, Balogun RA, Klingel R, Meyer E, et al. Guidelines on the use of therapeutic apheresis in clinical practice—evidence-based approach from the Writing Committee of the American Society for Apheresis: the eighth special issue. J Clin Apher. 2019;34:171–354. https://doi.org/10.1002/jca.21705
40. Joseph A, Rafat C, Zafrani L, Mariani-Kurkdjian P, Veyradier A, Hertig A, et al. Early differentiation of Shiga toxin–associated hemolytic uremic syndrome in critically ill adults with thrombotic microangiopathy syndromes. Crit Care Med. 2018;46:e904–11. https://doi.org/10.1097/CCM.0000000000003292
41. Lapeyraque A-L, Malina M, Fremeaux-Bacchi V, Boppel T, Kirschfink M, Oualha M, et al. Eculizumab in severe Shiga-toxin–associated HUS. N Engl J Med. 2011;364:2561–3. https://doi.org/10.1056/NEJMc1100859
42. Wong CS, Mooney JC, Brandt JR, Staples AO, Jelacic S, Boster DR, et al. Risk factors for the hemolytic uremic syndrome in children infected with *Escherichia coli* O157:H7: a multivariable analysis. Clin Infect Dis. 2012;55:33–41. https://doi.org/10.1093/cid/cis299
43. Nitschke M, Sayk F, Härtel C, Roseland RT, Hauswaldt S, Steinhoff J, et al. Association between azithromycin therapy and duration of bacterial shedding among patients with Shiga toxin–producing enteroaggregative Escherichia coli O104:H4. JAMA. 2012;307:1046–52. https://doi.org/10.1001/jama.2012.264

Address for correspondence: Paul Coppo, AP-HP.6 and Sorbonne Université, 184 rue du Faubourg Saint-Antoine, Assistance Publique–Hôpitaux de Paris, 75012 Paris, France; email: paul.coppo@aphp.fr

Fatal Human Infection with Evidence of Intrahost Variation of Eastern Equine Encephalitis Virus, Alabama, USA, 2019

Holly R. Hughes, Jason O. Velez, Emily H. Davis, Janeen Laven, Carolyn V. Gould, Amanda J. Panella, Amy J. Lambert, J. Erin Staples, Aaron C. Brault

Eastern equine encephalitis virus (EEEV) is an arbovirus in the family *Togaviridae*, genus *Alphavirus*, found in North America and associated with freshwater/hardwood swamps in the Atlantic, Gulf Coast, and Great Lakes regions. EEEV disease in humans is rare but causes substantial illness and death. To investigate the molecular epidemiology and microevolution of EEEV from a fatal case in Alabama, USA, in 2019, we used next-generation sequencing of serum and cerebrospinal fluid (CSF). Phylogenetic inference indicated that the infecting strain may be closely related to isolates from Florida detected during 2010–2014, suggesting potential seeding from Florida. EEEV detected in serum displayed a higher degree of variability with more single-nucleotide variants than that detected in the CSF. These data refine our knowledge of EEEV molecular epidemiologic dynamics in the Gulf Coast region and demonstrate potential quasispecies bottlenecking within the central nervous system of a human host.

In North America, eastern equine encephalitis virus (EEEV) causes disease in equids, domestic birds, and humans (*1*,*2*). The virus is maintained in an enzootic cycle between passerine avian amplification hosts and *Culiseta melanura* mosquitoes as the principal mosquito vectors (*3*). EEEV infections in humans and equids result from spillover from the enzootic transmission cycle or by the bites of bridge vectors that can become infected during epizootics. In humans and equids, viremia does not develop at sufficient levels to infect additional mosquito vectors; however, the disease can be severe because of the neurotropic nature of the virus (*4*).

In the New England region, cases of eastern equine encephalitis (EEE) resulting from EEEV infection in humans are seasonal and are typically reported during July–October (*5*); in Florida, EEEV transmission persists all year (*6*). The first case of EEE in a human was identified in Massachusetts in 1938 after an epizootic among horses (*2*). Before 2019, the last major EEE epidemic occurred in New Jersey in 1959; a total of 32 cases in humans were reported (*7*). During 2003–2018, an average of 8 (range 4–21) EEE cases/year in humans were reported to the Centers for Disease Control and Prevention (CDC) (*8*). Although reports of EEE in humans are rare and the proportion of inapparent infections is high (*7*), the case-fatality rate for patients with reported cases of neuroinvasive EEE is estimated to be 30% (*9*) and the rate of long-term sequalae in survivors is high, making EEEV infections a substantial public health concern. In 2019, an unprecedented epidemic of EEE across the eastern and upper midwestern United States resulted in 38 confirmed cases in humans, most in Massachusetts and Michigan (*8*).

EEEV is highly genetically conserved; a single major lineage has been circulating since 1933 (*10*). Phylogenetic studies have shown substantial genetic diversity among isolates of Madariaga virus, the virus most closely related to EEEV (*11*). A recent study demonstrated more EEEV genetic diversity among strains in Florida, most likely resulting from year-round transmission and more geographic mixing of EEEV than what is seen in northern states (*12*).

We investigated the molecular epidemiology of EEEV sequences from 1 patient infected with EEEV in Alabama, an area with historically limited genetic information about EEEV. In addition, we evaluated intrahost virus diversity of EEEV in the patient and report genetic diversity of virus in the blood compared with the central nervous system (CNS). All methods followed manufacturer's recommended protocols unless otherwise noted.

Author affiliation: Centers for Disease Control and Prevention, Fort Collins, Colorado, USA

DOI: https://doi.org/10.3201/eid2707.210315

Methods

The Patient

The patient was a woman in her 60s who had lymphoma, for which she was receiving rituximab. She was active and working outdoors until September 2019, when she experienced lethargy and malaise. Approximately 1 week after symptom onset, she was found at home unresponsive and was transferred to the hospital. Her evaluation at the hospital indicated suspected viral encephalitis, but test results for numerous viral and bacterial etiologies, including testing of cerebrospinal fluid (CSF) by BioFire panel (BioFire Diagnostics, LLC, https://www.biofiredx.com), were negative; CNS lymphoma also was ruled out. The patient received broad-spectrum antimicrobial drugs and intravenous immunoglobulin, but her condition did not improve. She lapsed into a coma and never regained consciousness. Life support was discontinued, and she died 43 days after initial illness onset.

Samples

We extracted RNA from 140 μL of serum and CSF from the patient by using the QIAamp Viral RNA Mini Kit (QIAGEN, https://www.qiagen.com). We performed real-time reverse transcription PCR (RT-PCR) to detect viral RNA from the endemic encephalitic arboviruses, West Nile virus (WNV), and EEEV. We performed EEEV real-time RT-PCR as previously described (*13*) by using 10 μL of RNA and a QuantiTect Probe RT-PCR Kit (QIAGEN).

Library Preparation and Sequencing

We generated complementary DNA by using the Ovation RNA-Seq System V2 (NuGen, https://www.nugen.com). For whole-genome sequencing, we used the Ion Torrent Personal Genomic Machine system. We prepared libraries by using the Ion Plus Fragment Library Kit barcoded with the Ion Xpress Barcoding Kit and quantified by using the Ion Library TaqMan Quantitation Kit (all by Thermo Fisher Scientific, https://www.thermofisher.com). We prepared sequencing templates by using the Hi-Q View OT2 kit with the Ion One Touch 2 system (both by Thermo Fisher Scientific) and completed sequencing by using a Hi-Q View Sequencing Kit (Thermo Fisher Scientific). We loaded templated ion sphere libraries onto 318 Chips V2 and sequenced them by using the Ion Torrent PGM system (both by Thermo Fisher Scientific). We deposited virus sequences from this study into GenBank (accession nos. MT782294 and MT782295).

Whole-Genome Analysis

We loaded Fastq files (quality phred Q>20) into the CLC genomic workbench version 12 (QIAGEN) and assembled genomes by using de novo assembly. We identified viral contigs by using BLAST (https://blast.ncbi.nlm.nih.gov/Blast.cgi) and completed alignments by using the de novo assembled consensus sequences (GenBank accession nos. MT782294 and MT782295) and Bowtie2 version 2.3.4.1 (https://github.com/BenLangmead/bowtie2) with paired-end, sensitive local parameters. We removed PCR duplicates with MarkDuplicates (Picard Tools; Broad Institute, https://broadinstitute.github.io/picard). We calculated mutational frequency by using custom R scripts over possible nucleotide variables (A, U, C, G, –) according to the method described by Matsushita et al. (*14*) and called variants by using default settings of the software LoFreq (v2.0) requiring 2% frequency with a minimum of 100 reads (*15*).

We inferred phylogenies by using MEGA v7 (*16*). We downloaded reference EEEV complete genomes from GenBank (December 4, 2019) and codon aligned complete coding sequences by using ClustalW (*16*). We completed phylogenetic inference by using a maximum-likelihood algorithm with 1,000 bootstrap replicates and the general time-reversible model with gamma distributed rate variation and invariable sites, as determined by the model fit test in MEGA (https://www.megasoftware.net). We used Bayesian inference with BEAST (https://beast.community) and a Markov chain Monte Carlo approach of 100 million generations to confirm the maximum-likelihood tree topologies.

Results

Encephalitic Arboviruses in Clinical Samples

Serum and CSF specimens collected on day 24 of the patient's illness were sent to the CDC Arboviral Diagnostic and Reference Laboratory (Division of Vector-Borne Diseases, National Center for Emerging and Zoonotic Infectious Diseases, Fort Collins, CO, USA), for further evaluation of potential arboviral etiologies. Serum was negative for IgM against La Crosse virus, Jamestown Canyon virus, Powassan virus, and EEEV; neutralizing antibodies against EEEV were not detected. Test results for WNV and Saint Louis encephalitis virus IgM performed at another laboratory were reportedly negative. CSF was negative for IgM against Powassan virus and EEEV. Because the patient was receiving rituximab therapy, which can suppress antibody production, real-time RT-PCR testing was performed and found to be negative for WNV RNA; however, EEEV RNA was detected in serum

and CSF. Quantification cycle (Cq) values were 27.9 (serum) and 20.5 (CSF).

Genomic and Phylogenetic Analyses

Complete genome sequences of EEEV were obtained from each specimen: serum (520× coverage) and CSF (2,689× coverage). The EEEV consensus sequence from the serum shared 99.79% nt identity with EEEV sequences from Florida isolated in 2010 (GenBank accession no. KU840313) and 2014 (GenBank accession no KU840338). The EEEV consensus sequence from the CSF shared 99.81% nt identity with these same reference sequences. Maximum-likelihood phylogenetic analysis supported these findings and placed the derived sequences from the serum and CSF in a well-supported clade with EEEV isolated from northern Florida in 2013 and 2014 (Figure 1). These data suggest that the virus sequences obtained in this study are similar to EEEV circulating in the southeastern United States since 2010.

Intrahost Variability of EEEV in Serum and CSF

Intrahost variability was measured by detecting single-nucleotide variants (SNVs) in each specimen (Table). We detected 19 SNVs in the serum: 11 in the nonstructural genes, 7 in the structural genes, and 1 in the 3′ untranslated region (UTR). Of the 19 SNVs identified in the serum, 4 were synonymous. In contrast, 12 SNVs were identified in the CSF: 3 in the nonstructural genes, 5 in the structural genes, and 4 in the 3′ UTR. Of the 12 SNVs in the CSF, 1 was synonymous. When comparing the serum and CSF, we identified 4 SNVs in both specimens: 1 synonymous SNV at position 1322 in nonstructural protein 1 (NSP1), 2 nonsynonymous SNVs at positions 4443 in NSP3 and 9200 in envelope protein 2 (E2), and 1 SNV in the 3′ UTR at position 11312.

Three consensus nucleotides found in the serum were not found in the CSF; however, the corresponding minor SNV populations at positions 775 (NSP1), 5291 (NSP3), and 8728 (E2) in the serum were detected in the CSF with 100% frequency. These consensus level viral populations in the serum resulted in 1 synonymous nucleotide substitution at nt 5921 in NSP3 and 2 nonsynonymous changes at 775 in NSP1-I251T and 8728 in E2-L62S compared with sequences from the CSF and reference EEEV isolates (Figure 2, panels A, B). These data suggest intrahost variability on minor viral populations as well as intrahost variability at the consensus level between the specimen sources.

Discussion

EEEV causes a severe meningoencephalitis in equids, domestic birds, and humans. In 2019, the number of reported cases in humans increased substantially; 38 cases were confirmed, in contrast with the annual average of 8. We confirmed EEEV infection in an immunocompromised person; deep sequencing of the viral RNA directly from the patient's serum and CSF showed genetic relatedness to recent EEEV isolates in

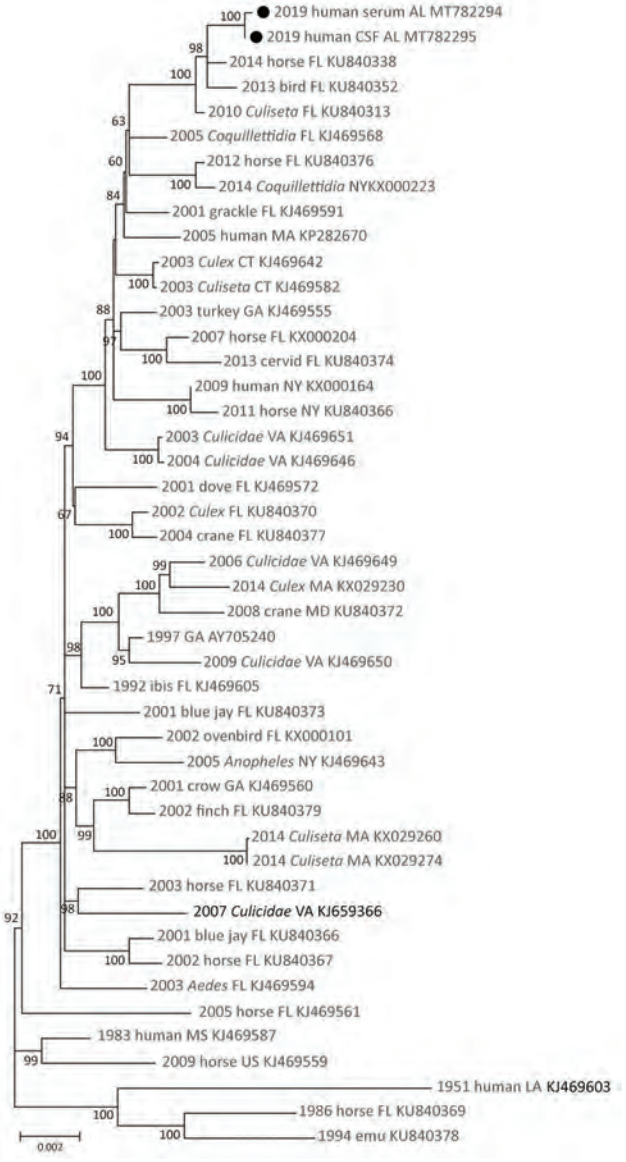

Figure 1. Maximum-likelihood phylogeny of eastern equine encephalitis virus from a woman in Alabama, USA, 2019 (solid circles), and reference sequences, based on complete coding region sequences. Nucleotide coding sequences of the full genome of eastern equine encephalitis viruses isolated during 1951–2019 were codon aligned and phylogenies inferred with general time reversible plus gamma plus proportion of invariable sites. Taxa are labeled with year of isolation, host, US state of isolation, and GenBank accession number. Branches are labeled with bootstrap support values as a percentage of 1,000 replicates. Branches with <50% bootstrap support are collapsed; only branches with >60% support are labeled. Branch lengths are drawn to scale and measured in the number of substitutions per site.

Table. Comparison of intrahost variability of eastern equine encephalitis virus variants in serum and cerebrospinal fluid from a woman in Alabama, USA, 2019*

Reference position†	Serum consensus/SNV	Serum SNV frequency, %	CSF consensus/SNV	CSF SNV frequency, %	Protein	Serum SNV amino acid substitution	CSF SNV aa substitution
646	T/C	4.42	T/–		NSP1	I208T	
775	C/T	14.40	T/–		NSP1	T251I	
778	T/A	9.13	T/–		NSP1	L252Q	
1322	T/C	12.18	T/C	6.52	NSP1	P433	P433
1326	A/C	5.46	A/–		NSP1	T435P	
2719	T/–		T/C	3.23	NSP2		L366P
2866	G/A	5.59	G/–		NSP2	R415H	
2871	G/C	6.74	G/–		NSP2	E417Q	
4443	T/C	7.75	T/C	7.34	NSP3	W147R	W147R
4445	G/A	14.05	G/–		NSP3	W147‡	
5291	T/C	4.21	C/–		NSP3	A429	
5546	G/–		G/A	4.87	Capsid		T514
7768	C/–		A/C	6.71	Capsid		A66V
7774	G/–		G/A	6.21	Capsid		R68H
8662	C/T	41.71	C/–		E2	A40V	
8728	C/T	6.38	T/–		E2	S62L	
8827	A/G	4.17	A/–		E2	H95R	
9195	A/G	4.29	A/–		E2	T218A	
9200	T/A	6.37	T/A	3.05	E2	D219E	D219E
9356	T/C	4.49	T/–		E2	P271	
10603	C/–		C/A	3.81	E1		T210N
11091	A/G	2.72	A/–		E1	S373G	
11303	A/–		T/C	4.82	3′ UTR		
11312	C/A	15.18	C/A	12.14	3′ UTR		
11450	T/–		T/C	6.90	3′ UTR		
11456	C/–		A/G	36.61	3′ UTR		

*Underlining indicates consensus nucleotide changes present in the serum compared with CSF sample. CSF, cerebrospinal fluid; NSP, nonstructural protein; SNV, single-nucleotide variants; UTR, untranslated region. Blank cells indicate not applicable in respective specimens.
†Reference genome position based on isolate with GenBank accession no. KX029239.
‡Stop codon.

northern Florida and uniquely demonstrated EEEV intrahost variability in a human.

Very few sequences of EEEV isolates from Alabama have been described. The sequences from our study cluster within the FL4 (*12*,*17*) monophyletic clade with EEEV isolates from northern Florida collected during 2010–2014. These data support findings of a previous study that evaluated partial coding sequences of 3 isolates from mosquitoes in Alabama that suggest EEEV gene flow between Alabama and Florida (*18*). Of note, the EEEV sequences derived in our study did not phylogenetically associate with those from similar geographic areas in the Florida panhandle, which have been shown to have a unique spatial structure (*17*). This finding suggests a potentially complex ecologic association unrelated to geographic proximity. Future surveillance of EEEV in the region will help clarify whether similar FL4 clade strains continue to circulate or become extinct, as has often been observed in northern states (*12*).

Advances in sequencing have improved our knowledge of intrahost virus variation, or quasispecies, in several arboviruses, including WNV (*19*,*20*), dengue viruses (*21*), Venezuelan equine encephalitis virus (*22*,*23*), and Ross River virus (*24*); however, few studies have evaluated intrahost genetic variation for EEEV (*25*). Sequencing reads from the serum sample exhibited more viral variation, and sequencing reads from the CSF specimen identified fewer SNVs, especially in coding regions. Our data suggest that EEEV might face a genetic bottleneck between the blood and central nervous system because the genetic variability in the CSF was more limited. The reduction in genetic variability in the CNS could potentially result from a genetic bottleneck and subsequent founder effect because of transmission across the blood–brain barrier as has been observed with poliovirus (*26*). Alternatively, the genetic variability could be indicative of continued selection for viruses capable of replication in neuronal cells, possibly resulting in neurovirulence (*27*).

In addition to intrahost quasispecies diversity, we also observed variation in the consensus sequences derived from each specimen. The consensus sequence derived from serum had 2 nonsynonymous nucleotide changes compared with that of the CSF. One amino acid change, NSP1-I251T, is located in an amphipathic peptide that has been shown to play a role in the membrane association of NSP1 (*28*), possible cell-to-cell transmission, and pathogenicity of alphaviruses (*29*,*30*). The second change, E2-L62S, is within the A domain in the wing region (*31*). This domain has been implicated in neutralization epitopes for several alphaviruses (*32*–*35*) and has also been

demonstrated to be involved with heparin sulfate receptor binding in neuronal cells (*36*,*37*).

When evaluating both intrahost virus variants and consensus-level majority variation, we found decreased variation in the CNS is not altogether unexpected because of potential bottlenecks and selection. It is noteworthy that consensus level amino acid changes observed in the serum are not reflected in the CNS. Stochastic generation of virus variants and lack of immune selection cannot explain fixation of 2 nonsynonymous amino acid changes in the peripheral compartment. It is possible that this scenario fits the quasispecies model of cooperative interaction in the virus population as described for poliovirus (*38*). Applying our observations to the quasispecies model (*39*) leads to the suggestion that the virus diversity in the periphery could contribute to systematic spread by maintaining the viral subpopulations that might facilitate CNS invasion and replication in this unique compartment. Although this study and observation are limited by a single description of EEEV in human serum, future surveillance and sequencing will add to our knowledge of EEEV disease and virus diversity.

The virus sequences generated in this study were derived from serum and CSF specimens from an immunocompromised person with no detectable serologic

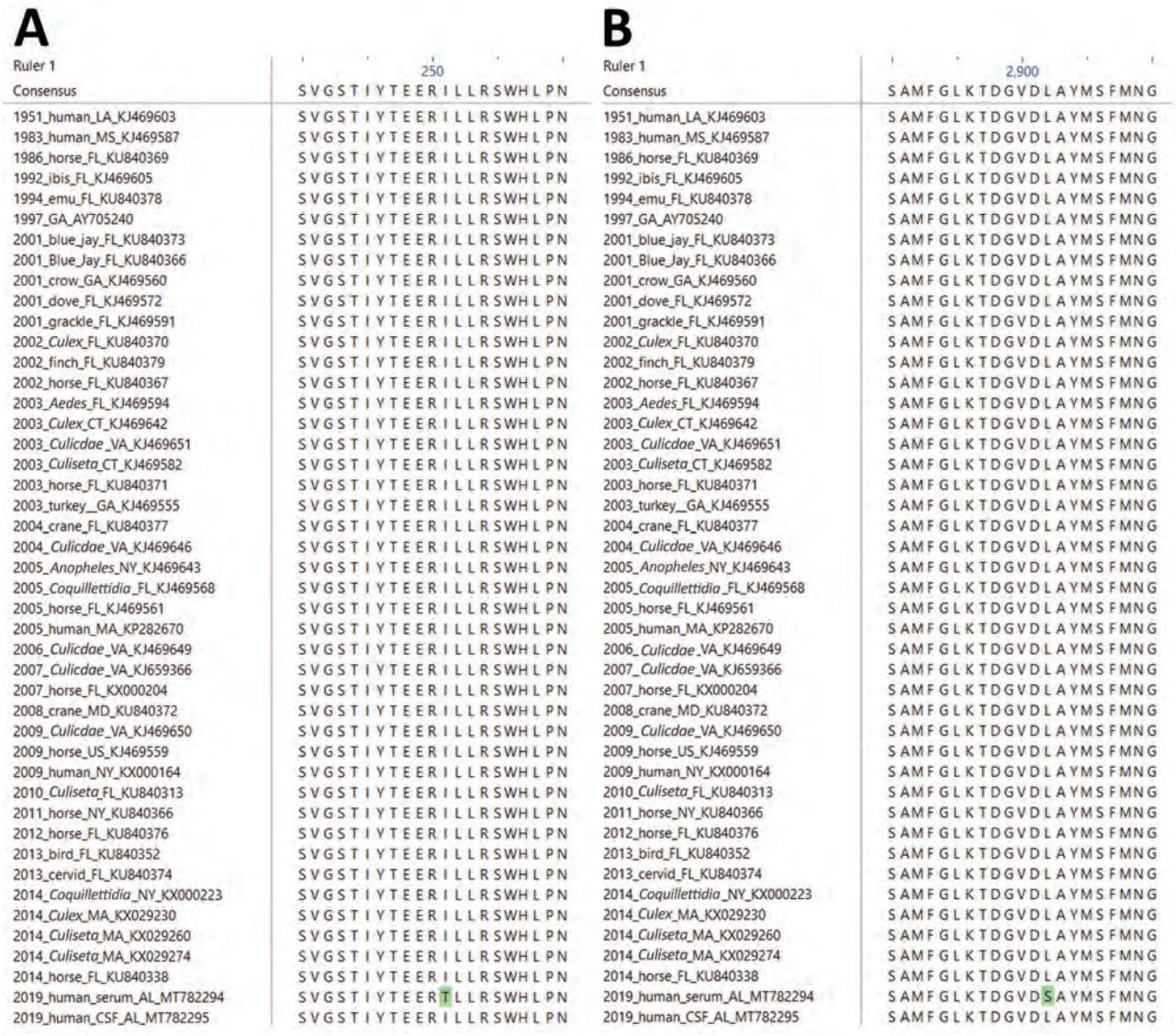

Figure 2. Amino acid sequence alignments depicting variation in the eastern equine encephalitis virus from a woman in Alabama, USA, 2019, compared with reference viruses. Open reading frames from 46 eastern equine encephalitis virus complete genomes were translated and aligned with ClustalW (*16*). Amino acid alignments show variants in the 2019 sequence in the nonstructural protein I251T (A) and structural E2 protein L62S (B). Green shading indicates changes unique to the virus sequence obtained from serum compared with cerebrospinal fluid. Reference viruses are labeled with year of isolation, host, state of isolation, and GenBank accession number.

antibody response to EEEV, probably because of rituximab therapy for lymphoma. Patients receiving B cell–depleting monoclonal antibody therapy may be predisposed to severe neuroinvasive disease and death after arbovirus infection. Cases have been associated with prolonged RNA detection in serum and CSF or brain tissue and lack of serologic response (*40*,*41*). This unique circumstance enabled us to sequence EEEV directly from the serum and CSF without amplification and report the complete EEEV sequence derived from human serum. The patient's Cq values of EEEV in serum were low, and viral genome diversity was broad. Although the relative Cq values observed in this study are similar to those found in *Cs. melanura* mosquitoes with high EEEV titers (*42*), they are below virus titers that have been observed in experimentally infected birds (*43*). It is unknown if the viral load in immunocompromised persons could lead to subsequent acquisition and transmission of the virus by a mosquito, but we can speculate that these persons could be hosts for mosquitoborne viruses, given higher viral loads and more prolonged viremias than those observed in dead-end hosts (*44*–*46*).

Acknowledgments

We thank Sherri Davidson and Emily McDonald for helping coordinate the transfer of specimens and relevant patient information.

About the Author

Dr. Hughes is a research microbiologist in the Diagnostic and Reference Team of the Arboviral Diseases Branch, Division of Vector-Borne Diseases, National Center for Emerging and Zoonotic Infectious Diseases, CDC, Fort Collins, Colorado. Her research focuses on next-generation sequencing and test development for clinical diagnosis.

References

1. Tully TN Jr, Shane SM, Poston RP, England JJ, Vice CC, Cho DY, et al. Eastern equine encephalitis in a flock of emus (*Dromaius novaehollandiae*). Avian Dis. 1992;36:808–12. https://doi.org/10.2307/1591790
2. Webster LT, Wright FH. Recovery of eastern equine encephalomyelitis virus from brain tissue of human cases of encephalitis in Massachusetts. Science. 1938;88:305–6. https://doi.org/10.1126/science.88.2283.305
3. Molaei G, Oliver J, Andreadis TG, Armstrong PM, Howard JJ. Molecular identification of blood-meal sources in *Culiseta melanura* and *Culiseta morsit*ans from an endemic focus of eastern equine encephalitis virus in New York. Am J Trop Med Hyg. 2006;75:1140–7. https://doi.org/10.4269/ajtmh.2006.75.1140
4. Moncayo AC, Edman JD. Toward the incrimination of epidemic vectors of eastern equine encephalomyelitis virus in Massachusetts: abundance of mosquito populations at epidemic foci. J Am Mosq Control Assoc. 1999;15:479–92.
5. Howard JJ, Morris CD, Emord DE, Grayson MA. Epizootiology of eastern equine encephalitis virus in upstate New York, USA. VII. Virus surveillance 1978–85, description of 1983 outbreak, and series conclusions. J Med Entomol. 1988;25:501–14. https://doi.org/10.1093/jmedent/25.6.501
6. Bigler WJ, Lassing EB, Buff EE, Prather EC, Beck EC, Hoff GL. Endemic eastern equine encephalomyelitis in Florida: a twenty-year analysis, 1955–1974. Am J Trop Med Hyg. 1976;25:884–90. https://doi.org/10.4269/ajtmh.1976.25.884
7. Goldfield M, Welsh JN, Taylor BF. The 1959 outbreak of Eastern encephalitis in New Jersey. 5. The inapparent infection:disease ratio. Am J Epidemiol. 1968;87:32–3. https://doi.org/10.1093/oxfordjournals.aje.a120807
8. Lindsey NP, Martin SW, Staples JE, Fischer M. Notes from the Field: multistate outbreak of eastern equine encephalitis virus—United States, 2019. MMWR Morb Mortal Wkly Rep. 2020;69:50–1. https://doi.org/10.15585/mmwr.mm6902a4
9. Lindsey NP, Staples JE, Fischer M. Eastern equine encephalitis virus in the United States, 2003–2016. Am J Trop Med Hyg. 2018;98:1472–7. https://doi.org/10.4269/ajtmh.17-0927
10. Arrigo NC, Adams AP, Weaver SC. Evolutionary patterns of eastern equine encephalitis virus in North versus South America suggest ecological differences and taxonomic revision. J Virol. 2010;84:1014–25. https://doi.org/10.1128/JVI.01586-09
11. Brault AC, Powers AM, Chavez CL, Lopez RN, Cachón MF, Gutierrez LF, et al. Genetic and antigenic diversity among eastern equine encephalitis viruses from North, Central, and South America. Am J Trop Med Hyg. 1999;61:579–86. https://doi.org/10.4269/ajtmh.1999.61.579
12. Tan Y, Lam TT, Heberlein-Larson LA, Smole SC, Auguste AJ, Hennigan S, et al. Large-scale complete-genome sequencing and phylodynamic analysis of eastern equine encephalitis virus reveals source-sink transmission dynamics in the United States. J Virol. 2018;92:e00074-18. https://doi.org/10.1128/JVI.00074-18
13. Lambert AJ, Martin DA, Lanciotti RS. Detection of North American eastern and western equine encephalitis viruses by nucleic acid amplification assays. J Clin Microbiol. 2003;41:379–85. https://doi.org/10.1128/JCM.41.1.379-385.2003
14. Matsushita H, Hasegawa K, Oda K, Yamamoto S, Nishijima A, Imai Y, et al. The frequency of neoantigens per somatic mutation rather than overall mutational load or number of predicted neoantigens per se is a prognostic factor in ovarian clear cell carcinoma. Oncoimmunology. 2017;6:e1338996. https://doi.org/10.1080/2162402X.2017.1338996
15. Wilm A, Aw PP, Bertrand D, Yeo GH, Ong SH, Wong CH, et al. LoFreq: a sequence-quality aware, ultra-sensitive variant caller for uncovering cell-population heterogeneity from high-throughput sequencing datasets. Nucleic Acids Res. 2012;40:11189–201. https://doi.org/10.1093/nar/gks918
16. Kumar S, Stecher G, Tamura K. MEGA7: Molecular Evolutionary Genetics Analysis version 7.0 for bigger datasets. Mol Biol Evol. 2016;33:1870–4. https://doi.org/10.1093/molbev/msw054
17. Heberlein-Larson LA, Tan Y, Stark LM, Cannons AC, Shilts MH, Unnasch TR, et al. Complex epidemiological dynamics of eastern equine encephalitis virus in Florida. Am J Trop Med Hyg. 2019;100:1266–74. https://doi.org/10.4269/ajtmh.18-0783
18. White GS, Pickett BE, Lefkowitz EJ, Johnson AG, Ottendorfer C, Stark LM, et al. Phylogenetic analysis of eastern equine encephalitis virus isolates from Florida. Am J Trop Med Hyg. 2011;84:709–17. https://doi.org/10.4269/ajtmh.2011.10-0267
19. Dridi M, Rosseel T, Orton R, Johnson P, Lecollinet S, Muylkens B, et al. Next-generation sequencing shows West Nile virus quasispecies diversification after a single passage in a carrion crow (*Corvus corone*) in vivo infection model. J Gen Virol. 2015;96:2999–3009. https://doi.org/10.1099/jgv.0.000231

20. Nelson CW, Sibley SD, Kolokotronis SO, Hamer GL, Newman CM, Anderson TK, et al. Selective constraint and adaptive potential of West Nile virus within and among naturally infected avian hosts and mosquito vectors. Virus Evol. 2018;4:vey013. https://doi.org/10.1093/ve/vey013
21. Ko HY, Li YT, Chao DY, Chang YC, Li ZT, Wang M, et al. Inter- and intra-host sequence diversity reveal the emergence of viral variants during an overwintering epidemic caused by dengue virus serotype 2 in southern Taiwan. PLoS Negl Trop Dis. 2018;12:e0006827. https://doi.org/10.1371/journal.pntd.0006827
22. Patterson EI, Khanipov K, Rojas MM, Kautz TF, Rockx-Brouwer D, Golovko G, et al. Mosquito bottlenecks alter viral mutant swarm in a tissue and time-dependent manner with contraction and expansion of variant positions and diversity. Virus Evol. 2018;4:vey001. https://doi.org/10.1093/ve/vey001
23. Forrester NL, Guerbois M, Adams AP, Liang X, Weaver SC. Analysis of intrahost variation in Venezuelan equine encephalitis virus reveals repeated deletions in the 6-kilodalton protein gene. J Virol. 2011;85:8709–17. https://doi.org/10.1128/JVI.00165-11
24. Liu WJ, Rourke MF, Holmes EC, Aaskov JG. Persistence of multiple genetic lineages within intrahost populations of Ross River virus. J Virol. 2011;85:5674–8. https://doi.org/10.1128/JVI.02622-10
25. Weaver SC, Bellew LA, Gousset L, Repik PM, Scott TW, Holland JJ. Diversity within natural populations of eastern equine encephalomyelitis virus. Virology. 1993;195:700–9. https://doi.org/10.1006/viro.1993.1421
26. Pfeiffer JK, Kirkegaard K. Bottleneck-mediated quasispecies restriction during spread of an RNA virus from inoculation site to brain. Proc Natl Acad Sci U S A. 2006;103:5520–5. https://doi.org/10.1073/pnas.0600834103
27. Gardner CL, Ebel GD, Ryman KD, Klimstra WB. Heparan sulfate binding by natural eastern equine encephalitis viruses promotes neurovirulence. Proc Natl Acad Sci U S A. 2011;108:16026–31. https://doi.org/10.1073/pnas.1110617108
28. Spuul P, Salonen A, Merits A, Jokitalo E, Kääriäinen L, Ahola T. Role of the amphipathic peptide of Semliki Forest virus replicase protein nsP1 in membrane association and virus replication. J Virol. 2007;81:872–83. https://doi.org/10.1128/JVI.01785-06
29. Ahola T, Kujala P, Tuittila M, Blom T, Laakkonen P, Hinkkanen A, et al. Effects of palmitoylation of replicase protein nsP1 on alphavirus infection. J Virol. 2000;74:6725–33. https://doi.org/10.1128/JVI.74.15.6725-6733.2000
30. Laakkonen P, Auvinen P, Kujala P, Kääriäinen L. Alphavirus replicase protein NSP1 induces filopodia and rearrangement of actin filaments. J Virol. 1998;72:10265–9. https://doi.org/10.1128/JVI.72.12.10265-10269.1998
31. Voss JE, Vaney MC, Duquerroy S, Vonrhein C, Girard-Blanc C, Crublet E, et al. Glycoprotein organization of chikungunya virus particles revealed by X-ray crystallography. Nature. 2010;468:709–12. https://doi.org/10.1038/nature09555
32. Kim AS, Austin SK, Gardner CL, Zuiani A, Reed DS, Trobaugh DW, et al. Protective antibodies against Eastern equine encephalitis virus bind to epitopes in domains A and B of the E2 glycoprotein. Nat Microbiol. 2019;4:187–97. https://doi.org/10.1038/s41564-018-0286-4
33. Pal P, Dowd KA, Brien JD, Edeling MA, Gorlatov S, Johnson S, et al. Development of a highly protective combination monoclonal antibody therapy against chikungunya virus. PLoS Pathog. 2013;9:e1003312. https://doi.org/10.1371/journal.ppat.1003312
34. Hasan SS, Sun C, Kim AS, Watanabe Y, Chen CL, Klose T, et al. Cryo-EM structures of eastern equine encephalitis virus reveal mechanisms of virus disassembly and antibody neutralization. Cell Rep. 2018;25:3136–3147.e5. https://doi.org/10.1016/j.celrep.2018.11.067
35. Jin J, Liss NM, Chen DH, Liao M, Fox JM, Shimak RM, et al. Neutralizing monoclonal antibodies block chikungunya virus entry and release by targeting an epitope critical to viral pathogenesis. Cell Rep. 2015;13:2553–64. https://doi.org/10.1016/j.celrep.2015.11.043
36. Bernard KA, Klimstra WB, Johnston RE. Mutations in the E2 glycoprotein of Venezuelan equine encephalitis virus confer heparan sulfate interaction, low morbidity, and rapid clearance from blood of mice. Virology. 2000;276:93–103. https://doi.org/10.1006/viro.2000.0546
37. Lee P, Knight R, Smit JM, Wilschut J, Griffin DE. A single mutation in the E2 glycoprotein important for neurovirulence influences binding of Sindbis virus to neuroblastoma cells. J Virol. 2002;76:6302–10. https://doi.org/10.1128/JVI.76.12.6302-631-.2002
38. Vignuzzi M, Stone JK, Arnold JJ, Cameron CE, Andino R. Quasispecies diversity determines pathogenesis through cooperative interactions in a viral population. Nature. 2006;439:344–8. PMID: 16327776
39. Biebricher CK, Eigen M. The error threshold. Virus Res. 2005; 107:117–27. https://doi.org/10.1016/j.virusres.2004.11.002
40. Solomon IH, Ciarlini PDSC, Santagata S, Ahmed AA, De Girolami U, Prasad S, et al. Fatal eastern equine encephalitis in a patient on maintenance rituximab: a case report. Open Forum Infect Dis. 2017;4:ofx021. https://doi.org/10.1093/ofid/ofx021
41. Solomon IH, Spera KM, Ryan SL, Helgager J, Andrici J, Zaki SR, et al. Fatal Powassan encephalitis (deer tick virus, lineage II) in a patient with fever and orchitis receiving rituximab. JAMA Neurol. 2018;75:746–50. https://doi.org/10.1001/jamaneurol.2018.0132
42. Armstrong PM, Andreadis TG. Eastern equine encephalitis virus in mosquitoes and their role as bridge vectors. Emerg Infect Dis. 2010;16:1869–74. https://doi.org/10.3201/eid1612.100640
43. Komar N, Dohm DJ, Turell MJ, Spielman A. Eastern equine encephalitis virus in birds: relative competence of European starlings (*Sturnus vulgaris*). Am J Trop Med Hyg. 1999;60:387–91. https://doi.org/10.4269/ajtmh.1999.60.387
44. de Souza Pereira BB, Darrigo Junior LG, de Mello Costa TC, Felix AC, Simoes BP, Stracieri AB, et al. Prolonged viremia in dengue virus infection in hematopoietic stem cell transplant recipients and patients with hematological malignancies. Transpl Infect Dis. 2017;19:e12721. https://doi.org/10.1111/tid.12721
45. Mateo R, Xiao SY, Guzman H, Lei H, Da Rosa AP, Tesh RB. Effects of immunosuppression on West Nile virus infection in hamsters. Am J Trop Med Hyg. 2006;75:356–62. https://doi.org/10.4269/ajtmh.2006.75.356
46. Huang C, Slater B, Rudd R, Parchuri N, Hull R, Dupuis M, et al. First isolation of West Nile virus from a patient with encephalitis in the United States. Emerg Infect Dis. 2002;8:1367–71. https://doi.org/10.3201/eid0812.020532

Address for correspondence: Holly Hughes, Centers for Disease Control and Prevention, 3156 Rampart Rd, Fort Collins, CO 80521, USA; email: ltr8@cdc.gov

Ethnically Disparate Disease Progression and Outcomes among Acute Rheumatic Fever Patients in New Zealand, 1989–2015

Jane Oliver, Oliver Robertson, Jane Zhang, Brooke L. Marsters, Dianne Sika-Paotonu, Susan Jack, Julie Bennett, Deborah A. Williamson, Nigel Wilson, Nevil Pierse, Michael G. Baker

We investigated outcomes for patients born after 1983 and hospitalized with initial acute rheumatic fever (ARF) in New Zealand during 1989–2012. We linked ARF progression outcome data (recurrent hospitalization for ARF, hospitalization for rheumatic heart disease [RHD], and death from circulatory causes) for 1989–2015. Retrospective analysis identified initial RHD patients <40 years of age who were hospitalized during 2010–2015 and previously hospitalized for ARF. Most (86.4%) of the 2,182 initial ARF patients did not experience disease progression by the end of 2015. Progression probability after 26.8 years of theoretical follow-up was 24.0%; probability of death, 1.0%. Progression was more rapid and ≈2 times more likely for indigenous Māori or Pacific Islander patients. Of 435 initial RHD patients, 82.2% had not been previously hospitalized for ARF. This young cohort demonstrated low mortality rates but considerable illness, especially among underserved populations. A national patient register could help monitor, prevent, and reduce ARF progression.

Acute rheumatic fever (ARF) is a rare inflammatory condition triggered in response to untreated group A *Streptococcus* infection. ARF rates peak among children 5–14 years of age (*1*). ARF may permanently damage cardiac valves, producing chronic rheumatic heart disease (RHD), a serious, sometimes fatal, condition that may require surgery (*2*). Approximately half the children who experience an initial episode of ARF sustain cardiac damage, which persists as RHD for ≈15%–50% (*3*). Repeated ARF attacks (recurrent ARF) can produce new, and worsen existing, cardiac damage. If long-term prophylaxis (intramuscular injections of benzathine penicillin G [BPG]) is not administered regularly, ≈50% of ARF patients will experience recurrent ARF (*4*). Secondary prophylaxis is complicated by access to healthcare, cultural appropriateness of care delivery, injection-related discomfort, and health literacy. RHD can also develop without any previously recognized ARF (*6*,*7*). The World Health Organization recommends establishing patient registers to assist with best-practice patient management in areas where ARF persists. New Zealand lacks a national ARF register, despite a significant disease burden (*5*).

In most high-income countries, ARF is rare; rates declined sharply from the 1960s. This decline is largely attributed to improved socioeconomic and living conditions that reduce group A *Streptococcus* infections and to increased use of antimicrobial drugs to treat infections before ARF onset (*1*,*8*–*10*). Pacific Islanders make up 7% of the New Zealand population; migration between New Zealand and other Pacific Island countries occurs regularly (*11*). ARF rates for indigenous Australian, New Zealand Māori, and Pacific Islander populations are among the highest in the world (*12*,*13*). In New Zealand, deaths from ARF are uncommon, but RHD causes ≈140 deaths and ≈600 hospitalizations annually; Māori and Pacific Islander persons are overrepresented (*14*).

In New Zealand, the National Health Index number (NHI), a unique identifier, can identify and link a person's information across health datasets.

Author affiliations: Murdoch Children's Research Institute, Melbourne, Victoria, Australia (J. Oliver); University of Otago, Wellington, New Zealand (J. Oliver, O. Robertson, J. Zhang, B.L. Marsters, S. Jack, J. Bennett, N. Pierse, M.G. Baker); University of Melbourne, Melbourne (J. Oliver, D.A. Williamson); University of Otago, Wellington (D. Sika-Paotonu); Victoria University of Wellington, Wellington (D. Sika-Paotonu); Southern District Health Board, Dunedin (S. Jack); Starship Child Health, Auckland (N. Wilson)

DOI: https://doi.org/10.3201/eid2707.203045

However, information regarding the extent to which ARF patients experience poor health outcomes is limited (*18*). Patient register data (which includes echocardiographic records) from Northern Territory, Australia, show that RHD developed within 10 years of a new ARF diagnosis for 61% of indigenous patients (*19*). In New Zealand, ARF is legally notifiable; however, considerable historic undernotification impairs the usefulness of surveillance data. Thus, epidemiologic analyses often rely on hospital admission data in the national minimum dataset (NMDS), which contains data on all publicly funded hospitalizations. The NDMS is affected by misdiagnosis and miscoding and is estimated to be 80% sensitive for detecting true ARF patients (*20*). NMDS specificity for identifying RHD is also an issue. Historically, patients who have valve disease without known cause were assigned International Classification of Diseases (ICD) codes for RHD (*21*). Analyses of ICD codes for RHD can thus overestimate true cases, particularly in high-income countries, where as few as 32% of patients assigned RHD codes have genuine probable/possible RHD (*22*). The ARF diagnosis can be complex and easy for clinicians to miss (*2*). Mild-to-moderate RHD may not necessitate hospital admission, and outpatient records are not compiled on a national level. Although it is recommended that persons with initial or recurrent ARF are hospitalized for optimal management (*2*), adult patients with minimal or no symptoms are often reluctant to be admitted. These issues make evaluating ARF prevention and control activities challenging (*5*).

The prognosis for patients with subclinical RHD is unclear. These patients may not experience clinically apparent ARF but rather experience cardiac changes consistent with RHD, detectable using echocardiography only. Without prophylaxis, some patients may experience further cardiac damage, eventually resulting in clinically evident RHD. Therefore, echocardiographic screening of high-risk children to identify subclinical RHD cases and provide prophylactic treatment/monitoring may be needed to effectively reduce the RHD burden (*23*,*24*).

Given the absence of a national patient register from which to monitor New Zealand ARF patient outcomes, our first aim was to quantify the proportion of patients with initial ARF who progressed to hospitalization with recurrent ARF or RHD or died from circulatory causes (circulatory death) and to investigate their risk for disease progression according to selected demographic and clinical characteristics. Our second aim was to determine the proportion of patients with initial RHD who were hospitalized with previous ARF. Ethics approval was provided by the University of Otago Human Ethics Committee (HD 17/452), including a waiver of consent to use deidentified health data.

Methods

Aim 1: Determining Progression of Initial ARF to Recurrent ARF, RHD Hospitalization, and Early Death

In New Zealand, NMDS data with universal use of the NHI are available from 1988 on (*25*).; we extracted hospital admission data for 1989–2015. We extracted mortality data for 1989–2015 from the national Mortality Collection, which classifies the underlying cause of death for all registered deaths (*26*). We excluded from analysis non–New Zealand residents and all hospital transfers.

RHD Dataset

We extracted NMDS data for patients hospitalized with RHD for the first time during 1989–2015 (Figure 1, Initial RHD). These patients had not previously received a diagnosis of RHD or a concurrent diagnosis of ARF.

Initial ARF Dataset

We extracted NMDS data for patients who were hospitalized and assigned a principal diagnosis of ARF during 1989–2012 (Figure 1, Initial ARF). To maximize data accuracy and completeness, we excluded patients born before January 1, 1984. Included patients would therefore have been ≤5 years of age at the start of the study period. Because ARF is very rare in children <4 years of age, all ARF hospitalizations would be captured in this cohort (*27*,*28*). To increase the average follow-up time, we excluded patients hospitalized for initial ARF after December 31, 2012. Consequently, the oldest possible participant age by the end of the follow-up period (December 31, 2015) was 31 years and the youngest possible age was 3 years.

We excluded persons who had concurrent RHD and initial ARF (Figure 2, panel A). Concurrent cases were identified when an encrypted NHI corresponding to an initial ARF hospitalization was matched to the RHD dataset and both hospitalizations occurred within 180 days of each other. The 180-day cutoff point was selected by using clinical advice from a pediatric cardiologist experienced in treating ARF and RHD. A data subset of initial ARF patients was created, as was a data subset of concurrent cases. Patients were considered to have had carditis if ICD codes 101, 102, 1020, 391, 392, or 3920 were listed with their initial ARF hospitalization.

Recurrent ARF Dataset

The encrypted NHI identified all repeated hospitalizations occurring within 180 days of each other for which ARF was the principal diagnosis during 1989–2015 (Figure 1, Recurrent ARF). A data subset for patients with recurrent ARF was created (Figure 2, panel A).

RHD Progression Dataset

We used the encrypted NHI to match persons in the initial ARF dataset with the RHD dataset (Figure 1, Progression to Initial RHD). We created a data subset of patients with initial ARF that progressed to hospitalization for RHD (Figure 2, panel A).

ARF Mortality Datasets

We used the encrypted NHI to match the initial ARF dataset with the Mortality Collection. When a match was made, we extracted the date and cause of death. We identified initial ARF patients who died before January 1, 2016. We noted when the primary cause of death was attributed to diseases of the circulatory system (Figure 1, Circulatory Death; codes 390–459 from ICD 9th Revision, 100–199 ICD 10th Revision). We created a data subset of initial ARF patients who died from circulatory causes (Figure 2, panel A).

Initial ARF: A hospitalization with a diagnostic code corresponding to ARF (ICD-9: 390–392, ICD-10: I00–I02) applied as principal diagnosis during the period 1989–2012, for patients who had never previously or concurrently been assigned a principal diagnosis of RHD (i.e. within 180 days of the initial ARF hospitalization), or previously been assigned a principal diagnosis of ARF, and were born after 31 Dec 1983.

Recurrent ARF: A hospitalization where a diagnostic code corresponding to ARF (ICD-9: 390–392, ICD-10: I00–I02) was applied as principal diagnosis at least 180 days following the initial ARF hospitalization.

Initial RHD: A hospitalization with a diagnostic code corresponding to RHD (ICD-9: 393–398, ICD-10: I05–I09) applied as principal diagnosis during the period 1989–2015, for patients who had never previously been assigned a principal diagnosis of RHD or concurrently been assigned a principal diagnosis of ARF (i.e. within 180 days of the initial RHD patient hospitalization).

Progression to Initial RHD: A hospitalization where a diagnostic code corresponding to initial RHD (ICD-9: 393–398, ICD-10: I05–I09) was applied as principal diagnosis at least 180 days following the initial ARF patient hospitalization.

Death: Individuals identified in the Mortality Collection during the period 1989–2015.

Circulatory death: Individuals with codes corresponding to diseases of the circulatory system listed as primary cause of death in the Mortality Collection (ICD-9: 390–459, ICD-10: I00–I99).

Progression (any): A recurrent ARF hospitalization, or a initial RHD hospitalization, or circulatory death, occurring during 1989–2015 following the initial ARF hospitalization.

Previous ARF: Hospitalization with ARF applied as a principal diagnosis (ICD-9: 390–392, ICD-10: I00–I02) at least 180 days prior to the initial RHD hospitalization.

National Health Index (NHI) number: A unique patient identifier widely used in NZ health data. The NHI encodes some information about selected demographic characteristics.

National Minimum Dataset (NMDS): A national dataset which collects information on all publicly funded hospitalizations in NZ.

Figure 1. Definitions of terms used in study of ethnically disparate disease progression and outcomes among acute rheumatic fever patients in New Zealand, 1989–2015.

Any Progression Dataset

We combined data subsets of patients with initial ARF who progressed to hospitalization with recurrent ARF or RHD, to circulatory death, or both (Figure 1, Progression [Any]). The resulting dataset identified initial ARF patients who experienced disease progression before January 1, 2016. We tabulated key demographic and clinical characteristics of patients who did and did not progress.

Aim 2: Determining Proportion of RHD Patients with Previous ARF

Initial RHD patients were identified in NMDS data when an ICD code corresponding to RHD (Figure 1, Initial RHD) was applied for the first time as a principal diagnosis during January 1, 2010–December 31, 2015. To maximize chances of detecting the first hospitalization with ARF/RHD as a primary diagnosis, we excluded RHD patients >39 years of age. We applied inclusion and exclusion criteria when identifying initial RHD patients who had and had not been hospitalized with previous ARF (Figure 2, panel B).

We used the 180-day separation to distinguish ARF progression from patients who concurrently had ARF and RHD (aim 1) and from patients with multiple ARF hospitalizations for their first ARF episode (aim 2). When observing ARF progression, patients with ICD code(s) corresponding to initial RHD as principal diagnosis <180 days from their initial ARF hospitalization were classified as having concurrent ARF and RHD (aim 1). When RHD preceded ARF, patients with diagnostic code(s) corresponding to ARF applied as principal diagnosis <180 days of their initial RHD hospitalization were classified as having concurrent ARF and RHD (aim 2).

Statistical Analyses

We used R software version 3.1.0 throughout our analysis (*29*). Demographic data analyzed included patient age at hospitalization, New Zealand resident status, sex, prioritized ethnicity, and 2006/2013 New Zealand Deprivation Index (NZDep06/NZDep13), all of which were encoded by the NHI. Prioritized ethnicity identifies persons belonging to multiple ethnic groups and reallocates a single ethnic group by using a prioritized order of Māori, Pacific Islander, Asian, and other (*30*).

The NZDep06/NZDep13 classification system measures socioeconomic deprivation in small geographic areas by using census data (*31*). Quintile 1 represents persons living in the least deprived neighborhoods; quintile 5, the most deprived neighborhoods.

To investigate whether reported proportions differed significantly between groups, we used the χ^2 test. We used the Mann-Whitney U test to compare differences in progression time from initial ARF hospitalization to RHD progression (aim 1) and time from preceding ARF to initial RHD hospitalization (aim 2). We used Kaplan-Meier modeling to estimate the probability of disease progression over a theoretical 9,791-day (i.e., 26.8-year) follow-up period by extrapolating observed progression rates. This period was the maximum time that any person in the dataset was observed. Outcomes were investigated individually and together as the "any progression" group. Observations were right censored at the end of the study period.

Generalized linear models calculated odds ratios (ORs) and 95% CIs of progression outcomes by selected characteristics. Cox-proportional hazard ratios (HRs) and 95% CIs described whether initial ARF patients with certain characteristics tended to experience disease progression sooner than others. We considered $p<0.05$ to be significant.

Results

Aim 1: Study Population

During 1989–2012, a total of 4,623 ARF patients were hospitalized with ARF for the first time; 2,182 met the inclusion criteria (Figure 2, panel A). The median follow-up time for this cohort was 10.4 years (range 3.0–26.8 years, interquartile range [IRQ] 6.4–15.3 years). Most initial ARF patients were 5–14 years of age (83.3%), male (57.9%), and of Māori (54.4%) or Pacific Islander (36.4%) ethnicity. Most (66.9%) were from NZDep06 quintile 5 (the most deprived neighborhoods). Just over half (51.9%) had carditis (Table 1).

Of the initial ARF patients hospitalized for RHD, 42% (125/298) had RHD concurrently and were excluded (aim 1). Similarly, of the initial RHD patients who experienced ARF, 46% (65/142) had concurrent ARF (aim 2) and were excluded. The time distribution to progression supports use of the 180-day cutoff (Appendix Figure 1, panels A, B, (https://wwwnc.cdc.gov/EID/article/27/7/20-3045-App1.pdf).

Aim 1A: Risk for Progression from Initial ARF to Recurrent ARF or RHD Hospitalization and Early Death

A total of 297 (13.6%) of the 2,182 patients with initial ARF experienced disease progression before January 1, 2016. Of these, 142 (6.5%) were hospitalized with recurrent ARF and 173 (7.9%) with RHD; 24 were hospitalized for both. Fifteen initial ARF patients died, 8 from circulatory causes (Figure 2, panel A).

The median time from initial ARF to recurrent ARF hospitalization was 3.2 years (IQR 1.9–8.4 years) and to RHD hospitalization was 4.0 years (IQR 1.9–8.4 years). The median time to circulatory death was 10.4 years (IQR 3.3–12.8 years).

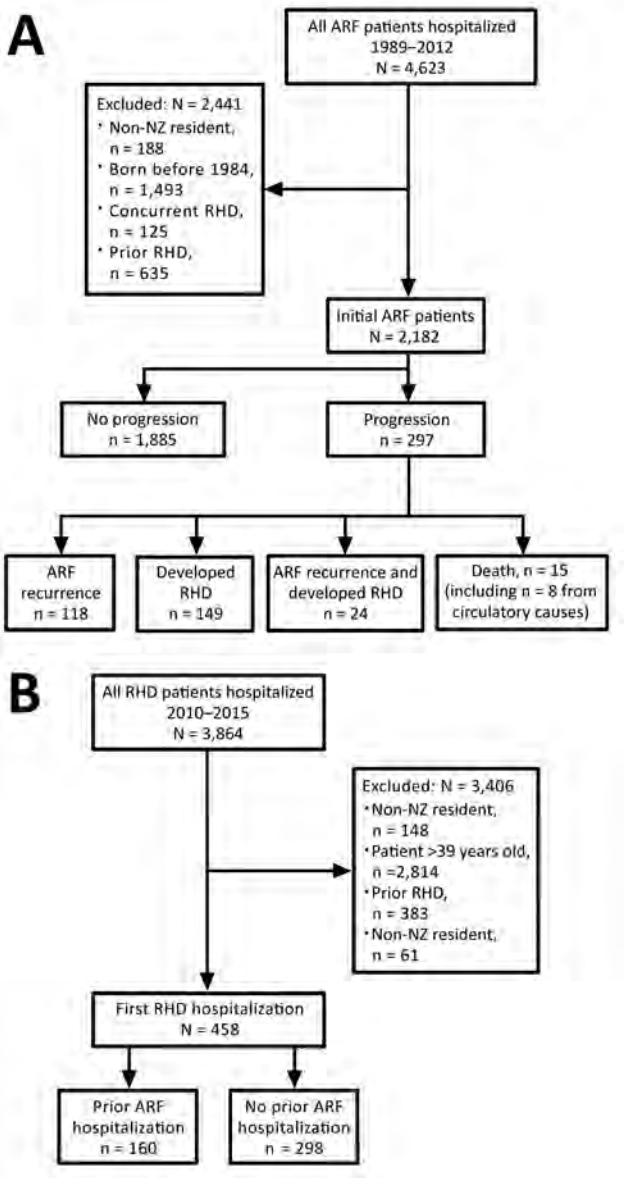

Figure 2. Progression of ARF and RHD among acute rheumatic fever patients in New Zealand, 1989–2015. A) Identification of patients with initial ARF and disease progression. B) Identification of patients with initial RHD and previous ARF. ARF, acute rheumatic fever; RHD, rheumatic heart disease.

Table 1. Key demographic and clinical characteristics of initial ARF patients born after December 31, 1983, and hospitalized during 1989–2012, New Zealand, outcomes through December 31, 2015*

Patient characteristics	All initial ARF patients, no.	No. (%) patients					
		Did not experience ARF progression	Experienced ARF progression	Recurrent ARF hospitalization	RHD hospitalization	Died from any cause	Died from circulatory causes
Total	2,182	1,885 (86.4)	297 (13.6)	142 (6.5)	173 (7.9)	15 (0.7)	8 (0.4)
Age group, y							
0–4	77	70 (90.9)	7 (9.1)	4 (5.2)	4 (5.2)	1 (1.3)	0
5–9	798	694 (87.0)	104 (13.0)	56 (7.0)	55 (6.9)	2 (0.3)	2 (0.3)
10–14	1,019	871 (85.5)	148 (14.5)	63 (6.2)	95 (9.3)	1 (0.1)	0
15–19	201	174 (86.6)	27 (13.4)	14 (7.0)	13 (6.5)	6 (3.0)	1 (0.5)
20–29	87	76 (87.4)	11 (12.6)	5 (5.7)	6 (6.9)	5 (5.7)	5 (5.7)
Sex							
M	1,264	1,123 (88.8)	141 (11.2)	72 (5.7)	78 (6.2)	10 (0.8)	5 (0.4)
F	918	762(83.0	156 (17.0)	70 (7.6)	95 (10.3)	5 (0.5)	3 (0.3)
Ethnicity (prioritized)							
Māori	1,189	1,025 (86.2)	164 (13.8)	80 (6.7)	97 (8.2)	8 (0.7)	4 (0.3)
Pacific Islander	795	681 (85.7)	114 (14.3	50 (6.3)	68 (8.6)	6 (0.8)	4 (0.5
European/other	198	179 (90.4)	19 (9.6)	12 6.1)	8 (4.0)	1 (0.5)	0
NZDep06 quintile							
1	68	59 (86.8)	9 (13.2)	5 (7.4)	9 (13.2)	0	0
2	102	88 (86.3)	14 (13.7)	6 (5.9)	5 (4.9)	0	0
3	187	155 (82.9)	32 (17.1)	11 (5.9)	12 (6.4)	2 (1.1)	2 (1.1)
4	353	315 (89.2)	38 (10.8)	19 (5.4)	22 (6.2)	3 (0.8)	1 (0.3)
5	14,60	1,259 (86.2)	201 (13.8)	99 (6.8)	124 (8.5)	10 (0.7)	5 (0.3)
Unknown	12	9 (75.0)	3 (25.0)	2 (16.7)	1 (8.3)	0	0
Carditis							
No	1,050	951 (90.6)	99 (9.4)	59 (5.6)	48 (4.6)	5 (0.5)	1 (0.1)
Yes	1,132	934 (82.5)	198 (17.5)	83 (7.3)	125 (11.0)	10 (0.9)	7 (0.6)

*ARF, acute rheumatic fever; NZDep06 index, 2006 New Zealand Deprivation Index; RHD, rheumatic heart disease.

The overall probability of experiencing disease progression (to hospitalization with recurrent ARF/RHD or to circulatory death) within a theoretical 9,791 days from the initial ARF hospitalization was 24.0%. When progression outcomes were considered individually, the probability of recurrent ARF hospitalization was 23.5%, as was the probability of being hospitalized for RHD. The risk for death was low: 1.0% (Figure 3).

Aim 1B: Risk Factors for Progression from Initial ARF

Risk for disease progression was higher for Māori (OR 1.68, 95% CI 1.10–2.67) and Pacific Islander (OR 2.12, 95% CI 1.37–3.39) patients than for persons of European or other ethnicities. Progression occurred sooner for Māori (HR 1.89, 95% CI 1.24–2.88) and Pacific Islander (HR 2.35, 95% CI 1.54–3.60) patients. Disease progression was twice as likely for patients with carditis (OR 2.00, 95% CI 1.57–2.54) than without carditis, and progression occurred sooner (HR 1.94, 95% CI 1.55–2.43). We noted no significant differences in risk for disease progression by sex, age, or NZDep 06 quintile (Table 2). No factors in Table 2 were found to be significant predictors of recurrent ARF.

Risk for disease progression to RHD hospitalization was higher for Māori (OR 2.09, 95% CI 1.09–4.52) and Pacific Islander (OR 3.64, 95% CI 1.91–7.86) patients than for patients of European or other ethnicities and occurred sooner (HR 2.54, 95% CI 1.27–5.10 for Māori; HR 2.53, 95% CI 1.27–5.05 for Pacific Islanders). Initial ARF patients with carditis were more likely to experience RHD (OR 5.19, 95% CI 3.52–7.89) than those without carditis. Patients with initial ARF whose condition progressed to recurrent ARF were more likely to experience progression to hospitalization for RHD than patients who did not experience recurrent ARF (OR 3.10, 95% CI 2.07-4.55). Small patient numbers meant that no factors predicted circulatory death, with the exception of carditis (OR 6.52, 95% CI 1.16–122.00; Appendix Table 2).

Aim 2: Proportion of Initial RHD Patients with Preceding ARF

A total of 3,836 patients were hospitalized with RHD during 2010–2015; of these, 435 patients with initial RHD met the inclusion criteria (Figure 2, panel B), 102 of whom were also included in the initial ARF dataset for aim 1. Most patients were female (229, 52.6%), Pacific Islander (207, 47.6%), or Māori (176, 40.5%) and were from the most deprived neighborhoods (271 [62.3%] NZDep13 quintile 5). Previous hospitalization for ARF (i.e., ≥180 days before initial RHD hospitalization) was detected for 77 patients (17.8%; Figure 2, panel B). Of the 335 initial RHD patients <30 years of age, 19.4% had been previously hospitalized for ARF.

Of the Māori patients, 21.6% were previously hospitalized for ARF, as were 18.4% of Pacific Islander patients. A significantly lower proportion (1.9%) of patients of European and other ethnicities were previously hospitalized for ARF ($p<2.2 \times 10^{-16}$). A lower proportion of female patients (11.4%) were previously hospitalized for ARF than were male patients (24.8%; $p = 2.565 \times 10^{-6}$). Of the patients from NZDep quintile 5, a total of 19.9% were previously hospitalized for ARF, as were 15.4% of patients from other quintiles ($p = 0.048$; Appendix Table 1). There was no difference in overall time of progression from initial ARF to RHD hospitalization compared with time from initial RHD going back to preceding ARF hospitalization ($p>0.05$; Appendix Figure 1).

Discussion

This study demonstrates concerning ethnic inequities in ARF progression. By the end of the study period, 14% of initial ARF patients (with no concurrent RHD) had experienced progression to recurrent ARF, RHD, or circulatory death. However, ARF progression was approximately twice as likely for Māori and Pacific Islander patients and occurred approximately twice more rapidly. It is concerning that of 435 initial RHD patients <40 years of age, <1 in 5 were hospitalized with preceding ARF, severely limiting opportunities for secondary prevention. Ethnic inequities in ARF progression add to extreme ethnic inequities in the burden of ARF (*27*,*28*). Possible reasons for increased illness among Māori and Pacific Islander patients include the inequitable distribution of the underlying determinants of health, such as access to health services, nutrition, and a healthy home environment (*32*,*33*). Genetic and immunologic factors may also contribute (*33*–*36*). Similar findings have been reported for indigenous patients in Australia (*18*).

That 14% of the initial ARF cohort experienced progression suggests failures in secondary prophylaxis to which Māori and Pacific Islander patients may experience barriers. We support creating a national patient register by drawing on data from regional registers. The goal would be to improve secondary prophylaxis uptake by coordinating treatment for patients who are frequently mobile. There is widespread support for a national register among stakeholders, which could be expanded to monitor patients' RHD status and health outcomes (*5*,*37*). Previous attempts to set up a national register have failed because of privacy concerns. A perceived lack of political will to implement such a register has been noted (*38*,*39*).

Disease progression for New Zealand ARF patients overall seems to be considerably less than that reported for indigenous patients in Australia (*19*). This difference probably reflects multiple factors, including difficulty delivering consistent medical treatment in remote areas and use of echocardiography outreach clinics in Australia (which may detect RHD sooner than when signs/symptoms otherwise come to medical attention) (*15*,*19*,*40*). Our findings may be specific to New Zealand.

Although we did not identify differences in ARF progression by sex, these differences have been reported elsewhere (*19*,*41*). Our finding that 12% of female patients with initial RHD were previously hospitalized with ARF, compared with 25% of male patients, may suggest that clinical manifestations and outcomes for female patients warrant investigation.

More than 80% of young initial RHD patients had not been previously hospitalized for ARF, which indicates that many ARF patients do not come to clinical attention and miss prophylactic treatment. Increasing public and clinician awareness of ARF, echocardiographic screening for high-risk children, and new diagnostic tools may improve case identification (*24*,*42*). If a clear prognostic benefit is demonstrated from echocardiography screening programs, this finding may strongly support the use of targeted screening among high-risk New Zealand children. It is unlikely that RHD detected through echocardiography screening

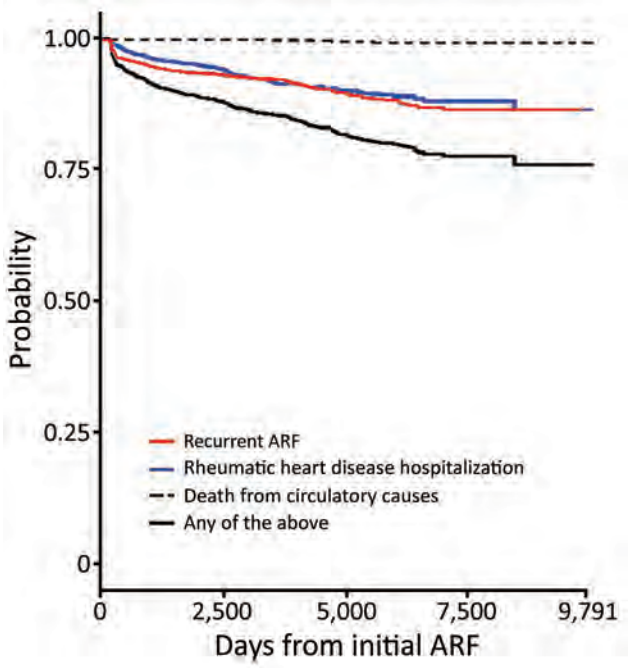

Figure 3. Probability of disease progression to recurrent ARF, hospitalization for rheumatic heart disease, or circulatory death after hospitalization for initial ARF >9,791 days among acute rheumatic fever patients in New Zealand, 1989–2015. ARF, acute rheumatic fever.

Table 2. Factors influencing the likelihood of disease progression to recurrent ARF, hospitalization for RHD, or circulatory death after hospitalization for initial ARF, New Zealand, 1989–2015*

Factor	Patient progression from initial ARF	
	Cox-proportional model, HR (95% CI)	Generalized linear model, OR (95% CI)
Age group, y		
<5	0.59 (0.24–1.4)	1.17 (0.45–3.01)
5–9	0.88 (0.46–1.7)	1.43 (0.75–3.01)
10–14	1.02 (0.54–1.9)	1.54 (0.82–3.23)
15–19	1.02 (0.50–2.1)	1.30 (0.62–2.92)
20–29	Referent	Referent
Sex		
F	1.01 (0.81–1.25)	1.02 (0.80–1.28)
M	Referent	Referent
Ethnicity		
Māori	**1.89 (1.24–2.88)**	**1.68 (1.10–2.67)**
Pacific Islander	**2.35 (1.54–3.60)**	**2.12 (1.37–3.39)**
European/other	Referent	Referent
NZDep06 quintile		
1	Referent	Referent
2	0.56 (0.25–1.23)	0.47 (0.19–1.09)
3	0.88 (0.47–1.66)	0.77 (0.39–1.58)
4	0.70 (0.38–1.27)	0.61 (0.32–1.21)
5	0.88 (0.51–1.50)	0.76 (0.42–1.43)
ARF diagnostic code denoting carditis		
Yes	**1.94 (1.55–2.43)**	**2.00 (1.57–2.54)**
No	Referent	Referent

*Boldface indicates statistical significance. ARF, acute rheumatic fever; HR, hazard ratio; NZDep06 index, 2006 New Zealand Deprivation Index; OR, odds ratio; RHD, rheumatic heart disease.

studies would have affected this analysis because they would receive outpatient assessment (*43*).

The reliance on hospital data is a major limitation of, and justification for, this study. In New Zealand, gaps in data completeness for ARF/RHD are closing; however, the study period is affected (*44*). Some patients may have been inappropriately included or missed from this analysis, or progression outcomes may be misclassified. This study markedly underestimates the proportion of ARF patients whose condition will ultimately progress because of limited follow-up time; furthermore, hospitalization data do not capture outpatients (*2*). Although a prospective study design would enable a more nuanced analysis of ARF progression, severe outcomes may take many years to develop (*16*). Repeat analyses of this study cohort will provide a more complete assessment of progression risk. Migration of RHD patients into New Zealand may account for some occurrences where no preceding ARF hospitalization was identified (*45*). The high (94%) proportion of children <10 years of age with initial RHD and no preceding/concurrent ARF hospitalization may result from miscoding (with ARF incorrectly coded as RHD; Appendix Table 1). Use of the ≥180-day window was supported when examining time intervals to progression (Appendix) and by the small number of studies reporting on ARF progression (*46*,*47*). A quality systematic patient audit would be valuable for assessing the validity of diagnostic coding. It would also be useful to audit a sample of initial RHD patients not previously hospitalized for ARF to see if diagnostic opportunities had been missed.

A key study strength is use of the encrypted NHI to identify persons within and between datasets, which permits inclusion of an entire national cohort. Hospitalization is the standard of care for all patients with suspected initial ARF in New Zealand (*2*). Ambulatory care data and prophylaxis data were not available (*2*). Published data on BPG adherence are inconsistently available. A regional study of 77 ARF patients identified 51% as fully adherent to BPG prophylaxis (*48*). An audit from Auckland (where ≈50% of patients reside) indicated that ≈96% of ARF patients were fully adherent in the 2 largest regions, but adherence fell from 93% in 1998 to 86% in 2000 in the smaller (Waitemata) region (*49*). The extent to which progression rates were affected by ARF patients' adherence to secondary prophylaxis in this analysis is unknown.

In summary, our study better defines ARF disease progression in New Zealand. After their initial ARF hospitalization, 14% of patients were hospitalized with recurrent ARF or RHD or died; that proportion will probably increase over time. Māori and Pacific Islander patients face an increased risk for ARF progression. Four fifths of initial RHD patients had no preceding ARF hospitalization recorded, thus limiting opportunities for prophylaxis. The need to enhance clinical care delivery for underserved groups is strongly indicated.

A national patient register may improve prophylaxis uptake, clinical service coordination, and sector performance monitoring. Further research into echocardiography screening is needed. Our results show a clear need to address the major modifiable determinants of health and equity; ARF and RHD represent indicators of progress that should be closely monitored.

Acknowledgments

We acknowledge Janine Ryland, who was a member of Brooke Marsters' advisory group.

This work was supported by a grant from the New Zealand Lotteries Health Commission, in the form of a PhD scholarship awarded to J.O. and a Health Research Council of New Zealand project grant providing support for M.G.B. and J.B. B.M. was supported by a Pacific Health Research Summer Studentship from the Health Research Council of New Zealand. D.A.W. is supported by a Fellowship from the National Health and Medical Research Council of Australia (GNT 1123854).

About the Author

Dr. Oliver is a postdoctoral research fellow and works as infectious disease researcher at the University of Melbourne and Murdoch Children's Research Institute. Her research focus is streptococcal diseases and Buruli ulcer. This study formed part of her doctoral thesis, which concerns acute rheumatic fever, its risk factors, and determinants.

References

1. Carapetis JR, Steer AC, Mulholland EK, Weber M. The global burden of group A streptococcal diseases. Lancet Infect Dis. 2005;5:685–94. https://doi.org/10.1016/S1473-3099(05)70267-X
2. Heart Foundation of New Zealand. New Zealand guidelines for rheumatic fever: diagnosis, management and secondary prevention of acute rheumatic fever and rheumatic heart disease: 2014 update. Auckland (New Zealand); The Foundation; 2014.
3. Caldas AM, Terreri MTA, Moises VA, Silva CM, Len CA, Carvalho AC, et al. What is the true frequency of carditis in acute rheumatic fever? A prospective clinical and Doppler blind study of 56 children with up to 60 months of follow-up evaluation. Pediatr Cardiol. 2008;29:1048–53. https://doi.org/10.1007/s00246-008-9242-z
4. Porth C. Essentials of pathophysiology: concepts of altered health states. Hagerstown (MD): Lippincott Williams & Wilkins; 2007.
5. Oliver J, Pierse N, Baker MG. Improving rheumatic fever surveillance in New Zealand: results of a surveillance sector review. BMC Public Health. 2014;14:528. https://doi.org/10.1186/1471-2458-14-528
6. Carapetis JR, Currie BJ, Good MF. Towards understanding the pathogenesis of rheumatic fever. Scand J Rheumatol. 1996;25:127–31, discussion 132–3. https://doi.org/10.3109/03009749609080000
7. Gemechu T, Mahmoud H, Parry EH, Phillips DI, Yacoub MH. Community-based prevalence study of rheumatic heart disease in rural Ethiopia. Eur J Prev Cardiol. 2017;24:717–23. https://doi.org/10.1177/2047487316687104
8. Nkomo VT. Epidemiology and prevention of valvular heart diseases and infective endocarditis in Africa. Heart. 2007;93:1510–9. https://doi.org/10.1136/hrt.2007.118810
9. Rizvi SF, Khan MA, Kundi A, Marsh DR, Samad A, Pasha O. Status of rheumatic heart disease in rural Pakistan. Heart. 2004;90:394–9. https://doi.org/10.1136/hrt.2003.025981
10. Zühlke L, Mirabel M, Marijon E. Congenital heart disease and rheumatic heart disease in Africa: recent advances and current priorities. Heart. 2013;99:1554–61. https://doi.org/10.1136/heartjnl-2013-303896
11. Statistics NZ. Pacific Peoples ethnic group [cited 2018 Feb 14]. http://archive.stats.govt.nz/Census/2013-census/profile-and-summary-reports/quickstats-culture-identity/pacific-peoples.aspx
12. Ralph AP, Carapetis JR. Group A streptococcal diseases and their global burden. In: Chhatwal GS, editor. Host-pathogen interactions in streptococcal diseases. Berlin: Springer-Verlag; 2013. p. 1–27.
13. Oliver J, Upton A, Jack SJ, Pierse N, Williamson DA, Baker MG. Distribution of streptococcal pharyngitis and acute rheumatic fever, Auckland, New Zealand, 2010–2016. Emerg Infect Dis. 2020;26:1113–21. https://doi.org/10.3201/eid2606.181462
14. Bennett J, Zhang J, Leung W, Jack S, Oliver J, Webb R, et al. Rising ethnic inequalities in acute rheumatic fever and rheumatic heart disease, New Zealand, 2000–2018. Emerg Infect Dis. 2021;27. https://doi.org/10.3201/eid2701.191791
15. Anderson RD, Pepine CJ. Gender differences in the treatment for acute myocardial infarction: bias or biology? Circulation. 2007;115:823–6. https://doi.org/10.1161/CIRCULATIONAHA.106.685859
16. Milne RJ, Lennon D, Stewart JM, Vander Hoorn S, Scuffham PA. Mortality and hospitalisation costs of rheumatic fever and rheumatic heart disease in New Zealand. J Paediatr Child Health. 2012;48:692–7. https://doi.org/10.1111/j.1440-1754.2012.02446.x
17. North RA, Sadler L, Stewart AW, McCowan LM, Kerr AR, White HD. Long-term survival and valve-related complications in young women with cardiac valve replacements. Circulation. 1999;99:2669–76. https://doi.org/10.1161/01.CIR.99.20.2669
18. He VY, Condon JR, Ralph AP, Zhao Y, Roberts K, de Dassel JL, et al. Long-term outcomes from acute rheumatic fever and rheumatic heart disease: a data-linkage and survival analysis approach. Circulation. 2016;134:222–32. https://doi.org/10.1161/CIRCULATIONAHA.115.020966
19. Lawrence JG, Carapetis JR, Griffiths K, Edwards K, Condon JR. Acute rheumatic fever and rheumatic heart disease: incidence and progression in the Northern Territory of Australia, 1997 to 2010. Circulation. 2013;128:492–501. https://doi.org/10.1161/CIRCULATIONAHA.113.001477
20. Oliver J, Pierse N, Baker MG. Estimating rheumatic fever incidence in New Zealand using multiple data sources. Epidemiol Infect. 2015;143:167–77. https://doi.org/10.1017/S0950268814000296
21. Fitz-Gerald JA, Ongzalima CO, Ng A, Greenland M, Sanfilippo FM, Hung J, et al. A validation study: how predictive is a diagnostic coding algorithm at identifying rheumatic heart disease in Western Australian hospital data? Heart Lung Circ. 2019. https://doi.org/10.1016/j.hlc.2019.08.020

22. Katzenellenbogen JM, Nedkoff L, Cannon J, Kruger D, Pretty F, Carapetis JR, et al. Low positive predictive value of International Classification of Diseases, 10th Revision codes in relation to rheumatic heart disease: a challenge for global surveillance. Intern Med J. 2019;49:400–3. https://doi.org/10.1111/imj.14221
23. Beaton A, Aliku T, Dewyer A, Jacobs M, Jiang J, Longenecker CT, et al. Latent rheumatic heart disease: identifying the children at highest risk of unfavorable outcome. Circulation. 2017;136:2233–44. https://doi.org/10.1161/CIRCULATIONAHA.117.029936
24. Engelman D, Mataika RL, Ah Kee M, Donath S, Parks T, Colquhoun SM, et al. Clinical outcomes for young people with screening-detected and clinically-diagnosed rheumatic heart disease in Fiji. Int J Cardiol. 2017;240:422–7. https://doi.org/10.1016/j.ijcard.2017.04.004
25. Ministry of Health. National minimum dataset (hospital events) [cited 2012 Sep 13]. http://www.health.govt.nz/nz-health-statistics/national-collections-and-surveys/collections/national-minimum-dataset-hospital-events
26. New Zealand Ministry of Health. Mortality Collection data dictionary [cited 2019 Mar 20]. https://www.health.govt.nz/system/files/documents/publications/mortality_data_dictionary_v1.6_final.pdf
27. Milne RJ, Lennon DR, Stewart JM, Vander Hoorn S, Scuffham PA. Incidence of acute rheumatic fever in New Zealand children and youth. J Paediatr Child Health. 2012;48:685–91. https://doi.org/10.1111/j.1440-1754.2012.02447.x
28. Jaine R, Baker M, Venugopal K. Epidemiology of acute rheumatic fever in New Zealand 1996-2005. J Paediatr Child Health. 2008;44:564–71. https://doi.org/10.1111/j.1440-1754.2008.01384.x
29. R Core Team. R: a language and environment for statistical computing. Vienna (Austria): R Foundation for Statistical Computing; 2014.
30. Ministry of Health. Ethnicity data protocols for the health and disability sector. Wellington (New Zealand); The Ministry; 2004.
31. Salmond CE, Crampton P. Development of New Zealand's deprivation index (NZDep) and its uptake as a national policy tool. Can J Public Health. 2012;103(Suppl 2):S7–11.
32. Hobbs M, Tomintz M, McCarthy J, Marek L, Vannier C, Campbell M, et al. Obesity risk in women of childbearing age in New Zealand: a nationally representative cross-sectional study. Int J Public Health. 2019;64:625–35. https://doi.org/10.1007/s00038-019-01239-8
33. Baker MG, Gurney J, Oliver J, Moreland NJ, Williamson DA, Pierse N, et al. Risk factors for acute rheumatic fever: literature review and protocol for a case-control study in New Zealand. Int J Environ Res Public Health. 2019;16:E4515. https://doi.org/10.3390/ijerph16224515
34. Hill S, Sarfati D, Robson B, Blakely T. Indigenous inequalities in cancer: what role for health care? ANZ J Surg. 2013;83:36–41. https://doi.org/10.1111/ans.12041
35. Cheng TO. How much of the recent decline in rheumatic heart disease in China can be explained by changes in cardiovascular risk factors? Int J Cardiol. 2009;132:300–2. https://doi.org/10.1016/j.ijcard.2008.06.087
36. Goodman A, Kajantie E, Osmond C, Eriksson J, Koupil I, Thornburg K, et al. The relationship between umbilical cord length and chronic rheumatic heart disease: a prospective cohort study. Eur J Prev Cardiol. 2015;22:1154–60. https://doi.org/10.1177/2047487314544082
37. Anderson A, Peat B, Ryland J, Ofanoa M, Burgess H, Malungahu G, et al. Mismatches between health service delivery and community expectations in the provision of secondary prophylaxis for rheumatic fever in New Zealand. Aust N Z J Public Health. 2019;43:294–9. https://doi.org/10.1111/1753-6405.12890
38. Thornley C, McNicholas A, Baker M, Lennon D. Rheumatic fever registers in New Zealand. New Zealand Public Health Report. 2001;8:41–4.
39. Oliver J, Pierse N, Baker MG. Improving rheumatic fever surveillance in New Zealand: results of a surveillance sector review. BMC Public Health. 2014;14:528. https://doi.org/10.1186/1471-2458-14-528
40. McDonald M, Towers RJ, Andrews RM, Carapetis JR, Currie BJ. Epidemiology of *Streptococcus dysgalactiae* subsp. *equisimilis* in tropical communities, Northern Australia. Emerg Infect Dis. 2007;13:1694–700. https://doi.org/10.3201/eid1311.061258
41. Ministry of Health. Cardiovascular disease (50+ years) [cited 2017 Nov 3]. http://www.health.govt.nz/nz-health-statistics/health-statistics-and-data-sets/Māori-health-data-and-stats/tatau-kura-tangata-health-older-Māori-chart-book/nga-mana-hauora-tutohu-health-status-indicators-50-years/cardiovascular-disease-50-years
42. Gauld R, Horsburgh S. Does a host country capture knowledge of migrant doctors and how might it? A study of UK doctors in New Zealand. Int J Public Health. 2016;61:1–8. https://doi.org/10.1007/s00038-015-0770-z
43. Webb RH, Wilson NJ, Lennon DR, Wilson EM, Nicholson RW, Gentles TL, et al. Optimising echocardiographic screening for rheumatic heart disease in New Zealand: not all valve disease is rheumatic. Cardiol Young. 2011;21:436–43. https://doi.org/10.1017/S1047951111000266
44. Oliver J, Pierse N, Williamson DA, Baker MG. Estimating the likely true changes in rheumatic fever incidence using two data sources. Epidemiol Infect. 2018;146:265–75. https://doi.org/10.1017/S0950268817002734
45. Darlington-Pollock F, Shackleton N, Norman P, Lee AC, Exeter D. Differences in the risk of cardiovascular disease for movers and stayers in New Zealand: a survival analysis. Int J Public Health. 2018;63:173–9. https://doi.org/10.1007/s00038-017-1011-4
46. Voss LM, Wilson NJ, Neutze JM, Whitlock RM, Ameratunga RV, Cairns LM, et al. Intravenous immunoglobulin in acute rheumatic fever: a randomized controlled trial. Circulation. 2001;103:401–6. https://doi.org/10.1161/01.CIR.103.3.401
47. Group CRFS. The treatment of acute rheumatic fever in children. A cooperative clinical trial of ACTH, cortisone and aspirin. Circulation. 1955;11:343–77. https://doi.org/10.1161/01.CIR.11.3.343
48. Oetzel JG, Lao C, Morley M, Penman K, Child M, Scott N, et al. Efficacy of an incentive intervention on secondary prophylaxis for young people with rheumatic fever: a multiple baseline study. BMC Public Health. 2019;19:385. https://doi.org/10.1186/s12889-019-6695-3
49. Grayson S, Horsburgh M, Lennon D. An Auckland regional audit of the nurse-led rheumatic fever secondary prophylaxis programme. N Z Med J. 2006;119:U2255.

Address for correspondence: Jane Oliver, University of Melbourne, 792 Elizabeth St, Melbourne, VIC 3000, Australia; email: jane.oliver@mcri.edu.au

Plasmodium falciparum kelch 13 Mutations, 9 Countries in Africa, 2014–2018

Sarah E. Schmedes,[1] Dhruviben Patel,[1] Simran Dhal, Julia Kelley, Samaly S. Svigel, Pedro Rafael Dimbu, Adicatou-Laï Adeothy, Gauthier Mesia Kahunu, Papy Mandoko Nkoli, Abdoul Habib Beavogui, Simon Kariuki, Don P. Mathanga, Ousmane Koita, Deus Ishengoma, Ally Mohamad, Moonga Hawela, Leah F. Moriarty, Aaron M. Samuels, Julie Gutman, Mateusz M. Plucinski, Venkatachalam Udhayakumar, Zhiyong Zhou, Naomi W. Lucchi, Meera Venkatesan, Eric S. Halsey, Eldin Talundzic

The spread of drug resistance to antimalarial treatments poses a serious public health risk globally. To combat this risk, molecular surveillance of drug resistance is imperative. We report the prevalence of mutations in the *Plasmodium falciparum kelch 13* propeller domain associated with partial artemisinin resistance, which we determined by using Sanger sequencing samples from patients enrolled in therapeutic efficacy studies from 9 sub-Saharan countries during 2014–2018. Of the 2,865 samples successfully sequenced before treatment (day of enrollment) and on the day of treatment failure, 29 (1.0%) samples contained 11 unique nonsynonymous mutations and 83 (2.9%) samples contained 27 unique synonymous mutations. Two samples from Kenya contained the S522C mutation, which has been associated with delayed parasite clearance; however, no samples contained validated or candidate artemisinin-resistance mutations.

Malaria remains a serious global health concern, causing ≈405,000 deaths annually, mainly in young children in Africa (*1*). Although substantial progress has been made over the past decade to reduce the global burden of malaria, several factors threaten these gains, including the emergence and spread of antimalarial drug resistance (*1*). Artemisinin-based combination therapies (ACTs) are the first-line treatment for uncomplicated malaria caused by *Plasmodium falciparum* parasites, as recommended by the World Health Organization (WHO) (*2*). Unfortunately, resistance to ACTs (i.e., delayed parasite clearance and clinical treatment failures) has emerged in the Greater Mekong Subregion of Southeast Asia, posing a considerable risk to malaria control in the region (*3*). Even though clinical resistance to ACTs has not been reported in Africa (*1*), the threat of its emergence remains.

Author affiliations: Association of Public Health Laboratories, Silver Spring, Maryland, USA (S.E. Schmedes); Centers for Disease Control and Prevention, Atlanta, Georgia, USA (S.E. Schmedes, D. Patel, S.S. Svigel, A.M. Samuels, J. Gutman, M.M. Plucinski, V. Udhayakumar, Z. Zhou, N.W. Lucchi, E. Talundzic); Williams Consulting LLC, Baltimore, Maryland, USA (D. Patel); The Wallace H. Coulter Department of Biomedical Engineering, Georgia Institute of Technology, Atlanta (S. Dahl); CDC Foundation, Atlanta (J. Kelley); National Malaria Control Program, Ministry of Health, Luanda, Angola (P.R. Dimbu); National Malaria Control Program, Ministry of Health, Porto-Novo, Benin (A.-L. Adeothy); University of Kinshasa, Kinshasa, Democratic Republic of the Congo (G.M. Kahunu); National Institute of Biomedical Research, Kinshasa (P.M. Nkoli); Maferinyah Rural Health Research Center, Mafèrinyah, Guinea (A.H. Beavogui); Kenya Medical Research Institute, Centre for Global Health Research, Kisumu, Kenya (S. Kariuki); University of Malawi College of Medicine, Blantyre, Malawi (D.P. Mathanga); University of Sciences, Techniques, and Technologies of Bamako, Bamako, Mali (O. Koita); Harvard T.H. Chan School of Public Health, Boston, Massachusetts, USA (D. Ishengoma); National Institute for Medical Research, Tanga Research Centre, Dar es Salaam, Tanzania (D. Ishengoma, A. Mohamad); Monash University Faculty of Pharmaceutical Sciences, Melbourne, Australia (D. Ishengoma); National Malaria Elimination Centre, Lusaka, Zambia (M. Hawela); US President's Malaria Initiative, Centers for Disease Control and Prevention, Atlanta (L.F. Moriarty, M.M. Plucinski E.S. Halsey,); US President's Malaria Initiative, US Agency for International Development, Washington, DC, USA (M. Venkatesan)

DOI: https://doi.org/10.3201/eid2707.203230

[1]These authors contributed equally to this article.

As part of antimalarial therapeutic efficacy activities, WHO recommends molecular surveillance of the *P. falciparum kelch 13* gene (*Pfk13*) (with focus on the propeller domain region), a molecular marker associated with delayed clearance of parasitemia after therapy with artemisinin monotherapy or an ACT (*3*–*7*). Because specific single-nucleotide polymorphisms (SNPs) within the propeller domain region of *Pfk13* continue to be discovered, WHO continues to update a list of these SNPs on the basis of association with delayed parasite clearance and reduced in vitro drug susceptibility (Table 1). Nine SNPs are currently considered validated by WHO to have delayed parasite clearance and in vitro data demonstrating partial resistance to artemisinin (*3*). WHO categorized 11 SNPs as candidate mutations, correlated with delayed parasite clearance but not validated with in vitro data (*3*). An additional 11 SNPs are listed by WHO as associated with delayed parasite clearance but without statistical significance because of limited data (*3*).

WHO recommends that malaria-endemic countries perform therapeutic efficacy studies (TESs) every 2 years to evaluate antimalarial treatments currently used in a particular region (*8*). Surveillance for molecular markers associated with antimalarial resistance is a recommended part of a TES to detect the presence of mutations associated with resistance (*8*). As part of the US President's Malaria Initiative, the Centers for Disease Control and Prevention (CDC) and the US Agency for International Development provide support to countries in Africa to perform TESs, including molecular characterization of antimalarial-resistance markers, through the PMI-supported Antimalarial Resistance Monitoring in Africa (PARMA) network (*9*). Established in 2015, this endeavor involves laboratory trainees in Africa who bring TES samples from their home country to the CDC (Atlanta, Georgia, USA) to receive advanced laboratory training and perform molecular testing for antimalarial-resistance mutations (*9*). In this article, we report *Pfk13* mutation data generated from samples analyzed and collected from TESs conducted in 9 countries in Africa during 2014–2018.

Methods

Samples, Ethics Statement, and TES Protocols

Before initiation, all work described in this article was approved by the respective institutional ethics review committee in each country and the Office of the Associate Director of Science of CDC's Center for Global Health and assigned the following tracking numbers: 2014–233a and 2014–233b (Angola), 2017–141 (Benin), 2018–035 (DRC), 2016–046 (Guinea), 6696.0 (Kenya), 6029.0 (Malawi), 2016–012a (Mali), 2015–073a (Tanzania), and 2016–200 (Zambia). Dried blood spots were collected from TESs conducted in 9 countries in Africa (Angola, Benin, the Democratic Republic of the Congo [DRC], Guinea, Kenya, Malawi, Mali, Tanzania, and Zambia; Table 2) during 2014–2018. The samples included those obtained pretreatment (at day of enrollment) and at day of treatment failure. Day of treatment failure samples came from patients experiencing a recrudescence or new infection during the follow-up period of (usually ending at 28 or 42 days) after administration of an ACT. TES and antimalarial molecular marker results for some of the data analyzed have been previously published for Angola (*10*–*12*), Kenya (*13*), and Tanzania (*14*). Results might differ slightly from previously published works because those works might not have reported results from all samples, might not have reported mutations in mixed infections, or might not have reported synonymous mutation results. Our study was a reanalysis of all available sequences using the same sequence data analysis quality filters, cut-offs, and quality scores for all countries.

Sequencing of *Pfk13* Propeller Domain Region

We extracted DNA from dried blood spots using the QIAamp Blood DNA Kit (QIAGEN, https://www.qiagen.com) according to the manufacturer's instructions. We amplified the propeller domain region from codon positions 389–649 by PCR and Sanger sequenced according to methods previously described (*15*).

Table 1. Mutations in the *Pfk13* gene and WHO classification related to *Plasmodium falciparum* artemisinin resistance*

Validated *Pfk13* mutations	Candidate *Pfk13* mutations	Non–statistically significant associated *Pfk13* mutations
F446I	P441L	D452E
N458Y	G449A	C469Y
M476I	C469F	K479I
Y493H	A481V	R515K
R539T	P527H	S522C
I543T	N537I	N537D
P553L	G538V	R575K
R561H	V568G	M579I
C580Y	P574L, F673I, A675V	D584V, P667T, H719N

*Adapted from an August 2018 WHO status report on artemisinin resistance and artemisinin-based combination therapy efficacy (*3*). *Pfk13*, *P. falciparum kelch 13*; WHO, World Health Organization.

Table 2. Summary of antimalarial therapeutic efficacy studies, 9 countries in Africa, 2002–2007*

Country	Sites	Treatments studied	Age of patients enrolled	Year	Total no. samples			ACTs introduced
					D0 + DF	D0	DF	
Angola	Benguela, Zaire, Lunda Sul	AL, ASAQ, DP	6 mo–12 y	2015	379	379	0	2005
				2017	76	38	38	2005
Benin	Klouanmey, Djougou	AL	6–59 mo	2017	194	175	19	2004
DRC	Kabondo, Kapolowe, Rutshuru, Mikalayi, Kimpese	AL, ASAQ, DP	6–59 mo	2017–2018	633	317	316	2006
Guinea	Maferinyah, Labè	AL	6–59 mo	2016	432	409	23	2004–2005
Kenya	Siaya County	AL, DP	6–59 mo	2016–2017	417	325	92	2006
Malawi	Machinga, Nkhotakota, Karonga	AL, ASAQ	6–59 mo	2014	27	8	19	2007
Mali	Dioro, Sèlinguè	AL, ASAQ	2–59 mo	2015–2016	410	320	90	2006
Tanzania	Kibaha, Ujiji, Mkuzi, Mlimba	AL	6 mo–10 y	2016	417	345	72	2006
Zambia	Gwembe, Katete, Mansa	AL, DP	>6 mo	2016	263	263	0	2002
Total					3,248	2,579	669	

*ACTs, artemisinin-based combination therapies; AL, artemether/lumefantrine; ASAQ, artesunate/amodiaquine; D0, day of enrollment (pretreatment); DF, day of failure; DP, dihydroartemisinin/piperaquine; DRC; Democratic Republic of the Congo.

Data Analysis

We analyzed sequence data by using Geneious Prime (Biomatters, https://www.geneious.com). We trimmed and quality filtered forward and reverse sequence reads for each sample (error probability limit 0.05, maximum low-quality bases 30) from the 3′ and 5′ ends to remove low-quality bases. We aligned trimmed sequences to the *Pfk13* National Center for Biotechnology Information gene reference no. PF3D7_1343700 (https://www.ncbi.nlm.nih.gov/gene/814205) and assessed for SNPs. We only considered SNPs if they had a Phred quality score of ≥30 and were present in both forward and reverse strands. Mixed infections were detected by using the heterozygous caller plug-in tool in Geneious with a threshold of ≥30%. A second analyst confirmed all SNP and heterozygous calls by manual technical review. We submitted all *Pfk13* sequences with SNPs reported in this study to GenBank (accession nos. MN072940–3042). We used R software version 4.0.1 (R Foundation for Statistical Computing, https://www.r-project.org) to generate a map showing the distribution of mutations in the 9 countries (Figure).

Results

We attempted *Pfk13* sequencing on 3,248 samples (2,579 pretreatment and 669 day of failure samples) from the 9 countries (Table 2); 2,865 were successfully sequenced (Table 3). Of those, 2,753 samples were wild-type. A total of 11 unique nonsynonymous mutations and 27 unique synonymous mutations were detected in 2,865 successfully sequenced pretreatment and day of failure samples from Angola, Benin, DRC, Guinea, Kenya, Malawi, Mali, Tanzania, and Zambia collected during 2014–2018 (Figure, Table 4; Appendix 1, https://wwwnc.cdc.gov/EID/article/27/7/20-3230-App1.pdf).

Of the 2,303 sequenced pretreatment samples, 2,213 were wild-type and 90 (3.9%) contained mutations (Table 3). Of the 90 pretreatment samples with mutations, 10 unique nonsynonymous mutations were present in 25 samples from 8 of the 9 countries assessed (Table 4) and 25 unique synonymous mutations were present in 65 samples from 8 of the 9 countries assessed (Appendix 1 Table 1). Two samples from Kenya contained the S522C mutation, reported by WHO as a less-frequent mutation associated with delayed parasite clearance but without statistical significance because of limited data (*3*). Both of these patients cleared their initial infection. A578S, the most commonly found mutation in Africa (not associated with resistance) (*3*), was the most common nonsynonymous mutation we identified. The mutation was found in 14 pretreatment isolates: 4 in Angola, 1 in DRC, 1 in Mali, 6 in Kenya, 1 in Tanzania, and 1 in Zambia (Table 4). No mutations were identified in the samples from Malawi. Eight of the 10 unique nonsynonymous mutations in the pretreatment samples have been reported previously in other countries, whereas 2 mutations, P419S (Guinea) and Q613R (Angola), were newly identified in our study. No WHO-validated or candidate *Pfk13* mutations were identified.

Of the 669 day of failure samples, 562 were successfully sequenced; 107 (16.0%) samples failed to amplify, produced poor-quality sequences, or both (Table 3). A total of 540 samples were wild-type. Two nonsynonymous mutations were found in 4 day of failure samples (Table 4) and 10 synonymous mutations (Appendix 1 Table 2) were identified in 18 day of failure samples from 4 countries. Of the nonsynonymous mutations in day of failure samples, 2 samples from Kenya and 1 sample from DRC contained the A578S mutation, and 1 sample from DRC contained the S477Y mutation (Table 4). We compiled the complete results of the

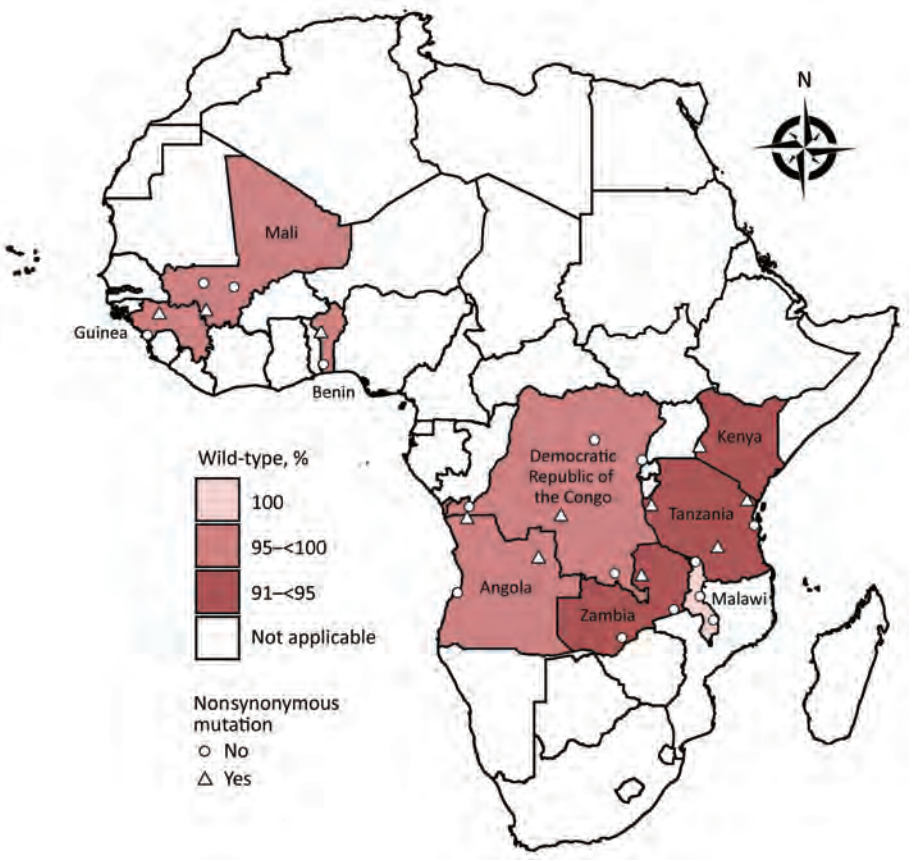

Figure. Prevalence of *Plasmodium falciparum kelch 13* mutations in pretreatment therapeutic efficacy study samples, 9 countries in Africa, 2014–2018. A total of 11 unique nonsynonymous and 27 unique synonymous mutations were detected in 2,865 successfully sequenced pretreatment and day of failure samples from Angola, Benin, Democratic Republic of the Congo, Guinea, Kenya, Malawi, Mali, Tanzania, and Zambia collected during 2014–2018. A total of 2,753 samples were wild-type. Data from Angola includes results from 2 therapeutic efficacy studies.

sequence data reanalysis (Appendix 2, https://wwwnc.cdc.gov/EID/article/27/7/20-3230-App2.xlsx).

Discussion

This work provides an update on *Pfk13* genetic markers in 9 countries in Africa with endemic malaria. Although clinical resistance to ACTs has yet to be confirmed in Africa (*1*), the early detection of *Pfk13* mutations through surveillance allows for swift action before resistance spreads widely. To date, all WHO-validated SNPs detected in Africa have been the result of independent emergence as opposed to spreading through imported cases from Southeast Asia (*21*). More than 200 *Pfk13* mutations have been identified in global samples (*3*,*18*,*21*), and ≥74 *Pfk13* nonsynonymous mutations have been reported in Africa (*22*,*23*). In this study, we report the presence of S522C in Kenya, a less frequent mutation that has been previously reported to be associated with delayed parasite clearance but lacking

Table 3. Summary of *Pfk13* gene mutations detected in *Plasmodium falciparum* pretreatment and DF samples, 9 countries in Africa, 2014–2018*

	No. samples pretreatment (DF)					
Country (year)	Total with sequencing attempted	Poor quality or no amplification	Successfully sequenced	Wild-type samples pretreatment	Other nonsynonymous mutations	Synonymous mutations
Angola (2015)	379 (0)	77 (0)	302 (0)	291 (0)	5 (0)	6 (0)
Angola (2017)	38 (38)	0 (2)	38 (36)	37 (36)	1 (0)	0 (0)
Benin (2017)	175 (19)	20 (1)	155 (18)	151 (18)	1 (0)	3 (0)
DRC (2017–2018)	317 (316)	13 (34)	304 (282)	295 (269)	1 (2)	8 (11)
Guinea (2016)	409 (23)	20 (1)	389 (22)	380 (22)	1 (0)	8 (0)
Kenya (2016–2017)	325 (92)	7 (4)	318 (88)	302 (85)	8 (2)	8 (1)
Malawi (2014)	8 (19)	1 (5)	7 (14)	7 (14)	0 (0)	0 (0)
Mali (2015–2016)	320 (90)	68 (48)	252 (42)	244 (39)	1 (0)	7 (3)
Tanzania (2016)	345 (72)	20 (12)	325 (60)	306 (57)	6 (0)	13 (3)
Zambia (2016)	263 (0)	50 (0)	213 (0)	200 (0)	1 (0)	12 (0)
Total	2,579 (669)	276 (107)	2,303 (562)	2,213 (540)	25 (4)	65 (18)

*DF, day of failure; DRC, Democratic Republic of the Congo; *Pfk13*, *Plasmodium falciparum kelch 13*.

Table 4. Summary of *Pfk13* nonsynonymous mutations detected in *Plasmodium falciparum* pretreatment and DF samples, 9 countries in Africa, 2014–2018*

Mutation	Country	Codon change	No. samples pretreatment (DF)	Country or region where previously reported (reference)
I416V	Tanzania	ATA → GTA	1 (0)	Tanzania (*14*)
P419S	Guinea	CCA → TCA	1 (0)	NA
E433D	Tanzania	GAA → GAC	1 (0)	Tanzania (*14*)
R471S	Tanzania	CGT → AGT	1 (0)	Tanzania (*14*)
S477Y	DRC	TCT → TAT	0 (1)	Grande Comore Island (*16*)
A504V	Angola (2017)	GCT → GTT	1 (0)	Gabon (*17*)
S522C	Kenya	AGT → TGT	2 (0)	Africa (*18*)
A569G	Benin	GCA → GGA	1 (0)	Gambia (*19*) and Niger (*20*)
A578S	Angola (2015)	GCT → TCT	4 (0)	Africa (*19*)
A578S	DRC	GCT → TCT	1 (1)	Africa (*19*)
A578S	Mali	GCT → TCT	1 (0)	Africa (*19*)
A578S	Kenya	GCT → TCT	6 (2)	Africa (*19*)
A578S	Tanzania	GCT → TCT	1 (0)	Africa (*19*)
A578S	Zambia	GCT → TCT	1 (0)	Africa (*19*)
Q613R	Angola (2015)	CAA → CGA	1 (0)	NA
Q613E	Tanzania	CAA → GAA	2 (0)	Tanzania (*14*)
Total			25 (4)	

*DF, day of failure; DRC, Democratic Republic of the Congo; NA, not available; *Pfk13*, *Plasmodium falciparum kelch 13*.

sufficient evidence to be considered a WHO-validated or candidate mutation (*3*).

As more molecular surveillance data are collected, previous results should be reinterpreted to determine the presence of WHO-reportable mutations because the importance of these mutations in drug resistance might change based on new data (*3*,*24*). Although we report only 1 mutation identified by WHO to possibly play a role in resistance, other detected mutations, such as the other nonsynonymous mutations with unknown resistance status reported in this study, might be deemed important in the future as more data are collected and validated. In 2017, WHO categorized only 5 mutations as validated (N458Y, Y493H, R539T, I543T, and 580Y) (*24*), but in 2018 the validated list was updated to include an additional 4 mutations, including F446I, P553L, and R561H (formerly candidate markers) and M476I (formerly reported as a less frequent variant associated with in vivo or in vitro test results) (*3*). In addition, the Worldwide Antimalarial Resistance Network tracks *Pfk13* mutations worldwide and strives to detect new associations of mutations with delayed parasite clearance, which might inform WHO classifications (*18*).

We report the presence of 11 unique nonsynonymous mutations in Angola, Benin, Guinea, DRC, Kenya, Mali, Tanzania, and Zambia; all were previously reported in the literature (Table 4) except P419S and Q613R. The most common nonsynonymous mutation observed in our study was A578S, a nonsynonymous mutation frequently described in Africa (*3*) and, to a lesser extent, Asia (e.g., Thailand [*19*] and Bangladesh [*25*]). WHO has reported that A578S is not associated with partial artemisinin resistance (*3*). Most mutations detected were synonymous mutations consistent with previous reports (*21*). Because synonymous mutations do not result in an amino acid change, they are not associated with resistance. Parasites from Africa have been shown to have a higher prevalence of synonymous mutations, which is not surprising given that *P. falciparum* originated in Africa and continues to have a high level of transmission in this region (*19*).

The results described in this article represent the collaborative output of the PARMA network, which originated in 2015 with the objectives of assisting countries in Africa in testing malaria samples from TESs for genetic markers associated with antimalarial resistance and supporting training and capacity building of collaborators in Africa (*9*). In 8 of the 9 countries included in this report (all but Angola), the *Pfk13* results were generated during a 6–8-week visit to CDC by trainees from a laboratory in the country where the TES was performed. Results were subsequently shared by the trainee's laboratory with their national malaria control program and other local stakeholders to make decisions related to antimalarial use. Although the *Pfk13* results we have described would not be cause for alarm or policy change, recent findings in Rwanda suggests a substantial presence of the *Pfk13* R561H mutation (*26*) that has evolved locally, highlighting the importance of molecular surveillance for early detection of emerging patterns of resistance. In this context, PARMA training visits generate a vast amount of data from TES samples, ranging from efficacy results to prevalence of other molecular markers (e.g., *P. falciparum* multidrug-resistant protein 1 and *P. falciparum* chloroquine-resistance transporter) to the

presence of *P. falciparum* histidine-rich protein 2 and 3 deletions (which might affect rapid diagnostic test performance). Generating phenotypic (i.e., efficacy) and genotypic data on the same sample provides an opportunity to identify novel mutations associated with resistance and enables detection of known mutations in samples with well-characterized efficacy outcomes. Because the PARMA network encourages standardization of laboratory methods and data reporting, such explorations might detect trends over time in a single country or produce insightful observations by using data from multiple countries. With the increased use of next-generation sequencing, the PARMA network has embarked on applying these principles of data generation, capacity building, networking, and standardization to this emerging technology (*27*). The ultimate goal of laboratories in Africa independently analyzing their own malaria samples.

This work was made possible with funding provided by the US President's Malaria Initiative (PMI) through PARMA. We also acknowledge partial support from the Advanced Molecular Detection Initiative at the CDC and partial support by the Bioinformatics Fellowship Program administered by the Association of Public Health Laboratories and funded by CDC. S.E.S. was supported by the Bioinformatics Fellowship Program. J.K. was supported in part by the CDC Foundation. D.P. was employed by Williams Consulting LLC, which provided support in the form of salary for D.P. D.S.I. was partly supported by the Developing Excellence in Leadership and Genetics Training for Malaria Elimination (DELGEME) in Sub-Saharan Africa program through the Developing Excellence in Leadership, Training and Science Africa Initiative (DELGEME grant no. 107740/Z/15/Z). The Developing Excellence in Leadership, Training and Science Africa Initiative is an independent funding scheme of the African Academy of Sciences' Alliance for Accelerating Excellence in Science in Africa and is supported by the New Partnership for Africa's Development Planning and Coordinating Agency with funding from the Wellcome Trust (DELGEME grant no. 107740/Z/15/Z) and government of the United Kingdom. The funders had no role in study design, data collection and analysis, decision to publish, or preparation of the manuscript.

About the Author

Dr. Schmedes is lead bioinformatician at the Florida Department of Health; her primary interests include developing and implementing bioinformatics methods for studying bacterial and viral pathogens of public health significance in the state of Florida. Dr. Talundzic is an informatics health scientist in the Center for Global Health at CDC; his primary interests include developing and implementing next generation sequencing and bioinformatics methods for studying *Plasmodium* parasites.

References

1. World Health Organization. World malaria report 2019 [cited 2020 May 15]. https://www.who.int/publications/i/item/9789241565721
2. World Health Organization. Guidelines for the treatment of malaria. 3rd edition. 2015 [cited 2020 May 15]. https://apps.who.int/iris/handle/10665/162441
3. World Health Organization. Artemisinin resistance and artemisinin-based combination therapy efficacy: status report. 2018 [cited 2020 May 15]. https://apps.who.int/iris/handle/10665/274362
4. Cheeseman IH, Miller BA, Nair S, Nkhoma S, Tan A, Tan JC, et al. A major genome region underlying artemisinin resistance in malaria. Science. 2012;336:79–82. https://doi.org/10.1126/science.1215966
5. Takala-Harrison S, Clark TG, Jacob CG, Cummings MP, Miotto O, Dondorp AM, et al. Genetic loci associated with delayed clearance of *Plasmodium falciparum* following artemisinin treatment in Southeast Asia. Proc Natl Acad Sci U S A. 2013;110:240–5. https://doi.org/10.1073/pnas.1211205110
6. Ariey F, Witkowski B, Amaratunga C, Beghain J, Langlois A-C, Khim N, et al. A molecular marker of artemisinin-resistant *Plasmodium falciparum* malaria. Nature. 2014;505:50–5. https://doi.org/10.1038/nature12876
7. Ashley EA, Dhorda M, Fairhurst RM, Amaratunga C, Lim P, Suon S, et al.; Tracking Resistance to Artemisinin Collaboration (TRAC). Spread of artemisinin resistance in *Plasmodium falciparum* malaria. N Engl J Med. 2014;371:411–23. https://doi.org/10.1056/NEJMoa1314981
8. World Health Organization. Methods for surveillance of antimalarial drug efficacy. 2009 [cited 2020 May 15]. https://www.who.int/malaria/publications/atoz/9789241597531/en
9. Halsey ES, Venkatesan M, Plucinski MM, Talundzic E, Lucchi NW, Zhou Z, et al. Capacity development through the US President's Malaria Initiative–Supported Antimalarial Resistance Monitoring in Africa Network. Emerg Infect Dis. 2017;23:S53–S56. https://doi.org/10.3201/eid2313.170366
10. Plucinski MM, Dimbu PR, Macaia AP, Ferreira CM, Samutondo C, Quivinja J, et al. Efficacy of artemether-lumefantrine, artesunate-amodiaquine, and dihydroartemisinin-piperaquine for treatment of uncomplicated *Plasmodium falciparum* malaria in Angola, 2015. Malar J. 2017;16:62. https://doi.org/10.1186/s12936-017-1712-4
11. Ljolje D, Dimbu PR, Kelley J, Goldman I, Nace D, Macaia A, et al. Prevalence of molecular markers of artemisinin and lumefantrine resistance among patients with uncomplicated *Plasmodium falciparum* malaria in three provinces in Angola, 2015. Malar J. 2018;17:84. https://doi.org/10.1186/s12936-018-2233-5
12. Davlantes E, Dimbu PR, Ferreira CM, Florinda Joao M, Pode D, Félix J, et al. Efficacy and safety of artemether-lumefantrine, artesunate-amodiaquine, and dihydroartemisinin-piperaquine for the treatment of uncomplicated *Plasmodium falciparum* malaria in three provinces in Angola, 2017. Malar J. 2018;17:144. https://doi.org/10.1186/s12936-018-2290-9

13. Chebore W, Zhou Z, Westercamp N, Otieno K, Shi YP, Sergent SB, et al. Assessment of molecular markers of anti-malarial drug resistance among children participating in a therapeutic efficacy study in western Kenya. Malar J. 2020;19:291. https://doi.org/10.1186/s12936-020-03358-7
14. Ishengoma DS, Mandara CI, Francis F, Talundzic E, Lucchi NW, Ngasala B, et al. Efficacy and safety of artemether-lumefantrine for the treatment of uncomplicated malaria and prevalence of Pfk13 and Pfmdr1 polymorphisms after a decade of using artemisinin-based combination therapy in mainland Tanzania. Malar J. 2019;18:88. https://doi.org/10.1186/s12936-019-2730-1
15. Talundzic E, Chenet SM, Goldman IF, Patel DS, Nelson JA, Plucinski MM, et al. Genetic analysis and species specific amplification of the artemisinin resistance-associated kelch propeller domain in *P. falciparum* and *P. vivax*. PLoS One. 2015;10:e0136099.
16. Huang B, Deng C, Yang T, Xue L, Wang Q, Huang S, et al. Polymorphisms of the artemisinin resistant marker (K13) in *Plasmodium falciparum* parasite populations of Grande Comore Island 10 years after artemisinin combination therapy. Parasit Vectors. 2015;8:634. https://doi.org/10.1186/s13071-015-1253-z
17. Voumbo-Matoumona DF, Kouna LC, Madamet M, Maghendji-Nzondo S, Pradines B, Lekana-Douki JB. Prevalence of *Plasmodium falciparum* antimalarial drug resistance genes in southeastern Gabon from 2011 to 2014. Infect Drug Resist. 2018;11:1329–38. https://doi.org/10.2147/IDR.S160164
18. WWARN K13 Genotype-Phenotype Study Group. Association of mutations in the *Plasmodium falciparum* Kelch13 gene (Pf3D7_1343700) with parasite clearance rates after artemisinin-based treatments—a WWARN individual patient data meta-analysis. BMC Med. 2019;17:1. https://doi.org/10.1186/s12916-018-1207-3
19. Ménard D, Khim N, Beghain J, Adegnika AA, Shafiul-Alam M, Amodu O, et al.; KARMA Consortium. A worldwide map of *Plasmodium falciparum* K13-propeller polymorphisms. N Engl J Med. 2016;374:2453–64. https://doi.org/10.1056/NEJMoa1513137
20. Laminou I, Lamine M, Arzika I, Mahamadou B, Gora D, Dieye A. Detection of *Plasmodium falciparum* K13 propeller A569G mutation after artesunate-amodiaquine treatment failure in Niger. J Adv Biol Biotechnol. 2018;18:1–8. https://doi.org/10.9734/JABB/2018/42872
21. MalariaGEN *Plasmodium falciparum* Community Project. Genomic epidemiology of artemisinin resistant malaria. eLife. 2016;5:e08714. https://doi.org/10.7554/eLife.08714
22. Ocan M, Akena D, Nsobya S, Kamya MR, Senono R, Kinengyere AA, et al. K13-propeller gene polymorphisms in *Plasmodium falciparum* parasite population in malaria affected countries: a systematic review of prevalence and risk factors. Malar J. 2019;18:60. https://doi.org/10.1186/s12936-019-2701-6
23. Conrad MD, Rosenthal PJ. Antimalarial drug resistance in Africa: the calm before the storm? Lancet Infect Dis. 2019; 19:e338–51. https://doi.org/10.1016/S1473-3099(19)30261-0
24. World Health Organization. Artemisinin and artemisinin-based combination therapy resistance: status report. 2017 [cited 2020 May 15]. https://apps.who.int/iris/handle/10665/255213
25. Mohon AN, Alam MS, Bayih AG, Folefoc A, Shahinas D, Haque R, et al. Mutations in *Plasmodium falciparum* K13 propeller gene from Bangladesh (2009–2013). Malar J. 2014;13:431. https://doi.org/10.1186/1475-2875-13-431
26. Uwimana A, Legrand E, Stokes BH, Ndikumana JM, Warsame M, Umulisa N, et al. Emergence and clonal expansion of in vitro artemisinin-resistant *Plasmodium falciparum* kelch13 R561H mutant parasites in Rwanda. Nat Med. 2020;26:1602–8. https://doi.org/10.1038/s41591-020-1005-2
27. Talundzic E, Ravishankar S, Kelley J, Patel D, Plucinski M, Schmedes S, et al. Next-generation sequencing and bioinformatics protocol for malaria drug resistance marker surveillance. Antimicrob Agents Chemother. 2018;62:e02474–17. https://doi.org/10.1128/AAC.02474-17

Address for correspondence: Eldin Talundzic, Centers for Disease Control and Prevention, 1600 Clifton Rd NE, Mailstop H23-10, Atlanta, GA 30329-4018, USA; email: etalundzic@cdc.gov

Transmission Dynamics of African Swine Fever Virus, South Korea, 2019

Dae Sung Yoo,[1] Younjung Kim,[1] Eune Sub Lee, Jun Sik Lim, Seong Keun Hong, Il Seob Lee, Chung Sik Jung, Ha Chung Yoon, Sung Hwan Wee, Dirk U. Pfeiffer, Guillaume Fournié

African swine fever (ASF) is a substantial concern for global food production and security. However, lack of epidemiologic data in affected areas has limited the knowledge of the main drivers of ASF virus (ASFV) transmission. To assess the role of vehicle movements and wild boar populations in spreading ASFV to pig farms in South Korea, we combined data generated by ASF surveillance on pig farms and of wild boars with nationwide global positioning system–based tracking data for vehicles involved in farming activities. Vehicle movements from infected premises were associated with a higher probability of ASFV incursion into a farm than was geographic proximity to ASFV-infected wild boar populations. Although ASFV can spill over from infected wild boars into domestic pigs, vehicles played a substantial role in spreading infection between farms, despite rapid on-farm detection and culling. This finding highlights the need for interventions targeting farm-to-farm and wildlife-to-farm interfaces.

African swine fever (ASF) is a highly contagious hemorrhagic viral disease that affects domestic pigs and wild boars. Since its introduction into China in 2018 (*1*) and subsequently into many other countries in Asia (*2*), most of the global pig population has been exposed to the ASF virus (ASFV). In the absence of vaccines and treatments, ASF control relies heavily on on-farm biosecurity and on early detection and containment of infected premises (IPs). It is, therefore, essential to identify and target major ASFV transmission routes. However, only a few studies have assessed the contribution of different transmission routes to ASF epidemics (*3*–*6*), probably because detailed epidemiologic data are lacking. Although those studies have contributed to knowledge of risk factors for ASFV infection, their findings are limited by possible bias resulting from underreporting of outbreaks, absence of information about contact patterns between farms, or both.

After ASFV is introduced into domestic pigs, contact between farms may contribute greatly to virus spread (*7*). Vehicles connect farms through the movements of animals, persons, feed, or medical supplies. Such vehicle movements may create conditions for large ASF epidemics on pig farms, as has been reported for other animal diseases (*8*–*10*). However, despite their probable epidemiologic role, the role of vehicle movements in shaping ASF epidemics has not been assessed. Moreover, although the role of livestock movements in the dynamics of several animal diseases has been assessed in a large body of modeling studies (*11*,*12*), other types of contact between farms, such as those mediated by vehicles involved in farming activities, have rarely been explicitly accounted for.

In 2019, South Korea experienced its first ASF outbreak, which affected domestic pigs and wild boars in the northernmost part of the country. At least 1 pig was positive for ASFV by reverse transcription PCR (*13*) on 14 farms (IPs) from September 17 through October 9. ASFV infection was also confirmed by reverse transcription PCR for 26 wild boars from October 3 through November 20. We assessed the contribution of vehicle movements and wild boars to the spread of ASFV to pig farms during the 2019 epidemic in South Korea by combining ASF case data and vehicle movement data generated by nationwide global positioning system (GPS) tracking.

Author affiliations: Animal and Plant Quarantine Agency, Gimcheon, South Korea (D.S. Yoo, E.S. Lee, S.K. Hong, I.S. Lee, C.S. Jung, H.C. Yoon, S.H. Wee); Jockey Club College of Veterinary Medicine and Life Sciences, City University of Hong Kong, Hong Kong, China (Y. Kim, D.U. Pfeiffer);Kangwon National University College of Veterinary Medicine, Chuncheon, South Korea (J.S. Lim); Royal Veterinary College, London, UK (D.U. Pfeiffer, G. Fournié)

DOI: https://doi.org/10.3201/eid2707.204230

[1]These authors contributed equally to this article.

Methods

Data

The Animal Plant and Quarantine Agency (https://www.qia.go.kr) provided the domestic pig farm registry and farm case data. The study population included all 6,340 registered pig farms (Figure 1). IPs were in 4 contiguous municipalities: Ganghwa Island (n = 5/35), Gimpo (n = 2/20), Paju (n = 5/93), and Yeoncheon (n = 2/80) (*13*). Any 2 IPs were <84 km apart (median 28.5 km) (Appendix Figure 1, https://wwwnc.cdc.gov/EID/article/27/7/20-4230-App1.pdf). By October 16 (i.e., 1 week after the last reported IP), 62.7% (143/228) herds in affected municipalities had been depopulated (Figures 2, 3).

Most (71.4%) IPs raised >1,000 pigs (Appendix Figure 2). Premises were either commercial (n = 12) or backyard (n = 2) farms: 10 breeding and fattening, 2 breeding, and 2 fattening farms. All IPs, except for 1 backyard farm, were registered. Of the 14 IPs, 11 were detected through farmers' reports of ASF-like clinical signs and 3 were detected by active surveillance. At the time of reporting, ≤5 pigs on each farm showed ASF-like clinical signs; these clinical signs were observed in ASFV-positive sows on 9 IPs.

Data on the movements of GPS-tracked vehicles involved in farming activities (e.g., private and government veterinary services; feed, manure, and livestock transport) were collated from the Korean

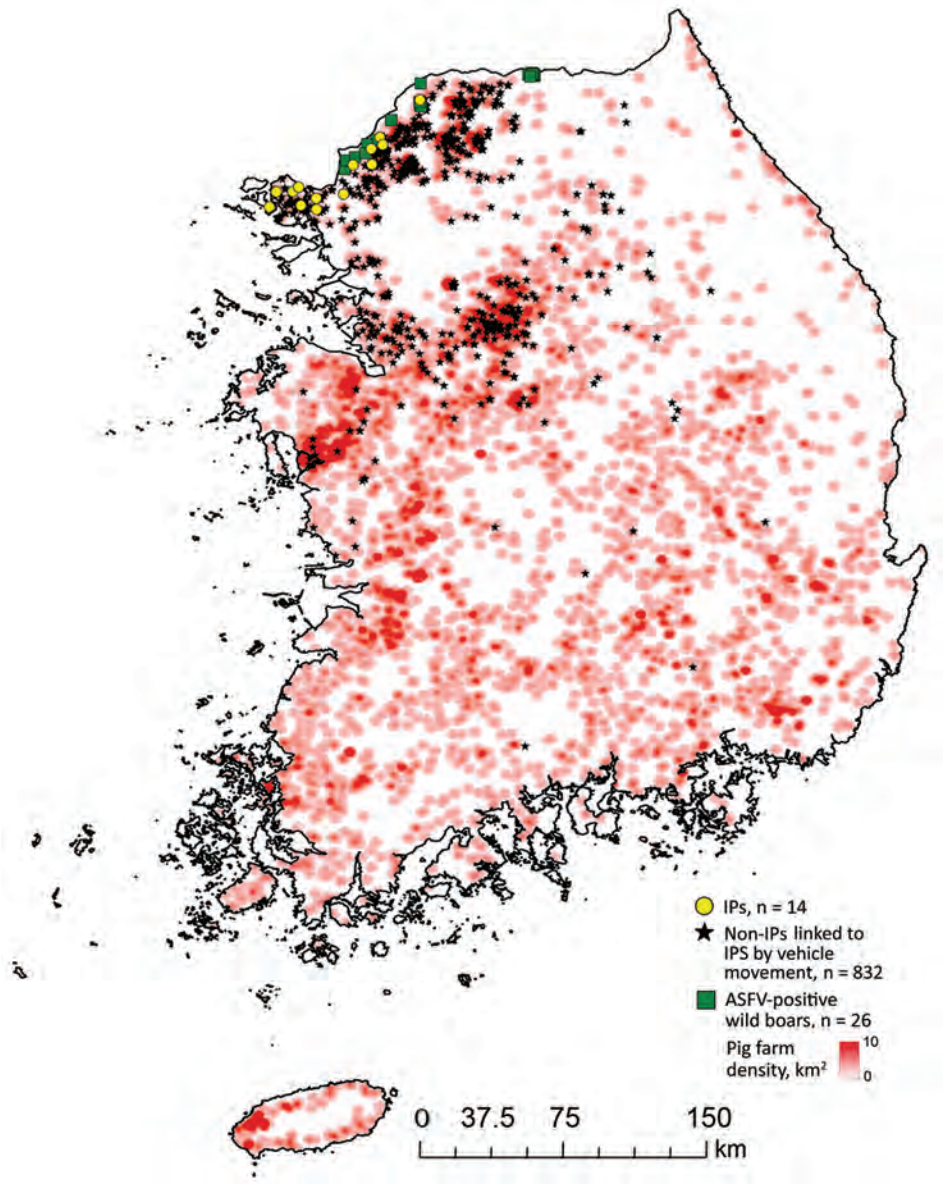

Figure 1. Spatial distribution of registered domestic pig farms in South Korea, indicating African swine fever–positive farms (IPs); ASFV-positive wild boars, confirmed during the study period (August 28–October 16, 2019); and pig farms visited by vehicles that had visited IPs ≥1 time during the study period. ASFV, African swine fever virus; IP, infected premises.

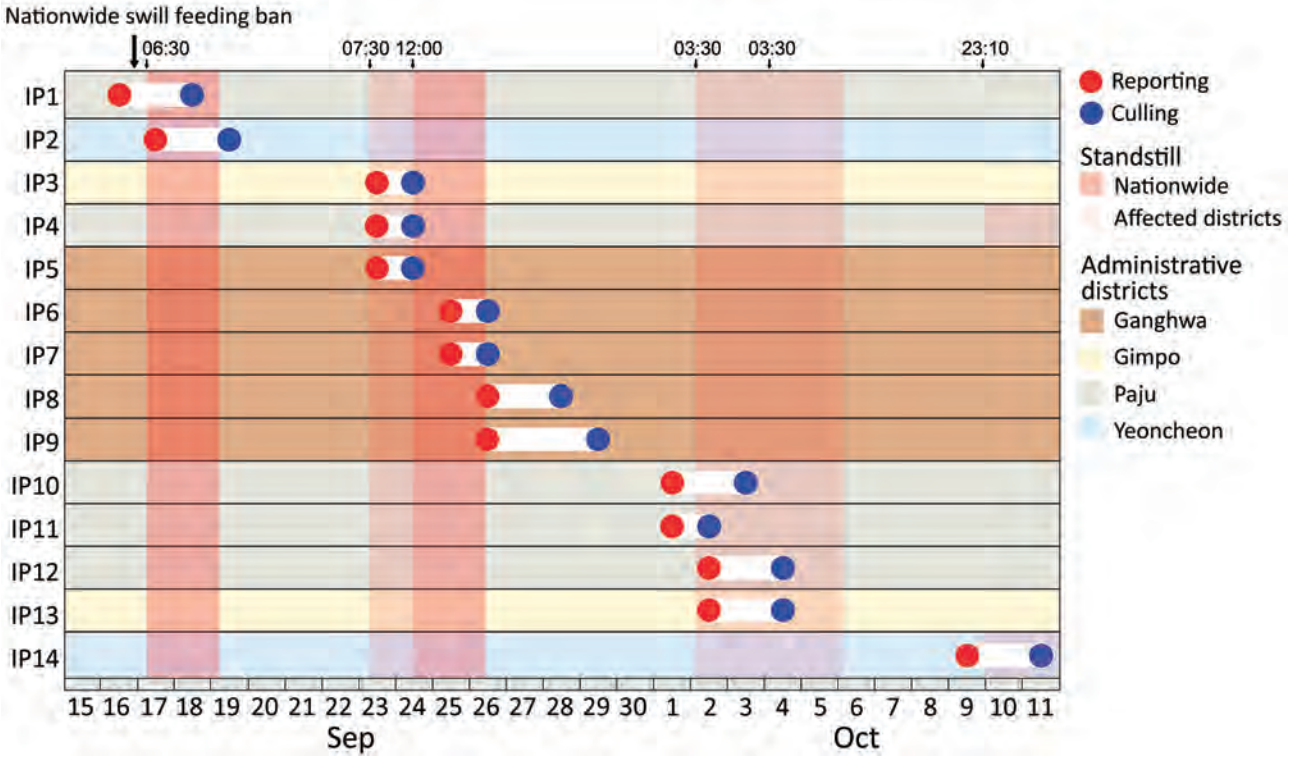

Figure 2. Timeline of reporting and culling of African swine fever virus IPs and control measures implemented during the African swine fever epidemic in South Korea, 2019. Reddish vertical shades represent movement restriction (standstill) imposed across the country (darker shades) or only in the affected municipalities (lighter shades). Numbers on the top represent the time when movement restriction was imposed. The colors of horizontal shades refer to IPs' municipalities. IPs were numbered in the order of reporting dates. Over the course of the epidemic, six 48-hour standstill periods (bans on movements of livestock, persons, vehicles, and supplies to farms and slaughterhouses) were enforced across the country or in affected municipalities. IP, infected premises.

Animal Health Information System (https://www.kahis.go.kr). Given the low number of symptomatic pigs at the time of reporting and the estimated incubation period in pigs (4–13 days) (*14*), we assumed that the length of time between farm infection and reporting was <20 days. In addition, because the law required that vehicles be disinfected before entering farms and when entering and exiting a city, town, or village, we assumed that ASFV-contaminated vehicles remained infectious for <1 week. On the basis of these assumptions, we considered all movements made by vehicles that entered IPs from August 28 (20 days before the first report of an infected premise) through October 16 (a week after the last report of an infected premise).

The Ministry of Environment (https://me.go.kr) provided data on cases in wild boars. From the first report of ASFV infection in domestic pigs, surveillance efforts for wild boars progressively increased by providing financial incentives for wild boar hunting, trapping, and carcass reporting and by testing for ASFV all wild boars caught or found dead (Appendix Figure 3). We assessed spatial clustering of wild boar cases by using an elliptic version of the spatial scan statistic in SatScan (https://www.satscan.org).

Bayesian Modeling

To test the hypothesis that vehicle movements and ASFV-infected wild boars were the main sources of infection for pig farms, we fit a model of ASFV transmission to the farm case data. A vehicle was considered potentially contaminating if it entered farm i within d days after having visited farm j while farm j was infectious. For a given farm on a given day, the overall force of infection was modeled as the sum of the risk for infection resulting from visits by potentially contaminating vehicles, the risk resulting from exposure to wild boars in the spatial clusters of ASFV-positive wild boars, and background risk. Two levels of background risk were considered, depending on the location of a farm: in municipalities where the virus had been detected or across the country. We estimated parameters by using a 2-stage Metropolis-Hastings Markov chain

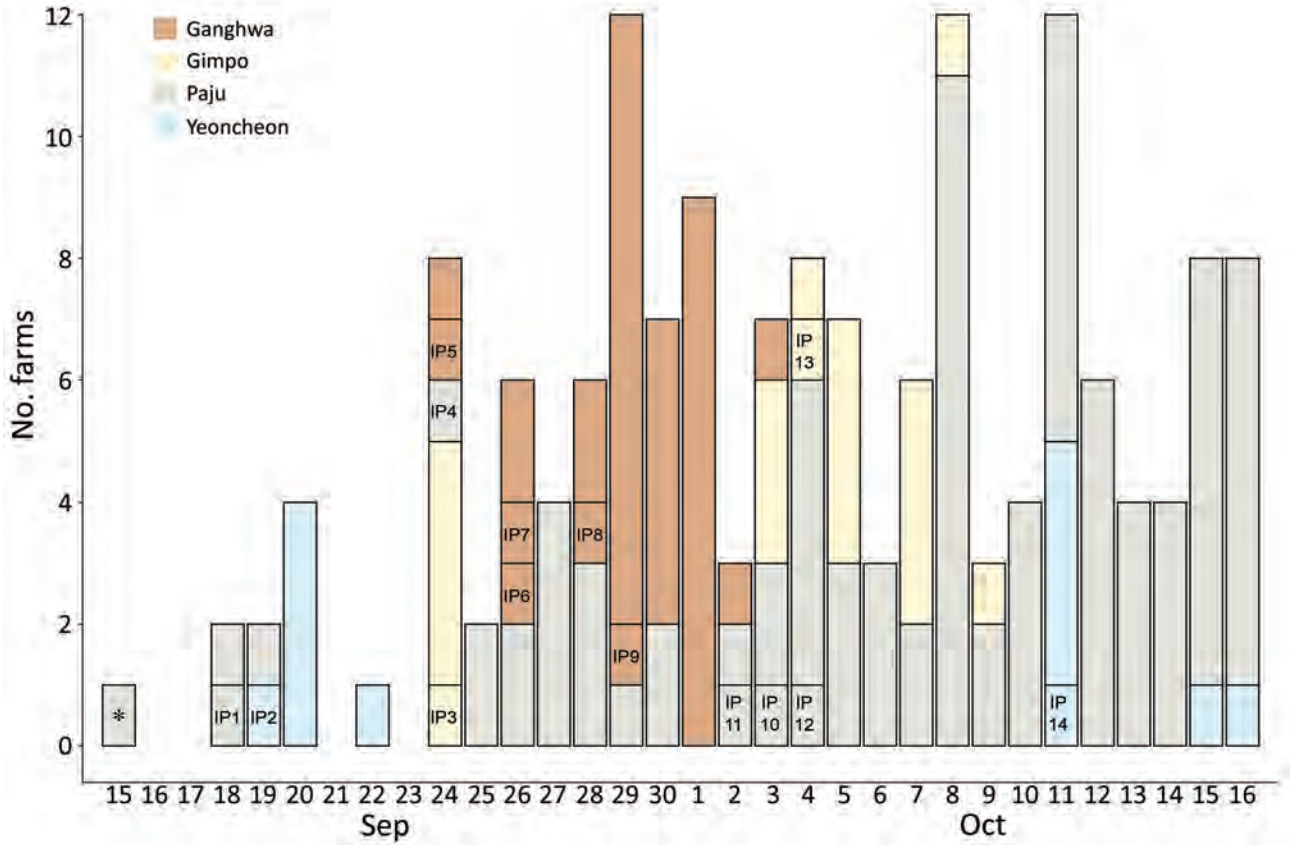

Figure 3. Number of farms registered in the government pig farm database that were emptied during the study period by culling or government purchase, South Korea, 2019. IP labels are shown on the day they were culled. Herds located within a 3-km radius around IPs and herds with an epidemiologic link to IPs (e.g., same ownership) were culled within 3 days after confirmation of African swine fever virus infection in IPs. As the epidemic developed, the government further depopulated remaining herds in affected municipalities as a preventive measure. *One farm stopped rearing pigs for reasons not associated with the epidemic. IP, infected premises.

Monte Carlo algorithm and, because infection dates were not observed, a data augmentation technique (*15*–*17*). The model accounting for the influence of vehicle movements and wild boars was compared with models accounting for only 1 of these epidemiologic factors or for only the constant background risk (null model) on the basis of their deviance information criterion (Appendix).

Results

Vehicle Movement Patterns

During the study period, 208 vehicles visited IPs, making 12,671 visits to 832 farms (infected and noninfected). A total of 156 vehicles made 2,824 farm visits within 3 days after having visited an IP (assuming that vehicles could remain contaminated for 3 days after visiting an IP); each vehicle made a median of 3 farm visits (interquartile range [IQR] 2–7). Of those farm visits, 255 (9.0%) involved other IPs and 2,569 (91.0%) involved 360 non-IPs (5.7% of farms in the country). The number of farm visits changed with the assumed duration of vehicle infectiousness (Figure 4), decreasing from 5 (IQR 2–9) to 2 (IQR 1–4) as the assumed duration of infectiousness decreased from 6 days to 1 day. However, the proportions of movements involving other IPs and non-IPs remained constant (Appendix Table 3). In terms of movements between IPs, 96 (37.6%) started from an IP within the 20-day period preceding the report of a suspected infection and reached another farm within 3 days, before the other farm reported a suspected infection. All these movements occurred between 5 (65.6%) IPs on Ganghwa Island or between 6 (34.4%) IPs off the island (Appendix Table 4). No vehicle movements were involved at 2 IPs (IP2 and IP11). Although another IP (IP14) was visited by such vehicles, the IP was not a source of potentially contaminating vehicle movements to other IPs, even with a vehicle infectiousness duration of 6 days (Appendix Figure 4).

Spatial Clustering of ASF-Positive Wild Boars

During September 21–November 20 in 95 of 226 municipalities, 1,292 wild boars were tested; the rate of testing increased over time (Appendix Figure 3). A total of 26 ASFV-positive wild boars were identified in Paju (n = 6/57), Yeoncheon (n = 8/130), and Cheorwon (n = 12/398) (Figure 5). Two clusters of ASFV-positive wild boars were identified. Of 36 wild boars tested in cluster 1 (10.7 km^2), 10 were ASFV positive, and of 131 in the larger cluster 2 (1,209.4 km^2), 13 were positive. Wild boars caught or found dead within these clusters were 21.8 (cluster 1) and 37.2 (cluster 2) times more likely to be ASFV-positive than were those outside these clusters ($p<0.001$ for all). Although there was no pig farm in cluster 1, there were 6 IPs and 112 non-IPs in cluster 2 (Figure 5). The distance between an infected premise and the nearest infected wild boar was 1.3–37.0 km (Appendix Figure 5).

The Model

For our results, we assumed that a vehicle remained infectious for 3 days after having left an IP. Changes in this parameter value did not largely affect interpretation of the results (Appendix).

When compared by using the deviance information criterion, the model accounting for vehicle movements and for exposure to wild boars in the spatial cluster was preferred over models accounting for only 1, or none, of those sources of infection (Table; Appendix Table 5). Indeed, exposure to these factors substantially increased the risk of farms becoming infected. The daily probability of infection on a farm increased 11.1-fold (95% highest density interval [HDI] 1.1–39.3) after the visit of a potentially contaminating vehicle, compared with a farm not visited by such a vehicle (Appendix Table 6). For a farm in the spatial cluster of ASFV-positive wild boars, the daily probability of becoming infected was 2.5 (95% HDI 1.0–7.7) times as high as for a farm outside this cluster (Appendix Table 6).

On the basis of the best-fit model, we estimated the force of infection exerted on IPs on their estimated infection dates and the proportion of ASFV incursions attributable to each transmission route. Vehicle movements accounted for 41.2% and exposure to wild boars in the spatial cluster for 24.0% of viral incursions; the background risk accounted for the remaining 34.8% (Appendix Table 7). The contribution of different transmission routes to ASFV incursion into IPs varied with the spatial location of the farms. Vehicle movements were the most likely route for ASFV introduction into IPs in the southwestern epidemic region. In contrast, ASFV was not likely to have been spread by vehicles in the northeastern epidemic region, where wild boars were estimated to be the main source of infection for IPs within the ASFV-positive wild boar cluster (Figure 5; Appendix Figures 6, 7). Indeed, the density of potentially contaminating vehicle movements differed greatly between these regions. After accounting for the posterior predictive

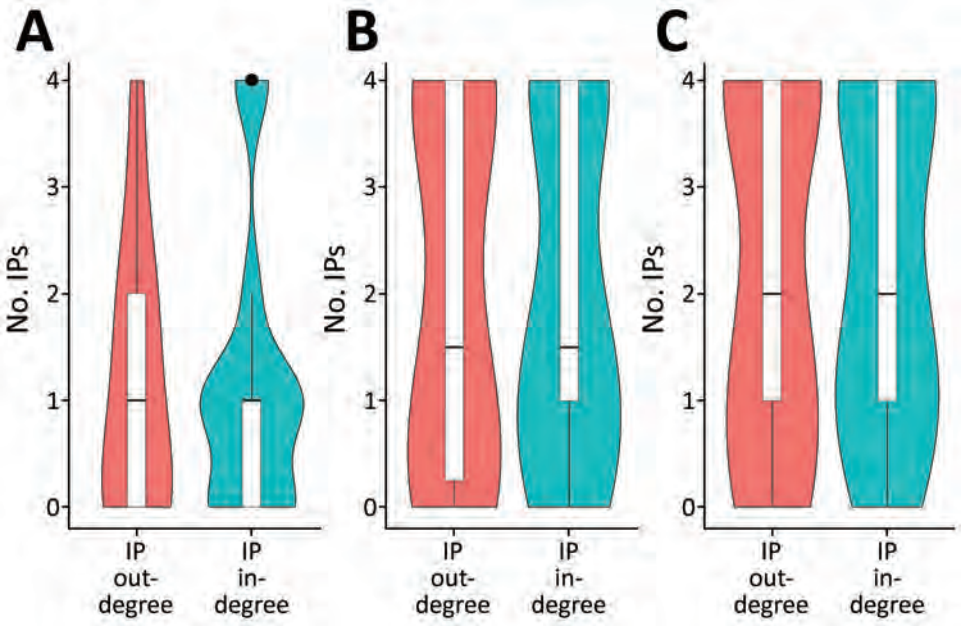

Figure 4. Distribution of the number of African swine fever virus–infected premises connections through vehicle movements, South Korea, 2019. IP out-degree represents the number of other IPs to which an IP sent ≥1 vehicle; IP in-degree represents the number of other IPs from which an IP received ≥1 vehicle. With 1-day (A), 3-day (B), or 6-day (C) assumptions for the duration of vehicle infectiousness, only the movements made up to 20 days before an exit farm reported suspicion of ASFV infection and before an entry farm reported suspicion of infection were considered. In the boxplots, center horizontal lines represent medians, and box limits represent upper and lower quartiles. Upper and lower whiskers extend to the largest and smallest values within 1.5× interquartile ranges. The point represents an outlier. ASFV, African swine fever virus; IP, infected premises.

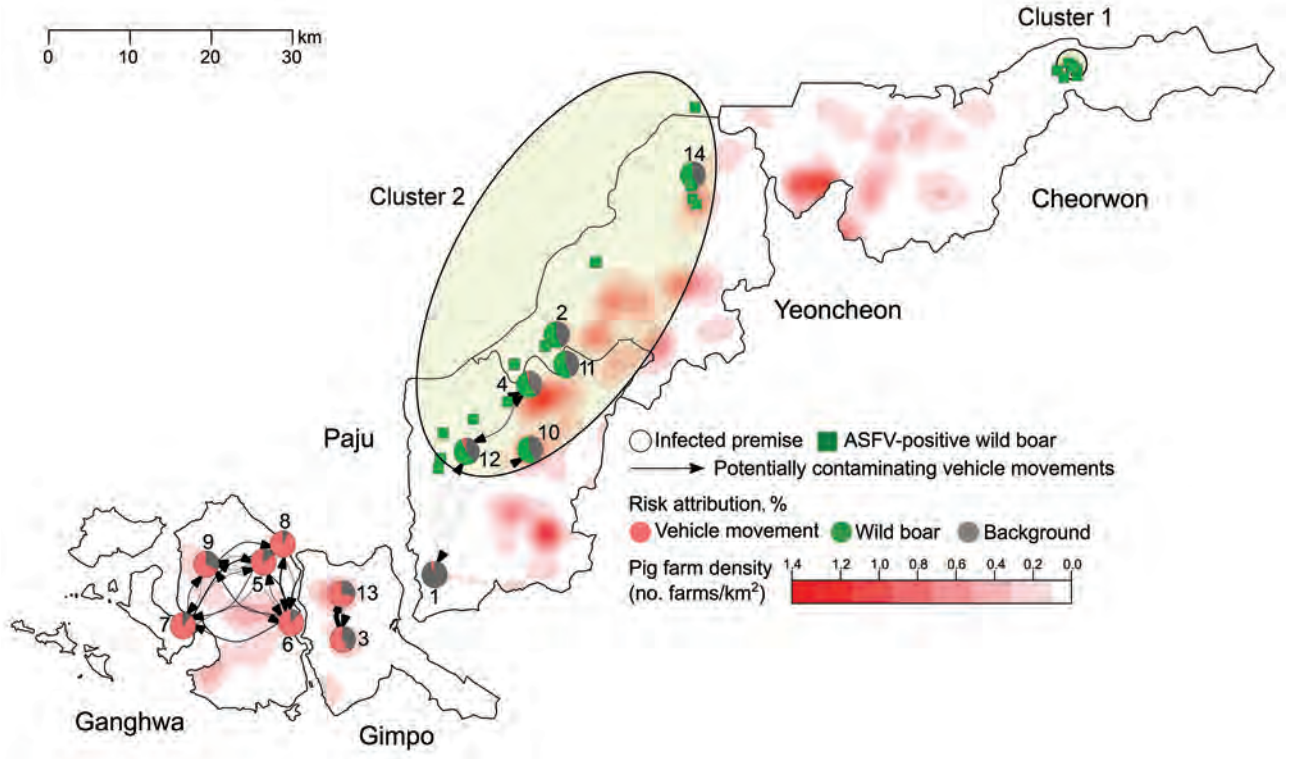

Figure 5. Spatial distribution of infected premises (IPs), non-IPs, African swine fever virus (ASFV)–positive wild boars, and potentially contaminating vehicle movements between IPs, South Korea, 2019. The duration of vehicle infectiousness was set to 3 days. Circles represent IPs; numbers represent the order of reporting dates. Pie charts show the estimated contribution of different transmission routes to the infection of each IP. Edge width is proportional to the number of potentially contaminating vehicle movements between IPs, weighted by the probability that an exit IP was infectious at the time of the vehicle departure. Edge arrows represent the direction of vehicle movements. Pig farm density is shown in reddish colors. Green squares represent the location of ASFV-positive wild boars; green-shaded ellipses represent spatial clusters.

probability that an infected premise was already infected when a vehicle left it, the estimated number of potentially contaminating vehicle movements was 36.6 between IPs and 891.6 from IPs to non-IPs (Appendix Table 8). Of those movements between IPs, 94.3% reached IPs in the southwestern (4.3 visits/infected premise) regions and 5.7% reached IPs in the northeastern (0.3 visits/infected premise) regions. Also, among farms visited by potentially contaminating vehicles, the force of infection resulting from these vehicle movements was much higher for IPs than for non-IPs (Appendix Figure 8). Together, these findings indicate that a dense network of potentially contaminating vehicle movements was formed between a small group of farms, despite the short length of time between farm infection and reporting (median 4.3 days, 95% HDI 1.0–15.8) (Table). To avoid an infected farm spreading ASFV to >1 other farm through vehicle movements, the average number of vehicles visiting a farm in a day and the average number of farms visited by a vehicle in a day should be limited to 1.3 (Figure 6).

Discussion

Our investigation of the role of vehicle movements and of wild boars in ASFV spread to pig farms during the 2019 epidemic in South Korea was made possible by the availability of vehicle movement data generated by integrated GPS tracking and case data on wild boars generated by enhanced ASFV surveillance. The model that accounted for the influence of vehicle movements and wild boars best explained the epidemic pattern, suggesting that both transmission routes contributed to ASFV spread.

Our model suggests that the main route of ASFV introduction into IPs in the southwestern epidemic region was through contaminated vehicles. Indeed, most IPs on Ganghwa Island and Gimpo were densely connected through vehicle movements. In particular, there were a large number of vehicle movements between the 5 IPs on Ganghwa Island (IPs 5–9) ≈1–9 days before a suspected ASFV infection was reported. These 5 IPs reported possible ASF outbreaks within a 4-day period; a small

Table. Posterior parameter estimates and posterior predictive length of time between infection and reporting of African swine fever, South Korea, 2019*

Parameters	Model output		
	Median (95% HDI)	G-R	DIC
Full model			
Potentially contaminating vehicle movement (P_v)	53.9 (7.4–113.4) × 10^{-4}	1.00	275.8 (null model: 284.6)
Wild boar cluster (P_w)	8.2 (0–19.0) × 10^{-4}	1.00	
Background (country, P_{B_1})	0.03 (0–0.1) × 10^{-4}	1.00	
Background (epidemic region, P_{B_2})	5.4 (1.1–11.2) × 10^{-4}	1.00	
Mean of the gamma distribution (α)	3.7 (1.0–8.8)	1.00	
Variance of the gamma distribution (β)	44.6 (5.2–113.5)	1.00	
Length of time between infection and reporting (D)†	4.3 (1.0–15.8)		

*DIC, deviance information criteria; G-R, Gelman-Rubin convergence diagnostic; HDI, highest density interval; P_v, risk for infection resulting from 1 potentially contaminating vehicle movement; P_w, daily risk for infection resulting from being located in an African swine fever virus–positive wild boar cluster; P_{B1}, daily background risk (country); P_{B2}, daily background risk (epidemic region).
†The distribution was obtained by simulating values from the gamma distribution, based on parameters α and β randomly sampled from their joint distribution.

number of pigs showed clinical signs at the time of reporting. This finding suggests that the high density of vehicle movements probably promoted virus transmission between these IPs. Vehicle movements may have increased ASFV spread more because of potentially less effective vehicle disinfection measures on the island. According to epidemiologic investigations, IPs on Ganghwa Island seemed to have insufficient disinfection facilities for vehicles and personnel. Moreover, although farms were relatively close together on this small island (total 302.4 km^2), most vehicle disinfection stations were near 2 bridges connecting the island to the mainland. Therefore, vehicle movements on the island were likely to bypass these stations.

It is unclear how the virus reached the southwestern epidemic region. No potentially contaminating vehicle movements from other affected municipalities were recorded, even when the infectious period for a contaminated vehicle was extended to 6 days. No wild boars were caught or found dead, and they were therefore unavailable for ASFV testing in either municipality. Although the lack of boars for testing does not exclude the possibility that ASFV circulated in the wild boar population, the number of wild boars may be relatively small and the risk for ASFV spread from wild boars to domestic pigs may be very low in this region. Alternatively, ASFV could have been introduced through vehicle movements not captured in this study. We accounted only for vehicle movements between farms; we did not account for vehicle movements involving other types of premises (e.g., slaughterhouses) that could have acted as a source of infection.

Our results suggest that exposure to ASFV-positive wild boars was the main source of infection for pig farms in the northeastern epidemic region. First, all IPs except 1 (IP1) in Paju and Yeoncheon were located in a cluster encompassing almost all ASFV-positive wild boars found in those municipalities. Second, unlike IPs in the southwestern region, several IPs in Paju and Yeoncheon were not connected, or were only weakly connected, to other IPs through vehicle movements. However, the way in which ASFV could have spread from wild boars to domestic pigs remains unclear. Pietschmann et al. (*18*) showed that ASFV transmission was possible from wild boars to domestic pigs housed in separate pens. Such contact was, however, unlikely to have occurred in this setting because the pigs were kept indoors in all but IP11, a backyard farm. Also, potential biological vectors (*Ornithodoros* spp. ticks) have not been reported in South Korea (*19*,*20*). Although the exact mode of ASFV transmission remains unknown, the potential for ASFV spread from infected wild boars must be addressed by ASF prevention and control efforts, a view that is supported by a previous study that linked epidemics in wild boars and domestic pigs in the Russian Federation (*3*).

The nationwide GPS vehicle tracking system provided a unique opportunity to investigate the role of vehicle movements in virus dissemination between farms. Although the estimated length of time from farm infection to reporting was short and several movement restriction (standstill) periods were enforced, a large number of vehicles had already visited IPs during their estimated infectious period and could have spread ASFV to other farms. The types of vehicles and the purpose of the farm visits were not made available for this study. Vehicles involved in farming activities were required by law to be disinfected at multiple sites (e.g., the entry point of a city, town, or village) during the epidemic and routinely disinfected at the farm entrance. These findings suggest that disinfection may have been suboptimal. Therefore, restrictions on vehicle movements should be prioritized in the event

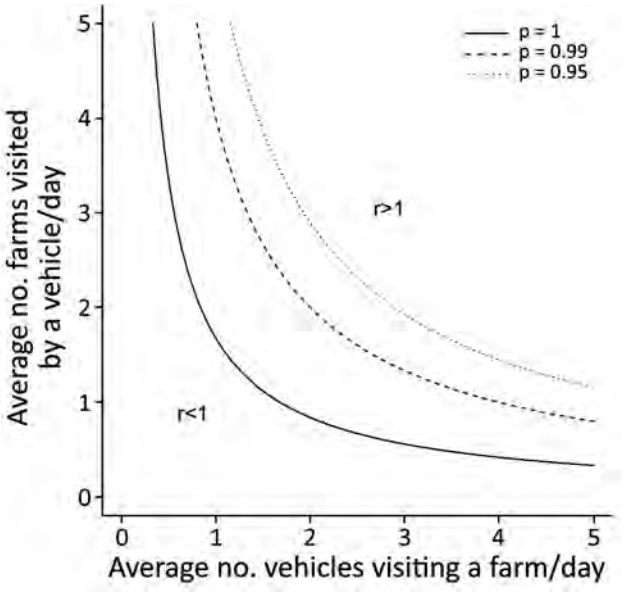

Figure 6. Expected number of secondary farm cases of African swine fever (r) caused by 1 infected farm through the movements of vehicles, South Korea, 2019. r is computed as a function of the average daily number of vehicles visiting a farm (x-axis) and the average daily number of farms visited by a vehicle (y-axis). Different lines represent different thresholds for the proportion of iterations in which r was <1 (p = 1, 0.99, or 0.95). Vehicles were assumed to remain infectious for 3 days after leaving an infected farm. Appendix Figure 9 (https://wwwnc.cdc.gov/EID/article/27/7/20-4230-App1.pdf) shows the results with different assumptions on the duration of vehicle infectiousness.

of virus introduction into areas where high on-farm biosecurity cannot be guaranteed. The availability of contact tracing data could reduce the negative effect of movement restrictions on farming activities by targeting those restrictions to premises that have been in contact with IPs. Active surveillance could also be focused on these premises, enabling even more timely case detection.

The background risk accounted for a substantial fraction of the force of infection exerted on several IPs. Swill feeding probably did not contribute to this background risk because it was banned at the start of the epidemic and, according to the outbreak investigations, did not seem to be practiced on IPs. Control measures were unlikely to have promoted ASFV dissemination. Pigs were culled within a few days after confirmation of diagnostic results, and carcasses were placed inside a fiber-reinforced plastic chamber and buried on the premise. Vehicles and personnel involved in these interventions were not allowed to visit non-IPs throughout the epidemic. Regular inspections of vehicles visiting feed and manure disposal plants suggested that most vehicles involved in farming activities were registered and therefore tracked by GPS. Nonetheless, some vehicle movements not captured in this study could have contributed to disease spread. For instance, we did not consider vehicle contamination from visiting other types of premises (e.g., slaughterhouses). Private vehicles were not GPS tracked, but outbreak investigations did not identify any connections between IPs through such vehicles. Wild boars may have also substantially contributed to the background risk. Although these findings strongly suggest that the prevalence of ASFV infection in wild boars was much higher within than outside the clusters, it was not possible to exclude the possibility that the virus might also have circulated at lower prevalence in wild boar populations outside the spatial clusters. This source of infection might have been plausible for some IPs for which most of the force of infection was attributed to background risk.

One limitation of this study is that the model did not consider the possible heterogeneity in the infectiousness of vehicles and the susceptibility of farms to ASFV infection. Farm visits may involve different types of contact with persons, equipment, and pigs, thereby presenting different transmission risks. In addition, farms with poor biosecurity could have been exposed to an increased risk for infection when visited by contaminated vehicles. The risk for infection from infected wild boars was also likely to have varied between farms because of different levels of on-farm biosecurity and proximity to wild boar habitats. In addition, although the model identified an excess risk for infection for farms within the spatial cluster of ASFV wild boar cases, the spatiotemporal heterogeneity in ASFV circulation among wild boars inside and outside the cluster may have been underestimated.

Another limitation is that the model assumed that the potential for a contaminated vehicle to transmit the infection remained constant throughout the vehicle's period of infectiousness. Yet because vehicles were supposed to be disinfected when entering a farm, their infectiousness may have decreased over time with each additional farm visited. Accounting for this process would probably have increased the estimated probability of virus incursion after a visit from a potentially contaminating vehicle. However, this process is unlikely to have influenced our conclusions because the contribution of vehicle movements to ASFV spread was not affected by variations in the assumed duration of vehicle infectiousness.

The possibility that some wild boars were infected while on IPs cannot be completely excluded. However, ASFV was probably circulating among wild boars before pig farms were infected, given that the first wild boar case was detected in the demilitarized zone where no civilians and farms are present, and North Korea had already reported the disease. Subsequently, the delayed detection of ASFV in wild boars probably resulted from the lower sensitivity of surveillance in wild animals compared with domestic animals and from increased surveillance efforts among wild boars after disease detection on farms. In addition, since the end of the study period (November 21, 2019), ASFV infection has been confirmed in >700 wild boars and on 3 pig farms (*2*), suggesting that ASFV can continue to circulate among wild boars in the absence of virus circulation among domestic pigs.

Our models did not account for within-farm transmission dynamics. Farm infectiousness was likely to vary over time, influencing between-farm transmission dynamics. However, given that a small number of pigs showed ASF-like clinical signs on all IPs at the time of reporting or detection, and that herds were culled within 1 or 2 days, the effect may have been limited.

In conclusion, our findings suggest that the movement of contaminated vehicles and infected wild boars contributed to the spread of ASFV to pig farms in South Korea. Although the ongoing circulation of ASFV in wild boars poses an ongoing risk for virus spillover onto pig farms, vehicle movements have the potential to cause large chains of transmission between farms. Therefore, the timely implementation of movement restrictions is critical for the rapid and effective management of ASFV epidemics. In this regard, the tracking of vehicles involved in farming activities could guide the targeting of restrictions to those at high risk for infection because of their recent contacts. High on-farm biosecurity and effective vehicle disinfection should be ensured, especially in areas where ASFV is circulating among wild boars.

This study was supported by the Animal and Plant Quarantine Agency, South Korea.

About the Author

Dr. Yoo is an epidemiologist at the Animal and Plant Quarantine Agency, the Ministry of Agriculture, Food and Rural Affairs, in South Korea. His research focuses mainly on providing epidemiologic advice with regard to prevention and control of animal infectious diseases.

References

1. Zhou X, Li N, Luo Y, Liu Y, Miao F, Chen T, et al. Emergence of African swine fever in China, 2018. Transbound Emerg Dis. 2018;65:1482–4. https://doi.org/10.1111/tbed.12989
2. World Organisation for Animal Health. OIE World Animal Health Information System [cited 2020 Nov 17]. https://wahis.oie.int
3. Vergne T, Gogin A, Pfeiffer DU. Statistical exploration of local transmission routes for African swine fever in pigs in the Russian Federation, 2007–2014. Transbound Emerg Dis. 2017;64:504–12. https://doi.org/10.1111/tbed.12391
4. Ma J, Chen H, Gao X, Xiao J, Wang H. African swine fever emerging in China: distribution characteristics and high-risk areas. Prev Vet Med. 2020;175:104861. https://doi.org/10.1016/j.prevetmed.2019.104861
5. Vergne T, Korennoy F, Combelles L, Gogin A, Pfeiffer DU. Modelling African swine fever presence and reported abundance in the Russian Federation using national surveillance data from 2007 to 2014. Spat Spatio-Temporal Epidemiol. 2016;19:70–7. https://doi.org/10.1016/j.sste.2016.06.002
6. Iglesias I, Rodríguez A, Feliziani F, Rolesu S, de la Torre A. Spatio-temporal analysis of African swine fever in Sardinia (2012–2014): trends in domestic pigs and wild boar. Transbound Emerg Dis. 2017;64:656–62. https://doi.org/10.1111/tbed.12408
7. Craft ME. Infectious disease transmission and contact networks in wildlife and livestock. Philos Trans R Soc Lond B Biol Sci. 2015;3701669. https://doi.org/10.1098/rstb.2014.0107
8. Fournié G, Guitian J, Desvaux S, Cuong VC, Dung H, Pfeiffer DU, et al. Interventions for avian influenza A (H5N1) risk management in live bird market networks. Proc Natl Acad Sci U S A. 2013;110:9177–82. https://doi.org/10.1073/pnas.1220815110
9. Green DM, Kiss IZ, Kao RR. Modelling the initial spread of foot-and-mouth disease through animal movements. Proc Biol Sci. 2006;273:2729–35. https://doi.org/10.1098/rspb.2006.3648
10. Kim Y, Dommergues L, M'sa AB, Mérot P, Cardinale E, Edmunds J, et al. Livestock trade network: potential for disease transmission and implications for risk-based surveillance on the island of Mayotte. Sci Rep. 2018;8:11550. https://doi.org/10.1038/s41598-018-29999-y
11. Green DM, Kiss IZ, Mitchell AP, Kao RR. Estimates for local and movement-based transmission of bovine tuberculosis in British cattle. Proc Biol Sci. 2008;275:1001–5. https://doi.org/10.1098/rspb.2007.1601
12. Gilbert M, Mitchell A, Bourn D, Mawdsley J, Clifton-Hadley R, Wint W. Cattle movements and bovine tuberculosis in Great Britain. Nature. 2005;435:491–6. https://doi.org/10.1038/nature03548
13. Yoon H, Hong SK, Lee I, Yoo DS, Jung CS, Lee E, et al. Clinical symptoms of African swine fever in domestic pig farms in the Republic of Korea, 2019. Transbound Emerg Dis. 2020 Mar 25 [Epub ahead of print]. https://doi.org/10.1111/tbed.13552
14. Guinat C, Reis AL, Netherton CL, Goatley L, Pfeiffer DU, Dixon L. Dynamics of African swine fever virus shedding and excretion in domestic pigs infected by intramuscular inoculation and contact transmission. Vet Res (Faisalabad). 2014;45:93. https://doi.org/10.1186/s13567-014-0093-8
15. Walker PG, Cauchemez S, Métras R, Dung H, Pfeiffer D, Ghani AC. A Bayesian approach to quantifying the effects of mass poultry vaccination upon the spatial and temporal dynamics of H5N1 in northern Vietnam. PLOS Comput

Biol. 2010;6:e1000683. https://doi.org/10.1371/journal.pcbi.1000683
16. Cauchemez S, Bhattarai A, Marchbanks TL, Fagan RP, Ostroff S, Ferguson NM, et al.; Pennsylvania H1N1 Working Group. Role of social networks in shaping disease transmission during a community outbreak of 2009 H1N1 pandemic influenza. Proc Natl Acad Sci U S A. 2011;108:2825–30. https://doi.org/10.1073/pnas.1008895108
17. Chapman LAC, Jewell CP, Spencer SEF, Pellis L, Datta S, Chowdhury R, et al. The role of case proximity in transmission of visceral leishmaniasis in a highly endemic village in Bangladesh. PLoS Negl Trop Dis. 2018;12:e0006453. https://doi.org/10.1371/journal.pntd.0006453
18. Pietschmann J, Guinat C, Beer M, Pronin V, Tauscher K, Petrov A, et al. Course and transmission characteristics of oral low-dose infection of domestic pigs and European wild boar with a Caucasian African swine fever virus isolate. Arch Virol. 2015;160:1657–67. https://doi.org/10.1007/s00705-015-2430-2
19. Chae JB, Kang JG, Kim HC, Chong ST, Lee IY, Shin NS, et al. Identification of tick species collected from wild boars and habitats of wild boars and domestic pigs in the Republic of Korea. Korean J Parasitol. 2017;55:185–91. https://doi.org/10.3347/kjp.2017.55.2.185
20. Chae JB, Cho YS, Cho YK, Kang JG, Shin NS, Chae JS. Epidemiological investigation of tick species from near domestic animal farms and cattle, goat, and wild boar in Korea. Korean J Parasitol. 2019;57:319–24. https://doi.org/10.3347/kjp.2019.57.3.319

Address for correspondence: Younjung Kim, City University of Hong Kong College of Veterinary Medicine and Life Sciences, Department of Infectious Diseases and Public Health, Room 1B-410, 4/F, Block 1, To Yuen Building, 31 To Yuen St, Kowloon, Hong Kong, China; email: younjung.kim@my.cityu.edu.hk

Cross-Sectional Serosurvey of Companion Animals Housed with SARS-CoV-2–Infected Owners, Italy

Barbara Colitti, Luigi Bertolotti, Alessandro Mannelli, Gianmarco Ferrara, Andrea Vercelli, Andrea Grassi, Claudio Trentin, Saverio Paltrinieri, Chiara Nogarol, Nicola Decaro, Emiliana Brocchi, Sergio Rosati

We conducted a serologic survey among dogs and cats in Italy to detect antibodies against severe acute respiratory syndrome virus 2 (SARS-CoV-2). We found that SARS-CoV-2 seroprevalence was higher among cats (16.2%) than dogs (2.3%). In addition, seroprevalence was higher among animals living in close contact with SARS-CoV-2–positive owners.

After emerging in Wuhan, China, in December 2019, coronavirus disease (COVID-19), caused by severe acute respiratory syndrome coronavirus 2 (SARS-CoV-2), rapidly became a serious threat to human health worldwide (*1*–*3*). Italy has experienced one of the highest rates of human deaths in the world (*4*).

Questions concerning the role of companion animals in the COVID-19 pandemic arose after a dog in Hong Kong reportedly tested positive for SARS-CoV-2 (*5*). In addition, the World Organisation for Animal Health defined COVID-19 as an emerging disease in animals and began promoting surveys on the prevalence of SARS-CoV-2 infections among animals (*6*). In this context, serologic tests are essential for rapid and accurate screening of animal populations.

Few studies have been conducted to clarify the effects domestic animals have in sustaining the SARS-CoV-2 transmission cycle (*5*,*7*–*9*; Q. Zhang et al., unpub. data, https://www.biorxiv.org/content/10.1101/2020.04.01.021196v1). Because Italy suffered high COVID-19 incidence rates and the country has >32 million companion animals, health authorities were interested in examining virus transmission between humans and animals. We conducted a cross-sectional serologic survey among domestic dogs and cats in Italy to identify a possible association between SARS-CoV-2 infection in humans and animals. We used serologic tests to detect specific antibodies from animals living in close contact with SARS-CoV-2–positive human patients.

The Study

Blood was collected from pets during routine activities performed by veterinary practitioners, who shared serum samples with us. Owners provided written consent for research purposes. We used 198 samples, 130 from dogs and 68 from cats, collected during the March–June 2020 COVID-19 epidemic in Italy and 100 serum samples, 65 from dogs and from 35 cats, collected in different regions of Italy before 2019 as prepandemic controls.

A recombinant antigen corresponding to the nucleocapsid (N) protein of SARS-CoV-2 has been expressed in human embryonic kidney 293T cells, which have been used to develop Eradikit COVID19-IgG (IN3diagnostic, https://www.in3diagnostic.com) a sensitive and specific ELISA to detect SARS-CoV-2 antibodies in human serum samples. However, our initial attempts to validate the specificity of this ELISA on pet serum samples were unsuccessful. We switched the reaction from solid-phase to solution-phase kinetics using the same antigen and the specificity improved. Thus, we used a novel immunoassay, xMAP (Luminex Corp., https://www.luminexcorp.com), which is based on paramagnetic beads. We developed a flow cytometry-based system and applied it to serum samples from cats and dogs.

To define the test's specificity, we analyzed preepidemic samples and expressed results as the mean

Author affiliations: University of Turin, Turin, Italy (B. Colitti, L. Bertolotti, A. Mannelli, S. Rosati); University of Naples, Naples, Italy (G. Ferrara); Clinica veterinaria Città di Torino, Turin, Italy (A. Vercelli); I-Vet srl Laboratorio di Analisi Veterinarie, Flero, Italy (A. Grassi); AUSL Valle d'Aosta, Aosta, Italy (C. Trentin); University of Milan, Milan, Italy (S. Paltrinieri); IN3Diagnostic, Turin (C. Nogarol); University of Bari, Bari, Italy (N. Decaro); Istituto Zooprofilattico Sperimentale della Lombardia e dell'Emilia Romagna, Brescia, Italy (E. Brocchi)

DOI: https://doi.org/10.3201/eid2707.203314

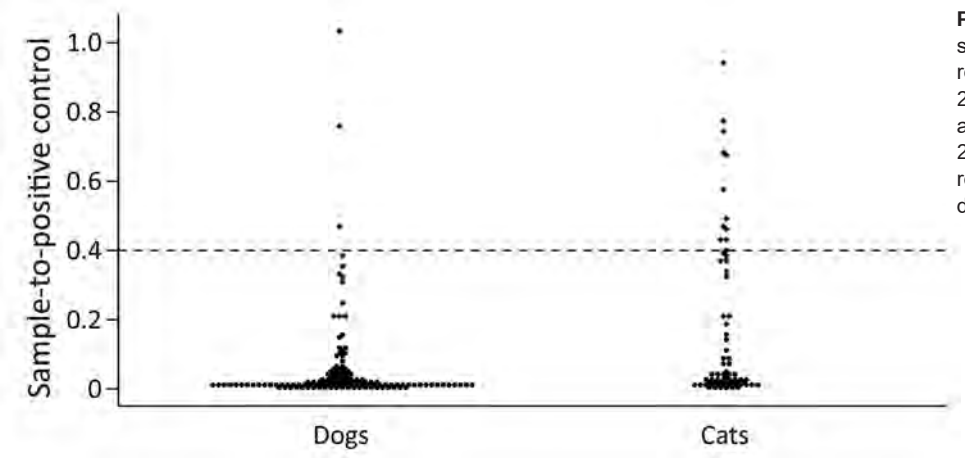

Figure 1. Distribution of sample-to-positive severe acute respiratory syndrome coronavirus 2 serology results among dogs and cats, Italy, March–June 2020. Horizontal dashed line represents the positive-negative discriminatory cutoff.

fluorescence intensity (MFI) ratio of a sample-to-positive control. On the basis of reactivity distribution, we set the discriminative cutoff to 40% MFI of the positive control. Using these specifications, we recorded diagnostic specificities of 96.5% (95% CI 87.9%–99.6%) for dog serum and 100.0% (95% CI 90.0%–100.0%) for cat serum.

Our choice of the viral N protein might raise concern because dogs and cats are susceptible to species-specific coronaviruses. The amino acid similarity between SARS-CoV-2 and the canine betacoronavirus, canine respiratory coronavirus, is slightly higher than canine and feline alphacoronaviruses (*10*), which could explain the suboptimal specificity obtained in pre-epidemic dog samples. In fact, 2 serum samples gave reactivity slightly over the cutoff value. However, when potential cross-reactivity of the N protein between SARS-CoV-2 and endemic human coronaviruses was evaluated, no reactivity was shown against human coronaviruses 229E, OC43, HKU1, or NL63 by western blot or ELISA (*11*), suggesting that similar results might be expected from phylogenetically related feline and canine coronaviruses (*12*).

Table 1. Seropositivity among cats and dogs tested for antibodies against severe acute respiratory syndrome coronavirus 2, Italy, March–June 2020

Level of analysis	% Positivity among pets
Individual animal	
Owners' status*	
Infected, n = 147	9.5
Not tested, n = 49	0
Animal species	
Cat, n = 68	16.2
Dog, n = 130	2.3
Living conditions†	
Indoor, n = 87	12.6
Outdoor, n = 51	3.9
Households tested, n = 156‡	
Owners' status	
Infected, n = 111	10.8
Not tested, n = 45	0
Cats tested in the household	
Yes, n = 51	19.6
No, n = 105	1.9
Dogs tested in the household	
Yes, n = 114	2.6
No, n = 42	21.4

*Information on owners' status was missing from 1 cat and 1 dog. Infected means positive molecular tests for the detection of SARS-Cov-2 in ≥1 owner in a household. Percent positivity at the household level was based on finding ≥1 seropositive animal.
†Information on pets' living conditions was missing for 43 dogs and 17 cats.
‡Households were considered positive if ≥1 pet was serologically positive. Households were divided into those in which ≥1 cat was tested and those in which ≥1 dog was tested.

Among samples collected during the epidemic period, 7.1% (14/198) tested positive by the serologic test. In all, 147 animals (54 cats and 93 dogs) lived in households with SARS-CoV-2–positive owners. All 14 seropositive animals lived with SARS-CoV-2–infected owners and percent positivity was greater among cats than dogs (Table 1; Figure 1). Among animals living with SARS-CoV-2–infected owners, 20.4% (11/54) of cats and 3.2% (3/93) of dogs were seropositive.

Exact logistic regression analysis indicated a positive association between owners' infections and seropositivity in individual animals, after adjusting for animal species (Figure 2). The odds of finding ≥1 seropositive animal in a household were positively associated with owners' infection and with an increasing number of tested cats (Table 2; Appendix, https://wwwnc.cdc.gov/EID/article/27/7/20-3314-App1.pdf). The association with owner infection was only statistically significant based on a 1-tailed hypothesis, whether the outcome was measured at the animal or household level.

Using exact logistic regression, we noted the percent of positive results was greater for animals living indoors only than for animals with access to the outside (odds ratio 3.4, 95% CI 0.71–35.9), but the association was not statistically significant (p = 0.15). Because information on living conditions was missing

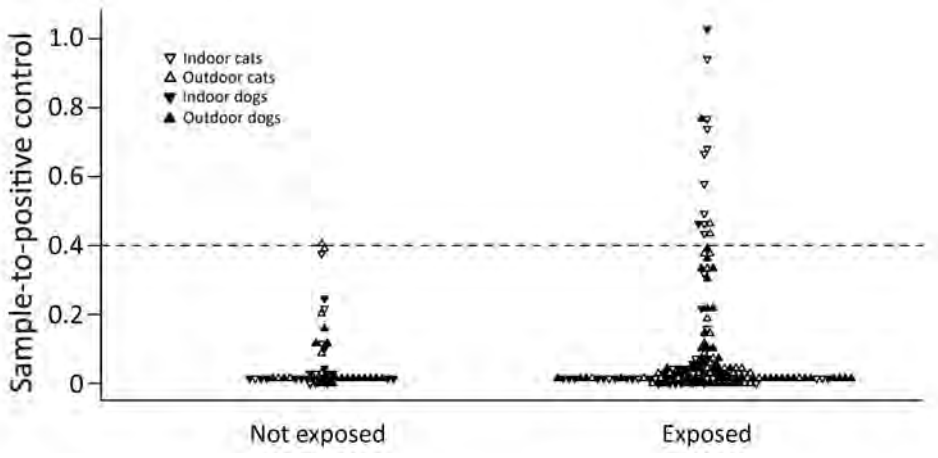

Figure 2. Distribution of sample-to-positive severe acute respiratory syndrome coronavirus 2 serology results among dogs and cats exposed and unexposed to positive owners, Italy, March–June 2020. Horizontal dashed line represents the positive-negative discriminatory cutoff.

for 60 animals, we did not include this factor in the exact logistic regression analysis (Tables 1, 2).

We found the proportion of serologic positivity increased with increasing length of exposure. We recorded the first SARS-CoV-2–positive animals 10 days after owners' diagnoses and all 14 seropositive cases were classified as positive after ≥54 days of exposure (Appendix).

Among 5/14 positive animals, owners reported that their pets experienced clinical signs concurrent with the owner's COVID-19 illness. In particular, a 10-year-old male dog showed respiratory signs (cough, sneezing) after which he had vomiting and diarrhea in concomitance with the onset of the owners' symptoms; a 1-year-old dog showed mild respiratory signs characterized by cough and sneezing; a 12-year-old female cat showed respiratory signs characterized by rhinitis with abundant nasal discharge. Furthermore, a 13-year-old female cat was hospitalized for a brachial cephalic thrombosis and a 3-year-old male cat was hospitalized for interstitial pneumonia. Of note, 3 asymptomatic SARS-CoV-2–positive cats belonged to a single-family cluster in which both owners tested positive and hospitalized.

Conclusions

We detected antibodies against the SARS-CoV-2 N protein in pets living with SARS-CoV-2–infected owners. A higher percentage of feline samples tested positive, confirming a higher susceptibility and prevalence in cats than in dogs reported in previous experiments (*10*,*13*). The susceptibility of cats to SARS-related human coronaviruses also was reported in 2003 when a study confirmed that cats were susceptible to infection and could transmit the virus to other in-contact animals (*14*). The association between seropositivity in animals and the confirmed SARS-CoV-2 infection in ≥1 of the animal's owners was statistically significant ($p<0.05$) based on a 1-sided test assuming the owner's infection could not reasonably exert a protective effect on pets' infection.

We could not draw conclusions concerning the direction of viral transmission in this cross-sectional study. Nevertheless, our results, coupled with the direction of the association between seropositivity and length of exposure to an infected owner and living indoors, suggest that the development of antibodies in pets might be a consequence of viral transmission from their owners. Additional studies with more statistical power could confirm these relationships.

Based on our results, future studies should focus on overcoming test limitations by improving specificity in dog serum samples through detailed epitope mapping of the N protein. Additional studies also should examine routes and risk factors for transmission of SARS-CoV-2 from infected persons to susceptible pets and the potential role of pets in the COVID-19 pandemic. Clinical and pathological consequences of SARS-CoV-2 infection in cats and dogs also warrant further research.

In conclusion, our study on companion animals housed with SARS-CoV-2–infected humans confirms the susceptibility of domestic cats under natural exposure. Our data statistically support other findings that cats are more susceptible than dogs

Table 2. Results of multivariable exact logistic regression of the association between severe acute respiratory syndrome coronavirus 2 seropositivity among cats and dogs and infected owners, Italy, March–June 2020

Level of analysis	Odds ratio (95% CI)	p value*
Individual animal		
Owners' status	6.1† (0.97–∞)	0.055
Cat vs. dog	7.6 (1.9–44.4)	0.002
Household		
Owners' status	5.8† (0.9–∞)	0.068
No. tested cats	2.5 (1.3–5.2)	0.008

*p value based on 2-tailed test.
†Median unbiased estimate.

and that living in contact with ≥1 SARS-CoV-2–infected person increases the risk for infection in pets. These results justify the need to adopt control measures in SARS-CoV-2–infected pet owners to reduce viral transmission to their companion animals.

Acknowledgments

We thank veterinary practitioners in Italy for their significant contributions from and help with sample collection. We also thank Alessandro Bellato for assisting with statistical analysis using Stata (StataCorp LLC, https://www.stata.com).

The study was carried out in compliance with the national legislation with authorization by the Ministry of Health Legislative Decree 26/2014 (authorization no. 694/2020-PR). Blood samples were collected during routine activities performed by veterinary practitioners. Written consent was obtained from all owners for research purposes.

About the Author

Dr. Colitti holds a research grant position in the Department of Veterinary Sciences, University of Turin, Italy. Her primary research interest is the diagnosis of animal infectious diseases.

References

1. Zhou P, Yang XL, Wang XG, Hu B, Zhang L, Zhang W, et al. A pneumonia outbreak associated with a new coronavirus of probable bat origin. Nature. 2020;579:270–3. https://doi.org/10.1038/s41586-020-2012-7
2. Zheng J. SARS-CoV-2: an emerging coronavirus that causes a global threat. Int J Biol Sci. 2020;16:1678–85. https://doi.org/10.7150/ijbs.45053
3. Wu F, Zhao S, Yu B, Chen YM, Wang W, Song ZG, et al. A new coronavirus associated with human respiratory disease in China. Nature. 2020;579:265–9. https://doi.org/10.1038/s41586-020-2008-3
4. World Health Organization. Coronavirus disease (COVID-19) dashboard 2020 [cited 2020 Nov 17]. https://covid19.who.int
5. Sit THC, Brackman CJ, Ip SM, Tam KWS, Law PYT, To EMW, et al. Infection of dogs with SARS-CoV-2. Nature. 2020;586:776–8. https://doi.org/10.1038/s41586-020-2334-5
6. World Organisation for Animal Health. Infection with SARS-Cov-2 in animals 2020; updated 2021 Jan [cited 2020 Nov 8]. https://www.oie.int/app/uploads/2021/03/en-factsheet-sars-cov-2.pdf
7. Shi J, Wen Z, Zhong G, Yang H, Wang C, Huang B, et al. Susceptibility of ferrets, cats, dogs, and other domesticated animals to SARS-coronavirus 2. Science. 2020;368:1016–20. https://doi.org/10.1126/science.abb7015
8. Halfmann PJ, Hatta M, Chiba S, Maemura T, Fan S, Takeda M, et al. Transmission of SARS-CoV-2 in domestic cats. N Engl J Med. 2020;383:592–4. https://doi.org/10.1056/NEJMc2013400
9. Bosco-Lauth AM, Hartwig AE, Porter SM, Gordy PW, Nehring M, Byas AD, et al. Experimental infection of domestic dogs and cats with SARS-CoV-2: Pathogenesis, transmission, and response to reexposure in cats. Proc Natl Acad Sci U S A. 2020;117:26382–8. https://doi.org/10.1073/pnas.2013102117
10. Sharun K, Sircar S, Malik YS, Singh RK, Dhama K. How close is SARS-CoV-2 to canine and feline coronaviruses? J Small Anim Pract. 2020;61:523–6. https://doi.org/10.1111/jsap.13207
11. Guo L, Ren L, Yang S, Xiao M, Chang D, Yang F, et al. Profiling early humoral response to diagnose novel coronavirus disease (COVID-19). Clin Infect Dis. 2020;71:778–85. https://doi.org/10.1093/cid/ciaa310
12. Lv H, Wu NC, Tsang OT-Y, Yuan M, Perera RAPM, Leung WS, et al. Cross-reactive antibody response between SARS-CoV-2 and SARS-CoV infections. Cell Rep. 2020;31:107725. PubMed https://doi.org/10.1016/j.celrep.2020.107725
13. Salajegheh Tazerji S, Magalhães Duarte P, Rahimi P, Shahabinejad F, Dhakal S, Singh Malik Y, et al. Transmission of severe acute respiratory syndrome coronavirus 2 (SARS-CoV-2) to animals: an updated review. J Transl Med. 2020;18:358. PubMed https://doi.org/0.1186/s12967-020-02534-2
14. Martina BE, Haagmans BL, Kuiken T, Fouchier RA, Rimmelzwaan GF, Van Amerongen G, et al. Virology: SARS virus infection of cats and ferrets. Nature. 2003;425:915. https://doi.org/10.1038/425915a

Address for correspondence: Barbara Colitti, University of Turin, Largo Paolo Braccini 2, 10095 Grugliasco, Turin, Italy; email: barbara.colitti@unito.it

Autochthonous *Thelazia callipaeda* Infection in Dog, New York, USA, 2020

A.B. Schwartz,[1] Manigandan Lejeune,[1] Guilherme G. Verocai, Rebecca Young, Paul H. Schwartz

We report a case of autochthonous infection of the eye worm *Thelazia callipaeda* in a dog in the northeastern United States. Integrated morphologic identification and molecular diagnosis confirmed the species. Phylogenetic analysis suggested introduction from Europe. The zoonotic potential of this parasite warrants broader surveillance and increased awareness among physicians and veterinarians.

Thelaziasis in dogs can be caused by 2 nematodes of the genus *Thelazia* (Nematoda: Spirurida): *T. callipaeda* and *T. californiensis* (*1*). The oriental eye worm (*T. callipaeda*) is a helminth that infects a variety of domestic and wild carnivores, lagomorphs, rodents, and primates (including humans) across Eurasia (*2*,*3*). In Europe, the *T. callipaeda* eye worm is an emergent vectorborne helminth that has spread steadily across all countries over the past 3 decades (*2*). The California eye worm (*T. californiensis*) has been reportedly found in wild and domestic carnivores, ungulates, lagomorphs, and humans; its range is limited to the western United States (*4*). Zoonotic infection of humans with a third species of eye worm (*T. gulosa*), which infects cattle, has recently been reported in the western United States (*5*). These 3 species of *Thelazia* eye worm with zoonotic potential are morphologically and biologically distinct (*1*,*5*,*6*).

Thelazia nematodes are found in the conjunctival recesses of the eye (*1*). Secretophagous dipteran intermediate hosts (*1*,*7*) ingest first-stage larvae (L1) while feeding from the definitive host's eyes. After metamorphosis, infective third-stage larvae (L3) are passed via the labelum onto the conjunctiva of another suitable host. L3 develop into adults that migrate to the conjunctival recess, lacrimal ducts, or both, resulting in conjunctivitis, ocular discharge, and blepharospasm. Female worms release more L1, seeding ocular secretions of the host, and conclude the life cycle (*1*,*2*). Intermediate hosts for *Thelazia* nematodes are dipteran flies of the genera *Phortica* for *T. callipaeda, Fannia* for *T. californiensis*, and *Musca* for *T. gulosa* (*1*,*5*,*7*,*8*). *P. variegata* fruit flies are widely distributed across Eurasia and have been found in multiple areas in the eastern United States (*9*). In North America, they have been experimentally proven to be competent vectors for *T. callipaeda* worms (*10*), supporting the potential occurrence of *T. callipaeda* infection in the United States (*2*). We report *T. callipaeda* eye worm infection detected in a dog in the Western Hemisphere in November 2020.

The Case

The patient was a 7.5-year-old Labrador retriever, with no relevant medical history. The dog routinely received heartworm preventive (Heartgard; Boehringer Ingelheim Pharmaceuticals, Inc., https://www.boehringer-ingelheim.com) and flea and tick preventive (NexGard [Boehringer Ingelheim Pharmaceuticals, Inc.] and Vectra [Ceva Animal Health, https://www.ceva.us]) in accordance with recommended dosing and had never traveled beyond Dutchess County, New York, USA. The dog was taken to a veterinarian because of a 3-week history of unilateral epiphora and blepharospasm. Treatment with an ophthalmic preparation (neomycin, polymyxin B, and dexamethasone) produced no demonstrable response. Subsequent nasolacrimal duct flushing with 0.3% gentamicin sulfate and 0.2% dexamethasone in physiological saline solution, followed by 100 μg/

Author affiliations: Marist College, Poughkeepsie, New York, USA (A.B. Schwartz); Animal College of Veterinary Medicine at Cornell University, Ithaca, New York, USA (M. Lejeune, R. Young); Texas A&M University College of Veterinary Medicine and Biological Sciences, College Station, Texas, USA (G.G. Verocai); Center for Veterinary Care Millbrook, PC, Millbrook, New York, USA (P.H. Schwartz)

DOI: https://doi.org/10.3201/eid2707.210019

[1]These authors contributed equally to this article.

mL ivermectin in physiological saline solution, led to recovery of 12 nematodes. After systemic ivermectin administration, no recurrence has been noted.

Four nematodes (3 female, 1 male) were morphologically identified as *T. callipaeda* eye worms on the basis of the cuticular transverse striations (CTS) pattern and vulva position (*1*,*6*). The 3 female worms were 12.7–13.9 mm long and 314–360 μm wide. The vulval opening was anterior to the esophageal intestinal junction, and in 1 specimen it was 610.86 μm from the cephalic end. The midbodies contained 150–190 CTS/mm, and the cephalic/caudal region contained 220–240 CTS/mm. The buccal capsule was wider than it was deep. Two protruding phasmids were visible at the tip of the tail, which did not taper unilaterally (Figure 1). The male worm was 8.9 mm long, and its width was not measured. The cephalic region contained 310 CTS/mm, and the midbody/caudal region contained 170 CTS/mm. The small spicules measured 147.73 μm; the large spicules, 1721.90 μm.

We subjected a female worm to DNA extraction and multilocus PCR (18S rRNA, 12S rRNA, and cytochrome oxidase c subunit 1 [*cox1*] gene markers) by using assays described previously (*4*,*11*), followed by sequencing. The partial sequences generated for 18S rRNA matched 99.7%, 12S rRNA 99.4%, and *cox1* genes 93.3%–100% of the corresponding genes of *T. callipaeda* worms in GenBank. We deposited the generated sequences in GenBank (accession no. MW570771 for 18S rRNA, MW575766 for 12S rRNA, and MW570733 for *cox1*). Molecular data unequivocally confirmed the parasite as *T. callipaeda*. Phylogenetic analysis of the *cox1* gene showed that the *T. callipaeda* eye worm found in North America belongs to the haplotype-1 prevalent in Europe (100% maximum identity), suggesting a possible source of introduction (Figure 2).

Conclusions

The discovery of an autochthonous case of *T. callipaeda* eye worm infection in the United States suggests its introduction and establishment on a continent where natural infection has not been documented. The report on the distribution of *P. variegata* fruit flies in the eastern United States and their competence for *T. callipaeda* eye worms has raised concern for eye worm infections in animals and humans in this region (*10*). Our finding is in line with previous predictions. Active surveillance of all susceptible hosts, coupled with ecologic niche modeling as conducted in Europe, can help gauge the extent of *T. callipaeda* eye worm spread in North America (*7*). Our findings should bring awareness about this invasive, zoonotic parasite to veterinary and medical ophthalmologists in the Americas. To curtail the potential spread in the United States, consideration should be given to US Department of Agriculture–imposed

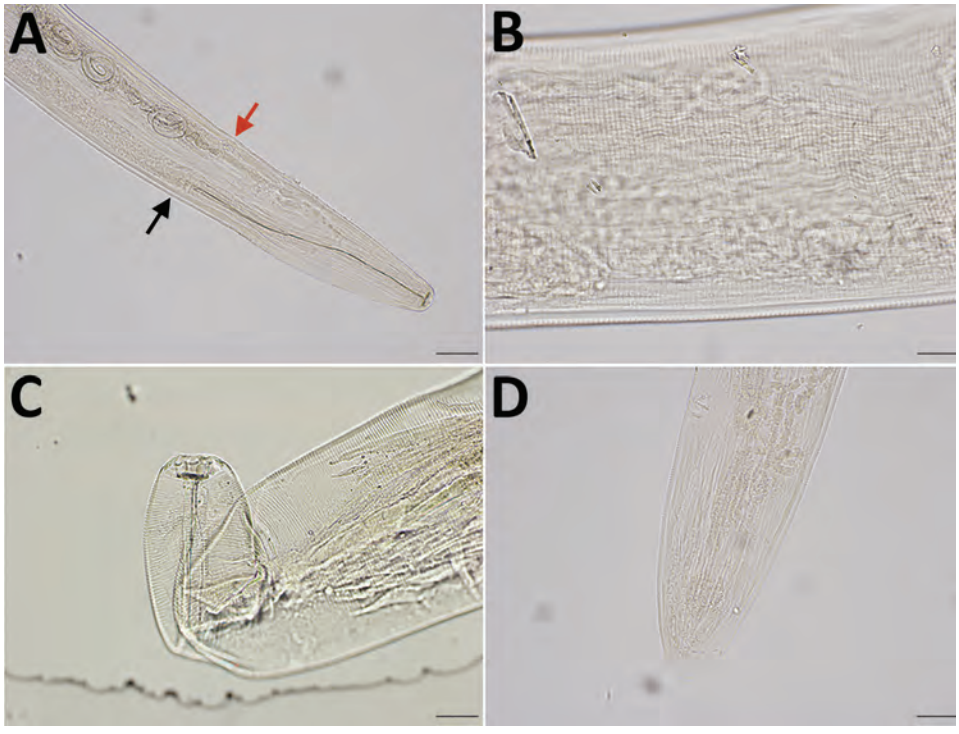

Figure 1. Integrated diagnostic approach for confirming *Thelazia callipaeda* nematodes: morphologic identification. Specimens were cleared in lactophenol before examination under an Olympus compound microscope (BX53) (https://www.olympus-lifescience.com). Images were taken with an Olympus DP73 camera, and morphometry was performed by using Olympus cellSens software. A) Cephalic end of a female worm. Black arrow indicates esophageal intestinal junction; red arrow indicates vulval opening. Original magnification ×100. B) Transverse striations (150–190/mm) in the cuticle of midbody region of a female worm. Original magnification ×200. C) Buccal cavity of a female worm, wider than deep. Note tightly spaced cuticular striations in the cephalic end. Original magnification ×200. D) Caudal end of female worm with protruding phasmids in the tip. The tail was not protruding unilaterally. Original magnification ×100.

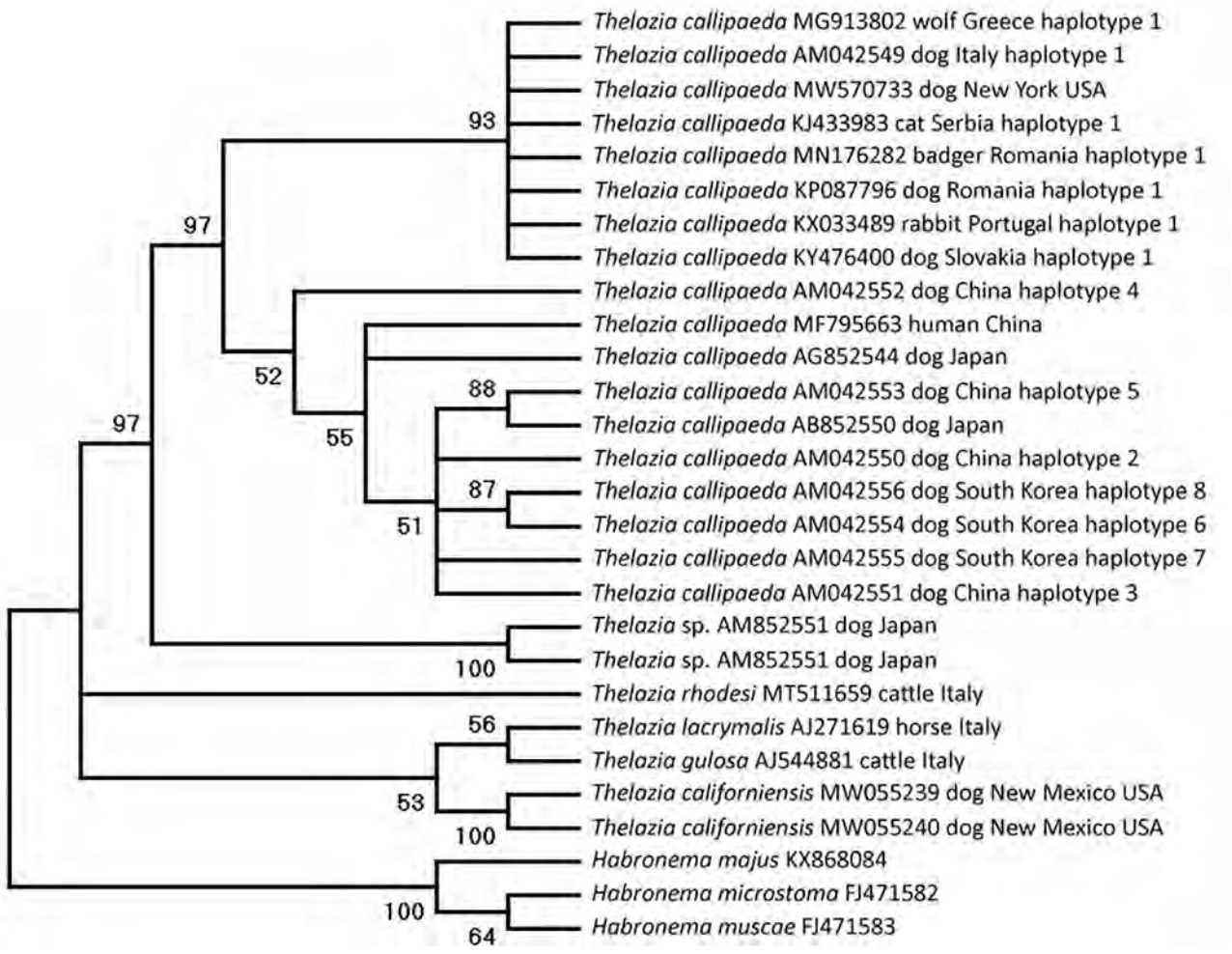

Figure 2. Phylogenetic relationship based on cytochrome oxidase c subunit 1 gene of *Thalazia callipaeda* nematode isolate from a dog in Dutchess County, New York, USA, 2020 (GenBank accession no. MW570733), and other related *Thelazia* species available in GenBank (accession numbers shown). Analysis was performed by using MEGAX (http://www.megasoftware.net) and the maximum-likelihood method, 1,000 bootstrap replicates; nodes with <50% support were condensed.

requirements for implementing broad and accurate parasite diagnostic methods and prophylactic anthelmintic treatment to mitigate the introduction of exotic parasites before relevant species are imported. The One Health model of cooperation among veterinarians, wildlife biologists, and physicians is vital for assessing the current distribution and mitigating the spread of this multihost parasite with zoonotic potential. As this case shows, emergence of *T. callipaeda* parasites requires increased awareness by both human medical and veterinary professionals.

Acknowledgments

We thank Caroline Sobotyk de Oliveira for her assistance depositing DNA sequences in GenBank, Domenico Otranto for his assistance with elucidating the potential extension of this emergent disease, and Antech Diagnostics for sharing information about cases of *Thelazia* infection identified in their laboratory.

About the Author

Ms. A.B. Schwartz is a graduate of Marist College with an interest in biopharmaceutical development; she will begin a master's degree in Public Health at Georgetown University in the fall of 2021.

References

1. Naem S. *Thelazia* species and conjunctivitis. In: Z. Pelikan, editor. Conjunctivitis—A Complex and Multifaceted Disorder. Rijeka (Croatia): Intech Open Access Press; 2011. p. 201–32.
2. Otranto D, Mendoza-Roldan JA, Dantas-Torres F. *Thelazia callipaeda*. Trends Parasitol. 2021;37:263–4. https://doi.org/10.1016/j.pt.2020.04.013

3. Otranto D, Traversa D. *Thelazia* eyeworm: an original endo- and ecto-parasitic nematode. Trends Parasitol. 2005;21:1–4. https://doi.org/10.1016/j.pt.2004.10.008
4. Sobotyk C, Foster T, Callahan RT, McLean NJ, Verocai GG. Zoonotic *Thelazia californiensis* in dogs from New Mexico, USA, and a review of North American cases in animals and humans. Vet Parasitol Reg Stud Rep. 2021;24:100553. https://doi.org/10.1016/j.vprsr.2021.100553
5. Bradbury RS, Gustafson DT, Sapp SGH, Fox M, de Almeida M, Boyce M, et al. A second case of human conjunctival infestation with *Thelazia gulosa* and a review of *T. gulosa* in North America. Clin Infect Dis. 2020;70:518–20.
6. Kofoid CA, Williams OL. The nematode *Thelazia californiensis* as a parasite of the eye of man in California. Arch Ophthalmol. 1935;13:176–80. https://doi.org/10.1001/archopht.1935.00840020036002
7. Otranto D, Brianti E, Cantacessi C, Lia RP, Máca J. The zoophilic fruitfly *Phortica variegata*: morphology, ecology and biological niche. Med Vet Entomol. 2006;20:358–64. https://doi.org/10.1111/j.1365-2915.2006.00643.x
8. Otranto D, Cantacessi C, Testini G, Lia RP. *Phortica variegata* as an intermediate host of *Thelazia callipaeda* under natural conditions: evidence for pathogen transmission by a male arthropod vector. Int J Parasitol. 2006;36:1167–73. https://doi.org/10.1016/j.ijpara.2006.06.006
9. Werner T, Jaenike J. The encyclopedia of north american drosophilids: drosophilids of the midwest and northeast, 2017 [cited 2021 May 10]. https://digitalcommons.mtu.edu/cgi/viewcontent.cgi?article=1000&context=oabooks
10. Otranto D, Iatta R, Lia RP, Cavalera MA, Màca J, Pombi M, et al. Competence of *Phortica variegata* from the United States as an intermediate host of the *Thelazia callipaeda* eyeworm. Am J Trop Med Hyg. 2018;98:1175–8. https://doi.org/10.4269/ajtmh.17-0956
11. Floyd RM, Rogers AD, Lambshead PJD, Smith CR. Nematode specific PCR primers for the 18S small subunit rRNA gene. Mol Ecol Notes. 2005;5:611–2. https://doi.org/10.1111/j.1471-8286.2005.01009.x

Address for correspondence: Paul H. Schwartz and A.B. Schwartz, Center for Veterinary Care Millbrook, PC, PO Box 518, Millbrook, NY 122545, USA: email: cvcroute343@gmail.com and alex.barnes.schwartz@gmail.com or hvsevc@gmail.com

COVID-19 Outbreak on a Passenger Ship and Assessment of Response Measures, Greece, 2020

Sophia Hatzianastasiou,[1] Varvara A. Mouchtouri,[1] Androula Pavli, Maria Tseroni, Spyros Sapounas, Charalampos Vasileiou, Katerina Dadouli, Maria Kyritsi, Michalis Koureas, Panagiotis Prezerakos, Matthaios Speletas, Georgios Panagiotakopoulos, Sotirios Tsiodras,[2] Christos Hadjichristodoulou[2]

We describe response measures to an outbreak involving 128 (33.4%) coronavirus disease cases (46.1% asymptomatic) among 383 persons onboard a passenger ship. Multivariate analysis indicated that dining in certain rooms and bar areas, nationality, working department (for crew members), and quarantining onboard the ship were significantly associated with infection.

On March 7, 2020, a passenger ship (2,500-passenger and 1,606-bed capacity) with 33 crew members sailed from Piraeus, Greece, to Cesme, Turkey, where an additional 350 crew members embarked on March 8, 2020 (*1*). For 21 days, the ship sailed without any disembarkations or embarkations until the first suspected coronavirus disease (COVID-19) case was reported to the health authority of the Piraeus port on March 28, 2020. We describe results of the outbreak investigation, including risk factors for transmission of severe acute respiratory syndrome coronavirus 2 (SARS-CoV-2).

The Study

We collected data by completing standardized forms through interviews and medical examination of all travelers onboard and by reviewing the ship records and logs. We used descriptive statistics to analyze the study variables and performed univariate and multivariate analyses.

In conducting clinical management of cases, we followed guidelines from the Hellenic National Public Health Organization (NPHO) for health measures on travelers and repatriation, which were based on the European Union Healthy Gateways Joint Action advice for management of COVID-19 cases onboard ships (*2*) (Appendix Table 1, https://wwwnc.cdc.gov/EID/article/27/7/21-0398-App1.pdf). NPHO and the Piraeus Port Health Authority provided passengers with information about using medical facemasks at all times when outside of their cabins, as well as handwashing, physical distancing, and cleaning and disinfecting cabins; ship officers supervised.

Food preparation and laundry and cleaning services were halted; travelers were instructed to clean their own cabins and store used linens in plastic bags. Cleaning and disinfection of the terminal was done by a private company under supervision of the Piraeus Port Health Authority, after all travelers disembarked the ship at the port of Piraeus. A catering company provided packaged meals; personal hygiene supplies were also provided (including facemasks and hand sanitizer). Methods and results of the environmental sampling have been published elsewhere (*3*).

We collected oropharyngeal specimens from all travelers onboard. Molecular tests for SARS-CoV-2 detection were performed by using the Cobas SARS-CoV-2 test qualitative assay and the Cobas 6800/8800 System (La Roche, https://www.roche.com). Serologic tests were performed on blood

Author affiliations: Hellenic National Public Health Organization, Athens, Greece (S. Hatzianastasiou, A. Pavli, M. Tseroni, S. Sapounas, G. Panagiotakopoulos); University of Thessaly Faculty of Medicine, Larisa, Greece (V.A. Mouchtouri, K. Dadouli, M. Kyritsi, M. Koureas, M. Speletas, C. Hadjichristodoulou); European Union Healthy Gateways Joint Action, Larisa (V.A. Mouchtouri, C. Hadjichristodoulou); Department of Hygiene Inspections of the Port of Piraeus, Region of Attica, Athens (C. Vasileiou); University of Peloponnese Department of Nursing, Tripoli, Greece (P. Prezerakos); University of Patras Faculty of Medicine, Patra, Greece (G. Panagiotakopoulos); National and Kapodistrian University Medical School, Athens (S. Tsiodras)

DOI: https://doi.org/10.3201/eid2707.210398

[1]These first authors contributed equally to this article.

[2]These senior authors contributed equally to this article..

specimens collected from 116 cases. Serum samples were initially tested with the Xiamen Boson Biotech (https://www.bosonbio.com) Rapid 2019-nCoV IgG/IgM Combo Test Card, a rapid lateral flow (immunochromatographic) test, and subsequently with the MAGLUMI800 chemiluminescence immunoassay (Snibe Diagnostic, https://www.snibe.com).

Our study was a public health response as part of activities of the Hellenic NPHO and local authorities (i.e., Piraeus Port Health Authority and Port Administration). Participants provided verbal informed consent for recording and processing of information during interviews, and written consent was obtained from participants for blood specimen analysis. All required ethics considerations were applied according to rules of the Hellenic NPHO and the Ministry of Health.

The first 3 symptomatic cases occurred on March 20 among travelers (passengers and crew) of different nationalities and working departments (hotel, dining room service, and housekeeping [cabin steward]). The peak of the outbreak occurred during March 30–April 1 (Figure). We conducted laboratory tests for SARS-CoV-2 and for antibodies during 3 follow-up examinations (Appendix Table 2).

Travelers who tested positive were isolated onboard (except the first case-patients, who were hospitalized, and 2 travelers who were isolated in hotels designated by the government of Greece for that purpose). All travelers onboard who tested negative were considered contacts and quarantined individually in quarantine facilities ashore (hotels designated by the government of Greece), except 36 crew members who tested negative but quarantined in separate decks and facilities onboard to ensure safe ship operation. We compiled characteristics of travelers, hospitalizations, and quarantine measures (Appendix Table 2), symptom frequency (Appendix Table 3), and results of univariate analysis for testing risk factors (Appendix Table 4). No deaths occurred; 7 patients were hospitalized, including the first patient, who was intubated.

We conducted multivariate analysis, in the form of binary logistic regression, using SPSS 25.0 (IBM, https://www.ibm.com). For all analyses, we used a 5% significance level. Multivariate analysis results indicated that test-negative travelers quarantined at hotels had lower odds of SARS-CoV-2 infection than those who quarantined onboard the ship (odds ratio 0.07, 95% CI 0.01–0.58). Travelers of nationality A who worked in the entertainment department had higher odds of infection (odds ratio 3.54, 95% CI 1.03–12.16). Multivariate analysis indicated that dining in certain rooms and bar areas, nationality, working department (for crew members), and quarantine onboard the ship significantly associated with infection (Table).

Conclusions

Our findings can be used in COVID-19 prevention and control preparedness plans for ports and ships. Ongoing transmission can occur onboard ships, affecting a large number of travelers, without any sign of symptoms for an extended period, especially in cases where most of the travelers are of young age. Assuming a serial interval number of 5 days and a reproduction number of 2.6, we could conclude that 1 infectious traveler embarked on the first or second day of the voyage, and 21 days later 120 travelers on board had been infected (*4*,*5*).

Active or passive surveillance for COVID-19 based on symptoms onboard ships alone cannot

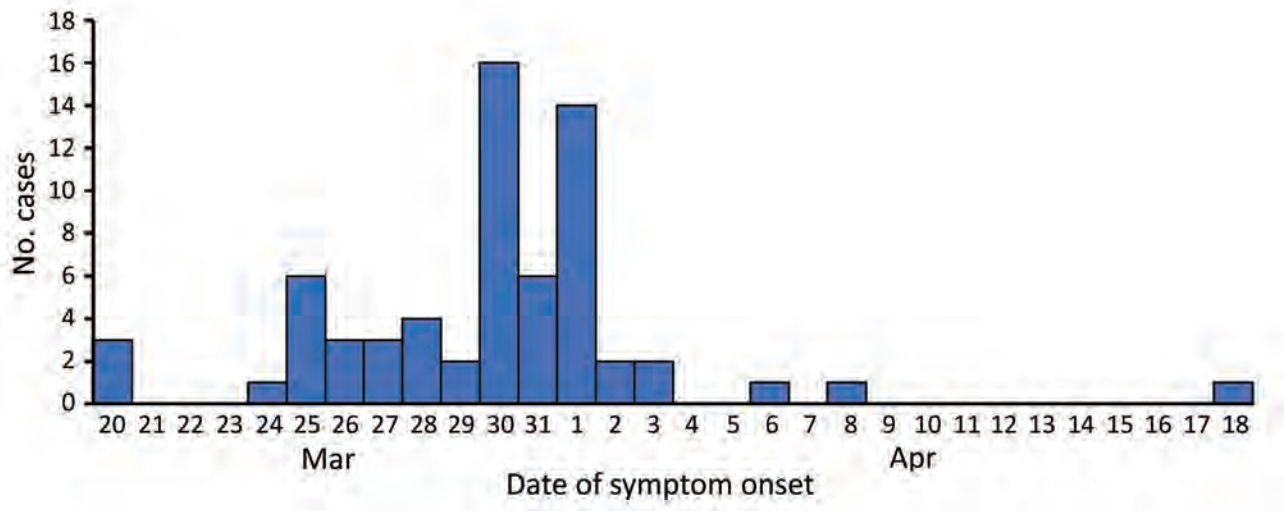

Figure. Epidemic curve for symptomatic coronavirus disease case-patients, by date of symptom onset, during an outbreak on a passenger ship, Greece, March 20–April 18, 2020. A total of 65 case-patients had a known date of symptom onset.

Table. Multivariate analysis of risk factors for SARS-CoV-2 infection during an outbreak on a passenger ship, Greece, March 20–April 18, 2020*

Factor	Area of work (for crew members)			Consuming meals and drinks in galley/dining area/bar A‡
	Food and beverage	Housekeeping and hotel	Other†	
Nationality				
A			Referent	
B	0.00 (0.00–0.00)	NA	NA	NA
C	1.20 (0.51–2.81)	**0.11 (0.02–0.75)**	**0.03 (0.002–0.42)**	**0.49 (0.24–0.99)**
D	0.81 (0.36–1.83)	0.23 (0.05–1.14)	NA	0.54 (0.27–1.08)
E	0.90 (0.25–3.21)	0.96 (0.10–9.27)	NA	0.94 (0.32–2.78)
Other†	1.51 (0.41–5.62)	1.02 (0.14–7.20)	0.22 (0.02–2.98)	1.52 (0.59–3.91)
Consuming meals and drinks in galley/dining area/bar A‡				
	Referent	**2.71 (1.34–5.46)**	**4.44 (1.81–10.95)**	NA

*A total of 120 passengers and crew tested positive during the first specimen collection and testing. Values in bold type are statistically significant. SARS-CoV-2, severe acute respiratory syndrome coronavirus 2; NA, not applicable.
†Entertainment, security, shop, hospital, other.
‡Meals and beverages were prepared and served in galley and dining room and café-bar A (for travelers who embarked at Cesme port) and in galley and dining room and café-bar B (for travelers who embarked at Piraeus port).

be effective for early COVID-19 outbreak detection because only a small proportion of cases can be identified when the disease has already spread widely. Screening of incoming travelers and preboarding and regular routine laboratory testing can be implemented in addition to surveillance (*6*). We advise laboratory diagnostic testing of passengers and crew for SARS-CoV-2 within 72 hours before embarkation and a second test the day of embarkation. In addition, for crew members, we advise a 10-day quarantine period before starting work and regular testing of all crew members on board every 7 days. The preparedness plans of ships and ports should ensure laboratory capacity for diagnosis of all persons onboard once an outbreak has been identified and frequent and regular testing until negative results are obtained in accordance with port policies (*7*).

Because of the large proportion of travelers who tested positive in this outbreak, the relevant authorities decided that COVID-19 case-patients would be isolated onboard the ship, whereas travelers who tested negative would disembark and quarantine individually in hotels. Individual quarantine and isolation in separate facilities was effective in preventing further spread (*2*,*6*,*8*–*11*). These measures contributed to preventing intra-cabin transmission, which was documented in other COVID-19 outbreaks onboard passenger ships (*12*,*13*). Halting food preparation and service, housekeeping activities in cabins, and laundry service stopped transmission onboard. This outcome is contrary to the outbreak management approach taken onboard another cruise ship, where crew continued working duties while passengers and crew were isolated in their cabins, resulting in further COVID-19 spread (*11*). In our study, logistic regression statistical analysis showed that quarantining travelers in hotels was a protective factor against SARS-CoV-2 infection compared with quarantining onboard the ship.

Crew members who worked in the entertainment department, were of a certain nationality, and consumed meals and drinks at specific dining and bar areas had a higher risk for infection. Dining areas and bars can be settings for COVID-19 transmission because of congregation of persons and because facemasks are not used while eating or drinking (*13*). Avoiding self-service, encouraging service of meals in cabins, staggering meal times, and reconfiguring dining room seating to ensure physical distancing are recommended to avoid possible transmission within ships' dining rooms (*2*,*11*,*14*).

A coordinated approach from a country's central government, in cooperation with local port authorities, is needed to define the maximum response capacities of each port and the maximum number of ships that can be allowed to call. This approach will help to avoid confining travelers on ships for quarantine and isolation and reduce the risk for spread onboard when outbreaks occur, in line with the World Health Organization's International Health Regulations, which are designed to prevent unnecessary interference with international traffic and trade (*7*).

Acknowledgments

We acknowledge the contribution of the Ministry of Health's COVID-19 Taskforce, the Ministry of Shipping and Island Policy, the Hellenic National Public Health Organization, the General Secretariat for Civil Protection; the National Center for Blood Donation in Athens, the Laboratory of Hygiene and Epidemiology of the University of Thessaly, the Department of Hygiene Inspections of the Port of Piraeus, Region of Attica, Athens, the custom authorities, and the Piraeus Port Authority. Moreover, we thank the ship medical doctor and all ship officers and crew members for their contribution.

About the Author

Dr. Hatzianastasiou is an internal medicine and infectious disease physician who works for the Department of Travel Medicine of the Hellenic National Public Health Organization. Her primary research interests include travel medicine. Dr. Mouchtouri is associate professor in the Department of Hygiene and Epidemiology of the University of Thessaly's Faculty of Medicine. She works for the European Union's Healthy Gateways Joint Action. Her primary research interests include the prevention and control of cross-border health threats.

References

1. MarineTraffic. 2021. Eleftherios Venizelos travel information [in Greek] [cited 2021 Mar 1]. https://www.marinetraffic.com/el/ais/details/ships/shipid:208272/mmsi:237628000/imo:7907673/vessel:el_venizelos
2. European Union Health Gateways. Advice for ship operators for preparedness and response to the outbreak of COVID-19. 2020 Feb 20 [cited 2021 Mar 1]. https://www.healthygateways.eu/Portals/0/plcdocs/EU_HEALTHY_GATEWAYS_COVID-19_MARITIME_20_2_2020_FINAL.pdf
3. Mouchtouri VA, Koureas M, Kyritsi M, Vontas A, Kourentis L, Sapounas S, et al. Environmental contamination of SARS-CoV-2 on surfaces, air-conditioner and ventilation systems. Int J Hyg Environ Health. 2020;230:113599. https://doi.org/10.1016/j.ijheh.2020.113599
4. Du Z, Xu X, Wu Y, Wang L, Cowling BJ, Meyers LA. Serial interval of COVID-19 among publicly reported confirmed cases. Emerg Infect Dis. 2020;26:1341–3. https://doi.org/10.3201/eid2606.200357
5. Zhang S, Diao M, Yu W, Pei L, Lin Z, Chen D. Estimation of the reproductive number of novel coronavirus (COVID-19) and the probable outbreak size on the Diamond Princess cruise ship: a data-driven analysis. Int J Infect Dis. 2020;93:201–4. https://doi.org/10.1016/j.ijid.2020.02.033
6. European Union Health Gateways. Interim advice for restarting cruise ship operations after lifting restrictive measures in response to the COVID-19 pandemic. 2020 Jun 30 [cited 2021 Mar 1]. https://www.healthygateways.eu/Portals/0/plcdocs/EU_HEALTHY_GATEWAYS_COVID-19_RESTARTING_CRUISES.pdf
7. World Health Organization. International Health Regulations [cited 2021 Mar 1]. https://www.who.int/health-topics/international-health-regulations
8. Rocklöv J, Sjödin H, Wilder-Smith A. COVID-19 outbreak on the Diamond Princess cruise ship: estimating the epidemic potential and effectiveness of public health countermeasures. J Travel Med. 2020;27:27. https://doi.org/10.1093/jtm/taaa030
9. Gupta A, Kunte R, Goyal N, Ray S, Singh K. A comparative analysis of control measures on-board ship against COVID-19 and similar novel viral respiratory disease outbreak: quarantine ship or disembark suspects? Med J Armed Forces India. 2020. https://doi.org/10.1016/j.mjafi.2020.06.003
10. Mouchtouri VA, Dirksen-Fischer M, Hadjichristodoulou C. Health measures to travellers and cruise ships in response to COVID-19. J Travel Med. 2020;27:27. https://doi.org/10.1093/jtm/taaa043
11. World Health Organization. Interim guidance for operational considerations for managing COVID-19 cases/outbreak on board ships 2020 [cited 2021 Mar 1]. https://www.who.int/publications-detail/operational-considerations-for-managing-covid-19-cases-outbreak-on-board-ships.
12. Plucinski MM, Wallace M, Uehara A, Kurbatova EV, Tobolowsky FA, Schneider ZD, et al. COVID-19 in Americans aboard the Diamond Princess cruise ship. Clin Infect Dis. 2020;ciaa1180. https://doi.org/10.1093/cid/ciaa1180
13. Kakimoto K, Kamiya H, Yamagishi T, Matsui T, Suzuki M, Wakita T. Initial investigation of transmission of COVID-19 among crew members during quarantine of a cruise ship—Yokohama, Japan, February 2020. MMWR Morb Mortal Wkly Rep. 2020;69:312–3. https://doi.org/10.15585/mmwr.mm6911e2
14. Centers for Disease Control and Prevention. Interim guidance for ships on managing suspected or confirmed cases of coronavirus disease 2019 (COVID-19) 2021 [cited 2021 Mar 1]. https://www.cdc.gov/quarantine/maritime/recommendations-for-ships.html

Address for correspondence: Christos Hadjichristodoulou, Laboratory of Hygiene and Epidemiology, Faculty of Medicine, University of Thessaly, 22 Papakyriazi St, 41222, Larissa, Greece; email: xhatzi@uth.gr

Emergence of SARS-CoV-2 B.1.1.7 Lineage at Outpatient Testing Site, Berlin, Germany, January–March 2021

Welmoed van Loon, Heike Rössig, Susen Burock, Jörg Hofmann, Julian Bernhard, Elisabeth Linzbach, Domenika Pettenkofer, Christian Schönfeld, Maximilian Gertler, Joachim Seybold, Tobias Kurth, Frank P. Mockenhaupt

Within 5 weeks in 2021, B.1.1.7 became the dominant severe acute respiratory syndrome coronavirus 2 lineage at an outpatient testing site in Berlin, Germany. Compared with outpatients with wild-type virus infection, patients with B.1.1.7 had similar cycle threshold values, more frequent sore throat and travel history, and less frequent anosmia/ageusia.

Severe acute respiratory syndrome coronavirus 2 (SARS-CoV-2) B.1.1.7 lineage (variant of concern [VOC] 202012/01 or 20I/501Y.V1) likely emerged during autumn 2020 in the United Kingdom and quickly became dominant there (E. Volz et al., unpub. data, https://www.medrxiv.org/content/10.1101/2020.12.30.20249034v2). B.1.1.7 carries multiple mutations and deletions, including 501Y and deletion ΔH69/ΔV70 (del69–70) in the spike protein. B.1.1.7 reportedly exhibits greater transmissibility and fatality in the community than non-VOC lineages (hereafter referred to as wild-type virus) (*1*; E. Volz et al., unpub. data). However, increased deaths were not seen in hospitalized patients (*2*).

The first patient infected with B.1.1.7 at the outpatient SARS-CoV-2 testing site of Charité–Universitätsmedizin Berlin was identified on January 18, 2021. We describe lineage prevalence over time and demographic and clinical characteristics in outpatients with B.1.1.7 or wild-type virus who sought care during January–March 2021. Ethics approval was obtained from Charité's Institutional Review Board (EA4/083/20).

Author affiliations: Charité–Universitätsmedizin Berlin, Berlin, Germany (W. van Loon, H. Rössig, S. Burock, J. Bernhard, E. Linzbach, D. Pettenkofer, C. Schönfeld, M. Gertler, J. Seybold, T. Kurth, F.P. Mockenhaupt); Labor Berlin–Charité Vivantes GmbH, Berlin (J. Hofmann)

DOI: https://doi.org/10.3201/eid2707.210845

The Study

Details of the testing site have been described (*3*). Physicians interviewed patients about demographics, medical history, and symptoms. If indicated, a combined oro-nasopharyngeal swab specimen was collected. Specimens were tested by using the cobas 6800/8800 assay (Roche Diagnostics, https://diagnostics.roche.com), targeting open reading frame 1ab and the envelope gene (*4*). All positive samples were typed for the N501Y and del69–70 polymorphisms by melting curve analysis. Variants including both polymorphisms were considered B.1.1.7.

During January 18–March 29, 2021, a total of 349 SARS-CoV-2–positive patients were seen at the testing site, and the proportion of B.1.1.7 increased from 2% to >90% (Figure 1). In total, 35.8% (125/349) of samples belonged to the wild-type lineage, 57.0% (199/349) were B.1.1.7, and 7.2% (25/349) were other non–wild-type variants (non-VOCs).

Six patients previously had received ≥1 SARS-CoV-2 vaccinations; all were infected with B.1.1.7 but were excluded from analysis because vaccination could interfere with viral dynamics and clinical manifestation (Appendix Table, https://wwwnc.cdc.gov/EID/article/27/7/21-0845-App1.pdf). We excluded patients carrying lineages other than wild-type or B.1.1.7. Half of the patients were female (49%); mean age was 36 (SD ±15) years. Almost all (97%) reported symptoms. Median symptom duration until testing was 3 (interquartile range 2–4) days. Symptoms were fatigue (72%), headache (69%), and muscle ache (60%). Fifteen percent reported travel outside Berlin in the previous 14 days,

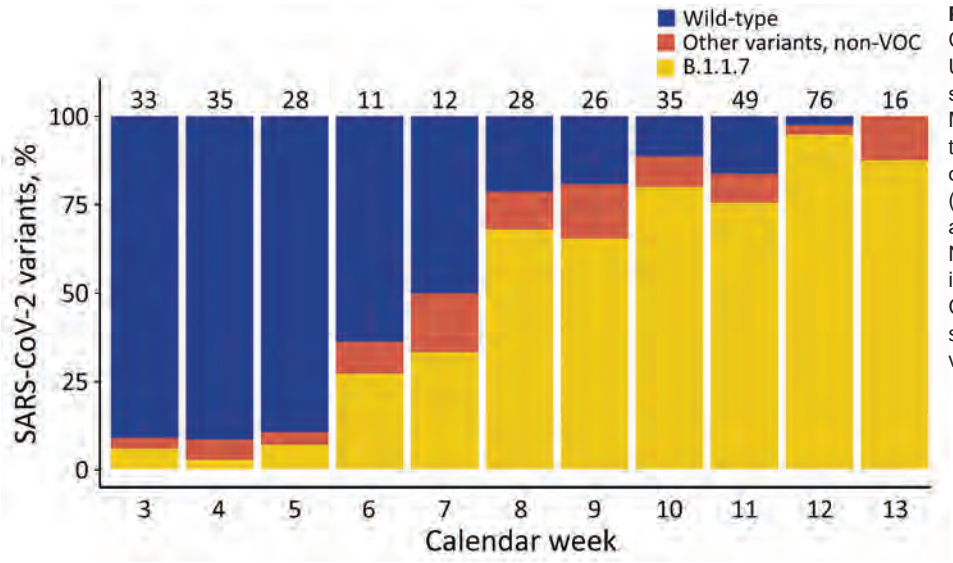

Figure 1. Proportion of SARS-CoV-2 lineages at the Charité–Universitätsmedizin Berlin testing site, Berlin, Germany, January–March 2021. The numbers on top of the bars indicate the total number of positive SARS-CoV-2 tests. Six (partially) vaccinated outpatients are included for completeness. Note that calendar week 13 only includes 1 day (March 29). SARS-CoV-2, severe acute respiratory syndrome coronavirus 2; VOC, variant of concern.

and half (49%) reported contact with a SARS-CoV-2–positive person (Table).

Most assessed characteristics did not substantially differ between patients with wild-type or B.1.1.7, including age, sex, leading symptoms, symptom duration, contact with a SARS-CoV-2–positive person, and time passed since contact (Table). However, B.1.1.7 patients had traveled more frequently than those with the wild-type strain (19% vs. 10%). Patients with B.1.1.7 more often reported sore throat than did patients with wild-type virus (54% vs. 42%) but less frequently reported anosmia or ageusia (24% vs. 38%) (Table).

Table. Characteristics of severe acute respiratory syndrome coronavirus 2–positive outpatients attending the Charité–Universitätsmedizin Berlin testing site, by lineages, Germany, January–March 2021*

Characteristic	Wild-type lineage	B.1.1.7 variant	OR (95% CI)
Total no.	125	193	NA
Sex			
M	69 (55.2)	94 (49.0)	
F	56 (44.8)	98 (51.0)	1.3 (0.8–2.0)
Mean age, y (±SD)	36.6 (±13.8)	34.8 (±15.9)	1.8 (−1.5 to 5.1)†
Any symptoms	122 (97.6)	186 (96.4)	0.7 (0.2–2.6)
Self-reported fever in previous 48 h	48 (38.4)	82 (42.5)	1.2 (0.8–1.9)
Median self-reported temperature in case of fever, °C (±SD)	38.3 (±0.6)	38.2 (±0.7)	0.1 (−0.2 to 0.4)§
Shortness of breath	12 (9.6)	26 (13.5)	1.5 (0.7–3.0)
Fatigue	92 (73.6)	138 (71.5)	0.9 (0.5–1.5)
Chest pain	3 (2.4)	2 (1.0)	0.4 (0.1–2.6)
Diarrhea	19 (15.2)	24 (12.4)	0.8 (0.4–1.5)
Anosmia or ageusia (loss of smell or taste)	47 (37.6)	46 (23.8)	0.5 (0.3–0.9)
Muscle aches	75 (60.0)	116 (60.1)	1.0 (0.6–1.6)
Sore throat	52 (41.6)	104 (53.9)	1.6 (1.0–2.6)
Cough	61 (48.8)	98 (50.8)	1.1 (0.7–1.7)
Headache	86 (68.8)	133 (68.9)	1.0 (0.6–1.6)
Chills	44 (35.2)	67 (34.7)	1.0 (0.6–1.6)
Rhinorrhea	76 (60.8)	102 (52.8)	0.7 (0.5–1.1)
Median duration of symptoms upon test, d (25%–75% quantile)	3.0 (2.0–4.8)	3.0 (2.0–4.0)	0.0 (−1.0 to 0.0)§
Contact with person with confirmed SARS-CoV-2 infection	60 (48.0)	97 (50.3)	1.1 (0.7–1.7)
Median time between contact with person with confirmed SARS-CoV-2 infection and test, d (25%–75% quantile)	4.0 (1.2–7.0)	4.0 (1.0–6.0)	0.0 (−1.5 to 3.0)‡
Travel outside Berlin region in previous 14 d	12 (9.6)	36 (18.7)	2.2 (1.1–4.3)
Median C_t value (25%–75% quantile)	20.2 (17.4–24.1)	20.1 (17.1–22.8)	0.1 (−0.9 to 1.6)‡
Symptom duration <7 d, no. patients (median C_t value [25%–75% quantile])	113 (19.9 [17.4–23.5])	171 (19.5 [16.6–22.6])	0.4 (−1.0 to 1.7)‡
Symptom duration ≥7 d, no. patients (median C_t value [25%–75% quantile])	6 (30.1 [26.1–31.3])	11 (26.2 [21.4–31.2])	3.9 (−5.6 to 10.0)‡

*Values are no. (%) except as indicated. C_t, cycle threshold; NA, not applicable; OR, odds ratio; SARS-CoV-2, severe acute respiratory syndrome coronavirus 2.
†Difference in means (95% CI).
‡Difference in medians (95% CI). The 95% CI for difference in medians was computed by a percentile bootstrap with 1,000 replications.

We observed no difference in cycle threshold (C_t) values for the envelope gene target between B.1.1.7 and wild-type samples (median 20.2 vs. 20.1) (Table). In patients reporting a symptom duration of ≥7 days, C_t values appeared to be lower for those with B.1.1.7 (26.2 vs. 30.1 for wild-type), but the difference was not significant (p = 0.7 by Mann–Whitney U test) (Table; Figure 2).

Finally, we explored which combination of variables in our dataset best described B.1.1.7 in a logistic regression applying a backward stepwise selection on the basis of the Akaike information criterion (Appendix). This work identified the best set of associated factors as the absence of anosmia or ageusia (p = 0.01), longer symptom duration (p = 0.02), sore throat (p = 0.05), lower C_t value (p = 0.07), travel in the previous 14 days (p = 0.08), lower age (p = 0.09), and absence of rhinorrhea (p = 0.12). We then used the bootstrap technique to repeat the variable selection in 1,000 replicated datasets and evaluated how often these variables were selected with the backward selection. This analysis resulted in anosmia or ageusia, 89%; symptom duration, 78%; travel, 73%; sore throat, 68%; C_t value, 66%; age, 56%; and rhinorrhea, 51%. Absence of anosmia or ageusia, longer symptom duration, and travel were selected most often, indicating their association with B.1.1.7 infection. We performed all analyses in R version 3.6.3 (https://cran.r-project.org).

Conclusions

The first B.1.1.7 case in Germany was recorded in late December 2020 (*5*). At our testing site, B.1.1.7 was observed 3 weeks later and replaced wild-type virus as the dominant strain within just 5 weeks. The rapid emergence and dominance of this lineage likely results from its increased transmissibility (E. Volz et al., unpub. data), which is potentially caused by spike protein polymorphisms (including 501Y) conferring enhanced mucosal binding (*6*); 681H, near a region vital for transmission (T.P. Peacock et al., unpub. data, https://doi.org/10.1101/2020.09.30.318311); and deletion 69–70, linked to immune escape (*7*). Viral replication in vitro does not differ from earlier strains (J.C. Brown et al., unpub. data, https://doi.org/10.1101/2021.02.24.432576).

Compared to the wild-type virus, B.1.1.7 is reportedly associated with more deaths in nonhospitalized patients but not in inpatients (*1*,*2*). In our young outpatient study population, we did not observe major, lineage-dependent differences in leading symptoms. Nevertheless, anosmia and ageusia, among the most specific coronavirus disease symptoms (*3*), were less common in patients with B.1.1.7., whereas sore throat was more common. A survey in the United Kingdom revealed patients with B.1.1.7 experienced anosmia and ageusia less frequently but more frequently experienced sore throat, cough, fatigue, myalgia, and fever (*8*). In contrast, no associations between SARS-CoV-2 B.1.1.7 and self-reported symptoms, disease duration, or hospital admissions were seen in another UK study (*9*). The main factors for B.1.1.7 infection prediction in our study appeared to be lack of anosmia or ageusia and longer symptom duration, in addition to recent travel. The association with recent travel at the time of B.1.1.7 spread is probably no longer relevant because B.1.1.7 is now the most common variant in Berlin and Germany.

With regard to C_t values, one study observed similar figures in patients with B.1.1.7 and wild-type lineages; however, a longer duration of PCR–positivity with B.1.1.7 was suggestive by repeated sampling over time (S.M. Kissler et al., unpub. data, https://doi.org/10.1101/2021.02.16.21251535). Likewise, longer persistence has been observed for B.1.1.7 (*10*), but lower

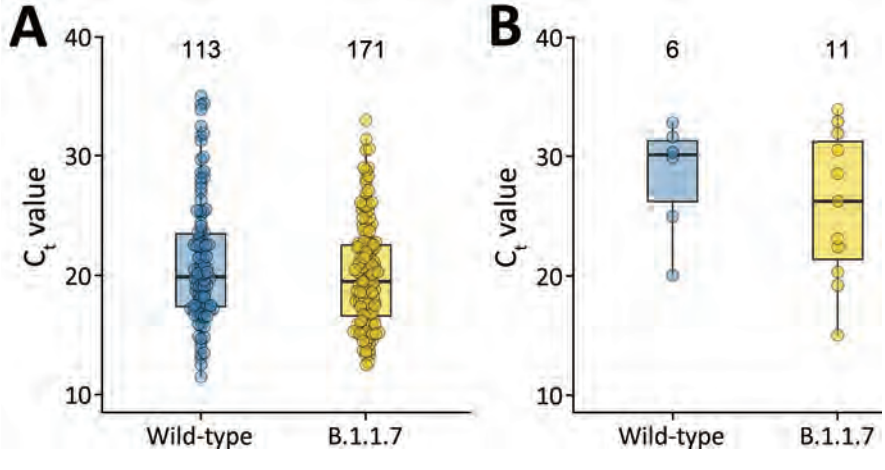

Figure 2. Comparison of median C_t values in severe acute respiratory syndrome coronavirus 2 wild-type and B.1.1.7 lineage by symptom duration, Berlin, Germany, January–March 2021. A) Symptom duration <7 days. B) Symptom duration >7 days. The boxplots indicate medians (center) and 25th (top) and 75th (bottom) percentiles (i.e., quartile [Q] 1 and Q3). The upper whiskers reach the largest value with a maximum Q3 +1.5 interquartile range. The lower whiskers reach the smallest value with a minimum Q1 –1.5 interquartile range. The numbers on top of the boxplots indicate the total number of observations included in the comparison. C_t, cycle threshold.

C_t values (indicating higher viral load) have been observed compared to wild-type samples. Lower C_t values were also seen in other studies on population (*11*) and inpatient levels (*2*). In our cross-sectional assessment of recently ill outpatients, we did not observe such differences. Still, increased transmissibility may result from the variant's prolonged excretion (*10*; S.M. Kissler et al., unpub. data). Test timing appears crucial for interpretation of C_t values. Outpatients are commonly tested earlier than inpatients. The combination of prolonged viral shedding with different test timing might explain increased viral load in B.1.1.7 samples in inpatients but not in recently ill outpatients. In outpatients with ≥7 days symptom duration, C_t values in B.1.1.7 samples were suggestively reduced. However, comparison groups were small. Our data enabled detection of a maximum effect size on overall C_t values, which corresponds to B.1.1.7 C_t values being 1.5 units below or 1.0 above those for wild-type virus.

The main limitation of our study was its limited subgroup sizes, which reduced the likelihood of detecting differences between rare characteristics. Other limitations are the 1-time assessment, subjective symptom duration, and the variable manifestation of SARS-CoV-2 infection (*3*). Strengths include standardized procedures conducted by trained medical staff and its prospective nature evaluating patient groups during the same period, reducing the likelihood of biases because of temporal effects.

In summary, SARS-CoV-2 VOC B.1.1.7 is now the dominant lineage in Berlin. In outpatients, no major difference in clinical manifestations has been observed.

This article was preprinted at https://www.medrxiv.org/content/10.1101/2021.04.15.21255389v1.

Acknowledgments

We thank the Corona Untersuchungsstelle staff at the Charité–Universitätsmedizin Berlin for their dedication and hard work during the coronavirus disease pandemic.

About the Author

Ms. Van Loon is a PhD student at the Research Group Malaria and Infectious Diseases Epidemiology, Institute of Tropical Medicine and International Health, Charité–Universitätsmedizin Berlin, Germany. Her primary research interests include the epidemiology of infectious diseases.

References

1. Davies NG, Jarvis CI, Edmunds WJ, Jewell NP, Diaz-Ordaz K, Keogh RH; CMMID COVID-19 Working Group. Increased mortality in community-tested cases of SARS-CoV-2 lineage B.1.1.7. Nature. 2021;1–5. https://doi.org/10.1038/s41586-021-03426-1
2. Frampton D, Rampling T, Cross A, Bailey H, Heaney J, Byott M, et al. Genomic characteristics and clinical effect of the emergent SARS-CoV-2 B.1.1.7 lineage in London, UK: a whole-genome sequencing and hospital-based cohort study. Lancet Infect Dis. 2021 Apr 12 [Epub ahead of print]. https://doi.org/10.1016/S1473-3099(21)00170-5
3. Maechler F, Gertler M, Hermes J, van Loon W, Schwab F, Piening B, et al. Epidemiological and clinical characteristics of SARS-CoV-2 infections at a testing site in Berlin, Germany, March and April 2020-a cross-sectional study. Clin Microbiol Infect. 2020;26:1685.e7–12. https://doi.org/10.1016/j.cmi.2020.08.017
4. Poljak M, Korva M, Knap Gašper N, Fujs Komloš K, Sagadin M, Uršič T, et al. Clinical evaluation of the cobas SARS-CoV-2 test and a diagnostic platform switch during 48 hours in the midst of the COVID-19 pandemic. J Clin Microbiol. 2020;58:e00599–20. https://doi.org/10.1128/JCM.00599-20
5. Robert Koch Institute. Coronavirus disease 2019 (COVID-19) daily situation report of the Robert Koch Institute. 2020 Dec 26 [cited 2021 Apr 3]. https://www.rki.de/DE/Content/InfAZ/N/Neuartiges_Coronavirus/Situationsberichte/Dez_2020/2020-12-26-en.pdf?__blob=publicationFile
6. Chan KK, Tan TJC, Narayanan KK, Procko E. An engineered decoy receptor for SARS-CoV-2 broadly binds protein S sequence variants. Sci Adv. 2021;7:eabf1738.
7. Kemp SA, Collier DA, Datir R, Ferreira IATM, Gayed S, Jahun A, et al. Neutralising antibodies in Spike mediated SARS-CoV-2 adaptation. Nature. 2021;592:277–82. https://doi.org/10.1038/s41586-021-03291-y
8. Office for National Statistics. Coronavirus (COVID-19) infection survey: characteristics of people testing positive for COVID-19 in England, 27 January 2021 [cited 2021 Apr 3]. https://www.ons.gov.uk/peoplepopulationandcommunity/healthandsocialcare/conditionsanddiseases/articles/coronaviruscovid19infectionsinthecommunityinengland/characteristicsofpeopletestingpositiveforcovid19inengland27january2021
9. Graham MS, Sudre CH, May A, Antonelli M, Murray B, Varsavsky T, et al.; COVID-19 Genomics UK (COG-UK) Consortium. Changes in symptomatology, reinfection, and transmissibility associated with the SARS-CoV-2 variant B.1.1.7: an ecological study. Lancet Public Health. 2021;6:e335–45. https://doi.org/10.1016/S2468-2667(21)00055-4
10. Calistri P, Amato L, Puglia I, Cito F, Di Giuseppe A, Danzetta ML, et al. Infection sustained by lineage B.1.1.7 of SARS-CoV-2 is characterised by longer persistence and higher viral RNA loads in nasopharyngeal swabs. Int J Infect Dis. 2021;105:753–5. https://doi.org/10.1016/j.ijid.2021.03.005
11. Kidd M, Richter A, Best A, Cumley N, Mirza J, Percival B, et al. S-variant SARS-CoV-2 lineage B1.1.7 is associated with significantly higher viral loads in samples tested by ThermoFisher TaqPath RT-qPCR. J Infect Dis. 2021 Feb 13 [Epub ahead of print]. https://doi.org/10.1093/infdis/jiab082

Address for correspondence: Welmoed van Loon, Institute of Tropical Medicine and International Health, Charité–Universitätsmedizin Berlin, Campus Virchow-Klinikum, Augustenburger Platz 1, 13353 Berlin, Germany; email: welmoed.van-loon@charite.de

Assessing Community Vulnerability over 3 Waves of COVID-19 Pandemic, Hong Kong, China

Qiuyan Liao, Meihong Dong, Jiehu Yuan, Richard Fielding, Benjamin J. Cowling, Irene Oi Ling Wong, Wendy Wing Tak Lam

We constructed a coronavirus disease community vulnerability index using micro district-level socioeconomic and demographic data and analyzed its correlations with case counts across the 3 pandemic waves in Hong Kong, China. We found that districts with greater vulnerability reported more cases in the third wave when widespread community outbreaks occurred.

The coronavirus disease (COVID-19) pandemic disproportionally affects socially disadvantaged populations because of economic, social, and demographic factors, as well as their health conditions and practices (*1*). Identifying vulnerable communities and effectively allocating ameliorating resources to them are necessary if policy makers are to manage the effects of COVID-19. Community vulnerability indexes (CVIs) have been increasingly used to assess community social vulnerability to a pandemic using community-level socioeconomic and demographic data (*2*–*7*). In the United States, greater CVI and vulnerability in domains of minority status, household composition, housing, transportation, and disability at the county level were significantly associated with greater risk of COVID-19 diagnosis (*3*,*4*). We aimed to construct a CVI more socioculturally adapted to metropolises in Asia to explain the impact of COVID-19 across more microgeographic units (i.e., districts) within a highly urbanized city, Hong Kong, China. We also analyzed the extent that CVI was correlated with the evolution of the COVID-19 pandemic in Hong Kong.

Author affiliations: University of Hong Kong, Hong Kong, China (Q. Liao, M. Dong, J. Yuan, R. Fielding, B.J. Cowling, I.O.L. Wong, W.W.T. Lam); Hong Kong Science and Technology Park, Hong Kong (B.J. Cowling)

DOI: https://doi.org/10.3201/eid2707.204076

The Study

Hong Kong has long been regarded as an epicenter for many infectious diseases and is predisposed to severe COVID-19 impact because of its dense and rapidly aging population (*8*,*9*). Geographically, Hong Kong comprises 3 main regions, New Territories, Kowloon, and Hong Kong Island, which are further subdivided into 18 administrative districts (*10*). As of August 31, 2020, Hong Kong had experienced 3 waves of COVID-19 (Appendix Figure 1, https://wwwnc.cdc.gov/EID/article/27/7/20-4076-App1.pdf), reporting 4,811 COVID-19 cases, including 89 deaths; 76.5% of cases occurred in wave 3 (*11*).

Following methods used by the Surgo Foundation (*6*), we first defined 5 domains that contributed to an overall CVI: socioeconomic status, household composition, housing condition, healthcare system, and epidemiologic factors. We included 22 indicators in the 5 domains for calculating domain CVI and overall CVI (Table 1). We first ranked each indicator by district, with a higher rank indicating greater vulnerability. Then, we calculated the percentile rank of each district over each indicator using the formula of percentile rank = (rank – 1)/(n – 1), where n refers to total geographic units (n = 18). A higher percentile rank indicates greater relative CVI of the district over the specific indicator. We then summed the percentile ranks over all indicators within each domain, reranked them to calculate domain CVIs, and summed the percentile ranks of all domains to calculate an overall CVI for each district. We assumed equal weights for indicators within domains and for the 5 domains within the overall CVI because of a lack of available evidence informing a more optimized weight scheme. Finally, we categorized all districts into very high (>80%), high (60%–80%), moderate (40%–60%), low (20%–40%), and very low (<20%) vulnerability on the basis of their domain and overall

Table 1. Domains and domain indictors for calculating community vulnerability index in the context of the coronavirus disease pandemic, Hong Kong*

Domain	Descriptions of the indicators
Socioeconomic status†	
Poverty	Proportion of persons below poverty line‡
Unemployment	Proportion of persons ≥15 years of age who are unemployed
Income	Median income per capita
Educational level	Proportion persons ≥15 years of age having education level below high school
Household composition†	
Persons ≥65 years of age	Proportion of persons ≥65 years of age
Persons ≤14 years of age	Proportion of persons ≤14 years of age
Single-parent households	Proportion of single-parent households among all households
Elderly living alone	Proportion of elderly (≥65 years of age) living alone
Housing conditions†	
Household density	Mean number of persons per household
Area of accommodation	Median floor area of accommodation per household
Healthcare system factors§	
Hospital beds	Proportion of hospital beds per 100,000 persons
Intensive care unit (ICU) beds	Proportion of ICU beds per 100,000 persons
Hospital labor	Proportion of hospital labor force (full-time staff employed by Hong Kong Hospital Authority) per 100,000 persons
Epidemiologic factors	
Population density¶	Estimated persons per square kilometre
Obesity#	Proportion of persons with BMI ≥25
Hypertension#	Proportion of persons with hypertension
Smoking#	Proportion of daily smokers
Persons employed in transportation sector†	Proportion of persons employed in transportation sector
Persons employed in accommodation and food catering sectors†	Proportion of persons employed in accommodation and food catering sectors
Working outside residency district†	Proportion of persons not working in the district of their residence
Entertainment venues**	Number of entertainment venues (e.g., bar, karaoke, wine, club house)
Non–Chinese ethnicities †	Proportion of persons with non–Chinese ethnicities

*All statistics were calculated at the residential district level of Hong Kong.
†Data from the 2016 Hong Kong population by-census data (https://www.censtatd.gov.hk/hkstat/sub/so459.jsp).
‡Monthly household income is below 50% of the median monthly household income in Hong Kong before any government interventions.
§Data from the 2018–2019 Hospital Authority Annual Report, Hong Kong (https://www3.ha.org.hk/data/HAStatistics/StatisticalReport/2018-2019).
¶Data from the Hong Kong Statistical Reports: Land area, mid-year population and population density by District Council district, 2019 edition (https://www.censtatd.gov.hk/hkstat/sub/sp150.jsp?productCode = D5320189).
#Data from the 2015 report of a major Family Project Cohort Study comprising ≈8,000 households in Hong Kong (https://familycohort.sph.hku.hk/en/knowledge_exchange.html).
**Data from OpenRice (https://www.openrice.com/en/hongkong), the most popular restaurant review app, which provides the largest database of food venues, bars and other entertainment venues in Hong Kong.

CVI. We calculated the Pearson correlations of indicator, domain, and overall CVI with COVID-19 case counts across districts and pandemic waves. We analyzed the differences in temporal trends of accumulated COVID-19 counts by districts of different vulnerability categories using Poisson regression models and plotted the results. We included 3,847 cases reported during January 23–August 31, 2020, for which a residence was locatable.

We plotted the spatial distribution of overall CVI and case counts (Figure 1) and domain CVI by districts (Appendix Figure 2). The 4 districts with very high vulnerability districts reported 1,333 COVID-19 cases, accounting for 34.6% (95% CI 33.1%–36.2%) of the total cases; the 4 districts with very low vulnerability reported 491 COVID-19 cases, 12.7% (95% CI 11.7%–13.9%) of the total. Of the 81 COVID-19–attributed deaths with recorded residence, 45.7% (95% CI 34.6%–57.1%) were reported in the 4 districts with very high vulnerability and 34.6% (95% CI 24.3%–46.0%) were reported in the 3 districts with high vulnerability. Only 2 COVID-19–attributed deaths were reported from the 7 very low or low-vulnerability districts.

By pandemic wave, the correlation between overall CVI and case counts was not significant for wave 1, negative in wave 2, and positive in wave 3, and, consequently, positive overall (Table 2). In wave 2, the case counts correlated negatively with most indicator and domain CVI but correlated positively with distribution of entertainment venues and non-Chinese ethnicities. In wave 3, the case counts correlated positively with most indicators and all domain CVIs but correlated negatively with non–Chinese ethnicities. Overall, community profile variables that correlated positively with case counts over the 3 waves included poverty, income, educational level, single-parent households, area of accommodation, hospital beds, population density, obesity, and working outside area of residency.

We plotted the temporal changes in cumulative cases by vulnerability categories (Figure 2). The Poisson regression model revealed an overall significant effect of vulnerability levels on cumulative cases (moderate vulnerability, $\beta = 0.17$, $p<0.001$; high/very high vulnerability, $\beta = 0.31$, $p<0.001$). By pandemic wave, districts of high/very high vulnerability reported fewer cases in the first 2 waves ($\beta = -0.45$, $p<0.001$) but significantly more cases in wave 3 ($\beta = 0.68$, $p<0.001$).

Conclusion

Adding to existing literature (*2*–*5*), our study indicates that community vulnerability is dynamic, changing with the evolution of the pandemic. In waves 1 and 2, COVID-19 cases were mainly imported cases, including those infecting students and domestic helpers returning from overseas, as well as business travelers (*12*). These cases were found mainly within more socially privileged families and thereby an inverse association between socioeconomic status and case counts was seen. In Hong Kong, 55% of persons with non–Chinese ethnicities are domestic helpers for more socially privileged families and another 25% are executives or professionals (*13*) who have greater work-from-home flexibility (*12*). Subsequently, after tightening measures for inbound travelers and because there were more work-from-home arrangements in wave 3, the positive correlation between non–Chinese ethnicities and vulnerability to COVID-19 infection in waves 1 and 2 shifted to be negative. Entertainment venues constituted a primary exposure setting that spread COVID-19 in waves 1 and 2 (*14*) but ceased to be a major contributor to community vulnerability in wave 3 after these venues were closed. In wave 3, socioeconomic deprivation, poor housing, and dense household composition, as well as epidemiologic factors that facilitate viral transmission, became more key contributors to community vulnerability to COVID-19 infection. By April 2021, Hong Kong had experienced another pandemic wave (wave 4), characterized, again, by cases mainly in younger persons with higher socioeconomic status, linking to the largest local cluster (dancing/singing studio cluster) and the second largest cluster (fitness center outbreak) (*10*). Updated analyses found that socioeconomic deprivation and poor housing were no longer major contributors, whereas entertainment

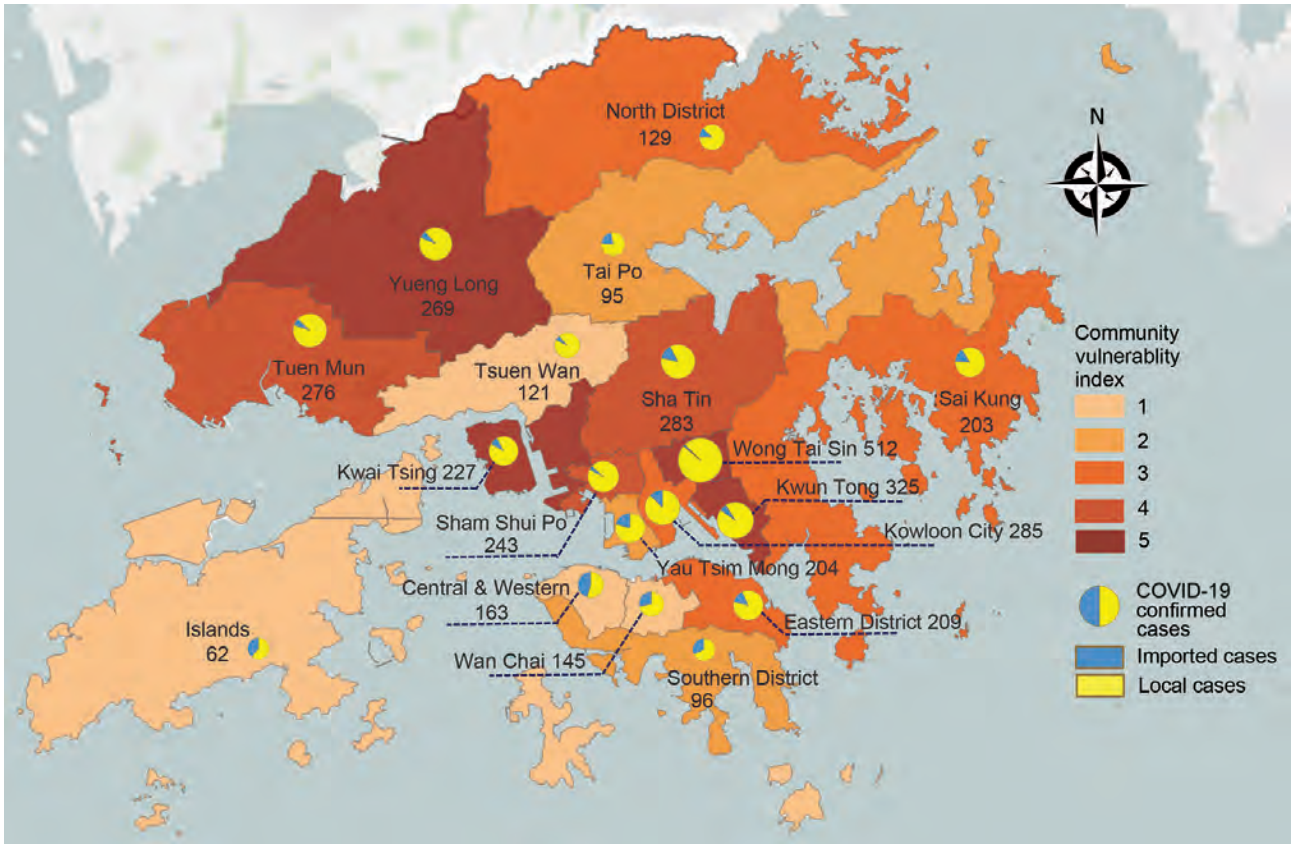

Figure 1. Distributions of community vulnerability index and total case counts of COVID-19 across administrative districts of Hong Kong as of August 31, 2020. COVID-19, coronavirus disease.

Table 2. Pearson correlations of indicator, domain, and overall community vulnerability index for coronavirus disease confirmed cases across 3 pandemic waves, as of August 31, 2020, Hong Kong

Domains and indicators	Wave 1	Wave 2	Wave 3	Overall
Overall index	0.31	−0.49*	0.77‡	0.71†
Socioeconomic status	0.01	−0.59*	0.68†	0.58*
Poverty	0.26	−0.43	0.75‡	0.71†
Unemployment	−0.10	−0.64†	0.50*	0.38
Income	0.02	−0.65†	0.60[b]	0.48*
Educational level	−0.06	−0.70†	0.64†	0.51*
Household composition	0.14	−0.51*	0.57*	0.49*
Persons ≥65 years of age	0.59*	0.09	0.30	0.37
Persons ≤14 years of age	−0.36	−0.48*	−0.11	−0.25
Single-parent households	0.25	−0.44	0.73†	0.68†
Elderly living alone	−0.09	−0.28	0.45	0.41
Housing condition	0.16	−0.42	0.49*	0.43
Household density	0.07	−0.20	−0.01	−0.05
Area of accommodation	0.08	−0.32	0.65†	0.62†
Healthcare system factors	0.48*	−0.07	0.47	0.50*
Hospital beds	0.45	−0.33	0.59*	0.57*
ICU beds	0.41	0.16	0.39	0.47
Hospital labor	0.50*	−0.01	0.37	0.41
Epidemiologic factors	0.45	−0.37	0.68[†]	0.66[†]
Population density	0.45	0.17	0.51*	0.60[†]
Obesity	0.43	−0.32	0.53*	0.51*
Hypertension	0.54*	0.01	0.41	0.46
Smoking	−0.06	−0.51*	0.19	0.08
Employed in transportation sector	−0.22	−0.71†	0.26	0.10
Employed in accommodation and food catering sectors	−0.02	−0.51*	0.48*	0.39
Working outside residency district	−0.10	−0.56*	0.59*	0.49*
Entertainment venues	0.34	0.63†	0.04	0.21
Non–Chinese ethnicities	0.002	0.66†	−0.71†	−0.60†

*p<0.05
†p<0.01
‡p<0.001

venues again became strong contributors to community vulnerability in wave 4 (Appendix Table).

Overall, our study indicates that a COVID-19 CVI can be applied to district-level data within a city to help city-level policy makers in resource allocation planning, but these measures should be viewed as dynamic at different pandemic stages. For instance, infection control and prevention measures should be intensified, perhaps by more strict or substantial social distancing in community settings with entertainment venues where persons may remove their face masks to exercise, dance, or eat and drink when community incidence is lower to minimize pandemic resurgence, whereas more material resources can be allocated to support social distancing measures among more socially disadvantaged communities when widespread community outbreaks occur. Our analysis focused on the correlation of CVI with COVID-19 case counts rather than infection risk (i.e., incidence) or severity (e.g.,

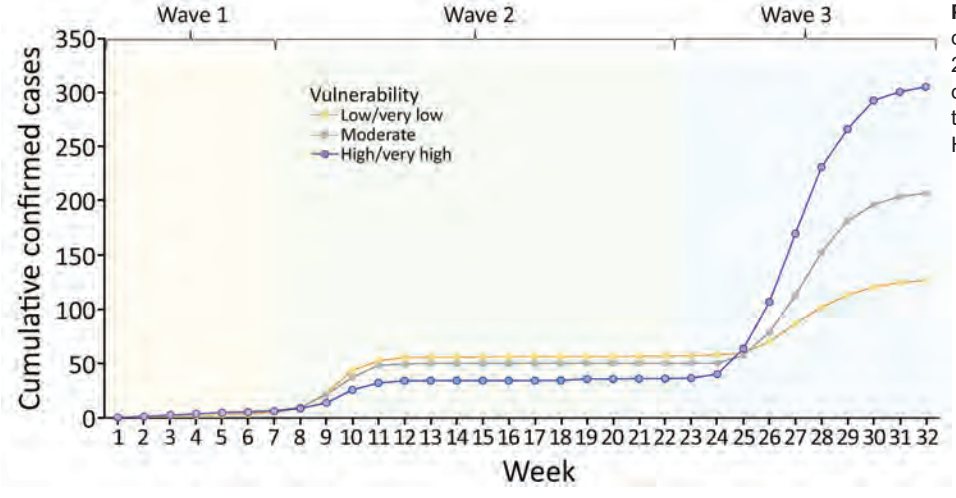

Figure 2. Cumulative coronavirus disease cases as of August 31, 2020, by week and districts of different vulnerability levels since the first case was reported in Hong Kong.

fatalities) because of the relatively small number of cases and COVID-19 mortality in Hong Kong. However, because symptoms are generally mild in most cases, the magnitude of the pandemic impact is a key determinant for resource allocation.

About the Author

Dr. Liao is an assistant professor of behavioral sciences and public health at the University of Hong Kong. Her research interests include public risk perception and risk communication in the context of communicable and noncommunicable diseases.

References

1. The Lancet. Redefining vulnerability in the era of COVID-19. Lancet. 2020;395:1089. https://doi.org/10.1016/S0140-6736(20)30757-1
2. Acharya R, Porwal A. A vulnerability index for the management of and response to the COVID-19 epidemic in India: an ecological study. Lancet Glob Health. 2020;8:e1142–51. https://doi.org/10.1016/S2214-109X(20)30300-4
3. Khazanchi R, Beiter ER, Gondi S, Beckman AL, Bilinski A, Ganguli I. County-level association of social vulnerability with COVID-19 cases and deaths in the USA. J Gen Intern Med. 2020;35:2784–7. https://doi.org/10.1007/s11606-020-05882-3
4. Karaye IM, Horney JA. The impact of social vulnerability on COVID-19 in the U.S.: an analysis of spatially varying relationships. Am J Prev Med. 2020;59:317–25. https://doi.org/10.1016/j.amepre.2020.06.006
5. Kim SJ, Bostwick W. Social vulnerability and racial inequality in COVID-19 deaths in Chicago. Health Educ Behav. 2020;47:509–13. https://doi.org/10.1177/1090198120929677
6. Surgo Foundation. The U.S. COVID-19 community vulnerability index (CCVI) [cited 2020 Sep 11]. https://precisionforcovid.org/ccvi
7. Amram O, Amiri S, Lutz RB, Rajan B, Monsivais P. Development of a vulnerability index for diagnosis with the novel coronavirus, COVID-19, in Washington State, USA. Health Place. 2020;64:102377. https://doi.org/10.1016/j.healthplace.2020.102377
8. Hong Kong Census and Statistics Department. Statistics by subject: Hong Kong in figures [cited 2020 Sep 2]. https://www.censtatd.gov.hk/hkstat/hkif/index.jsp
9. Hong Kong Census and Statistics Department. 2016 population by-census [cited 2020 Sep 3]. https://www.censtatd.gov.hk/hkstat/sub/so459.jsp
10. Hong Kong Home Affairs Department. Hong Kong: the facts—district administration [cited 2020 Sep 4]. https://www.gov.hk/en/about/abouthk/factsheets/docs/district_admin.pdf
11. Hong Kong Center for Health Protection. Latest situation of cases of COVID-19 (as of 10 April 2021) [cited 2021 Apr 11]. https://www.chp.gov.hk/files/pdf/local_situation_covid19_en.pdf
12. Yang B, Wu P, Lau EHY, Wong JY, Ho F, Gao H, et al. Changing disparities in coronavirus disease 2019 (COVID-19) burden in the ethnically homogeneous population of Hong Kong through pandemic waves: an observational study. Clin Infect Dis. 2021 Jan 6 [Epub ahead of print]. https://doi.org/10.1093/cid/ciab002
13. Hong Kong Census and Statistics Department. 2016 Population by-census thematic report: ethnic minorities [cited 2021 Apr 11]. https://www.bycensus2016.gov.hk/data/16bc-ethnic-minorities.pdf
14. Wong NS, Lee SS, Kwan TH, Yeoh E-K. Settings of virus exposure and their implications in the propagation of transmission networks in a COVID-19 outbreak. Lancet Reg Health West Pac. 2020;4:100052. https://doi.org/10.1016/j.lanwpc.2020.100052

Address for correspondence: Qiuyan Liao, School of Public Health, Li Ka Shing Faculty of Medicine, The University of Hong Kong, 7 Sassoon Rd, Pokfulam, Hong Kong, China; email: qyliao11@hku.hk

Anthrenus sp. and an Uncommon Cluster of Dermatitis

Loïc Simon, Fériel Boukari, Halilou Almou Oumarou, Thomas Hubiche, Pierre Marty, Christelle Pomares, Pascal Delaunay

We report patients in their homes in France who had cutaneous lesions caused by *Anthrenus* sp. larvae during the end of winter and into spring. These lesions mimic bites but are allergic reactions to larvae hairs pegged in the skin. These lesions should be distinguished from bites of bed bugs or fleas.

Among all biting insects, some are responsible only for bite lesions, and others are also vectors of diseases (*1*–*3*). In both instances, these insects are a physical nuisance and sometimes a psychological one. The most-described biting insects found in human dwellings are bed bugs, which are transmitted by travel and movement of persons; and fleas, which are transmitted by household pets (*3*,*4*). We describe patients requesting a dermatologic consultation for skin lesions caused by hairs of *Anthrenus* sp. (carpet beetle) larvae.

The Study

During January–March 2020, a total of 11 patients (6 children 7–17 years of age and 5 adults 19–58 years of age) from 7 families living in southern France (Nice area) consulted with the Department of Dermatology, Centre Hospitalier Universitaire de Nice (Nice, France). Each person had a several-week history of multiple skin lesions. Clinical examinations showed 7–35 (median 17) isolated erythematous urticarial papules/patient. These papules were pruritic, and lasted ≈1 week before disappearing slowly; new papules then appeared. Erythematous papular lesions always appeared first in 1 family member. Then, in all cases, dermatitis progressively affected some, but not all, family members. Lesions and absence of other symptoms did not evoke a specific dermatologic condition. Because the scattering of symptoms among family members was compatible with insect infestation, patients were referred to the Department of Medical Entomology for further examination.

No recent history of travel, purchase of secondhand items, or presence of infected pets (confirmed by veterinarians) were reported by the families. Examinations indicated that lesions were located mostly under clothing: on the thighs, arms, chest, and abdomen (Figure 1). Careful inspection of beds and sofas by the families did not find bed bugs or fleas. In addition, the fact that the lesions were scattered all over the body, mainly under clothing, was not typical for bed bugs and fleas (Table) (*4*). In this context, the medical entomologist visited 2 homes and looked for mites or insects responsible for the dermatitis. He confirmed the absence of bed bugs and fleas, and rapidly found larvae and adult insects in clothing, fabric, and upholstery inside the homes (Figure 2, panels A–C). These larvae and adult insects were later identified as specimens of *Anthrenus* sp. by using a 40× binocular magnifier (Figure 2, panel D). For the other families, he asked the patients to look for *Anthrenus* sp. in these same places, showing them pictures of carpet beetle adults and larvae (*5*). All families found similar larvae and adult insects and brought them to the medical entomologist, who confirmed *Anthrenus* sp. by morphology.

Anthrenus sp., better known as the carpet beetle, belongs to the order Coleoptera and family Dermestidae. Adults have a length of ≈3–4 mm, feed on nectar and pollen, and are harmless to humans. During autumn, female beetles search for hot areas and lay their eggs in dark places and cracks, making furniture one of their favorite spots (*6*,*7*). The larvae, which have a length of 4 mm, hatch at the end of winter or during spring. They usually live in dark drawers and cupboards. Larvae feed on dried organic matter from plant or animal residues, such as

Author affiliations: Centre Hospitalier Universitaire de Nice, Nice, France (L. Simon, F. Boukari, H. Almou Oumarou, T. Hubiche, P. Marty, C. Pomares, P. Delaunay); Université Côte d'Azur, Nice (L. Simon, P. Marty, C. Pomares); Université de Montpellier, Montpellier, France (P. Delaunay)

DOI: https://doi.org/10.3201/eid2707.203245

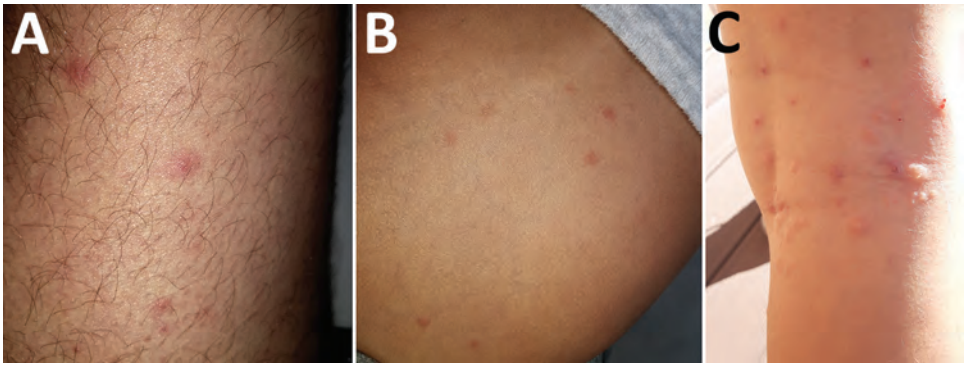

Figure 1. Aspects of lesions caused by larvae of *Anthrenus* sp. carpet beetles on 3 members of the same family, France. A) Thigh of a 33-year-old man; B) abdomen of a 5-year-old boy; C) leg of an 8-year-old girl (who scratched lesions).

wool, dust, dead skin cells, feathers, and hairs; thus, they are commonly found in wardrobes, on stuffed animals, mattresses, or under carpets (*6*,*7*). Larvae never infest living animals. The larvae of many species of carpet beetles are covered with spear-headed hairs. These hairs are disseminated throughout the interior of a home by a natural air stream or an air conditioning system.

We observed for 1 child from the first family a large number of lesions (35 papules), probably caused by the air conditioning unit located above her bed. Two kinds of hairs coexist on these insect larvae. One hair is fine and has a terminal arrow, and the other hair is thick and has scales (Figure 2, panel E). Among the hairs of the *Anthrenus* sp. larvae, only the fine prickly hairs are responsible for lesions. Their spear-headed shape enable them to get stuck in the skin or respiratory mucosa, leading to hypersensitivity reactions in the hosts (*8*). Few cases of dermatitis caused by *Anthrenus* sp. beetles have been described (*6*,*9*,*10*). Even rare cases of asthma could be linked to the presence of carpet beetle larvae in the house (*11*).

Several steps (excluding insecticides) were recommended to quickly help the 7 families eliminate their lesions and clean their homes. All patients were given antihistamines and topical corticoids. Clothing that had direct skin contact and was to be worn in the next few days was washed to eliminate larvae hairs and stored after drying in airtight bags to protect them from the environment. In the homes, places where *Anthrenus* sp. beetles were found were inspected and cleaned. Insects were removed mechanically. Mattresses and other infested areas were vacuumed, and the vacuum bag was put in a plastic bag in the trash. Air conditioning systems present in the infested rooms were cleaned to prevent larvae hairs from spreading.

After observance of the above protocol, skin lesions healed in all affected adults and children in 3 days. A month later, no other lesions were observed in the 7 families.

Conclusions

In our medical experience, infestations by *Anthrenus* sp. beetles have been sporadic. We observed a large number of cases during a short period, and a new case of *Anthrenus* sp. infestation was being investigated when this manuscript was being written. The families described in this report lived either in houses or apartments. They were not geographically near each other, but they all lived near parks or green spaces in urban or periurban areas.

Table. Characteristics of 3 insects found in dwellings during a study of *Anthrenus* sp. and an uncommon cluster of dermatitis*

	Configuration of skin lesions							
Insect pest	Body part affected	Location in clothes	Grouping	Time of year	Harmful stage of insect	Location in housing	Treatment for housing	Evolution without treatment
Bed bugs	Face, hands, feet	Uncovered areas	Frequently 3 or 4	Any season	All	Beds, sofas	Steam >60°C with or without insecticide	Exponential
Fleas	Buttocks, legs	Covered or uncovered areas	Frequently 3 or 4	Any season	Adult	Adults: animals; larvae: carpets, sofas	Animal treatment, vacuum carpets and sofas	Depending on presence of infected animal
Anthrenus sp.	No specific parts	Mostly covered areas	Isolated	Late winter, early spring	Larval	Baseboards, wardrobes, mattresses, old carpets, drawers	Vacuum and cleaning of air conditioning systems	Possible spontaneous healing at end of spring

*Treatment for all patients was antihistamines and topical corticoids.

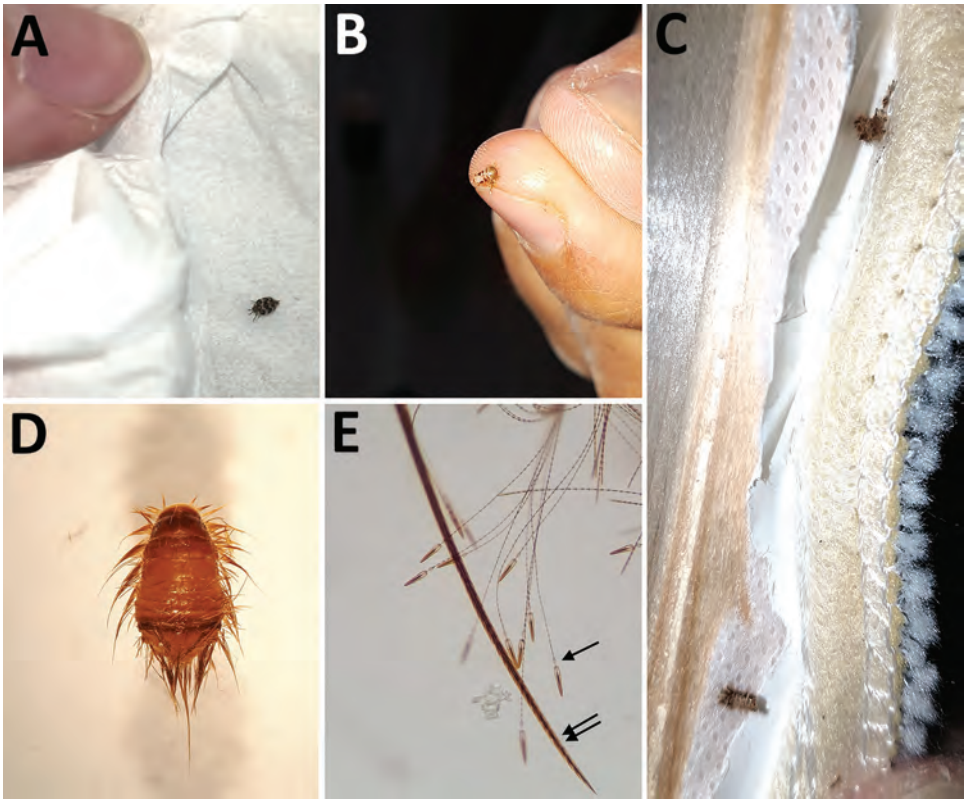

Figure 2. Stages of *Anthrenus* sp. carpet beetle. A) Adult stage (length 4 mm); B, C) larval stage (length 4 mm) found inside clothing and upholstery fabric; D) larvae (original magnification ×40); and E) larvae (original magnification ×200) showing fine hairs (single arrow) that have a spear-headed shape, are responsible for human hypersensitivity, and are invisible to the naked eye. Double arrow indicates thick larvae hair.

Proper detection and identification of specimens is a key step in controlling insect pests. *Anthrenus* sp. larvae are responsible for allergic cutaneous reactions (not bites) caused by hairs hooked in the skin, leading to lesions found under clothing in members of the same household. The environment should be investigated for this carpet beetle in the case of skin lesions mimicking arthropod bites without a central blister. Reactions to larvae hairs are different from 1 family member to another, and ≥1 of these family members frequently have no symptoms.

Dermatitis caused by *Anthrenus* sp. larvae is underdiagnosed or confused with dermatitis caused by bed bugs or fleas. These erroneous diagnoses can lead to use of insecticides and thus to unnecessary, tiring, expensive, and toxic procedures. Dermatitis caused by *Anthrenus* sp. larvae has clinical and environmental characteristics relevant to ruling out other entomologic causes. It is useful to know that lesions caused by this insect are isolated and located mostly under clothing. Also, these insects are found in late winter or during spring, and bed bugs or fleas are not found contemporaneously. This insect pest has been uncommon in human medicine, and these cases could indicate its emergence. Physicians and dermatologists should be better aware of this insect.

Acknowledgment

We thank Alissa Majoor for assistance with language editing of the manuscript.

About the Author

Dr. Simon is a parasitologist in the department of Parasitology–Mycology and Medical Entomology, University Hospital Center of Nice, Nice, France. His primary research interests include vector-borne parasitic diseases and host–pathogen interactions.

References

1. Charrel RN, Berenger J-M, Laroche M, Ayhan N, Bitam I, Delaunay P, et al. Neglected vector-borne bacterial diseases and arboviruses in the Mediterranean area. New Microbes New Infect. 2018;26:S31–6. https://doi.org/10.1016/j.nmni.2018.08.015
2. Laroche M, Bérenger J-M, Delaunay P, Charrel R, Pradines B, Berger F, et al. Medical entomology: a reemerging field of research to better understand vector-borne infectious diseases. Clin Infect Dis. 2017;65(suppl_1):S30–8. https://doi.org/10.1093/cid/cix463
3. Steen CJ, Carbonaro PA, Schwartz RA. Arthropods in dermatology. J Am Acad Dermatol. 2004;50:819–42, quiz 842–4. https://doi.org/10.1016/j.jaad.2003.12.019
4. Bernardeschi C, Le Cleach L, Delaunay P, Chosidow O. Bed bug infestation. BMJ. 2013;346(jan22 1):f138. https://doi.org/10.1136/bmj.f138
5. Larva of *Anthrenus verbasci*, 2020 [cited 2020 Apr 24]. https://fr.wikipedia.org/w/index.php?title=Anthrenus_verbasci&oldid=166281282

6. Hoverson K, Wohltmann WE, Pollack RJ, Schissel DJ. Dermestid dermatitis in a 2-year-old girl: case report and review of the literature. Pediatr Dermatol. 2015;32:e228–33. https://doi.org/10.1111/pde.12641
7. Jurecka W, Gebhart W, Mainitz M. *Anthrenus* sp.: the paraffin block eater bug. Am J Dermatopathol. 1987;9:204–7. https://doi.org/10.1097/00000372-198706000-00004
8. Ruzzier E, Kadej M, Battisti A. Occurrence, ecological function and medical importance of dermestid beetle hastisetae. PeerJ. 2020;8:e8340. https://doi.org/10.7717/peerj.8340
9. Ahmed AR, Moy R, Barr AR, Price Z. Carpet beetle dermatitis. J Am Acad Dermatol. 1981;5:428–32. https://doi.org/10.1016/S0190-9622(81)70104-X
10. MacArthur KM, Richardson V, Novoa RA, Stewart CL, Rosenbach M. Carpet beetle dermatitis: a possibly under-recognized entity. Int J Dermatol. 2016;55:577–9. https://doi.org/10.1111/ijd.12952
11. Johansson SG, Wüthrich B, Zortea-Caflisch C. Nightly asthma caused by allergens in silk-filled bed quilts: clinical and immunologic studies. J Allergy Clin Immunol. 1985;75:452–9. https://doi.org/10.1016/S0091-6749(85)80017-8

Address for correspondence: Loïc Simon, Service de Parasitologie Mycologie, Centre Hospitalier Universitaire de Nice, Hôpital l'Archet, 151 Route Saint-Antoine de Ginestière, CS 23079, 06202 Nice CEDEX 3, France; email: simon.l@chu-nice.fr

Multisystem Inflammatory Syndrome after SARS-CoV-2 Infection and COVID-19 Vaccination

Mark B. Salzman, Cheng-Wei Huang, Christopher M. O'Brien, Rhina D. Castillo

We report 3 patients in California, USA, who experienced multisystem inflammatory syndrome (MIS) after immunization and severe acute respiratory syndrome coronavirus 2 infection. During the same period, 3 adults who were not vaccinated had MIS develop at a time when ≈7% of the adult patient population had received ≥1 vaccine.

Multisystem inflammatory syndrome (MIS) in children (MIS-C) and adults (MIS-A) are febrile syndromes with elevated inflammatory markers that usually manifest 2–6 weeks after a severe acute respiratory syndrome 2 (SARS-CoV-2) infection (*1*–*3*). The Brighton Collaboration Case Definition for MIS-C/A was recently published to be used in the evaluation of patients after SARS-CoV-2 immunization (*3*); some scientists are concerned that vaccination against SARS-CoV-2 can trigger MIS-C/A. We report 6 cases of MIS from a large integrated health system in Southern California, USA; 3 of those patients received SARS-CoV-2 vaccination shortly before seeking care for MIS. All 6 patients met the Brighton Collaboration Level 1 of diagnostic certainty for a definitive case and had MIS illness onset between January 15–February 15, 2021. The Chief Compliance Officer for the Southern California Permanente Medical Group reviewed this case series and confirmed that it was compliant with the Health Insurance Portability and Accountability Act for publication.

The Study

Patient 1 was a 20-year-old Hispanic woman who sought care for 3 days of a diffuse body rash, tactile fever, sore throat, mild neck discomfort, and fatigue. There was no cough, congestion, headache, or abdominal pain. She had vomiting and diarrhea, which had subsided 8 days before admission. She received her first dose of SARS-CoV-2 vaccine 15 days before admission. She had no known coronavirus disease (COVID-19) exposure but was SARS-CoV-2 PCR and nucleocapsid IgG positive. She was hypotensive at arrival to the emergency department, requiring inotropic support. She had elevated troponin and brain natriuretic peptide (BNP) with a left ventricular ejection fraction initially mildly reduced at 45% but 30%–35% the following day. She responded well to therapy with intravenous immunoglobulin (IVIG) and methylprednisolone (Table 1).

Patient 2 was a 40-year-old Hispanic man who sought care after 6 days of episodic fevers up to 101.7°F. Associated symptoms included dyspnea on exertion, headache, neck pain, lethargy, abdominal pain, and diarrhea. No chest pain was present. He had a history of SARS-CoV-2 vaccination and laboratory-confirmed mild to moderate COVID-19, both within 48 days before seeking care (Figure). His exam was notable for sweats, diffuse abdominal pain on palpation, tachycardia, and tachypnea. Patient 2 fulfilled Brighton Level 1 criteria for MIS-A with documented fevers, gastrointestinal and neurologic symptoms, elevated inflammatory and cardiac markers, and electrocardiogram changes that were concerning for myocarditis (*3*). He responded well to treatment with dexamethasone (Table 1).

Patient 3 was an 18-year-old Asian American man who sought care at the emergency department with a history of 3 days of fever as high as 104°F with headache, vomiting, diarrhea, and abdominal cramping (Figure). He denied any upper respiratory symptoms. He had a history of a laboratory-confirmed COVID-19 infection 6 weeks before the onset of symptoms and received the first dose of

Author affiliations: Kaiser Permanente West Los Angeles Medical Center, Los Angeles, California, USA (M.B. Salzman); Kaiser Permanente Los Angeles Medical Center, Los Angeles (C.-W. Huang); Kaiser Permanente Zion Medical Center, San Diego, California, USA (C.M. O'Brien); Kaiser Permanente Tustin Ranch Medical Offices, Tustin, California, USA (R.D. Castillo)

DOI: https://doi.org/10.3201/eid2707.210594

the SARS-CoV-2 vaccine 18 days before the onset of symptoms. In the emergency department, he was found to be hyponatremic and hypotensive (Table 1). His examination was notable for tachycardia and abdominal tenderness. He had elevated inflammatory markers, thrombocytopenia, and lymphopenia. Echocardiogram revealed mild to moderate reduced systolic function with an ejection fraction

Table 1. Demographic, laboratory, and clinical characteristics of 3 patients who had multisystem inflammatory syndrome after SARS-CoV-2 immunization, Southern California, USA

Characteristic	Patient 1	Patient 2	Patient 3
Age, y/sex	20 y/F	40 y/M	18 y/M
Race/ethnicity	Hispanic/Latina	Hispanic/Latino	Asian/Filipino
Underlying conditions	Asthma	Depression, hyperlipidemia	Asthma
Symptoms	Fever and rash for 3 d, diarrhea, vomiting, cardiogenic shock, acute renal failure	6 d of fevers, malaise, diarrhea, neck pain, headache, lethargy	3 d of fever, 2 d of abdominal pain, diarrhea, vomiting and headache
Initial vital signs	Pulse: 130 beats/min, BP 73/56 mm Hg, RR 20 breaths/min, temp 99.4°F, repeat temp 101.4, O2 sats 99% on RA; BMI: 27.85	Pulse 102 beats/min, BP 136/88 mm Hg, RR 20 breaths/min, temp 99.2°F, O2 sats 97% on RA; BMI: 28.89	Pulse 96 beats/min, BP 98/58 mm Hg, RR 20 breaths/min, temp 97.9°F, sats 97% on RA; BMI: 23.99
Treatment	Vasopressors × 3 d, IVIG 100 g, methylprednisolone 1 g/d for 3 d, heparin, broad spectrum antibiotics, remdesivir	Dexamethasone 6 mg/d for 10 d, ceftriaxone, azithromycin, enoxaparin	IVIG 100 g, methylprednisolone 1 g/d for 3 d, anakinra 100 mg/d for 3 d, broad-spectrum antibiotics, aspirin
Imaging	TTE: normal LV, mildly reduced EF 45% which decreased to 30%–35% the next day; chest radiograph: subtle bibasilar ground glass opacities	EKG: ST depression and T wave inversion in inferior leads; TTE: normal LV; EF: 50%–55%; CT angiogram: no pulmonary embolism, minimal ground glass opacities	TTE: normal LV size with mild to moderately reduced EF 40%–45%, right ventricle mildly dilated with normal systolic function; chest radiograph: right pleural effusion; CT abdomen and pelvis: hepatomegaly, splenomegaly, small ascites; pericholecystic fluid; retroperitoneal adenopathy.
Length of hospital stay	8 d	3 d	9 d
First vaccine	12 d before symptom onset	42 d before symptom onset	19 d before symptom onset
Second vaccine	NA	4 d before symptom onset	NA
Previously known COVID-19 disease	No	34 d before symptom onset	43 d before symptom onset
Initial lab results (reference range)			
Serum leukocytes, × 1,000/mcL (4.5–14.5)	32.3	11.3	7
Lymphocytes absolute, × 1,000/mcL (1.5–6.8)	0.55	0.94	0.26
Neutrophils absolute, × 1,000/mcL (1.5–8.00)	31.75	12.68	6.28
Platelets, × 1,000/mcL (130–400)	155	312	63
Creatinine, mg/dL (≤1.00)	2.64	1.12	1.12
C-reactive protein, mg/L (<7.4)	378	199.4	185.5
D-dimer, µg FEU/mL (≤0.49)	3.01	1.15	3.44
Ferritin, ng/mL (17–168)	533	1,079.7	3,002
Fibrinogen, mg/dL (218–441)	801	875	693
Troponin, ng/mL (≤0.03)	1.54	0.37	0.06
BNP, pg/mL (≤99)	1,498	672	106
LDH, U/L (≤279)	251	156	291
AST, U/L (≤34)	43	55	59
ALT, U/L (<63)	28	83	58
Procalcitonin, ng/mL (0.0–0.1)	160.92	0.01	4.41
SARS-COV-2 nucleocapsid IgG qualitative	Positive	Positive	Positive
SARS-COV-2 PCR	Positive	Positive	Negative
Blood culture	Negative × 2	Negative × 2	Negative × 2
Urine culture	Negative	Not done	Negative (after antibiotics)
Bacterial GI PCR panel	Negative	Not done	Negative

*All patients received the Pfizer-BioNTech vaccine (https://www.pfizer.com). ALT, alanine aminotransferase; AST, aspartate aminotransferase; BMI, body mass index; BNP, brain natriuretic peptide; BP, blood pressure; CT, computed tomography; EF, ejection fraction; EKG, electrocardiogram; GI, gastrointestinal; IVIG, intravenous immunoglobulin; LDH, lactate dehydrogenase; LV, left ventricle; MR, mitral regurgitation; NA, not applicable; RA, room air; RR, respiratory rate; SARS-CoV-2, severe acute respiratory syndrome coronavirus 2; sats, saturations; temp, temperature; TR, tricuspid regurgitation; TTE, transthoracic echocardiogram.

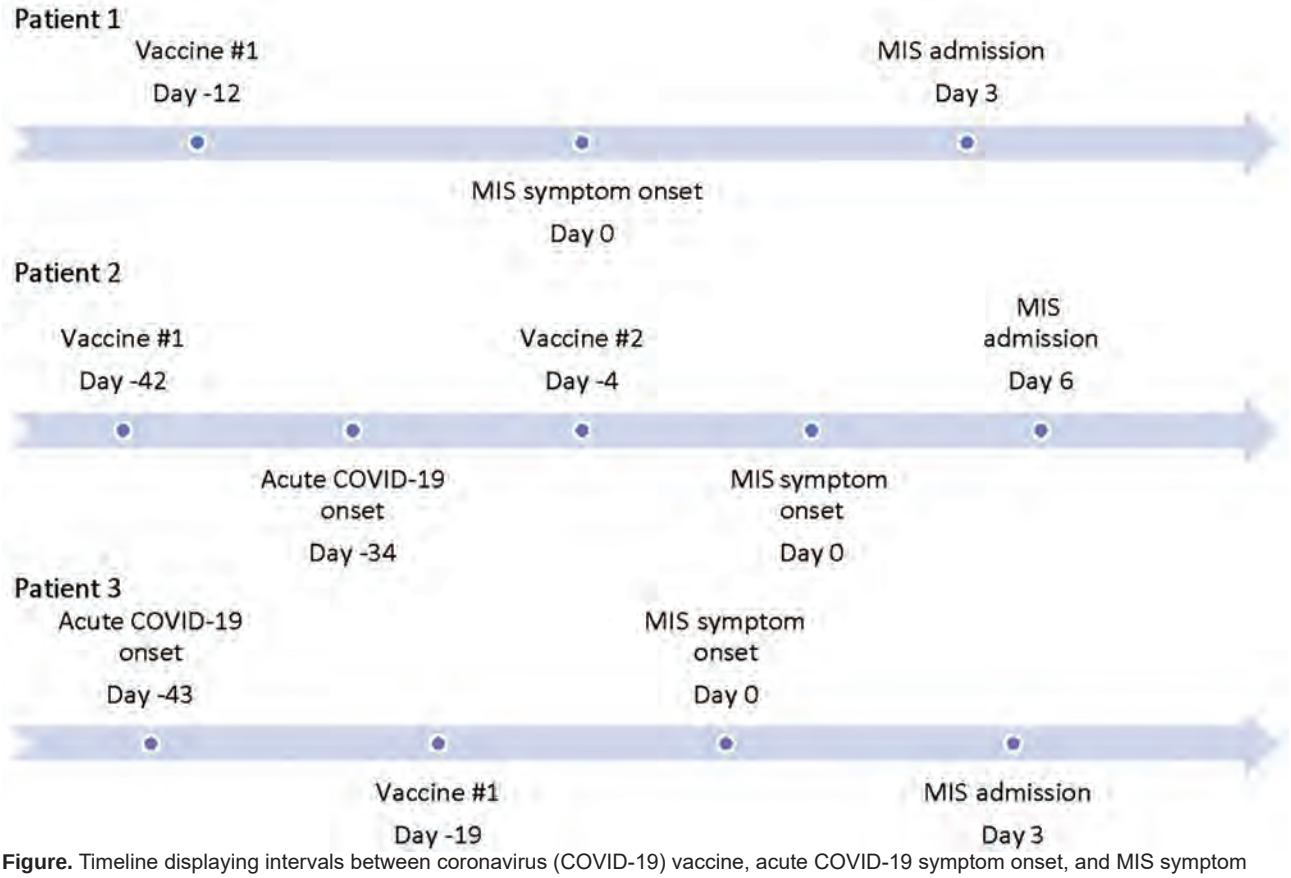

Figure. Timeline displaying intervals between coronavirus (COVID-19) vaccine, acute COVID-19 symptom onset, and MIS symptom onset in patients in California, USA. MIS, multisystem inflammatory syndrome.

of 40%–45%. He responded well to therapy with methylprednisolone, IVIG, and anakinra.

Patient 4 was a 62-year-old Asian American man who sought care at the emergency department for fever lasting 5 days. For 6 days he had had nausea and vomiting, which developed 23 days after a laboratory-confirmed mild to moderate acute COVID-19 illness that subsided after 1 week. He also had 4 days of bilateral hearing loss. He was hypotensive, requiring inotropic support. He had thrombocytopenia, elevated inflammatory markers, and elevated troponin with diffuse ST elevations on electrocardiogram (Table 2). He responded well to treatment with methylprednisolone, including improvement in his hearing loss.

Patient 5 was a 29-year-old Hispanic woman who experienced fever, chills, headache, and nausea 28 days after a laboratory-confirmed acute COVID-19 illness. She sought care at the emergency department with hypotension requiring inotropic support. Clinicians diagnosed MIS-A on the basis of conjunctivitis, evidence of colitis on abdominal imaging, elevated inflammatory markers, lymphopenia, and elevated BNP. She responded well to treatment with methylprednisolone and IVIG (Table 2).

Patient 6 was a 23-year old Hispanic man who experienced fever and abdominal pain 38 days after a laboratory-confirmed mild to moderate acute COVID-19 illness. He was hypotensive, requiring inotropic support. He had mesenteric adenitis on abdominal imaging. He had elevated inflammatory markers, neutrophilia, lymphopenia, and a left ventricular ejection fracture of 20% on echocardiogram. He was treated with IVIG and methylprednisolone (Table 2). He died 12 days after admission.

Conclusions

At the time of our study, our medical group was only vaccinating healthcare workers and patients ≥75 years of age. The 3 patients that were immunized qualified for early vaccination because they either worked or volunteered in a healthcare setting. These cases occurred ≈1 month after the peak surge of COVID-19 cases in Southern California. At the time these patients sought care, only ≈7% of the adult (≥18 years of age) population who were

Table 2. Demographic, laboratory, and clinical characteristics of patients who had multisystem inflammatory syndrome without SARS-CoV-2 immunization, California, USA

Characteristic	Patient 4	Patient 5	Patient 6
Age/sex	62 y/M	29 y/F	23 y/M
Race/ethnicity	Asian	Hispanic/Latina	Hispanic/Latino
Underlying conditions	Hyperlipidemia, gout, atrial fibrillation	Obesity	Asthma, obesity
Signs and symptoms	6 d of fever, vomiting, abdominal pain, 4 d of hearing loss; shock, acute renal failure	4 d of fever, headaches, vomiting, abdominal pain; conjunctivitis, shock, acute kidney injury	4 d of fever, abdominal pain, diarrhea, cough, SOB; shock
Initial vital signs	Pulse 121 beats/min, BP 112/63 mm Hg, RR 20 breaths/min, temp 101.6°F, O2 sats 98%; within 1 h in ER: BP 70/56 mm Hg, pulse 112 beats/min, RR 28 breaths/min, O2 sat 97%; BMI: 28.1	Pulse 140 beats/min, BP 102/71 mm Hg (61/48 mm Hg after 5 h of being in ER), RR 20, temp 105.2°F, O2 sats 99%; BMI: 31.63	Pulse 125 beats/min, BP 87/27 mm Hg, temp 98.2°F, O2 sats 98% on RA; BMI: 40.3
Treatment	Vasopressors, methylprednisolone 125 mg every 6 h, broad spectrum antibiotics, enoxaparin	Vasopressors, methylprednisolone 30 mg every 12 h, IVIG 100 g, heparin, ceftriaxone, ciprofloxacin	Vasopressors, IVIG 2 g/kg, methylprednisolone 1 g daily for 3 d, broad spectrum antibiotics
Imaging	EKG: diffuse ST elevation; TTE: mild concentric LVH, mild LV systolic dysfunction, EF 50%; CT angiogram: no evidence of embolus; increased interstitial markings and hazy ground glass changes, small bilateral pleural effusions; 6 mm pericardiac effusion; ultrasound: right popliteal DVT	TTE: LVEF 50%–55%, mild TR regurgitation, abdominal CT with colitis and enlarged lymph nodes	EKG: sinus tachycardia, no ST changes; TTE: LVEF 20%, global hypokinesis, abdominal CT with mesenteric adenitis
Length of hospital stay	7 d	10 d	12 d; deceased
First vaccine	NA	NA	NA
Second vaccine	NA	NA	NA
Previously known COVID-19	23 days before symptom onset	28 d before symptom onset	38 d before symptom onset
Initial lab results (reference ranges)			
Serum leukocytes, × 1,000/mcL (4.5–14.5)	18.4	10.2	6.8
Lymphocytes absolute, × 1,000/mcL (1.5–6.8)	0.00	0.35	0.52
Neutrophils absolute, × 1,000/mcL (1.5–8.00)	17.66	9.66	14.35
Platelets, × 1,000/mcL (130–400)	102	170	185
Creatinine, mg/dL (≤1.00)	2.24	0.78	2.49
C-reactive protein, mg/L (<7.4)	351.7	364.9	246.3
D-dimer, µg FEU/mL (≤0.49)	7.21	5.79	>4
Ferritin, ng/mL (17–168)	5,032	606	1,273 at admission, >18,000 at its peak 2 days later
Fibrinogen, mg/dL (218–441)	N/A	N/A	454
Troponin, ng/mL (≤0.03)	0.85	0.06	<0.02
BNP, pg/mL (≤99)	931	331	228
LDH, U/L (≤279)	267	N/A	224
AST, U/L (≤34)	38	N/A	42
ALT, U/L (<63)	40	55 8	88
Procalcitonin, ng/mL (0.0–0.1)	Not done	8.15	29.37
SARS-COV-2 nucleocapsid IgG qualitative	Not done	Positive	Not done
SARS-COV-2 PCR	Positive	Negative	Positive
Blood culture	Negative x 2	Negative x 4	Negative x 9
Urine culture	Negative (after antibiotics)	Negative (after antibiotics)	Negative (after antibiotics)
Bacterial GI PCR panel	Not done	Negative	Not done

*ALT, alanine aminotransferase; AST, aspartate aminotransferase; BMI, body mass index; BNP, brain natriuretic peptide; BP, blood pressure; CT, computed tomography; COVID-19, coronavirus disease; DVT, deep venous thrombosis; EF, ejection fraction; EKG, electrocardiogram; GI, gastrointestinal; IVIG, intravenous immunoglobulin; LDH, lactate dehydrogenase; LV, left ventricle; MR, mitral regurgitation; NA, not applicable; RA, room air; RR, respiratory rate; SARS-CoV-2, severe acute respiratory syndrome coronavirus 2; sats, saturations; temp, temperature; TR, tricuspid regurgitation; TTE, transthoracic echocardiogram.

members of the Kaiser Permanente patient group (≈3,776,000 members) had received ≥1 SARS-CoV-2 vaccine, whereas 3 of the 6 patients in this study who had MIS were vaccinated. These 6 patients were hospitalized at 5 of the 15 Kaiser Permanente medical centers across Southern California. We believe the temporal association after SARS-CoV-2 immunization is worth noting, given the theoretical concern of MIS-C/A after vaccination (*3*). We did not identify any patients with MIS after vaccination who did not have recent SARS-CoV-2 infection. It is possible that other case-patients in our member population were hospitalized outside of our 15 medical centers and thus were not captured for this case series.

Overall, MIS is rare in adults. In comparison we treated >50 children with MIS-C during January 2021–February 2021 and >100 since May 2020 among a pediatric population of 960,000.

The Centers for Disease Control and Prevention (CDC) allows for vaccination after a SARS-CoV-2 infection after recovery from the acute illness and after the isolation period, with no recommended minimal interval between infection and vaccination (*4*). Most cases of MIS-C/A occur 2–6 weeks after an exposure or infection (*1*–*3*), although we have seen several children brought for care as late as 8–10 weeks after a confirmed infection or exposure. We need to continue to monitor for MIS-C/A after SARS-CoV-2 infection and immunization as more of the population are vaccinated, especially as vaccines are administered to children who are at higher risk for MIS. CDC and the US Food and Drug Administration co-manage VAERS (the Vaccine Adverse Event Reporting System), which is being used to monitor for adverse events after COVID-19 vaccines. MIS-C/A is listed as a postvaccination adverse event of special interest (*5*) and should be reported to VAERS (*6*).

About the Author

Dr. Salzman is a pediatric infectious diseases physician and assistant chief of the Department of Pediatrics at Kaiser Permanente West Los Angeles Medical Center, Los Angeles, California. He is also the regional lead physician in pediatric infectious diseases for the Southern California Permanente Medical Group.

References

1. Morris SB, Schwartz NG, Patel P, Abbo L, Beauchamps L, Balan S, et al. Case series of multisystem inflammatory syndrome in adults associated with SARS-CoV-2 infection—United Kingdom and United States, March–August 2020. MMWR Morb Mortal Wkly Rep. 2020;69:1450–6. https://doi.org/10.15585/mmwr.mm6940e1
2. Godfred-Cato S, Bryant B, Leung J, Oster ME, Conklin L, Abrams J, et al.; California MIS-C Response Team. COVID-19–associated multisystem inflammatory syndrome in children—United States, March–July 2020. MMWR Morb Mortal Wkly Rep. 2020;69:1074–80. https://doi.org/10.15585/mmwr.mm6932e2
3. Vogel TP, Top KA, Karatzios C, Hilmers DC, Tapia LI, Moceri P, et al. Multisystem inflammatory syndrome in children and adults (MIS-C/A): case definition & guidelines for data collection, analysis, and presentation of immunization safety data. Vaccine. 2021 Feb 25 [Epub ahead of print]. https://doi.org/10.1016/jvaccine.2021.01.054
4. US Centers for Disease Control and Prevention. Interim clinical considerations for use of COVID-19 vaccines currently authorized in the United States. April 27, 2021 [cited 2021 May 12]. https://www.cdc.gov/vaccines/covid-19/info-by-product/clinical-considerations.html
5. US Centers for Disease Control and Prevention. Vaccine Adverse Event Reporting System (VAERS) standard operating procedure for COVID-19 (as of 29 January 2021). 2021 [cited 2021 May 12]. https://www.cdc.gov/vaccinesafety/pdf/VAERS-v2-SOP.pdf
6. US Department of Health and Human Services; Vaccine Adverse Event Reporting System. COVID-19 vaccine EUA reporting requirements for providers. https://vaers.hhs.gov/index.html

Address for correspondence: Mark B. Salzman, Department of Pediatrics, Kaiser Permanente West Los Angeles Medical Center, 6041 Cadillac Ave, Los Angeles, CA 90034, USA; email: mark.b.salzman@kp.org

Pneumococcal Disease Outbreak at a State Prison, Alabama, USA, September 1–October 10, 2018[1]

Guillermo V. Sanchez, Constance L. Bourne, Sherri L. Davidson, Mark Ellis, Leora R. Feldstein, Katherine Fay, Nicole E. Brown, Evelyn F. Geeter, Lytasha L. Foster, Charlotte Gilmore, Mary G. McIntyre, Burnestine Taylor, Srinivasan Velusamy, Sopio Chochua, Almea M. Matanock

A pneumococcal disease outbreak caused by *Streptococcus pneumoniae* serotype 12F occurred in a state prison in Alabama, USA. Among 1,276 inmates, 40 cases were identified (3 confirmed, 2 probable, 35 suspected). Close living quarters, substance use, and underlying conditions likely contributed to disease risk. Prophylaxis for close contacts included azithromycin and 23-valent pneumococcal polysaccharide vaccine.

Streptococcus pneumoniae (pneumococcus) causes a spectrum of disease ranging from mild respiratory infections to severe disease, including meningitis, sepsis, and pneumonia (*1*). Invasive pneumococcal disease (IPD) occurs when pneumococcus invades normally sterile sites. Pneumococcus is transmitted person-to-person primarily through respiratory droplets and is a leading cause of vaccine-preventable illness and death (*2*). Pneumococcal colonization is a precursor to disease but does not always result in disease (*3*). Pneumococcal conjugate vaccine (PCV) is highly effective in preventing pneumonia in adults (*4*), and pneumococcal disease incidence has declined since the introduction of PCV (*5*). IPD outbreaks are rare but can occur in settings with close person-to-person contact, such as homeless shelters (*6*) and healthcare facilities, in which underlying conditions can increase disease risk (*7*).

On September 19, 2018, the Alabama Department of Public Health (Montgomery, AL) was notified of an IPD case after identification of *S. pneumoniae* in a blood culture from an ill patient incarcerated at a state prison. On September 24, a second case of IPD was reported in another inmate who received a diagnosis of meningitis and sepsis and died that morning. We investigated this outbreak to determine its extent, identify cases among staff and inmates, and recommend prophylactic measures to reduce spread.

The Study

At the time of the outbreak, facility A, a medium-security state prison, housed 1,276 male inmates across 6 dormitories (original capacity 650 inmates; 2018 reported capacity of 1,650 inmates) (*8*,*9*). Each dormitory contained multiple large rooms with 4–6 rows of beds for 190–255 inmates. Group activities allowed mixing of inmates from different dorms until the outbreak was recognized; activities were suspended around September 26. A clinic within facility A with a 52-member staff, including 2 nurse practitioners and a physician, provided services to inmates through self or employee referral.

A suspected case was defined as respiratory or meningeal symptoms consistent with pneumococcal disease in an incarcerated person or a person in prolonged or close contact with anyone incarcerated at facility A during September 1–October 10, 2018 (Appendix, https://wwwnc.cdc.gov/EID/article/27/7/20-3678-App1.pdf). Probable cases were defined as suspected cases with radiographic-confirmed pneumonia, clinical sepsis, or cerebrospinal fluid analysis suggestive of bacterial meningitis with unknown etiology. Confirmed cases were

Author affiliations: Centers for Disease Control and Prevention, Atlanta, Georgia, USA (G.V. Sanchez, L.R. Feldstein, K. Fay, N.E. Brown, S. Velusamy, S. Chochua, A.M. Matanock); Alabama Department of Public Health, Montgomery, Alabama, USA (G.V. Sanchez, C.L. Bourne, S.L. Davidson, M. Ellis, E.F. Geeter, L.L. Foster, C. Gilmore, M.G. McIntyre, B. Taylor)

DOI: https://doi.org/10.3201/eid2707.203678

[1]Preliminary results from this study were presented at the Centers for Disease Control and Prevention 2019 Epidemic Intelligence Service conference, April 29–May 2, 2019, Atlanta, Georgia, USA.

defined as suspected cases with *S. pneumoniae* isolation or positive urinary antigen test.

We conducted retrospective case finding among inmates who were seen in the clinic during September 1–September 29 and prospective surveillance during September 30–October 10. Cases in which inmates reported respiratory illness, altered mental status, headache, or fever and those without a listed chief complaint were flagged for medical chart review. Inmates whose medical records indicated signs or symptoms of pneumococcal disease were interviewed by using a standardized questionnaire to identify clinical characteristics, risk factors, and epidemiologic links with confirmed cases. For prospective surveillance, we screened all inmates who experienced respiratory symptoms for pneumococcus and influenza by using nasopharyngeal swabs. We tested influenza-negative swab specimens for other respiratory pathogens by using the BioFire FilmArray Respiratory Panel (bioMérieux, https://www.biomerieux.com). We performed pneumococcal serotyping on nasopharyngeal swab specimens from which *S. pneumoniae* was isolated. We calculated attack rates by dividing the number of identified cases by the at-risk population (i.e., all dormitory residents). Specimen culture and antibiotic susceptibility testing was performed at laboratories in the hospitals in which patients received care and confirmed at the Centers for Disease Control and Prevention. Sterile body fluids and nasopharyngeal swab specimens were sent to Centers for Disease Control and Prevention for species detection, confirmation, and serotyping by using real-time reverse transcription PCR. Bacterial serotyping and whole-genome sequencing (WGS) were performed on pneumococcal isolates collected from confirmed cases. We analyzed single-nucleotide polymorphisms identified through WGS to verify temporal relatedness of the isolates.

Through retrospective case finding, 96 medical chart reviews and 52 inmate interviews identified 40 cases (3 confirmed, 2 probable, and 35 suspected; Figure) for attack rates of 3% (40/1,276) within facility A and 5% (14/255) within dormitory X. All confirmed cases occurred in inmates living in dormitory X. Suspected cases were identified among inmates in all 6 dormitories. No pattern of temporal spread was observed among dormitories. Of suspected cases, 26% (9/35) reported lower respiratory symptoms (chest pain, shortness of breath, or fever with cough) (Table 1). Underlying conditions for which 23-valent pneumococcal polysaccharide vaccine (PPSV23) is routinely recommended (excluding smoking tobacco) (*10*) were reported in 2/5 (40%) confirmed or probable cases and 6/35 (17%) suspected cases. In 3/35 (9%) suspected cases, patients were immunocompromised. Of the 28/40 (70%) patients who reported smoking cigarettes, half (14/28, 50%) reported sharing cigarettes.

Blood (n = 5) or cerebrospinal fluid (n = 4) specimens were collected from 5 patients. Three *S. pneumoniae* isolates were identified from 3 patients (2 from cerebrospinal fluid, 1 from blood); all 3 were serotype 12F. WGS demonstrated a 2–5 single-nucleotide polymorphism difference among isolates, indicating all confirmed cases were closely related. Antimicrobial susceptibility testing confirmed isolate susceptibility.

During prospective surveillance, we collected nasopharyngeal swab specimens from 2 inmates; *S. infantis* serotype 13 was detected in 1 specimen and adenovirus only in the other. No additional cases were identified. Prophylaxis with PPSV23, which protects against serotype 12F, and 2 doses of azithromycin were offered to inmates and close contacts living in or assigned to dormitory X, clinic staff, and prison employees (Table 2).

Conclusions

This investigation highlights the outbreak potential of *S. pneumoniae* and demonstrates that correctional facilities remain at risk for pneumococcal outbreaks after PCV introduction in the United States. The last

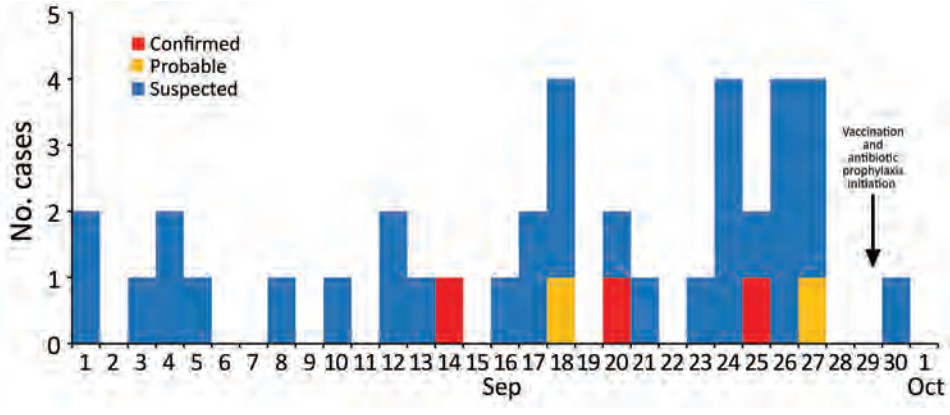

Figure. Epidemic curve of identified cases among inmates in study of pneumococcal disease outbreak at a state prison, Alabama, USA, September 1–October 10, 2018. Date of first symptom onset is shown. Healthcare unit visit date was used when symptom onset date was not known. Two suspected cases without a clear onset date were excluded from this graph.

Table 1. Patient demographics, signs, symptoms, and *Streptococcus pneumoniae* risk factors by case classification in study of pneumococcal disease outbreak at a state prison, Alabama, USA, September 1–October 10, 2018*

Demographics	Confirmed cases, n = 3	Probable cases, n = 2	Suspected cases, n = 35
Median age, y (range)	46 (44–61)	42 (26–58)	39 (23–64)
Race			
Black	3 (100)	0	14 (40)
White	0	2 (100)	13 (37)
Unknown	0	0	8 (23)
Signs or symptoms			
Fever	2 (67)	1 (50)	15 (43)
Cough	2 (67)	1 (50)	19 (54)
Shortness of breath	1 (33)	2 (100)	4 (11)
Chest pain	1 (33)	1 (50)	6 (17)
Headache	1 (33)	0	11 (31)
Neck stiffness	2 (67)	0	1 (3)
Altered mental status	3 (100)	1 (50)	0
Congestion	0	0	6 (17)
Clinical features and risk factors			
Immunocompromising condition†	0	0	3 (9)
Chronic medical condition‡	1 (33)	1 (50)	6 (17)
Substance use: cigarettes, alcohol, or illicit drugs	2 (67)	0	27 (77)
Assigned housing			
Dormitory X	3 (100)	0	11 (31)
Dormitory Y	0	1 (50)	8 (23)
Other dormitories: U, V, W, Z	0	0	16 (46)
Healthcare unit	0	1 (50)	0

*Values are no. (%) except as indicated. Table includes composite statistics from both inmate interviews and medical chart abstractions. All identified cases occurred in inmates; no cases were identified among staff members.
†Includes immune suppression, chronic renal failure, HIV, solid organ transplant, asplenia, sickle cell disease and other hemoglobinopathies, and malignancy excluding skin cancer (Centers for Disease Control and Prevention Adult Vaccine Schedule, https://www.cdc.gov/vaccines/acip).
‡Includes chronic heart, liver, kidney, lung diseases, and diabetes mellitus; excludes documented substance abuse, Hepatitis C infection, and chronic osteomyelitis (Centers for Disease Control and Prevention Adult Vaccine Schedule, https://www.cdc.gov/vaccines/acip).

documented pneumococcal disease outbreak at a US correctional facility also involved serotype 12F and occurred in 1989 in a crowded Texas jail, in which 46 inmates experienced pneumonia, meningitis, or sepsis over a 4-week period (*11*). Unlike jails, which have an average detention length of <2 months, prisons have lower rates of inmate turnover because they are designed for long-term incarceration; the average detention among US state prisoners in 2016 was 2.6 years (*12*). However, jails and prisons are similar in that they share risk factors for outbreaks, such as potential overcrowding and increased medical and behavioral risk factors for communicable diseases (*13*). Decreases in pneumococcal disease have been observed during outbreaks after administering prophylactic antibiotics and PPSV23 to high-risk persons (*6*,*7*,*11*,*14*). Risk for pneumococcal disease outbreaks in prisons can be minimized by offering inmates vaccinations per Advisory Committee on Immunization Practices recommendations, which recommend PPSV23 for persons with chronic heart, liver, or lung disease (*15*). Risk can be further reduced by minimizing inmate crowding, eliminating indoor smoking, and ensuring adequate ventilation (*11*).

Table 2. Administration of pneumococcal polysaccharide vaccine and antibiotic prophylaxis to reduce *Streptococcus pneumoniae* transmission in prison inmates during a pneumococcal disease outbreak, Alabama, USA, September 29–October 10, 2018*

Prophylaxis type	Status	No. (%)		
		Inmates, n = 264†	Medical staff, n = 52	Prison employees, n = 72
PPSV23 vaccine	Received	206 (78)	32 (62)	62 (86)
	Declined	58 (22)	18 (35)	8 (11)
	Absent or unknown	0	2 (4)	2 (3)
Dose 1: azithromycin 500 mg‡	Received	232 (88)	11 (21)	70 (97)
	Declined	15 (6)	6 (12)	0
	Absent or unknown	17 (6)	35 (67)	2 (3)
Dose 2: azithromycin 1000 mg	Received	246 (93)	35 (67)	46(64)
	Declined	18 (7)	16 (31)	4 (6)
	Absent or unknown	0	1 (2)	22 (31)

*Because of rounding, all cells might not sum to 100%. PPSV23, 23-valent pneumococcal polysaccharide vaccine.
†Inmates assigned to dormitory X (n = 255) or living in dormitory X without an assignment (n = 9) were offered prophylaxis. Not all inmates lived or slept in the dorm to which they were assigned.
‡Initial antibiotic prophylaxis dosing was chosen by the Alabama Department of Corrections as 500 mg offered on September 29 and a planned second dose of 500 mg 1 week later. This dose would have provided less antibiotic coverage than previous outbreak regimens. Based on Alabama Department of Health recommendations, a higher, single dose of azithromycin (1,000 mg) was offered during October 3–October 10.

One limitation of this study was that risk factor information was collected by self-reporting and might be underestimated. Disease etiology was not confirmed for most cases because few patients had confirmatory laboratory testing for respiratory pathogens. Dormitories were not assessed for space, capacity, or ventilation.

Pneumococcal colonization among inmates could not be widely assessed. We observed decreases in pneumococcal disease after prophylaxis administration, but we cannot determine the direct impact of prophylaxis since *S. pneumoniae* serotype 12F carriage was not measured. Pneumococcal carriage studies among incarcerated populations could further our understanding of pneumococcal disease in correctional facilities.

In our outbreak investigation of pneumococcal disease in a state prison, we observed decreases in disease after prophylaxis with PPSV23 and azithromycin. Increased pneumococcal disease risk might have resulted from close living quarters, substance use, and underlying conditions. Improved pneumococcal disease surveillance and proactive vaccination of at-risk inmates in accordance with Advisory Committee on Immunization Practices recommendations might mitigate risk for and scale of future outbreaks.

Acknowledgments

We thank the Alabama Department of Corrections for collaboration during this investigation.

About the Author

Mr. Sanchez is an Epidemic Intelligence Service officer with the National Center for Emerging and Zoonotic Infectious Diseases, Centers for Disease Control and Prevention, assigned to the Alabama Department of Public Health. His research interests include antibiotic resistance, antibiotic stewardship, and healthcare-associated infections.

References

1. Simell B, Auranen K, Käyhty H, Goldblatt D, Dagan R, O'Brien KL; Pneumococcal Carriage Group. The fundamental link between pneumococcal carriage and disease. Expert Rev Vaccines. 2012;11:841–55. https://doi.org/10.1586/erv.12.53
2. Centers for Disease Control and Prevention. Pneumococcal disease: types of infection [cited 2019 Nov 14]. https://www.cdc.gov/pneumococcal/about/infection-types.html
3. Bogaert D, De Groot R, Hermans PWM. Streptococcus pneumoniae colonisation: the key to pneumococcal disease. Lancet Infect Dis. 2004;4:144–54. https://doi.org/10.1016/S1473-3099(04)00938-7
4. Bonten MJM, Huijts SM, Bolkenbaas M, Webber C, Patterson S, Gault S, et al. Polysaccharide conjugate vaccine against pneumococcal pneumonia in adults. N Engl J Med. 2015;372:1114–25. https://doi.org/10.1056/NEJMoa1408544
5. Shiri T, McCarthy ND, Petrou S. The impact of childhood pneumococcal vaccination on hospital admissions in England: a whole population observational study. BMC Infect Dis. 2019;19:510. https://doi.org/10.1186/s12879-019-4119-8
6. Romney MG, Hull MW, Gustafson R, Sandhu J, Champagne S, Wong T, et al. Large community outbreak of *Streptococcus pneumoniae* serotype 5 invasive infection in an impoverished, urban population. Clin Infect Dis. 2008;47:768–74. https://doi.org/10.1086/591128
7. Fleming-Dutra K, Mbaeyi C, Link-Gelles R, Alexander N, Guh A, Forbes E, et al. *Streptococcus pneumoniae* serotype 15A in psychiatric unit, Rhode Island, USA, 2010-2011. Emerg Infect Dis. 2012;18:1889–93. https://doi.org/10.3201/eid1811.120454
8. Dunn JS, Thomas KT. Alabama Department of Corrections Monthly Statistical Report. September 2018 [cited 2020 Feb 5]. http://www.doc.state.al.us/docs/MonthlyRpts/2018-09.pdf
9. Alabama Department of Corrections. Ventress Correctional Facility [cited 2019 Feb 20]. http://www.doc.state.al.us/facility?loc=38
10. Centers for Disease Control and Prevention. Pneumococcal vaccine timing for adults [cited 2018 Oct 1]. https://www.cdc.gov/vaccines/vpd/pneumo/downloads/pneumo-vaccine-timing.pdf
11. Hoge CW, Reichler MR, Dominguez EA, Bremer JC, Mastro TD, Hendricks KA, et al. An epidemic of pneumococcal disease in an overcrowded, inadequately ventilated jail. N Engl J Med. 1994;331:643–8. https://doi.org/10.1056/NEJM199409083311004
12. Kaeble D. Time served in state prison, 2016. November 2018 [cited 2020 Feb 5]. https://www.bjs.gov/content/pub/pdf/tssp16.pdf
13. Binswanger IA, Krueger PM, Steiner JF. Prevalence of chronic medical conditions among jail and prison inmates in the USA compared with the general population. J Epidemiol Community Health. 2009;63:912–9. https://doi.org/10.1136/jech.2009.090662
14. Crum NF, Wallace MR, Lamb CR, Conlin AMS, Amundson DE, Olson PE, et al. Halting a pneumococcal pneumonia outbreak among United States Marine Corps trainees. Am J Prev Med. 2003;25:107–11. https://doi.org/10.1016/S0749-3797(03)00114-4
15. Centers for Disease Control and Prevention. Advisory Committee on Immunization Practices (ACIP) [cited 2019 Nov 14]. https://www.cdc.gov/vaccines/acip/index.html

Address for correspondence: Guillermo V. Sanchez, Centers for Disease Control and Prevention, 1600 Clifton Rd NE, Mailstop H16-3, Atlanta, GA 30329, USA; email: gsanchez@cdc.gov

Cluster of Oseltamivir-Resistant and Hemagglutinin Antigenically Drifted Influenza A(H1N1)pdm09 Viruses, Texas, USA, January 2020

Teena Mohan,[1] Ha T. Nguyen,[1] Krista Kniss, Vasiliy P. Mishin, Angiezel A. Merced-Morales, Jennifer Laplante, Kirsten St. George, Patricia Blevins, Anton Chesnokov, Juan A. De La Cruz, Rebecca Kondor, David E. Wentworth, Larisa V. Gubareva

Four cases of oseltamivir-resistant influenza A(H1N1) pdm09 virus infection were detected among inhabitants of a border detention center in Texas, USA. Hemagglutinin of these viruses belongs to 6B.1A5A-156K subclade, which may enable viral escape from preexisting immunity. Our finding highlights the necessity to monitor both drug resistance and antigenic drift of circulating viruses.

Resistance to antiviral drugs for influenza is an ongoing public health concern. The neuraminidase (NA) inhibitor oseltamivir is the most prescribed antiviral drug for controlling influenza. However, during 2007–2009, oseltamivir-resistant influenza A(H1N1) viruses rapidly spread worldwide (*1*). Molecular mechanisms implicated in this event were acquisition of NA-permissive mutations that alleviated deleterious fitness effects of the resistance-conferring mutation NA-H275Y (N1 numbering) (*2*); changes that improved balance of hemagglutinin (HA) and NA activities (*3*); and a "hitchhiking" mechanism, in which HA antigenic drift promoted the spread of oseltamivir-resistant viruses (*4*). Oseltamivir-resistant H1N1 viruses were later displaced by the 2009 pandemic virus, influenza A(H1N1)pdm09 (pH1N1), which was antigenically distinct and oseltamivir sensitive (*5*). The emergence and transmission of oseltamivir-resistant pH1N1 carrying a NA-H275Y mutation was first reported early in the 2009 pandemic (*6*). In the following years, transmission of oseltamivir-resistant viruses within healthcare settings and communities, or between close contacts, was occasionally observed (*1*); clusters were reported in Australia in 2011 (*7*) and Japan in 2013 (*8*). Despite these incidents, widespread circulation of oseltamivir-resistant viruses has yet to occur.

The Study

The Centers for Disease Control and Prevention (CDC) receives influenza-positive specimens collected globally for virological surveillance. Viral genomes are analyzed using next-generation sequencing (NGS) to identify strains of epidemiologic, virologic, and clinical importance (*9*). To supplement US national antiviral surveillance, pyrosequencing is used by public health laboratories to screen additional viruses either in-house or by the National Influenza Reference Center (*10*).

During the 2019–20 influenza season, the pH1N1 subtype predominated in the United States. Later in the season, fewer influenza samples were identified, likely because of COVID-19 pandemic mitigation strategies. Of 951 pH1N1 isolates collected nationwide during October 2019–September 2020, 4 (0.4%) had the NA-H275Y marker. Supplemental surveillance, conducted on 282 viruses from 18 states collected November 2019–March 2020, detected another 6 (2.1%) NA-H275Y viruses, bringing the total detected nationwide to 10 (10/1,233;

Author affiliations: Centers for Disease Control and Prevention, Atlanta, Georgia, USA (T. Mohan, H.T. Nguyen, K. Kniss, V.P. Mishin, A.A. Merced-Morales, A. Chesnokov, J.A. De La Cruz, R. Kondor, D.E. Wentworth, L.V. Gubareva); General Dynamics Information Technology, Atlanta (T. Mohan, H.T. Nguyen); New York State Department of Health, Albany, New York, USA (J. Laplante, K. St. George); San Antonio Metropolitan Health District, San Antonio, Texas, USA (P. Blevins)

DOI: https://doi.org/10.3201/eid2707.204593

[1]These authors contributed equally to this article.

0.8%). Of these, 4 (7.7%) were detected among 52 viruses from Texas.

An investigation into a potential epidemiologic link revealed that these 4 virus isolates were collected from the same location, a border detention center in Webb County, Texas, on the same day (January 24, 2020). In January 2020, an influenza outbreak took place there; 8 cases were reported during January 19–28, 2020. All patients showed similar symptoms, such as fever, cough, sore throat, and body aches. Oseltamivir was prescribed on the same day, following specimen collection. Only 4 nasopharyngeal specimens from this outbreak were available for analysis; these samples were collected from men 25–59 years of age. San Antonio Metropolitan Health District Laboratory (San Antonio, TX, USA) conducted the initial diagnostic testing by real-time reverse transcription PCR and determined the cycle threshold (C_t) values as 16.7–25.9, indicating relatively high viral loads. NGS analysis showed that the viruses had the oseltamivir resistance-conferring mutation, NA-H275Y. To expand testing, the San Antonio Laboratory submitted to CDC all remaining pH1N1 positive respiratory specimens (n = 36), collected from Webb County residents during November 2019–March 2020. These specimens were collected from 19 male and 17 female patients with a median age of 6 years (range 0–65 years); C_t values were 21.1–37.5. Pyrosequencing analysis concluded that there were no additional specimens with the NA-H275Y mutation.

A unique genomic signature can help in tracing the origin and spread of viruses in an outbreak. NGS analysis (*11*) revealed that the codon-complete genomes of the 4 cluster viruses were identical at a nucleotide level. Although the chain of transmission is unknown, considering the close-contact setting, this finding might suggest that an oseltamivir-resistant virus was transmitted from a single source. The cluster viruses shared 2 rare substitutions, PB1-Q687H and PB2-R251G, the combination of which was not found in other sequences from the National Center for Biotechnology Information and GISAID (https://www.gisaid.org; accessed October 22, 2020). Therefore, this virus has a unique genomic signature that has not been detected in viruses collected in Texas or elsewhere.

We isolated the 4 cluster viruses and propagated them in MDCK cells, followed by sequence confirmation. We tested the virus isolates for susceptibility to NA inhibitors using the NA inhibition assay (*10*) and they showed highly reduced inhibition by oseltamivir (≈1,300-fold) and peramivir (≈350-fold), and normal inhibition by zanamivir and laninamivir (Table 1). Markers associated with resistance to the polymerase inhibitor, baloxavir, were not detected. To confirm baloxavir susceptibility, we tested viruses by a high-content imaging-based neutralization test (HINT) (*12*). The concentrations of drug needed to inhibit infection by 50% fell in a low nanomolar range (mean 1.86 nM, SD 0.26), consistent with a susceptible phenotype.

HA phylogenetic analysis placed the cluster viruses into the 6B.1A5A-156K subclade, which shares additional amino acid substitutions K130N, L161I, V250A in HA1 and E179D in HA2 (Figure 1, panel A). HA substitutions at residue 156 have been sporadically detected and shown to affect antigenicity, but no widespread circulation of such viruses was observed before summer 2019. In the United States, viruses with HA-5A-156K were first detected in fall 2019 and prevailed among pH1N1 by February 2020. Conversely, the circulation of another recently emerged subclade, 6B.1A5A-187A, 189E, had decreased by winter 2020. A/Hawaii/70/2019 virus (HI/70) from subclade 5A-187A, 189E, was selected as a pH1N1 vaccine component for the 2020–21 Northern Hemisphere influenza season; A/Wisconsin/588/2019

Table 1. Susceptibility to NA inhibitors of influenza A(H1N1)pdm09 virus isolates from border detention center inhabitants, Texas, USA, January 2020*

Virus	NA resistance marker	Mean IC_{50} ± SD, nM (fold difference)			
		Zanamivir	Oseltamivir	Peramivir	Laninamivir
Test					
A/Texas/26/2020	H275Y	0.29 ± 0.01 (2)	200.99 ± 21.56 (1,182)	23.34 ± 6.18 (333)	0.53 ± 0.04 (2)
A/Texas/136/2020	H275Y	0.32 ± 0.00 (2)	247.44 ± 20.52 (1,456)	25.09 ± 1.08 (358)	0.59 ± 0.04 (3)
A/Texas/137/2020	H275Y	0.33 ± 0.04 (2)	229.50 ± 35.77 (1,350)	23.32 ± 0.29 (333)	0.56 ± 0.03 (3)
A/Texas/138/2020	H275Y	0.31 ± 0.02 (2)	228.41 ± 27.05 (1,344)	24.15 ± 1.10 (345)	0.51 ± 0.02 (2)
Reference					
A/Illinois/45/2019	Wildtype	0.19	0.17	0.07	0.22
A/Alabama/03/2020	H275Y	0.27 (1)	139.71 (822)	12.43 (178)	0.47 (2)

*The drug susceptibility of MDCK-grown viruses was determined using a NA inhibition assay. Reference viruses are from the Centers for Disease Control and Prevention Neuraminidase Inhibitor Susceptibility Reference Virus Panel version 3.0 (Atlanta, GA, USA). IC_{50} fold increase was determined by comparing to wild-type reference virus IC_{50}. According to the World Health Organization Antiviral Working Group criteria, an increase below 10-fold constitutes normal inhibition, an increase of 10–100-fold is considered as reduced inhibition and an increase >100-fold is classified as highly reduced inhibition. IC_{50}, concentration of drug needed to inhibit NA by 50%; NA, neuraminidase.

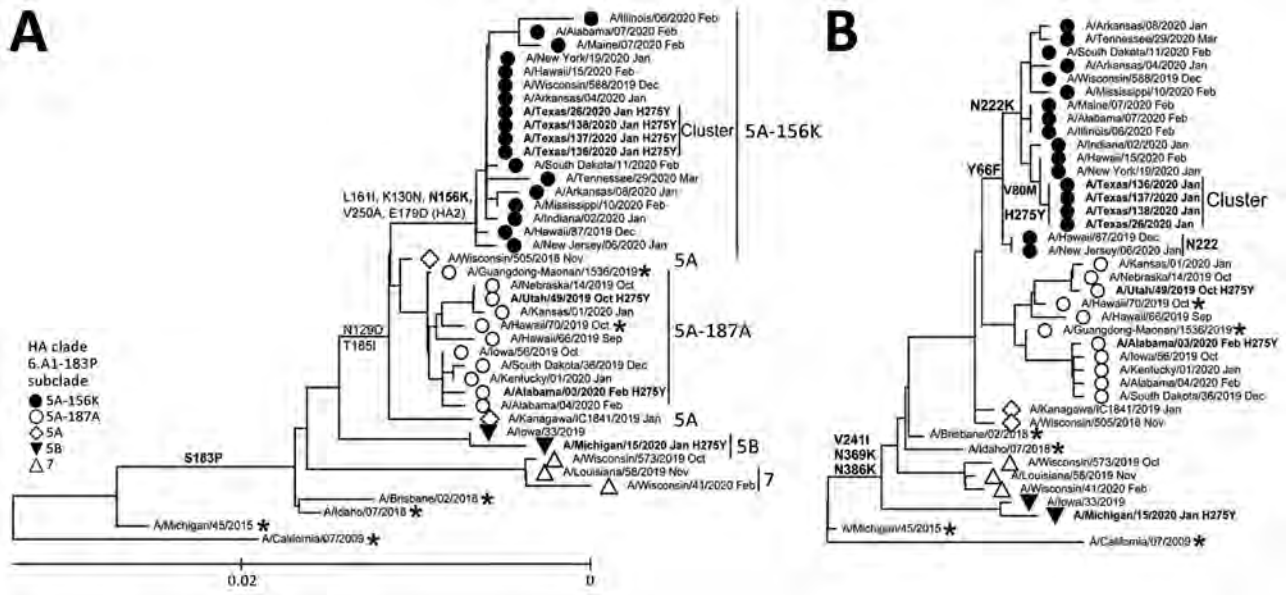

Figure 1. Evolutionary relationships of the HA (A) and NA (B) genes of influenza A(H1N1)pdm09 viruses circulating in the United States during the 2019–20 influenza season compared with reference viruses. We generated phylogenetic trees using MEGA software version 10.1.8 (http://www.megasoftware.net) and the bootstrap method (1,000 replications). We computed evolutionary distances by using the maximum composite likelihood model. Analysis included 40 representative A(H1N1)pdm09 HA and NA gene sequences. Boldface indicates oseltamivir-resistant viruses carrying NA-H275Y substitution; asterisks indicate vaccine viruses. A/California/07/2009 virus (the first A(H1N1)pdm09 vaccine) is used as a reference for ancestry (root) and numbering. Scale bar represents nucleotide substitutions per site. HA, hemagglutinin; NA, neuraminidase.

(WI/588), representing 5A-156K, was selected for the 2021 Southern Hemisphere vaccine.

We assessed the antigenicity of pH1N1 viruses representing distinct HA genetic groups circulating in the United States for antigenic relatedness by HINT and hemagglutination inhibition (HI) assays, using postinfection ferret antiserum (*13*,*14*). We used viruses A/Idaho/07/2019 (ID/07), HI/70, and WI/588, representing recent vaccines, and their homologous ferret antiserum as references. In the HINT assay, we found that the antiserum raised to ID/07 showed poor reactivity (65–78-fold reduction) to viruses with HA-N156K, including the cluster. The HI/70 antiserum reacted even more poorly (315–429-fold) against this group but maintained good reactivity to other HA groups. Antiserum raised to WI/588 (5A-156K) had very high titers against viruses of the same group, including the cluster, and reacted poorly (40–612-fold) to viruses of other groups (Table 2). Results obtained by the

Table 2. Antigenicity of influenza A(H1N1)pdm09 viruses representing distinct HA genetic groups, United States, 2019–2020*

Virus	HA subclade 6B.1A	Ferret antiserum, titers (fold)					
		HINT assay			HI assay		
		ID/07	HI/70	WI/588	ID/07	HI/70	WI/588
Reference							
A/Idaho/07/2018	3	*28,421* ***(1)***	23,464 **(3)**	543 **(250)**	*2,560* ***(1)***	2,560 **(1)**	160 **(16)**
A/Hawaii/70/2019	5A-187A, 189E	15,132 **(2)**	*69,032* ***(1)***	238 **(570)**	1,280 **(2)**	*2,560* ***(1)***	160 **(16)**
A/Wisconsin/588/2019	5A-156K	592 **(48)**	552 **(125)**	*135,765* ***(1)***	80 **(32)**	80 **(32)**	*2,560* ***(1)***
Test							
n = 2	5B	60,007 **(2)**	83,978 **(1)**	3,402 **(40)**	2,560 **(1)**	5,120 **(1)**	Not tested
n = 7	7	37,410 **(1)**	35,135 **(2)**	784 **(173)**	2,560 **(1)**	2,560 **(1)**	80 **(32)**
n = 22	5A-187A, 189E	24,863 **(1)**	88,411 **(1)**	222 **(612)**	1,280 **(2)**	2,560 **(1)**	80 **(32)**
n = 21	5A-156K	399 **(71)**	190 **(363)**	207,958 **(1)**	320 **(8)**	320 **(8)**	5,120 **(1)**

*The antigenicity of MDCK-grown influenza A(H1N1)pdm09 viruses, representing different HA genetic groups, was tested by the HINT and HI assays, using postinfection ferret antiserum, generated from the influenza A(H1N1)pdm09 vaccine candidate viruses for the Northern Hemisphere during 2019–2020 (A/Idaho/07/2019; ID/07) and 2020–21 (A/Hawaii/70/2019; HI/70), and the Southern Hemisphere for the 2021 (A/Wisconsin/588/2019; WI/588) seasons. In the HINT assay, the neutralization titers were determined by calculating the antiserum dilution factor needed to reduce the infected cell population by 50% (average titers are shown) and the HI titers were expressed as the reciprocal of the highest serum dilution that inhibit the hemagglutination of 4 HA units of virus (median titers are shown). Italics indicate homologous titers; boldface indicates fold changes determined by comparing HINT or HI titers to the respective homologous titers. HA, hemagglutinin; HI, hemagglutination inhibition; HINT, high-content imaging-based neutralization test.

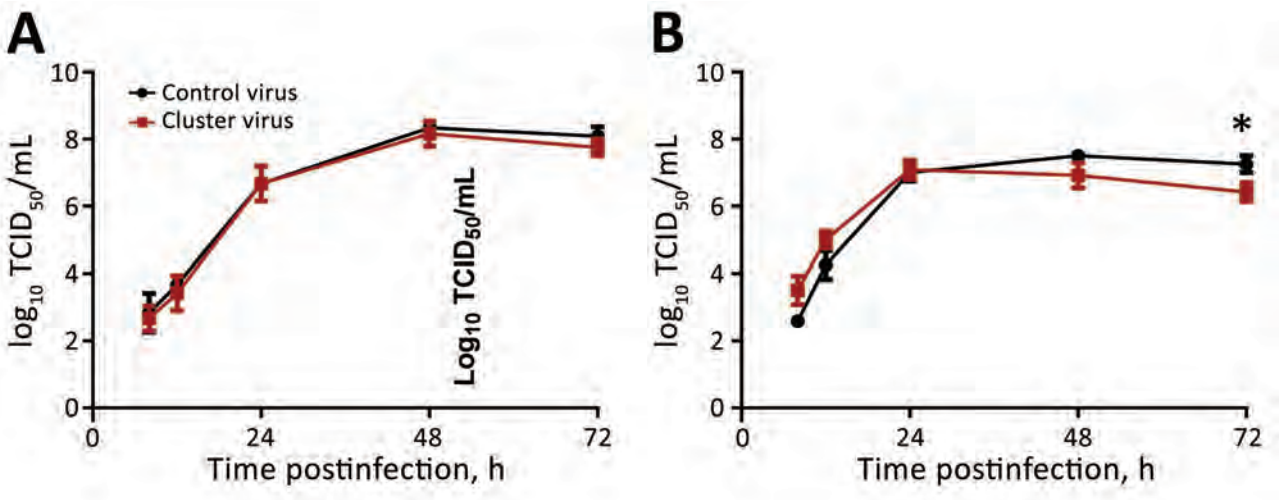

Figure 2. In vitro replicative fitness of influenza A(H1N1)pdm09 cluster and control viruses. The growth kinetics of the 2 viruses, the cluster virus A/Texas/137/2020, and A/New York/19/2020, were assessed using MDCK (A) and hCK (B) cell lines. These viruses have identical HA and NA amino acid sequences, except the H275Y substitution in NA. Cell monolayers were infected at a multiplicity of infection of 0.002 and the supernatants were harvested at 8, 12, 24, 48, and 72 hours postinoculation. Infectious virus titers were determined and expressed as $\log_{10}$ $TCID_{50}$/mL. The lower limit of virus detection is 1.75 $\log_{10}$ $TCID_{50}$/mL. Data are shown as mean ±SD; we used the unpaired *t*-test with Welch's correction for statistical comparisons (asterisk indicates $p<0.05$). The hCK cell line was kindly provided by Dr. Y. Kawaoka (University of Wisconsin, Madison, WI, USA) per material transfer agreement. HA, hemagglutinin; hCK, humanized MDCK cells; NA, neuraminidase; $TCID_{50}$, median tissue culture infectious dose.

conventional HI assay corroborated the HA antigenic drift detected by HINT (Table 2). While analyzing antigenicity of pH1N1, it is prudent to consider that ferret antiserum may preferentially detect changes at HA antigenic site Sa, where N156K resides, compared with site Sb, where D187A is located (*15*). Nevertheless, the findings of this study and other reports indicate that viruses carrying HA-N156K may escape humoral immunity elicited by previous infections and vaccinations.

We assessed the in vitro replicative fitness of the cluster virus A/Texas/137/2020, and A/New York/19/2020, which has identical HA and NA amino acid sequences except for NA-H275Y. These 2 viruses had very similar growth kinetics in MDCK and humanized MDCK (hCK) cells. In MDCK cells, the growth curves were alike at all time points (Figure 2, panel A). In hCK cells, the NA-H275Y-containing virus had better growth at 8 hours, but its titers tapered off slightly at later times (Figure 2, panel B).

Phylogenetic analysis of NA (Figure 1, panel B) showed that the cluster viruses had NA similar to the majority of viruses in the 5A-156K group, including characteristic substitutions NA-Y66F and NA-N222K. However, their NA contained a rare substitution, NA-V80M. Studies to evaluate the effects of these changes on HA–NA functional balance are ongoing.

Conclusions

Although no evidence of oseltamivir-resistant virus transmission outside the detention center was found, the properties of the cluster viruses are concerning. They belong to an HA antigenically drifted group, and escape from preexisting immunity may contribute to the spread of oseltamivir-resistant viruses in coming seasons.

Acknowledgments

We thank the Association of Public Health Laboratories for active support of the national and state-level influenza antiviral surveillance and the San Antonio Metropolitan Health LRN Laboratory staff for their technical contributions. We greatly value the contributions to the study made by the Virus Reference Team, Genomics and Diagnostics Team, and Genomic Analysis Activity in the Virology, Surveillance, and Diagnosis Branch of the Influenza Division, National Center for Immunization and Respiratory Diseases, CDC.

About the Author

Dr. Mohan is a member of the Molecular Epidemiology Team in the Virology, Surveillance, and Diagnosis Branch of the Influenza Division, National Center for Immunization and Respiratory Diseases, CDC. Her research interests include the molecular mechanisms of influenza virus resistance to antiviral medications and the effect of resistance mutations on viral fitness in vitro and in vivo.

References

1. McKimm-Breschkin JL. Influenza neuraminidase inhibitors: antiviral action and mechanisms of resistance. Influenza Other Respir Viruses. 2013;7(Suppl 1):25–36. https://doi.org/10.1111/irv.12047
2. Bloom JD, Gong LI, Baltimore D. Permissive secondary mutations enable the evolution of influenza oseltamivir resistance. Science. 2010;328:1272–5. https://doi.org/10.1126/science.1187816
3. Neverov AD, Kryazhimskiy S, Plotkin JB, Bazykin GA. Coordinated evolution of influenza A surface proteins. PLoS Genet. 2015;11:e1005404. https://doi.org/10.1371/journal.pgen.1005404
4. Wu WL, Lau SY, Chen Y, Wang G, Mok BW, Wen X, et al. The 2008–2009 H1N1 influenza virus exhibits reduced susceptibility to antibody inhibition: implications for the prevalence of oseltamivir resistant variant viruses. Antiviral Res. 2012;93:144–53. https://doi.org/10.1016/j.antiviral.2011.11.006
5. Garten RJ, Davis CT, Russell CA, Shu B, Lindstrom S, Balish A, et al. Antigenic and genetic characteristics of swine-origin 2009 A(H1N1) influenza viruses circulating in humans. Science. 2009;325:197–201. https://doi.org/10.1126/science.1176225
6. Centers for Disease Control and Prevention (CDC). Oseltamivir-resistant 2009 pandemic influenza A (H1N1) virus infection in two summer campers receiving prophylaxis—North Carolina, 2009. MMWR Morb Mortal Wkly Rep. 2009;58:969–72.
7. Hurt AC, Hardie K, Wilson NJ, Deng YM, Osbourn M, Leang SK, et al. Characteristics of a widespread community cluster of H275Y oseltamivir-resistant A(H1N1)pdm09 influenza in Australia. J Infect Dis. 2012;206:148–57. https://doi.org/10.1093/infdis/jis337
8. Takashita E, Ejima M, Itoh R, Miura M, Ohnishi A, Nishimura H, et al. A community cluster of influenza A(H1N1)pdm09 virus exhibiting cross-resistance to oseltamivir and peramivir in Japan, November to December 2013. Euro Surveill. 2014;19:20666. https://doi.org/10.2807/1560-7917.ES2014.19.1.20666
9. Jester B, Schwerzmann J, Mustaquim D, Aden T, Brammer L, Humes R, et al. Mapping of the US domestic influenza virologic surveillance landscape. Emerg Infect Dis. 2018;24:1300–6. https://doi.org/10.3201/eid2407.180028
10. Okomo-Adhiambo M, Fry AM, Su S, Nguyen HT, Elal AA, Negron E, et al.; 2013–14 US Influenza Antiviral Working Group. Oseltamivir-resistant influenza A(H1N1)pdm09 viruses, United States, 2013–14. Emerg Infect Dis. 2015;21:136–41. https://doi.org/10.3201/eid2101.141006
11. Shepard SS, Meno S, Bahl J, Wilson MM, Barnes J, Neuhaus E. Viral deep sequencing needs an adaptive approach: IRMA, the iterative refinement meta-assembler. BMC Genomics. 2016;17:708. https://doi.org/10.1186/s12864-016-3030-6
12. Gubareva LV, Mishin VP, Patel MC, Chesnokov A, Nguyen HT, De La Cruz J, et al. Assessing baloxavir susceptibility of influenza viruses circulating in the United States during the 2016/17 and 2017/18 seasons. Euro Surveill. 2019;24:1800666. https://doi.org/10.2807/1560-7917.ES.2019.24.3.1800666
13. Jorquera PA, Mishin VP, Chesnokov A, Nguyen HT, Mann B, Garten R, et al. Insights into the antigenic advancement of influenza A(H3N2) viruses, 2011-2018. Sci Rep. 2019;9:2676. https://doi.org/10.1038/s41598-019-39276-1
14. Melidou A, Pereyaslov D, Hungnes O, Prosenc K, Alm E, Adlhoch C, et al.; WHO European Region Influenza Surveillance Network; WHO European Region Influenza Surveillance Network Author List. Virological surveillance of influenza viruses in the WHO European region in 2019/20—impact of the COVID-19 pandemic. Euro Surveill. 2020;25:2001822. https://doi.org/10.2807/1560-7917.ES.2020.25.46.2001822
15. Liu STH, Behzadi MA, Sun W, Freyn AW, Liu WC, Broecker F, et al. Antigenic sites in influenza H1 hemagglutinin display species-specific immunodominance. J Clin Invest. 2018;128:4992–6. https://doi.org/10.1172/JCI122895

Address for correspondence: Larisa V. Gubareva, Centers for Disease Control and Prevention, 1600 Clifton Rd NE, Mailstop H17-5, Atlanta, GA 30329-4027, USA; email: lgubareva@cdc.gov

Trypanosoma cruzi in Nonischemic Cardiomyopathy Patients, Houston, Texas, USA

Melissa S. Nolan, David Aguilar,[1] Arunima Misra,[2] Sarah M. Gunter, Tim Erickson, Rodion Gorchakov,[3] Hilda Rivera, Susan P. Montgomery, Kristy O. Murray

To investigate possible cardiac manifestations of Chagas disease, we tested 97 Latinx patients with nonischemic cardiomyopathy in Houston, Texas, USA, for *Trypanosoma cruzi* infection. We noted a high prevalence of underdiagnosed infection and discrepant results in clinical diagnostic assays. Latinx cardiac patients in the United States would benefit from laboratory screening for *T. cruzi* infection.

The clinical manifestations of Chagas disease, caused by infection with the *Trypanosoma cruzi* parasite, are cardiac in approximately one third of patients. Without treatment, the parasite alternates between the trypomastigote and amastigote forms and causes direct smooth muscle tissue damage, myocardial fibrosis, chronic activation of inflammatory pathways, and autonomic dysfunction (*1*). This process can lead to progressive heart failure years later for some patients. Chagas cardiomyopathy patients can seek treatment for malignant ventricular arrhythmias, aneurysms, thromboembolism, or sudden cardiac death (*2*). Despite advances in our understanding of the pathogenic pathways, why some patients have onset of progressive cardiac disease whereas others remain in a persistent subclinical indeterminate disease remain unknown. Identifying infection status early, before the onset of heart failure, is critical because chemotherapeutics are most efficacious in the acute and early stages of infection.

Author affiliations: University of South Carolina, Columbia, South Carolina, USA (M.S. Nolan), Baylor College of Medicine, Houston, Texas, USA (M.S. Nolan, D. Aguilar, A. Misra, S.M. Gunter, T. Erickson, R. Gorchakov, K.O. Murray), Harris Health System–Ben Taub Hospital, Houston (A. Misra), Centers for Disease Control and Prevention, Atlanta, Georgia, USA (H. Rivera, S.P. Montgomery)

DOI: https://doi.org/10.3201/eid2707.203244

In the United States, ≈300,000 persons are infected with *T. cruzi* parasites (*3*), and <1% have received treatment (*4*). Because of low physician awareness (*5*), Chagas disease often is underdiagnosed or misdiagnosed. Previous cardiac patient seroprevalence studies in New York, NY, and Los Angeles, CA, suggest that the rate of undiagnosed *T. cruzi* infection is particularly high (13%–19%) among Latin American immigrants with dilated cardiomyopathy (*6*,*7*). However, the extent of *T. cruzi* infection in the United States beyond these 2 metropolitan areas is largely unknown. We assessed the utility of *T. cruzi* diagnostic surveillance for Latinx patients with nonischemic cardiomyopathy who sought clinical care in a large tertiary care facility in Houston, Texas, USA.

The Study

During August 2015–July 2017, we recruited cardiac patients for Chagas disease surveillance from Harris Health System–Ben Taub Hospital, a large county-funded tertiary care facility in Houston. Patients with known nonischemic cardiomyopathy who sought treatment at the outpatient cardiac clinic or who were admitted to a cardiac inpatient unit were invited to participate in our study. Inclusion criteria required a recorded ejection fraction <50% within the past year and a recent negative ischemic work-up based on stress echocardiography or invasive coronary angiography. We excluded patients of non-Latinx ethnicity and those who were currently incarcerated, had prior *T. cruzi* serologic testing, had evidence of acute coronary syndrome suspected to be of Takotsubo

[1]Current affiliation: University of Texas Health Science Center, Houston, Texas, USA.

[2]Current affiliation: Michael E. Debakey Veterans Affairs Medical Center, Houston, Texas, USA.

[3]Current affiliation: King Abdullah University of Science and Technology, Thuwal, Saudia Arabia.

origin, or had documentation of an alternative etiology for their nonischemic cardiomyopathy (e.g., peripartum, genetic, or alcoholic cardiomyopathy). Consent forms were available in English and Spanish, and licensed translators ensured that all potentially eligible participants were invited to participate. This protocol was reviewed and approved by the Baylor College of Medicine Institutional Review Board (protocol no. H-36761).

After consent, participating patients provided a blood sample for *T. cruzi* diagnostic testing and completed a risk factor questionnaire. The 5-page questionnaire was administered by a study team member and included sections on residential and travel histories, potential triatomine exposures and sources, current health symptoms and health behaviors, clinical family history, and knowledge, attitudes, and practices regarding Chagas disease. Initial *T. cruzi* diagnostic testing included *T. cruzi*–specific antibody testing using Chagas STAT-PAK Assay (Chembio Diagnostic Systems, Inc., https://chembio.com) and Hemagen Chagas Kit (Hemagen Diagnostics, Inc., https://www.hemagen.com). Confirmation of positive and discordant results were then performed by using Chagatest ELISA Recombinante 3.0 (Wiener Laboratorios S.A.I.C., https://www.wiener-lab.com) and TESA blot by the Centers for Disease Control and Prevention.

During the 2-year study period, 97 patients with nonischemic cardiomyopathy were enrolled out of 132 eligible patients; 35 refused to participate because of lack of interest. The average age of participants was 52 years (range 28–91 years); 38% of participants were female and 62% male. Birth countries for the cohort were Mexico (53%), United States (14%), El Salvador (12%), Honduras (9%), Guatemala (4%), and other Latin America Spanish-speaking countries (8%). Patients born in the United States originated from Texas (n = 9), New York (n = 2), Indiana (n = 1), and Oregon (n = 1). Of the cohort, 43% reported having previously seen the triatomine vector; 20/42 (48%) reported sightings in Texas, compared with 31/42 (74%) in a Chagas-endemic Latin American country. Furthermore, 12% of the cohort reported a history of triatomine bites. Despite high triatomine recognition, only 8% of the patient cohort had ever heard of Chagas disease, and only half of these patients could correctly state how Chagas disease is acquired.

Overall, 7% of Latinx nonischemic cardiomyopathy patients seeking treatment for heart failure management were confirmed positive for *T. cruzi* infection by Centers for Disease Control and Prevention Wiener EIA and TESA blot confirmation testing. Discordant test results were common (Table), complicating the clinical decision-making process. All 7 patients who had laboratory-confirmed Chagas cardiomyopathy were born in a Latin America country: El Salvador (n = 4), Honduras (n = 1), Mexico (n = 1), and Venezuela (n = 1). All 7 confirmed positive patients had mothers who were born in or had lived in a Latin America country. Three had lived in a house with a dirt floor and 2 with a palm leaf thatched roof, which are both known risks for triatomine infestations (*8*,*9*). One participant had received a blood transfusion in

Table. Characteristics of patients enrolled in a cross-sectional study of *Trypanosoma cruzi* infections in Latinx cardiomyopathy patients at a tertiary care facility† and results of 4 diagnostic assays, Houston, Texas, USA, 2015–2017*

			True	BCM testing		CDC testing	
ID	Age, y/sex	State, country of birth	positive†§	Stat-Pak	Hemagen	Weiner EIA	TESA blot
CM-013	79/F	Guerrero, Mexico	No	Faint positive	–	–	NP
CM-014	66/M	La Union, El Salvador	Yes	+	+	+	+
CM-017	62/M	San Salvador, El Salvador	Yes	+	+	+	+
CM-037	73/F	El Salvador‡	Yes	Faint positive	–	+	+
CM-048	54/M	Texas, USA	No	Faint Positive	–	–	NP
CM-058	68/F	Michoacan, Mexico	No	-	+	–	NP
CM-082	70/F	Tegucigalpa, Honduras	Yes	+	+	+	+
CM-116	34/M	Acapulco, Mexico	No	Faint positive	–	–	NP
CM-121	77/M	Maracay, Venezuela	Yes	+	+	+	+
CM-143	42/M	San Miguel, El Salvador	Yes	+	+	+	+
CM-155	73/M	Unreported‡	No	Faint positive	–	–	NP
CM-174	78/M	Guerrero, Mexico	Yes	+	+	+	+
CM-197	62/M	Tamaulipas, Mexico	No	+	–	–	NP
CM-243	54/M	Durango, Mexico	No	Faint positive	–	–	NP

*All patients were of White race and Latinx ethnicity. A total of 83 patients tested negative by STAT-PAK (Chembio Diagnostic Systems, Inc., https://chembio.com) and Hemagen (Hemagen Diagnostics, Inc., https://www.hemagen.com). This table displays the 14 patients who tested positive on ≥1 of the screener assays, whose samples where then sent to CDC for testing. None of the 83 patients who tested negative by the 2 screening assays had samples sent to CDC for confirmation testing. BCM, Baylor College of Medicine; CDC, Centers for Disease Control and Prevention; EIA, enzyme immunoassay; ID, identification; NP, not performed; –, negative; +, positive.
†True positive refers to the CDC guidelines recommending a minimum of ≥2 positive test results using ≥2 different diagnostic assay techniques (https://www.cdc.gov/parasites/chagas/healthprofessionals/dx.html).
‡Participants choose not to answer state, country of birth, or both because of personal concerns.

their home country. Two were polyparous mothers, and none of their children had been tested for Chagas disease. Only 2 of the 7 patients with Chagas cardiomyopathy had ever heard of Chagas disease, and only 1 of these patients knew how Chagas disease was acquired.

Conclusions

Our study adds to the growing body of evidence supporting *T. cruzi* surveillance of Latinx patients with nonischemic cardiomyopathy or other risk factors for *T. cruzi* infection in the United States. *T. cruzi* infection accounts for a considerable proportion of nonischemic cardiomyopathy in foreign-born Latinx patients (7%–19%) (*4*,*5*), and the timely diagnosis of their infection is imperative.

Our investigation has a few limitations, including the inability to perform additional cardiac imaging and diagnostic studies or follow patients long-term to evaluate prospective identification of underlying etiology. As highlighted by our discordant results, further work is needed to develop a highly specific diagnostic test to prevent clinical confusion regarding accurate disease status. Determining the underlying etiology has a benefit for Chagas cardiomyopathy patients despite the limited efficacy of treatment with antiparasitics (benznidazole and nifurtimox). Patients with Chagas cardiomyopathy might be recommended for heart transplant (*10*) and can positively respond to implantable cardioverter-defibrillator placement (*11*) and amiodarone (*12*). Awareness of infection could lead to testing of at-risk family members who might respond favorably to early treatment.

Acknowledgments

We thank Kaila Fagerstrom for assisting with patient recruitment.

This project was funded by the National Institutes of Health, National Institute of Allergy and Infectious Diseases (grant no. R21 AI114877-01).

About the Author

Dr. Nolan is an assistant professor of epidemiology at the University of South Carolina's Arnold School of Public Health. Her research program focuses on the clinical epidemiology of vectorborne and parasitic diseases of the Americas.

References

1. Bern C, Messenger LA, Whitman JD, Maguire JH. Chagas disease in the United States: a public health approach. Clin Microbiol Rev. 2019 Nov 27;33(1):e00023-19. doi: 10.1128/CMR.00023-19. PMID: 31776135
2. Pino-Marín A, Medina-Rincón GJ, Gallo-Bernal S, Duran-Crane A, Arango Duque ÁI, Rodríguez MJ, Medina-Mur R, Manrique FT, Forero JF, Medina HM. Chagas cardiomyopathy: from Romaña sign to heart failure and sudden cardiac death. Pathogens. 2021 Apr 22;10(5):505. doi: 10.3390/pathogens10050505. PMID: 33922366
3. Manne-Goehler J, Umeh CA, Montgomery SP, Wirtz VJ. Estimating the burden of Chagas disease in the United States. PLoS Negl Trop Dis. 2016;10:e0005033. https://doi.org/10.1371/journal.pntd.0005033
4. Manne-Goehler J, Reich MR, Wirtz VJ. Access to care for Chagas disease in the United States: a health systems analysis. Am J Trop Med Hyg. 2015;93:108–13. https://doi.org/10.4269/ajtmh.14-0826
5. Stimpert KK, Montgomery SP. Physician awareness of Chagas disease, USA. Emerg Infect Dis. 2010;16:871–2. https://doi.org/10.3201/eid1605.091440
6. Traina MI, Sanchez DR, Hernandez S, Bradfield JS, Labedi MR, Ngab TA, et al. Prevalence and impact of Chagas disease among Latin American immigrants with nonischemic cardiomyopathy in Los Angeles, California. Circ Heart Fail. 2015;8:938–43. https://doi.org/10.1161/CIRCHEARTFAILURE.115.002229
7. Kapelusznik L, Varela D, Montgomery SP, Shah AN, Steurer FJ, Rubinstein D, et al. Chagas disease in Latin American immigrants with dilated cardiomyopathy in New York City. Clin Infect Dis. 2013;57:e7. https://doi.org/10.1093/cid/cit199
8. Bustamante DM, De Urioste-Stone SM, Juárez JG, Pennington PM. Ecological, social and biological risk factors for continued *Trypanosoma cruzi* transmission by *Triatoma dimidiata* in Guatemala. PLoS One. 2014;9:e104599. https://doi.org/10.1371/journal.pone.0104599
9. Rabinovich JE, Gürtler RE, Leal JA, Feliciangeli D. Density estimates of the domestic vector of Chagas disease, *Rhodnius prolixus* Stål (Hemiptera: Reduviidae), in rural houses in Venezuela. Bull World Health Organ. 1995;73:347–57.
10. Benatti RD, Oliveira GH, Bacal F. Heart transplantation for Chagas cardiomyopathy. J Heart Lung Transplant. 2017;36:597–603. https://doi.org/10.1016/j.healun.2017.02.006
11. Pavão MLRC, Arfelli E, Scorzoni-Filho A, Rassi A Jr, Pazin-Filho A, Pavão RB, et al. Long-term follow-up of Chagas heart disease patients receiving an implantable cardioverter-defibrillator for secondary prevention. Pacing Clin Electrophysiol. 2018;41:583–8. https://doi.org/10.1111/pace.13333
12. Stein C, Migliavaca CB, Colpani V, da Rosa PR, Sganzerla D, Giordani NE, et al. Amiodarone for arrhythmia in patients with Chagas disease: a systematic review and individual patient data meta-analysis. PLoS Negl Trop Dis. 2018;12:e0006742. https://doi.org/10.1371/journal.pntd.0006742

Address for correspondence: Melissa Nolan, University of South Carolina, 915 Greene St, Ste 435D, Columbia, SC 29208, USA; email: msnolan@mailbox.sc.edu

Polymicrobial Infections Among Patients with Vascular Q Fever, France, 2004–2020

Mathilde Puges, Xavier Bérard, Caroline Caradu, Maïlys Ducours, Carole Eldin, Mathilde Carrer, Noémie Sauvage, Marc-Olivier Vareil, Laure Alleman, Fatima M'Zali, Sabine Pereyre, Charles Cazanave

We report 5 cases of vascular Q fever complicated by polymicrobial superinfection in patients who had no risk factors for acute Q fever. Q fever was diagnosed by serologic and molecular assays for *Coxiella burnetii*. We confirmed additional infections using conventional graft cultures.

Vascular Q fever, which is caused by *Coxiella burnetii*, is well-described disease; recent publications on the topic include large studies in France and the Netherlands (*1*–*3*). Unlike other vascular graft and endograft infections, especially of aortic and aortoenteric fistulas, vascular Q fever is usually caused by a single microorganism. However, when clinical samples (e.g., blood, vascular graft tissue) test positive for bacterial infection, no recommendation exists for screening for additional microorganisms. Researchers have documented ≥5 cases of vascular Q fever complicated by polymicrobial superinfection, all involving a single co-infecting species: *Bacteroides fragilis*, *Streptococcus* spp., *S. anginosus*, *Yersinia enterocolitica*, or *Klebsiella pneumoniae* (*4*–*6*). Researchers also have documented several cases of Q fever endocarditis complicated by an additional microorganism: *Enterococcus faecalis*, *S. viridans*, *S. mitis*, *S. gallolyticus*, *S. salivarius*, *S. crispatus*, *S. gordonii*, or *Staphylococcus aureus* (*7*–*10*). We describe 5 cases of vascular Q fever complicated by polymicrobial superinfection.

Author affiliations: Centre Hospitalier Universitaire de Bordeaux, Bordeaux, France (M. Puges, X. Bérard, C. Caradu, M. Ducours, M. Carrer, N. Sauvage, S. Pereyre, C. Cazanave); IHU-Méditerranée Infection, Marseille, France (C. Eldin); Aix Marseille University, IRD, AP-HM, SSA, VITROME, Marseille (C. Eldin); Centre Hospitalier de la Côte Basque, Bayonne, France (M.-O. Vareil, L. Alleman); University of Bordeaux, Bordeaux (F. M'Zali, S. Pereyre, C. Cazanave)

DOI: https://doi.org/10.3201/eid2707.210282

The Study

We retrospectively screened the Bordeaux University Hospital Vascular Infections database for patients with chronic Q fever treated at Bordeaux University Hospital (BUH; Bordeaux, France) or Bayonne District Hospital (Bayonne, France) during January 2004–June 2020. To be included in the study, patients had to have a *C. burnetii* phase I IgG titer >6,400 or molecular detection in blood or infected tissues, as well as clinical signs of a vascular infection or evidence from computed tomography or nuclear imaging scans (*6*). We conducted an immunofluorescence assay for *C. burnetii* at BUH and Bayonne Hospital, then sent the samples to the French National Reference Center (Marseille, France) for species confirmation (*6*). When patients had borderline or positive *C. burnetii* serologic results (phase I IgG titer ≥100), we also conducted PCR on an arterial biopsy or vascular graft sample. PCR also was conducted at the French National Reference Center as previously described (*6*). In accordance with national legislation, surviving patients did not object to the analysis of their data for research purposes.

Of 425 patients with vascular infections during January 2004–June 2020, 16 had Q fever, including 7 since 2019, when BUH and Bayonne Hospital began conducting systematic Q fever serologic assays for all patients with vascular infections. In total, 5 patients (1 with aortitis and 4 with vascular graft and endograft infections) had vascular Q fever complicated by polymicrobial superinfection in the abdominal aorta (Table 1, https://wwwnc.cdc.gov/EID/article/27/7/21-0282-T1.htm). Of the 5 cases, 4 had occurred since 2015. All 5 patients had undergone surgery; 4 had an aortoduodenal fistula, and the remainder had intimate contact between the aortic graft and the duodenum.

In total, 4 patients had *C. burnetii* phase I IgG titers ≥100 and <6,400. Patient 3 had a borderline result; therefore, that patient's sample was not sent to

the French National Reference Center for species confirmation (Tables 1, 2). Four patients tested positive by PCR on vascular or graft samples, whereas patient 5 tested positive by PCR on a vertebral biopsy (Table 1). We conducted PCR on serum samples from 2 patients; the samples tested negative for *C. burnetii*. None of the patients had risk factors for acute Q fever, such as contact with animals, consumption of raw milk, or tick bites. Three of the patients lived in the countryside of the Nouvelle-Aquitaine region. We isolated 2–10 additional microorganisms using conventional graft cultures, identifying concurrent bacteremia in 3 patients (patients 2, 3, and 4) (Table 1). All isolated microorganisms were common commensals of the oral or gut microflora. Only patient 3 had a fungal co-infection (*Candida albicans*).

Patients 3 and 5 had been treated for previous episodes of vascular Q fever; their infections relapsed after the end of treatment. Patient 3 had been treated with hydroxychloroquine and doxycycline for 2 years for a Q fever aortic graft infection. The infected graft was not removed, and the infection relapsed 2 months after the end of treatment. Patient 5 had Q fever aortitis and spondylodiscitis 4 years before this episode. He had been treated with hydroxychloroquine and doxycycline for 18 months and had received an aortic graft implantation. However, the infection in the aortic graft relapsed 2 years after the end of treatment.

In total, 3 patients died of vascular graft and endograft infections; another died of a different cause. Patients 1, 3, and 4 were treated with hydroxychloroquine and doxycycline. Only patients 1 and 3 completed the 18-month therapy; the other patients died before or during treatment (Table 1). All patients also had a 6-week course of antimicrobial therapy for the other identified microorganisms.

Conclusions

We identified 5 cases of vascular Q fever complicated by polymicrobial superinfection in patients with no documented risk factors for acute Q fever. Q fever was diagnosed by serologic and molecular assays. We isolated additional microorganisms from clinical samples from 5 of 16 patients with vascular fever, suggesting that co-infections might be more common than previously thought. Furthermore, 4 of the cases complicated by polymicrobial superinfection were diagnosed during the past 5 years, suggesting that this condition might be emergent.

All patients had an aortoduodenal fistula or intimate contact between the aortic graft and the duodenum. The role of *C. burnetii* in vascular fistulas is well-described, especially in aortoenteric fistulas but also in aortobronchial, aortocaval, and arteriocutaneous fistulas (*2*,*11*–*13*). Death rates among patients with chronic Q fever complicated by arterial fistula are higher than among those without fistulas (*2*). Aortoenteric fistulas arise from infection and inflammation of the aortic wall or the perigraft tissues created by *C. burnetii* infection, which erodes the adjacent digestive tract. Diagnostic delays might contribute to fistula development; therefore, earlier detection of vascular Q fever might reduce the incidence of these complications.

We found that 31% of patients with vascular Q fever in this study also had an aortoenteric fistula, a concurrent condition that might have contributed to superinfection. This rate is higher than that suggested by previously published studies on vascular Q fever and aortoenteric fistulas (*2*). We might have found a higher rate because we have conducted systematic Q fever screening in every patient with vascular infection since 2019.

Table 2. Serologic assay results of patients with vascular Q fever complicated by polymicrobial infections, France, 2014–2020*

Serologic results, time of assay†	Patient (month of Q fever diagnosis)				
	1 (2015 Apr)	2 (2020 Jun)	3 (2015 Jul)	4 (2019 Sep)	5 (2010 Dec)
Before Q fever diagnosis	NA	NA	NA	NA	2007 Aug 9: 1,600/0/0–3,200/0/0; 2007 Aug 29: 1,600/0/0–3,200/0/0; 2007 Nov: 1,600/0/0–3,200/0/0; 2008 May: 800/0/0–1,600/0/0
At Q fever diagnosis	2015 Apr: 800/0/200–100/0/0	2020 Jun 15: 100/0/0–100/0/0; 2020 Jun 17: 100/0/0–100/0/0	Borderline	2019 Sep: 1,600/0/800–1,600/0/800	2010 Dec: 400/0/100–800/0/200
After Q fever diagnosis	2015 Jul: 800/0/200–400/0/0; 2016 Aug: 800/0/400–200/0/0; 2017 Dec: 400/0/200–200/0/100	NA‡	NA	NA‡	NA‡

*NA, not available.
†Values are titers against *C. burnetti* phase I–phase II (IgG/IgM/IgA).
‡Values NA because of patient death: patient 2 died on day 37, patient 4 died on day 27, and patient 5 died on day 12.

In conclusion, we report a small case series of vascular Q fever complicated by polymicrobial superinfection. Our findings support systematic screening for *C. burnetii* in patients with vascular infections, especially when an arterial fistula is suspected or confirmed. We believe these screenings should be conducted even when more common microorganisms are isolated by culture. The screening should not be limited to patients with risk factors for acute Q fever. The patients in this study had low *C. burnetti* phase I IgG titers (none >6,400) and all had vascular Q fever confirmed by molecular diagnosis. Low phase I IgG titers have been described in acute Q fever endocarditis (*10*,*14*), suggesting that some of our patients might have had acute rather than chronic vascular Q fever. Therefore, physicians should conduct PCR selective for *C. burnetii* on vascular grafts or arterial biopsies when patients with a vascular infection have a phase I IgG titer ≥100. However, this low cutoff might impair specificity and positive predictive value (*15*) and should be further investigated. We highlight that vascular Q fever requires a specific and prolonged therapy, including surgery, to prevent relapse and other complications. We emphasize the need for systematic *C. burnetii* screening in patients with vascular infections, even when cultures test positive for other microbes.

About the Author

Dr. Puges is an infectious diseases physician at Bordeaux University Hospital in Bordeaux, France. Her primary research interests include vascular infections and implant-related infections.

References

1. Broos PPHL, Hagenaars JCJP, Kampschreur LM, Wever PC, Bleeker-Rovers CP, Koning OHJ, et al. Vascular complications and surgical interventions after world's largest Q fever outbreak. J Vasc Surg. 2015;62:1273–80. https://doi.org/10.1016/j.jvs.2015.06.217
2. Karhof S, van Roeden SE, Oosterheert JJ, Bleeker-Rovers CP, Renders NHM, de Borst GJ, et al. Primary and secondary arterial fistulas during chronic Q fever. J Vasc Surg. 2018;68:1906–1913.e1. https://doi.org/10.1016/j.jvs.2018.01.044
3. Botelho-Nevers E, Fournier P-E, Richet H, Fenollar F, Lepidi H, Foucault C, et al. *Coxiella burnetii* infection of aortic aneurysms or vascular grafts: report of 30 new cases and evaluation of outcome. Eur J Clin Microbiol Infect Dis. 2007;26:635–40. https://doi.org/10.1007/s10096-007-0357-6
4. Dvorak S, Bizzini A. *Streptococcus anginosus* and *Coxiella burnetii* vascular graft co-infection. IDCases. 2020;19:e00697. https://doi.org/10.1016/j.idcr.2020.e00697
5. Bisharat N, Minuhin I. Prosthetic vascular graft infections between blood and concordance of graft culture pathogen. Am J Med Sci. 2012;344:431–5. https://doi.org/10.1097/MAJ.0b013e3182442eb3
6. Eldin C, Mélenotte C, Mediannikov O, Ghigo E, Million M, Edouard S, et al. From Q fever to *Coxiella burnetii* infection: a paradigm change. Clin Microbiol Rev. 2017;30:115–90. https://doi.org/10.1128/CMR.00045-16
7. Million M, Thuny F, Richet H, Raoult D. Long-term outcome of Q fever endocarditis: a 26-year personal survey. Lancet Infect Dis. 2010;10:527–35. https://doi.org/10.1016/S1473-3099(10)70135-3
8. Rovery C, Granel B, Casalta J-P, Lepidi H, Habib G, Raoult D. Coinfection with *Coxiella burnetii* in infectious endocarditis. Clin Microbiol Infect. 2009;15:190–1. https://doi.org/10.1111/j.1469-0691.2008.02221.x
9. Kampschreur LM, Oosterheert JJ, de Vries Feyens CA, Delsing CE, Hermans MHA, van Sluisveld ILL, et al. Chronic Q fever–related dual-pathogen endocarditis: case series of three patients. J Clin Microbiol. 2011;49:1692–4. https://doi.org/10.1128/JCM.02596-10
10. Younis S, Stein M, Reisfeld S. Screening for Q fever during other bacterial endocarditis in endemic areas: our experience with three patients. Case Rep Infect Dis. 2019;2019:9890659.
11. Prinsen J-HS, Boersma D, van Loenhout R, van Schaik PM, Verhoeven BA. Persistent endoleak after endovascular aneurysm repair for acute Q-fever–infected aortocaval fistula. Vascular. 2015;23:645–7. https://doi.org/10.1177/1708538114562658
12. Sigterman TA, Bendermacher BLW, Welten RJTJ, Krasznai A, Bouwman LH. Primary aortoduodenal fistula and Q-fever. Vasc Med. 2013;18:347–9. https://doi.org/10.1177/1358863X13508337
13. Mejia A, Toursarkissian B, Hagino RT, Myers JG, Sykes MT. Primary aortoduodenal fistula and Q fever: an underrecognized association? Ann Vasc Surg. 2000;14:271–3. https://doi.org/10.1007/s100169910046
14. Melenotte C, Epelboin L, Million M, Hubert S, Monsec T, Djossou F, et al. Acute Q fever endocarditis: a paradigm shift following the systematic use of transthoracic echocardiography during acute Q fever. Clin Infect Dis. 2019;69:1987–95.
15. Kampschreur LM, Oosterheert JJ, Koop AMC, Wegdam-Blans MCA, Delsing CE, Bleeker-Rovers CP, et al. Microbiological challenges in the diagnosis of chronic Q fever. Clin Vaccine Immunol. 2012;19:787–90. https://doi.org/10.1128/CVI.05724-11

Address for correspondence: Mathilde Puges, Service des Maladies Infectieuses et Tropicales, Hôpital Pellegrin, Place Amélie Raba Léon, Bordeaux, F-33076, France; email: mathilde.puges@chu-bordeaux.fr

Prevalence of Middle East Respiratory Syndrome Coronavirus in Dromedary Camels, Tunisia

Simone Eckstein, Rosina Ehmann, Abderraouf Gritli, Houcine Ben Yahia, Manuel Diehl, Roman Wölfel, Mohamed Ben Rhaiem, Kilian Stoecker,[1] Susann Handrick,[1] Mohamed Ben Moussa[1]

Free-roaming camels, especially those crossing national borders, pose a high risk for spreading Middle East respiratory syndrome coronavirus (MERS-CoV). To prevent outbreaks, active surveillance is necessary. We found that a high percentage of dromedaries in Tunisia are MERS-CoV seropositive (80.4%) or actively infected (19.8%), indicating extensive MERS-CoV circulation in Northern Africa.

Middle East respiratory syndrome (MERS) coronavirus (MERS-CoV) has the highest lethality of all know human coronaviruses; the case-fatality rate is 34.3% (*1*). The virus, first isolated in Saudi Arabia in 2012 (*2*), most likely originates from bats (*3*). However, several studies suggest that the zoonosis is mainly transmitted to humans by dromedary camels (*Camelus dromedarius*) (*4*–*6*).

As of January 2020, a total of 2,519 human MERS-CoV infections and 866 related deaths had been reported to the World Health Organization from 27 countries. Most of these cases (84.2%), including 788 related deaths, occurred in Saudi Arabia (*1*).

Given the close trading links between the Middle East and Africa, the risk for transferring the zoonosis is high. Tunisia is not a popular trading location, which makes undocumented transfers of dromedary camels within the country or with neighboring countries difficult to track. Only 3 human MERS cases have been imported from Qatar (*7*), and no autochthonous MERS-CoV infections have been reported for Tunisia. However, severe underestimation of human MERS cases is highly probable because of the broad range of manifestations, from asymptomatic infection to acute pneumonia.

Furthermore, epidemiologic surveillance of MERS-CoV is limited in Tunisia, and no respective data for neighboring countries is publicly available. Two studies analyzing MERS-CoV prevalence in dromedaries in Tunisia reported high seropositivity of the sampled animals (49.0% and 87.3%) (*8*,*9*). However, those studies analyzed dromedary camels from livestock markets, slaughterhouses, and meat farms, without representing natural habitats. This limitation complicates drawing realistic conclusions about geographic and age-dependent distributions. We investigated the prevalence of MERS-CoV in dromedary camels in Tunisia primarily by sampling animals that roam freely through the desert during summer to determine an authentic representation of the distribution pattern.

The Study

Winter is mating and birthing season for dromedary camels. Therefore, animals kept for milk and meat production gather in areas that provide access to salty plants and other minerals. This environment provides an optimal opportunity to catch and examine large numbers of animals from different herds and origins, given that the camels that roam freely through the desert the rest of the year congregate simultaneously.

In January 2020, we collected serum samples and nasal swabs of 382 gathered animals in Tunisia. We sampled an additional 119 camels used for transport or patrol purposes, all of which were males and kept enclosed. The specimens were collected from 20 different locations within the Kebili Governorate (Table; Figure 1, panel A). Furthermore, serum samples of 22 camel keepers and 2 veterinarians were obtained. We

Author affiliations: Bundeswehr Institute of Microbiology, Munich, Germany (S. Eckstein, R. Ehmann, M. Diehl, R. Wölfel, K. Stoecker, S. Handrick), Ministry of National Defense, General Directorate of Military Health, Veterinary Service, Tunis, Tunisia (A. Gritli, H. Ben Yahia, M. Ben Rhaiem), Military Hospital of Instruction of Tunis Department of Virology, Tunis (M. Ben Moussa)

DOI: https://doi.org/10.3201/eid2707.204873

[1]These authors contributed equally to this article.

have compiled details of our sampling and testing methods (Appendix, https://wwwnc.cdc.gov/EID/article/27/720-4873-App1.pdf).

We analyzed all 501 dromedary serum samples for MERS-CoV–specific antibodies by ELISA and found 80.4% to be seropositive for MERS-CoV IgG. At 85.7%, MERS-CoV seropositivity was higher in female than in male camels (65.6%) (Table; Figure 1, panel A).

Although none of the calves (0–6 months of age) and 4.9% of the juvenile camels (6–24 months of age) were seropositive for antibodies against MERS-CoV, relative seropositivity increased with age (Table). None of the camel keepers or veterinarians was seropositive, indicating no previous MERS-CoV infection.

Screening the dromedary nasal swab specimens for active virus infections with real-time reverse transcription PCR revealed MERS-CoV RNA in 19.8%. However, cycle thresholds >30 (for all but 6 samples) indicated low virus concentrations. Female animals (23.0%) actively shed MERS-CoV RNA, whereas only 10.7% of the male camel specimens were PCR-positive. In contrast to the immunologic findings, a high percentage (40%) of juvenile camels (<2 years of age) shed MERS-CoV RNA, compared with 17.8% of the adult camels that tested positive (Table, Figure 1, panel A)

In summary, 433 of 501 dromedaries tested positive for MERS-CoV. A total of 334 animals were seropositive for MERS-CoV IgG but did not shed MERS-CoV RNA. Of these, 30 dromedary swab specimens contained MERS-CoV RNA, but no specific antibodies were found in the respective serum samples. Sixty-nine PCR-positive dromedary camels also had

Table. MERS-CoV IgG seropositivity and viral RNA presence in dromedary camels, by selected sampling parameters, Tunisia*

Sampling parameter	No. dromedaries	ELISA serologic testing, no. (%) positive for MERS-CoV IgG	Molecular biology rRT-PCR, no. (%) positive for MERS-CoV RNA
Sex			
M	131	86 (65.6)	14 (10.7)
F	370	317 (85.7)	85 (23.0)
p value		<0.05	<0.01
Age group			
Juvenile	45	2 (4.4)	18 (40.0)
0–6 mo	4	0 (0)	1 (25.0)
6–24 mo	41	2 (4.9)	17 (41.5)
Adult	456	401 (87.9)	81 (17.8)
2–6 y	81	62 (76.5)	19 (23.5)
6–12 y	179	157 (87.7)	28 (15.6)
12–25 y	190	176 (87.9)	32 (16.8)
>25 y	6	6 (100)	2 (33.3)
p value, juvenile compared with adult		<0.00001	<0.01
Sampling site			
Ksar Ghilane, n = 6	211	154 (73.0)	49 (23.2)
Site 1	28	20 (71.4)	7 (25.0)
Site 2	20	8 (40.0)	0 (0)
Site 3	30	26 (86.7)	6 (20.0)
Site 4	20	19 (95.0)	1 (5.0)
Site 5	73	50 (68.5)	25 (34.2)
Site 6	40	31 (77.5)	10 (25.0)
Bazma, n = 7	168	152 (90.5)	32 (19.1)
Site 1	25	24 (96.0)	2 (8.0)
Site 2	30	25 (83.3)	8 (26.7)
Site 3	15	13 (86.7)	3 (20.0)
Site 4	15	14 (93.3)	1 (6.7)
Site 5	21	20 (95.2)	4 (19.0)
Site 6	16	13 (81.3)	6 (37.5)
Site 7	46	43 (93.5)	8 (17.4)
Douz, n = 5	53	32 (60.4)	4 (7.5)
Site 1a	4	3 (75.0)	0 (0)
Site 1b	4	0 (0)	0 (0)
Site 2	24	18 (75.0)	3 (12.5)
Site 3	18	10 (55.6)	1 (5.6)
Site 4	3	1 (33.3)	0 (0)
Mahrouga, n = 2	69	65 (94.2)	14 (20.3)
Site 1	42	40 (95.2)	3 (7.1)
Site 2	27	25 (92.6)	11 (40.7)
p value for comparisons among all 4 main sites		0.05	Not significant
Total	501	403 (80.4)	99 (19.8)

*MERS-CoV, Middle East respiratory syndrome coronavirus; rRT-PCR, real-time reverse transcription PCR.

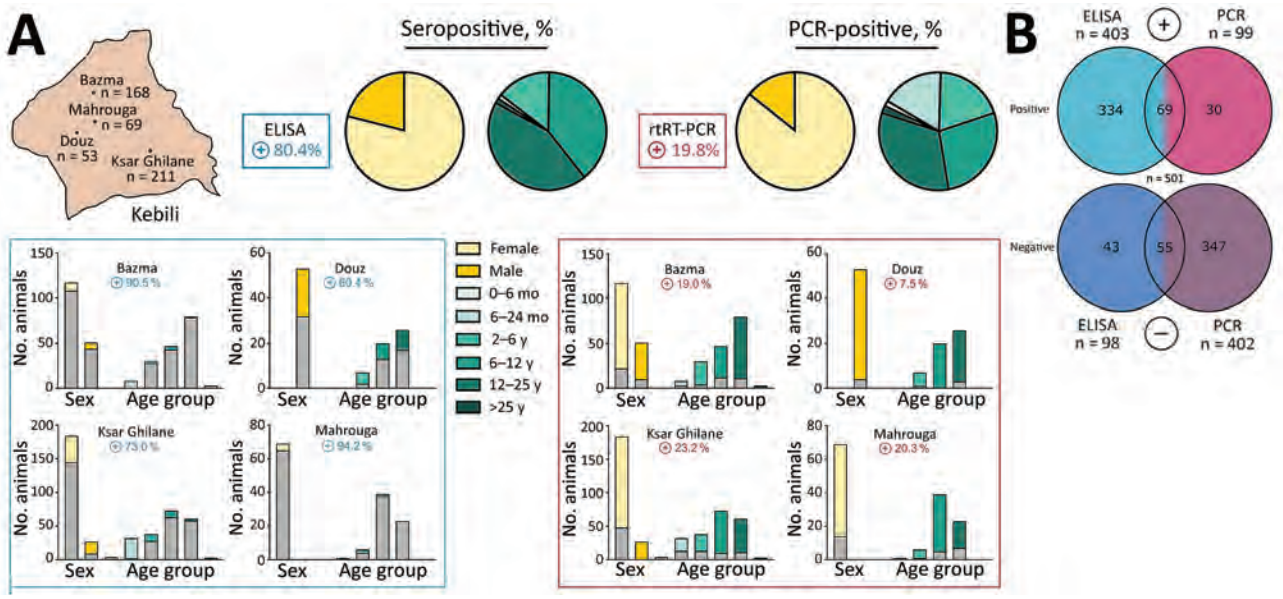

Figure 1. MERS-CoV prevalence in dromedary camels, Tunisia. A) Overview of seropositive and PCR-positive dromedaries from 4 different sampling areas (Appendix, https://wwwnc.cdc.gov/EID/article/27/720-4873-App1.pdf), by sex and age group. Blues boxes represent seropositive dromedaries and purple boxes PCR-positive dromedaries. Bars in chart represent total number of sampled animals; gray-shaded bar sections represent total number of MERS-CoV–positive animals. In the Douz area, all dromedary camels sampled were used for patrol or transport purposes and were exclusively adult male animals. B) Distribution of ELISA (blue) and PCR (purple) results, by number. Bright colors represent positive results, dark colors negative results; 2-colored areas represent animals that are either positive for both ELISA and PCR or negative for both. MERS-CoV, Middle East respiratory syndrome coronavirus;

MERS-CoV antibodies, indicating reinfection (Figure 1, panel B).

Attempts to cultivate the virus from all respective PCR-positive swab specimens were unsuccessful, most likely because of the low virus concentrations in the samples. Presumably, whole-genome sequencing did not work for the same reasons. However, we performed Sanger sequencing of cDNAs obtained from PCR-positive samples with the highest viral concentrations and subsequently conducted phylogenetic analysis with a 720-bp fragment of the spike receptor-binding protein. The analyzed nucleotide sequences from the dromedaries in Tunisia differ from previously published MERS-CoV sequences and therefore form a separate group distinct from strains found in Arabia. Two MERS-CoV isolates in Egypt, however, cluster in the same clade (Figure 2).

Conclusions

On the continent of Africa, active surveillance, longitudinal studies, and epidemiologic monitoring are scarce, and little is known about the prevalence and circulation of MERS-CoV in many regions. Whether MERS-CoV lineages in Africa have a lower tendency to cross the species barrier and infect humans is not fully understood. Therefore, closing the gaps in surveillance and virus prevalence data remains a focus for all regions with dromedary camel populations.

Seroprevalence studies in Egypt, Ethiopia, Nigeria, and Kenya all indicate MERS-CoV circulation within camel herds, reporting seropositivity rates ranging from 30% to 100% (*10*). For dromedaries in Tunisia, only 2 studies have been published, reporting 49% and 87.3% MERS-CoV seropositive animals and only 0.7% active viral shed (*8*,*9*).

However, most studies focus on locations where large numbers of camels congregate (e.g., abattoirs, large-scale farms, harbors, or livestock markets). At these locations, dromedaries are kept at a substantially increased population density compared with their normal habitats. This practice, referred to as crowding, increases stress for individual animals (*11*). Under these circumstances, increased intensive animal contact can lead to higher transmission rates of various microorganisms. Crowding, in combination with animal transport, is known to promote infections of the upper and lower respiratory tract, especially in cattle (*12*). In contrast, the camels investigated in our study represent a rare example of MERS-CoV prevalence in animal groups with a natural herd structure in northern Africa.

We found extensive MERS-CoV IgG seropositivity (80.4%) and high ratios of MERS-CoV RNA (19.8%) among dromedaries in Tunisia. Compared with adult animals, juvenile camels were more likely to have active MERS-CoV infections and less MERS-CoV IgG in their serum samples. Furthermore, some dromedaries appeared to have MERS-CoV reinfections, explained by the fact that coronaviruses tend to establish endemic infection patterns with high seroprevalence and low but continuous viral shedding in their natural host (*13*). Waning antibodies in combination with antigenic drift of the virus fosters reinfection events (*14*).

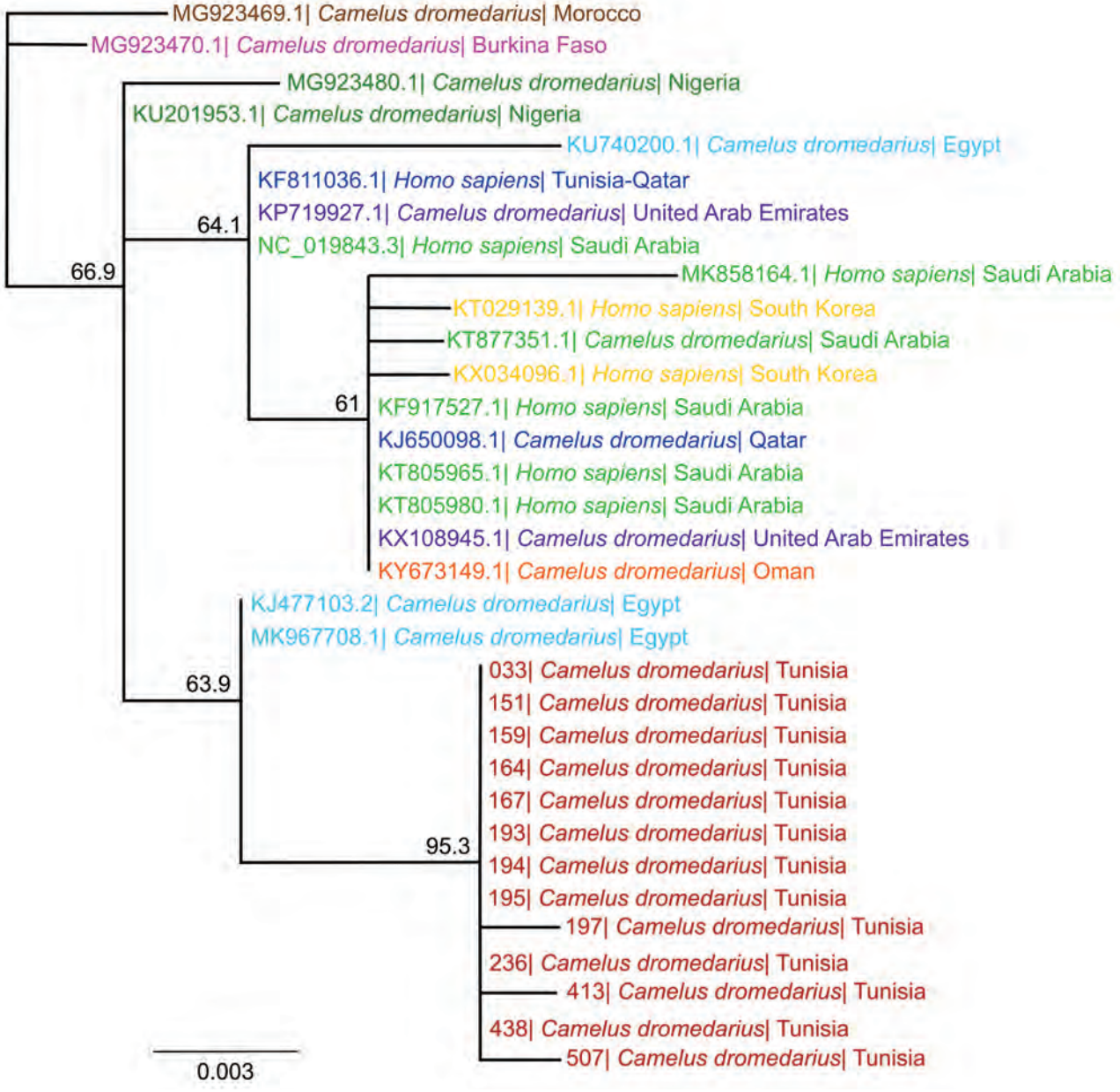

Figure 2. Phylogenetic analysis of MERS-CoV samples from dromedary camels in Tunisia, conducted by using the spike RBD. We used 720-bp fragments of the MERS-CoV spike RBD amplified from nasal swab samples of 13 dromedary camels and published RBD sequences of representative MERS-CoV strains from other countries to create the phylogenetic tree using Geneious Prime Tree Builder (Geneious Biologics, https://www.geneious.com). Branches are shaded by country: red represents sequences from Tunisia (this study); brown represents Morocco, pink Burkina Faso, dark green Nigeria, blue Egypt, dark blue Qatar, green Saudi Arabia, yellow South Korea, purple United Arab Emirates, and orange Oman. GenBank accession numbers are provided for reference sequences. Numbers indicate bootstrap values (1,000 pseudo-replicates). Scale bar indicates sequence divergence (% nucleotide substitutions). MERS-CoV, Middle East respiratory syndrome coronavirus; RBD, receptor-binding protein.

A limitation of our study is that the low sample size of humans tested, comprising 22 camel keepers and 2 veterinarians (data not shown), precludes drawing generalized conclusions. Furthermore, no nasal swab specimens were collected from camel keepers to check for active MERS infections. Also, no phenotypic or whole-genome analysis of MERS-CoV strains from the dromedary camels was possible because virus growth and next-generation sequencing were not successful because of low viral concentrations.

In conclusion, the high seroprevalence of MERS-CoV antibodies and the active shed of MERS-CoV RNA indicate the widespread nature of the virus in dromedaries in Tunisia. However, more extensive studies in the human and dromedary camel populations and in-depth whole-genome sequence analysis of circulating MERS-CoV strains are required to increase epidemiologic understanding of the disease and its infection dynamics.

Acknowledgments

We thank the Deutsche Gesellschaft für Internationale Zusammenarbeit for their support by planning and organizing the study. Furthermore, we gratefully acknowledge the camel keepers in Tunisia for their participation.

This work is part of Medical Biological Defense Research Program of the Bundeswehr Medical Service and was supported by the Enable and Enhance Initiative of the federal government of Germany (Ertüchtigungsinitiative der Deutschen Bundesregierung, grant no. OR12-370.43 ERT TUN IMB).

About the Author

Dr. Eckstein is a scientist at the Bundeswehr Institute of Microbiology. Her research interests include viral and bacterial zoonoses in North Africa.

References

1. World Health Organization. MERS situation update: January 2020 [cited 2020 Dec 1]. https://vlibrary.emro.who.int/idr_records/mers-situation-update-january2020
2. Zaki AM, van Boheemen S, Bestebroer TM, Osterhaus AD, Fouchier RA. Isolation of a novel coronavirus from a man with pneumonia in Saudi Arabia. N Engl J Med. 2012;367:1814–20. https://doi.org/10.1056/NEJMoa1211721
3. Anthony SJ, Gilardi K, Menachery VD, Goldstein T, Ssebide B, Mbabazi R, et al. Further evidence for bats as the evolutionary source of Middle East respiratory syndrome coronavirus. MBio. 2017;8:e00373–17. https://doi.org/10.1128/mBio.00373-17
4. Reusken CB, Haagmans BL, Müller MA, Gutierrez C, Godeke GJ, Meyer B, et al. Middle East respiratory syndrome coronavirus neutralising serum antibodies in dromedary camels: a comparative serological study. Lancet Infect Dis. 2013;13:859–66. https://doi.org/10.1016/S1473-3099(13)70164-6
5. Azhar EI, El-Kafrawy SA, Farraj SA, Hassan AM, Al-Saeed MS, Hashem AM, et al. Evidence for camel-to-human transmission of MERS coronavirus. N Engl J Med. 2014;370:2499–505. https://doi.org/10.1056/NEJMoa1401505
6. Azhar EI, Hashem AM, El-Kafrawy SA, Sohrab SS, Aburizaiza AS, Farraj SA, et al. Detection of the Middle East respiratory syndrome coronavirus genome in an air sample originating from a camel barn owned by an infected patient. MBio. 2014;5:e01450–14. https://doi.org/10.1128/mBio.01450-14
7. Abroug F, Slim A, Ouanes-Besbes L, Hadj Kacem MA, Dachraoui F, Ouanes I, et al.; World Health Organization Global Outbreak Alert and Response Network Middle East Respiratory Syndrome Coronavirus International Investigation Team. Family cluster of Middle East respiratory syndrome coronavirus infections, Tunisia, 2013. Emerg Infect Dis. 2014;20:1527–30. https://doi.org/10.3201/eid2009.140378
8. Reusken CB, Messadi L, Feyisa A, Ularamu H, Godeke GJ, Danmarwa A, et al. Geographic distribution of MERS coronavirus among dromedary camels, Africa. Emerg Infect Dis. 2014;20:1370–4. https://doi.org/10.3201/eid2008.140590
9. Kandeil A, Gomaa M, Nageh A, Shehata MM, Kayed AE, Sabir JSM, et al. Middle East respiratory syndrome coronavirus (MERS-CoV) in dromedary camels in Africa and Middle East. Viruses. 2019;11:717. https://doi.org/10.3390/v11080717
10. Dighe A, Jombart T, Van Kerkhove MD, Ferguson N. A systematic review of MERS-CoV seroprevalence and RNA prevalence in dromedary camels: implications for animal vaccination. Epidemics. 2019;29:100350. https://doi.org/10.1016/j.epidem.2019.100350
11. Proudfoot K, Habing G. Social stress as a cause of diseases in farm animals: current knowledge and future directions. Vet J. 2015;206:15–21. https://doi.org/10.1016/j.tvjl.2015.05.024
12. Yates WD. A review of infectious bovine rhinotracheitis, shipping fever pneumonia and viral-bacterial synergism in respiratory disease of cattle. Can J Comp Med. 1982;46:225–63.
13. Addie DD, Schaap IAT, Nicolson L, Jarrett O. Persistence and transmission of natural type I feline coronavirus infection. J Gen Virol. 2003;84:2735–44. https://doi.org/10.1099/vir.0.19129-0
14. Herrewegh AA, Mähler M, Hedrich HJ, Haagmans BL, Egberink HF, Horzinek MC, et al. Persistence and evolution of feline coronavirus in a closed cat-breeding colony. Virology. 1997;234:349–63. https://doi.org/10.1006/viro.1997.8663

Address for correspondence: Kilian Stoecker, Bundeswehr Institute of Microbiology, Neuherbergstr. 11, 80937 Munich, Germany; email: KilianStoecker@bundeswehr.org

Retrospective Study of Kyasanur Forest Disease and Deaths among Nonhuman Primates, India, 1957–2020

Sulagna Chakraborty, William E. Sander, Brian F. Allan, Flavia C.D. Andrade

Kyasanur Forest disease (KFD) is a tickborne hemorrhagic disease affecting primates along the Western Ghats mountain range in India. Our retrospective study indicated that ≥3,314 monkey deaths attributed to KFD were reported in KFD-endemic states in India during 1957–2020. These data can help guide surveillance to protect animal and human health.

Kyasanur Forest disease (KFD) is a highly infectious tickborne disease affecting humans and monkeys. The etiologic agent of this disease is the Kyasanur Forest disease virus (KFDV), a flavivirus. Since its discovery in 1957 in Karnataka State, India, KFD has expanded to 5 states along the western coastline in India (*1*) and ≈10,000 reported cases of KFD in humans, averaging 400–500 cases annually (*2*). After an incubation period of 3–8 days, primary clinical symptoms include fever, myalgia, and gastrointestinal and bleeding problems. In a small subset of patients, a second phase of the disease can include neurologic manifestations and fever. If the disease is detected early, symptomatic supportive care can improve recovery from the disease. Case-fatality rates range from 3% to 15% (*1*,*3*). The primary vectors of KFDV are *Haemaphysalis spinigera* and *H. turturis* ticks, which are endemic to southern India and transmit the virus to monkeys and humans (*4*). Larvae and nymphs of these ticks feed on monkeys when the monkeys are ground foraging, providing routes of infection and spread. In addition, KFDV can be transmitted transovarially in these ticks (Figure 1).

Macaca radiata and *Semnopithecus entellus* are 2 monkey species in the KFD-endemic region frequently associated with KFD; these monkeys can succumb to the virus quickly (*3*). For monkeys, KFDV causes nonspecific and degenerative changes in abdominal organs, hemorrhage, and encephalitis. Experimentally infected monkeys have diarrhea, bradycardia, and hypotension and ultimately die (*5*). Monkey migration might expand KFDV geographic distribution, in which infected ticks are carried across state borders through connected natural areas (*1*,*3*,*4*). Although reporting of monkey deaths from KFD during the past 60 years has been unsystematic and inconsistent, the data provide valuable information. We summarize reports of monkey deaths connected with KFD in India and evaluate the utility of reporting KFD occurrence in monkeys for human disease surveillance.

The Study

We conducted a retrospective review of scientific literature through Web of Science, PubMed Central, and Google Scholar and included data from ProMED Mail, newspapers, and government reports issued during 1957–2020. The search keywords included KFD, KFDV, monkey fever, Kyasanur Forest disease, and mankan kayla (a local term in Karnataka, India). We used 55 peer-reviewed journal articles, 109 Pro-MED Mail reports, 1 report by the Karnataka State government, and 1 newspaper report to generate estimates. We created a database from all information sources; our final dataset (Table 1) contains the most updated information for all years from the available data.

Information on monkey deaths caused by KFD is limited, particularly for species-specific deaths. Our review of all data sources indicates that ≥3,314 monkey deaths associated with KFD were reported during 1957–2020 (Table 1). However, only a subset of deaths were tested for KFDV. During this period, 760 monkeys underwent necropsy, and 334 were laboratory-confirmed to have KFDV infection (Appendix).

Author affiliation: University of Illinois Urbana–Champaign, Urbana–Champaign, Illinois, USA

DOI: https://doi.org/10.3201/eid2707.210463

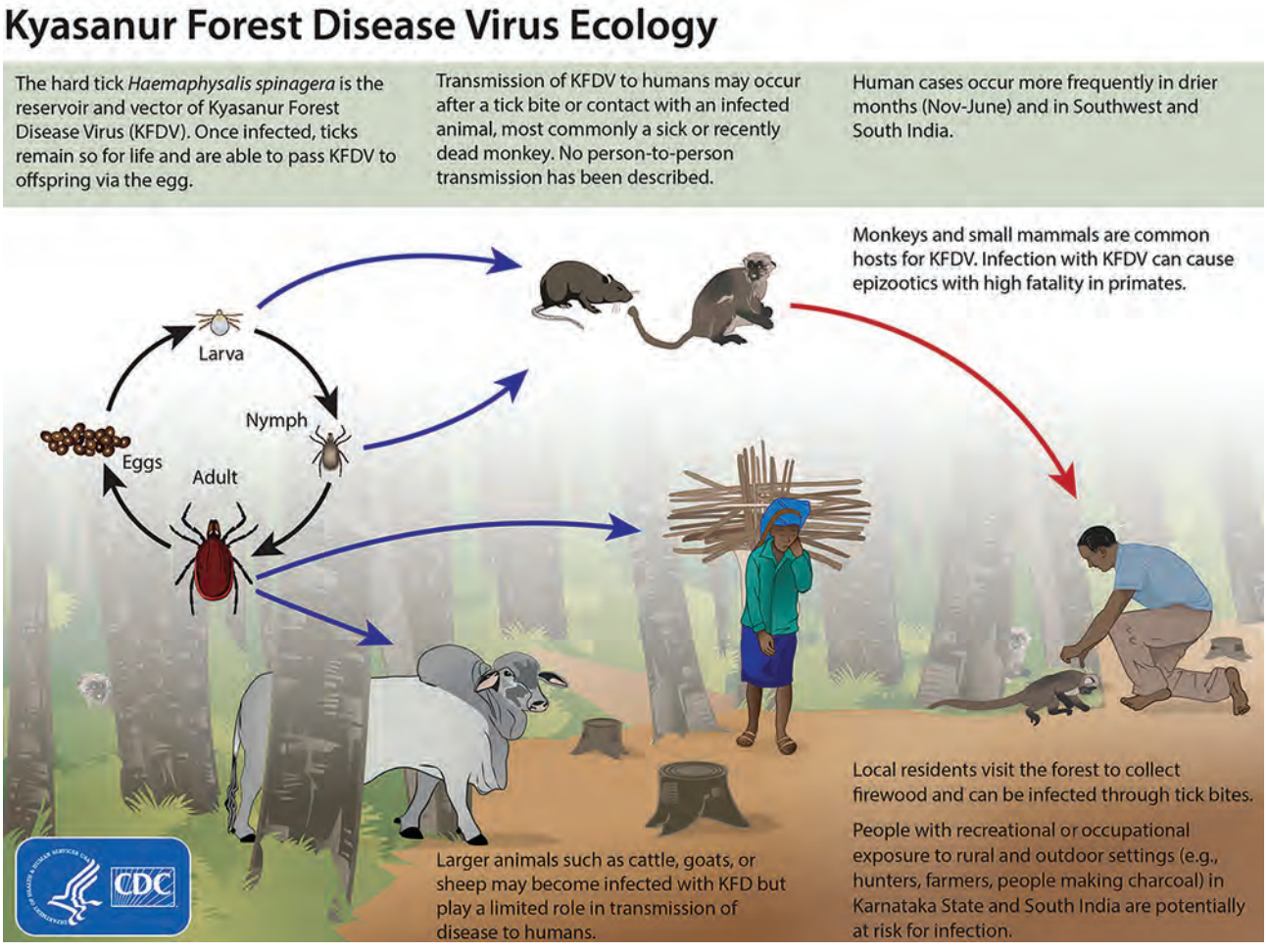

Figure 1. Ecology of Kyasanur Forest disease virus. Reproduced from https://www.cdc.gov/vhf/kyasanur/resources/virus-ecology.html.

Of the reported monkey deaths, a total of 1,676 deaths occurred in *S. entellus* monkeys and 400 deaths occurred in *M. radiata* monkeys; species were not reported for the remaining 1,238 deaths.

We found an early report of KFD in monkeys outside of Karnataka in Tamil Nadu state in 2012, which could be linked to an outbreak of human cases at the Bandipur Tiger Reserve in 2012. Monkeys from Karnataka might have entered Tamil Nadu carrying the virus or infected ticks. Subsequently, KFD in monkeys was reported in Kerala state in 2014 and Goa and Maharashtra states in 2016. Substantial overlap occurred between reported monkey deaths and human cases of KFD (Figure 2). We identified the drivers behind KFD transmission and geographic expansion based on the literature (Table 2).

Higher mortality rates occurred among *S. entellus* monkeys (81% of 1,159 deaths) than among *M. radiata* monkeys during 1957–1964 (*7*). Most monkey deaths were reported in evergreen and semievergreen forests in the Western Ghats (*8*). We found no other information associating the frequency of monkey deaths to habitat.

The abundance of these primate species in the area of interest is difficult to determine because of limited studies with inconsistent sampling methods. In Karnataka, higher encounter rates with *M. radiata* monkeys were reported in wet evergreen forests and human-inhabited areas (*9*). *M. radiata* monkeys were encountered mainly in the Western Ghats and the Southern Plateau, whereas *S. entellus* monkeys were abundant in the Western Ghats and Northern Plains. Based on a 2001 Environmenta Information System bulletin (*10*), the national population of *M. radiata* monkeys in India was ≈150,000 and that of *S. entellus* monkeys was ≈300,000. Both species have suffered population decline because of habitat loss, translocation, and hunting, and minimal efforts have been undertaken to conserve these species (*9*,*11*).

Conclusions

Our study highlights the need for consistent surveillance of monkey deaths. Monkey deaths caused by KFDV are harbingers of human cases (*1*,*3*,*4*), making these animals potential sentinels for KFD (*6*). Therefore, determining these primate species' relative susceptibility to KFDV to evaluate the potential to use monkey deaths for surveillance is essential. In laboratory experiments, higher mortality rates have been reported in *S. entellus* than *M. radiata* monkeys (*12*). Patil et al. (*13*) experimentally infected *M. radiata* monkeys with KFDV and found that only 20% of these primates had onset of severe clinical signs, but all exhibited viral shedding and a humoral immune response. Thus, other factors might contribute to KFD mortality rates under natural conditions, and *M. radiata* monkeys might be less susceptible to KFD than previously thought. KFDV infection can often be subclinical in nature, explaining why fewer deaths have been observed for *M. radiata* than *S. entellus* monkeys. By shedding the virus through body secretions, *M. radiata* monkeys might aid in expanding KFDV into new areas. This phenomenon underscores the need for conducting serum or fecal surveillance of primates to determine KFDV epidemiology and transmission.

Most human cases of KFD are typically reported during December–May, the same period during which monkey deaths generally occur. Local public health authorities often undertake precautionary measures on the basis of monkey deaths, including spraying acaricide around areas with monkey carcasses and vaccination of persons within a 5-km

Table 1. Monkey deaths attributed to Kyasanur Forest disease in the southwestern states of India, 1957–2020*

Year	Total no. monkey deaths	No. monkey deaths, state of occurrence
1957 Jan–Sep	105	105, KN
1957–1958 Oct–Sep	92	92, KN
1958–1959	290	290, KN
1959–1960	187	187, KN
1960–1961	80	80, KN
1961–1962	114	114, KN
1962–1963	147	147, KN
1963–1964	144	144, KN
1964–1965	109	109, KN
1965–1966	191	191, KN
1967–1968	126	126, KN
1968–1969	138	138, KN
1969–1970	135	135, KN
1970–1971	88	88, KN
1971–1972	75	75, KN
1972–1973	101	101, KN
1973–1974	83	83, KN
1975–1981	No data	No data
1982–1983	>35	<35, KN
1983–1997	No data	No data
1998	Dead monkeys reported	No figure reported† for KN
1999	No data	No data
2000	Several dead monkeys reported	No figure reported for KN
2001–2002	No data	No data
2003	132	132, KN
2004	86	86, KN
2005	53	53, KN
2006	61	61, KN
2007	19	19, KN
2008	23	23, KN
2009	86	86, KN
2010	28	28, KN
2011	>35	<35, KN
2012	≥64	39-64, KN; No figure reported for TN
2013	50	50, KN
2014	≥131	31, KN; <100, KL
2015	60	42, KN; 18, KL
2016	72	3, MH; 69, GA
2017	≥81	<51, KL; <10, GA
2018	≥76	<76, KN; No figure reported for KL or MH
2019	≥15	15, KN; No figure reported for KL
2020	≥2	2, KN; No figure reported for KL

*GA, Goa; KL, Kerala; KN, Karnataka; MH, Maharashtra; TN, Tamil Nadu.
†No figure reported indicates that monkey deaths were reported in a state but an exact number was not provided.

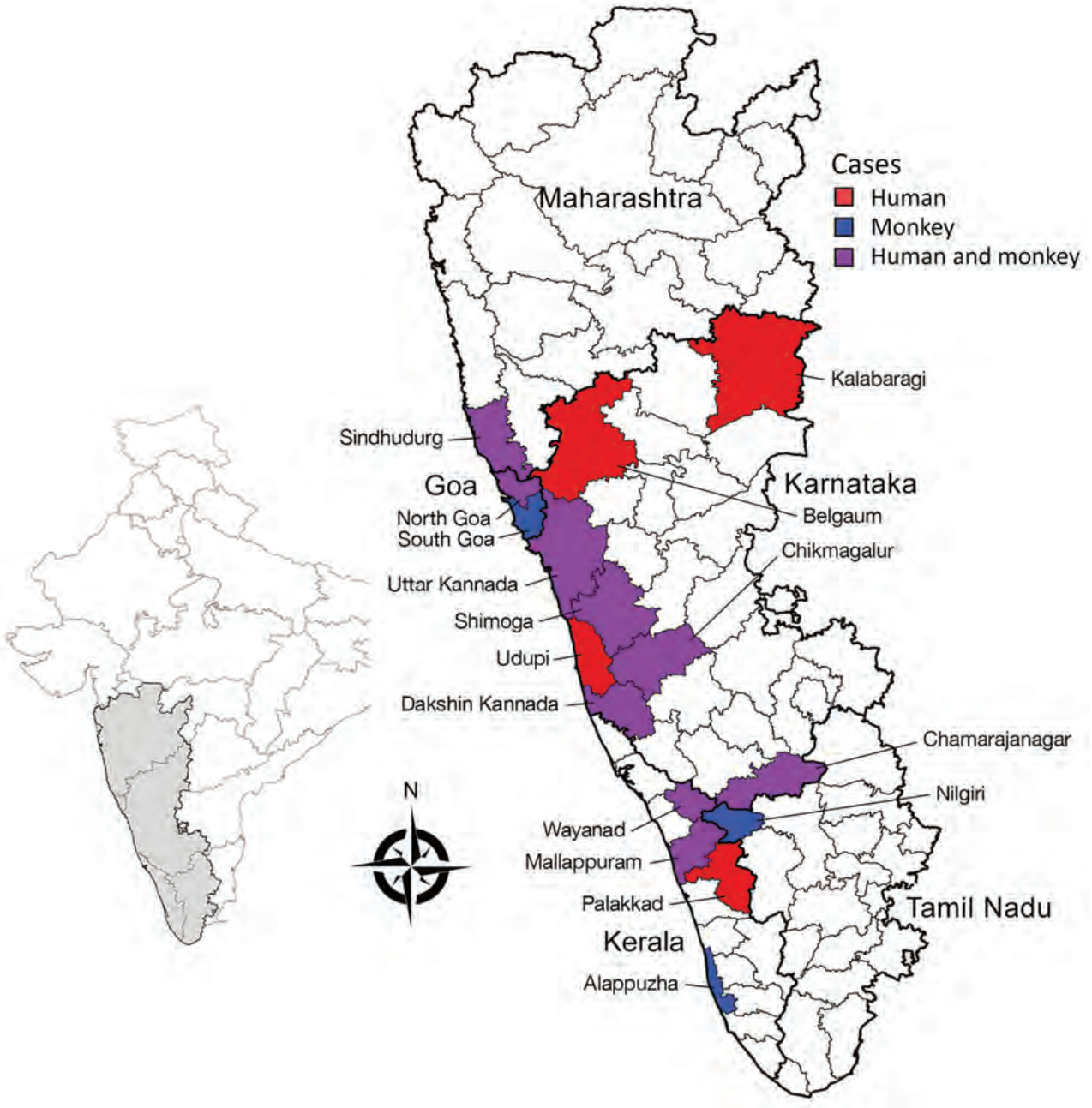

Figure 2. Hotspot areas for human cases and monkey deaths attributable to Kyasanur Forest disease, India,1957–2020. Inset map shows the region in context of the Indian subcontinent.

radius (*6*,*14*). The importance of animals as sentinels of infectious diseases, environmental hazards, and acts of bioterrorism is well documented (*15*). Because monkey deaths are used as sentinels for KFD, establishing year-round surveillance systems that consistently report KFD-related monkey deaths by date, location, and species is essential to better understand the epidemiology of the disease and design appropriate public health measures.

One limitation of our review is the inconsistency and gaps in the availability of reported monkey deaths caused by KFD. Few studies report monkey mortality data or provide specific monkey deaths by location, year, and species, so assessing whether mortality rates have changed over time is difficult. Another limitation is the incomplete data on testing and diagnoses of monkey carcasses for KFDV because of challenges such as distance to the testing site and delays in discovery.

Table 2. Information about potential drivers of Kyasanur Forest Disease transmission based on review of available literature

Drivers	Source of information (reference)
Large-scale deforestation for various reasons (e.g., paddy fields and plantations)	Ajesh et al., 2017 (*1*); Pattnaik, 2006 (*3*)
Human encroachment into forested areas	Pattnaik, 2006 (*3*); Murhekar et al., 2015 (*6*)
Humidity in paddy fields ideal for tick survival	Pattnaik, 2006 (*3*)
Vector ticks can survive in various kinds of biotypes	Sadanandane et al., 2018 (*4*)
Number of small mammalian animals that act as reservoirs for the virus and for the vector tick	Pattnaik, 2006 (*3*)
Movement of monkeys into new areas	Chakraborty et al., 2019 (*2*); Pattnaik, 2006 (*3*)
Cattle may act as amplifying hosts for Kyasanur Forest disease virus and help in maintenance and propagation of the tick vector (handling of cows might also be a risk factor)	Chakraborty et al., 2019 (*2*)

Further research is needed to develop serosurveys specific to KFDV among monkeys, determine species-specific vulnerability to KFDV, and assess whether KFDV can spread through routes other than tick transmission. Testing capacity in KFD-endemic states should be strengthened to conduct timely monkey necropsies, providing more information on the prevalence of KFD in these sentinel animals, to elucidate the epidemiology of KFDV and protect monkey and human health.

Funding for this study was obtained through the University of Illinois Campus Research Board and was supported by the Cooperative State Research, Education, and Extension Service of the US Department of Agriculture (project no. ILLU 875-952).

About the Author

Ms. Chakraborty is a doctoral candidate in the Program in Ecology Evolution and Conservation Biology at the University of Illinois, Urbana–Champaign. Her research interests include the ecology and epidemiology of vectorborne diseases and One Health approaches in disease surveillance and prevention.

References

1. Ajesh K, Nagaraja BK, Sreejith K. Kyasanur Forest disease virus breaking the endemic barrier: an investigation into ecological effects on disease emergence and future outlook. Zoonoses Public Health. 2017;64:e73–80. https://doi.org/10.1111/zph.12349
2. Chakraborty S, Andrade FCD, Ghosh S, Uelmen J, Ruiz MO. Historical expansion of Kyasanur Forest disease in India from 1957 to 2017: a retrospective analysis. Geohealth. 2019;3:44–55. https://doi.org/10.1029/2018GH000164
3. Pattnaik P. Kyasanur Forest disease: an epidemiological view in India. Rev Med Virol. 2006;16:151–65. https://doi.org/10.1002/rmv.495
4. Sadanandane C, Gokhale MD, Elango A, Yadav P, Mourya DT, Jambulingam P. Prevalence and spatial distribution of *Ixodid* tick populations in the forest fringes of Western Ghats reported with human cases of Kyasanur Forest disease and monkey deaths in South India. Exp Appl Acarol. 2018;75:135–42. https://doi.org/10.1007/s10493-018-0223-5
5. Pavri K. Clinical, clinicopathologic, and hematologic features of Kyasanur Forest disease. Rev Infect Dis. 1989;11(Suppl 4):S854–9. https://doi.org/10.1093/clinids/11.Supplement_4.S854
6. Murhekar MV, Kasabi GS, Mehendale SM, Mourya DT, Yadav PD, Tandale BV. On the transmission pattern of Kyasanur Forest disease (KFD) in India. Infect Dis Poverty. 2015;4:37. https://doi.org/10.1186/s40249-015-0066-9
7. Goverdhan MK, Rajagopalan PK, Narasimha Murthy DP, Upadhyaya S, Boshell-M J, Trapido H, et al. Epizootiology of Kyasanur Forest disease in wild monkeys of Shimoga District, Mysore State (1957–1964). Indian J Med Res. 1974;62:497–510.
8. Mehla R, Kumar SR, Yadav P, Barde PV, Yergolkar PN, Erickson BR, et al. Recent ancestry of Kyasanur Forest disease virus. Emerg Infect Dis. 2009;15:1431–7. https://doi.org/10.3201/eid1509.080759
9. Kumara HN, Singh M, Kumar S, Sinha A. Distribution, abundance, group size and demography of dark-bellied bonnet macaque *Macaca radiata* in Karnataka, South India. Curr Sci. 2010;99:663–7.
10. Sinha A. The bonnet macaque revisited: ecology, demography and behavior. Environmental Information System bulletin: Wildlife and Protected Areas. 2001;1:32–41.
11. Kumara HN, Kumar S, Singh M. Of how much concern are the 'least concern' species? Distribution and conservation status of bonnet macaques, rhesus macaques and Hanuman langurs in Karnataka, India. Primates. 2010;51:37–42. https://doi.org/10.1007/s10329-009-0168-8
12. Technical Information Bulletin—Indian Council on Medical Research. Kyasanur Forest disease 1957–1964. Poona (India): Virus Research Centre.; 1964.
13. Patil DR, Yadav PD, Shete A, Chaubal G, Mohandas S, Sahay RR, et al. Study of Kyasanur Forest disease viremia, antibody kinetics, and virus infection in target organs of *Macaca radiata*. Sci Rep. 2020;10:12561. https://doi.org/10.1038/s41598-020-67599-x
14. Kasabi GS, Murhekar MV, Sandhya VK, Raghunandan R, Kiran SK, Channabasappa GH, et al. Coverage and effectiveness of Kyasanur Forest disease (KFD) vaccine in Karnataka, South India, 2005–10. PLoS Negl Trop Dis. 2013;7:e2025. https://doi.org/10.1371/journal.pntd.0002025
15. Neo JPS, Tan BH. The use of animals as a surveillance tool for monitoring environmental health hazards, human health hazards and bioterrorism. Vet Microbiol. 2017;203:40–8. https://doi.org/10.1016/j.vetmic.2017.02.007

Address for correspondence: William Sander, University of Illinois Urbana–Champaign, 1008 W Hazelwood Dr, Urbana, IL 61802, USA; email: wsander@illinois.edu

Prolonged SARS-CoV-2 RNA Shedding from Therapy Cat after Cluster Outbreak in Retirement Home

Claudia Schulz,[1] Claudia Wylezich,[1] Kerstin Wernike, Magdalena Gründl, Alexandra Dangel, Christine Baechlein, Donata Hoffmann, Susanne Röhrs, Sabrina Hepner, Nikolaus Ackermann, Andreas Sing, Isabelle Pink, Beate Länger, Holger A. Volk, Paul Becher, Gerd Sutter, Antonie Neubauer-Juric, Maren von Köckritz-Blickwede, Martin Beer, Asisa Volz

Author affiliations: University of Veterinary Medicine Hanover, Hanover, Germany (C. Schulz, C. Baechlein, S. Röhrs, B. Länger, H.A. Volk, P. Becher, M. von Köckritz-Blickwede, A. Volz); Friedrich-Loeffler-Institut, Greifswald-Insel Riems, Germany (C. Wylezich, K. Wernike, D. Hoffmann, M. Beer); Local Health Authority Cham, Cham, Germany (M. Gründl); Bavarian Health and Food Safety Authority, Oberschleißheim, Germany (A. Dangel, S. Hepner, N. Ackermann, A. Sing, A. Neubauer-Juric); Hanover Medical School, Hanover (I. Pink); Ludwig Maximilian University Munich, Munich, Germany (G. Sutter)

DOI: https://doi.org/10.3201/eid2707.204670

We report a therapy cat in a nursing home in Germany infected with severe acute respiratory syndrome coronavirus 2 during a cluster outbreak in the home residents. Although we confirmed prolonged presence of virus RNA in the asymptomatic cat, genome sequencing showed no further role of the cat in human infections on site.

Cats are susceptible to severe acute respiratory syndrome coronavirus 2 (SARS-CoV-2) infection and can transmit the virus to other cats (*1*–*3*). However, the pathophysiology and epidemiologic impact of SARS-CoV-2 infection of pets remain poorly understood (*4*). We report 3 therapy cats living in a retirement home in Germany for which evidence indicated naturally occurring human-to-cat transmission during SARS-CoV-2 outbreaks.

A total of 21 confirmed human SARS-CoV-2 infections occurred in the outbreaks, including 3 deaths. Six infected care and administrative personnel showed mild or no symptoms; 15 infected residents showed typical signs of coronavirus disease, including fever and severe respiratory disease (cough, pneumonia, and dyspnea). The first outbreak occurred on the home's ground floor at the end of March 2020 (Appendix Figure 1, panel A, https://wwwnc.cdc.gov/EID/article/27/7/20-4670-App1.pdf); it is assumed that the virus was introduced through care personnel. One SARS-CoV-2–positive resident (90 years of age, given a diagnosis on April 4, 2020), already bedridden, died on April 12. He had been in close contact with cat K8, which snuggled in his face.

A strict hygienic plan was implemented to contain the initial outbreak, including using separate personnel for each floor. No visitors were allowed. All residents were kept in their rooms without social contact between them. Despite isolation, the cats still had access to all areas and to the outside.

At the end of April, residents of the first floor showed typical COVID-19 symptoms. We tested oropharyngeal swab specimens from the cats on April 29 (surveillance day 1) (Appendix Figure 1, panel A). Although 2 cats (K4 and K9) showed negative results, 1 (K8) showed positive results for SARS-CoV-2 RNA by quantitative reverse transcription PCR specific for partial envelope protein gene (Table; Appendix Figure 1, panel C).

Because of epidemiologic connections, we speculated whether K8 could have been involved in spreading SARS-CoV-2 to the first floor. We isolated the cats in a Biosafety Level 3 facility for surveillance (Appendix Figure 1, panel A) and tested them again on May 4. K8 was positive for SARS-CoV-2 RNA and had lower quantification cycle values (Table; Appendix Figure 1, panels B, C). Cats were housed in single cages during the first 4 days of quarantine (surveillance days 6–10), then moved into 1 combined cage system (surveillance day 11). After 15 days (surveillance day 21), cats were transferred to floor housing under Biosafety Level 3 conditions and permitted free movement and contact. Testing at regular intervals of conjunctival, fecal, and oropharyngeal swab specimens showed that K4 and K9 remained negative, whereas K8 was positive for SARS-CoV-2 RNA until day 21 of surveillance. K8 also had positive quantification cycle values (range 26.3–38.5; values <40 were considered positive) (Appendix Figure 1, panel B) and ≈5.7×10^4 to 5.0×10^3 RNA copies/mL (Appendix Figure 1, panel C).

Subsequently, we detected no viral RNA in swab samples through day 73.

These PCR results demonstrated an extended period of SARS-CoV-2 infection of the positive cat. When serum samples were analyzed for SARS-CoV-2–neutralizing antibodies (*5*), K8 showed a positive titer (range 1:20–1:52) (Appendix Figure 1, panel D). Multispecies ELISA results showed serum antibodies against the receptor-binding domain (*5*). Titers peaked by day 35 and decreased but remained positive until the end of surveillance (Appendix Figure 1,

[1]These authors contributed equally to this article.

Table. Overview of cat swab specimen and blood sampling regimen for prolonged SARS-CoV-2 RNA shedding from therapy cat after cluster outbreak in retirement home, Germany*

Day of surveillance	Sample type	Cq values by RdRp/RdRp gene screen	Cq values by E/E/S gene screen
1	OPS	ND/ND	ND/35.56/36.15†
6	OPS	ND/ND	ND/26.34/27.06†
7	OPS	29.66/31.40	30.52/ND
9	OPS, CS, FS, BS	37.48/no Cq	36.23/ND
11	OPS, CS, FS	30.95/34.80	34.66/ND
13	OPS, CS, FS, BS	32.63/35.50	35.98/ND
15	OPS, CS, FS	31.17/35.10	36.96/ND
17	OPS, CS, FS, BS	33.12/36.50	35.92/ND
19	OPS, CS, FS	No Cq/no Cq	No Cq/ND
21	OPS, CS, FS, BS	No Cq/38.80	No Cq/ND
28	OPS, CS, FS, **BS**	No Cq/no Cq	ND/ND
31	OPS, CS, FS	No Cq/no Cq	No Cq/ND
35	OPS, CS, FS, BS	No Cq/no Cq	ND/ND
38	OPS, CS, FS	No Cq/no Cq	ND/ND
42	OPS, CS, FS, BS	No Cq/no Cq	ND/ND
45	OPS, CS, FS	No Cq/no Cq	ND/ND
49	OPS, CS, FS, BS	No Cq/no Cq	ND/ND
69	BS	No Cq/no Cq	ND/ND
73	OPS, CS, FS, BS	No Cq/no Cq	ND/ND

*Results are given for virus-positive cat K8. At day 28, serum samples for analysis of blood were collected (in bold). PCRs were performed between day 1 and day 6 by using the RealStar SARS-CoV-2 RT-PCR Kit 1.0 (Altona Diagnostics, https://www.altona-diagnostics.com) for initial diagnosis (E gene screen and SARS-CoV-2 specific spike gene), and from day 7 by using an RdRP gene SARS-2-IP4 quantitative real-time PCR (World Health Organization–recommended assay) and an E gene-specific PCR (see details in Appendix, https://wwwnc.cdc.gov/EID/article/27/7/20-4670-App1.pdf). The 2 results in the RdRp and E gene columns indicate that these assays were performed independently in 2 different laboratories (University of Veterinary Medicine Hannover and Friedrich-Loeffler Institut). BS, blood sample; CS, conjunctival swab; Cq, quantification cycle; E, envelope; FS, fecal swab; ND, not done; OPS, oropharyngeal swab; RdRP, RNA-dependent RNA polymerase; S, spike protein; SARS-CoV-2, severe acute respiratory syndrome coronavirus 2.
†Indicates a third test result for the S gene.

panel E). K4 and K9 remained SARS-CoV-2 seronegative (Appendix Figure 1, panels D, E).

To examine the effects of potential co-infections, we analyzed common feline viral infections. All cats were negative for feline leukemia virus. However, K8 was positive for feline immunodeficiency virus (FIV)–specific antibodies, and K4 and K9 were positive for feline coronavirus–specific antibodies. The marginal serologic reactivity of K8 indicated that this cat was not previously infected with feline coronavirus (Appendix Figure 2).

SARS-CoV-2 genome sequences obtained from K8 and related human cases in the retirement home (1 from the first outbreak and 3 from the second outbreak) differed from each other by 3 ambiguous sites, indicating low-frequency variants within K8, leading to viral quasispecies. Sequences from the second outbreak included a constant C→T change (Appendix Figure, panel F). These data support direct human-to-cat-transmission during the first outbreak but not zoonotic SARS-CoV-2 transmission from K8 because of the constant viral sequence difference within the second outbreak series.

Our data showed human-to-cat SARS-CoV-2 transmission in a community-acquired cluster outbreak that had multiple infection events. We demonstrated prolonged shedding of SARS-CoV-2 RNA up to day 21 after the first detection, in contrast to a recent study in a naturally infected cat (RNA-positive for 11 days) (*6*). We hypothesize a longer period of RNA shedding (>21 days) because we do not know the day of infection before the start of cat surveillance. Prolonged SARS-CoV-2 RNA shedding could be related to immune status of individual animals or co-infections or immunosuppression as reported for humans (*7*–*9*).

Our sequencing data do not suggest zoonotic spillback from the SARS-CoV-2–infected cat to humans, as reported elsewhere (*3*,*10*). However, reinfections, prolonged virus replication, and transmission events in cats cannot be excluded, in particular if one considers emergence of SARS-CoV-2 variants that have potentially increased host range or ability to escape preexisting immunity. Thus, cats should be considered in surveillance and control measures.

Acknowledgments

We thank Reinhold Schoirer for expert help with initial SARS-CoV-2 diagnosis in the cats; Giuseppe Valenza, Jürgen Christian, and Nelly Scuda for expert help with human SARS-CoV-2 diagnosis; Dirk Höper for expert help in uploading genome sequences; Patrick Zitzow, Bianka Hillmann, Inga Grotha, and Nelia Libowski for excellent technical support; Saskia Oppermann, Darren Markillie, and Monika Berg for dedicated animal care and exceptional support; and Arbor Biosciences for providing SARS-CoV-2 baits for virus enrichment.

This study was supported by the German Federal Ministry of Food and Agriculture through the Federal Office for Agriculture and Food (project ZooSeq, grant no. 2819114019).

About the Author

Dr. Schulz is a postdoctoral researcher at University of Veterinary Medicine Hanover, Hanover, Germany. Her primary research interests are the pathogenesis and epidemiology of emerging and vector-borne diseases in the wildlife–livestock and human–animal interfaces.

References

1. Gaudreault NN, Trujillo JD, Carossino M, Meekins DA, Morozov I, Madden DW, et al. SARS-CoV-2 infection, disease and transmission in domestic cats. Emerg Microbes Infect. 2020;9:2322–32. https://doi.org/10.1080/22221751.2020.1833687
2. Halfmann PJ, Hatta M, Chiba S, Maemura T, Fan S, Takeda M, et al. Transmission of SARS-CoV-2 in domestic cats. N Engl J Med. 2020;383:592–4. https://doi.org/10.1056/NEJMc2013400
3. Barrs VR, Peiris M, Tam KW, Law PY, Brackman CJ, To EM, et al. SARS-CoV-2 in quarantined domestic cats from COVID-19 households or close contacts, Hong Kong, China. Emerg Infect Dis. 2020;26:3071–4. https://doi.org/10.3201/eid2612.202786
4. Sit TH, Brackman CJ, Ip SM, Tam KW, Law PY, To EM, et al. Infection of dogs with SARS-CoV-2. Nature. 2020;586:776–8. https://doi.org/10.1038/s41586-020-2334-5
5. Wernike K, Aebischer A, Michelitsch A, Hoffmann D, Freuling C, Balkema-Buschmann A, et al. Multi-species ELISA for the detection of antibodies against SARS-CoV-2 in animals. Transbound Emerg Dis. 2020;Nov 15:1–7. https://doi.org/10.1111/tbed.13926
6. Garigliany M, Van Laere AS, Clercx C, Giet D, Escriou N, Huon C, et al. SARS-CoV-2 natural transmission from human to cat, Belgium, March 2020. Emerg Infect Dis. 2020;26:3069–71. https://doi.org/10.3201/eid2612.202223
7. Yousaf M, Hameed M, Alsoub H, Khatib M, Jamal W, Ahmad M. COVID-19: Prolonged viral shedding in an HIV patient with literature review of risk factors for prolonged viral shedding and its implications for isolation strategies. Clin Case Rep. 2021;9:1397–401. https://doi.org/10.1002/ccr3.3786
8. Ambrosioni J, Blanco JL, Reyes-Urueña JM, Davies MA, Sued O, Marcos MA, et al.; COVID-19 in HIV Investigators. Overview of SARS-CoV-2 infection in adults living with HIV. Lancet HIV. 2021;8:e294–305. https://doi.org/10.1016/S2352-3018(21)00070-9
9. Tarhini H, Recoing A, Bridier-Nahmias A, Rahi M, Lambert C, Martres P, et al. Long term SARS-CoV-2 infectiousness among three immunocompromised patients: from prolonged viral shedding to SARS-CoV-2 superinfection. J Infect Dis. 2021;Feb 8:jiab075. https://doi.org/10.1093/infdis/jiab075
10. Sailleau C, Dumarest M, Vanhomwegen J, Delaplace M, Caro V, Kwasiborski A, et al. First detection and genome sequencing of SARS-CoV-2 in an infected cat in France. Transbound Emerg Dis. 2020;67:2324–8. https://doi.org/10.1111/tbed.13659

Address for correspondence: Asisa Volz, Institute of Virology, University of Veterinary Medicine Hannover, Buenteweg 17, 30559 Hanover, Lower Saxony, Germany; email: asisa.volz@tiho-hannover.de

Effects of COVID-19 Vaccination Timing and Risk Prioritization on Mortality Rates, United States

Xutong Wang, Zhanwei Du, Kaitlyn E. Johnson, Remy F. Pasco, Spencer J. Fox, Michael Lachmann, Jason S. McLellan, Lauren Ancel Meyers

Author affiliations: The University of Texas at Austin, Austin, Texas, USA (X. Wang, Z. Du, K.E. Johnson, R.F. Pasco, S.J. Fox, J.S. McLellan, L.A. Meyers); The University of Hong Kong, Hong Kong, China (Z. Du); Hong Kong Science and Technology Park, Hong Kong (Z. Du); Santa Fe Institute, Santa Fe, New Mexico, USA (M. Lachmann, L.A. Meyers)

DOI: https://doi.org/10.3201/eid2707.210118

During rollout of coronavirus disease vaccination, policymakers have faced critical trade-offs. Using a mathematical model of transmission, we found that timing of vaccination rollout would be expected to have a substantially greater effect on mortality rate than risk-based prioritization and uptake and that prioritizing first doses over second doses may be lifesaving.

In December 2020, the US government issued emergency use authorization for two 2-dose severe acute respiratory syndrome coronavirus 2 (SARS-CoV-2) vaccines, both estimated to be >94% efficacious in preventing symptomatic coronavirus disease (COVID-19) (*1*–*3*). The Advisory Committee on Immunization Practices immediately recommended the prioritization of frontline workers and high-risk subgroups (*4*). As of February 14, 2021, ≈52 million doses have been administered (*5*). We used a mathematical model of COVID-19 transmission to evaluate the effects of vaccine timing, risk prioritization, number of doses administered, and uptake rates on population-level mortality rates (Figure).

Focusing on Austin, Texas, USA, we projected COVID-19 deaths over 8 months for both an infection-blocking vaccine that prevents infection upon exposure (assuming 95% reduction in susceptibility in vaccinated persons) and a symptom-blocking vaccine that prevents symptoms upon infection (assuming 95% reduction in symptomatic ratio in vaccinated persons). Vaccination would begin on January 15 or February 15, with 10,000 vaccines administered weekly and allocated to cities pro rata. We compare 3 strategies: no priority groups; 1 of 3 priority groups vaccinated before the general public (adults >65 years of age, adults who have high-risk underlying

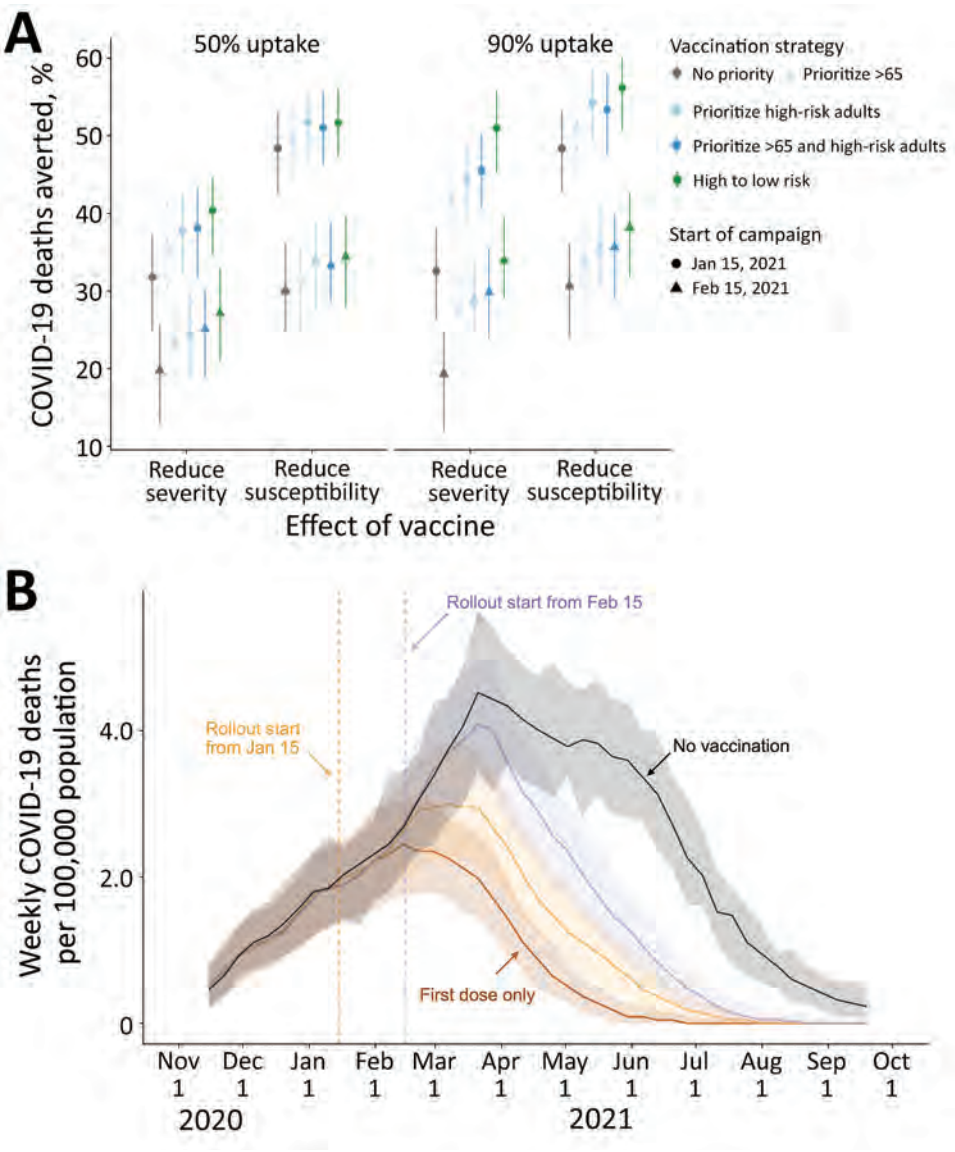

Figure. Projected COVID-19 deaths and deaths averted in the Austin–Round Rock Metropolitan Statistical Area (Austin, TX, USA) under various vaccine rollout scenarios for November 8, 2020–September 17, 2021. A) COVID-19 deaths averted after January 15, 2021, under combinations of vaccine uptake of 50% (left) or 90% (right); type of protection, either infection blocking (reducing susceptibility) or symptom blocking (reducing severity); rollout dates, either January 15 (circles) or February 15 (triangles); and risk prioritization, either no priority (gray), prioritize all adults >65 years of age (light blue), adults with high-risk underlying conditions (medium blue), or the combination of the two (dark blue), or a 10-phase risk-ordered strategy (green) that sequentially vaccinates >65 y high risk, 50–64 y high risk, >65 y low risk, 18–49 y high risk, 50–64 y low risk, 18–49 y low risk, 0–4 y high risk, 5–17 y high risk, 0–4 y low risk, 5–17 y low risk. Points and whiskers indicate the median and 95% CI across 200 paired stochastic simulations. B) Weekly incident COVID-19 deaths per 100,000 population, assuming intermediate (70%) uptake (*6*) without vaccine (black) or under a 10-phase risk-based rollout of a 95% efficacious infection-blocking vaccine, starting either January 15 (orange) or February 15 (purple). The brown line assumes that only first doses are administered starting January 15. Solid lines and shading indicate the median and 95% CI across 200 stochastic simulations. COVID-19, coronavirus disease.

conditions, or both); and 10 phases that vaccinate age–risk groups in order of risk for severe COVID-19 outcomes. Stochastic simulations assumed that 7.6% of the overall population of the Austin–Round Rock Metropolitan Statistical Area were immunized by infection before January 15.

If a perfectly risk-prioritized (10-phase) rollout of an infection-blocking vaccine were to begin January 15, we estimated that 52% (95% CI 47%–56%) of deaths would be averted relative to the baseline of no vaccines, assuming 50% uptake, or 56% (95% CI 51%–60%) of deaths averted assuming 90% uptake (Figure, panel A). If rollout were delayed 1 month, 34% (95% CI 28%–40%) of deaths would be averted at 50% uptake, or 38% (95% CI 32%–43%) at 90% uptake. Under low (50%) uptake, prioritization has minimal benefit. Under high uptake (90%), the 10-stage strategy is optimal, followed by prioritizing adults >65 years of age and high-risk younger adults.

Expected differences are magnified with a symptom-blocking vaccine. For a January 15 start and 50% uptake, the risk-prioritized 10-phase strategy would avert 40% (95% CI 35%–45%) of deaths, whereas unprioritized rollout would avert 32% (95% CI 25%–37%). If a single dose with 82% efficacy (*1*,*2*) is administered under the 10-phase strategy, we would

expect a 50% (95% CI 45%–54%) reduction in mortality for a symptom-blocking vaccine and 66% (95% CI 63%–70%) reduction for an infection-blocking vaccine (Appendix Table 1, https://wwwnc.cdc.gov/EID/article/27/7/21-0118-App1.pdf).

These projections validate the prioritizing of high-risk groups. In a pessimistic scenario in which a symptom-blocking vaccine rollout began in February 2021 with 50% uptake, prioritizing high-risk adults and adults >65 would avert ≈17,000 (95% CI 0–36,000) more deaths in the United States than a nonprioritized campaign. Given the state of the pandemic in early 2021, we expected vaccine delays to cost more lives than either imperfect prioritization or vaccine hesitancy.

The United Kingdom and Belgium have prioritized first doses over second doses (*7*), in an effort to provide partial immunity to more persons. The United States has publicly resisted this approach, citing the lack of clinical trial data validating the approach (*8*). We found that providing a single (82% efficacious) dose would be expected to save more lives than the corresponding 2-dose strategy, because partially immunizing a large number confers a greater degree of population-level protection than more fully immunizing half as many. Although a 1-dose campaign may accelerate herd immunity and require far fewer resources than a 2-dose campaign, we strongly caution that additional data and single-dose trials are needed to establish efficacy. If the single-dose efficacy is <82%, then we would expect the difference between a single-dose strategy and the corresponding 2-dose strategy to be smaller. We expect similar reductions in mortality rate from both strategies when the single-dose efficacy is 52% (*2*) (Appendix Figure 7). We note that low-efficacy vaccines may increase the risk for vaccine-resistant variants (*9*) and that there may be political, commercial, and societal barriers to shifting priorities mid-campaign (*10*).

We assumed that vaccines provide lasting immunity and block either infection or symptoms, whereas the reality may be a hybrid of both (Appendix Table 2, Figure 2), along with riskier behavior stemming from pandemic weariness or overconfidence in the vaccination campaign. Our estimates reflect conditions in the United States in early 2021, as cases were surging toward a pandemic peak in the absence of effective mitigation. The estimated public health benefits of vaccines decrease under higher COVID-19 transmission rates that might occur with relaxed mitigation measures, lower levels of immunity before the rollout, or the emergence of more transmissible SARS-CoV-2 variants including B.1.1.7 (Appendix).

Risk prioritization is a valid approach for maximizing the impact of vaccines, but not at the expense of vaccination speed. Our projections suggest 2 immediate strategies: hybrid distributions that combine active outreach to priority groups with passive distribution to the general public; and distribution of single doses to as much of the population as possible, foregoing plans to hold second doses in reserve.

Acknowledgments

We thank Matthew Biggerstaff for critical discussions and parameter guidance.

This research was supported by grants from the US National Institutes of Health (grant no. R01 AI151176) and the US Centers for Disease Control and Prevention (grant no. U01 IP001136) and a donation from Love, Tito's (the philanthropic arm of Tito's Homemade Vodka, Austin, TX, USA) to the University of Texas to support the modeling of COVID-19 mitigation strategies.

About the Author

Dr. Wang completed this work as a PhD candidate at the University of Texas at Austin, under the supervision of Lauren Ancel Meyers. Her research interest is on mathematical and statistical modeling of infectious disease dynamics.

References

1. Vaccines and Related Biological Products Advisory Committee. FDA briefing document: Moderna COVID-19 vaccine. December 17, 2020 [cited 2021 May 7]. https://www.fda.gov/media/144434/download
2. Vaccines and Related Biological Products Advisory Committee. FDA briefing document: Pfizer BioNTech COVID-19 vaccine. December 10, 2020 [cited 2021 May 7]. https://www.fda.gov/media/144245/download
3. US Food and Drug Administration. COVID-19 vaccines. [cited 2021 Feb 17]. https://www.fda.gov/emergency-preparedness-and-response/coronavirus-disease-2019-covid-19/covid-19-vaccines
4. Dooling K, McClung N, Chamberland M, Marin M, Wallace M, Bell BP, et al. The Advisory Committee on Immunization Practices' interim recommendation for allocating initial supplies of COVID-19 vaccine—United States, 2020. MMWR Morb Mortal Wkly Rep. 2020;69:1857–9. https://doi.org/10.15585/mmwr.mm6949e1
5. US Centers for Disease Control and Prevention. Vaccines for COVID-19. 2021 [cited 2021 Feb 15]. https://www.cdc.gov/coronavirus/2019-ncov/vaccines/index.html
6. Tyson A, Johnson C, Funk C. US public now divided over whether to get COVID-19 vaccine. 2020 [cited 2020 Dec 14]. https://www.pewresearch.org/science/2020/09/17/u-s-public-now-divided-over-whether-to-get-covid-19-vaccine/
7. Pancevski B. UK delays second COVID-19 vaccine dose as Europe ponders how to speed up immunization. 2020

[cited 2021 Jan 13]. https://www.wsj.com/articles/u-k-delays-second-covid-19-vaccine-dose-as-europe-ponders-how-to-speed-up-immunization-11609334172
8. US Food and Drug Administration. FDA statement on following the authorized dosing schedules for COVID-19 vaccines. January 4, 2021 [cited 2021 Jan 14]. https://www.fda.gov/news-events/press-announcements/fda-statement-following-authorized-dosing-schedules-covid-19-vaccines
9. Livingston EH. Necessity of 2 doses of the Pfizer and Moderna COVID-19 vaccines. JAMA. 2021;325:898. 10.1001/jama.2021.1375 https://doi.org/10.1001/jama.2021.1375
10. Science advisers: publish evidence behind COVID vaccine dosing strategy. Nature. 2021;589:169–70. https://doi.org/10.1038/d41586-021-00045-8

Address for correspondence: Lauren Ancel Meyers, Department of Integrative Biology, 1 University Station C0990; Austin, TX 78712, USA; email: laurenmeyers@austin.utexas.edu

SARS-CoV-2 Aerosol Exhaled by Experimentally Infected Cynomolgus Monkeys

Chunmao Zhang,[1] Zhendong Guo,[1] Zongzheng Zhao,[1] Tiecheng Wang, Liang Li, Faming Miao, Cheng Zhang, Yuanguo Li, Yuwei Gao

Author affiliations: College of Veterinary Medicine at Hebei Agricultural University, Baoding, China. (C. Zhang); Military Veterinary Research Institute, Changchun, China (C. Zhang, Z. Guo, Z. Zhao, T. Wang, L. Li, F. Miao, C. Zhang, Y. Li, Y. Gao)

DOI: https://doi.org/10.3201/eid2707.203948

We analyzed size of severe acute respiratory coronavirus 2 (SARS-CoV-2) aerosol particles shed by experimentally infected cynomolgus monkeys. Most exhaled particles were small, and virus was mainly released early during infection. By postinfection day 6, no virus was detected in breath, but air in the isolator contained large quantities of aerosolized virus.

Although airborne transmission of severe acute respiratory syndrome coronavirus 2 (SARS-CoV-2) has been proven possible among humans (*1*), cats (*2*), ferrets (*3*), and Syrian hamsters (*4*), the relative roles of droplets and aerosols in the airborne transmission of SARS-CoV-2 remain controversial. A recent study showed that coronavirus disease (COVID-19) patients exhaled millions of SARS-CoV-2 particles during early infection stages (*5*). However, the size distribution of SARS-CoV-2 aerosol particles in exhaled breath of COVID-19 patients is not clear.

To analyze size distribution of SARS-CoV-2 aerosols shed by cynomolgus monkeys, we inoculated 3 monkeys with SARS-CoV-2 via a combination of intranasal, intratracheal, and ocular routes. Monkeys were kept in individual cages placed in an isolator (biosafety housing with HEPA filters and independent ventilation system). The exhaled breath and air in the isolator were collected by a 6-stage Andersen sampler (https://tisch-env.com) at postinfection days 2, 4, and 6, and we quantified the viral RNA copies in samples (Appendix, https://wwwnc.cdc.gov/EID/article/27/7/20-3948-App1.pdf). We also determined size distribution of SARS-CoV-2 particles.

The virus particles monkeys exhaled peaked at postinfection day 2 and ranged from 11,578 to 28,336 RNA copies during a 40-minute period. On average, each monkey exhaled 503 virus particles/min and 209.5 virus particles/L of exhaled breath. At postinfection day 4, the number of exhaled virus particles decreased substantially, ranging from 3,369 to 5,134 RNA copies during a 40-minute period. On average, each monkey exhaled 106 virus particles/min and 44 virus particles/L of breath. At postinfection day 6, no viral RNA was detected in exhaled breath (Figure, panel A; Appendix Figure 1). At postinfection days 2, 4, and 6, viral RNA was detected in air within the isolator housing the monkeys; we detected 6,182–13,608 RNA copies during a 30-minute period (Figure, panel C).

We measured size distribution of SARS-CoV-2 aerosol particles shed by the monkeys. In exhaled breath of inoculated monkeys and in air in the isolator, viral RNA was detected in all size bins, 0.65–2.1 mm, 2.1–4.7 mm, and >4.7 mm, at postinfection days 2 and 4; most were concentrated in the 2.1–4.7-mm bin (Figure, panels B, D; Appendix Tables 1, 2). For exhaled breath, virus particles in each of the 3 size bins accounted for 27.4%, 49.6%, and 23.0% of the total virus copies/40 min, respectively; for air in the isolator, virus particles in each of the 3 size bins accounted for 3.8%, 75.0%, and 21.2% of the total virus copies/30 min, respectively (Appendix Tables 1, 2, Figure 3). Most virus particles were in the smaller particle size range (0.65–4.7 mm), accounting for 77% to 79% of the total virus particles shed by the monkeys; droplets (>4.7 mm) accounted for ≈21%– 23% (Appendix Tables 1, 2, Figure 3). We tried to isolate live virus by sequentially passaging

[1]These authors contributed equally to this article.

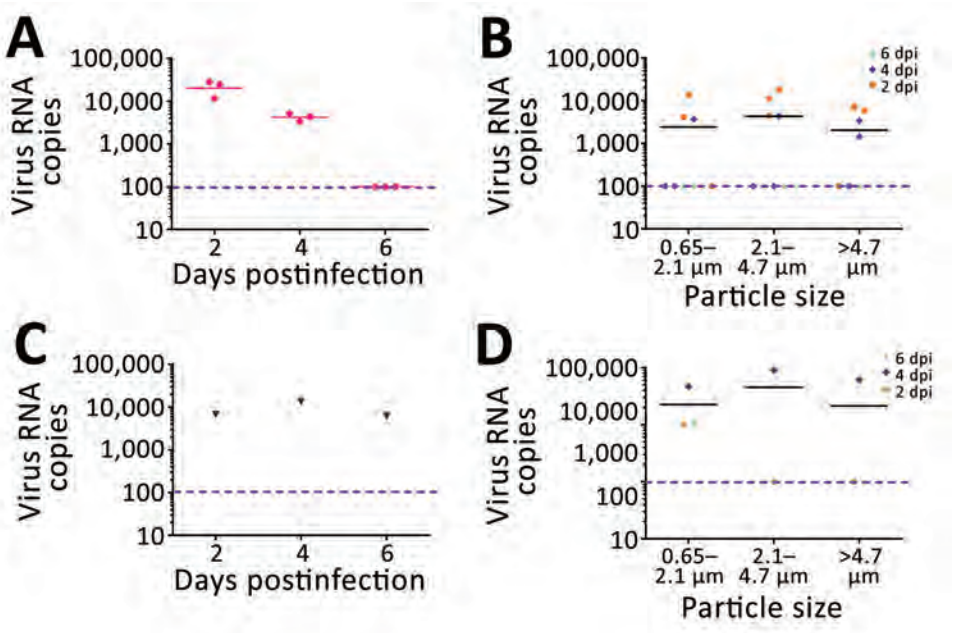

Figure. Viral RNA copies and size distribution of severe acute respiratory syndrome coronavirus 2 aerosols shed by experimentally infected cynomolgus monkeys. A) Viral RNA copies in aerosols directly expelled during 40 minutes of breathing. B) Size distribution of virus aerosols directly expelled during 40 minutes of breathing. C) Viral RNA copies in aerosols from the housing isolator during 30 minutes of sampling. D) Size distribution of virus aerosols in the isolator during 30 minutes of sampling. dpi, days postinfection. The pink dotted line indicates the limit of detection.

these samples in Vero-E6 cells 3 times (Appendix) but obtained no live virus and observed no cytopathic effects; the reasons for this failure are unknown.

The World Health Organization cites the 2 main transmission routes of SARS-CoV-2 as large respiratory droplets and contact transmission. However, we found that monkeys infected with SARS-CoV-2 emitted large quantities of virus aerosol particles, most of which were smaller (<4.7 μm). Ma et al. showed that COVID-19 patients exhaled millions of SARS-CoV-2 particles/hour (*5*), far more than that noted for monkeys. This variation may result from biological differences between humans and monkeys and different sampling methods. Respiration is much slower in monkeys (2.4 L/min) than in humans (12 L/min). In addition, during sampling, monkeys were anesthetized and breathed slowly through their nostrils, possibly emitting fewer virus particles than when awake. The size of airborne particles determines how the virus is transmitted. Droplets (>4.7 μm) can travel limited distances; smaller particles (<4.7 μm) stay airborne longer and spread widely (*6*,*7*). Our findings suggest that aerosol transmission might contribute to SARS-CoV-2 spread. Personal protection requires wearing face masks, maintaining social distancing, and reducing gatherings. Infection risk in enclosed spaces is lowered by natural wind or mechanical airflow ventilation.

Cynomolgus monkeys infected with SARS-CoV-2 emitted most virus particles in early infection stages; particles decreased substantially at postinfection day 6. Zhou et al. demonstrated that COVID-19 patients emitted fewer virus particles when they were recovering and ready for discharge than did those in early infection stages (*8*). At postinfection day 6, no virus was detected in the breath of monkeys, but air in the isolator housing the monkeys still contained large quantities of aerosolized virus. These different seemingly noncoherent observations can be attributed to monkey activity, air flow, and some virus aerosol residues exhaled by monkeys for a relatively long period before sampling. Recently, Asadi et al. showed that aerosolized fomites (microscopic particles) played a role in influenza virus transmission between guinea pigs (*9*). SARS-CoV-2 may be carried and transmitted between humans by aerosolized fomites. Most SARS-CoV-2 aerosol particles exhaled by the cynomolgus monkeys in this study were smaller, suggesting that aerosols might be a route for SARS-CoV-2 transmission.

Acknowledgments

We thank the staff at the Biosafety Level 3 laboratories of Military Veterinary Research Institute for their support and help.

This research was supported by the National Natural Science Foundation of China (32000134) and the National Major Research and Development Program (2020YFC0840800).

About the Author

Drs. Chunmao Zhang, Guo, and Zhao are investigators at the Military Veterinary Research Institute. Their primary interests are pathogenicity and airborne transmissibility of respiratory viruses, especially influenza viruses.

References

1. Anderson EL, Turnham P, Griffin JR, Clarke CC. Consideration of the aerosol transmission for COVID-19 and public health. Risk Anal. 2020;40:902–7. https://doi.org/10.1111/risa.13500
2. Shi J, Wen Z, Zhong G, Yang H, Wang C, Huang B, et al. Susceptibility of ferrets, cats, dogs, and other domesticated animals to SARS-coronavirus 2. Science. 2020;368:1016–20. https://doi.org/10.1126/science.abb7015
3. Kim YI, Kim SG, Kim SM, Kim EH, Park SJ, Yu KM, et al. Infection and rapid transmission of SARS-CoV-2 in ferrets. Cell Host Microbe. 2020;27:704–709.e2. https://doi.org/10.1016/j.chom.2020.03.023
4. Sia SF, Yan LM, Chin AWH, Fung K, Choy KT, Wong AYL, et al. Pathogenesis and transmission of SARS-CoV-2 in golden hamsters. Nature. 2020;583:834–8. https://doi.org/10.1038/s41586-020-2342-5
5. Ma J, Qi X, Chen H, Li X, Zhang Z, Wang H, et al. Coronavirus disease 2019 patients in earlier stages exhaled millions of severe acute respiratory syndrome coronavirus 2 per hour. Clin Infect Dis. 2020;ciaa1283. https://doi.org/10.1093/cid/ciaa1283
6. Bischoff WE, Swett K, Leng I, Peters TR. Exposure to influenza virus aerosols during routine patient care. J Infect Dis. 2013;207:1037–46. https://doi.org/10.1093/infdis/jis773
7. Brankston G, Gitterman L, Hirji Z, Lemieux C, Gardam M. Transmission of influenza A in human beings. Lancet Infect Dis. 2007;7:257–65. https://doi.org/10.1016/S1473-3099(07)70029-4
8. Zhou L, Yao M, Zhang X, Hu B, Li X, Chen H, et al. Breath-, air- and surface-borne SARS-CoV-2 in hospitals. J Aerosol Sci. 2021;152:105693. https://doi.org/10.1016/j.jaerosci.2020.105693
9. Asadi S, Gaaloul Ben Hnia N, Barre RS, Wexler AS, Ristenpart WD, Bouvier NM. Influenza A virus is transmissible via aerosolized fomites. Nat Commun. 2020;11:4062. https://doi.org/10.1038/s41467-020-17888-w

Address for correspondence: Yuwei Gao, Military Veterinary Research Institute, 666 Liuying West Rd, Changchun, 130122, China; email:gaoyuwei@gmail.com

Possible Human-to-Dog Transmission of SARS-CoV-2, Italy, 2020

Nicola Decaro, Gabriele Vaccari, Alessio Lorusso, Eleonora Lorusso, Luca De Sabato, Edward I. Patterson, Ilaria Di Bartolo, Grant L. Hughes, Liana Teodori, Costantina Desario, Barbara Colitti, Dominga Ricci, Domenico Buonavoglia, Sergio Rosati, Vito Martella, Cesare Cammà, Umberto Agrimi, Gabriella Elia

Author affiliations: University of Bari, Valenzano, Italy (N. Decaro, E. Lorusso, C. Desario, D. Buonavoglia, V. Martella, G. Elia); Istituto Superiore di Sanità, Rome, Italy (G. Vaccari, L. De Sabato, I. Di Bartolo, U. Agrimi); Istituto Zooprofilattico Sperimentale dell'Abruzzo e del Molise "G. Caporale," Teramo, Italy (A. Lorusso, L. Teodori, C. Cammà); Liverpool School of Tropical Medicine, Liverpool, UK (E.I. Patterson, G.L. Hughes); University of Turin, Turin, Italy (B. Colitti, S. Rosati); Ambulatorio Veterinario Dott.ssa Ricci Dominga, Andria, Italy (D. Ricci)

DOI: https://doi.org/10.3201/eid2707.204959

We detected severe acute respiratory syndrome coronavirus 2 in an otherwise healthy poodle living with 4 family members who had coronavirus disease. We observed antibodies in serum samples taken from the dog, indicating seroconversion. Full-length genome sequencing showed that the canine and human viruses were identical, suggesting human-to-animal transmission.

Coronavirus disease (COVID-19), caused by infection with severe acute respiratory syndrome coronavirus 2 (SARS-CoV-2), emerged in humans in Wuhan, China, in late December 2019, probably because of spillover from an unidentified animal host (*1*). Dogs and cats, to which some coronaviruses are endemic (*2*), are also susceptible to SARS-CoV-2 infection (*3*,*4*). Although the spread of SARS-CoV-2 is maintained mainly by human-to-human transmission, the epidemiologic implications of animal susceptibility remain uncertain (*4*). We characterized the full genome of a SARS-CoV-2 isolate detected in a dog.

A female poodle, who was 1.5 years of age, lived with 4 family members in Bitonto, Italy. All family members had signs and symptoms of COVID-19, the illness caused by SARS-CoV-2 infection. High temperature (37.5°C–38.5°C), coughing, anosmia, and ageusia developed in the mother, who was 54 years of age, on October 31, 2020. The woman tested positive for SARS-CoV-2 by a rapid antigen test conducted on November 3, 2020. The local health authority

collected nasopharyngeal swab samples and used molecular testing to confirm SARS-CoV-2 infection in the woman's husband and 2 daughters. Clinical signs in the other family members ranged from mild fatigue and high temperatures (37.5°C–37.8°C) in the daughters to moderate respiratory signs and persistent high temperature (37.8°C–38.6°C) in the husband. This study was approved by the Ethics Committee of the Department of Veterinary Medicine at the University of Bari (approval no. 15/2020).

On November 4, 2020, the owners collected oral and nasal swab samples from the family's poodle according to our instructions. The pooled samples tested positive for SARS-CoV-2 by real-time reverse transcription PCR selective for the N gene (*5*). During the next 11 days, the owners collected nasal, oral, and rectal swab samples from the dog. Of 20 samples collected during November 6–15, a total of 4 samples (all of which were collected during November 6–9) tested positive for SARS-CoV-2 (Table). Viral shedding occurred at low titers. We did not isolate the virus. The dog did not show any clinical signs, and no other pets lived in the household.

We tested a serum sample collected by the dog's veterinarian on November 27 with 2 commercial multispecies ELISA tests: ID Screen SARS-CoV-2 Double Antigen Multi-species ELISA (ID.vet, https://www.id-vet.com) and Eradikit COVID19-Multispecies (In3Diagnostic, http://www.in3diagnostic.com). We also conducted a plaque reduction neutralization test (PRNT) (*4*) and a virus neutralization test (VNT) (*6*). We detected antibodies with the Eradikit (23%), PRNT (1:80), and VNT (1:10). We used serologic assays to confirm the presence of antibodies against SARS-CoV-2 in an additional serum sample collected on December 12, 2020; the antibody titers were 1:80 for PRNT and 1:20 for VNT (Table).

We submitted the positive pooled oral and nasal swab samples from the dog and the oropharyngeal swab sample from the index patient, all of which were collected on November 4, for next-generation sequencing (*7*). Next-generation sequencing obtained total reads of 929,736 with a mean coverage of 4,300× for the index patient and 969,837 with a mean coverage of 1,800× for the dog. Complete genomes were obtained using the pipeline SARS-CoV-2 RECoVERY in the Galaxy public server ARIES (Istituto Superiore di Sanità, https://w3.iss.it/site/aries). The 2 SARS-CoV-2 genomes shared 100% nucleotide identity. The Pangolin COVID-19 Lineage Assigner (https://pangolin.cog-uk.io) and Nextclade (https://clades.nextstrain.org) assigned the sequences to the lineage B.1.177 (denoted by Nextclade as 20A.EU1) in Europe. Phylogenetic analysis confirmed the clustering of the 2 strains within the GV clade and the B.1.177 lineage already detected in Italy (Figure).

Despite the massive number of persons with SARS-CoV-2, only a few cases of active infection in pets have been reported (*3*). SARS-CoV-2–specific antibodies in pets have been reported on a few occasions, and higher seroprevalence rates have been found in animals from households in which family members have COVID-19 (*4*,*6*,*8*). The scarce reports of natural infection in dogs reflect their low susceptibility to SARS-CoV-2; for this infection, dogs are asymptomatic, produce limited titers, and have a reduced

Table. Molecular and serologic testing of dog with severe acute respiratory syndrome coronavirus 2 infection, Italy, 2020*

Date of sample collection	Real-time reverse transcription PCR C_t values			Serologic assay results			
	Oral	Nasal	Rectal	ELISA ID.vet†	ELISA In3Diagnostic‡	$PRNT_{80}$§	VNT¶
2020 Nov 4	35.7**	35.7**	ND	ND	ND	ND	ND
2020 Nov 6	ND	37.64	ND	ND	ND	ND	ND
2020 Nov 7	35.61	–	ND	ND	ND	ND	ND
2020 Nov 8	ND	–	40.71	ND	ND	ND	ND
2020 Nov 9	ND	–	36.04	ND	ND	ND	ND
2020 Nov 10	–	–	–	ND	ND	ND	ND
2020 Nov 11	–	–	ND	ND	ND	ND	ND
2020 Nov 12	–	–	ND	ND	ND	ND	ND
2020 Nov 13	–	–	ND	ND	ND	ND	ND
2020 Nov 14	–	–	ND	ND	ND	ND	ND
2020 Nov 15	–	–	ND	ND	ND	ND	ND
2020 Nov 27	ND	ND	ND	–	+ (23%)††	1:80	1:10
2020 Dec 12	ND	ND	ND	–	–	1:80	1:20

*C_t, cycle threshold; ND, not done; $PRNT_{80}$, 80% plaque reduction neutralization test; VNT, virus neutralization test; –, negative; +, positive.
†ID Screen SARS-CoV-2 Double Antigen Multi-species ELISA (ID.vet, https://www.id-vet.com).
‡Eradikit COVID19-Multispecies (In3Diagnostic, http://www.in3diagnostic.com).
§Antibody titer expressed as the highest serum dilution with 80% reduction in plaques in inoculated VERO-E6 cells compared with the control.1:20 was the lowest serum dilution tested.
¶Antibody titer expressed as the highest serum dilution preventing the appearance of cytopathic effect in inoculated VERO-E6 cells. 1:10 was the lowest serum dilution tested.
**Pooled oral and nasal swab specimens.
††Ratio between the optical densities of the tested serum and the positive control (cutoff value = 20%).

Figure. Maximum-likelihood tree comparing 108 strains of severe acute respiratory syndrome coronavirus 2 circulating among humans and canines. Tree shows 107 complete genomes downloaded from the GISAID database (https://www.gisaid.org) and the strains sequenced from an infected dog and family member in Italy (bold red text). The tree was built with IQ-TREE version 1.6.10 (http://www.iqtree.org) using the best fit model indicated by the Model Finder with 1,000 bootstrap replicates. Text at nodes indicates bootstrap values >70. Brackets to the right indicate clades. Scale bar indicates number of nucleotide substitutions per site.

duration of viral shedding (*9*). Upon experimental infection, dogs shed SARS-CoV-2 at lower titers and for a shorter period than cats (*10*). Patterson et al. (*4*) found no actively infected dog or cat in a sampled population of 494 pets, including 67 dogs from households in which family members had COVID-19; however, SARS-CoV-2–specific antibodies were detected in a small proportion of pets (*4*). Delayed sampling of animals, caused by restrictions on human and animal movement during the pandemic, probably contributed to the negative results of molecular testing in that study. The infected poodle we report was monitored after the identification of the index case in the family, enabling the detection of SARS-CoV-2 RNA in swab samples collected during the observational follow-up. Because the canine virus shared 100% nucleotide identity with the virus detected in the index case, we believe human-to-dog transmission of the virus probably occurred in the household.

Acknowledgments

We are grateful to Maria Stella Lucente, Cristiana Catella, Carlo Armenise, and Arturo Gentile for their excellent technical assistance. We thank Marco Crescenzi, Manuela Marra, and Maria Carollo for the Next Generation Sequencing through Ion GeneStudio S5 System.

N.D. was supported by grants of Fondazione CARIPLO—Misura a sostegno dello sviluppo di collaborazioni per l'identificazione di terapie e sistemi di diagnostica, protezione e analisi per contrastare l'emergenza Coronavirus e altre emergenze virali del future, project "Genetic characterization of SARS-CoV2 and serological investigation in humans and pets to define cats and dogs role in the COVID-19 pandemic (COVIDinPET)". A.L was supported by the Italian Ministry of Health Ricerca Corrente 2020 "PanCO: epidemiologia e patogenesi dei coronavirus umani ed animali" and Ricerca Strategica 2020 "Suscettibilità dei mammiferi a SARS-COV-2: rischi di zoonosi inversa e possibilità in medicina traslazionale."

About the Author

Dr. Decaro is professor in the Department of Veterinary Medicine at the University of Bari in Valenzano, Italy. His research interests include the study of viral pathogens of dogs and cats, especially coronaviruses and parvoviruses.

References

1. Lorusso A, Calistri P, Petrini A, Savini G, Decaro N. Novel coronavirus (SARS-CoV-2) epidemic: a veterinary perspective. Vet Ital. 2020;56:5–10. https://doi.org/10.12834/VetIt.2173.11599.1
2. Decaro N, Lorusso A. Novel human coronavirus (SARS-CoV-2): a lesson from animal coronaviruses. Vet Microbiol. 2020;244:108693. https://doi.org/10.1016/j.vetmic.2020.108693
3. Bosco-Lauth AM, Hartwig AE, Porter SM, Gordy PW, Nehring M, Byas AD, et al. Experimental infection of domestic dogs and cats with SARS-CoV-2: pathogenesis, transmission, and response to reexposure in cats. Proc Natl Acad Sci U S A. 2020;117:26382–8. https://doi.org/10.1073/pnas.2013102117
4. Patterson EI, Elia G, Grassi A, Giordano A, Desario C, Medardo M, et al. Evidence of exposure to SARS-CoV-2 in cats and dogs from households in Italy. Nat Commun. 2020;11:6231. https://doi.org/10.1038/s41467-020-20097-0
5. Corman VM, Landt O, Kaiser M, Molenkamp R, Meijer A, Chu DK, et al. Detection of 2019 novel coronavirus (2019-nCoV) by real-time RT-PCR [Erratum in: Euro Surveill. 2020;25: 20200409c] [Erratum in: Euro Surveill. 2020;25:2007303]. Euro Surveill. 2020;25:2000045. https://doi.org/10.2807/1560-7917.ES.2020.25.3.2000045
6. Zhang Q, Zhang H, Gao J, Huang K, Yang Y, Hui X, et al. A serological survey of SARS-CoV-2 in cat in Wuhan. Emerg Microbes Infect. 2020;9:2013–9. https://doi.org/10.1080/22221751.2020.1817796
7. Di Giallonardo F, Duchene S, Puglia I, Curini V, Profeta F, Cammà C, et al. Genomic epidemiology of the first wave of SARS-CoV-2 in Italy. Viruses. 2020;12:1438. https://doi.org/10.3390/v12121438
8. Fritz M, Rosolen B, Krafft E, Becquart P, Elguero E, Vratskikh O, et al. High prevalence of SARS-CoV-2 antibodies in pets from COVID-19+ households. One Health. 2020;11:100192. https://doi.org/10.1016/j.onehlt.2020.100192
9. Sit THC, Brackman CJ, Ip SM, Tam KWS, Law PYT, To EMW, et al. Infection of dogs with SARS-CoV-2. Nature. 2020;586:776–8. https://doi.org/10.1038/s41586-020-2334-5
10. Shi J, Wen Z, Zhong G, Yang H, Wang C, Huang B, et al. Susceptibility of ferrets, cats, dogs, and other domesticated animals to SARS-coronavirus 2. Science. 2020;368:1016–20. https://doi.org/10.1126/science.abb7015

Address for correspondence: Nicola Decaro, Department of Veterinary Medicine, University of Bari, Strada provinciale per Casamassima Km 3, 70010 Valenzano (Bari), Italy; email: nicola.decaro@uniba.it.

Postoperative *Paenibacillus thiaminolyticus* Wound Infection, Switzerland

Riccardo Di Micco, Matthias Schneider, Reto Nüesch

Author affiliations: Spital Schwyz, Schwyz, Switzerland (R. Di Micco, M. Schneider, R. Nüesch); University of Basel, Basel, Switzerland (R. Nüesch)

DOI: https://doi.org/10.3201/eid2707.203348

Paenibacillus thiaminolyticus is a nonvirulent organism found in human and ruminant microbiota. However, *P. thiaminolyticus* can act as an opportunistic pathogen in humans. We describe a case of abdominal wall hematoma secondarily infected by *P. thiaminolyticus*. Our findings emphasize the risk for unusual *Paenibacillus* infections in otherwise healthy persons.

The genus *Paenibacillus* comprises a growing number of species of rod-shaped, motile bacteria with peritrichous flagella (*1*). *Paenibacillus* species share 89.6% similarity of 16S rDNA gene sequences and grow as nonpigmented colonies on tryptic soy agar (*1*). Best known as a nearly ubiquitous environmental bacteria, many *Paenibacillus* species are potential opportunistic pathogens in humans (*2*). We report a case of isolated surgical site infection caused by *P. thiaminolyticus* in an otherwise healthy patient.

A 33-year-old woman came to the emergency department with a fever and reported having a painful and fluctuating abdominal wall mass for 3 days. She had undergone lipoabdominoplasty in a different hospital 7 days earlier. Laboratory tests showed anemia (hemoglobin 88 g/L, hematocrit 0.24 L/L) and isolated C-reactive protein elevation (117 mg/L). Computed tomography of the abdomen demonstrated a fluid collection in the abdominal wall measuring 22 × 9.5 × 5 cm. The patient was admitted for observation. Blood cultures performed at 38.5°C showed no bacterial growth.

Empirical intravenous antimicrobial drug therapy for suspected infected hematoma was initiated with amoxicillin/clavulanate (2.2 g 3×/d), according to local hospital guidelines. Under antimicrobial drug treatment, the patient's fever resolved, but her abdominal pain persisted.

On day 3, we aspirated a sample of the fluid collection in the abdominal wall for microbiological examination. The aspirate was cultured on blood agar incubated at 35°C with 5% CO_2 for 48 h; on MacConkey

agar incubated at 35°C, aerobic, for 24 h; and on selective anaerobic agar at 35°C, anaerobic, for 5 days. All 3 yielded a pure culture of gram variable rod-shaped bacteria. We used Biotyper matrix-assisted laser desorption/ionization time-of-flight (MALDI-TOF) mass spectrometry (Bruker Corporation, https://www.bruker.com) and the Bruker mass spectra database, which returned *P. thiaminolyticus* with a best-match score of 2.07 (a score ≥2 means identification at the species level) (*3*,*4*).

On day 7, the patient had bleeding at the surgical site, and we performed a surgical evacuation with drainage of the fluid collection. We took an intraoperative microbiological swab specimen and ran another MALDI-TOF mass spectrometry analysis, which confirmed the pathogen as *P. thiaminolyticus* with a best match score of 2.17.

After evacuation of the hematoma, the patient rapidly recovered. Because no specific clinical breakpoints have been established for *Paenibacillus* spp., we used nonspecies related clinical breakpoints from the European Committee on Antimicrobial Susceptibility Testing pharmacokinetics and pharmacodynamics (Table). Intravenous antimicrobial drug therapy was continued for a total of 10 days. On day 14, the patient was discharged with oral amoxicillin/clavulanate (1 g 3×/d) for another 2 weeks. We decided to perform a clinical and laboratory follow up at 2, 4, and 8 weeks after discharge. After 2 months, the surgical wound had healed, and the patient was well and without sequelae.

Of the 49 species of *Paenibacillus* known to cause symptomatic infection in humans, the most commonly reported are *P. alvei*, *P. phoenicis*, *P. macerans*, *P. lautus*, *P. timonensis*, *P. provencensis*, and *P. thiaminloyticus* (*2*). Clinical manifestation in patients is heterogeneous, ranging from paucisymptomatic to severe sepsis. The bacteria usually are found in blood with manifest bacteremia (*2*). In this case, *P. thiaminolyticus* was found in the aspirates of the infected abdominal wall hematoma but not in blood cultures or other body compartments.

Because *Paenibacillus* spp. are possible laboratory contaminants (*5*), the organisms should be detected in multiple sets to rule out contamination. The absence of clear, discriminating phenotypical features calls for molecular biology methods to identify the bacterium, such as MALDI-TOF mass spectrometry or, when in doubt, 16S rRNA gene sequencing (*4*).

P. thiaminolyticus is reported as potentially resistant to ampicillin alone (*2*), vancomycin (*2*), and clindamycin (*6*). In this case, the bacterium showed tetracycline resistance. Consequently, antimicrobial susceptibility testing is necessary. According to the antibiograms reported in the literature, empiric therapy with trimethoprim/sulfamethoxazole or amoxicillin/clavulanate is recommended. Although this patient's condition improved with intravenous antimicrobial drug therapy, clinical resolution occurred only after surgical evacuation of the abdominal wall fluid collection. Because of reports of persistent infections (*7*), patients should be monitored after treatment.

P. thiaminolyticus was identified in human feces in 1951 (*8*). Anecdotally, its thiaminase activity can reduce available thiamin necessary for energy metabolism in the central nervous system, causing polioencephalomalacia in ruminants (*9*). So far, no human disease syndrome has been related explicitly to *P. thiaminolyticus*. In 2008, *P. thiaminolyticus* was reported as the causative agent of bacteremia of unknown origin in a dialysis patient with multiple underlying conditions and a long-term catheter (*6*). Since then, 3 other isolates were reported in blood (*2*), vitreous humor (*2*), and cerebrospinal fluid (*10*).

In summary, this case is a reminder of the existence of a rare potential pathogen in our microbiota, although the causality might be discussed because *Paenibacillus* spp. remain mostly environmental bacteria. Therefore, identification relies on MALDI-TOF mass spectrometry or 16S rRNA gene sequencing. Surgical debridement of the infection focus also is recommended. The microorganism shows a variable antimicrobial susceptibility profile, and trimethoprim/sulfamethoxazole and amoxicillin/clavulanate are possible first choice empiric therapies after successful identification.

Table. Comparison of MIC and SS of antimicrobial drugs in blood 4 hours after intravenous administration to treat *Paenibacillus thiaminolyticus* in a patient, Switzerland*

Antimicrobial drug†	MIC	SSC
Amoxicillin/clavulanate	0.064 mg/L	1.2 mg/L
Tetracycline	12 mg/L	2.8 mg/L
Trimethoprim/sulfamethoxazole‡	<0.094 mg/L	1.5–3 mg/L
Clindamycin	0.38 mg/L	23 mg/L
Ciprofloxacin	0.19 mg/L	4.56 mg/L

*No specific clinical breakpoints have been established for *Paenibacillus* spp. We used European Committee on Antimicrobial Susceptibility Testing pharmacokinetics and pharmacodynamics to determine antimicrobial susceptibility. SSC, steady state concentration.
†Antimicrobial drugs were administered at the recommended doses reported in the manufacturer the data sheets (compendium.ch, https://compendium.ch).
‡Trimethoprim/sulfamethoxazole is dose dependent.

Acknowledgments

We thank the patient for permission to share and publish her case. We also thank the clinical microbiology team of Kantonsspital Luzern for their assistance with biotyping.

About the Author

Dr. Di Micco is a general surgery resident at Spital Schwyz, Switzerland. His principal research interests are translational medicine, abdominal surgery, and prevention of surgical wound infections.

References

1. Grady EN, MacDonald J, Liu L, Richman A, Yuan ZC. Current knowledge and perspectives of *Paenibacillus*: a review. Microb Cell Fact. 2016;15:203. https://doi.org/10.1186/s12934-016-0603-7
2. Sáez-Nieto JA, Medina-Pascual MJ, Carrasco G, Garrido N, Fernandez-Torres MA, Villalón P, et al. *Paenibacillus* spp. isolated from human and environmental samples in Spain: detection of 11 new species. New Microbes New Infect. 2017;19:19–27. https://doi.org/10.1016/j.nmni.2017.05.006
3. Saffert RT, Cunningham SA, Ihde SM, Monson Jobe KE, Mandrekar J, Patel R. Comparison of Bruker Biotyper matrix-assisted laser desorption ionization-time of flight mass spectrometer to BD Phoenix automated microbiology system for identification of gram-negative bacilli. J Clin Microbiol. 2011;49:887–92. https://doi.org/10.1128/JCM.01890-10
4. Celandroni F, Salvetti S, Gueye SA, Mazzantini D, Lupetti A, Senesi S, et al. Identification and pathogenic potential of clinical bacillus and *Paenibacillus* isolates. PLoS One. 2016;11:e0152831. https://doi.org/10.1371/journal.pone.0152831
5. Noskin GA, Suriano T, Collins S, Sesler S, Peterson LR. *Paenibacillus macerans* pseudobacteremia resulting from contaminated blood culture bottles in a neonatal intensive care unit. Am J Infect Control. 2001;29:126–9. https://doi.org/10.1067/mic.2001.111535
6. Ouyang J, Pei Z, Lutwick L, Dalal S, Yang L, Cassai N, et al. Case report: *Paenibacillus thiaminolyticus*: a new cause of human infection, inducing bacteremia in a patient on hemodialysis. Ann Clin Lab Sci. 2008;38:393–400.
7. Szaniawski MA, Spivak AM. Recurrent *Paenibacillus* infection. Oxf Med Case Reports. 2019;2019:omz034.
8. Kuno Y. *Bacillus thiaminolyticus*, a new thiamin-decomposing bacterium. Proc Jpn Acad. 1951;27:362–5. https://doi.org/10.2183/pjab1945.27.362
9. Haven TR, Caldwell DR, Jensen R. Role of predominant rumen bacteria in the cause of polioencephalomalacia (cerebrocortical necrosis) in cattle. Am J Vet Res. 1983;44:1451–5.
10. Hehnly C, Zhang L, Paulson JN, Almeida M, von Bredow B, Wijetunge DSS, et al. Complete genome sequences of the human pathogen *Paenibacillus thiaminolyticus* Mbale and type strain *P. thiaminolyticus* NRRL B-4156. Microbiol Resour Announc. 2020;9:e00181-20. https://doi.org/10.1128/MRA.00181-20

Address for correspondence: Reto Nüesch, Department of Internal Medicine, Spital Schwyz, 10 Waldeggstrasse, 6430 Schwyz, Switzerland; email: reto.nueesch@spital-schwyz.ch

Confirmed Cases of Ophidiomycosis in Museum Specimens from as Early as 1945, United States

Jeffrey M. Lorch, Steven J. Price, Julia S. Lankton, Andrea N. Drayer

Author affiliations: US Geological Survey National Wildlife Health Center, Madison, Wisconsin, USA (J.M. Lorch, J.S. Lankton); University of Kentucky, Lexington, Kentucky, USA (S.J. Price, A.N. Drayer)

DOI: https://doi.org/10.3201/eid2707.204864

Ophidiomycosis represents a conservation threat to wild snake populations. The disease was reported in North America early in the 21st century, but the history of ophidiomycosis has not been investigated. We examined museum specimens and confirmed cases of ophidiomycosis >50 years before the disease's reported emergence.

Emerging fungal pathogens of wildlife are recognized as major threats to global biodiversity, causing population declines and extinction events in a variety of host species (*1*). *Ophidiomyces ophidiicola*, the causative agent of ophidiomycosis, is one such pathogen recognized as a conservation threat to wild snakes (*2*). The disease first gained attention in 2008 when fatal infections emerged in eastern massasauga rattlesnakes (*Sistrurus catenatus*) in Illinois, USA (*3*), and has since been documented throughout North America and Europe (*2*,*4*). The earliest retrospective detection of *O. ophidiicola* in snakes was from 2000 (*5*). We report the earliest known confirmed cases of ophidiomycosis in free-living snakes in the United States, dating back to 1945.

We investigated the historical occurrence of ophidiomycosis in snakes in the United States by examining specimens preserved in formalin or ethanol at the University of Wisconsin Zoological Museum (UWZM; Madison, WI, USA) and Morehead State University Museum Collection (Morehead, KY, USA). We visually examined 524 specimens representing 30 snake species from 19 states in the eastern United States collected during 1900–2012 (Appendix 1, https://wwwnc.cdc.gov/EID/article/27/7/20-4864-App1.xlsx). To reduce risk for cross-contamination, we first examined snakes for clinical signs of ophidiomycosis within the glass jars in which they were stored. When specimens were removed from the jars for sampling, new gloves were worn to handle

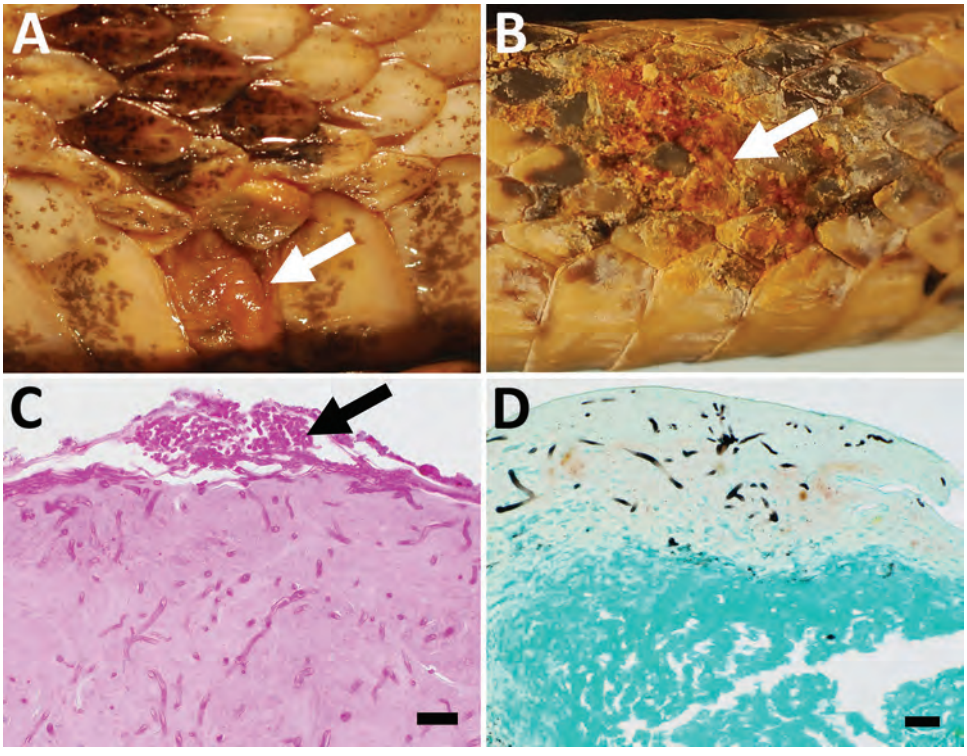

Figure. Gross and histologic lesions in museum snake specimens with confirmed ophidiomycosis, United States. A, B) *Crotalus horridus* (A; University of Wisconsin Zoology Museum [UWZH] accession no. 22773) and *Cemophora coccinea* (B; UWZH accession no. 13822) specimens with thickened necrotic scales (arrows). C, D) Histologic sections of lesioned skin from the same *C. horridus* (C; UWZH accession no. 22773) and *C. coccinea* (D; UWZH accession no. 13822) specimens showing arthroconidia (arrow) and intralesional fungal hyphae consistent with *Ophidiomyces ophidiicola* infection. Scale bars indicate 20 µm.

each snake. We observed clinical signs consistent with ophidiomycosis (Figure) in 47 (9.0%) snakes (*6*). These specimens represented 12 species from 7 states with collection dates ranging from 1929 to 1983 (Appendix 1).

Clinical signs of ophidiomycosis are not pathognomonic, and a confirmed diagnosis requires compatible histopathologic lesions and the detection of *O. ophidiicola* (*6*). Because these confirmatory steps involve destructive sampling of museum material, we selected a subset of snakes (n = 12) for these analyses. We targeted specimens with large (>0.5 cm^2) or multiple skin lesions from distant geographic areas and collected ≥25 years before the reported 2008 emergence of ophidiomycosis (*3*) (Table). From selected snakes, we excised and formalin-fixed portions of lesioned skin, routinely processed them for light microscopy, and stained with periodic acid-Schiff and Grocott methenamine silver methods. We also collected small pieces of lesioned skin (≈4 mm^2) for PCR-based detection of *O. ophidiicola*. We extracted DNA from dehydrated tissue by using the Gentra Puregene Tissue Kit (QIAGEN, https://www.qiagen.com); we used 10 µL of the kit-provided proteinase K per sample.

Table. Museum snake specimens with clinical signs of ophidiomycosis that were subjected to histopathologic examination and PCR specific for *Ophidiomyces ophidiicola*, United States*

Snake species	Museum accession no.	Museum collection	State collected	Date collected	Ophidiomycosis histopathology	PCR result†	Ophidiomycosis diagnosis‡
Crotalus horridus	UWZH 22773	UWZM	WI	1958 Aug	Positive	Positive	Confirmed
C. horridus	UWZH 23927	UWZM	TN	1973 Apr 13	Positive	Negative	Apparent
C. horridus	UWZH 23930	UWZM	TN	1973 Apr 13	Positive	Negative	Apparent
Cemophora coccinea	UWZH 13833	UWZM	FL	1945	Positive	Positive	Confirmed
Lampropeltis triangulum	UWZH 22583	UWZM	WI	1982 Apr 25	Positive	Negative	Apparent
Pantherophis spiloides	UWZH 23931	UWZM	TN	1973 Apr 13	Positive	Positive	Confirmed
Agkistrodon contortrix	582	MSUMC	KY	1979 Oct 29	Equivocal§	Negative	Possible
Coluber constrictor	603	MSUMC	KY	1980 May 6	Positive	Negative	Apparent
C. constrictor	632	MSUMC	KY	1980 May 16	Negative	Negative	Possible
Regina septemvittata	496	MSUMC	KY	1979 May 30	Equivocal	Negative	Possible
R. septemvittata	511	MSUMC	KY	1979 Jun 2	Equivocal	Negative	Possible
R. septemvittata	634	MSUMC	KY	1980 May 18	Equivocal	Negative	Possible

*MSUMC, Morehead State University Museum Collection; *Oo*, *Ophidiomyces ophidiicola*; UWZM, University of Wisconsin Zoology Museum.
†Samples are listed as positive if ≥1 PCR assay targeting the internal transcribed spacer region or mitochondrial NADH dehydrogenase subunit 1 gene was positive. See Appendix 1 (https://wwwnc.cdc.gov/EID/article/27/7/20-4864-App1.xlsx) for assay-specific results.
‡Based on Baker et al. (*6*).
§Equivocal indicates some histologic features consistent with ophidiomycosis were present but ≥1 diagnostic features were not observed (Appendix 1).

Negative controls consisted of blank extractions. For PCR, we used existing primers that specifically target the internal transcribed spacer region (ITS) of *O. ophidiicola* (*6*) and a newly designed PCR assay that targets mitochondrial NADH dehydrogenase subunit 1 (nad1) (Appendix 2, https://wwwnc.cdc.gov/EID/article/27/7/20-4864-App2.pdf). We targeted these 2 loci, which exist at high copy numbers in the genome, because amplifiable DNA was expected to be at low abundance in the preserved specimens. We cloned and sequenced PCR amplicons of the appropriate size to confirm the presence of *O. ophidiicola*. We conducted tissue collection, DNA extraction, and PCR under strict protocols (e.g., unidirectional workflow and regular decontamination of work surfaces and equipment) to prevent contamination of samples.

Of the 12 snakes subjected to histopathological analyses, 7 (58.3%) had microscopic lesions with intralesional fungi consistent with ophidiomycosis (*6*) (Table; Figure). We detected DNA from *O. ophidiicola* in 3 (50%) of the 6 specimens from UWZM that had been stored in 70% ethanol (Table). We did not detect DNA of *O. ophidiicola* in snakes from the Morehead State University Museum Collection (n = 6), likely because these specimens were stored long-term in formalin, which is known to affect the recovery of amplifiable nucleic acid. These results highlight the importance of targeting specimens stored in ethanol rather than formalin for molecular-based detection of pathogens in archival material.

We amplified the ITS target from 2 of the 3 specimens and nad1 target from all 3 specimens; these sequences were 100% identical to existing *O. ophidiicola* sequences in GenBank. The 3 additional specimens from UWZM were strongly suspected to represent cases of ophidiomycosis on the basis of the presence of arthroconidia in histologic sections of lesioned skin (*6*); however, fungal DNA from these specimens may not have been suitable for PCR amplification. Negative controls performed as expected. The 3 PCR-positive specimens met the diagnostic criteria for confirmed cases of ophidiomycosis (*6*); they were collected in Florida in 1945, Wisconsin in 1958, and Tennessee in 1973 (Table). These cases predate the earliest previously known detection of *O. ophidiicola* in free-living snakes in North America by as much as 55 years (*5*).

Museum specimens can provide crucial insights into the history of emerging infectious diseases. Preserved animal specimens have been used to trace the origin and spread of other fungal pathogens, such as *Pseudogymnoascus destructans* (white-nose syndrome in bats) and *Batrachochytrium* spp. (chytridiomycosis in amphibians) (*8*–*10*). By using a similar approach, we demonstrate that ophidiomycosis was circulating in the eastern United States for decades before its recognition as an emerging disease. Future work focusing on how such factors as climate change, environmental disturbance, and underlying health of snake populations influence ophidiomycosis dynamics might reveal the mechanism by which ophidiomycosis is emerging (*2*).

Acknowledgments

We thank the University of Wisconsin Zoological Museum and Morehead State University Museum Collection for allowing us to examine and destructively sample specimens.

This work was funded by the US Geological Survey and McIntire-Stennis Cooperative Forestry Research Program (#1014910).

Data for this study are available at https://doi.org/10.5066/P9FLC1XK.

About the Author

Dr. Lorch is a diagnostic microbiologist and research scientist at the US Geological Survey National Wildlife Health Center, Madison, Wisconsin. His research focuses on emerging infectious diseases of wildlife and the development of molecular tools for use in wildlife disease diagnostics.

References

1. Fisher MC, Henk DA, Briggs CJ, Brownstein JS, Madoff LC, McCraw SL, et al. Emerging fungal threats to animal, plant and ecosystem health. Nature. 2012;484:186–94. https://doi.org/10.1038/nature10947
2. Lorch JM, Knowles S, Lankton JS, Michell K, Edwards JL, Kapfer JM, et al. Snake fungal disease: an emerging threat to wild snakes. Philos Trans R Soc Lond B Biol Sci. 2016;371(1709):20150457.
3. Allender MC, Dreslik M, Wylie S, Phillips C, Wylie DB, Maddox C, et al. *Chrysosporium* sp. infection in eastern massasauga rattlesnakes. Emerg Infect Dis. 2011;17:2383–4. https://doi.org/10.3201/eid1712.110240
4. Franklinos LHV, Lorch JM, Bohuski E, Rodriguez-Ramos Fernandez J, Wright ON, Fitzpatrick L, et al. Emerging fungal pathogen *Ophidiomyces ophiodiicola* in wild European snakes. Sci Rep. 2017;7:3844. https://doi.org/10.1038/s41598-017-03352-1
5. Allender MC, Phillips CA, Baker SJ, Wylie DB, Narotsky A, Dreslik MJ. Hematology in an eastern massasauga (*Sistrurus catenatus*) population and the emergence of *Ophidiomyces* in Illinois, USA. J Wildl Dis. 2016;52:258–69. https://doi.org/10.7589/2015-02-049
6. Baker SJ, Haynes E, Gramhofer M, Stanford K, Bailey S, Christman M, et al. Case definition and diagnostic testing for snake fungal disease. Herpetol Rev. 2019;50:279–85.
7. Bohuski E, Lorch JM, Griffin KM, Blehert DS. TaqMan real-time polymerase chain reaction for detection of *Ophidiomyces*

ophiodiicola, the fungus associated with snake fungal disease. BMC Vet Res. 2015;11:95. https://doi.org/10.1186/s12917-015-0407-8
8. Martel A, Blooi M, Adriaensen C, Van Rooij P, Beukema W, Fisher MC, et al. Wildlife disease. Recent introduction of a chytrid fungus endangers Western Palearctic salamanders. Science. 2014;346:630–1. https://doi.org/10.1126/science.1258268
9. Burrowes PA, De la Riva I. Unraveling the historical prevalence of the invasive chytrid fungus in the Bolivian Andes: implications in recent amphibian declines. Biol Invasions. 2017;19:1781–94. https://doi.org/10.1007/s10530-017-1390-8
10. Campana MG, Kurata NP, Foster JT, Helgen LE, Reeder DM, Fleischer RC, et al. White-Nose Syndrome Fungus in a 1918 bat specimen from France. Emerg Infect Dis. 2017;23:1611–2. https://doi.org/10.3201/eid2309.170875

Address for correspondence: Jeffrey M. Lorch, US Geological Survey National Wildlife Health Center, 6006 Schroeder Rd, Madison, WI 53711, USA; email: jlorch@usgs.gov

Buffalopox Disease in Livestock and Milkers, India

Parimal Roy, Andrew Chandramohan

Author affiliation: Tamil Nadu Veterinary and Animal Sciences University, Chennai, India

DOI: https://doi.org/10.3201/eid2707.202111

Buffalopox outbreaks caused by vaccinia virus were observed in villages of Tamil Nadu, India, among lactating buffaloes and cows. Milkers also had lesions on their fingers. Because vaccinia virus is known to have extended its host range in Brazil, we recommend continuous surveillance to understand cross-species transmission and to curtail disease effects.

In India, sporadic outbreaks of buffalopox, which can be caused by vaccinia virus (VACV), have been reported among cattle and buffaloes (*1*–*3*) and also in humans (*3*). We describe an outbreak affecting 120 lactating buffaloes and 40 lactating cows in Kannivadi, Navapatti, Alathuranpatti, Maniakaranpatti, Muthukumaranpatti, S.Pudur, and E.Chittor, Dindigul district; and in Krishnarayapuram, Karur district, in Tamil Nadu, India in 2004. Pock lesions (0.5–1 cm diameter) were seen over the bodies of lactating buffaloes but restricted to only the udder and teats of lactating cows (Figure, panel A). Buffalopox did not cause death in the animals we reviewed; it affected more buffaloes (30%–50%) than cows (20%–30%). Suckling calves developed pock lesions on the forehead, lips, and mouth. Three milkers who worked with the affected animals experienced multiple pock lesions (1 cm diameter) on the fingers, interdigital webs, wrist and forearm (Figure, panel B) and generalized effects including fever (100°F) and enlargement of axillary lymph nodes.

To investigate the causative agent, we used existing clinical samples. Scab samples were collected randomly from 20 affected animals (both buffaloes and cows). We examined scab suspensions under transmission electron microscope (EM) at 80 KV and inoculated the suspension in BHK21 cell line for virus isolation. We examined scab homogenates and cell culture fluid by PCR for differential diagnosis of cowpox virus and VACV infection (*4*). EM revealed typical brick-shaped pox virus particles of ≈290 × 270 nm with irregularly arranged superficial filaments formed by tubules (Figure, panel C). After 2 blind passages, we noticed in BHK21 cell lines cytopathogenic effects such as cellular rounding, cellular fusion, and intracytoplasmic inclusion bodies (Figure, panel D) after 48–60 hours of infection; PCR analysis revealed the causative agent to be VACV.

During the global eradication of smallpox, strains of VACV were used as vaccine. VACV infection sometimes transmitted from the vasicular lesion of vaccinae to domestic animals, usually cattle; in turn, infected animals transmitted VACV to susceptible humans (*5*). Several outbreaks in cattle and humans that were thought to be cowpox were in fact caused by VACV (*1*,*6*,*7*). The infected animals were treated with parenteral injection of antimicrobial drugs for 1 week to control secondary bacterial infection and an antiinflammatory drug for 3 days to reduce pain and inflammation. Animal workers were also advised to clean the animals' lesions with 1% potassium permanganate solution followed by tropical application over the pock lesions with indigenous product of neem leaf extract and turmeric powder suspended in glycerin. Individual animals recovered in ≈1 month. Similarly affected humans were diagnosed at primary healthcare centers and treated with oral antimicrobial drugs and analgesics for 1 week, which reduced pain and pustules. Healing was complete in 3 weeks' time.

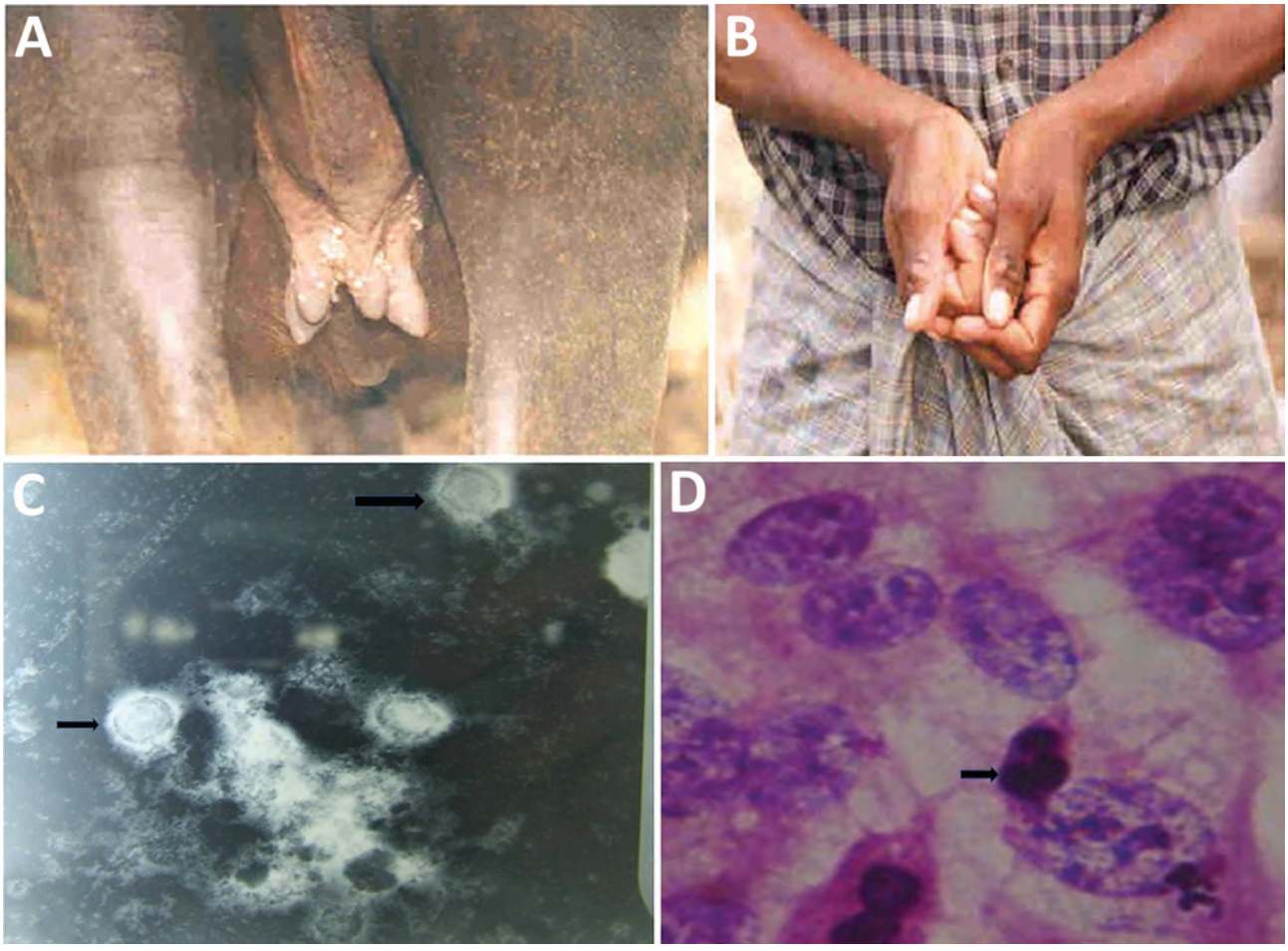

Figure. Buffalopox outbreak caused by vaccinia virus, Tamil Nadu, India. A) Buffalopox lesions on the udder and teats and over the body of a buffalo. B) Suspected buffalopox in a milker; lesions are visible on the fingers and forearms. C) Electron micrograph of vaccinia virus (arrows; magnification ×20,000). D) Hematoxylin and eosin stain (magnification ×1,000) shows cellular rounding and cell fusion and intracytoplasmic inclusion bodies (arrow). PCR revealed vaccinia virus infection.

The outbreaks resulted in financial loss to the farmers because of mastitis and loss of milk production. The outbreaks also created public health concern because of human infection. The source of infection could not be identified; it is possible that VACV could be lurking in rodents, as reported earlier (*8*), and causing sporadic outbreaks. More recently, Lima et al. reported that host range of VACV in Brazil has extended over the period 1960–2018; VACV has been detected in rodents, primates, and several species of domesticated animals as well as humans (*9*). Thus, continuous surveillance and the study of genetic diversity of VACV and its pathogenic attributes will be helpful to understand its founder effects and host diversity. Awareness among the stakeholders and steps taken for biosecurity will reduce the transmission of disease in animals and humans.

Acknowledgments

We thank Central Referral Laboratory, Chennai, and S. Marimuthu (DAH) and the late S. Poneerselvam for providing clinical samples and information. We thank the director of the Centre for Animal Health Studies, Tamil Nadu Veterinary and Animal Sciences University for providing necessary facilities.

About the Author

Dr. Roy is a professor in Central University Laboratory, Tamil Nadu Veterinary and Animal Sciences University, Chennai, India. His research interests are livestock and poultry disease epidemiology and zoonoses.

References

1. Dumbell K, Richardson M. Virological investigations of specimens from buffaloes affected by buffalopox in Maharashtra State, India, between 1985 and 1987. Arch Virol. 1993;128:257–67. https://doi.org/10.1007/BF01309438

2. Singh RK, Hosamani M, Balamurugan V, Satheesh CC, Shingal KR, Tatwarti SB, et al. An outbreak of buffalopox in buffalo (*Bubalus bubalis*) dairy herds in Aurangabad, India. Rev Sci Tech. 2006;25:981–7. https://doi.org/10.20506/rst.25.3.1708
3. Gurav YK, Raut CG, Yadav PD, Tandale BV, Sivaram A, Pore MD, et al. Buffalopox outbreak in humans and animals in Western Maharashtra, India. Prev Vet Med. 2011;100:242–7. https://doi.org/10.1016/j.prevetmed.2011.03.008
4. Ropp SL, Jin Q, Knight JC, Massung RF, Esposito JJ. PCR strategy for identification and differentiation of small pox and other orthopoxviruses. J Clin Microbiol. 1995;33:2069–76. https://doi.org/10.1128/JCM.33.8.2069-2076.1995
5. Fenner F, Henderson DA, Arita , Jezek Z, Ladnyi ID. Smallpox and its eradication. Geneva: World Health Organization; 1988.
6. Lum GS, Soriano F, Trejos A, Llerena J. Vaccinia epidemic and epizootic in El Salvador. Am J Trop Med Hyg. 1967;16:332–8. https://doi.org/10.4269/ajtmh.1967.16.332
7. Topciu V, Luca I, Moldovan E, Stoianovici V, Plavoşin L, Milin D, et al. Transmission of vaccinia virus from vaccinated milkers to cattle. Virologie. 1976;27:279–82.
8. De Souza Lopes S, Lacerda JPG, Fonseca IEM, Castro DP, Forattini OP, Rabello EX. Cotia virus: a new agent isolated from sentinel mice in São Paulo, Brazil. Am J Trop Med Hyg. 1965;14:156–7. https://doi.org/10.4269/ajtmh.1965.14.156
9. Lima MT, Oliveira GP, Afonso JAB, Souto RJC, de Mendonça CL, Dantas AFM, et al. An update on the known host range of the Brazilian vaccinia virus: an outbreak in buffalo calves. Front Microbiol. 2019;9:3327. https://doi.org/10.3389/fmicb.2018.03327

Address for correspondence: Parimal Roy, Tamil Nadu Veterinary and Animal Sciences University, Chennai, Tamil Nadu, India; email: parimalroy580@gmail.com

Anthemosoma garnhami in an HIV-Infected Man from Zimbabwe Living in South Africa

David Stead, Desiree du Plessis, Lisa Ming Sun, John Frean

Author affiliations: Walter Sisulu University, Mthatha, South Africa (D.F. Stead); Cecilia Makiwane Hospital, East London, South Africa (D.F. Stead); National Institute for Communicable Diseases, Johannesburg, South Africa (D. du Plessis, L. Ming Sun, J. Frean); University of the Witwatersrand, Johannesburg (J. Frean)

DOI: https://doi.org/10.3201/eid2707.204759

An HIV-positive man from Zimbabwe living in South Africa sought treatment for multiple clinical signs, including fever, weight loss, anemia, and splenomegaly. We identified in his blood an African rodent piroplasm, *Anthemosoma garnhami*, related to *Babesia* species. This finding extends the known geographic and host range of *A. garnhami*.

A 24-year-old man from Zimbabwe who had been living in East London, South Africa, for 13 years attended a primary health care clinic in East London complaining of a 3-month period of generalized body pains, drenching night sweats, and weight loss. He had no notable previous medical history. The attending nurse diagnosed HIV infection by rapid test, collected sputum for an Xpert MTB/RIF test (Cepheid, https://www.cepheid.com), and requested blood screening as preparation before initiating combination antiretroviral therapy. Malaria-like objects found on the blood smear prompted referral for specialist opinion at Cecilia Makiwane Hospital in Mdantsane, South Africa. This case report was approved by the Human Research Committee of the Faculty of Health Sciences, Walter Sisulu University, Mthatha, South Africa (protocol no. 126/2020). The patient granted written informed consent for publication of the case report.

The patient shared a house with another adult (no animals) and worked as a construction laborer. Four months before seeking treatment, he returned from a 2-month home visit to Masvingo Province in Zimbabwe. He did not recall tick bites but reported that goats and cattle lived in the village he visited.

At hospital admission, the patient was wasted (40 kg), generally weak, afebrile, and markedly pale; he had oral candidiasis. His enlarged, smooth, nontender spleen was palpable to ≈10 cm below the costal margin in the midclavicular line. No other findings were remarkable. Laboratory results (Table) showed evidence of likely hypersplenism-related pancytopenia, hemolysis, mildly raised transaminases, and advanced HIV infection. The abnormal blood smear showed intraerythrocytic parasites, initially thought to be malarial. However, concurrent rapid malaria antigen tests were negative, and the smears and whole blood sample were sent to a national parasitology reference laboratory for further assessment. On the basis of microscopic examination of Giemsa-stained blood smears (Figure), we diagnosed babesiosis accompanied by hemolytic anemia.

We started the patient on a 10-day course of oral clindamycin and quinine (each 600 mg every 8 h). Blood transfusion was not needed. After 2 weeks, all

Table. Laboratory findings over time for an HIV-positive patient from Zimbabwe living in South Africa who was infected with the rodent piroplasm *Anthemosoma garnhami*

Laboratory test	Dates					Reference values
	2019 May 31	2019 Jun 7*	2019 Jun 20	2020 Aug 31†	2020 Nov 11	
Hemoglobin, g/L	45	40	92	59	96	132–173
Mean cell volume, × 10^{15}/L	82	73	84	81	84	80–99
Leukocyte count, × 10^9/L	0.34	2.4	3.6	2.2	3.8	4–11
Platelet count, × 10^9/L	123	140	184	56	103	137–373
Reticulocytes, %		5.6				0.5–1.5
Creatinine, mg/dL		0.79				0.5–1.5
Total bilirubin, mg/dL		0.41				0.3–1.0
Aspartate transaminase, U/L		111				10–30
Alanine transaminase, U/L	19	47				10–40
Lactate dehydrogenase, U/L		922				100–200
Haptoglobin, g/L		<0.1				0.3–2.0
CD4, cells/mm^3	70			195		500–1,200
HIV ELISA	Positive					
Sputum Xpert MTB/RIF‡	Negative					

*Date of treatment initiation.
†Date of recrudescence and retreatment initiation.
‡*Mycobacterium tuberculosis* and rifampin resistance testing (Cepheid, https://www.cepheid.com).

symptoms improved markedly; splenomegaly was reduced to 5 cm below the costal margin and hemoglobin substantially improved. We subsequently initiated tenofovir, emtricitabine/efavirenz combination antiretroviral therapy, and trimethoprim/sulfamethoxazole prophylaxis; the patient responded well in the hospital antiretroviral unit.

DNA extracted from anticoagulated whole blood tested negative for *Plasmodium* spp. by multiplex real-time PCR for malaria. We used a nested conventional PCR assay for the *Babesia* species 18S RNA gene (*1*) and applied bidirectional Sanger sequencing to the 400-bp product, showing sequences shared across members of order Piroplasmida. We used PCR with 18S RNA universal primers to refine this result. (*2*). The ≈1,700 bp product sequence (GenBank accession no. MW276138) had 99.15% identity and a subsequent sequence (accession no. MW276139) from a recrudescence, 99.03% identity with the murine piroplasm *Anthemosoma garnhami* (accession no. MH093637.1; Appendix Figure, https://wwwnc.cdc.gov/EID/article/27/7/20-4759-App1.pdf).

The patient returned for treatment 14 months later. He had not traveled outside of South Africa since his initial treatment. He was again pale and had an enlarged spleen. His hemoglobin was 59 g/L, and we again observed intraerythrocytic piroplasms on the blood smear. His CD4 count was now 195 cells/mm^3

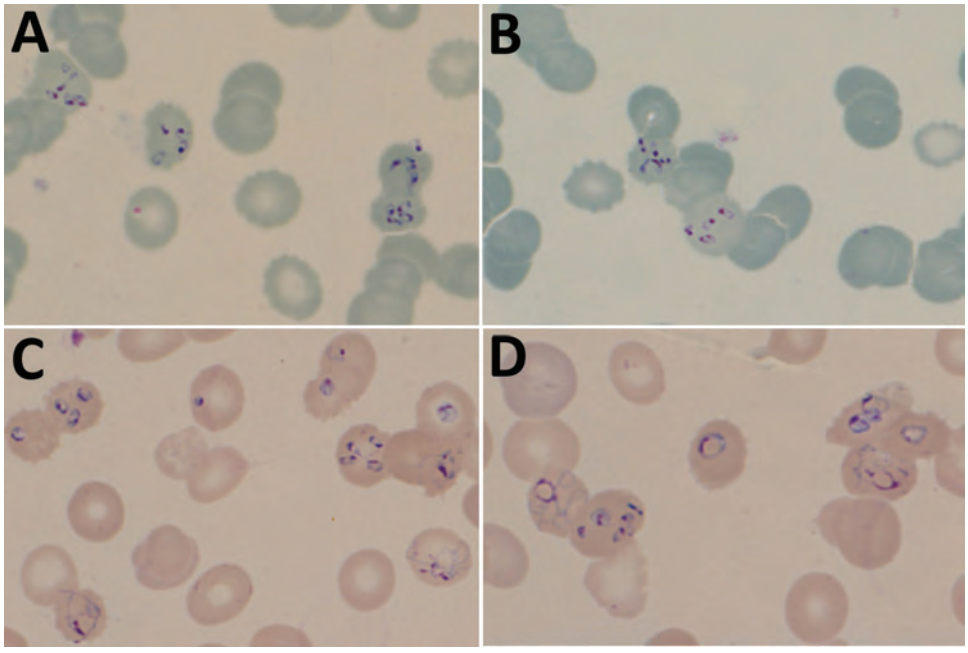

Figure. Thin blood film photographs showing *Babesia*-like early tetrads (panels A, B) and pleiomorphic later-stage parasites (panels C, D) in an HIV-positive patient from Zimbabwe living in South Africa. The multiply infected erythrocytes and unusual morphology suggested nonmalaria parasites and were later determined to be the rodent piroplasm *Anthemosoma garnhami*, related to *Babesia* spp. Slides stained with 10% Giemsa, pH 7.2, for 20 min; original magnification ×1,000.

and HIV viral load 304 copies/mL. He was admitted for intravenous clindamycin and oral quinine (each 600 mg every 8 h) as part of a 6-week treatment plan. The patient responded well clinically and hematologically to treatment (Table).

A. garnhami is an erythrocytic murine parasite, first described in spiny mice (*Acomys percivali*) in Ethiopia in 1969 (*3*). Because it shares characteristics with Haemosporidia and Piroplasmida, its classification was long debated, but on the basis of ribosomal RNA analysis of archived *A. garnhami* samples, it was finally assigned to the piroplasms, as the sole species of the family Anthemosomatidae (*3*). The parasite was identified again in 2 different rodent species in Namibia (*4*,*5*). Ixodid ticks serve as vectors of piroplasms and therefore are likely vectors for *A. garnhami*; experiments failed to demonstrate transmission by several tick and mosquito species (*3*). *A. garnhami* is closely related to the babesids in the Piroplasmida order, hence the similar microscopic appearance and the good clinical response in this case to clindamycin and quinine, drugs used to treat *Babesia* spp. Babesiosis in immunocompromised patients, including those with HIV, is more severe and more likely to recur (*6*). The recrudescing clinical course of this *A. garnhami* infection was probably exacerbated by the patient's advanced HIV disease.

Our report establishes a likely epizootologic similarity between *A. garnhami* and *Babesia* spp., suggesting the potential for *A. garnhami* to cause zoonotic infections in humans. Although babesiosis in domestic animals is common in Africa and *B. microti* has been found in nonhuman primates in East Africa (*7*), only single reports from southern Africa (*8*) and Equatorial Guinea (*9*) have described human *Babesia* spp. infections. The conjunction of high concentrations of ticks, animals, malaria, and HIV-infected humans in Africa make it possible for piroplasm infections to be misdiagnosed as malaria, which poses potentially serious clinical consequences for immunocompromised patients.

Acknowledgments

We are grateful to Michelle Bosman for the initial laboratory investigations and to Marinda Oosthuizen, Ilse Vorster, and Milana Troski for the gift of *Babesia* spp. DNA extracts.

About the Author

Dr. Stead is the head of the Division of Infectious Diseases in the Departments of Medicine at Frere and Cecilia Makiwane hospitals and senior lecturer in the Department of Medicine at the Walter Sisulu University Health Sciences Faculty. His primary research interests are tuberculosis diagnostics, HIV-related opportunistic infections, and severe acute respiratory syndrome coronavirus 2 healthcare worker infections.

References

1. Wei Q, Tsuji M, Zamoto A, Kohsaki M, Matsui T, Shiota T, et al. Human babesiosis in Japan: isolation of *Babesia microti*-like parasites from an asymptomatic transfusion donor and from a rodent from an area where babesiosis is endemic. J Clin Microbiol. 2001;39:2178–83. https://doi.org/10.1128/JCM.39.6.2178-2183.2001
2. Medlin L, Elwood HJ, Stickel S, Sogin ML. The characterization of enzymatically amplified eukaryotic 16S-like rRNA-coding regions. Gene. 1988;71:491–9. https://doi.org/10.1016/0378-1119(88)90066-2
3. Chavatte JM, Karadjian G, Landau I. Half a century after its discovery, new insights on *Anthemosoma garnhami* (Sporozoa, Piroplasmida): morphology, molecular characterisation and phylogenetic position. Parasitol Res. 2018;117:3917–25. https://doi.org/10.1007/s00436-018-6101-6
4. Gunders AE. *Anthemosoma* sp. isolated from *Aethomys namaquensis* in Namibia [conference abstract]. S Afr J Sci. 1985;81:48.
5. Gunders AE. *Anthemosoma* sp. from *Thallomys paedulcus* (Sundevall, 1847) from Namibia—a new host record [conference abstract]. S Afr J Sci. 1986;82:652.
6. Vannier E, Krause PJ. Human babesiosis. N Engl J Med. 2012;366:2397–407. https://doi.org/10.1056/NEJMra1202018
7. Maamun JM, Suleman MA, Akinyi M, Ozwara H, Kariuki T, Carlsson HE. Prevalence of *Babesia microti* in free-ranging baboons and African green monkeys. J Parasitol. 2011;97:63–7. https://doi.org/10.1645/GE-2391.1
8. Bush JB, Isaäcson M, Mohamed AS, Potgieter FT, de Waal DT. Human babesiosis—a preliminary report of 2 suspected cases in South Africa. S Afr Med J. 1990;78:699.
9. Arsuaga M, González LM, Padial ES, Dinkessa AW, Sevilla E, Trigo E, et al. Misdiagnosis of babesiosis as malaria, Equatorial Guinea, 2014. Emerg Infect Dis. 2018;24:1588–9. https://doi.org/10.3201/eid2408.180180

Address for correspondence: John Frean, National Institute for Communicable Diseases, Parasitology Reference Laboratory, P/Bag X4, Sandringham, Johannesburg 2131, South Africa; email: johnf@nicd.ac.za

Natural SARS-CoV-2 Infection in Kept Ferrets, Spain

Christian Gortázar, Sandra Barroso-Arévalo, Elisa Ferreras-Colino, Julio Isla, Gabriela de la Fuente, Belén Rivera, Lucas Domínguez, José de la Fuente, José M. Sánchez-Vizcaíno

Author affiliations: Instituto de Investigación en Recursos Cinegéticos, Consejo Superior de Investigaciones Científicas, Universidad de Castilla–La Mancha, Ciudad Real, Spain (C. Gortázar, E. Ferreras-Colino, J. de la Fuente); Universidad Complutense de Madrid, Madrid, Spain (S. Barroso-Arévalo, B. Rivera, L. Domínguez, J.M. Sánchez-Vizcaíno); Sabiotec, Ciudad Real (J. Isla, G. de la Fuente); Oklahoma State University, Stillwater, Oklahoma, USA (J. de la Fuente)

DOI: https://doi.org/10.3201/eid2707.210096

We found severe acute respiratory syndrome coronavirus 2 RNA in 6 (8.4%) of 71 ferrets in central Spain and isolated and sequenced virus from 1 oral and 1 rectal swab specimen. Natural infection occurs in kept ferrets when virus circulation among humans is high. However, small ferret collections probably cannot maintain virus circulation.

Natural infection of animals with severe acute respiratory syndrome coronavirus 2 (SARS-CoV-2) has been reported in pet cats and dogs, zoo felids and apes, and mustelids belonging to the subfamily Mustelinae (*1*). Among mustelids, natural SARS-CoV-2 infections have been recorded in farmed American mink (*Neovison vison*) and sporadically in wild mink (https://promedmail.org/promed-post/?id=8015608) and in a kept pet ferret (*Mustela putorius furo*) from an infected household in Slovenia (https://english.sta.si/2838759/first-case-of-coronavirus-positive-pet-confirmed-in-slovenia). Ferrets are common laboratory models, and experimental infections have evidenced their susceptibility to and ability to transmit the virus to other ferrets. SARS-CoV-2 is shed for up to 8 days postinfection (dpi) in nasal washes, saliva, urine, and feces and is effectively transmitted to naive ferrets by direct contact and through the air (*2*,*3*). Experimentally infected ferrets display either no clinical signs or exhibit elevated body temperature and loss of appetite (*2*,*4*).

Ferrets are common pets (https://www.avma.org/resources-tools/reports-statistics/us-pet-ownership-statistics) and are also used as work animals for rabbit control. However, whether SARS-CoV-2 circulates among kept ferret populations and whether ferrets could contribute to virus maintenance remains unknown.

We studied 71 ferrets belonging to 7 owners; the ferrets were used as working animals for rabbit hunting in Ciudad Real Province, central Spain. All 71 ferrets were included in the study, and none showed clinical signs of any illness. Group sizes ranged from 4 to 21 (mean 10). Twenty ferrets belonging to groups 1 and 2 were resampled 66 days after initial sampling. Information on coronavirus disease in the owners was not available. Sampling took place during August–November 2020. Animal sampling procedures were approved by the Madrid Animal Research Ethics Committee (approval no. CM14/2020). We collected 1 oropharyngeal and 1 rectal swab specimen (DeltaSwab Virus 3 mL; Deltalab, https://www.deltalab.es) from each ferret for RNA extraction.

We detected SARS-CoV-2–specific RNA by using a quantitative reverse transcription PCR assay (qRT-PCR). In brief, we extracted RNA by using the KingFisher Flex System (ThermoFisher, https://www.thermofisher.com). We conducted SARS-CoV-2 RNA detection by using the envelope protein–encoding gene and 2 targets (IP2 and IP4) of the RNA-dependent RNA polymerase gene (*RdRp*) (Appendix Table, https://wwwnc.cdc.gov/EID/article/27/7/21-0096-App1.pdf).

Specimens considered positive by qRT-PCR were subjected to virus isolation in Vero E6 cells. We cultured cells in RPMI-1640 Medium (Sigma Aldrich, https://www.sigmaaldrich.com) supplemented with Gibco 10% fetal bovine serum (ThermoFisher), 100 IU/mL penicillin, and 100 μg/mL streptomycin. We cultured cells in 96-well plates at 37°C with 5% CO_2 for 24–48 h. We then inoculated cells with 10 μL of the oronasal or fecal swab samples. We used mock-inoculated cells as negative controls. We maintained cultured cells with daily observation of virus-induced cytopathic effect and cellular death. After 6 days, cell cultures were frozen, thawed, and subjected to 3

Table. Kept ferrets testing qRT-PCR–positive for SARS-CoV-2, by sample type, Spain*

Animal ID	Sample type	Lowest C_t value†
Ferret 1 G1-H6	Rectal swab	34.5
Ferret 2 G1-H17	Nasal swab	37.29
Ferret 3 G2-H5	Nasal swab	35.38
Ferret 4 G5-H11	Nasal swab	39.83
Ferret 5 G7-H7	Nasal swab	30.59
Ferret 6 G7-H9	Nasal swab	38.91

*C_t, cycle threshold; qRT-PCR, quantitative reverse-transcription PCR; SARS-CoV-2, severe acute respiratory syndrome coronavirus 2.
†A C_t cutoff of 40 was used. A result was considered positive for SARS-CoV-2 when the sample showed a positive qRT-PCR result for ≥2 of the 3 analyzed targets.

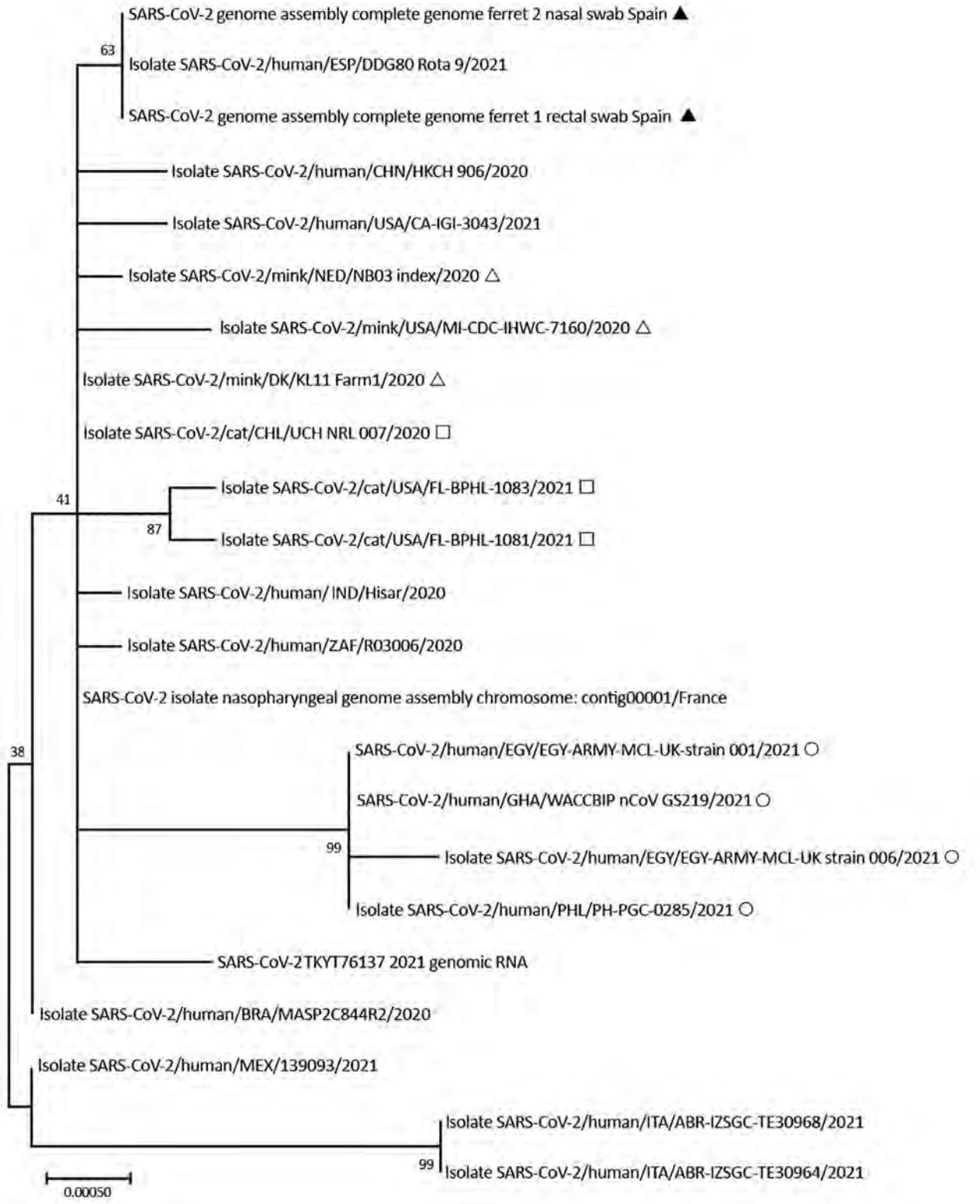

Figure. Phylogenetic analysis of SARS-CoV-2 indicating that spike sequences from kept ferrets were similar and clustered with a SARS-CoV-2 genome from Spain that was included in the alignment. Black triangle indicates ferret, open triangle indicates mink; open square indicates cat; open circle indicates human (B1.1.7). Scale bar indicates number of substitutions per site. BRA, Brazil; CHL, Chile; CHN, China; DK, Denmark; EGY, Egypt; ESP, Spain; GHA, Ghana; IND, India; ITA, Italy; MEX, Mexico; NED, Netherlands; PHL, Philippines; SARS-CoV-2, severe acute respiratory syndrome coronavirus 2;TKY, Turkey; UK, United Kingdom; USA, United States; ZAF, South Africa.

passages with inoculation of fresh Vero E6 cells with the lysates described. We performed SARS-CoV-2 molecular detection by using qRT-PCR on the supernatants from every passage to confirm presence or absence of the virus in the cell culture.

We obtained sequences from 2 positive samples with 38 primer sets (*5*) and performed sequence analysis by using the Sequencing Analysis 5.3.1 (ThermoFisher), and we used SeqScape 2.5 (ThermoFisher) for sequence assembly, using the SARS-CoV-2 isolate Wuhan-Hu-1 complete genome (GenBank accession no. NC_045512) as reference. We performed phylogenetic analysis by using MEGA X (*6*). We used MUSCLE (*7*) to align spike proteins from the sequences with published sequences.

We found SARS-CoV-2 RNA in swab samples from 6 (8.4%) of the 71 ferrets (Table), belonging to 4 of the 7 groups of ferrets investigated. The likelihood of a swab specimen testing positive was unrelated with age group (<1 vs. ≥1 year old), sex, and site of sample collection (oral vs. rectal) ($p>0.2$ by Fisher 2-tailed exact test). We confirmed qRT-PCR results by sequencing the positive PCR product. None of the 20 resampled ferrets was PCR-positive, including 1 ferret that had tested positive 2 months earlier by oropharyngeal swab specimen (cycle threshold 35.38).

We isolated SARS-CoV-2 from the rectal swab specimen of ferret 1 (GenBank accession no. SUB9578702-MZ082987) and the nasal swab specimen of ferret 2 (accession no. SUB9585789-MZ099821) (Table). Phylogenetic analysis showed that spike sequences from ferrets were similar and clustered with a genome from Spain that was included in the alignment (Figure). Ferret sequences had no mutations identified in variants of concern, such as deletions (69–70del and 145del) or mutations (N501Y, A570D, and D614G).

We conclude that natural SARS-CoV-2 infection in kept ferrets does occur in circumstances of high viral circulation in the human population (*8*). However, the high cycle thresholds observed and the lack of virus-positive ferrets at resampling suggest that small ferret populations are less able to maintain prolonged virus circulation than large, farmed mink populations (*9*,*10*). Specific guidance on SARS-CoV-2 in ferrets has been made available in the United Kingdom (http://apha.defra.gov.uk/documents/guidance-sars-cov-2-ferrets.pdf) and the United States (https://www.cdc.gov/coronavirus/2019-ncov/animals/pet-store.html).

This article was preprinted at https://doi.org/10.1101/2021.01.14.426652.

This study received funding from the Instituto de Salud Carlos III (grant no. COV20/01385). E.F.C. was supported by a grant from Universidad de Castilla–La Mancha, Spain.

About the Author

Prof. Gortázar heads the SaBio research group at the Spanish Wildlife Research Institute (Instituto de Investigación en Recursos Cinegéticos). His research interests include the epidemiology and control of infections shared between wildlife, livestock, and human beings.

References

1. Delahay RJ, de la Fuente J, Smith GC, Sharun K, Snary EL, Flores Girón L, et al. Assessing the risks of SARS-CoV-2 in wildlife. One Health Outlook. 2021;3:7. https://doi.org/10.1186/s42522-021-00039-6
2. Kim Y-I, Kim S-G, Kim S-M, Kim E-H, Park S-J, Yu K-M, et al. Infection and rapid transmission of SARS-CoV-2 in ferrets. Cell Host Microbe. 2020;27:704–709.e2. https://doi.org/10.1016/j.chom.2020.03.023
3. Richard M, Kok A, de Meulder D, Bestebroer TM, Lamers MM, Okba NMA, et al. SARS-CoV-2 is transmitted via contact and via the air between ferrets. Nat Commun. 2020;11:3496. https://doi.org/10.1038/s41467-020-17367-2
4. Shi J, Wen Z, Zhong G, Yang H, Wang C, Huang B, et al. Susceptibility of ferrets, cats, dogs, and other domesticated animals to SARS-coronavirus 2. Science. 2020;368:1016–20. https://doi.org/10.1126/science.abb7015
5. Tamura K. Estimation of the number of nucleotide substitutions when there are strong transition-transversion and G+C-content biases. Mol Biol Evol. 1992;9:678–87.
6. Kumar S, Stecher G, Li M, Knyaz C, Tamura K. MEGA X: Molecular Evolutionary Genetics Analysis across computing platforms. Mol Biol Evol. 2018;35:1547–9. https://doi.org/10.1093/molbev/msy096
7. Thompson JD, Plewniak F, Poch O. A comprehensive comparison of multiple sequence alignment programs. Nucleic Acids Res. 1999;27:2682–90. https://doi.org/10.1093/nar/27.13.2682
8. Fernández-de-Mera IG, Rodríguez Del-Río FJ, de la Fuente J, Pérez-Sancho M, Hervás D, Moreno I, et al. Detection of environmental SARS-CoV-2 RNA in a high prevalence setting in Spain. Transbound Emerg Dis. 2021;68:1487–92. https://doi.org/10.1111/tbed.13817
9. Koopmans M. SARS-CoV-2 and the human-animal interface: outbreaks on mink farms. Lancet Infect Dis. 2021;21:18–9. https://doi.org/10.1016/S1473-3099(20)30912-9
10. European Food Safety Authority and European Centre for Disease Prevention and Control, Boklund A, Gortazar C, Pasquali P, Roberts H, Nielsen SS, et al. Scientific opinion on the monitoring of SARS-CoV-2 infection in mustelids. EFSA J. 2021;19:e06459.

Address for correspondence: Christian Gortázar, SaBio research group at IREC (Instituto de Investigación en Recursos Cinegéticos) (CSIC-UCLM), Ronda de Toledo 12, 13003 Ciudad Real, Spain; email: christian.gortazar@uclm.es

Occupational Exposure to Zoonotic Tuberculosis Caused by *Mycobacterium caprae*, Northern Greece, 2019

Dimitrios Papaventsis, George Dougas, Ourania Kalkouni, Simona Karabela, Katerina Manika

Author affiliations: Sotiria Chest Diseases Hospital, Athens, Greece (D. Papaventsis, S. Karabela); National Public Health Organization, Athens (G. Dougas, O. Kalkouni); G. Papanikolaou Hospital, Thessaloniki, Greece (K. Manika)

DOI: https://doi.org/10.3201/eid2707.204399

Pulmonary tuberculosis caused by *Mycobacterium caprae* was diagnosed in a 65-year-old goat breeder from northern Greece. This case represents a documented occupational transmission of *M. caprae* and highlights the importance of enhanced laboratory screening and increased surveillance for zoonotic tuberculosis control.

Mycobacterium caprae, a member of *Mycobacterium tuberculosis* complex (MTBC), causes caprine tuberculosis (TB) (*1*). *M. caprae* has been isolated mainly in continental Europe and infects animals and humans (*2*–*4*). Although clinically indistinguishable from *M. tuberculosis* or *M. bovis*, *M. caprae* causes nearly one third of *M. bovis*–associated TB cases (*5*). Bovine TB control and pasteurization have made zoonotic TB rare; however, occupational risk exists for livestock farmers, veterinarians, slaughterhouse workers, butchers, and other persons working in close contact with livestock.

In August 2019, a 65-year-old male goat breeder from northern Greece was admitted to the Aristotle University Pulmonology Department at G. Papanikolaou Hospital (Thessaloniki, Greece) for weight loss, productive cough, and fever <38.5°C that was not responding to a 10-day regimen of cefuroxime. He was a frequent smoker, reported chronic alcohol abuse, and had no other medical history. He reported living in the goat shelter, occasionally consuming unpasteurized milk, and having no contact with or hunting practices involving other animal species. Laboratory tests showed normocytic anemia (hemoglobin 10.4 g/dL) and an erythrocyte sedimentation rate of 112 mm/h. Chest radiograph and computed tomography scans revealed upper lobe cavities and infiltrations, predominantly on the left side (Figure, panels A–C). A tuberculin skin test result was 12 mm in size. TB was suspected; sputum samples were sent for molecular and bacteriologic testing to the National Reference Laboratory for Mycobacteria at Sotiria Chest Diseases Hospital (Athens, Greece). Acid-fast stain results were positive and MTBC detected by using TRCReady-80 (Tosoh Corp., https://www.tosoh.com). We determined drug sensitivity on a strain grown on sodium pyruvate-LJ medium by Genotype MTBDRplus (Hain LifeScience, https://www.hain-lifescience.de) and on solid media. We documented sensitivity to first-line anti-TB drugs and pyrazinamide. Because of the patient's occupation, laboratory investigation included zoonotic species. GenoType MTBC differentiated the isolate as *M. bovis* subspecies *caprae*.

We used the optimized 24-loci Genoscreen MIRU-VNTR (mycobacterial interspersed repetitive unit–variable-number tandem-repeat) Typing Kit (Genoscreen, https://www.genoscreen.fr) on crude DNA, using 6 quadruplex PCR and fluorescent primers with capillary electrophoresis. Identification was performed with the MIRU-VNTR*plus* database (*6*). Because no match was detected after initial best-match analysis, we used a tree-based identification scheme by applying the UPGMA method and using the database reference strains. Identification was confirmed with a unique MIRU-VNTR pattern (M.caprae_Kilkis:255326322553434243231432) showing close phylogenetic match with *M. caprae* reference strains from central and eastern Europe and clear genetic distance from the Iberian cluster, mainly characterized by absence of spoligotype spacers 30–33 (*3*) (Appendix Figure, https://wwwnc.cdc.gov/EID/article/27/7/20-4399-App1.pdf).

The patient received a standard anti-TB regimen for 9 months and responded favorably. Cultures and acid-fast bacilli turned negative 10 days after treatment and were negative 2.5 months after treatment. Erythrocyte sedimentation rate dropped to 25 mm/h, and the patient gained 17 kg. Chest radiograph and computed tomography scans showed remarkable improvement (Figure, panels D–F). Contact tracing did not reveal further human cases. Veterinary investigation identified no tuberculin skin test reactors among >300 goats of the epidemiologically linked herd.

Zoonotic TB causes an estimated 147,000 new human cases and 12,500 deaths annually worldwide (*7*). Zoonotic TB is a reemerging and underrecognized infection in Europe; 170 confirmed human cases were reported in 2018 (0.05 cases/100,000 population) (*4*). Among countries not officially TB-free, Greece, Ireland, and Spain reported a plateaued prevalence of 2%–5% in cattle herds over the past decade (*4*). The actual global burden of *M. caprae* disease is further underestimated because of differences in laboratory

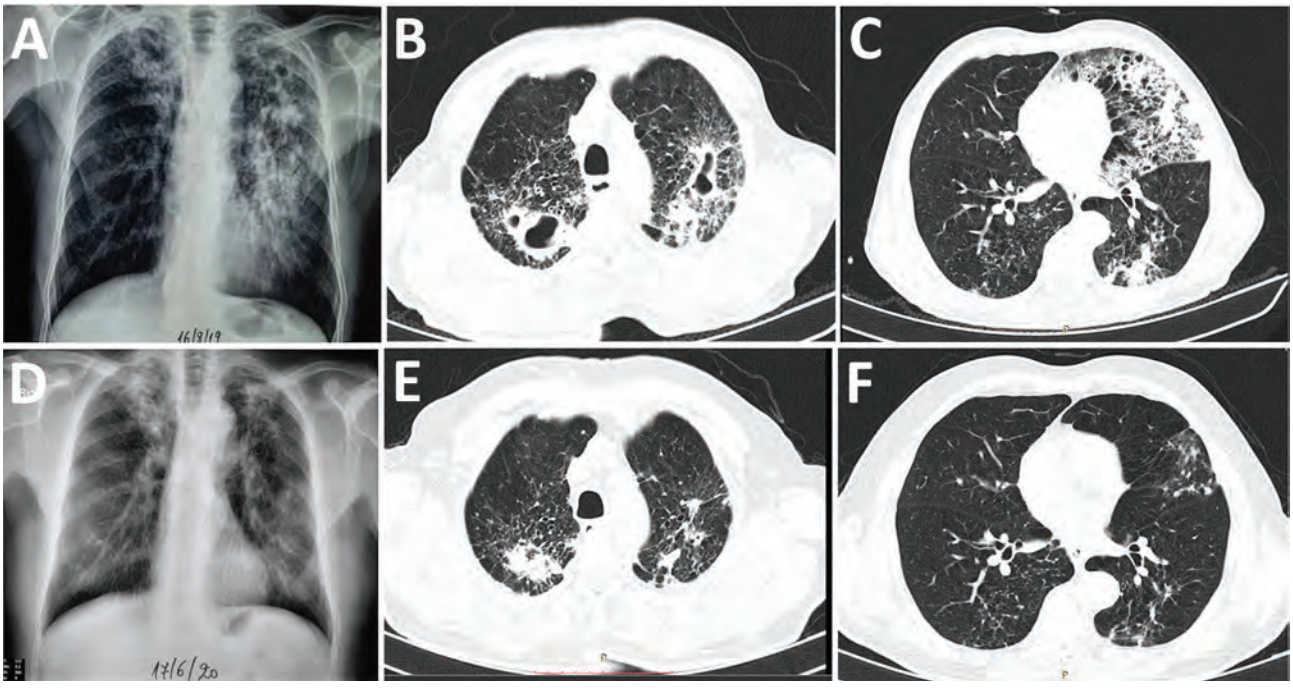

Figure. Comparison of chest radiographs and computed tomography scans before and after the end of treatment for a 65-year-old male goat breeder infected with *Mycobacterium caprae*, northern Greece, 2019. Multiple cavity infiltrations and opacities are shown on the chest radiographs (A) and the computed tomography scan (B, C), mainly in the left upper lobe. After treatment, significant improvement is shown by cavity closure and recession of opacities and infiltration on the chest radiograph (D) and on the chest computed tomography scans (E, F).

capacity and lack of routine surveillance data. Zoonotic TB is a public health hazard, resulting in serious economic losses and having a substantial effect on poor and marginalized communities (*7*).

Contaminated food and airborne transmission pose considerable risks to persons in contact with infected animals or animal products (*7*). In this study, caprine TB was occupationally acquired by a goat farmer with a history of routine close contact with livestock. Pyrazinamide sensitivity and lung localization could have caused an initial misdiagnosis of *M. tuberculosis* infection. Since 2019, enhanced laboratory screening and surveillance for high-risk patients related to animal breeding have been used in Greece. Timely application of bacteriologic and genotyping techniques, less frequently used in routine laboratory investigation until recently, highlighted the role of *M. caprae* as a human pathogen. MIRU-VNTR revealed a unique isolate similar to patterns reported in animals in Eastern Europe and the Balkans (*3*,*8*). Data on *M. caprae* zoonotic TB in Greece are limited. A dairy goat farm outbreak in northern Greece was the first documented in 2005; *M. caprae* caused pneumonia among animals, and the mortality rate reached 92% (*9*). Further, Neonakis et al. (*10*) reported a human *M. bovis* isolate identified as *M. bovis* subsp. *caprae* in a GenoType MTBC assay evaluation study.

M. caprae, a recently identified separate MTBC species, should be carefully addressed nationally and internationally. Key risk populations in countries not officially TB-free and with sizeable goat populations must be identified, occupational history sought, testing capacity extended, and monitoring and reporting improved. A One Health approach that highlights interdependence of human and animal health sectors is needed to curb the spread of this pathogen.

Acknowledgments

We thank all members of the staff involved in the investigation of this study at the National Reference Laboratory for Mycobacteria, Sotiria Chest Diseases Hospital, Athens; the National Public Health Organization, Athens; the Aristotle University Pulmonary Department, G. Papanikolaou Hospital, Thessaloniki; the General Directorate of Veterinary Medicine, Athens; and the Directorate of Public Health, Kilkis Prefecture, Kilkis, Greece.

About the Author

Dr. Papaventsis is a medical director in Clinical Microbiology–Laboratory Medicine at the National Reference Laboratory for Mycobacteria, Sotiria Chest

Diseases Hospital, Athens, Greece. His research interests include molecular diagnosis and genotyping of tuberculosis and infections caused by nontuberculous mycobacteria.

References

1. Aranaz A, Cousins D, Mateos A, Domínguez L. Elevation of *Mycobacterium tuberculosis* subsp. *caprae* Aranaz et al. 1999 to species rank as *Mycobacterium caprae* comb. nov., sp. nov. Int J Syst Evol Microbiol. 2003;53:1785–9. https://doi.org/10.1099/ijs.0.02532-0
2. Prodinger WM, Brandstätter A, Naumann L, Pacciarini M, Kubica T, Boschiroli ML, et al. Characterization of *Mycobacterium caprae* isolates from Europe by mycobacterial interspersed repetitive unit genotyping. J Clin Microbiol. 2005;43:4984–92. https://doi.org/10.1128/JCM.43.10.4984-4992.2005
3. Rodríguez S, Bezos J, Romero B, de Juan L, Álvarez J, Castellanos E, et al.; Spanish Network on Surveillance and Monitoring of Animal Tuberculosis. *Mycobacterium caprae* infection in livestock and wildlife, Spain. Emerg Infect Dis. 2011;17:532–5. https://doi.org/10.3201/eid1703.100618
4. European Food Safety Authority. The European Union One Health 2018 zoonoses report. EFSA J. 2019;17:5926 [cited 2019 Dec 12]. https://www.efsa.europa.eu/en/efsajournal/pub/5926
5. Kubica T, Rüsch-Gerdes S, Niemann S. *Mycobacterium bovis* subsp. *caprae* caused one-third of human *M. bovis*–associated tuberculosis cases reported in Germany between 1999 and 2001. J Clin Microbiol. 2003;41:3070–7. https://doi.org/10.1128/JCM.41.7.3070-3077.2003
6. Allix-Béguec C, Harmsen D, Weniger T, Supply P, Niemann S. Evaluation and strategy for use of MIRU-VNTRplus, a multifunctional database for online analysis of genotyping data and phylogenetic identification of *Mycobacterium tuberculosis* complex isolates. J Clin Microbiol. 2008;46:2692–9. https://doi.org/10.1128/JCM.00540-08
7. World Organization for Animal Health, World Health Organization, Food and Agricultural Organization of the United Nations. Roadmap for zoonotic tuberculosis. 2017 [cited 2020 Oct 23]. http://www.oie.int/fileadmin/Home/eng/Our_scientific_expertise/docs/pdf/Tuberculosis/Roadmap_zoonotic_TB.pdf
8. Valcheva V, Savova-Lalkovska T, Vyazovaya A, Dimitrova A, Bonovska M, Najdenski H. First insight into phylogeography of *Mycobacterium bovis* and *M. caprae* from cattle in Bulgaria. Infect Genet Evol. 2020;81:104240. https://doi.org/10.1016/j.meegid.2020.104240
9. Ikonomopoulos J, Aranaz A, Balaskas C, Sechi L, Gazouli M. Outbreak of acute tuberculosis in a goat herd; first case of *Mycobacterium caprae* isolation in Greece. Online J Vet Res. 2006;10:108–15.
10. Neonakis IK, Gitti Z, Petinaki E, Maraki S, Spandidos DA. Evaluation of the GenoType MTBC assay for differentiating 120 clinical *Mycobacterium tuberculosis* complex isolates. Eur J Clin Microbiol Infect Dis. 2007;26:151–2. https://doi.org/10.1007/s10096-007-0255-y

Address for correspondence: Dimitrios Papaventsis, National Reference Laboratory for Mycobacteria, Sotiria Chest Diseases Hospital, 152 Mesogeion Ave, Athens 11527, Greece; email: papaventsis.d@sotiria.gr, dpapaventsis@gmail.com

Outbreak of Rabbit Hemorrhagic Disease Virus 2 Infection, Ghana

Aruna Ambagala, Patrick Ababio, Lindsey Lamboo, Melissa Goolia, Oliver Lung, Yohannes Berhane, Theophilus Odoom

Author affiliations: National Centre for Foreign Animal Disease, Canadian Food Inspection Agency, Winnipeg, Manitoba, Canada (A. Ambagala, L. Lamboo, M. Goolia, O. Lung, Y. Berhane); Veterinary Services Directorate, Accra Laboratory, Accra, Ghana (P. Ababio, T. Odoom)

DOI: https://doi.org/10.3201/eid2707.210005

In September 2019, high mortality in commercial rabbits was reported in the Greater Accra Region of Ghana. Rabbit hemorrhagic disease virus 2 phylogenetically related to isolates from 2015–2017 outbreaks in the Netherlands was confirmed as the causative agent. The virus has not yet been detected in native rabbits in Ghana.

Rabbit hemorrhagic disease (RHD) is an acute, fatal, highly contagious viral hepatitis in European rabbits (*Oryctolagus cuniculus*) (*1*). It causes severe economic losses in the rabbit meat and fur industries and can have a substantial negative ecological impact on wild rabbit populations and their predators. The causative agent, RHD virus (RHDV; family *Caliciviridae*, genus *Lagovirus*) has a single-stranded positive-sense RNA genome ≈7.4 kb in length. Pathogenic RHDV strains exist in 2 main genotypes, GI.1 and GI.2 (RHDV2). RHDV GI.1 has several variants: GI.1a (proposed as G6/RHDVa), GI.1b (G1), GI.1c (G2), and GI.1d (G3–G5) (*2*). It is considered enzootic in domestic and wild European rabbits in Asia and Europe; sporadic outbreaks occur in the Americas, Middle East, and Africa (*1*). RHDV2 GI.2, a variant first reported in France in 2010 (*3*), differs antigenically from RHDV GI.1 and is therefore considered a distinct serotype. RHDV2, which has replaced RHDV GI.1 in many countries in Europe, infects rabbits of all ages and crosses the species barrier to affect non-European rabbit species (*4*).

Rabbit production, because of its low costs, has been promoted to reduce poverty in Africa but has been threatened by RHD outbreaks since the late 1980s. In 2015, RHDV2 was detected on Tenerife in the Canary Islands (*5*). In April 2017, an outbreak was reported in northern Morocco (*6*) caused by a recombinant GI.1b/GI.1b/GI.2 RHDV2 strain closely related to isolates identified in Portugal in 2014.

During 2015–2018, RHDV2 strains similar to those circulating in France, Portugal, Spain, and Finland were isolated in field rabbits in Tunisia (*7*). Recently, rabbit farms in West Africa have been severely affected by RHD. Using competitive ELISA, researchers in Benin in July 2015 confirmed an RHD outbreak in the coastal city Cotonou (*8*). In February 2016, several RHD outbreaks detected by using real-time reverse transcription PCR (rRT-PCR) in Korhogo in northern Côte d'Ivoire, were resolved but the virus and

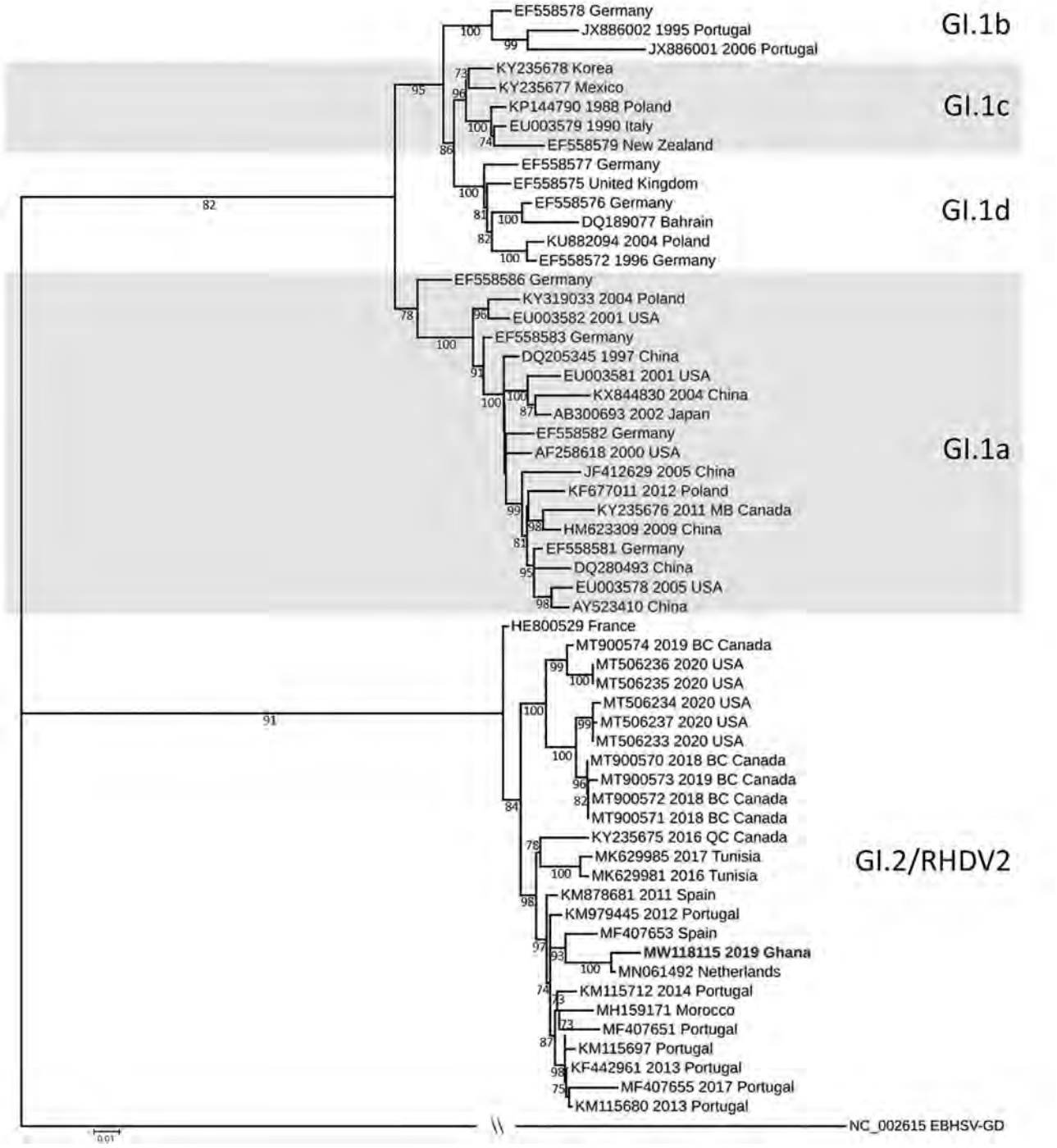

Figure. Maximum-likelihood phylogenetic tree of the viral protein 60 region of rabbit hemorrhagic disease virus from Ghana (boldface) and reference sequences. We downloaded sequences directly from or extracted them from the whole genome sequences downloaded from GenBank. We aligned sequences in Geneious Prime (Geneious, https://www.geneious.com) and constructed the phylogenetic tree with the IQ-TREE Web server (http://iqtree.cibiv.univie.ac.at), using 1,000 bootstrap replicates as indicated in the tree. We then visualized the phylogenetic tree using iTOL (https://itol.embl.de). Scale bar indicates branch length.

rabbit species were not well characterized (*8*). On June 3, 2020, Senegal reported its first RHDV2 outbreak, which killed many farmed Flemish giant, checkered giant, and Fauve de Bourgogne rabbits (*8*). Nigeria's first reported outbreak started in September 2020 at rabbit farms in Kwara and Oya, southwestern states bordering Benin (*8*).

A September 2019 RHDV2 outbreak sickened 11,350 rabbits and killed ≈6,000 in commercial rabbit farms in Dansoman, Korle-Bu, Mamprobi, and Banana Inn in the Ablekuma Central District, Greater Accra Region, Ghana. Clinical signs included dullness, anorexia, convulsion, dyspnea, bloody nasal discharge, mucus in feces, and paralysis. Postmortem examinations revealed multifocal petechial hemorrhages in multiple organs, congested and edematous lungs, pulmonary edema with tracheal foam, splenomegaly, and pale livers with areas of necrosis. Tissue samples from affected animals submitted to the Accra Veterinary Laboratory tested positive for RHDV2. The disease quickly spread to other areas of Ghana, including the Ashanti Central Eastern, Bono, and Ahafo regions. We sent 35 rRT-PCR–positive liver, lung, and spleen samples from different regions of Ghana (Appendix Figure 1, https://wwwnc.cdc.gov/EID/article/27/7/21-0005-App1.pdf) to the National Centre for Foreign Animal Disease in Winnipeg, Manitoba, Canada, where rRT-PCR testing confirmed RHDV2 (*9*).

We extracted nucleic acid from 1 of the samples (RHDV2 Ghana-15 2019; Dansoman, Ghana) with a cycle threshold of 12.73 and subjected it to whole-genome sequencing on an Illumina MiSeq instrument (https://www.illumina.com) after targeted cDNA conversion as described elsewhere (*10*) with modifications. The whole genome sequence (GenBank accession no. MW118115) closely resembled (98.84%) that of RHDV2 isolate RHDV-NL2016 (accession no. MN061492) from the 2015–2017 outbreak in the Netherlands (Appendix Figure 2). We later subjected 14 additional independent samples from different locations in the greater Accra region to whole-genome sequencing (accession no. MW789232–245) and found they were ≥99.73% identical at the nucleotide level to RHDV2 Ghana-15 2019, suggesting that this outbreak was caused by a single incursion.

The viral protein 60 gene of RHDV2 Ghana-15 2019 showed 98.73% identity to the same gene in the isolate from the Netherlands (accession no. MN061492), 96.32% to the isolate (accession no. MF407653) from Spain, and only 94.70% to the isolate from Tunisia (accession no. MK629981; Figure). No sequence information was available from the previous RHDV2 outbreaks in West Africa, and therefore it is not possible to comment on the relatedness of the recent RHDV2 outbreaks in this region. Introduction of RHDV2 at the port cities in West Africa suggests that the virus likely entered each country through imported rabbits or rabbit byproducts and was not spread by rabbits moving across land borders. The outbreak in Ghana continues, and the Ghana Veterinary Authority is considering vaccination to protect local rabbit populations. So far, no RHD cases have been reported in native rabbits in Ghana, but the lack of infections could be simply because native rabbits have not yet been exposed to the virus, which could change in the future.

Acknowledgments

This study was supported by the Canadian Food Inspection Agency and the Ministry of Food and Agriculture of Ghana. The authors thanks Dr. Paul Polku (Accra Metropolitan Veterinary Officer), Dr. Fenteng Danso (Epidemiology Unit) and Dr. Patrick Amponsah (Kumasi Veterinary Laboratory) at the Ministry of Food and Agriculture of Ghana for their help with sample collection.

About the Author

Dr. Ambagala is the section head and the World Organization for Animal Health–designated expert on classical swine fever at the Canadian Food Inspection Agency–National Centre for Foreign Animal Disease, in Winnipeg. Dr. Ambagala's research focuses on the detection, prevention, and control of imported and emerging viral diseases of farm animals.

References

1. Abrantes J, van der Loo W, Le Pendu J, Esteves PJ. Rabbit haemorrhagic disease (RHD) and rabbit haemorrhagic disease virus (RHDV): a review. Vet Res (Faisalabad). 2012;43:12. https://doi.org/10.1186/1297-9716-43-12
2. Le Pendu J, Abrantes J, Bertagnoli S, Guitton JS, Le Gall-Reculé G, Lopes AM, et al. Proposal for a unified classification system and nomenclature of lagoviruses. J Gen Virol. 2017;98:1658–66. https://doi.org/10.1099/jgv.0.000840
3. Le Gall-Reculé G, Zwingelstein F, Boucher S, Le Normand B, Plassiart G, Portejoie Y, et al. Detection of a new variant of rabbit haemorrhagic disease virus in France. Vet Rec. 2011;168:137–8. https://doi.org/10.1136/vr.d697
4. Rouco C, Aguayo-Adán JA, Santoro S, Abrantes J, Delibes-Mateos M. Worldwide rapid spread of the novel rabbit haemorrhagic disease virus (GI.2/RHDV2/b). Transbound Emerg Dis. 2019;66:1762–4. https://doi.org/10.1111/tbed.13189
5. Martin-Alonso A, Martin-Carrillo N, Garcia-Livia K, Valladares B, Foronda P. Emerging rabbit haemorrhagic disease virus 2 (RHDV2) at the gates of the African continent. Infect Genet Evol. 2016;44:46–50. https://doi.org/10.1016/j.meegid.2016.06.034

6. Lopes AM, Rouco C, Esteves PJ, Abrantes J. GI.1b/GI.1b/GI.2 recombinant rabbit hemorrhagic disease virus 2 (Lagovirus europaeus/GI.2) in Morocco, Africa. Arch Virol. 2019;164:279–83. https://doi.org/10.1007/s00705-018-4052-y
7. Rahali N, Sghaier S, Kbaier H, Zanati A, Bahloul C. Genetic characterization and phylogenetic analysis of rabbit hemorrhagic disease virus isolated in Tunisia from 2015 to 2018. Arch Virol. 2019;164:2327–32. https://doi.org/10.1007/s00705-019-04311-z
8. World Organisation for Animal Health. World Animal Health Information System [cited 2021 Jan 3]. https://wahis.oie.int
9. Duarte MD, Carvalho CL, Barros SC, Henriques AM, Ramos F, Fagulha T, et al. A real time Taqman RT-PCR for the detection of rabbit hemorrhagic disease virus 2 (RHDV2). J Virol Methods. 2015;219:90–5. https://doi.org/10.1016/j.jviromet.2015.03.017
10. Logan G, Freimanis GL, King DJ, Valdazo-González B, Bachanek-Bankowska K, Sanderson ND, et al. A universal protocol to generate consensus level genome sequences for foot-and-mouth disease virus and other positive-sense polyadenylated RNA viruses using the Illumina MiSeq. BMC Genomics. 2014;15:828. https://doi.org/10.1186/1471-2164-15-828

Address for correspondence: Aruna Ambagala, CFIA-National Centre for Foreign Animal Disease, 1015 Arlington St, Winnipeg, MB R3E 3M4, Canada; email: aruna.ambagala@canada.ca

Parmigianino. *Portrait of Antea,* c. 1531–1534. Oil on canvas. 53.1 in × 34.6 in. Museo di Capodimonte, Naples, Italy, by kind permission of Ministero della Cultura–Museo e Real Bosco di Capodimonte.

SARS-CoV-2, Mannerism, Marten, Mink, and Man

Mark Swancutt and Terence Chorba

Girolamo Francesco Maria Mazzola (1503–1540), known as Parmigianino (the little one from Parma), was a painter and printmaker. He was born into a family of painters in Parma, Italy, in what was then the Duchy of Milan, and died in Cremona, in northern Italy. He was among the first and most prominent artists of the Mannerist school of art of the Late Renaissance that came after the High Renaissance. The High Renaissance is known for the works of Raphael and the early works of Michelangelo, and its art is treasured for perfection of elegance and qualities of balance, proportion, and absolute beauty. In Mannerism, compositions are said to be exaggerated, almost to a fault, as a reaction to the art of the High Renaissance or perhaps as an attempt to improve on it. In general,

Author affiliations: Fulton County Board of Health, Atlanta, Georgia, USA (M. Swancutt); Centers for Disease Control and Prevention, Atlanta (T. Chorba)

DOI: https://doi.org/10.3201/eid2707.AC2707

Mannerism is characterized by realist but decorous art in which there is subtle, unsettling elongation of figures with stylized features and poses.

Among Parmigianino's more renowned works is a portrait painting from 1531–1534 of a young woman, Antea, which appears on this month's cover. It is unknown whether the painting is an image of a specific person or a stylized composition. We behold a beautiful young woman facing forward, with elongated bodily proportions, as is characteristic of Mannerist works. With a small oval head set upon a large torso and wide shoulders, her arms and hands appear exaggerated in size, as if the parts of her body were proportioned for different paintings. Yet despite these physical disproportions, the viewer has an impression of great beauty, a testimony to the subtlety and success of this Mannerist portrait. Contributing to the incongruousness of the image of this young lady, she is clad in the garments of an older woman, or a woman of an age with which we more commonly associate wealth; Antea is bejeweled, fingering a gold chain with her left hand, and dressed luxuriously. Among her layers of garments are a gold blouse with a fine white apron, a detailed gold satin dress, leather gloves, and a marten fur stole complete with the animal's head, on which the nose is pierced with a ring still attached to a chain.

For millennia, people have worn animal furs, first for survival and protection and later for fashion. In European populations, the wearing of furs of Mustelidae, a family of carnivorous mammals, has been popular. Among the many mustelids are wolverines, weasels (including ermines), otter, badgers, marten (including sables), ferrets, and mink. Since the early Middle Ages, the quest for furs of these animals has played a role in European national expansion into areas where fur-bearing mustelids were populous, including Russia's expansion into Siberia and France and England's expansion into North America. More recently, as with animals of many other species, mustelid fur farming, principally of mink, has become widely practiced in North America and Europe.

We are currently in the midst of a global pandemic caused by SARS-CoV-2, a *Betacoronavirus* related to coronaviruses found in horseshoe bats. SARS-CoV-2 infection spilled over as a zoonosis, perhaps through an intermediate animal, into humans in Hubei, China, a circumstance that was first identified in December 2019. As of May 25, 2021, approximately 168 million cases of SARS-CoV-2 infection and 3.5 million deaths in humans had been reported worldwide. SARS-CoV-2 infection has also naturally spread as a zoonosis from humans to dogs, domestic cats, captive felids (cats) in zoos and sanctuaries, gorillas in zoos, farmed mink, and recently, to pet ferrets. Recent experimental research has shown that many mammals can be infected with the virus, including cats, dogs, bank voles, deer mice, fruit bats, ferrets, hamsters, mink, skunks, pigs, rabbits, raccoon dogs, tree shrews, white-tailed deer, rhesus macaques, and cynomolgus macaques.

Extensive spillback of SARS-CoV-2 from humans to mink on mink farms was first reported in April 2020 in the Netherlands. Mink-to-human transmission has been documented in the Netherlands, Denmark, and Poland and is suspected to have occurred in the United States. In January 2021, a combined report of the Food and Agriculture Organization of the United Nations, the World Organisation for Animal Health (OIE), and the World Health Organization presented data from OIE and other sources from 36 countries with mink farming industries and documented widespread virus transmission, in both Europe and North America. Because of concerns that mink farm populations could serve as a reservoir for ongoing coronaviruses transmission and result in development of mutations that would undermine the effectiveness of SARS-CoV-2 vaccines, large-scale culling of these animals has been pursued by Denmark, the Netherlands, and Spain. Coronavirus variants have been identified in mink farms, including one with three amino-acid changes and two deletions in the spike protein. The escape of mink from farms into the wild is quite common; in one region of Denmark, 79% of wild mink have been found to be escapees. Presence of phylogenetically related SARS-CoV-2 in farmed mink and in free-ranging mink was first reported in Utah, USA, in December 2020. As with any zoonotic pathogen, the transmission of SARS-CoV-2 between animals and people emphasizes the importance of the One Health concept in the global approach to diseases that affect people and animals living in our shared environment.

Just as aspects of the figures in Mannerist paintings often need explanation that can be complicated, difficult, and anxiety provoking, the issues surrounding fur farming for fashion, potential exchange of SARS-CoV-2 between human populations and various animal species, and the massive culling of the commercial mink population are also complex and controversial. However, it appears that in addition to all the human-to-human contact prevention measures needed to control and eliminate SARS-CoV-2 transmission, interventions that reduce contact of humans or domestic (or farmed) animals with bats or other susceptible wild animals will be needed to avert future spillover with pandemic potential. Like the rat-borne Black Plague of the mid-14th century

that ravaged the Italian states where Parmigianino executed his magnificent portrayal of Antea with her luxurious mustelid stole a century and a half later, the current coronavirus pandemic underscores again how we share pathogens with other species. With more than 1 million deaths and 1 billion infections attributed annually to zoonotic infections before the SARS-CoV-2 pandemic, we are challenged to assess and mitigate the potential risks of coronavirus transmission posed by fur farms, to both humans and other animals. These are but two facets of the multifaceted public health goal of One Health, noted by CDC, "of achieving optimal health outcomes recognizing the interconnection between people, animals, plants, and their shared environment."

Bibliography

1. Centers for Disease Control and Prevention. COVID-19 and animals: mink and SARS-CoV-19 [cited 2021 Apr 20]. https://www.cdc.gov/coronavirus/2019-ncov/daily-life-coping/animals.html
2. Centers for Disease Control and Prevention. One Health basics [cited 2021 Apr 19]. https://www.cdc.gov/onehealth/basics/index.html
3. Delahay RJ, de la Fuente J, Smith GC, Sharun K, Snary EL, Flores Girón L, et al. Assessing the risks of SARS-CoV-2 in wildlife. One Health Outlook. 2021;3:7. https://doi.org/10.1186/s42522-021-00039-6
4. Ghai RR, Carpenter A, Liew AY, Martin KB, Herring MK, Gerber SI, et al. Animal reservoirs and hosts for emerging alphacoronaviruses and betacoronaviruses. Emerg Infect Dis. 2021;27:1015–22. https://doi.org/10.3201/eid2704.203945
5. Giner J, Villanueva-Saz S, Tobajas AP, Pérez MD, González A, Verde M, et al. SARS-CoV-2 seroprevalence in household domestic ferrets (Mustela putorius furo). Animals (Basel). 2021;11:667. PubMed https://doi.org/10.3390/ani11030667
6. Gombrich EH. Art and illusion: a study in the psychology of pictorial representation. Princeton (NJ): Princeton University Press; 1956.
7. Hammer AS, Quaade ML, Rasmussen TB, Fonager J, Rasmussen M, Mundbjerg K, et al. SARS-CoV-2 transmission between mink (Neovison vison) and humans, Denmark. Emerg Infect Dis. 2021;27:547–51. https://doi.org/10.3201/eid2702.203794
8. Karesh WB, Dobson A, Lloyd-Smith JO, Lubroth J, Dixon MA, Bennett M, et al. Ecology of zoonoses: natural and unnatural histories. Lancet. 2012;380:1936–45. https://doi.org/10.1016/S0140-6736(12)61678-X
9. Koslov M. US confirms world's first SARS-CoV-2 cases in gorillas. Jan 12, 2021 [cited 2012 Apr 20]. https://www.the-scientist.com/news-opinion/us-confirms-worlds-first-sars-cov-2-cases-in-gorillas-68347
10. Neilson C. Parmigianino's Antea: a beautiful artifice. New York: The Frick Collection; 2008.
11. Pagh S, Pertoldi C, Petersen HH, Jensen TH, Hansen MS, Madsen S, et al. Methods for the identification of farm escapees in feral mink (Neovison vison) populations. PLoS One. 2019;14:e0224559. https://doi.org/10.1371/journal.pone.0224559
12. Landauro I. COVID-19 update (319): Spain (AR) animal, farmed mink, 1st rep. ProMed Archive no. 20200717.7584560 [cited 2021 Apr 20]. https://promedmail.org/promed-post/?id=20200717.7584560
13. Ayudhya SSN, Kuiken T. Reverse zoonosis of COVID-19: lessons from the 2009 influenza pandemic. Vet Pathol. 2021;58:234–42. https://doi.org/10.1177/0300985820979843
14. World Health Organization. SARS-CoV-2 in animals used for fur farming [cited 2021 Apr 19]. https://www.who.int/publications/i/item/WHO-2019-nCoV-fur-farming-risk-assessment-2021.1
15. Zhou P, Shi ZL. SARS-CoV-2 spillover events. Science. 2021; 371:120–2. PubMed https://doi.org/10.1126/science.abf6097

Address for correspondence: Terence Chorba, Centers for Disease Control and Prevention, 1600 Clifton Rd NE, Mailstop US12-4, Atlanta, GA 30329-4027, USA; email: tlc2@cdc.gov

EMERGING INFECTIOUS DISEASES®

Upcoming Issue

- Considerations for Implementing a Successful Coronavirus Disease Vaccination Program in Africa
- *Mycobacterium microti* Infections in Free-Ranging Red Deer (*Cervus elaphus*)
- Severe Arboviral Encephalitis Observed among 4 Human Cases of Eastern Equine Encephalitis, Connecticut, USA, 2019
- Spatial, Ecologic, and Clinical Epidemiology of Community-Onset, Ceftriaxone-Resistant Enterobacteriaceae, Cook County, Illinois, USA
- Fungemia and other Fungal Infections Associated with Use of *Saccharomyces boulardii* Probiotic Supplements
- Peridomestic Mammal Susceptibility to Severe Acute Respiratory Syndrome Coronavirus 2 Infection
- Social Distancing, Mask Use, and Transmission of Severe Acute Respiratory Syndrome Coronavirus 2, Brazil, April–June 2020
- Transmission Dynamics of SARS-CoV-2 in High-Density Settings, Minnesota, USA, March–June 2020
- Intense and Mild First Wave of COVID-19, The Gambia
- Epidemiology and Spatial Emergence of Anaplasmosis, New York, USA, 2010–2018
- Natural Human Infections with *Plasmodium cynomolgi*, *Plasmodium inui*, and 4 other Simian Malaria Parasites, Malaysia
- SARS-CoV-2 Prevalence among Outpatients during a Period of Community Transmission in 6 Districts in Zambia, July 2020
- Weekly SARS-CoV-2 Sentinel Surveillance in Primary Schools, Kindergartens, and Nurseries, Germany, June–November 2020
- Zoonotic Soil-Transmitted Helminths in Free-Roaming Dogs, Kiribati, Western Pacific
- Outbreak of SARS-CoV-2 B.1.1.7 Lineage after Vaccination in Long-Term Care Facility, Germany, February–March 2021
- Delayed Antibody and T-Cell Response to BNT162b2 Vaccination in the Elderly, Germany
- SARS-CoV-2 Superspread in Fitness Center, Hong Kong, China, March 2021
- Persistence of SARS-CoV-2–Specific IgG in Children 6 Months After Infection, Australia
- Plague Transmission from Corpses and Carcasses

Complete list of articles in the August issue at http://www.cdc.gov/eid/upcoming.htm

Earning CME Credit

To obtain credit, you should first read the journal article. After reading the article, you should be able to answer the following, related, multiple-choice questions. To complete the questions (with a minimum 75% passing score) and earn continuing medical education (CME) credit, please go to http://www.medscape.org/journal/eid. Credit cannot be obtained for tests completed on paper, although you may use the worksheet below to keep a record of your answers.

You must be a registered user on http://www.medscape.org. If you are not registered on http://www.medscape.org, please click on the "Register" link on the right hand side of the website.

Only one answer is correct for each question. Once you successfully answer all post-test questions, you will be able to view and/or print your certificate. For questions regarding this activity, contact the accredited provider, CME@medscape.net. For technical assistance, contact CME@medscape.net. American Medical Association's Physician's Recognition Award (AMA PRA) credits are accepted in the US as evidence of participation in CME activities. For further information on this award, please go to https://www.ama-assn.org. The AMA has determined that physicians not licensed in the US who participate in this CME activity are eligible for AMA PRA Category 1 Credits™. Through agreements that the AMA has made with agencies in some countries, AMA PRA credit may be acceptable as evidence of participation in CME activities. If you are not licensed in the US, please complete the questions online, print the AMA PRA CME credit certificate, and present it to your national medical association for review.

Article Title

Non–*C. difficile* Clostridioides Bacteremia in Intensive Care Patients, France

CME Questions

1. Which of the following statements regarding the background of patients admitted to the intensive care unit (ICU) with Clostridioides bacteremia (CB) in the current study is most accurate?

A. Approximately half of patients with CB had no underlying comorbidities
B. >40% of patients with CB had cancer
C. >60% of patients had recent surgery or trauma
D. Septic shock at the time of admission was rare

2. Which of the following statements regarding the clinical presentation of patients with CB in the current study is most accurate?

A. Digestive symptoms were the most common presenting symptoms
B. Myonecrosis was present at admission in most patients
C. Most patients had evidence of acute hemolysis
D. Most patients had evidence of acute leukopenia

3. Which of the following statements regarding the microbiology of CB among patients in the current study was most accurate?

A. *C. perfringens* was isolated from > 30% of patients
B. < 10% of cases were polymicrobial
C. The rate of Clostridioides resistance to β-lactam antibiotics exceeded 50%
D. Patients treated with clindamycin experienced lower mortality rates compared with other antibiotics

4. All of the following factors were associated with a higher risk for death due to CB in the current study EXCEPT:

A. Older age
B. Higher Sequential Organ Failure Assessment (SOFA) score
C. Male sex
D. The presence of hemolysis

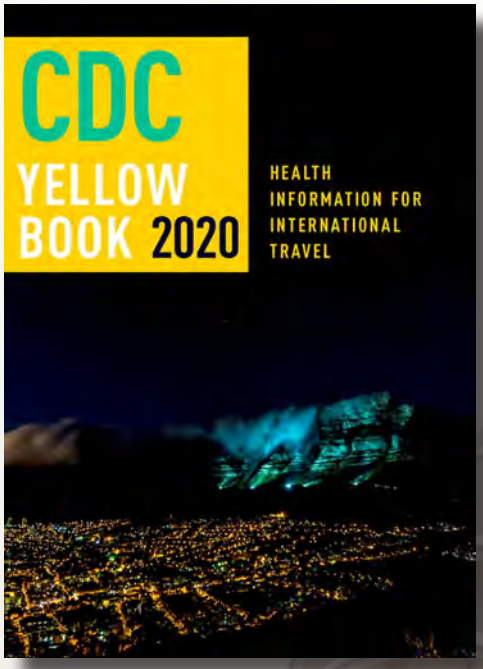

Available Now
Yellow Book 2020

The fully revised and updated CDC Yellow Book 2020: Health Information for International Travel codifies the US government's most current health guidelines and information for clinicians advising international travelers, including pretravel vaccine recommendations, destination-specific health advice, and easy-to-reference maps, tables, and charts.

ISBN: 978-0-19-006597-3 | $115.00 | May 2019 | Hardback | 720 pages

ISBN: 978-0-19-092893-3 | $55.00 | May 2019 | Paperback | 687 pages

Yellow Book 2020 includes important travel medicine updates

- **The latest information on emerging infectious disease threats, such as Zika, Ebola, and henipaviruses**
- **Considerations for treating infectious diseases in the face of increasing antimicrobial resistance**
- **Legal issues facing clinicians who provide travel health care**
- **Special considerations for unique types of travel, such as wilderness expeditions, work-related travel, and study abroad**

OXFORD
UNIVERSITY PRESS

Order your copy at:
www.oup.com/academic